Rhenium- and Technetium-tricarbonyl Core-based Supramolecular Metallocavitands and Helicates

A Thesis Submitted for the Degree of

DOCTOR OF PHILOSOPHY

By

MAMINA BHOL

School of Chemistry
University Of Hyderabad
Hyderabad 500046
INDIA

JULY 2022

Dedicated to
My FAMILY

CONTENTS

STATEMENT

I hereby declare that the matter embodied in this thesis is the result of investigations carried out by me in the School of Chemistry, University of Hyderabad, Hyderabad, under the supervision of **Prof. M. Sathiyendiran**.

In keeping with the general practice of reporting scientific observations, due acknowledgments have been made wherever the work described is based on the findings of other investigators.

15/07/2022
Hyderabad
JULY 2022

Mamina Bhol
Mamina Bhol
(16CHPH14)

DECLARATION

I, **Mamina Bhol**, hereby declare that this thesis entitled **"Rhenium- and Technetium-tricarbonyl Core-based Supramolecular Metallocavitands and Helicates"** submitted by me under the guidance and supervision of **Prof. M. Sathiyendiran**, is a bonafide research work which is also free from plagiarism. I also declare that it has not been submitted previously in part or in full to this university or any other university or institution for the award of any degree or diploma. I hereby agree that my thesis can be deposited in Shodhganga/INFLIBNET.

A report on plagiarism statistics from the University Librarian is enclosed.

Date: 15-07-2022

Name: Mamina Bhol

Reg. No.: 16CHPH14

Mamina Bhol

Signature of the student

M. Sathiyendiran.

Signature of the Supervisor

Dr. M.Sathiyendiran
Professor
School of Chemistry
University of Hyderabad
Hyderabad - 500 046, India.

UNIVERSITY OF HYDERABAD
Prof. M. Sathiyendiran

SCHOOL OF CHEMISTRY
HYDERABAD-500046, INDIA

Phone: +91-40-2313-4811 (Office), 2313-4911 (Lab) E-mail: msathi@uohyd.ac.in

CERTIFICATE

This is to certify that the thesis entitled **"Rhenium- and Technetium-tricarbonyl Core- based Supramolecular Metallocavitands and Helicates"** submitted by **Mamina Bhol** bearing registration number **16CHPH14** in partial fulfillment of the requirements for the award of the Doctor of Philosophy (Ph. D.) is a bonafide work carried out by her under my supervision and guidance in the School of Chemistry, University of Hyderabad. This thesis is free from plagiarism and has not been submitted previously in part or in full to this or any other University or Institution for the award of any degree or diploma. Further, the student has five publications before submission of the thesis for adjudication and has produced shreds of evidence for the same in the form of reprints.

Parts of this thesis have been published as the following articles:

1. **M. Bhol**, B. Shankar, M. Sathiyendiran, *Dalton Trans.* **2018**, *47*, 4494-4500 (***Chapter 2***).
2. **M. Bhol**, G. Claude, M. Roca Jungfer, U. Abram, M. Sathiyendiran, *Inorg. Chem.* **2022**, *61*, 5173-5177 (***Chapter 4***).
3. **M. Bhol**, B. Shankar, M. Sathiyendiran, *Inorg. Chem.* **2022**, DOI: 10.1021/acs.inorgchem.2c02061 (***Chapter 3***).

She has also made presentations in the following conferences:

1. **Poster:** *NMSTC-2017: National Meeting of Synthetic and Theoretical Chemists***,** University of Hyderabad, Telangana, India; 2017 Oct. 13-14.
2. **Poster:** *ICCCS-2017: 8th International Collaborative & Cooperative Chemistry Symposium*, University of Hyderabad, Telangana, India; 2017 Dec 18-19.
3. **Poster:** *CHEMFEST-2018: 15th Annual in- House Symposium*, University of Hyderabad, Telangana, India; 2018 Mar. 9-10 **(Best Poster Award)**.
4. **Poster:** *CHEMFEST-2019: 16th Annual in- House Symposium*, University of Hyderabad, Telangana, India; 2019 Feb. 22-23 **(Best Poster Award).**
5. **Oral:** *ACST-2019: International Conference on Advances in Chemical Sciences and Technologies*, National Institute of Technology, Warangal, India; 2019 Sep. 23-25.

6. **Poster**: *MTIC 2019: International Conference on Modern Trends In Inorganic Chemistry-XVIII,* Indian Institute of Technology Guwahati, Assam, India; 2019 Dec.11-14.
7. **Poster:** *CHEMFEST-2020: 17th Annual in- House Symposium,* University of Hyderabad, Telangana, India; 2020 Feb. 27-28.
8. **Oral:** *CHEMFEST-2020: 19th Annual in- House Symposium,* University of Hyderabad, Telangana, India; 2022 Apr. 22-23 **(Best Oral Presentation Award by RSC).**

Further the student has passed the following courses towards the fulfilment of coursework requirement for Ph. D.

Sl. No.	Course No.	Title of the Course	No. of Credits	Result
1.	CY801	Research Proposal	3	Pass
2.	CY805	Instrumental Methods-A	3	Pass
3.	CY806	Instrumental Methods-B	3	Pass
4.	CY451	Main Group & Inner Transition Elements	3	Pass

Hyderabad
JULY 2022

M. Sathiyendiran
Prof. M. Sathiyendiran
(Thesis Supervisor)

Dr. M.Sathiyendiran
Professor
School of Chemistry
University of Hyderabad
Hyderabad - 500 046, India.

Dean
School of Chemistry
University of Hyderabad
Hyderabad- 500046, INDIA

Dean
SCHOOL OF CHEMISTRY
University of Hyderabad
Hyderabad-500 046

ACKNOWLEDGEMENTS

I would like to express my sincere gratitude to my Ph.D. supervisor Prof. M. Sathiyendiran for his valuable guidance, helpful suggestions, and constructive criticisms during my Ph.D. research work.

I wish to extend my gratitude to my doctoral committee members, Prof. S. Pal and Prof. V. Bhaskar, for their insightful suggestions and encouragement.

I want to thank present and former deans, School of Chemistry, University of Hyderabad, and all the faculty members of the school of chemistry for their help and support on various occasions.

My special thanks to Prof. Ulrich Abram (Institute for Chemistry and Biochemistry, Freie Universität Berlin) for giving me an excellent opportunity to work with him on ^{99}Tc-chemistry. I am highly grateful to him for his valuable guidance, immense support, and great care during my research stay in Berlin.

I want to acknowledge University Grant Commission, Delhi (National Fellowship), and Erasmus+ Exchange Program, Berlin (Erasmus+ Grant) for financial support during my Ph.D. research tenure.

I want to extend my thanks to all non-teaching members of the school of chemistry, especially Mr. Abram for his help in official work (School Office), Mr. Durgesh and Mr. Mahender (NMR, School of Chemistry), Mr. A.V. R. Kumar, and Mr. Mahesh Rathod (SC-XRD, School of Chemistry), Mrs. Asia Parwez and Dr. Manasi Dalai (HRMS, School of Chemistry), and Mr. Anand (IR, School of Chemistry), for their keen help, assistance, and cooperation with instruments during my research work.

I am very much glad to thank my teachers of undergraduate and postgraduate programs who have sown the seeds of chemistry in my mind.

I would also like to thank all my lab seniors, Dr. Bhaskaran Shankar, Dr. P. Rajakannu, Dr. C. Kiran Kumar, Dr. Sruthi Bayya, and Dr. Amritanjali Tiwari, for their constructive comments and helpful discussion. I am very grateful to all my colleagues, Soumya, Isha, Moon, Upasana, Reema, and Vengadesh, for their help and for creating a pleasant research environment and making it a memorable and enjoyable journey. I extend my thanks to all the project students who worked with me, Bhuvana, Neha, Diya, Rasagna, Saranya, and Nitha.

I am grateful to everyone from Prof. Abrams's group for a great time during my research stay at FUB, especially to Dr. Max Roca Jungfer, Guilhem Claude, Bruna, Moritz Ernst, and Jonas Genz for the great and friendly working atmosphere. I am also grateful to Dr. Adelheid Hagenbach for her helpfulness, loving gesture, and support, and Ms. Jacqueline Grewe and Mr. Falk Wenzlaff for their help with the technical stuff.

I express my most profound appreciation to Dr. Majhi Shankar, Dr. Anil Kumar Gunnam, Dr. Rajendra Kumar Mallick, Dr. N. Tanmaya Kumar, Dr. Arijit Saha, Ms. Suchismita Subhadarshini, Ms. Sameeta Sahoo, Ms. Sipra Sucharita Sahoo, Ms. Mou Mondal, Hema, Gourachand, Suman, Smrutipragyan, Pradipta, Uma, Sailendra, Satya, Chiru, Baikuntha, Biswa, Saritha, Priya, Soumya, Smrutilipi, Sachi, Abhipsa, Sabnam, Manas, Aradhana, Arijit and Manoj for being a great bunch of people, and providing a friendly and homely atmosphere during my stay in the campus. Especially I would like to thank Dr. Anil Kumar Gunnam and Dr. N Tanmaya Kumar, who always had an open ear for my worries and guided me through my Ph.D. studies.

I thank Dr. K. Sathish Kumar, Dr. Sudhir Mittapalli, Dr. M. Sateesh, Dr. Suryanarayana Allu, Dr. R. Amaleswari, Dr. N. Senthilnathan, Jyotsna, Pritam, Irfan, Nilanjan, Suman, Soutric, Akram, Sarada, Mr. Alim, and Shanti for their help and support on several occasions.

Special warmest thanks to Prachi, Jubu, Thoi, Jay, Bandita, Ilu, Shubham, Debjyoti, Kamala, and Smruti for always being there for me through thick and thin. This endeavor would not have been possible without you people's unconditional love, generosity, and immense support. I am incredibly fortunate to have you people in my life.

Most importantly, I thank my family members, whose continuous care, strong emotional support, and prayer encouraged me throughout my academic research and daily life.

This dissertation is the conclusion of an incredible journey, full of beautiful and difficult moments which made me grow as a strong person besides as a researcher. Finally, I thank God Almighty for his grace and blessings.

Mamina Bhol

JULY 2022

List of abbreviations and symbols

SCCs	Supramolecular coordination complexes
fac	facial
Re	Rhenium
Tc	Technetium
2D	Two Dimensional
3D	Three Dimensional
DMSO	Dimethyl Sulfoxide
THF	Tetrahydrofuran
DMF	N,N-Dimethylformamide
DCM	Dichloromethane
$CHCl_3$	Chloroform
$CDCl_3$	Deuterated Chloroform
CD_2Cl_2	Deuterated Dichloromethane
DMSO-d_6	Deuterated Dimethyl Sulphoxide
MLCT	Metal-to-Ligand Charge Transfer
LLCT	Ligand-to-Ligand Charge Transfer
ILCT	Intra-Ligand Charge Transfer
UV-Vis	Ultraviolet-Visible
ATR-IR	Attenuated Total Reflectance Infrared spectroscopy
FT-IR	Fourier-transform Infrared Spectroscopy
NMR	Nuclear Magnetic Resonance
DOSY	Diffusion Ordered Spectroscopy
ESI- HR-MS	Electron Spray Ionization High Resolution Mass Spectrometry
SCXRD	Single Crystal X-Ray Diffraction
DNA	Deoxyribonucleic acid
Ppm	Parts per million

Å	Angstrom
hr	Hour
m/z	Mass to charge ratio
mg	Milligram
mL	Millilitre
nm	Nanometer
δ	Chemical shift
Hz	Hertz
MHz	Megahertz
λ_{abs}	Absorption wavelength
λ_{max}	Absorption maxima
λ_{exc}	Excitation wavelength
λ_{em}	Emission wavelength
J	Coupling constant
K	Binding constant
KOH	Potassium hydroxide
NaH	Sodium hydride
AcOH	Acetic acid
HBr	Hydrobromic acid
NaCl	Sodium Chloride
Na_2SO_4	Sodium Sulphate
KBr	Potassium bromide
H_2-dhbq	2,5-dihydroxy-1,4-benzoquinone
H_2-dhaq	1,4-dihydroxy-9,10-anthraquinone
H_2-dhnq	6,11-dihydroxy-5,12-naphthacenedione
H_2-CA	Chloranilic acid

SYNOPSIS

The thesis entitled "**Rhenium- and Technetium-tricarbonyl Core-based Supramolecular Metallocavitands and Helicates**" consists of six chapters.

Chapter 1: Introduction

Chapter 1 begins with the general introduction of supramolecular chemistry and its two main branches, i.e., host-guest chemistry and self-assembly. Further, the developments and applications of metallosupramolecular chemistry, including metallacalixarene and metallo- helicate/ mesocates, are discussed with a very short classification of calixarenes, helicates, and mesocates. The chapter highlights the rhenium and technetium-based metallocycles, their basic design principle, and mainly literature survey and discussion on various aspects of the chemistry of $Re(CO)_3$ core-based metallacalix[n]arenes (n = 3, 4), metallo-helicates, meso-helicates, and $Tc(CO)_3$ core based metallocycles.

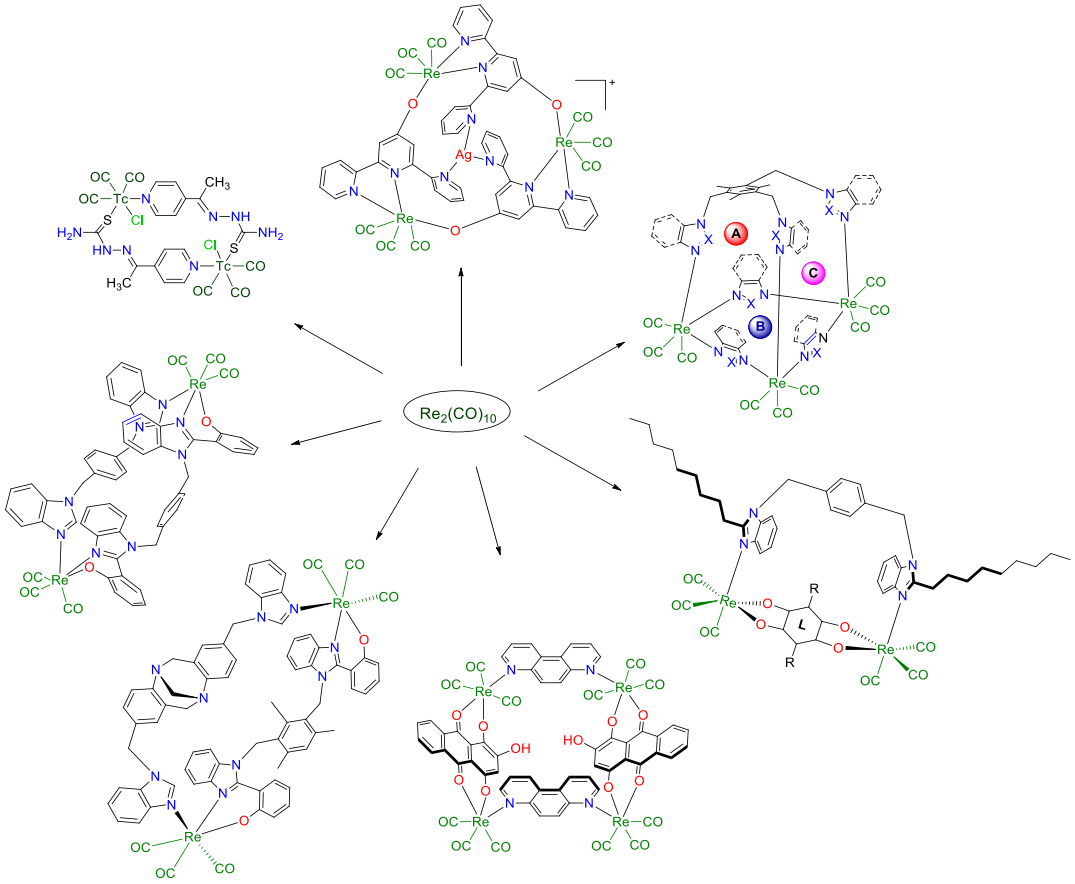

Scheme 1. Various known examples of M(I) core-based (M = Re/Tc) metallacycles.

Chapter 2: Re(I)-based Irregular Pentagonal-shaped Metallocavitands: Self-Assembly and Molecular Recognition Studies.

This chapter describes the design and synthesis of three new neutral ditopic flexible N-donor ligands (L^n = (L^1 = bis(4-(naphtho[2,3-d]imidazol-1-ylmethyl)phenyl)methane, L^2 = bis(4-(benzimidazol-1-ylmethyl)phenyl)methane and L^3 = bis(4-(2-nonyl benzimidazol-1-ylmethyl)phenyl)methane)) possessing bis(4-methylphenyl)methane spacer with multi-arene fused imidazole donor unit. The L^n were further utilized to develop metallocavitands analogous of calix[5]arene framework with larger cavity. The metallocavitands **1-4** were assembled from $Re_2(CO)_{10}$, rigid bis-chelating donor (H_2-dhaq = 1,4-dihydroxy-9,10-anthraquinone and H_2-CA = chloranilic acid) and L^n via solvothermal approach. The ligands and metallocavitands were characterized by analytical and spectroscopic methods and further **1** and **4** were confirmed by single crystal X-ray diffraction analysis which reveals that a toluene molecule is residing in the hydrophobic cavity. The L^n and **1-4** are emissive at room temperature. The internal cavity of the metallocavitand acts as host for aromatic guest molecules. The host-guest interaction properties of **1** with various nitroaromatic and polyaromatic hydrocarbons were studied by emission spectroscopic method. The study provides a way to prepare metallocavitands with a tunable cavity and functional group via simple one-pot method.

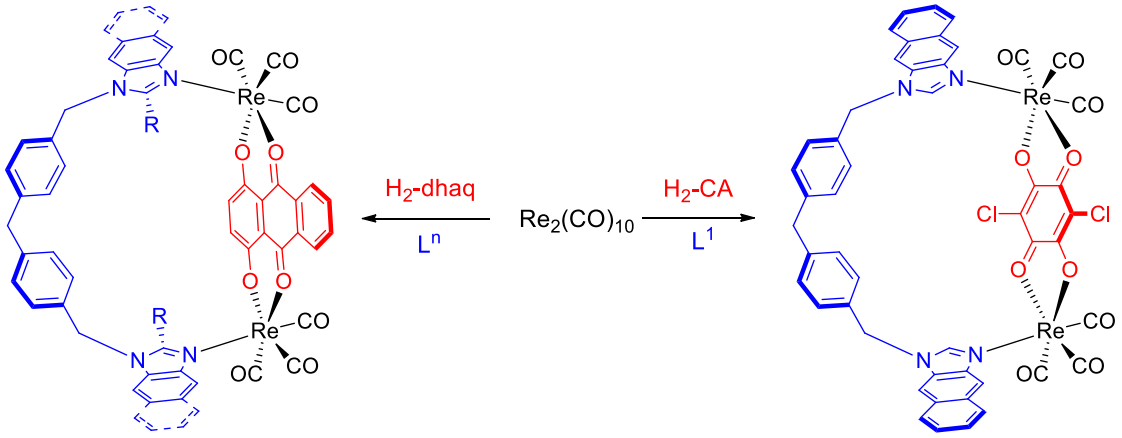

1, $L^n = L^1$, R = H; N donor = naphthanoimidazolyl
2, $L^n = L^2$, R = H; N donor = benzimidazolyl
3, $L^n = L^3$, R = -$(CH_2)_8$–CH_3; N donor = benzimidazolyl

4

Scheme 2. Synthesis of irregular pentagonal-shaped metallocavitands.

Chapter 3: Rhenium(I) Based Heteroleptic Pentagonal Toroid-Shaped Metallocavitands: Self-Assembly and Molecular Recognition Studies.

In chapter 3, a family of neutral, heteroleptic, dinuclear M_2LL'-type pentagonal toroid-shaped metallomacrocycles (**1–8**) were synthesized using $Re_2(CO)_{10}$, rigid bis-chelating ligands and flexible ditopic N donor ligands in a one-pot solvothermal self-assembly approach. The ligands and the metallomacrocycles were characterized using ATR-IR, ESI-MS, NMR, UV-Vis, and emission spectroscopic methods. The molecular structures of **1**, **2**, **4**, **6**, and **7** were confirmed by X-ray diffraction study. The solid-state structures of the supramolecules reveal that they can accommodate acetone, mesitylene, toluene and chlorobenzene like guest molecules inside their internal cavity. The photo-physical properties of the ligands and the metallomacrocycles were studied. The host-guest recognition properties of metallocavitands **1**, **2**, **7**, and **8** as a model host with phenol- and nitrobenzene-derivatives as guest molecules were studied by emission spectroscopic methods.

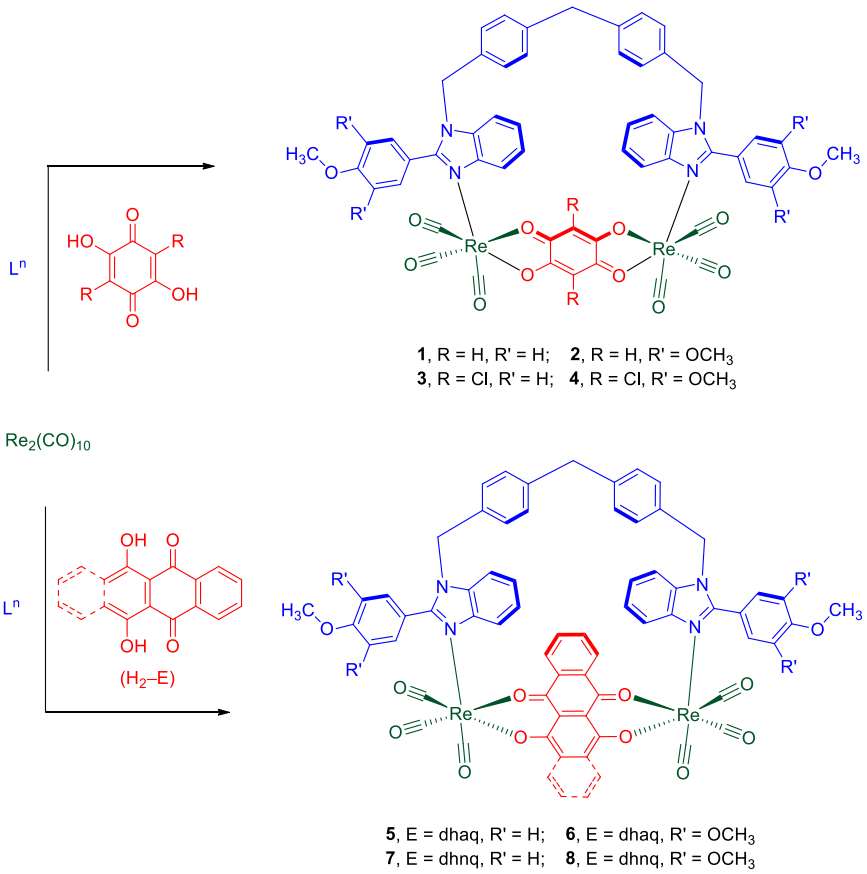

Scheme 3. Synthesis of pentagonal toroid -shaped metallocavitands.

Chapter 4: Calix[4]arene-Analogous Technetium and Rhenium Core-based Supramolecules

In chapter 4, two new type of neutral flexible bidentate nitrogen donor ligands (L^1 and L^2) consisting of four arene units covalently joined *via* methylene units with bismesitylene spacer were designed and synthesized. The L^n were further utilized to self-assemble calix[4]arene-analogous technetium supramolecules (**1**-**2**) using $(NBu_4)[Tc_2(\mu\text{-}Cl)_3(CO)_6]$. The neutral homoleptic technetium macrocycles adopt a partial cone/cone-shaped conformation in the solid-state. These supramolecules are the first example of *fac*-$[Tc(CO)_3]^+$ core-based metallacalix[4]arenes and second example of *fac*-$[Tc(CO)_3]^+$ core-based metallomacrocycles. Structurally similar *fac*-$[Re(CO)_3]^+$ core-based macrocycles (**3**-**4**) were also prepared using $[Re(CO)_5X]$ (where X = Cl or Br) and L^1 or L^2. The products were characterized spectroscopically and by X-ray analysis. The solid-state structures of the supramolecules reveal that these molecules adopt bowl-shaped structures. The molecular recognition studies of rhenium macrocycles were studied using emission spectroscopic methods.

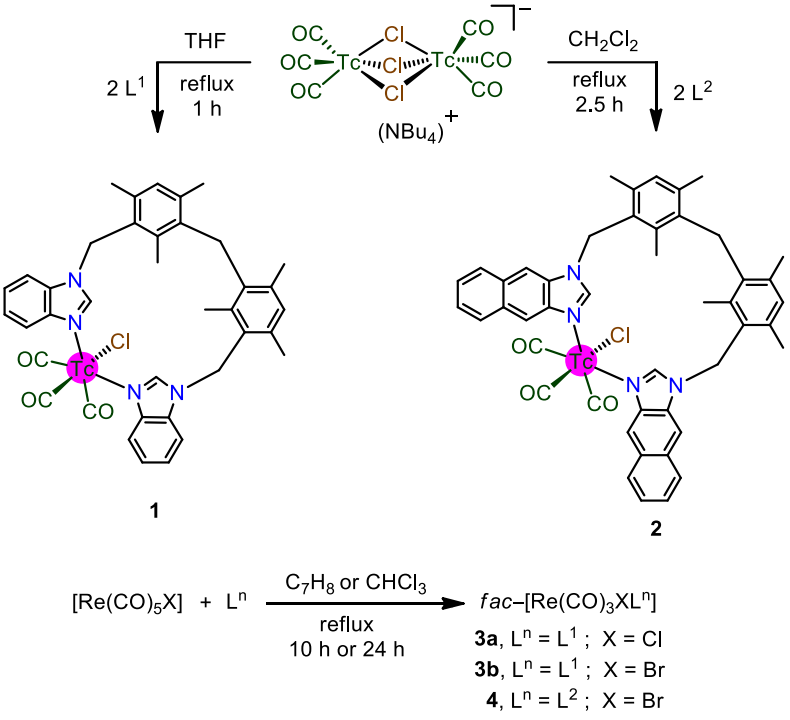

Scheme 4. Synthesis of calix[4]arene-analogous *fac*-$M(CO)_3$ (M = Tc/ Re) core-based supramolecules.

Chapter 5: Self-Assembly and Photophysical Properties of Rheniumtricarbonyl-Based Helicates and Mesocates

In Chapter 5, five rhenium tricarbonyl core-based supramolecular coordination complexes (SCCs) (**1**–**5**) were assembled using $Re_2(CO)_{10}$, rigid/flexible bis-chelating ligands (L^1, L^2), and flexible ditopic N donor ligands (L^3, L^4, L^5, L^6) via a one-pot approach. The metallosupramolecules were characterized spectroscopically and by X-ray analysis. The supramolecular structures of the complexes closely remain in the solution based on the ^{1}H NMR and ESI-mass analysis. Single-crystal X-ray analysis reveals that the dinuclear SCCs adopt heteroleptic double-stranded helical and mesocate architectures in the solid-state. The photophysical properties of the complexes were studied both in solution and solid state. All the supramolecules display emissions both in solution and solid state.

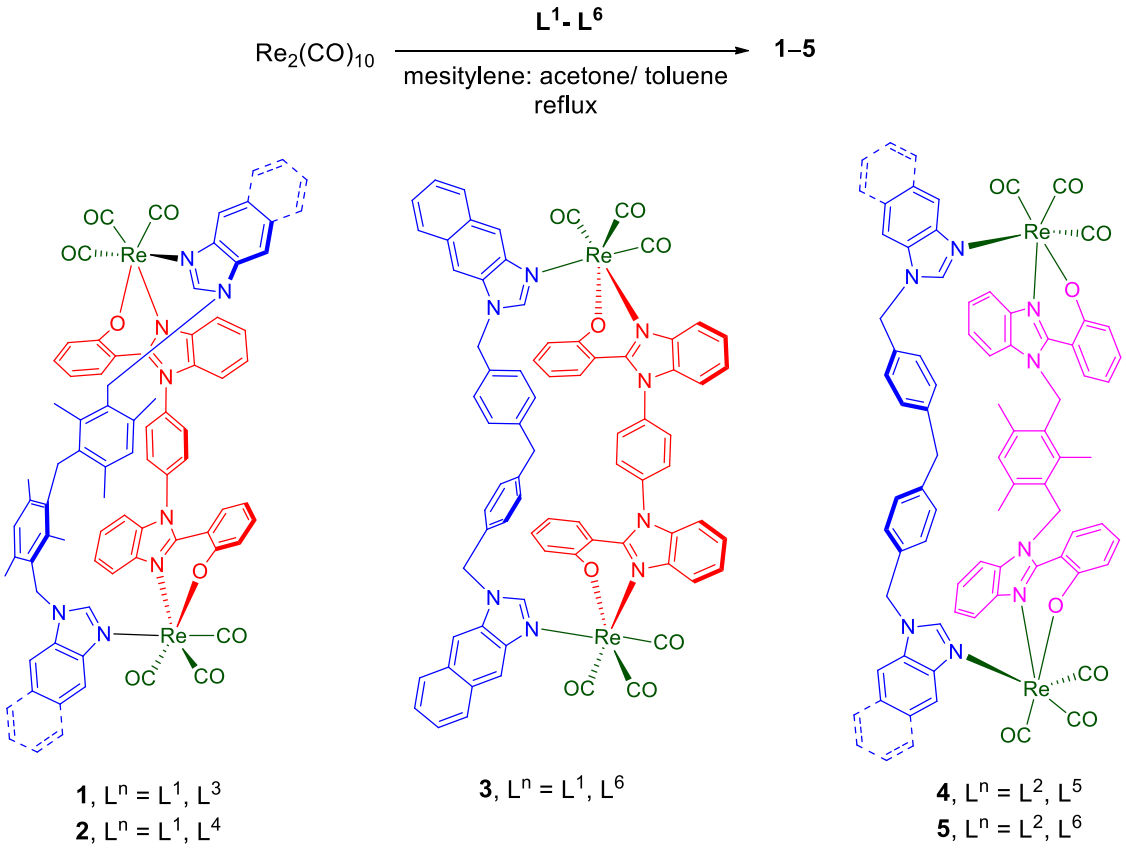

Scheme 5. Synthesis of $Re(CO)_3$ core-based Helicates (**1-2**) and Mesocates (**3-5**).

Chapter 6: Conclusion and Future Perspective

The thesis is summarized, and the possible future direction of the work is also discussed in this chapter. A series of new neutral, flexible bidentate nitrogen donor ligands with diarylmethane spacers were designed and synthesized. Further the nitrogen donor ligands were utilized to construct various sizes and shapes of [*fac*-$M(CO)_3]^+$ (M = Re/Tc) core-based supramolecular architectures, including rhenium- or technetium-based mononuclear homoleptic metallacalix[4]arenes, dinuclear rhenium heteroleptic metallacalix[5]arenes, and dinuclear rhenium heterostranded helicates and mesohelicates. Host-guest studies were carried out for rhenium-based metallacalix[n]arenes (n = 4, 5) by using emission spectroscopy.

Chapter 1

Introduction

1.1. Supramolecular chemistry

The field of supramolecular chemistry mainly focuses on the chemistry aspects of molecular assemblies and on intermolecular bonds.[1] Jean-Marie Lehn defines supramolecular chemistry as the "Chemistry beyond the molecules" as it deals with intermolecular interactions.[1] Supramolecular chemistry can also be called as "Lego block chemistry", where each molecular building block can be compared to a lego brick. Various intermolecular interactions such as hydrogen bonding, metal coordination, π···π interaction, Van der Waals forces, electrostatic and hydrophobic or solvatophilic interactions are responsible for holding these discrete molecular units together.[1-3]

Supramolecular chemistry is mainly divided into two main categories, i.e., host-guest chemistry and self-assembly.[1,3] Host-guest chemistry involves the study of large host molecules having a convergent binding site, capable of encapsulating small guest molecules with divergent binding sites through non-covalent interactions and best regarded as lock and key principle given by Emili Fischer in 1894. [3-5] In host- guest chemistry both should have mutual spatially and electronically complementary binding sites to form a supramolecules like a perfect fitting pieces of jigsaw puzzle.[4] Lehn and co-workers first introduced the concept of "self-assembly" which describes the spontaneous and reversible association of two or more units to make highly ordered non-covalently bound aggregate. [1a, 3, 6] Self-assembly is the main synthetic method for the design of metallo-supramolecular complexes, where the predesigned ligands and metal precursor units organize themselves into a stable, structurally well-defined aggregate. [7a]

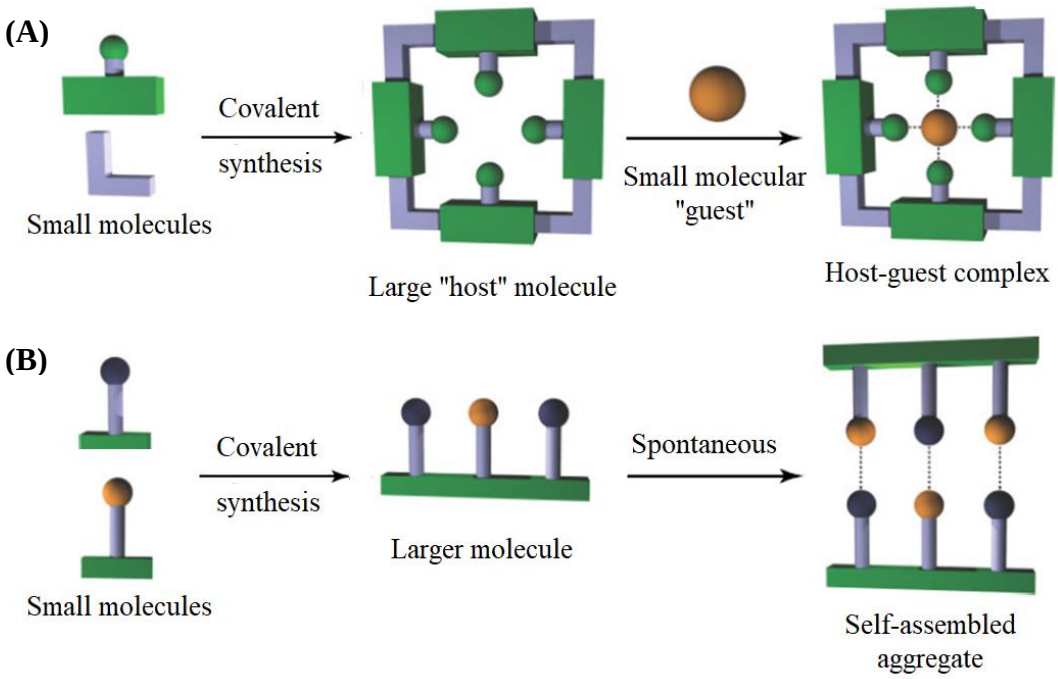

Figure 1.1. Supramolecular systems developed from molecular building blocks (binding sites are represented by circles); (A) host–guest complex (B) self-assembly between complementary molecules.[3]

1.2. Metallosupramolecular chemistry

Supramolecular assemblies, which involve the interaction between the metal ions and the predesigned organic ligand strands, are termed as metallo-supramolecular chemistry.[7] The appropriate choice of metal source and predesigned ligand plays an important role in tuning the shape and size of metallamacrocycles.[8] The metal ion's coordination preference, shape, and bonding mode of the ligands control the self-assembly of metallacycles.[8] The lability and reversibility of the metal-ligand coordination bond are crucial elements for the assembly of supramolecular complexes due to the possibility of formation of both kinetic and thermodynamic products. Some well-known examples of discrete metallo-supramolecular assemblies include metallacycles,[8-9] metallocavitands,[8c] helicates,[10-11] polygon/polyhedra,[8f,12,13] tetrahedra,[8e,13] cages,[8e,14] grids,[15] ladder/rack[15b,c] catenane,[16] rotaxane,[16] knot,[16b,17] links,[16c,17] and various other architectures. The metallacycles offer the benefits of the properties of metal-ligand bonds along with photophysical, redox generated features and photochemical as a result of the metal-ligand orbital overlap. Supramolecular metallacycles can be assembled by using several synthetic approaches, including orthogonal bonding, directional-bonding, symmetry interactions, weak-link, and rigidity modulated

approaches.[8e,14a,d,15c] Out of all the class of discrete metallo-supramolecules calixarene shaped metallocavitands and supramolecular helicates has gained special attention in the supramolecular chemistry field due to their potential application in molecular recognition including DNA recognition, selective reactivity, catalysis, bioimaging, selective sensors for biological analytes, anticancer agents and photo-sensitizers. [8b-e, 9,11]

1.3. Calixarenes and metallacalixarenes

David Gutsche and co-workers first introduced the word calixarene in 1975.[18] Calix[n]arenes are the organic macrocycles or cyclic oligomers obtained spontaneously via phenol-formaldehyde condensation under alkaline conditions.[18-19] The word calix comes from the resemblance of the shape of calyx krater vases of ancient Greece, and the term arene refers to the repeating aryl groups.[18] Calixarenes possess a hydrophobic wide upper rim and a hydrophilic narrow lower rim, and a central annulus (cavity) in their molecular architectures.

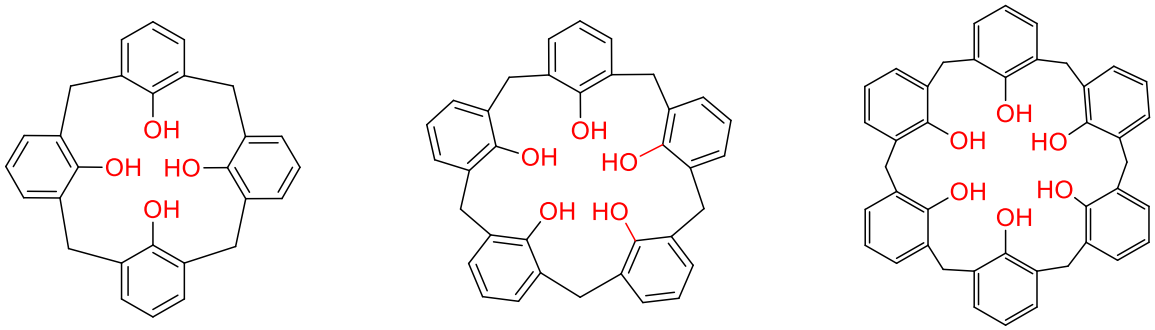

Calix[4]arene Calix[5]arene Calix[6]arene

Figure 1.2. Various types of calixarenes.

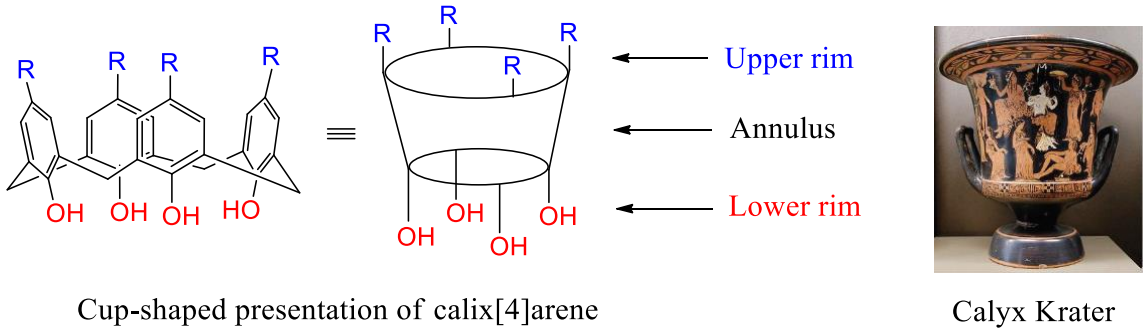

Cup-shaped presentation of calix[4]arene Calyx Krater

Figure 1.3. Structure and pictorial presentation of the shape of calix[4]arene.

Calixarenes have hydrophobic cavities that can accommodate ions or smaller guest molecules and fit in to the class of cavitands recognized in host-guest chemistry. The easy rotation of $-CH_2-Ar-CH_2-$ leads to have four limiting calixarene conformations, including cone, partial cone, 1,2-alternate and 1,3-alternate.[18]

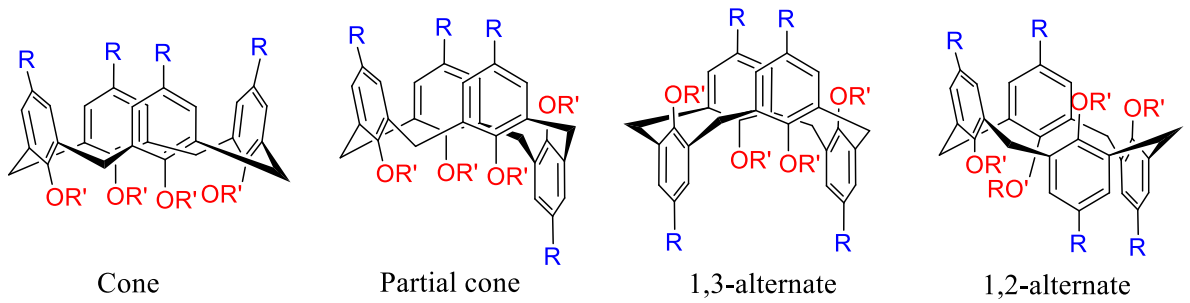

Figure 1.4. Various conformations of calix[4]arene.

Bernhard Lippert first coined the name "metallacalixarenes" in 1992, and compared the structures of self-assembled palladium and platinum discrete organic macrocycles derived from the nucleobases, theophylline and, guanine to the classical calixarene structure.[20] Thus, metallacalixarenes can defined as a class of metallacycles whose structures are similar to classic calixarene, where metal core replace the $-CH_2-$ groups and phenol rings are replaced by aromatic units, mimicking the calixarene walls.[20]

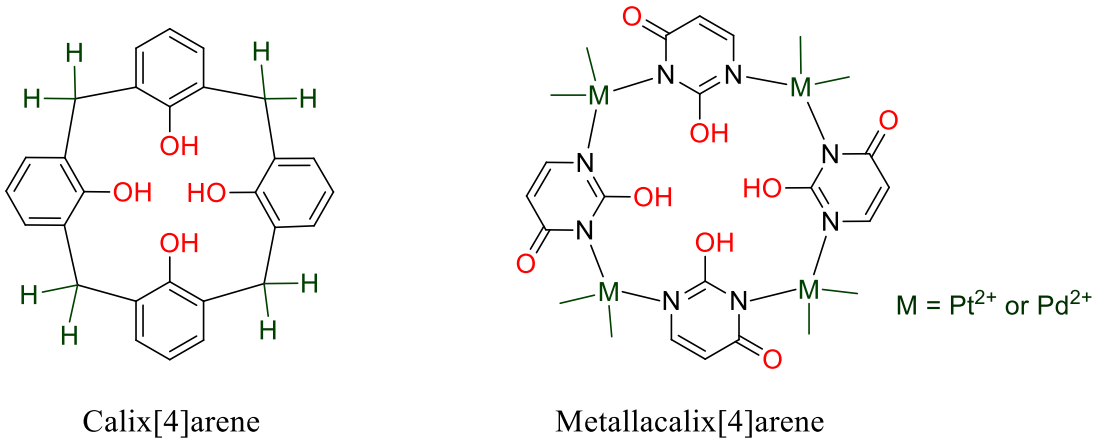

Figure 1.5. Schematic representation of the structural resemblance between a classical calix[4]arene (left) and a metallacalix[4]arene (right).

1.4. Molecular helicates and mesocates

Jean-Marie Lehn and co-workers first introduced the term "helicate" in 1987 to describe polynuclear copper double-stranded helical complexes containing 2,2'-bipyridine binding groups joined through bridging motifs as ligand strands.[10a] The term helicate is coined from the greek word helix (spiral, twist or winding) with suffix "–ate" which refer to the complexes between metal ions and pre-organized ligand strands.[10d] The supramolecular helicates are the discrete complexes where ligand strands are wrapped around the metal-metal helical axis in a helical fashion and ligands adopt a more linear "S" type conformation.[10,11a,21] The "C" type conformation of the ligands in complexes leads to meso-helicate structure, where ligand strands are arranged in a side-by-side manner with respect to the helical axis.[11a,21] Spacers are responsible for the size of cavity and the chirality of the helicate. Helicate architectures can be categorized by defining structural nature of helicate.[21] On the basis of number of metal ions; helicates can be mononuclear, dinuclear or trinucluear.[10d] Number of ligand strands defines the double, triple or quadruple stranded helicates.[10b-e] In homostranded helicates the ligand strands are identical whereas in heterostranded helicates the strands are different.[10d] The binding domains on the ligand strands can be same or different which give on to the formation of homotopic or heterotopic helicates.[10d] The parallel or antiparallel alignment of heterotopic strands leads to head-to-head or head-to-tail manner, respectively.[10d] When the coordination sphere of the metal ion is satisfied by the binding units of the ligand strands, they are referred as saturated helicates whereas they are described as unsaturated helicates when supplementary ligands are coordinated to the metal centres to enable their steriochemical requirments.[10d]

1.5. Rhenium-based metallamacrocycles

Among several synthetic approaches involving various metal precursors, the *fac*-$Re(CO)_3$ core based metallamacrocycles exhibit a distinctive class of stable, functional and robust metal-based cyclic architectures to form neutral 2D and 3D metallacycles.[22-24] We are mainly interested in the *fac*-$Re(CO)_3$ core based neutral metallamacrocycles because these SCCs display potential applications in molecular recognition, as photoluminescence quenching probes, cavity controlled catalysis, anticancer agents, photo- and electro-chemical sensing.[22-24.]

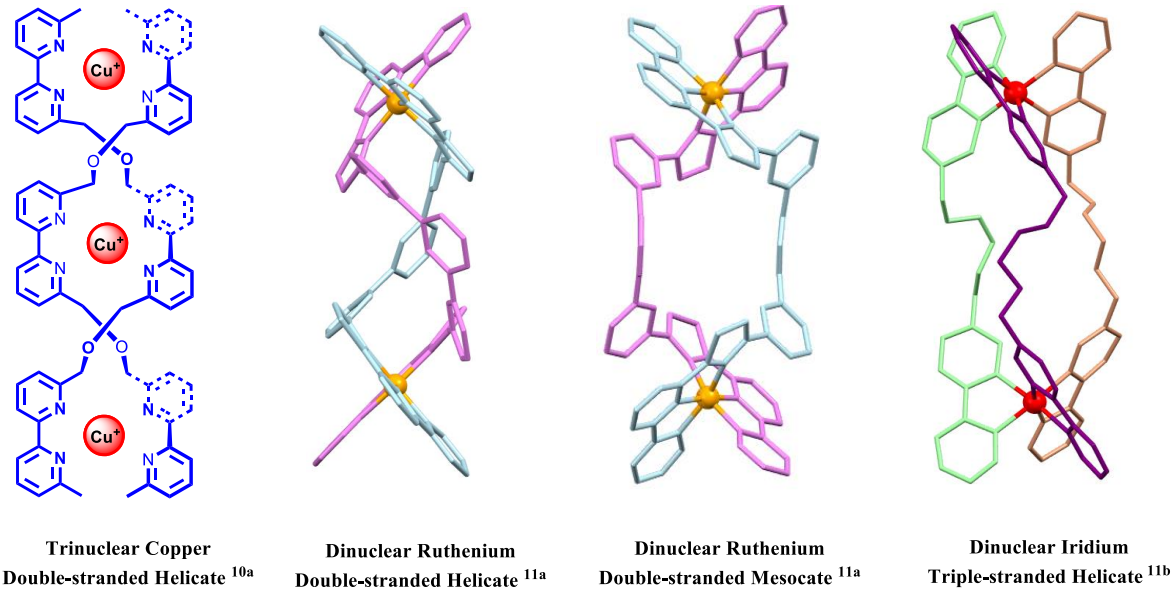

Figure 1.6. Various examples of helicates and mesocate.

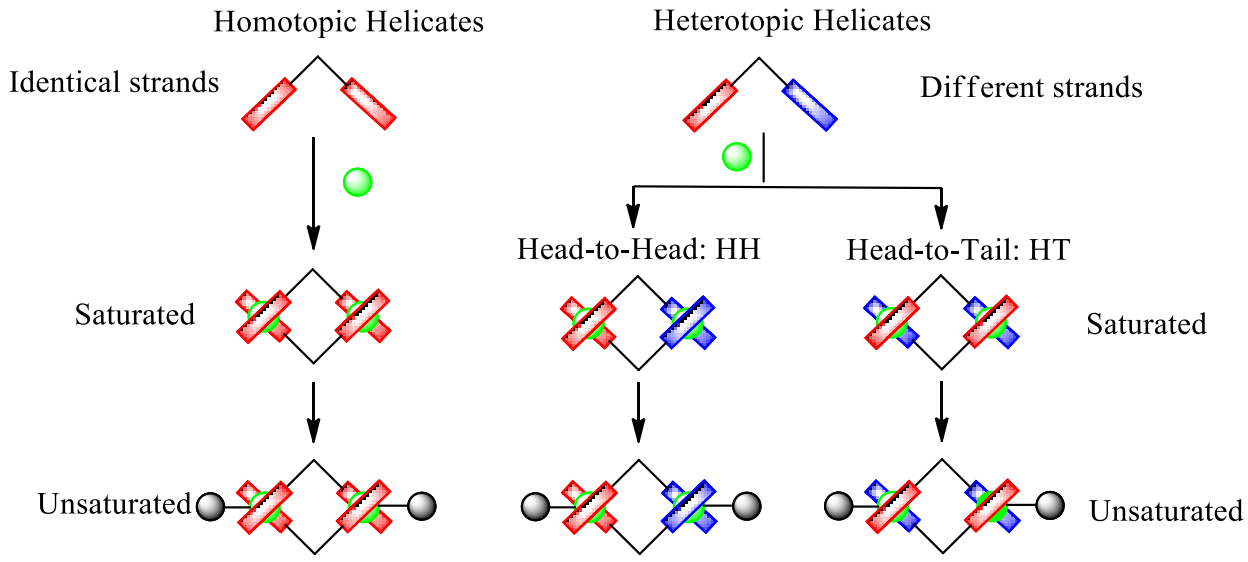

Figure 1.7. Classification of self-assembled helicates.

The *fac*-$Re(CO)_3$ fragment is kinetically inert and biocompatible which makes it as a very significant unit in medicinal field. Due to virtually identical chemical and physical properties of Re and Tc (Atomic radii: Re- 1.37 Å; Tc- 1.36 Å, lipophilicity, ionic mobility, and formal charge), advances in the *fac*-$Re(CO)_3$ based chemistry might be exploited for the designing and development of new *fac*-$^{99m}Tc(CO)_3$ core based radiopharmaceuticals as diagnostic and therapeutic agents.[25] Known examples of different shapes of *fac*-$Re(CO)_3$ core based cyclic supramolecular architectures are (M = Re(I); M′ = other metal ions) mononuclear-ML, dinuclear-$MM'L_2$, M_2LL', M_2L_2; trinuclear- M_3L_3, M_3L_3L', $M_3M'L_3$; tetranuclear squares-M_4L, M_4L_4, $M_4LL'_2$; rectangles-$M_4L_2L'_2$, $M_4L_2L'_4$; bowls-$M_4L_2L'_2$; gondolas-$M_4L_2L'_2$; calixarene-M_2LL'; bicycles-M_4L_2L', $M_6L_2L'_3$; spheroids-$M_6LL'_6$; wheel-$M_6L_2L'_6$; hexanuclear prisms- $M_6L_2L'_6$, $M_6L_2L'_3$; and octanuclear prisms-$M_8L_2L'_8$, $M_8L_2L'_4$.

1.5.1. General synthetic methods for rhenium-based metallamacrocycles

Rhenium carbonyl metal precursors such as $Re_2(CO)_{10}$, $Re(CO)_5OTf$, $Re(CO)_5Br$, $Re(CO)_5Cl$, and $[Re(CO)_3(dmso\text{-}O)_3](CF_3SO_3)$ are mostly used to synthesize various *fac*-$Re(CO)_3$ core based metallacycles along with organic ligand strands.[22-24] Two dimensional rhenium metallacycles can be synthesized by using the metal precursors such as $Re(CO)_5OTf$, $Re(CO)_5Br$, and $Re(CO)_5Cl$, which provides the ditopic metal-acceptor *fac*-$[Re(CO)_3X]$ (X= Br/Cl) core with *cis* bis-coordinating vacant sites that can assist two neutral organic donors. The dinuclear $Re_2(CO)_{10}$ metal precursor provides tritopic metal acceptor *fac*-$Re(CO)_3$ core having three vacant sites along with an angle of 90^o. Neutral 3D metallacycles can be self-assembled by combining *fac*-$Re(CO)_3$ core and suitable ditopic or tritopic neutral ligands with two electron donor along with a three electron donor bis-chelating anionic units. The organic ligand strands used to construct rhenium metallacycles are mainly nitrogen, phosphorous donors and other ligands such as thiols, alcohols, selenols and anionic organic bis-chelating motifs. The heteroleptic or homoleptic metallacycles can be achieved by the appropriate choice of nitrogen donors with/without ancillary ligands and rhenium metal precursors. Further these supramolecules can be obtained by one-step or two-step or by multi-step approaches.

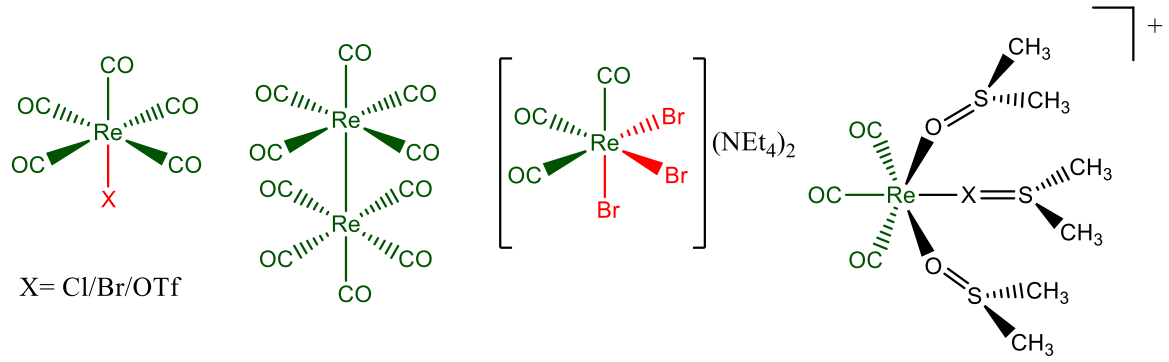

Figure 1.8. Various rheniumcarbonyl core-based starting materials used for the construction of *fac*-[Re(CO)$_3$] core-based SCCs.

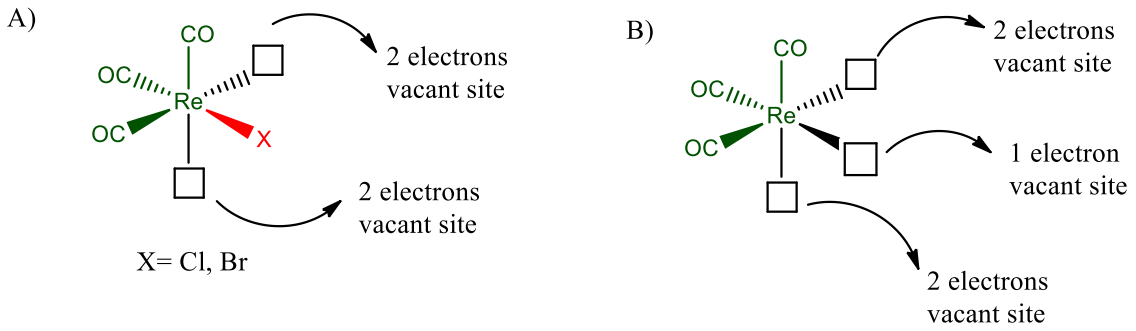

Figure 1.9. Different types of vacant coordination sites available on *fac*–Re(CO)$_3$ core.

1.6. Technetium-based metallamacrocycles

The design and synthesis of stable and kinetically inert *fac*-[M(CO)$_3$]$^+$ (M = ^{99m}Tc/ $^{186/188}$Re) core-based complexes have been gaining continuous research interest for the development of new radiopharmaceuticals as diagnostic and therapeutic agents.[25-26] ^{99m}Tc is still the workhorse of nuclear diagnostics due to its ideal nuclear decay properties ($t_{1/2}$ = 6.02 h, pure γ emitter, Eγ = 140 keV, 89%), whereas the beta-emitting rhenium nuclides ^{188}Re ($t_{1/2}$ = 17 h, E_β = 2.12 MeV) and ^{186}Re ($t_{1/2}$ = 89.3 h, E_β = 1.07 MeV) possess potential for therapy.[25] Iso-structural technetium and rhenium complexes are good candidates for nuclear medical theranostics. The known synthetic approaches for making *fac*-[Re(CO)$_3$]$^+$ core-based discrete supramolecules can be applied to create structurally analogous *fac*-[Tc(CO)$_3$]$^+$ core-based supramolecules.[22-24] Technetium carbonyl metal precursors such as (NBu$_4$)[Tc$_2$(μ–Cl)$_3$(CO)$_6$], (NEt$_4$)$_2$[TcCl$_3$(CO)$_3$], and [Tc(CO)$_3$(H$_2$O)$_3$]$^+$ are mostly used to synthesize various

fac-$Tc(CO)_3$ core-based complexes along with organic ligands.[25-27] The synthesis of *fac*-$[Tc(CO)_3]^+$ core-based macrocycles may result in a new class of supramolecules that may find potential utility in the medicinal fields due to the combined properties of the technetium(I) tricarbonyl core and discrete 2D/3D supramolecular structures.

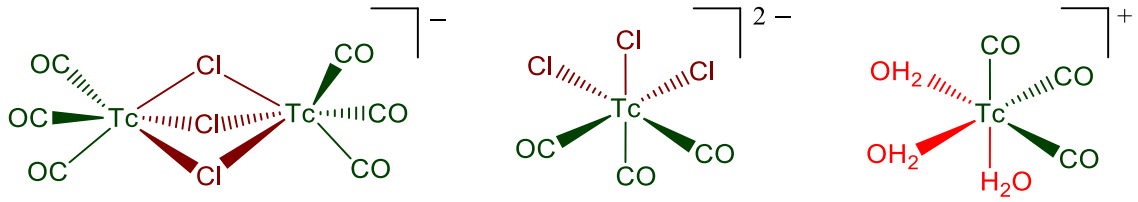

Figure 1.10. Various technetiumcarbonyl core-based starting materials used for the construction of *fac*-$[Tc(CO)_3]^+$ core-based complexes.

1.7. Molecular Recognition

One of the utmost important achievements of supramolecular chemistry is the design and synthesis of molecular architectures which can encapsulate and recognize guest molecules selectively and detect signals for the presence of specific guest molecules. Various non-covalent interactions like van der Waals interactions, hydrogen-bonding, and electrostatic interactions are involved and govern the ability of supramolecular complexes to act as a host for molecular recognition. Metallo-supramolecules are of great interest due to their ease of synthesis from simple complementary units. In particular, *fac*-$Re(CO)_3$ metal core-based metallacycles have been proved to be potential hosts for various guest molecules, including, cations, anions, and aromatic molecules, where the right choice of ligand motifs can easily tune the dimension of the internal cavity. Potential applications of supramolecular coordination complexes in molecular recognition have encouraged the design and synthesis of molecules that can be used therapeutically by interacting with biological systems as anticancer drugs.

The following sections cover the literature survey and discussion on various aspects of the chemistry of $Re(CO)_3$ core-based metallacalix[n]arenes (n = 3, 4), helicates, and meso-helicates and $Tc(CO)_3$ core-based cyclic systems.

1.8. $Re(CO)_3$ core-based metallacalix[3]arenes

Few rheniumtricarbonyl-based supramolecules with calix[3]arene shaped structures are known. These molecules have hydrophobic cavity suitable to accommodate neutral molecules and ions. The mononuclear complex *fac*-$[ReBr(C_7H_4N_3O_2)(CO)_3][NEt]_4$ (**1**), which was obtained from $[ReBr_3(CO)_3][NEt_4]_2$, 3-hydroxy-1,2,3-benzotriazine-4(3H)-one (**2**), and KOH in methanol.[28] This mononuclear complex (**1**) transformed to cyclic metallacalix[3]arene (**3**) by abstraction of coordinated bromide and counter cation by using $AgBr_4$. This ionic trirhenium metallacalix[3]arene acts as host for boron tetrabromide ion.[28]

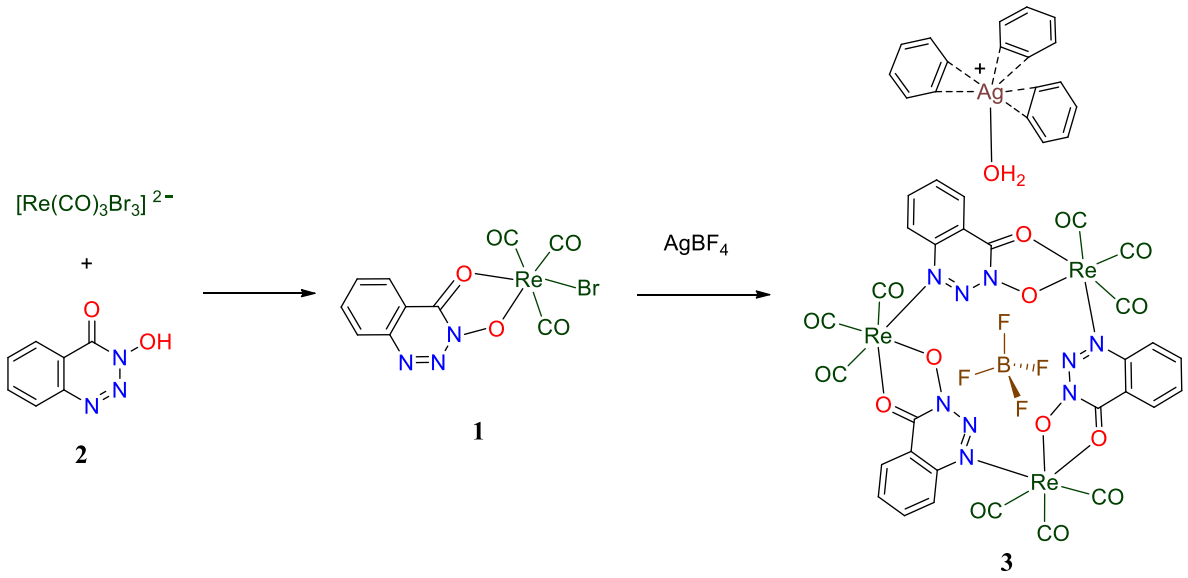

Figure 1.11. Synthesis of ionic trirhenium metallacalix[3]arene.

The reaction of bispyridylpyridone (**4**) with $[Re(CO)_5X]$ (X = Br, Cl) resulted in calix[3]arene analogous trinuclear rhenium metallacycles (**5** and **6**) which acts as a molecular vessel. [29] The pyridyl pendants are coordinated to a silver ion and form a propeller-shaped stopper to the molecular vessel. Upon irradiation at 405 nm, the Ag ion detaches from the system and the resulting neutral host-system is useful for silver ions transport through cell membrane. On cupper binding this luminescent vessel suggests that it can be a potential as PET imaging agents/biomedical fluorescence.

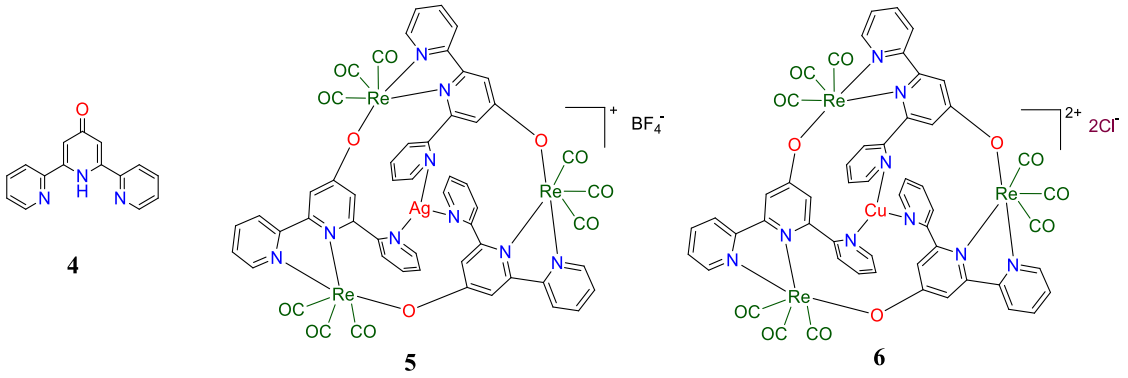

Figure 1.12. Trinuclear rhenium metallacalix[3]arenes.

Pyrazolonaterhenium(I) complexes were synthesised by treating $[ReX(CO)_5]$ (X = Cl, Br), with thiosemicarbazones ligands (**7** and **8**) obtained from β-keto esters in refluxing toluene which resulted in the cyclization of the ligand to give an unexcpected homoleptic metallacalix[3]arenes (**9** and **10**).[30] Another example of trinuclear rhenium metallacalix[3]arene (**11**) were self-assembled from the one pot reflux reaction of $[Re(CO)_5X]$ (X = Cl, Br), triethylamine and, 2-pyridyltetrazolate (**12**) in toluene. They adopt partial cone conformations and possess good luminescent properties and showed reversible three electron oxidation.[31]

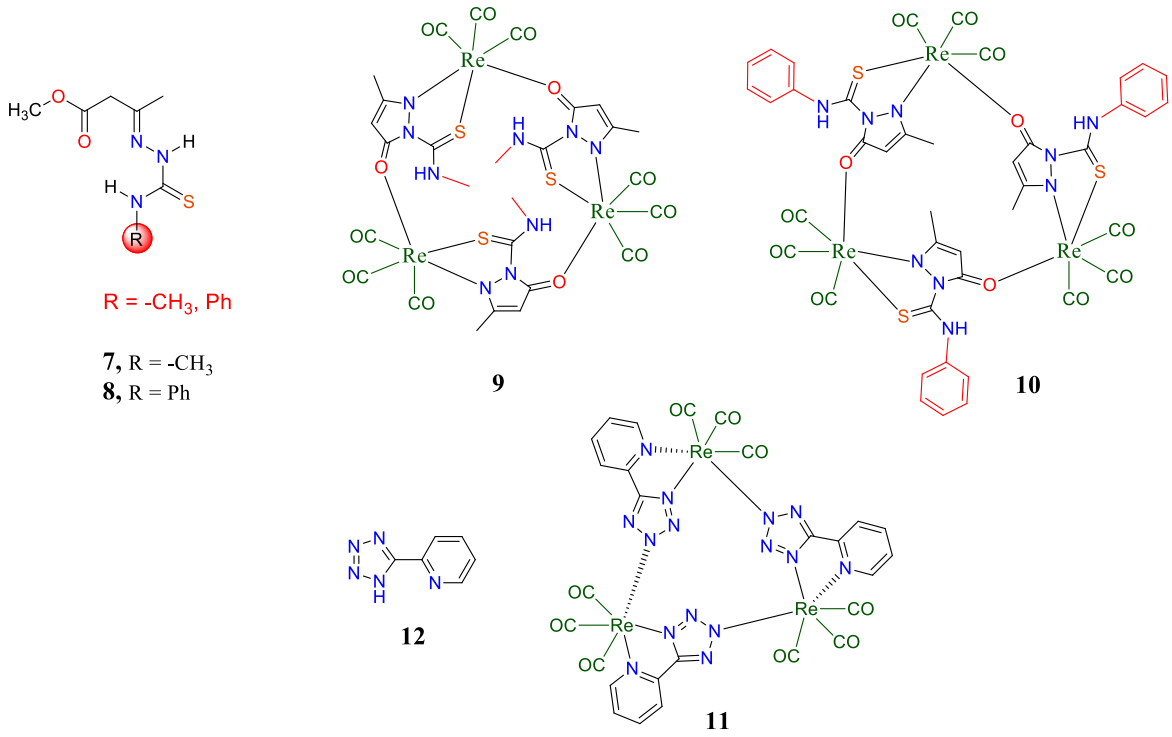

Figure 1.13. Thiosemicarbazones and 2-pyridyltetrazolate ligand based trinuclear rhenium metallacalix[3]arenes.

It is well known that the combination of imidazole (H-L) and Cu(I) or Pd(II) ions provide cyclic trinuclear M_3L_3 metallacycles. The neutral rheniumtetracarbonyl-based trinuclear metallacalix[3]arene (**13**) was obtained from $Re_2(CO)_{10}$ and 1,1-carbonyldiimidazole ligand (**14**).[32] The complex adopts calix-shaped structure and has two recognition units. The wide hydrophobic cavity can accommodate spherical shaped guest molecule. The other recognition unit is exocyclic receptor site provided by the lower rim of the metallacalix[3]arene where three imidazolate motifs deliver three set of *exo* C-H bonds that act as hydrogen-bond donors to the anions.

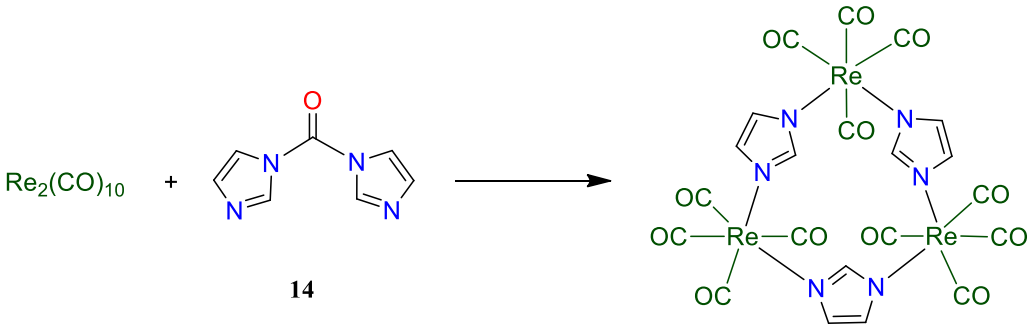

Figure 1.14. Synthesis of $Re(CO)_4$ core-based trinuclear metallacalix[3]arene.

Capped metallacalix[3]arenes (**15-19**) with additional recognition unit were obtained by combining $Re_2(CO)_{10}$ and imidazole (**20**) or benzimidazole (**21**) or benzotriazole (**22**) with flexible tritopic ligands [1,3,5-tris(imidazol-1-ylmethyl)-2,4,6-trimethylbenzene (**23**), , 1,3,5-tris(benzimidazol-1-ylmethyl)-2,4,6-trimethylbenzene (**24**), 1,3,5-tris(benzimidazol-1-ylmethyl)- benzene (**25**)].[33-35] These metallamacrocycles contain two types of exocyclic cavity (**26** and **27**) and one type of endocyclic cavity (**28**) .The exocyclic receptor site (**26**) provided by the lower rim of the metallacalix[3]arenes where three imidazolate motifs deliver three set of *exo* C-H bonds that act as hydrogen-bond donors to the anions.

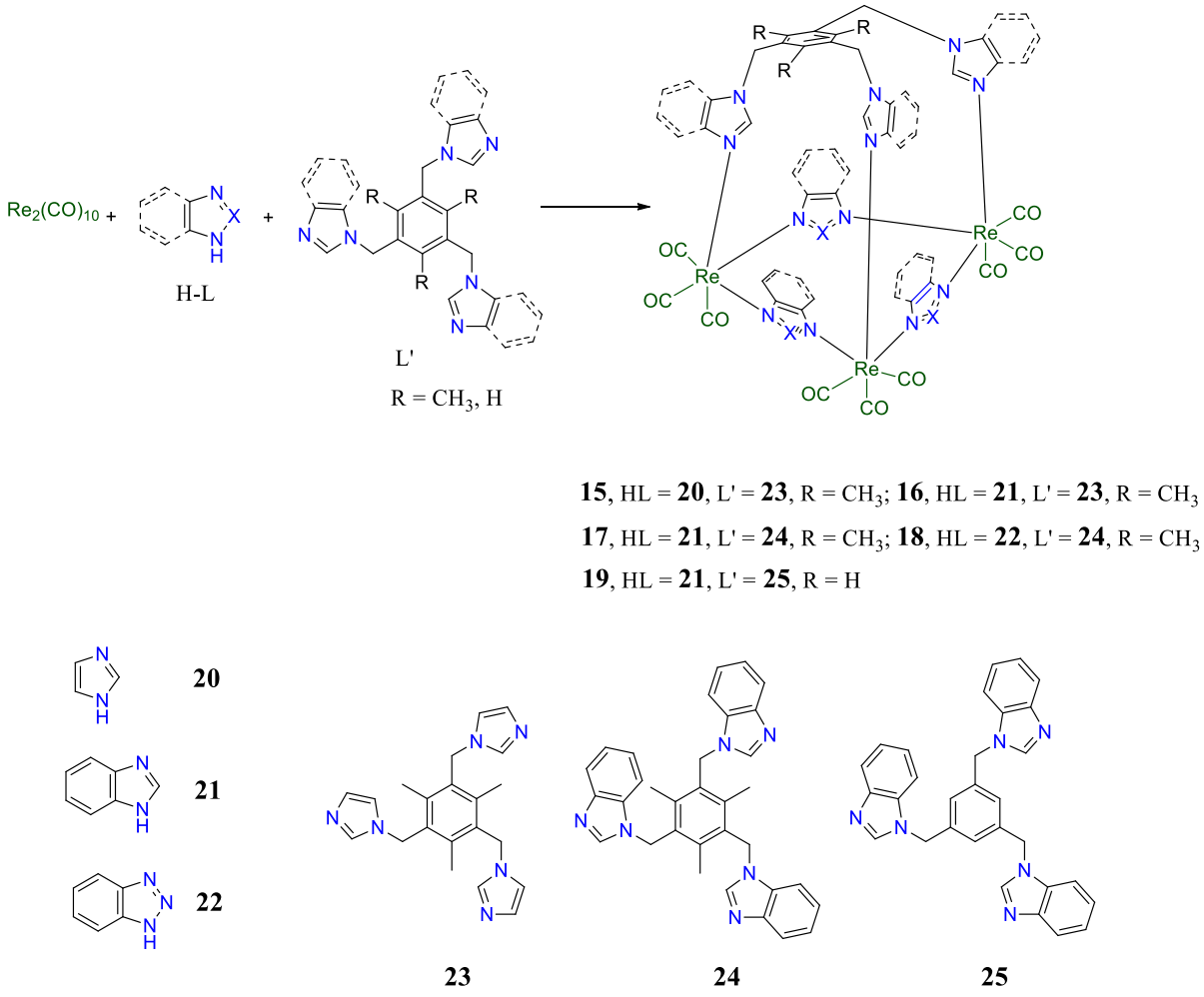

Figure 1.15. Synthesis of rhenium-based M_3L_3L'-type metallacycles.

Coordination of the flexible neutral tripodal nitrogen donor ligand governs the arrangement of three benzimidazolium units in such a fashion that three set of *exo* C-H bonds may act as hydrogen-bond donors to the anions whereas, three benzimidazolate motifs from the cone-shaped metallacalix[3]arene unit in **19** delivers three set of *exo* C-H bonds that may act as the hydrogen-bond donors to the anion and neutral molecules. The metallacalix[3]arene **19** contains three additional exocyclic cavity around the molecule.

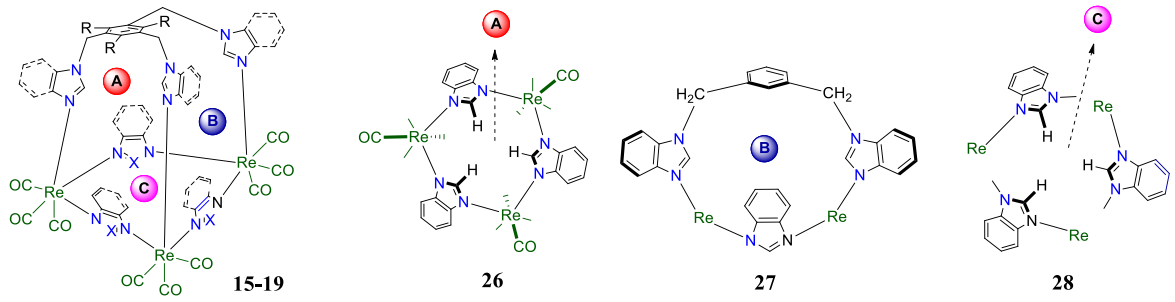

Figure 1.16. Different types of cavity frameworks in metallacycles **15-19**.

1.9. $Re(CO)_3$ core-based spheroids with metallacalix[3]arenes and metallacalix[4]arenes units.

In order to increase the number of molecular receptor units in one metallacycle, hexatopic flexible ligand (**29**) instead of tritopic ligands (**23-25**) were chosen as one of the basic building units. These ligands were treated with rigid imidazole/benzimidazole/ benzotriazole (**20-22**) and $Re_2(CO)_{10}$ to obtain multiple molecular receptor containing spheroid-shaped metallacycles (**30-32**).[36] The molecules have two metallacalix[3]arene units (**33**) and six- metallacalix[4]arene motifs (**34**). Further each cavity in the spheroid has ability to accommodate guest molecules, which is evident from X-ray structure.

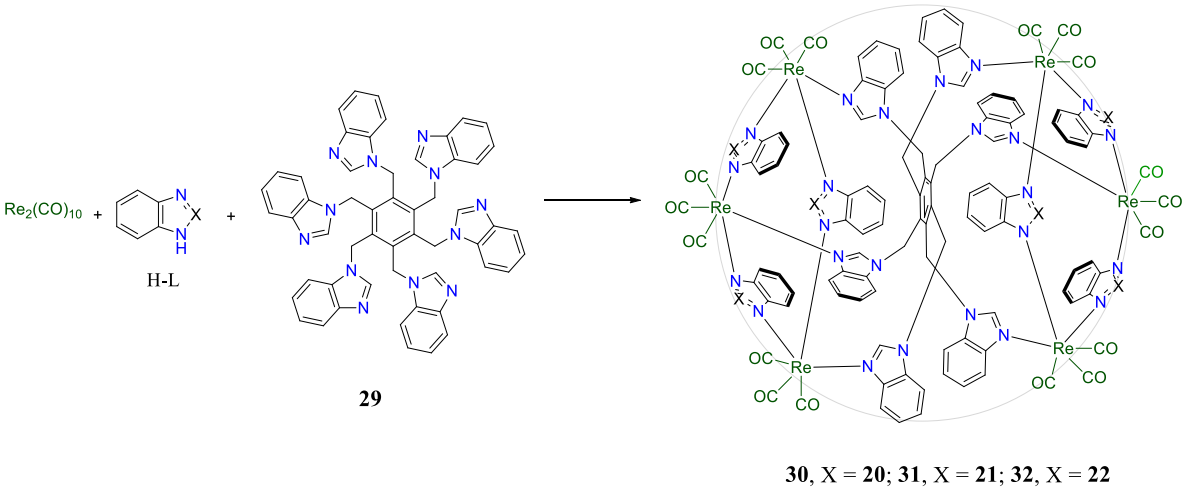

Figure 1.17. Synthesis of $Re(CO)_3$ core-based hexanuclear spheroid metallocavitands.

Further, the size of the calix[4]arenes cavity in **31** can be easily tuned by modulating heteroleptic coordinating units from benzimidazoly to naphthoimidazolyl.[37] The functionality of the metallacalix[3]arene motifs (**33**) in the spheroids can be tuned by modulating the heteroarene units. For example, the metallacalix[3]arene unit containing imidazolate/benzimidazolate structural building unit may act as hydrogen bond donors and able to accommodate neutral and anionic guest molecules. When the heteroarene unit is benzotriazole, the metallacalix[3]arene unit contains nitrogen atoms and is suitable to accommodate neutral molecule or cation.

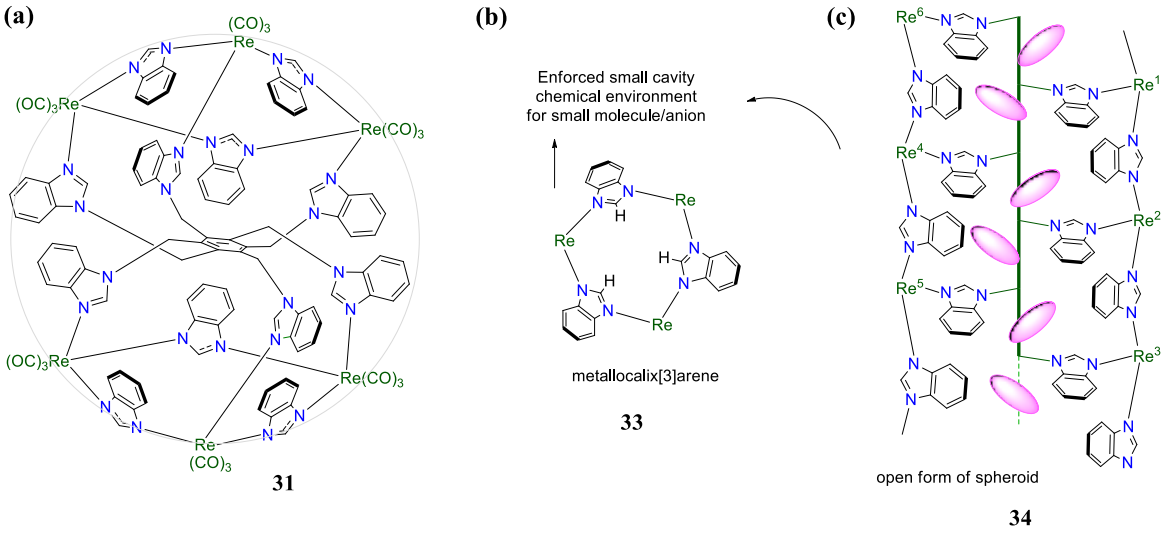

Figure 1.18. (a) Spheroid cage **31**; (b) metallacalix[3]arene motif with enforced small cavity; (c) open form of spheroid showing six metallacalix[4]arene cavities with guest molecules (pink).

1.10. $Re(CO)_3$ core-based homoleptic tetranuclear metallacalix[4]arene.

Calix[4]arene is a cyclic organic molecule and contains four arene motifs and four methylene groups. The alternate arrangement of these motifs provides bowl-shaped structure with wider upper cyclic cavity and narrow lower cavity.[18] Calix[4]arenes have the ability to accommodate various guest molecules in their hydrophobic internal cavity. Ligands containing calix[4]arene spacer are rarely used for making $Re(CO)_3$-core based metallacycle, in particular metallocavitand. In principle, large depth cavity containing metallacycles can be achieved from the calix[4]arene spacer-based nitrogen donor ligands (**35**).[38] Larger size

cavity containing tetranuclear metallocavitand (**36**) was designed and synthesized using $[Re(CO)_5Br]$ and orthotopic nitrogen donor with calix[4]arene spacer (octatopic nitrogen donor). The ligand is designed in such a way that calix[4]arene spacer has four symmetrically arranged 3,8-phenathroline cores. Each 3,8-phenathroline core acts as rigid ditopic bridging donor. All together there are four symmetrically arranged ditopic nitrogen donor like 4,4'-bipyridine which binds with four rhenium cores resulting in the funnel shaped cavity containing metallacalix[4]arene. The cyclic framework is stabilized by hydrogen bonding interactions that occur between water molecule and two adjacent nitrogen donors. The hydrophobic cavity is large and accommodates various guest molecules with the binding constant (K = ~ 1 × 10^2 M^{-1}).

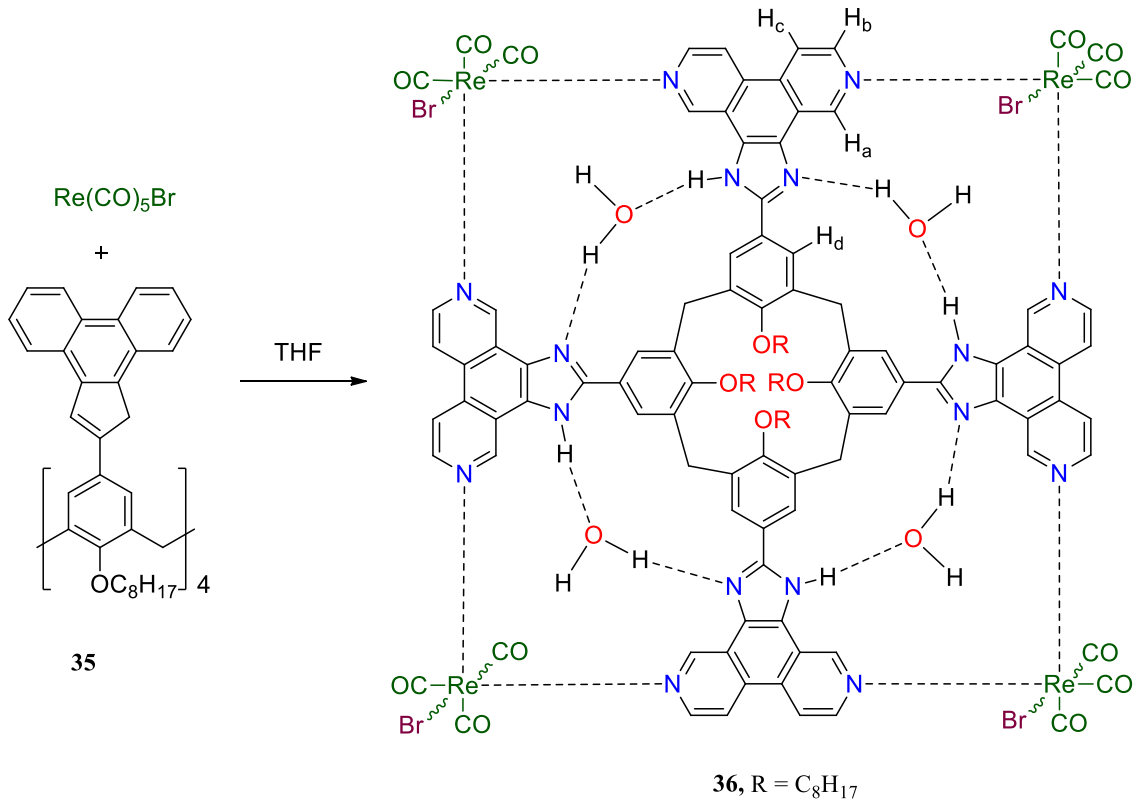

Figure 1.19. Synthesis of rhenium metallobridged cavitand.

Another example of tetranuclear homoleptic metallacalix[4]arene (**37**) is formed by treating $[Re(CO)_5Cl]$ with methyl acetoacetate (**38**) which resulted in cyclization of the ligand to give pyrazolone as bis-chelating five electron donor and coordinated to *fac*-$Re(CO)_3$ core through their S and N_3 atoms.[30]

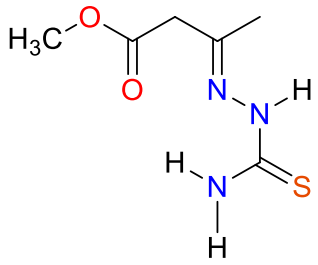

38

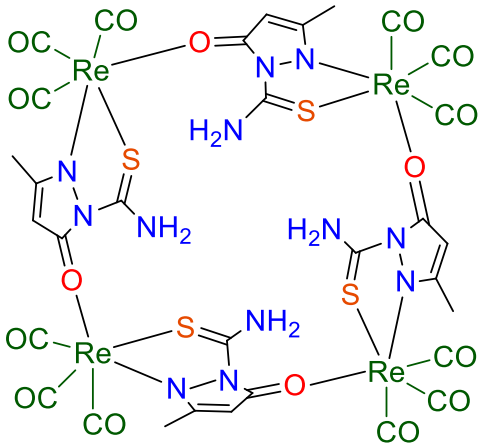

37

Figure 1.20. Homoleptic tetranuclear rhenium metallacalix[4]arene.

1.11. $Re(CO)_3$ core-based heteroleptic dirhenium metallacalix[4]arenes

The *fac*-$Re(CO)_3$ core based neutral, heteroleptic dinuclear metallacalix[4]arene supramolecules (**39-50**) are synthesized using rigid bis-chelating ligands, flexible ditopic ligand containing "phenylene($-CH_2-$heterocycle)$_2$" framework and $Re_2(CO)_{10}$ *via* reflux method or one pot solvothermal approach.[39] The flexible ligands (**L^1-L^2**) used for making these metallacalixarenes can be prepared easily by simple condensation of phenyl-dibromide and heteroarene N-donor motifs. Further, the functional groups of the metallacalixarenes can be tuned by the introducing suitable functional unit on hetero(arene) motifs in the flexible ligands.

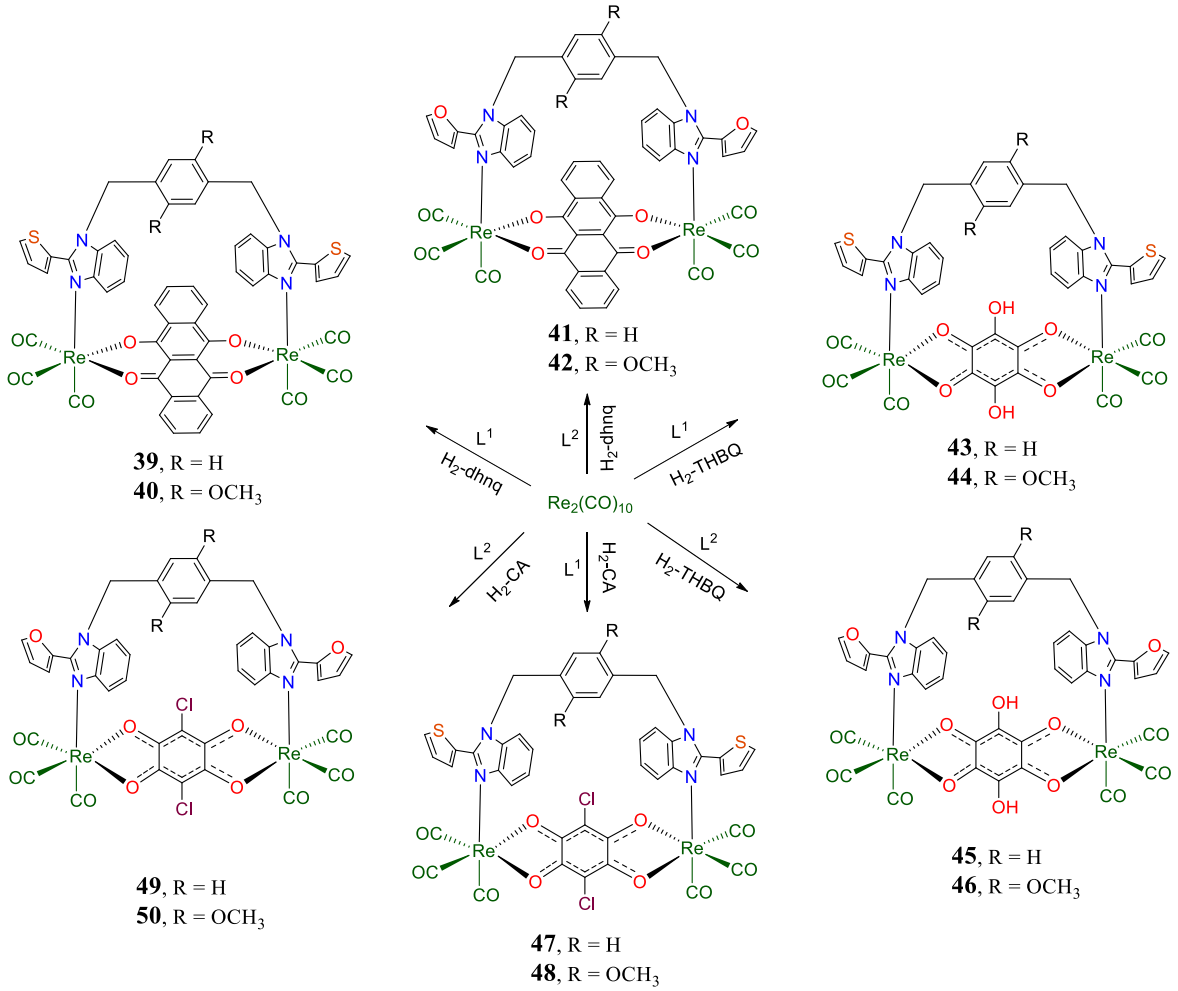

Figure 1.21. One-pot synthesis of functional dirhenium metallacalix[4]arenes.

The hydrophobic cavity present in these metallamacrocycles can accommodate small guest molecules. However the solid-state structural evidence for accommodating guest molecules inside cavity of these metallocavitands is rare. Ditopic ligand (**51**) was used with bis-chelating motifs (**52-55**) to self-assemble metallacalix[4]arenes (**56-59**) *via* one-pot approach.[40] Metallacalix[4]arene **56** accommodates toluene as a guest molecule in its internal cavity, and the methyl groups of toluene are directed towards its hydrophobic cavity.

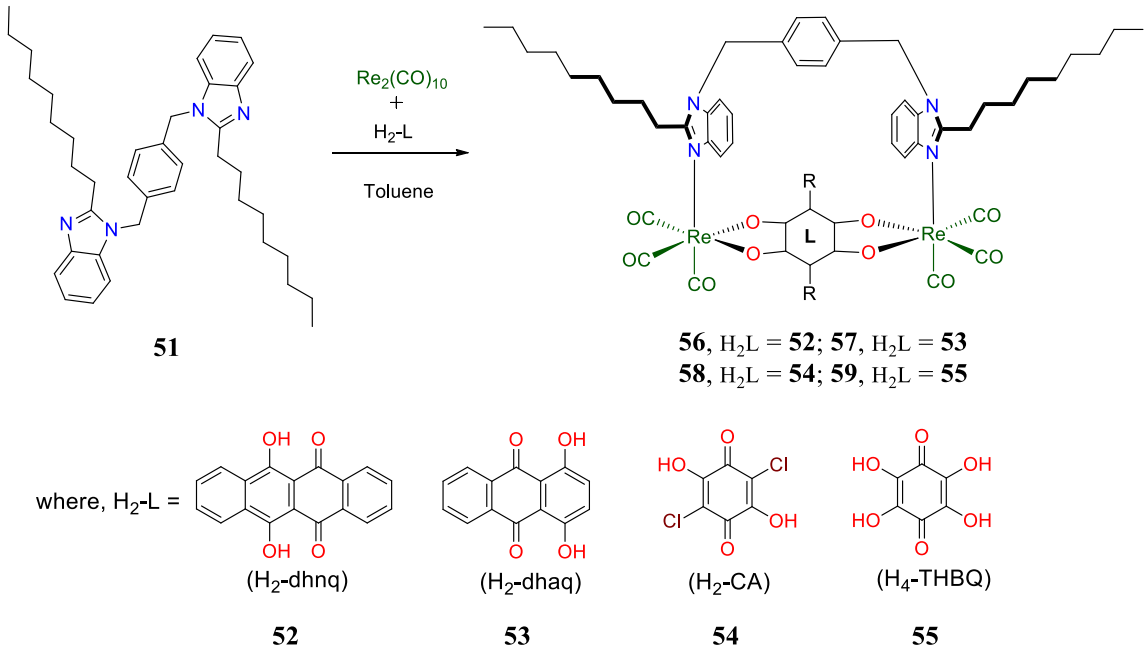

Figure 1.22. Self-assembly of heteroleptic dirhenium metallacalix[4]arenes.

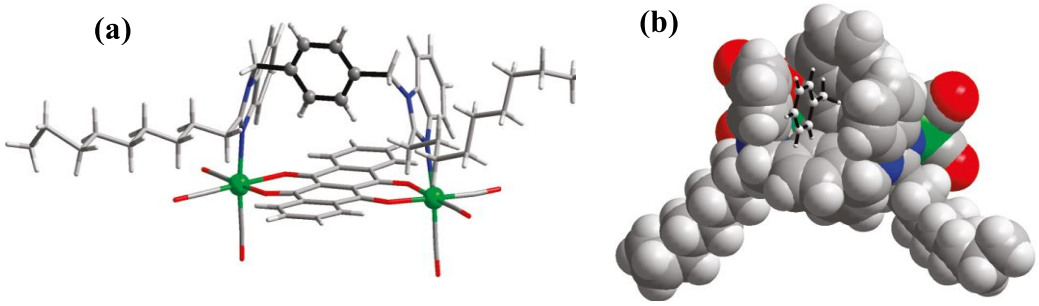

Figure 1.23. (a) Solid-state structure of metallacycle **56**, (b) space-filling representation of **56** with guest toluene (ball-and-stick model)

The *fac*-$Re(CO)_3$ core-based complexes having –SMe decorated heteroleptic metallacalix[4]arene are very rare. First example of –SMe decorated dirhenium–based metallacalix[4]arenes (**60**-**64**) were self-assembled from flexible tritopic donor ligands (1,3-bis(2-methylmercaptobenzimidazol-1-ylmethyl)benzene,1,3-bis(2-methylmercaptobenzimidazol-1-ylmethyl)-2,4,6-trimethylbenzene, 1,4-bis(2-methylmercaptobenzimidazol-1-ylmethyl)benzene,1,4-bis(2-methylmercaptobenzimidazol-1-ylmethyl)-2,5-dimethylbenzene, 1,4-bis(2-methylmercaptobenzimidazol-1-ylmethyl)-2,5-dimethoxybenzene, L^3-L^7), chlorinilic acid and $Re_2(CO)_{10}$. Each metallacycle has two thiomethyl groups on the cyclic rim.[41]

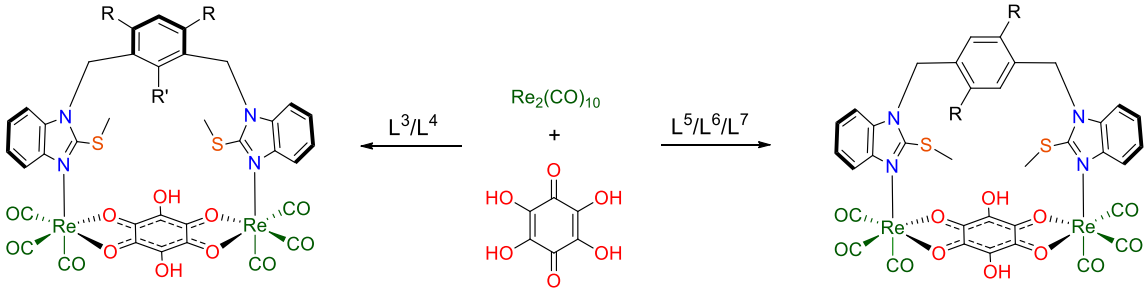

60, R = H
61, R = Me

62, R = H
63, R = Me
64, R = OMe

Figure 1.24. Self-assembly of 2-methylmercaptobenzimidazolyl ligand based dinuclear rhenium metallacalix[4]arenes.

Flexible tritopic ligands containing *m*-phenylene(CH_2-heterocycle)$_3$ framework have the ability to form dinuclear heteroleptic metallacalix[4]arenes adorned with free functionalized hetroarene motifs. Ligand 1,3,5-tri(2-(methylthio)benzimidazol-1-ylmethyl)-2,4,6-trimethylbenzene (**65**) was used to prepare functionalized dinuclear metallocavitands (**66**-**68**) in the presence of additional framework units 2,2′-biimidazole (**69**) or tetrahydroxy-1,4-quinone (**55**) or 6,11-dihydroxy- 5,12-naphthacenedione (**52**) with $Re_2(CO)_{10}$. In addition to the internal cavity suitable to accommodate guest molecules, these molecules possess functional units on the rim which have potential to interact with bio-systems. [42]

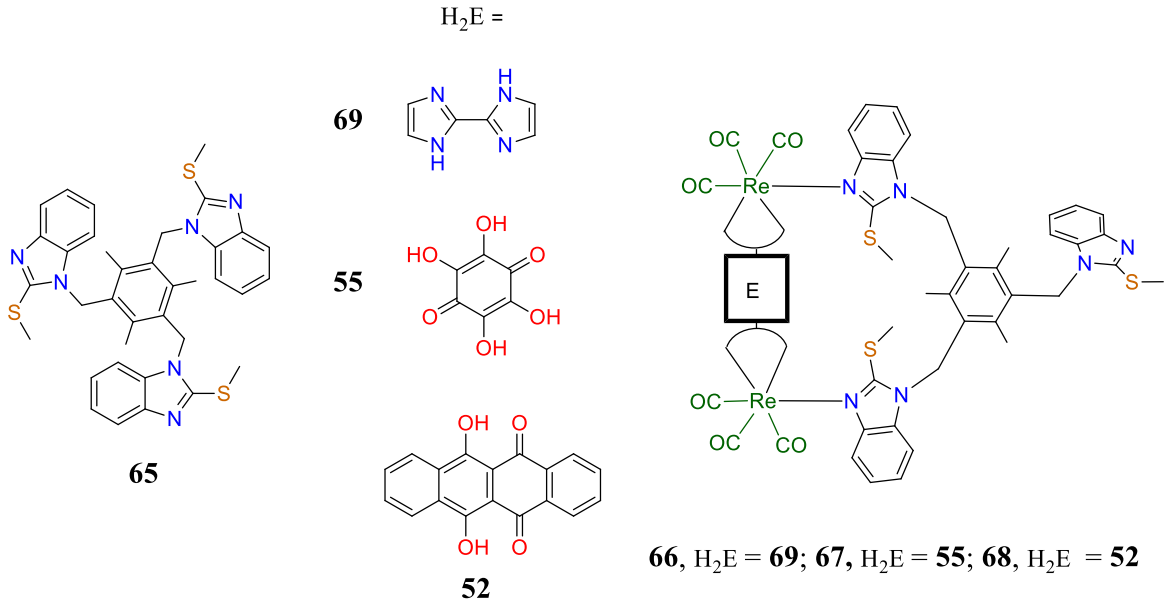

66, H_2E = **69**; **67**, H_2E = **55**; **68**, H_2E = **52**

Figure 1.25. One-pot self-assembly of functionalized dinuclear rhenium metallocavitands.

The above synthetic approach was extended to thiophene-functionalized nitrogen donor ligand 1,3,5-tri(2-(thiophene-2-yl)benzimidazol-1-ylmethyl)-2,4,6-trimethylbenzene (**70**), treated with tetrahydroxy 1,4-benzoquinone bis-chelating anionic donor (**71**) and $Re_2(CO)_{10}$ to get thiophene motifs decorated dinuclear metallacalix[4]arene (**72**). [42]

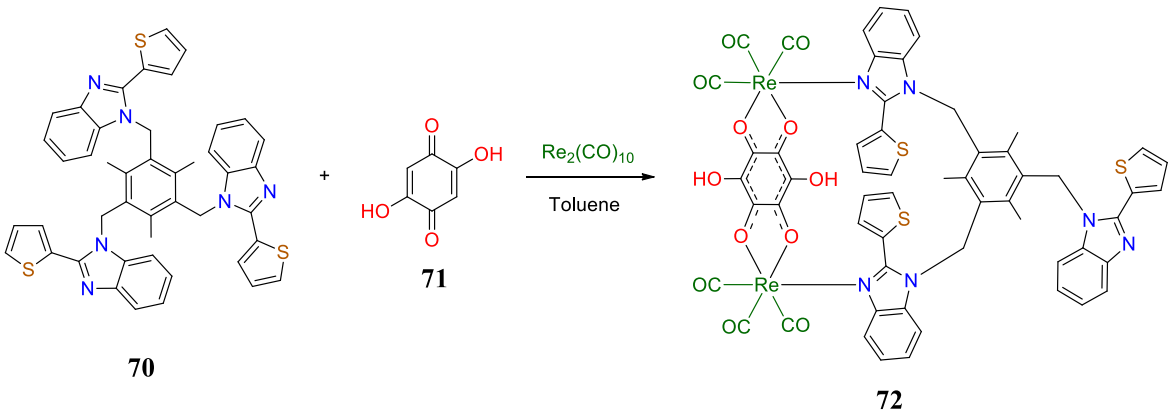

Figure 1.26. Thiophene motifs decorated dinuclear rhenium metallacalix[4]arene.

1.12. $Re(CO)_3$ core-based heteroleptic tetrarhenium metallacalix[4]arenes.

Tetranuclear rhenium metallacalix[4]arenes (**73-76**) with larger inner cavity can be self-assembled by using three component ($Re_2(CO)_{10}$, 4,7-phenanthroline, and bis-chelating donor) *via* self-assembly approach.[43] The choice of neutral ditopic N-donor ligand is crucial in dictating the bowl structure in these combinations. The 4,7-phenanthroline is rigid ditopic N-donor and has the binding angle of ~120^o. The bis-chelating ligands have to orient in a V-shaped arrangement to adjust the angle to be suitable for octahedral geometry around the metal core. This geometrical arrangement leads to the perfect bowl-shaped structure. These metallacalix[4]arenes are neutral, heteroleptic and have inner cavity suitable to accommodate guest molecules. The solvent molecules used to prepare these metallacalix[4]arenes are accommodated in the cavity. Physical properties such as colors, solubility, functionality of metallacalix[4]arenes can be tuned by modulating the bis-chelating ligands. The molecular recognition studies show that these cavitands can act as host for naphthalene, anthracene, phenathroline and pyrene like guest molecules.

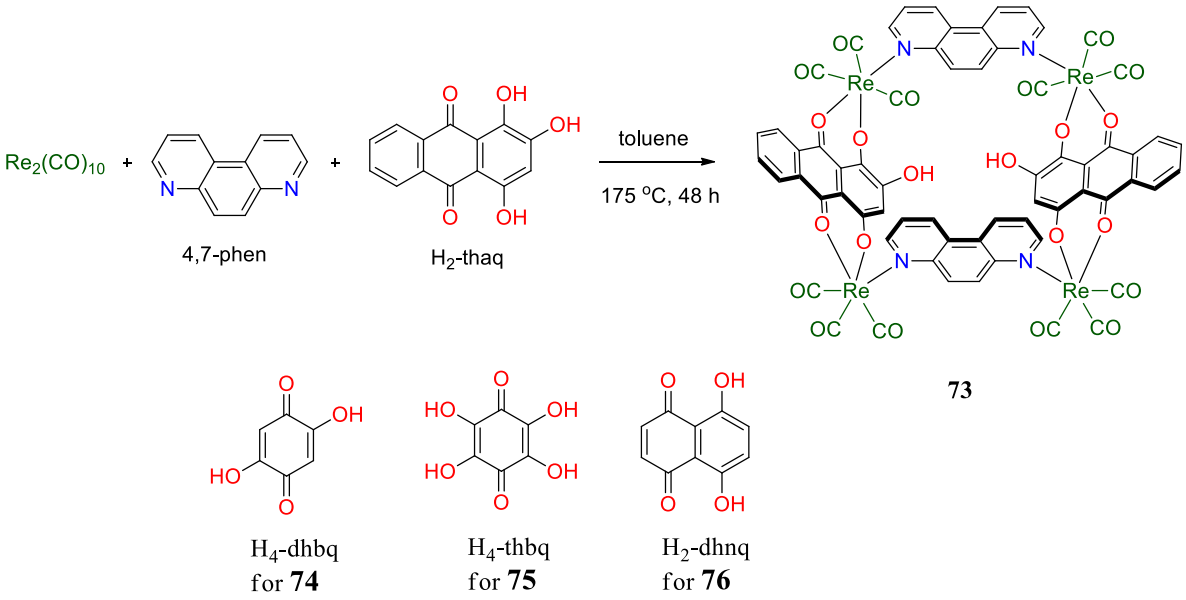

Figure 1.27. Self-assembly of syceelike tetrarhenium metallocavitands.

Metallocavitands **74** and **75** are utilized as evanescent wave infrared molecular sensors for the selective recognition of odorous amino compounds in air.[44] The selective and sensitive detection of amino compounds by the hydrophobic pocket of the metallocavitands found to follow the order as: aromatic amine > aliphatic primary amine ~ cyclo-amine > aliphatic secondary amine > aliphatic tertiaryamine. The cavity size and the hydrogen bonding donors present on the framework of the metallocavitands determine selective trapping of amine guest molecules.

1.13. $Re(CO)_3$ core-based heteroleptic bismetallacalix[4]arenes.

The *fac*-[$Re(CO)_3$] core-based supramolecule having two dinuclear heteroleptic metallacalix[4]arene motifs is very rare. First example of rhenium core containing bis metallacalix[4]arene units (**77**) was self-assembled from flexible tritopic donor1,3,5-tri(2-methylmercaptobenzimidazol-1-ylmethyl)-2,4,6-trimethylbenzene (**63**), chlorinilic acid and $Re_2(CO)_{10}$.[45] Each metallacycle has two thiomethyl groups on the cyclic rim. The hydrophobic cavity on the metallacycle can accommodate small guest molecules.

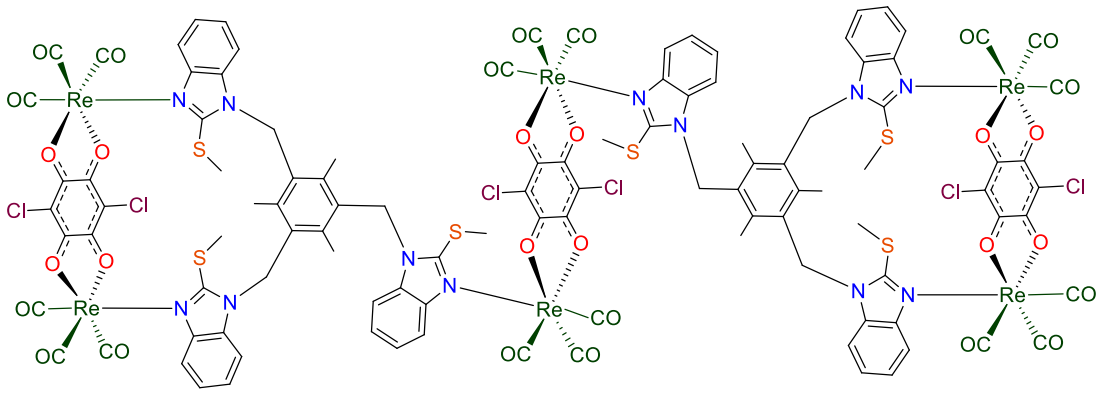

77

Figure 1.28. $Re(CO)_3$ core-based bismetallacalix[4]arenes.

The nitrogen donor ligands play a crucial role in determining the supramolecular architectures. Flexible tetratopic ligand structural framework (**78**) provides suitable coordination angle for the formation of dinuclear bis-metallacalix[4]arene supramolecules **79-80**) when combined with chlorinilc acid and $Re_2(CO)_{10}$.[46] The central phenylene unit of the tetratopic ligand share for both the metalllacalix[4]arene. By tuning the bis-chelating motif, the cavity size of each metallacalix[4]arene can be varied.

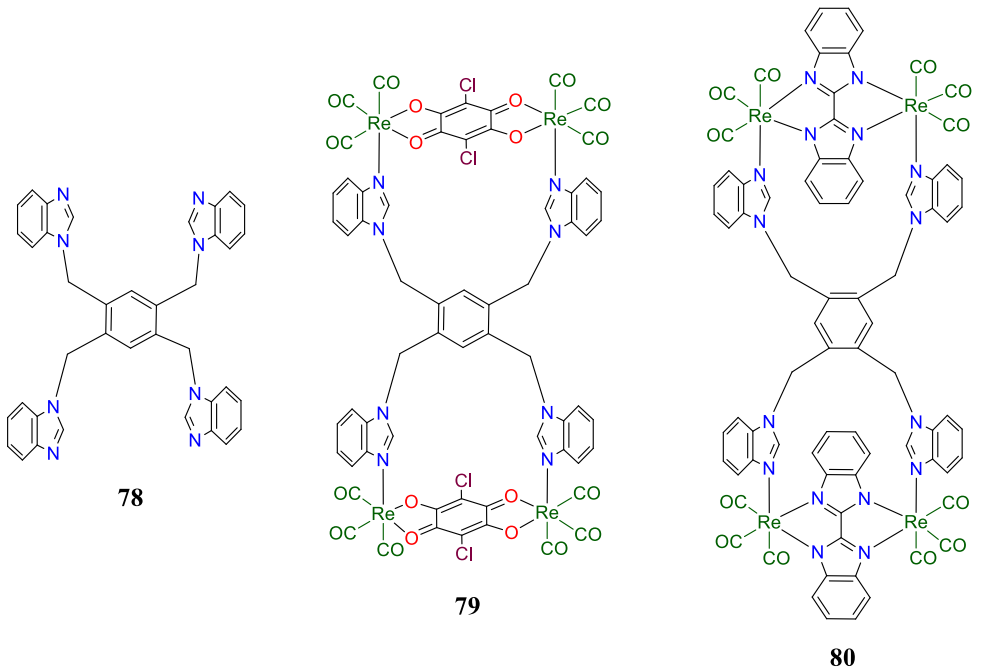

78 **79** **80**

Figure 1.29. Rhenium core-based dinuclear bis-metallacalix[4]arene supramolecules.

Other examples for bis-metallacalix[4]arenes (**81-82**) were synthesized using flexible tetratopic nitrogen donor ligand (**83**), 1,4-dihydroxy-9,10-anthraquinone (**51**), or 11-dihydroxy-5,12-naphthacenedione (**50**) with $Re_2(CO)_{10}$ via solvothermal approach.[47] The tetratopic ligand was designed in such a way it acts as a two ditopic N-donor ligands. Two dinuclear metallacalix[4]arenes in the complexes were connected via a C-C bond; therefore it can be best considered as bridgeless bis-metallacalix[4]arenes.

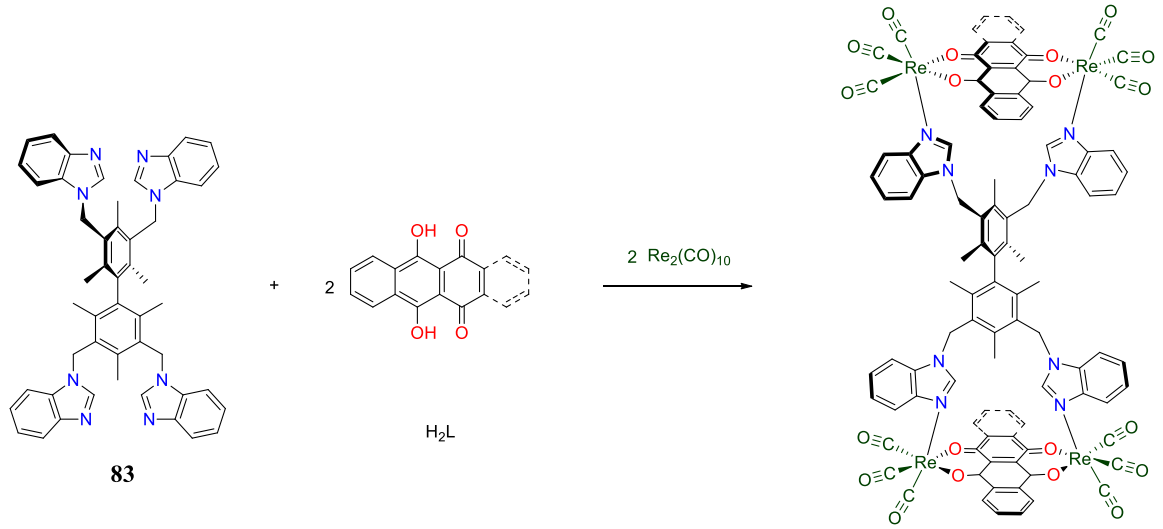

Figure 1.30. One-pot self-assembly of rhenium bridgeless bis-metallacalix[4]arenes.

1.14. $Re(CO)_3$ core-based helicates and mesocates.

The combination of two types of flexible ligands i.e., neutral flexible bis-monodentate nitrogen donor ligand (**84**) and bis-bidentate NO donor ligand (**85**), incorporating a flexible *p*-xylene motif ($-CH_2-Ph-CH_2-$) between two donors and $Re_2(CO)_{10}$ were used for assembling dinuclear heteroleptic helicate (**86**).[48] The spacer *p*-phenylene motif in both the ligands (**84-85**) plays an important role in adopting helical structure. This was evident when the spacer motif in the ligand strands was changed to *m*-xylene motif (**87-88**) which results in the mesohelical structure (**89**). These metallacycles exhibit fluorescence and phosphorescence both in solution and solid state.

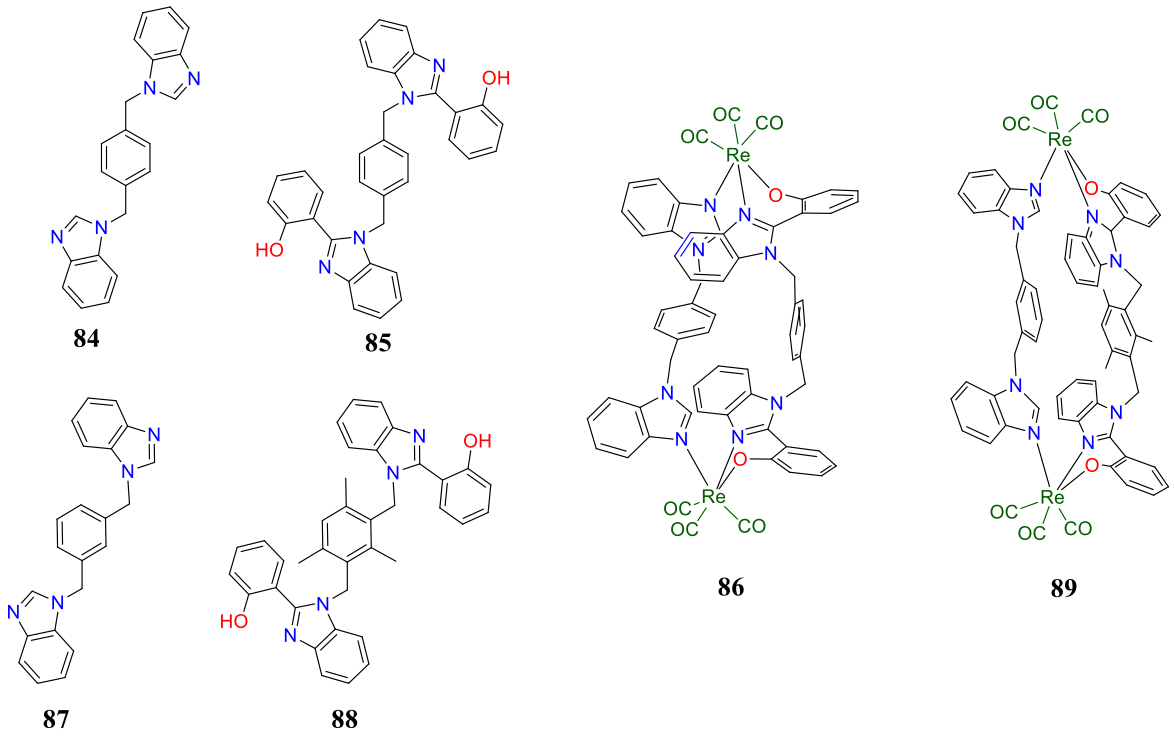

Figure 1.31. Dirhenium(I)-double-heterostranded helicates and mesocates.

Changing or modulating the bis(bidentate) NO donor ligands (**85** and **88**) can influence the resulting architectures. By treating the orthogonal tritopic *fac*-Re(CO)$_3$ metal acceptor with flexible bis-chelating dianionic OO-donor (**90**) and flexible bis-monodentate nitrogen donors (**84** and **87**) in toluene *via* one-pot solvothermal synthesis results in heteroleptic, neutral dinuclear helicates (**91**-**92**).[49]

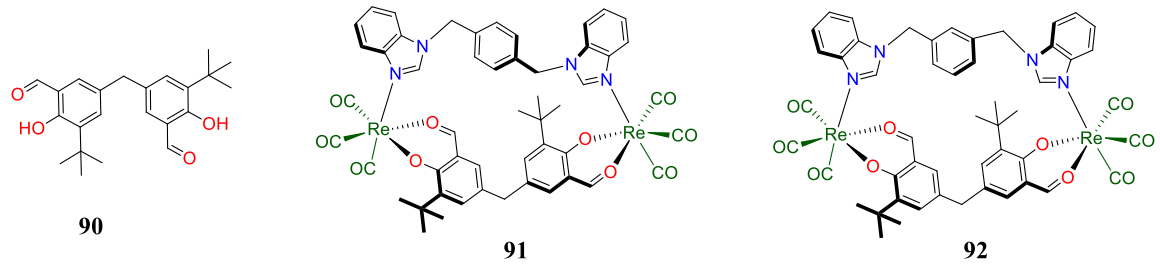

Figure 1.32. Dinuclear rhenium unsaturated double-stranded helicates.

Modulating the central spacer motif from *p*-phenylene spacer in **84** and **87** to Troger's base spacer motif in the neutral ditopic N-donor ligand (**93**) and treated with **85** or **88** and

$Re_2(CO)_{10}$ in toluene results in Re(I)-based dinuclear double hetero-stranded helicates (**94-95**). [50]

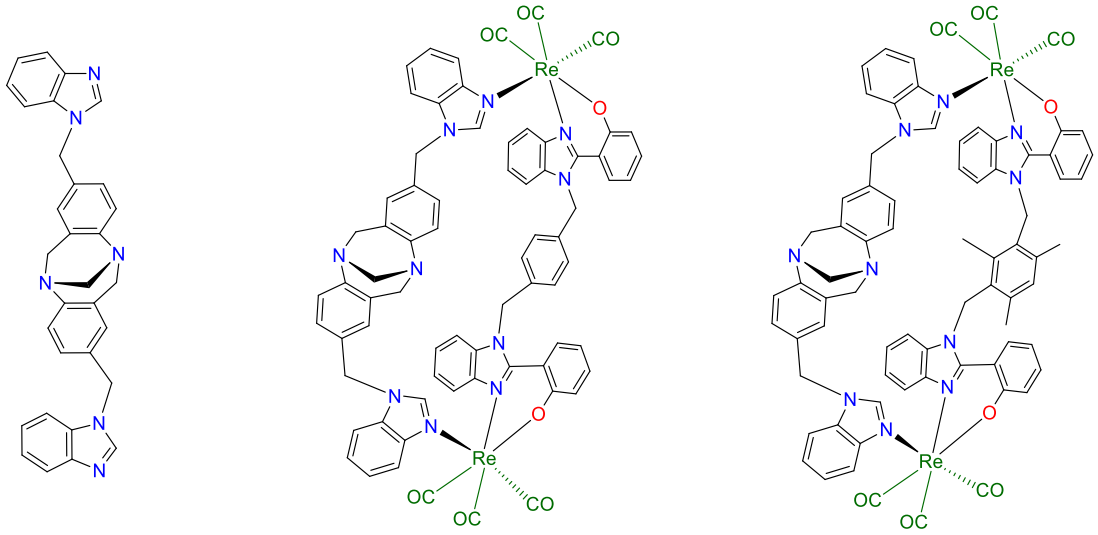

Figure 1.33. Re(I)-based dinuclear heteroleptic double-stranded helicates.

1.15. $Tc(CO)_3$ core-based cyclic complex

To the best of our knowledge, *fac*-[{$Tc(CO)_3Cl$}$_2$(ptc)$_2$] (ptc = 4-pyridyl-thiosemicarbazone = C_6H_5N-$C(CH_3)$=N-NH-C(S)-NH_2) (**96**), is the only known example for a metallamacrocycle based on the *fac*-$[Tc(CO)_3]^+$ core and formed by treating $(NEt_4)_2[Tc(CO)_3Cl_3]$ with ptc ligand (**97**) in acetonitrile.[51] In solid state the neighboring molecules are held by hydrogen bonds, and acetonitrile solvent molecules occupy the channels formed along the b-axis.

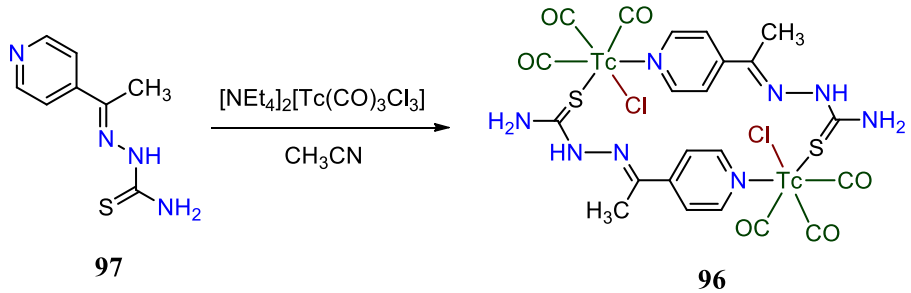

Figure 1.34. Synthesis of $Tc(CO)_3$ core-based metallamacrocycle.

1.16. Scope of the present thesis

It is clear from the preceding section that *fac*-[$Re(CO)_3$] core-based metallacalix[4]arenes have gained attention in the field of supramolecular chemistry owing to their interesting properties in the fields of molecular recognition, catalysis, selective reactivity and biology. The flexible benzimidazolyl and its structural analogous based ditopic N-donors have attracted attention as versatile structural framework for making cavity-containing *fac*-[$Re(CO)_3$] core-based metallacalix[4]arenes. The terminal heteroarene N-donor and phenelyne spacer in the ditopic flexible ligands act as aromatic/heteroaromatic walls of the metallacalixarenes. The bis-chelating organic ligands also act as one of the structural frameworks of the rhenium metallacalix[4]arenes. Although a variety of dirhenium heteroleptic, neutral metallacalixarenes can be obtained by using flexible ditopic N- donor ligands containing phenylene spacer, the hydrophobic cavity in the metallacalixarenes is small to accommodate guest moleculescompletely or partially. There is a lot of scope to modulate the ditopic benzimidazolyl/benzimidazolyl derivatives based nitrogen donor ligands by incorporating diphenylmethane as a spacer to prepare larger size cavity containing dinuclear rhenium metallacalixarenes. Functionalization on the lower rim of the bigger cavitands can result in longer hydrophobic cavity containing metallocavitands. The designed metallocavitands with increased width and depth may accommodate aromatic guest molecules and other potential guest molecules entirely inside their hydrophobic cavity. The anionic bis-chelating units used as structural framework to construct metallocavitands are rigid having an angle of 180 between the two chelating units. The use of the semi-rigid or flexible anionic donors possessing a longer binding length and an angular chelating angle may result in either metallocavitands with bigger hydrophobic cavity or helicate/meso-helicate kind of architectures.

The present thesis describes the design and synthesis of a series of new diotopic N-donor ligands with diarylmethanespacer and several *fac*-[$M(CO)_3$] (M = Re/ Tc) core-based mononuclear homoleptic metallacalix[4]arenes, and *fac*-[$Re(CO)_3$] core-based dinuclear heteroleptic metallacalix[5]arenes, dinuclear heterostranded helicates and meso-helicates.

1.17. References

1. Lehn, J.-M. Supramolecular Chemistry–Concepts and Perspectives, VCH, Weinheim, **1995**. (b) Lehn, J. M. *Angew. Chem. Int. Ed. Engl.* **1988,** *27*, 89-112. (c) Lehn, J. –M. Supramolecular chemistry and self-assembly special feature: Toward complex matter: Supramolecular chemistry and self-organization. *Proc. Nat. Acad. Sci. USA*, **2002**, *99*, 4763-4768.
2. Steed, J. W.; Atwood, J. L.; Gale, P. A. In *Definition and emergence of supramolecular chemistry*, John Wiley & Sons Ltd, 2012; pp 3-7.
3. Steed, J. W.; Turner, D. R.; Wallace, K. J. *Core Concepts in Supramolecular Chemistry and Nanochemistry*, John Wiley & Sons. Chichester, 2007.
4. Kyba, E. P.; Helgeson, R. C.; Madan, K.; Gokel, G. W.; Tarnowski, T. L.; Moore, S. S.; Cram, D. J. Host-guest complexation. 1. Concept and illustration. *J. Am. Chem. Soc*. **1977**, *99*, 2564-2571.
5. (a) Fischer, E. *Berichte de Deutschen Chemischen Gasellschaft.* **1894**, *27*, 2985-2993. (b) *Koshland, D. E.;* The Key–Lock Theory and the Induced Fit Theory. *Angew. Chem., Int. Ed.* **1995**, *33*, 2375-2378.
6. Lehn, J.-M.; Rigault, A.; Seigel, J.; Harrowfield, J.; Chevrier, B.; Moras, D. *Proc. Natl. Acad. Sci. USA*, **1987**, *84*, 2565-2569.
7. (a) Steel, P. J. Metallosupramolecular Chemistry; What is it?. *Chem. N. Z.* **2003**, *67*, 57-60. (b) Steel, P. J. Metallosupramolecular Chemistry; What now. *Chem. N. Z.* **2011**, *75*, 194-197. (c) Dance, I. What is supramolecular?. *New J. Chem*. **2003**, *27*, 1-2.
8. (a) Lippert, B.; Sanz Miguel, P. J. Metallatriangles and metallasquares: the diversity behind structurally characterized examples and the crucial role of ligand symmetry. *Chem. Soc. Rev*. **2011,** *40*, 4475-4487 and references therein. (b) Gao, W. -X.; Zhang. H. N.; Jin, G. -X. Supramolecular catalysis based on discrete heterometallic coordinationdriven metallacycles and metallacages. *Coord. Chem. Rev*. **2019**, *386*, 69-84. (c) Frischmann, P. D.; MacLachlan, M. J. Metallocavitands: an emerging class of functional multimetallic host molecules. *Chem. Soc. Rev.* **2013**, *42*, 871-890 and references therein. (d) Cook, T. R.; Stang, P. J. Recent Developments in the Preparation and Chemistry of Metallacycles and Metallacages via Coordination. *Chem. Rev.* **2015**, *115*, 7001-7045. (e) Chakrabarty, R.; Mukherjee, P. S.; Stang, P. J. Supramolecular Coordination: Self-Assembly of Finite Two-and Three-Dimensional Ensembles. *Chem.*

Rev. **2011**, *111*, 6810-6818. 69-84. (f) Stang, P. J.; Olenyuk, B. Self-Assembly, Symmetry, and Molecular Architecture: Coordination as the Motif in the Rational Design of Supramolecular Metallacyclic Polygons and Polyhedra. *Acc. Chem. Res.*, **1998**, *30*, 502-518.

9. (a) Barea, E.; Navarro J. A. R.; Salas J. M.; Quiros, M.; Willermann, M.; Lippert, B. Chiral Pyrimidine Metallacalixarenes: Synthesis, Structure and Host–Guest Chemistry. *Chem. – Eur. J.* **2003**, *9*, 4414-4421. (b) Galindo, M. A.; Olea, D.; Romero, M. A.; Gomez, J.; del Castillo, P.; Hannon, M. J.; Rodger, A.; Zamora, F.; Navarro, J. A. R. Design and Non-Covalent DNA Binding of Platinum(II) Metallacalix[4]arenes. *Chem. – Eur. J.* **2007**, *13*, 5075-5081. (c) Galindo, M. A.; Galli, S., Navarro, J. A. R.; Angustias Romero, M.; Formation of heterotopic metallacalix[n]arenes (n = 3, 4, 6) containing ethylenediaminepalladium(ii) metal fragments and 4,7-phenanthroline and 2-pyrimidinolate bridges. Synthesis, structure and host–guest chemistry. *Dalton Trans*. **2004**, 2780-2785. (d) Galindo, M. A.; Houlton, A.; Clegg, W.; Harrington, R. W.; Dobado, J.; Santoyo-Gonzalez, F.; Linares, F.; Romero, M. A.; Navarro, J. A. R. Electrochemically and photochemically active Palladium(ii) heterotopic metallacalix[3]arenes. *Chem. Commun*. **2008**, 3735-3737. (e) Xu, G. F.; Gamez, P.; Teat, S. J.; Tang, J. Praseodymium(iii)-based bis-metallacalix[4]arene with host–guest behavior. *Dalton Trans*. **2010**, *39*, 4353-4357. (f) Díaz-Ramírez, M. L.; Huggins, H.; Donnadieu, B.; Lopez, N.; Muñoz-Hernández, M. -Á. The Quest for Large Group 13 Metallacalixarenes Based on Benzymidazolyl Ligands and Al and Ga Alkyls. *Eur. J. Inorg. Chem*. **2021**, 3896-3902.
10. (a) Lehn, J. M.; Rigault, A.; Siegel, J.; Harrowfield, J.; Chevrier, B.; Moras, D. Spontaneous assembly of double-stranded helicates from oligobipyridine ligands and copper(I) cations: Structure of an inorganic double helix. *Proc. Natl. Acad. Sci. USA*. **1987**, *84*, 2565-2569. (b) Hannon, M. J.; Childs, L. J. Helices and Helicates: Beautiful Supramolecular Motifs with Emerging Applications. *J. Supramol. Chem*. **2004**, *16*, 7-22. (c) Albrecht, M. Let's Twist Again–Double-Stranded, Triple-Stranded, and Circular Helicates *Chem. Rev*. **2001**, *101*, 3457–3498. (d) Piguet, C.; Bernardinelli, G.; Hopfgartner, G.; Helicates as Versatile Supramolecular Complexes. *Chem. Rev*. **1997**, *97*, 2005-2062 and references there in. (e) Paneerselvan, A. P.; Mishra, S. S.; Chand, D. K. Linear and circular helicates: A brief review. *J. Chem. Sci*. **2018**, *130*, 1–18.
11. (a) Allison, S. J.; Cooke, D.; Davidson, F. S.; Elliott, P. I. P.; Faulkner, R. A.; Griffiths, H. B. S.; Harper, O. J.; Hussain, O.; Owen-Lynch, P. J.; Phillips, R. M.; Rice, C. R.;

Shepherd, S. L.; Wheelhouse, R. T. Ruthenium-Containing Linear Helicates and Mesocates with Tuneable p53-Selective Cytotoxicity in Colorectal Cancer Cells. *Angew. Chem. Int. Ed*. **2018**, *57*, 9799-9804. (b) Li, X.; Wu, J.; Wang, L.; He, C.; Chen, L.; Jiao, Y.; Duan, C. Mitochondrial DNA-targeted Ir^{III}-Containing Metallohelices with Tunable Photodynamic Therapy Efficacy in Cancer Cells. *Angew. Chem. Int. Ed*. **2020**, *59*, 6420-6427. (c) Li, X.; Shi, Z.; Wu, J.; Wu, J.; C, He.; Haoa, X.; Duan, C. Lighting up metallohelices: from DNA binders to chemotherapy and photodynamic therapy *Chem. Commun*. **2020**, 56, 7537-7548.

12. (a) Young, N. J.; Hay, B. P Structural design principles for self-assembled coordination polygons and polyhedral. *Chem. Commun.* **2013**, *49*, 1354-1379. (b) Stang, P. J.; Olenyuk, B. Self-Assembly, Symmetry, and Molecular Architecture: Coordination as the Motif in the Rational Design of Supramolecular Metallacyclic Polygons and Polyhedra. *Acc. Chem. Res.* **1997**, *30*, 502-518.
13. (a) Zhang, D.; Ronson, T. K.; Nitschke, J. R. Functional Capsules via Subcomponent Self-Assembly. *Acc. Chem. Res.* 2018, *5*, 2423-2436. (b) Wu, Z.; Zhou, K.; Ivanow, A. V.; Yusobov M.; Verpoort, F. The simplest and fascinating metal–organic polyhedra: Tetrahedra. *Coord. Chem. Rev.* **201**7, *353*, 180-200.
14. (a) Seidel, S. R.; Stang, P. J. High-Symmetry Coordination Cages via Self-Assembly. *Acc. Chem. Res.* **2002**, *35*, 972-983. (b) Zhang, Y. Y.; Gao, W. X.; Lin, L.; Jin, G. X.; Recent advances in the construction and applications of heterometallic macrocycles and cages. *Coord. Chem. Rev.* **2017**, *344*, 323-344. (c) Therrien, B. Arene Ruthenium Cages: Boxes Full of Surprises. *Eur. J. Inorg. Chem.* **2009**, 2445-2453.(d) Fujita, M.; Umemoto, K.; Yoshizawa, M.; Fujita, N.; Kusukawa, T.; Biradha, K. Molecular paneling *via* coordination. *Chem. Commun*. **2001**, 509‑518.
15. (a) Ruben, M.; Rojo, J.; Romero-Salguero, F.J.; Uppadine, L. H.; Lehn, J.-M. Grid-Type Metal Ion Architectures: Functional Metallosupramolecular Arrays. *Angew. Chem. Int. Ed*. **2004**, 43, 3644-3662. (b) Stadler, A.-M.; Kyritsakas, N.; Graff, R.; Lehn, J.-M. Formation of Rack- and Grid-Type Metallosupramolecular Architectures and Generation of Molecular Motion by Reversible Uncoiling of Helical Ligand Strands. *Chem. Eur. J*. **2006**, 12, 4503-4522. (c) Swiegers, G. F.; Malefetse, T. J. New Self-Assembled Structural Motifs in Coordination Chemistry. *Chem. Rev*. **2000**, *100*, 3483–3538.
16. (a) Sauvage, J. P. Transition Metal-Containing Rotaxanes and Catenanes in Motion: Toward Molecular Machines and Motors. *Acc. Chem. Res*. **1998**, *31*, 611-619.

(b) Sauvage, J. P. *Angew.* From Chemical Topology to Molecular Machines (Nobel Lecture). *Chem. Int. Ed.* **2017**, *56*, 11080-11093. (c) Huang, S. L.; Andy Hor, T. S.; Jin, G. X. Metallacyclic assembly of interlocked superstructures. *Coord. Chem. Rev.* **2017**, *333*, 1-26.

17. Forgan, R. S.; Sauvage, J. P.; Stoddart, J. F. Chemical Topology: Complex Molecular Knots, Links, and Entanglements. *Chem. Rev.* **2011**, *111*, 5434-5464.
18. (a) Gutsche, C. D. Calixarenes, *Monographs in Supramolecular Chemistry*, Stoddart, J. F. Ed., The Royal Society of Chemistry, Cambridge, United Kingdom, 1989. (b) Gutsche, C. D. Calixarenes: an introduction. Cambridge: Royal Society of chemistry, 2008.
19. Gutsche, C. D.; Muthukrishnan, R. Calixarenes.1.Analysis of the Product Mixtures Produced by the Base-Catalyzed Condensation of Formaldehyde with Para-Substituted Phenols. *J. Org. Chem.* **1978,** *43*, 4905.
20. Kulesza, J.; Barros, B. S.; Júniora S. A. Organic‑inorganic hybrid materials: Metallacalixarenes. Synthesis and applications. *Coord. Chem. Rev*. **2013**, *257*, 2192–2212.
21. (a) Cooke, D. J.; Cross, J. M.; Fennessy, R. V.; Harding, L. P.; Rice, C. R.; Slater, C. Steric control of the formation of dinuclear double helicate and dinuclear meso-helicate assemblies. *Chem. Commun*. **2013**, *49*, 7785-7787. (b) Xu, J.; Parac, T. N.; Raymond, K. N. meso myths: what drives assembly of helical versus meso[M_2L_3]clusters?. *Angew. Chem. Int. Ed*. **1999**, 38, 2878-2882. (c) Martínez-Calvo, M.; Romero M. J.; Pedrido. R.; González-Noya A. M.; Zaragozac. G. Bermejoa. M. R. Metal self-recognition: a pathway to control the formation of dihelicates and mesocates *Dalton Trans*. **2012**, *41*, 13395-13404. (d) Zhanga, Z.; Dolphin, D. A triple-stranded helicate and mesocate from the same metal and ligand. *Chem. Commun*. **2009**, 6931-6933. (e) Cui, F.; Li, S.; Jia, C.; Mathieson, J. S.; Cronin, L.; Yang, X.-J.; Wu, B. Anion-Dependent Formation of Helicates versus Mesocates of Triple-Stranded M_2L_3 (M = Fe^{2+}, Cu^{2+}) Complexes. *Inorg. Chem*. **2012**, *51*, 179–187.
22. (a) Bauer, E. B.; Haase, A. A.; Reich, R. M.; Crans, D. C.; Kühn, F. E. Organometallic and coordination rhenium compounds and their potential in cancer therapy. *Coord. Chem. Rev.* **2019**, *393*, 79-117. (b) Haase, A. A.; Bauer, E. B.; Kühn, F. E.; Crans, D. C. Speciation and toxicity of rhenium salts, organometallics and coordination complexes. *Coord. Chem. Rev*. **2019**, *394*, 135-161. (c) Dinolfo, P. H.; Hupp, J. T. Supramolecular coordination chemistry and functional microporous molecular materials. *Chem. Mater*.

2001, *13*, 3113–3125. (d) Hupp, J. T. Rhenium-Linked Multiporphyrin Assemblies: Synthesis and Properties. *Struct. Bonding*, **2006**, *121*, 145-165. (e) Gupta, D.; Sathiyendiran, M. Rhenium-Carbonyl-Based Supramolecular Coordination Complexes: Synthesis, Structure and Properties. *ChemistrySelect* **2018**, *3*, 7439-7458 and references cited therein.

23. (a) Ramakrishna, B.; Nagarajaprakash, R.; Veena, V.; Sakthivel, N.; Manimaran. B. Self-assembly of oxamidato bridged ester functionalised dirhenium metallastirrups: synthesis, characterisation and cytotoxicity studies. *Dalton Trans.* **2015**, *44*, 17629-17638. (b) Orsa, D. K.; Haynes, G. K.; Pramanik, S. K.; Iwunze, M. O.; Greco, G. E.; Krause, J. A.; Ho, D.; Williams, A. L.; Hill, D. A.; Mandal, S. K. Synthesis, characterization, and fluorescence and cytotoxicity studies of a tetrarhenium molecular rectangle. *Inorg. Chem. Commun.* **2007**, *10*, 821-824. (c) Balasingham, R. G.; Thorp-Greenwood, F. L.; Williams, C. F.; Coogan, M. P.; Pope, S. J. A. Biologically Compatible, Phosphorescent Dimetallic Rhenium Complexes Linked through Functionalized Alkyl Chains: Syntheses, Spectroscopic Properties, and Applications in Imaging Microscopy. *Inorg. Chem*. **2012**, *51*, 1419−1426.(d) Govindarajan, R.; Nagarajaprakash, R.; Veena,V.; Sakthivel, N.; Manimaran, B. One-pot reaction of amide functionalized Re(I) based dinuclear metallacycles: Synthesis, characterization and evaluation for anticancer potential. *Polyhedron*. **2018**, *139*, 229–236.
24. (a) Rohacova, J.; Ishitani, O. Photofunctional Multinuclear Rhenium(I) diimine Carbonyl Complexes. *Dalton Trans*. **2017**, *46*, 8899–8919. (b) Thanasekaran, P.; Lee, C. C.; Lu, K. L. One-Step Orthogonal-Bonding Approach to the Self-Assembly of Neutral Rhenium-Based Metallacycles: Synthesis, Structures, Photophysics, and Sensing Applications. *Acc. Chem. Res*. **2012**, *45*, 1403–1418. (c) Sato, S.; Ishitani, O. Photochemical reactions of fac-rhenium(I) tricarbonyl complexes and their application for synthesis. *Coord. Chem. Rev*. **2015**, *282–283*, 50–59.
25. (a) Alberto, R.; Schibli, R.; Waibel, R.; Abram, U.; Schubiger, A. P. Basic aqueous chemistry of $[M(OH_2)_3(CO)_3]^+$ (M = Re, Tc) directed towards radiopharmaceutical application. *Coord. Chem. Rev*. **1999**, *190-192*, 901-919. (b) Waibel, R.; Alberto, R.; Willuda, J.; Finnern, R.; Schibli, R.; Stichelberger, A.; Egli, A.; Abram, U.; Mach, J. –P.; Plückthun, A.; Schubiger, P. A. Stable one-step technetium-99m labeling of His-tagged recombinant proteins with a novel Tc(I)–carbonyl complex. *Nature Biotechnol*. **1999**, *17*, 897-901. (c) Abram, U.; Alberto, R. Technetium and rhenium: coordination chemistry and nuclear medical applications. *J. Braz. Chem. Soc.* **2006**, *17*, 1486-1500. (d)

Papagiannopoulou, D. Technetium-99m radiochemistry for pharmaceutical applications. *J. Labelled Comp. Radiopharm.* **2017**, *60*, 502-520. (e) Makris, G.; Bandari, R. P.; Kuchuk, M.; Jurisson, S. S.; Smith, C. J.; Hennkens, H. M. Development and Preclinical Evaluation of ^{99m}Tc- and ^{186}Re-Labeled NOTA and NODAGA Bioconjugates Demonstrating Matched Pair Targeting of GRPR-Expressing Tumors. *Mol. Imaging Biol.* **2021**, *23*, 52-61.

26. (a) Alberto, R. The "Carbonyl Story" and Beyond; Experiences, Lessons and Implications. *ChemMedChem*. **2012**, *16*, 84-91 (b) Morais, M.; Paulo, A.; Gano, L.; Santos, I.; Correia, J. D. G. Target-specific $Tc(CO)_3$-complexes for *in vivo* imaging *J. Organomet. Chem.* **2013**, *744*, 125-139. (c) Gasser, G.; Metzler Nolte, N. The potential of organometallic complexes in medicinal chemistry. *Cur. Opinion Chem. Biol*. **2012**, *16*, 84-91. (d) Bhattachrayya, S.; Dixon, M. Metallic radionuclides in the development of diagnostic and therapeutic radiopharmaceuticals. *Dalton Trans.* **2011**, *40*, 6112-6128. (e) Kasten, B. B.; Ma, X.; Cheng, K.; Bu, L.; Slocumb, W. S.; Hayes, T. R.; Trabue, S.; Cheng. Z.; Benny, P. D. Isothiocyanate-Functionalized Bifunctional Chelates and *fac*-$[M^I(CO)_3]^+$ (M = Re, ^{99m}Tc) Complexes for Targeting uPAR in Prostate Cancer. *Bioconjug. Chem*. **2016**, *27*, 130-142. (f) Imstepf, S.; Pierroz, V.; Raposinho, P.; Felber, M.; Fox, T.; Fernandes, C.; Gasser, G.; Santos, I.; Alberto, R. Towards ^{99m}Tc-based imaging agents with effective doxorubicin mimetics: a molecular and cellular study. *Dalton Trans*. **2016**, *45*, 13025-13033.
27. Hildebrandt, S. $(NBu_4)[Tc_2(\mu\text{-}Cl)_3(CO)_6]$ als Startverbindung für Technetiumtricarbonylkomplexe. PhD Thesis, FU Berlin, **2018**.
28. Brasey, T.; Buryak, A.; Scopelliti, R.; Severin K. Synthesis of a Metallamacrocyclic $Re(CO)_3$ Complex Using a Tridentate Bridging Ligand. *Eur. J. Inorg. Chem.* **2004**, 964-967.
29. Thorp-Greenwood, F. L.; Fernández-Moreira, V.; Millet, C. O.; Williams, C. F.; Cable, J.; Court, J. B.; Hayes, A. J.; Lloyd D.; Coogan, M. P. A 'Sleeping Trojan Horse' which transports metal ions into cells, localises in nucleoli, and has potential for bimodal fluorescence/PET imaging. *Chem. Commun*. **2011**, *47*, 3096-3098.
30. Barbazán, P.; Carballo, R.; Casas, J. S.; García-Martínez, E.; Pereiras-Gabián, G.; Sánchez, A.;Vázquez-López, E. M. Synthesis and Characterization of New Trimeric Rhenium(I) Complexes. The Influence of Steric Factors on the Size of Pyrazolonaterhenium(I) Metallomacrocycles. *Inorg. Chem*. **2006**, *45*, 7323-7330.

31. Wright, P. J.; Muzzioli, S.; Skelton, B. W.; Raiteri, P.; Lee, J.; Koutsantonis, G.; Silvester, D. S.; Stagni, Stefano.; Massi M. One-step assembly of Re(I) tricarbonyl 2-pyridyltetrazolato metallacalix[3]arene with aqua emission and reversible three-electron oxidation. *Dalton Trans.* **2013**, *42*, 8188-8191.
32. Lin, S.-M.; Velayudham, M.; Tsai, C.-H.; Chang, C.-H.; Lee, C.-C.; Luo, T.-T.; Thanasekaran, P.; Lu. K.-L. A Molecular Triangle as a Precursor Toward the Assembly of a Jar-Shaped Metallasupramolecule. *Organometallics* **2014**, *33*, 40-44.
33. Shankar, B.; Hussain, F.; Sathiyendiran, M. Synthesis of rhenium-based M3L3L0-type metallacycle from benzimidazole and flexible tri(benzimidazole) ligands. *J. Organomet. Chem*. **2012**, *719*, 26-29.
34. Shankar, B.; Elumalai, P.; Shanmugam, R.; Sathiyendiran, M. Neutral heteroleptic rhenium-based M3L3L0 type metallacycles: Synthesis, structural characterization and DFT/TDDFT studies.
35. Kedia, M.; Priyatharsini, M.; Sathiyashiva, S. D.; Shankar, B.; Krishnakumar, R.V.; Sathiyendiran, M. Prototype rhenium metallocavitand with four exocyclic cavities for small molecules. *J. Organomet. Chem*. **2022**, *959*, 122123.
36. Shankar, B.; Elumalai, P.; Sathiyashivan, S. D.; Sathiyendiran, M. Spheroid Metallocavitands with Eight Calixarene-Shaped Receptors on the Surface. *Inorg. Chem*. **2014**, *53*, 10018-10020.
37. Shankar, B.; Marimuthu, R.; Sathiyashivan, S. D.; Sathiyendiran, M. Spheroid Metallacycles and Metallocavitands with Calixarene- and/or Cleft-Shaped Receptors on the Surface. *Inorg. Chem*. **2016**, *55*, 4537-4544.
38. Botana, E.; Da Silva, E.; Benet-Buchholz, J., Ballester, P.; de Mendoza, J. Inclusion of Cavitands and Calix[4]arenes into a Metallobridged para-(1*H*-Imidazo[4,5-f][3,8]phenanthrolin-2-yl)-Expanded Calix[4]arene. *Angew. Chem. Int. Ed*. **2007**, 46, 198-201.
39. Rajakannu, P.; Mobin, S. M. Sathiyendiran, M. Thiophene/furan units decorated unsymmetrical dinuclear metallocalix[4]arenes. *J. Organomet. Chem*. **2014**, *771*, 68-77.
40. Rajakannu, P.; Shankar, B.; Yadav, A.; Shanmugam, R.; Gupta, D.; Hussain, F.; Chang, C.-H.; Sathiyendiran, M.; Lu, K.-L. Adaptation toward Restricted Conformational Dynamics: From the Series of Neutral Molecular Rotors. *Organometallics* **2011**, *30*, 3168-3176.

41. Rajakannu, P.; Elumalai, P.; Mobin, S. M.; Lu, K.-L.; Sathiyendiran, M. Hard and soft-donors decorated rhenium based metallocavitands. *J. Organomet. Chem*. **2013**, *743*, 17-23.
42. Rajakannu, P.; Elumalai, P.; Shankar, B.; Hussain, F.; Sathiyendiran, M. Rhenium(I) based metallocalix[4]arenes decorated with free functionalized benzimidazolyl units. *Dalton Trans*. **2013**, *42*, 11359-11362.
43. Sathiyendiran, M.; Tsai, C. -C.; Thanasekaran, P.; Luo, T. -T.; Yang, C. -I.; Lee, G. -H.; Peng, S. -M.; Lu, K. -L. Organometallic Calixarenes: Syceelike Tetrarhenium(I) Cavitands with Tunable Size, Color, Functionality, and Coin–Slot Complexation. *Chem. Eur. J.* **2011**, *17*, 3343-3346.
44. Huang, G. G.; Lee, C. J.; Yang, J.; Lu, Z. Z.; Sathiyendiran, M.; Huang, C. Y.; Kao, Y. C.; Lee, G. H.; Lu, K. L. Cavity-containing rhenium metallacycle treated evanescent wave infrared chemical sensors for the selective determination of odorous amines in the atmosphere. *Sens. Actuators B: Chem*. **2018**, *254*, 424-430.
45. Rajakannu, P.; Elumalai, P.; Hussain, F.; Sathiyendiran, M. Rhenium-based bicyclic supramolecule with calixarene-shaped bowls. *J. Organomet. Chem*. **2013**, *725*, 1-4.
46. Chuang, C.-H.; Sathiyendiran, M.; Tseng, Y.-H.; Wu, J.-Y.; Hsu, K.-C.; Hung, C.-H.; Wen, Y.-S.; Lu, K.-L. Rigidity-Modulated Approach toward the Construction of Metallacycles from a Flexible Tetratopic Ligand. *Organometallics* **2010**, *29*, 283-285.
47. Elumalai, P.; Kanagaraj, R.; Marimuthu, R.; Shankar, B.; Kalita, A. C.; Sathiyendiran, M. Rhenium(I)-based bridgeless double metallocalix[4]arenes. *Dalton Trans.* **2015**, *44*, 11274-11277.
48. Shankar, B.; Sahu, S.; Deibel, N.; Schweinfurth, D.; Sarkar, B.; Elumalai, P.; Gupta, D.; Hussain, F.; Krishnamoorthy, G.; Sathiyendiran, M. Luminescent Dirhenium(I)-Double-Heterostranded Helicate and Mesocate. *Inorg. Chem*. **2014**, *53*, 922−930.
49. Shankar, B.; Elumalai, P.; Jackmil, P. J.; Kumar, P.; Singh, S.; Sathiyendiran, M. Synthesis of rhenium-based M_2LL^0-type supramolecular coordination complexes from flexible ligands. *J. Organomet. Chem.* **2013**, *743*, 109-113.
50. Saxena, P.; Shankar, B.; Sathyanarayana, A.; Prabusankar G.; Sathiyendiran, M. Rhenium(i)-based Double-heterostranded Helicates. *Chimia.* **2015**, *69*, 675–677.
51. Pereiras-Gabián, G.; Vázquez-López, E. M.; Braband, H.; Abram, U. Mono- and Dinuclear Tricarbonyltechnetium(I) Complexes with Thiosemicarbazones. *Inorg. Chem*. **2005**, *44*, 834-836.

Chapter 2

Re(I)-based Irregular Pentagonal-shaped Metallocavitands: Self-Assembly and Molecular Recognition Studies

Abstract

Neutral ditopic flexible N-donor ligands (L^n = (L^1 = bis(4-(naphtho[2,3-d]imidazol-1-ylmethyl)phenyl)methane, L^2 = bis(4-(benzimidazol-1-ylmethyl)phenyl)methane and L^3 = bis(4-(2-nonyl benzimidazol-1-ylmethyl)phenyl)methane)) possessing bis(4-methylphenyl)methane spacer with multi-arene fused imidazole donor unit were designed and synthesized. The L^n were utilized to develop metollacavitands analogous of pillar[5]arene framework with larger cavity. The metallocavitands **1-4** were assembled from $Re_2(CO)_{10}$, rigid bis-chelating donor (H_2-dhaq = 1,4-dihydroxy-9,10-anthraquinone and H_2-CA = chloranilic acid) and L^n via solvothermal approach. The ligands and metollacavitands were characterized by analytical and spectroscopic methods and further **1** and **4** were confirmed by single crystal X-ray diffraction analysis which reveals that a toluene molecule is residing in the hydrophobic cavity. The L^n and **1-4** are emissive at room temperature. The internal cavity of the metallocavitand acts as host for aromatic guest molecules. The host-guest interaction properties of **1** with various aromatic (anthracene (An), naphthalene (Np)) and nitroaromatic molecules (nitrobenzene (NB), 2-nitrotoluene (2-NT), 4-nitrotoluene (4-NT) and 2,4-dinitrotoluene (DNT)) were studied by emission spectroscopic method.

This work has been published in *Dalton Trans*. **2018**, *47*, 4494 -4500.

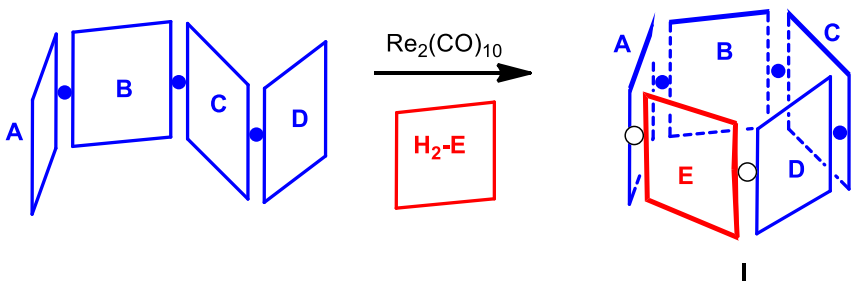

I

2.1. Introduction

The design and synthesis of metallocavitands similar to calixarenes have been growing due to their interest in the field of molecular recognition, catalysis, selective reactivity and biology.[1-4] Most of the studies in this area are focused on making neutral/ionic metallacalix[*n*]arenes (n = 3 and 4) to tune the hydrophobic cavity and functional groups at the rim.[5-8] Further, various approaches various metal ions and organic building units have been attempted to modulate the properties. Up to now, attempt to make neutral metallocavitand framework similar to calix[*5*]arene is scarce. It is expected that the metallocavitand may display properties similar to the calix[5]arene and is conformationally rigid and has larger hydrophobic cavity than the metallocavitand which is similar to calix[4]arene framework.[9-10] Herein, we report a simple synthetic approach for metallocavitand with larger cavity. The neutral heteroleptic metallocavitand was assembled using $Re_2(CO)_{10}$, rigid bis-chelating donors and a flexible ditopic N-donor possessing bis(4-methylphenyl)methane spacer, via solvothermal approach. Though the approach is similar to dirhenium-based metallacalix[4]arene i.e., combination of ditopic ligands containing a "phenylene(C*H*$_2$-hydrocycle)$_2$" flexible framework, rigid bis-chelating donor, and $Re_2(CO)_{10}$, this approach uses "C*H*$_2$-(phenylene-C*H*$_2$-heterocycle)$_2$" that results metallocavitand framework with solvent accessible hydrophobic cavity (Scheme 2.2-2.3).[12]

2.2. Experimental

2.2.1 Materials and Methods

Starting materials such as $Re_2(CO)_{10}$, H_2-dhaq, H_2-CA, benzimidazole(H-bimz), 2,3-diaminonaphthalene, diphenylmethane, phosphoric acid, paraformaldehyde, 30-33% HBr in AcOH, glacial acetic acid, formic acid and KOH were obtained from commercial sources and used as received. Naphthanoimidazole (H-nimz) and bis(4-(bromomethyl)phenyl)methane were prepared by using reported procedure.[13] Toluene and mesitylene were purified and distilled by conventional procedure. Spectroscopic grade solvent were used for analysis. FT-IR spectra were recorded on a Nicolet 380 FT-IR Spectrometer and Bruker ALPHA II FTIR Spectrometer. ^{1}H NMR spectra were recorded on a Bruker Avance III 500 and 400 MHz spectrometers. HR-MS spectra were recorded on a Bruker maXis mass spectrometer.

Elemental analysis data were performed on a Flash EA 1112 Series CHNS analyzer. UV-Vis and Fluorescence spectra were recorded on Shimadzu UV-VIS-NIR (UV-3600) spectrophotometer and Horiba Jobin Yvon (Fluoromax-4) spectrophotometer, respectively.

2.2.2 Synthesis of ligands and complexes.

Synthesis of bis(4-(naphtho[2,3-d]imidazol-1-ylmethyl)phenyl)methane (L^1).

A mixture of powdered KOH (0.1001 g, 1.784 mmol) and H-nimz (0.3 g, 1.784 mmol) in DMF (10 mL) was stirred at room temperature for 3 h. Bis(4-(bromomethyl)phenyl)methane (0.3157 g, 0.892 mmol) was added to the solution. The reaction mixture was then stirred continuously for 24 h. The residue was poured into ice cold water (300 mL). The resulting gray precipitate was filtered, washed several times with water, and air dried. The crude was purified by column chromatography (ethyl acetate/hexane, 4/6, v/v). Yield: 69% (324 mg). ^{1}H NMR (400 MHz, DMSO-d_6): δ 8.61 (s, 2H, H^2), 8.22 (s, 2H, H^9), 8.01-7.99 (m, 2H, H^8), 7.96 (s, 2H, H^4), 7.91-7.89 (m, 2H, H^5), 7.38-7.35 (m, 4H, $H^{7,6}$), 7.23 (d, J_{HH} = 8.16 Hz, 4H, $H^{14,11}$), 7.14 (d, J_{HH} = 8.16 Hz, 4H, $H^{13,12}$), 5.50 (s, 4H, H^{10}, -CH_2-), and 3.82 (s, 2H, H^{15}, -CH_2-). ESI (HR-MS). Calcd for $C_{37}H_{28}N_4$ $[M+H]^+$: *m/z* 529.2387. Found: *m/z* 529.2395. Anal. Calcd for $C_{37}H_{28}N_4$: C, 84.06; H, 5.34; N, 10.60. Found: C, 84.17; H, 5.39; N, 10.48.

Synthesis of bis(4-(benzimidazol-1-ylmethyl)phenyl)methane (L^2).

A mixture of powdered KOH (0.239 g, 4.232 mmol) and H-bimz (0.5 g, 4.232 mmol) in DMF (10 mL) was stirred at room temperature for 3 h. Bis(4-(bromomethyl)phenyl)methane (0.750 g, 2.116 mmol) was added to the solution. The reaction mixture was then stirred continuously for 48 h. The residue was poured into ice cold water (300 mL) and filtered. The resulting sticky white precipitate was washed with hexane and air dried. The crude was purified by column chromatography (methanol/chloroform, 2.5/97.5, v/v). Yield: 51% (462 mg). ^{1}H NMR (500 MHz, DMSO-d_6): δ 8.36 (s, 2H, H^2), 7.65-7.62 (m, 2H, H^7), 7.50-7.47 (m, 2H, H^4), 7.20-7.16 (m, 8H, $H^{12,9,6,5}$), 7.15-7.13 (m, 4H, $H^{11,10}$), 5.41 (s, 4H, H^8, -CH_2-), and 3.83 (s, 2H, H^{13}, -CH_2-). ESI (HR-MS). Calcd for $C_{29}H_{24}N_4$ $[M+H]^+$: *m/z* 429.2079. Found: *m/z* 429.2119. Anal. Calcd for $C_{29}H_{24}N_4$: C, 81.28; H, 5.65; N, 13.07. Found: C, 81.12; H, 5.58; N, 13.21.

Synthesis of bis(4-(2-nonyl benzimidazol-1-ylmethyl)phenyl)methane)) (L^3).

A mixture of powdered KOH (0.115 g, 2.046 mmol) and H-nbimz (0.5 g, 2.046 mmol) in DMF (10 mL) was stirred at room temperature for 3 h. Bis(4-(bromomethyl)phenyl)methane (0.362 g, 1.023 mmol) was added to the solution. The reaction mixture was then stirred continuously for 24 h. The residue was poured into water and chloroform mixture, and stirred for overnight. The organic layer was extracted, washed with saturated NaCl solution, dried over Na_2SO_4 and concentrated. The sticky precipitate was purified by column chromatography (hexane) to afford yellow coloured liquid. The resulting product was left open and the powder was obtained after 7-10 days. The powder was washed with hexane and dried. Yield: 48% (334 mg). ^{1}H NMR (500 MHz, DMSO-d_6): δ 7.56-7.54 (m, 2H, H^7), 7.41-7.39 (m, 2H, H^4), 7.13-7.09 (m, 8H, $H^{12,9,6,5}$), 6.95 (d, J_{HH} = 8.1 Hz, 4H, $H^{11,10}$), 5.40 (s, 4H, H^8, -CH_2-), and 3.82 (s, 2H, H^{13}, -CH_2-), 2.79-2.75 (t, J_{HH} = 7.6 Hz, 4H, H^{14}), 1.67-1.61 (m, 4H, H^{15}), 1.18 (s, 24H, H^{16-21}), and 0.84-0.81 (t, J_{HH} = 6.8 Hz, 6H, H^{22}). ESI (HR-MS). Calcd for $C_{47}H_{60}N_4$ $[M+H]^+$: *m/z* 681.4896. Found: *m/z* 681.4952. Anal. Calcd for $C_{47}H_{60}N_4$: C, 82.89; H, 8.88; N, 8.23. Found: C, 82.76; H, 8.32; N, 8.79.

Synthesis of [{(CO)$_3$Re(μ−dhaq)Re(CO)$_3$}(μ−L^1)] (1).

A mixture of $Re_2(CO)_{10}$ (100 mg, 0.1532 mmol), H_2-dhaq (36.80 mg, 0.1532 mmol), L^1 (80.99 mg, 0.1532 mmol), and toluene (10 mL) in a Teflon flask was placed in a steel bomb. The bomb was kept in an oven at 160 °C for 48 h and cooled to 30 °C. Compound **1** was obtained as dark coloured crystals and powder. The product was filtered, washed with hexane and air-dried. Yield: 76% (153 mg). ^{1}H NMR (400 MHz, DMSO-d_6): δ 9.32 (s, 2H, H^2), 8.52-8.49 (m, 4H, $H^{9,a}$), 8.31 (s, 2H, H^4), 8.13-8.10 (m, 2H, H^8), 8.03-8.00 (m, 2H, H^b), 7.93-7.91 (m, 2H, H^5), 7.43-7.40 (m, 4H, $H^{6,7}$), 7.15 (s, 2H, H^c), 7.08 (d, J_{HH} = 8.21 Hz, 4H, $H^{14,11}$), 6.80 (d, J_{HH} = 8.21 Hz, 4H, $H^{13,12}$), 5.55-5.35 (m, H^{10}, -CH_2-), and 3.64-3.54 (m, H^{15}, -CH_2-). ESI (HR-MS). Calcd for $C_{57}H_{34}N_4O_{10}Re_2$ $[M+H]^+$: *m/z* 1309.1465. Found: *m/z* 1309.1463. Anal. Calcd for $C_{57}H_{34}N_4O_{10}Re_2$: C, 52.37; H, 2.62; N, 4.29. Found: C, 52.43; H, 2.58; N, 4.35. FT-IR (KBr, cm^{-1}): 2011 (s), 1913 (s), and 1856 (s).

Synthesis of [{(CO)$_3$Re(μ−dhaq)Re(CO)$_3$}(μ−L^2)] (2).

A mixture of $Re_2(CO)_{10}$ (50 mg, 0.0766 mmol), H_2-dhaq (18.4 mg, 0.0766 mmol), L^2 (32.83 mg, 0.0766 mmol), and mesitylene (30 mL) was refluxed for 6 h. The product was filtered in hot condition, washed with hexane and air-dried. Compound **2** was obtained as dark coloured

powder. Yield: 49% (45 mg). ^{1}H NMR (500 MHz, DMSO-d_6): δ 9.13 (s, 2H, H^2), 8.52-8.50 (m, 2H, H^a), 8.04-8.03 (m, 2H, H^b), 7.98-7.96 (d, J_{HH} = 7.45 Hz, 2H, H^7), 7.83-7.82 (d, J_{HH} = 7.35 Hz, 2H, H^4), 7.36-7.30 (m, 4H, H^{6,5}), 7.10-7.09 (d, J_{HH} = 8.1 Hz, 4H, H^{12,9}), 7.06 (s, 2H, H^c), 6.84-6.82 (d, J_{HH} = 8.1 Hz, 4H, H^{11,10}), 5.50-5.32 (m, 4H, H^8, -CH_2-), and 3.65-3.58 (m, 2H, H^{13}, -CH_2-). Anal. Calcd for $C_{49}H_{30}N_4O_{10}Re_2$: C, 48.75; H, 2.50; N, 4.64. Found: C, 48.82; H, 2.56; N, 4.58. FT-IR (KBr, cm^{-1}): 2007 (s), and 1864 (s).

Synthesis of [{(CO)$_3$Re(μ−dhaq)Re(CO)$_3$}(μ−L^3)] (3).

A mixture of $Re_2(CO)_{10}$ (50 mg, 0.0766 mmol), H_2-dhaq (18.4 mg, 0.0766 mmol), L^3 (52 mg, 0.0766 mmol), and mesitylene (30 mL) was refluxed for 6 h. The resulting liquid was concentrated, washed with distilled hexane and air-dried. Compound **3** as dark coloured powder was obtained. Yield: 65% (73 mg). ^{1}H NMR (500 MHz, DMSO-d_6): δ 8.36-8.34 (m, 2H, H^a), 7.94-7.92 (m, 2H, H^b), 7.56-7.54 (m, 2H, H^7), 7.41-7.39 (m, 2H, H^4), 7.29 (s, 2H, H^c), 7.13-7.09 (m, 8H, H^{12,9,6,5}), 6.96-6.95 (d, J_{HH} = 8.1 Hz, 4H, H^{11,10}), 5.39 (s, 4H, H^8, -CH_2-), and 3.83 (s, 2H, H^{13}, -CH_2-), 2.79-2.76 (t, J_{HH} = 7.5 Hz, 4H, H^{14}), 1.68-1.62 (m, 4H, H^{15}), 1.18 (s, 24H, H$^{16-21}$), and 0.84-0.82 (t, J_{HH} = 6.85 Hz, 6H, H^{22}). Anal. Calcd for $C_{67}H_{66}N_4O_{10}Re_2$: C, 55.13; H, 4.56; N, 3.84. Found: C, 55.23; H, 4.48; N, 3.81. FT-IR (KBr, cm^{-1}): 2010 (s), and 1874 (s).

Synthesis of [{(CO)$_3$Re(μ−CA)Re(CO)$_3$}(μ−L^1)] (4).

Dark coloured crystals and powder of **4** were obtained by following the procedure similar to that for **1**, using a mixture of $Re_2(CO)_{10}$ (100 mg, 0.1532 mmol), H_2-CA (32 mg, 0.1532 mmol), L^1 (80.60 mg, 0.1532 mmol), and toluene (10 mL) in a Teflon flask. Yield: 57% (112.4 mg), (Major isomer). ^{1}H NMR (500 MHz, DMSO-d_6): δ 8.66 (s, 2H, H^2), 8.22 (s, 2H, H^9), 8.11-7.98 (m, 2H, H^8), 7.97 (s, 2H, H^4), 7.92-7.89 (m, 2H, H^5), 7.47-7.32 (m, 4H, H^{7,6}), 7.27-7.21 (m, 4H, H^{14,11}), 7.19-7.12 (m, 4H, H$^{13-12}$), 5.51 (m, 4H, H^{10}, -CH_2-), and 3.82 (m, 2H, H^{15}, -CH_2-). ESI (HR-MS). Calcd for $C_{49}H_{28}N_4Cl_2O_{10}Re_2$ [M+H]$^+$: *m/z* 1277.0366. Found: *m/z* 1277.0356. Anal. Calcd for $C_{49}H_{28}N_4Cl_2O_{10}Re_2$: C, 46.12; H, 2.21; N, 4.39. Found: C, 46.18; H, 2.25; N, 4.32. FT-IR (KBr, cm^{-1}): 2017 (s), and 1890 (s).

2.2.3 Host-Guest Studies.

Quenching experiments of host **1** in the presence of aromatic nitro compounds (Nitrobenzene, NB; 2-Nitrotoluene, 2-NT; 4-Nitrotoluene, 4-NT; 2,4- dinitrotoluene, 2,4-DNT) and planar

aromatic compounds (Benzene, Bn; Mesitylene, Ms; Naphthalene, Np; Anthracene, An) were carried out by fluorescence spectroscopic method. The solvent (DMSO) used in this study was of spectroscopic grade and used as received. Aromatic guests stock solutions (NB; 1.7×10^{-2} M for 2-NT, 4-NT and 2,4-DNT; 1.7×10^{-1} M for Bn and Ms; 0.14×10^{-2} M for Np; 0.17×10^{-3} M for An) were prepared in DMSO. Complex **1** stock solutions (1.92×10^{-4} M for NB, 2-NT, 4-NT and 2,4-DNT; 1.92×10^{-4} M for both Bn and Ms; 2.13×10^{-4} M for Np; 1.92×10^{-4} M for An) were prepared in DMSO. Test solutions were prepared by the addition of an appropriate aliquot (0.02-3mL) of each guest stock into 5ml standard volumetric flask followed by placing 1 mL of stock solution of host **1** and then diluting the solution to 5 mL with DMSO. The excitation wavelengths (λ_{exc}) were 336 nm for NB, 2-NT and 4-NT and 2,4-DNT; 350 nm for Bn; 325 nm for Ms; 290 nm for Np and 336 nm for An. The slit width was 5 nm for both the excitation and emission. The binding characteristics of host **1** with guest molecules were determined by the emission spectroscopic method. The binding constants were calculated on the basis of the Benesi-Hildebrand equation [$1/\Delta I = 1/\Delta I_{max} + (1/ K[G] \Delta I_{max})$]**;** here $\Delta I = I–I_{min}$, $\Delta I_{max} = I_0–I_{min}$, I_0 is the emission intensity of free host **1,** I is the intensity measured with guest, I_{min} is the intensity measured with an excess of guest, K is the binding constant, and [G] is the concentrations of guest molecules.

2.3. Results and discussion

2.3.1 Synthesis, characterization, and molecular structure of ligands L^1- L^3.

Neutral nitrogen donor ligands (L^1-L^3) were obtained using bis(4-bromomethylphenyl)methane and heterocyclic motif (naphthanoimidazole, H-nimz; benzimidazole, H-bimz; 2-nonylbenzimidazole, H-nbimz) in the presence of base.[11]

The ^{1}H NMR spectra of L^n displayed single set of signals for all the protons. In particular, two singlet signals in the aliphatic region corresponds to two methylene protons (~5-6 ppm for N-C*H*$_2$-C and ~3.5-4.0 ppm for C-C*H*$_2$-C), suggesting formation of the ligands and are flexible in solution i.e., various conformers which interconvert each other in the solution. Ligand L^1 takes M-shaped conformation mode in the solid state ligand L^2 adopts *cis*-conformation. Two nimz units of L^1 are arranged *anti*-cofacially, whereas two bimz motifs of L^2 are in *syn*-orientation**.**

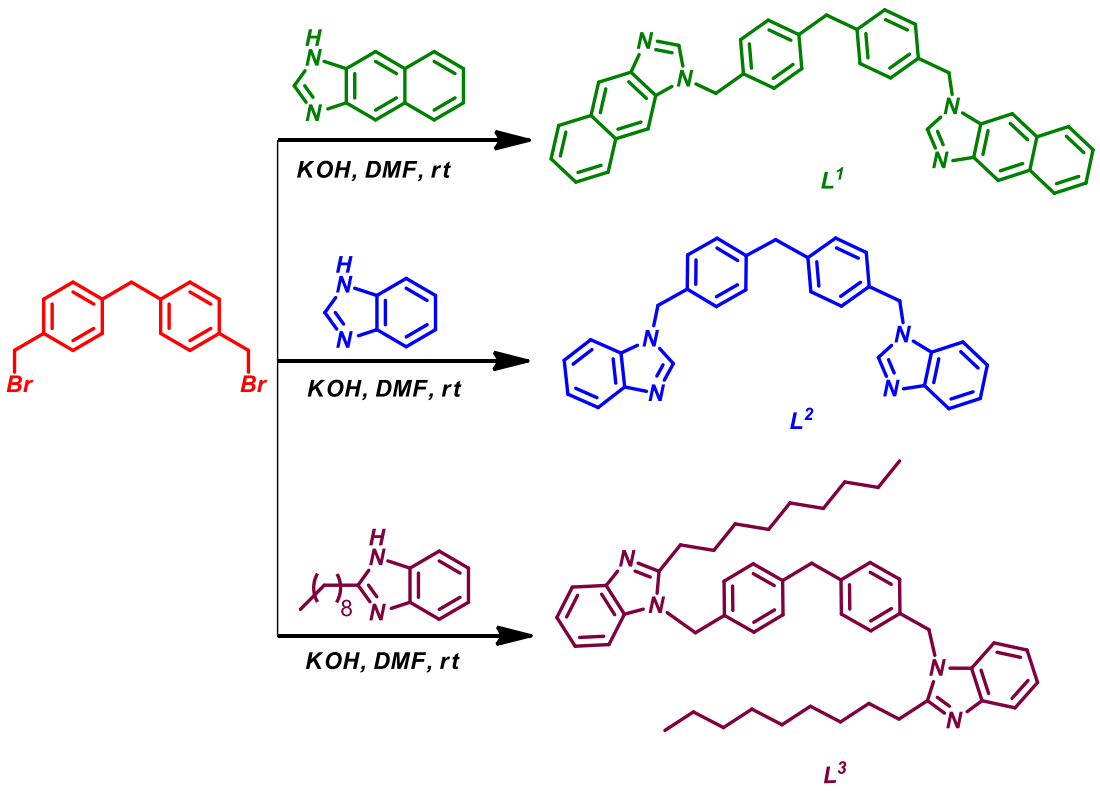

Scheme 2.1 Synthesis of ligands L^1-L^3.

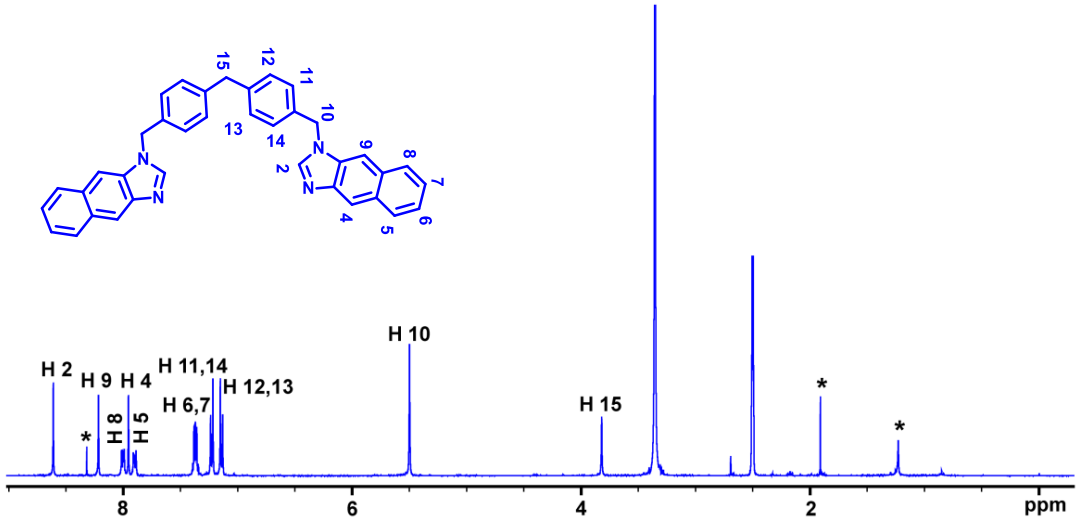

Figure 2.1. ^{1}H NMR spectrum of L^1 in DMSO- d_6 (* is solvent).

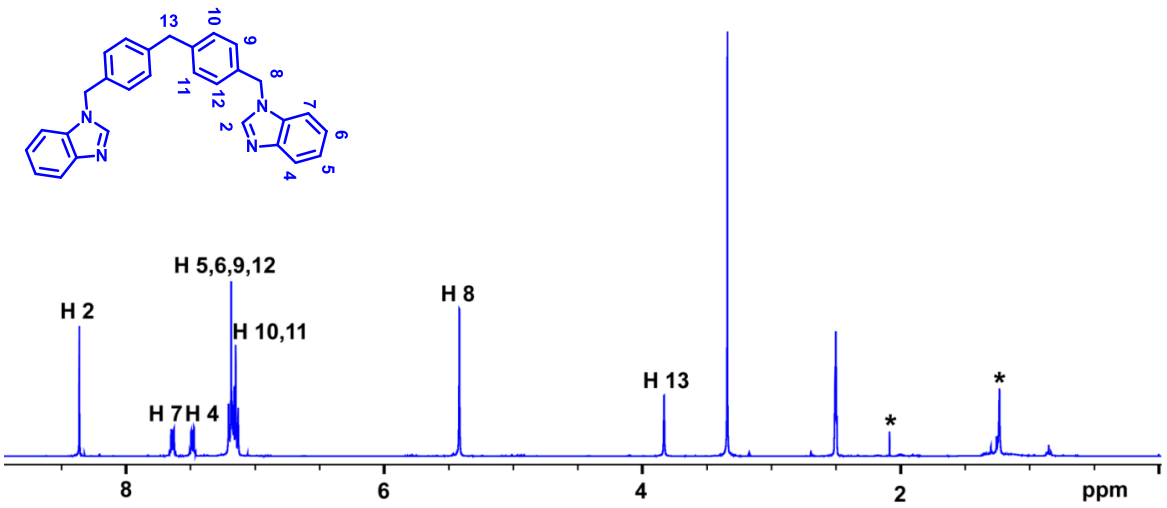

Figure 2.2. ^{1}H NMR spectrum of L^{2} in DMSO- d_6 (* is solvent).

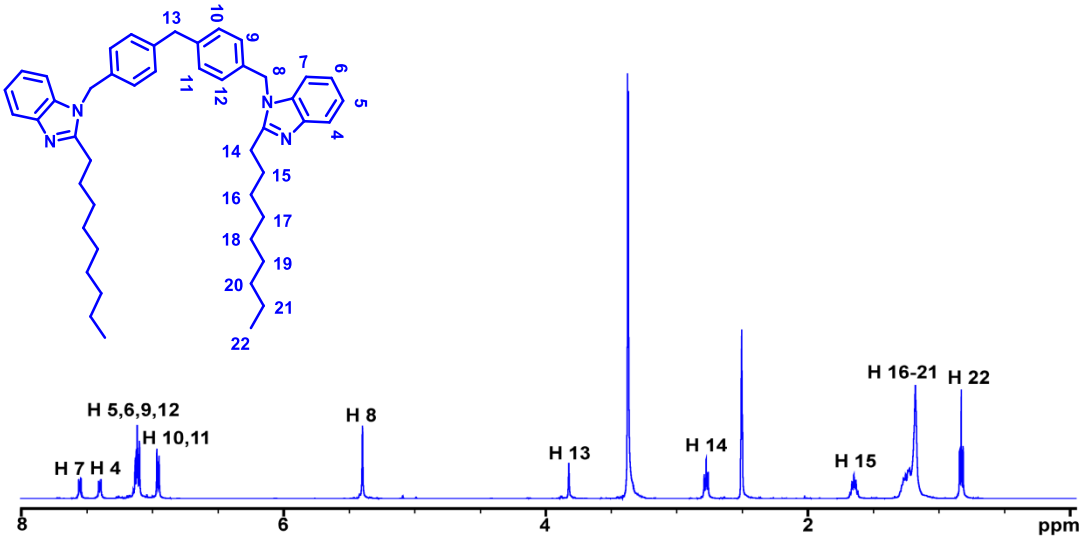

Figure 2.3. ^{1}H NMR spectrum of L^{3} in DMSO- d_6.

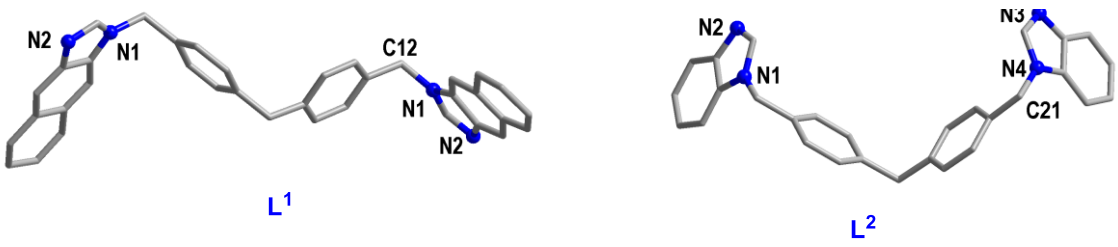

Figure 2.4. Molecular structures of L^{1} and L^{2} (H-atoms are omitted for clarity).

2.3.2 Synthesis and characterization of metallocavitands (1-4).

The treatment of $Re_2(CO)_{10}$, 1,4-dihydroxy-9,10-anthraquinone (H_2-dhaq)/chloranilicacid (H_2-CA), L^n and toluene or mesitylene yielded metallocavitands (**1-4**) with toluene molecule (Scheme 2.3).[11] The complexes are air and moisture stable, and moderately soluble in polar organic solvents. The FT-IR spectra of **1-4** showed strong bands around 2017–1856 cm^{-1}, characteristic of the *fac*-$Re(CO)_3$ units in the asymmetric environment.[1]

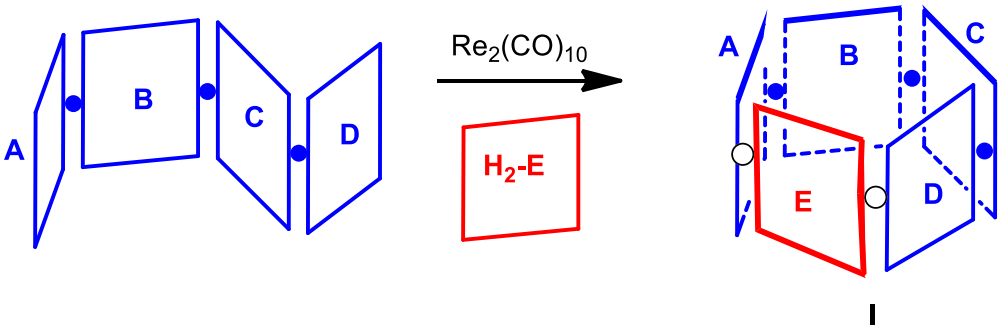

I

Scheme 2.2. Synthesis of an irregular pentagonal-shaped metallocavitand (**I**). A = D = heterocyclic nitrogen donor; B = C = phenylene; H_2E = bis-chelating unit; ● = CH_2; o = *fac*-$Re(CO)_3$.

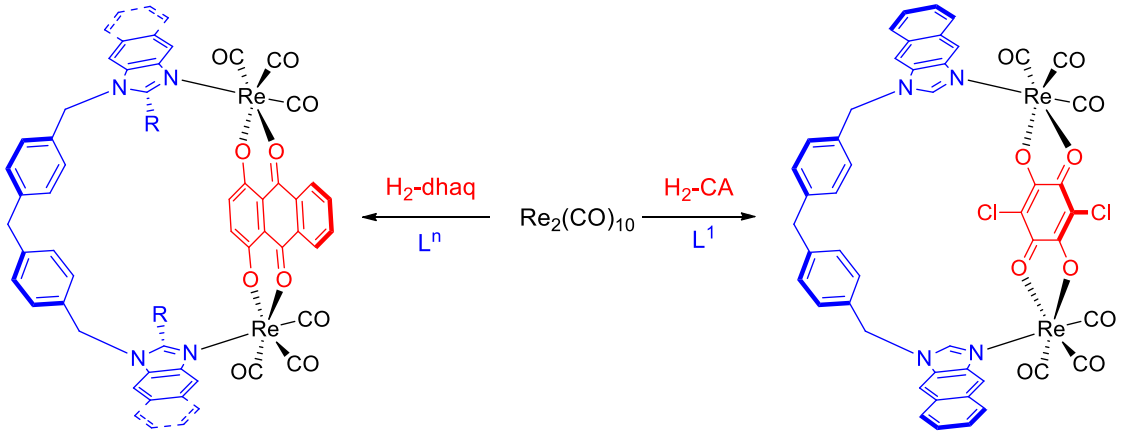

1, $L^n = L^1$, R = H; N donor = naphthanoimidazolyl
2, $L^n = L^2$, R = H; N donor = benzimidazolyl
3, $L^n = L^3$, R = $-(CH_2)_8-CH_3$; N donor = benzimidazolyl

4

Scheme 2.3. Synthesis of **1-4**.

The ^{1}H NMR spectra of **1** and **2** displayed a single set of chemical resonances for protons of both L^{n} and dhaq in a 1:1 integration ratio, ascribed to M_2LL'-type complexes. The proton of N-C*H*-N in **1** and **2** was significantly downfield shifted relative to uncoordinated L^{1}/L^{2}, confirms the coordination of N to rhenium. The methylene protons (N-CH_2-C and C-CH_2-C) of **1** and **2** were appeared as multiplets, suggesting the rigidity of L^{1}/L^{2} in the complexes. Remaining protons of L^{n} and dhaq motifs were shifted in relative to those protons in the uncoordinated ligands. In the case of **3**, no shift in the peaks for the protons of L^{3} compared to those protons in free L^{3} while the peaks for the protons of dhaq unit were shifted compared to those protons in uncoordinated H_2-dhaq. Complex **4** displays two types of ^{1}H NMR pattern for protons of L^{1}. The pattern of major peaks resembled to the ligand proton peaks with slight downfield shift. The minor peaks resembled to the peaks of L^{1} in **1**. We suggest that **4** exists as various conformers i.e. two major conformers, and more than two minor conformers, in solution.[11a]

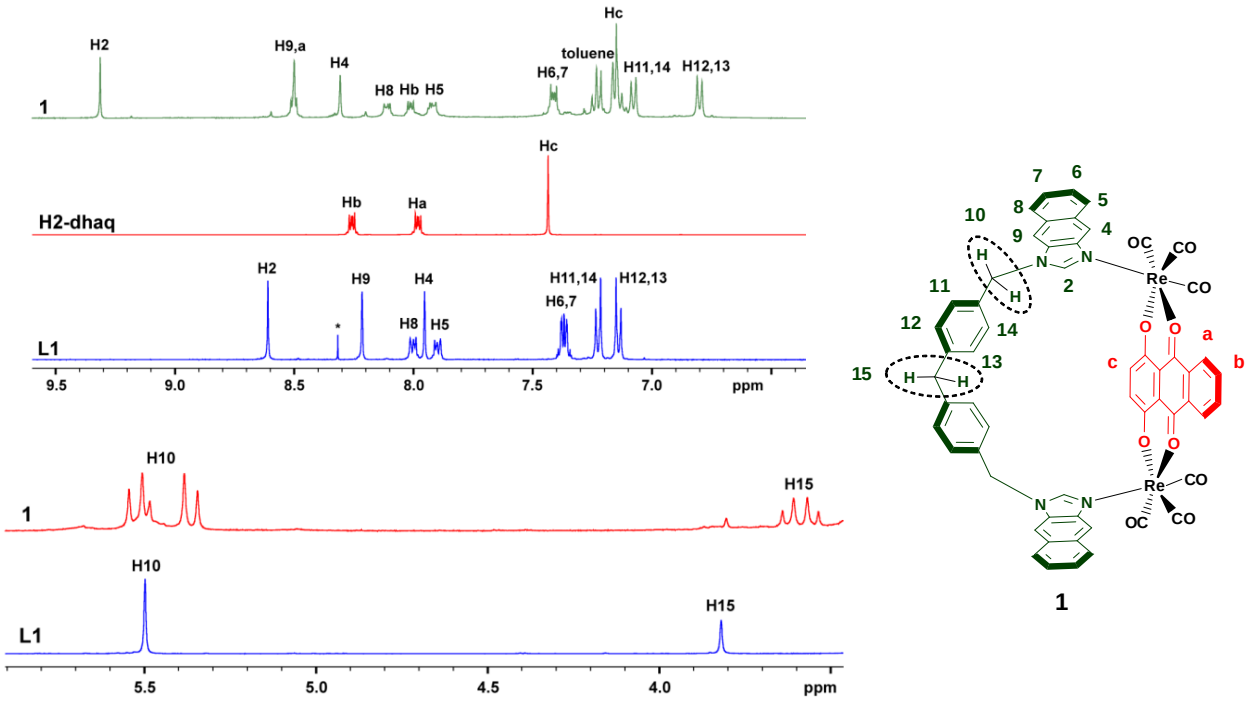

Figure 2.5. Partial ^{1}H NMR spectra of **1**, H_2-dhaq and L^{1} in DMSO-d_6.

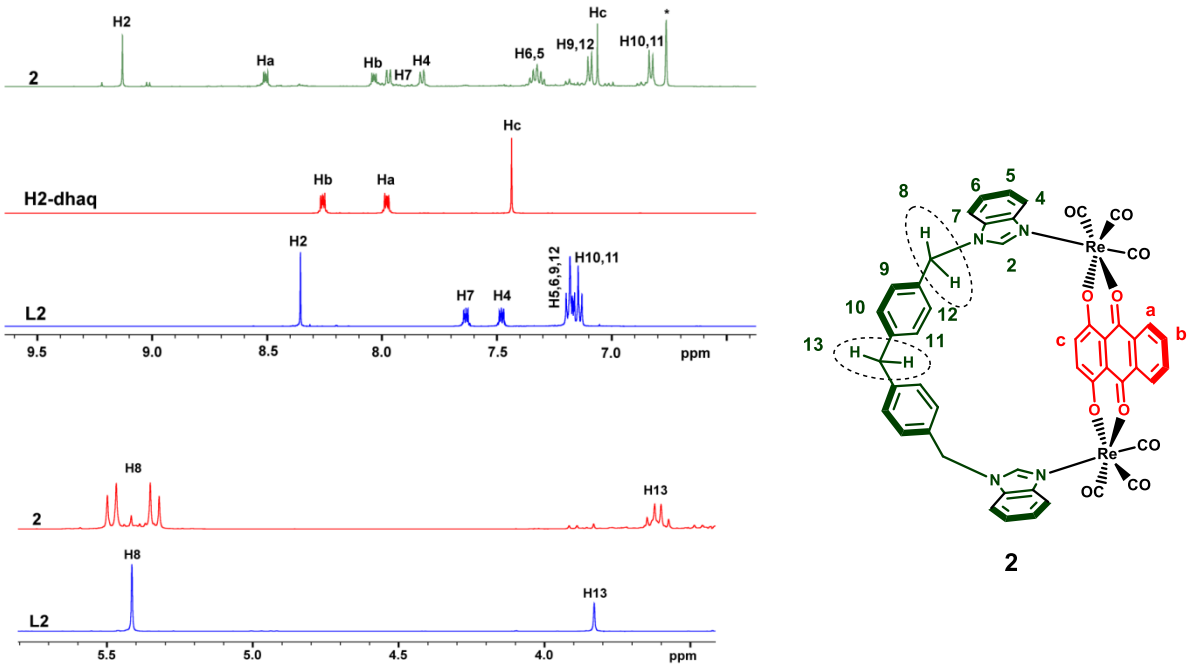

Figure 2.6. Partial ^{1}H NMR spectra of **2**, H_2-dhaq and L^2 in DMSO-d_6.

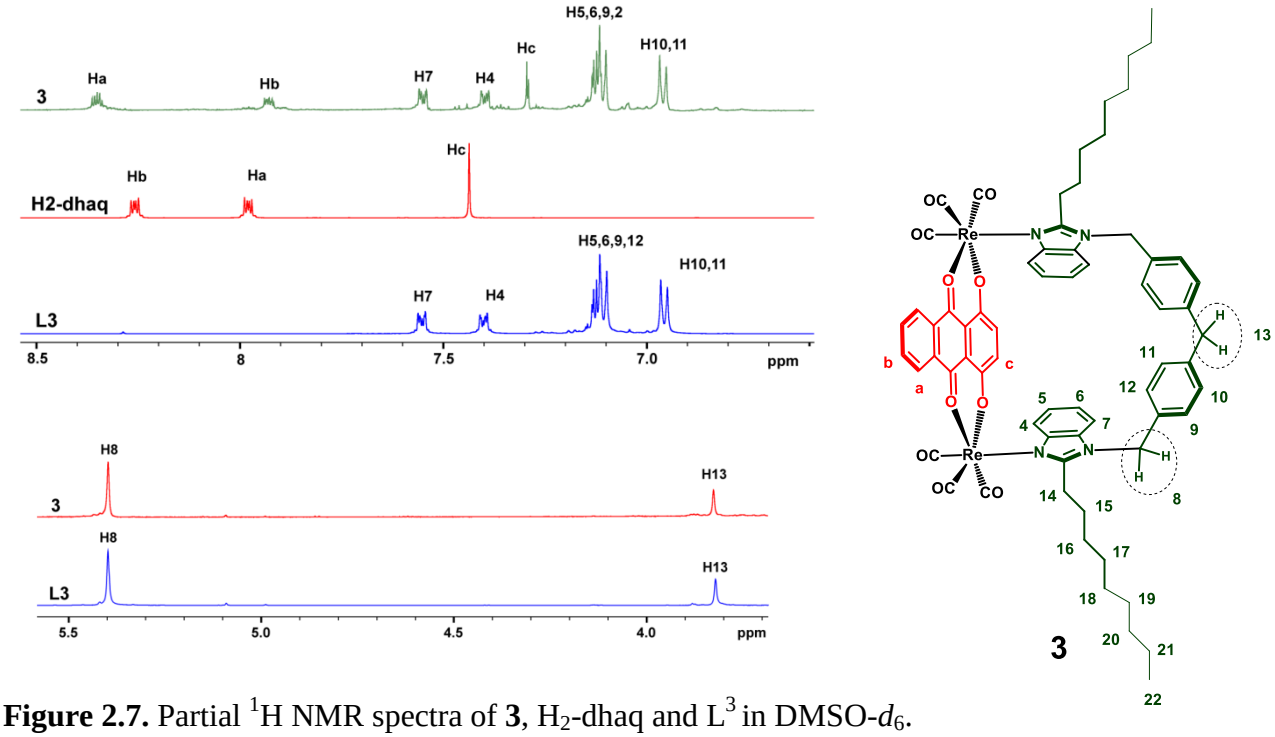

Figure 2.7. Partial ^{1}H NMR spectra of **3**, H_2-dhaq and L^3 in DMSO-d_6.

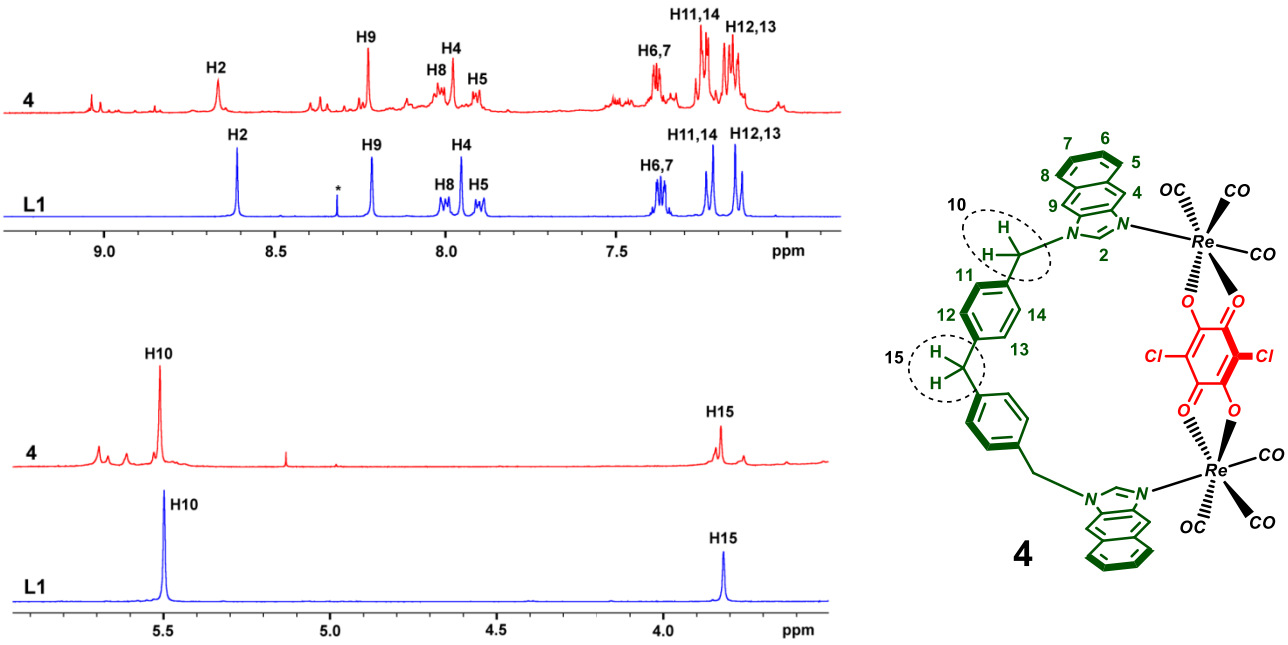

Figure 2.8. Partial ^{1}H NMR spectra of **4** and L^{1} in DMSO-d_6.

2.3.3 Molecular structure of metallocavitands (1 and 4).

The result of SCXRD study showed that **1** adopts M_2LL'-type of SCC with irregular pentagon (Fig. 2.9). The cyclic assembly of **1** can be viewed as [2+1+1] assembly of two *fac*-Re(CO)$_3$ cores, one dianionic dhaq^{2-} motif, and one neutral nitrogen donor ligand L^1. The arrangement of five organic units i.e., "Re–dhaq^{2-}–Re–nimz–C*H*$_2$–phenylene–C*H*$_2$–phenylene–C*H*$_2$–nimz", provide distorted pentagonal-shaped structure i.e three methylene units (–C^{1}H$_2$–, –C^{2}H$_2$–, –C^{3}H$_2$–) and two Re atoms are related to five vertices and dhaq^{2-}, two nimz units and two phenylene units are the edges. The dimensions of **1** are 8.390 Å (Re···Re), 5.679 Å (Re^2···C^{12}{CH$_2$}), 5.875 Å (C^{12}{CH$_2$}···C^{19}{CH$_2$}), 5.820 Å (C^{19}{CH$_2$}···C^{26}{CH$_2$}), and 5.665 Å (C^{26}{CH$_2$}···Re^1) including van der Waals radii. The height of structure of **1** is 8.7 Å (length of nimz unit). Among the five pentagonal walls, two phenylene walls are tilted oppositely with dihedral angle 115.7°. The remaining three walls are perpendicular to the plane created by five vertices with the dihedral angle of 88.5°, 88.63° and 88.47°. The five interior angles of pentagonal structure are 100°, 95°, 112°, 115° and 117°, and the sum of the pentagonal angle is 540°. It is noteworthy to mention that pentagonal shaped metal-directed SCCs are very limited.

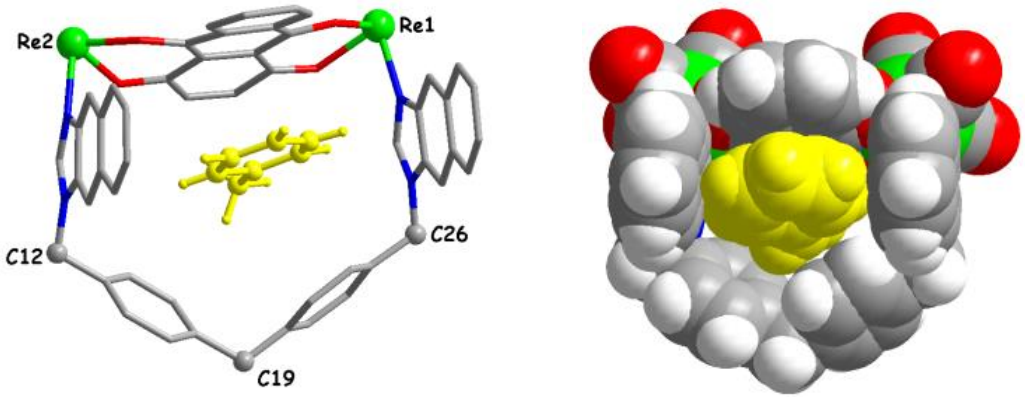

Figure 2.9. Molecular structure of **1** (left: H atoms and six CO units were removed to show cyclic framework; right: space-filling view of **1**. C = gray, H = white, N = blue, O = red, Re = green, toluene = yellow.

Complex **4** adopts a similar structure like that of **1** (Fig. 2.10). The distances between the vertices of pentagonal structure of **4** are similar to those found in **1** except Re···Re distance (8.13 Å) which is 0.26 Å shorter than Re···Re distance in **1**. The major differences found among these two complexes are the orientation of two nimz units in the cyclic framework. The two nimz units of **1** are cofacial with the dihedral angle of 6.598 Å. The distance of centre of nimz to centre of another nimz is 9.52 Å in **1**. However, two nimz in **4** are tilted in such a way that the edges of the six-membered core of nimz are close to each other with the dihedral of angle of 32.672°. The shortest non-bonded distance between two nimz in **4** is 4.745 Å which is above the five vertices plane and longest distance (9 Å) is below to the plane. The electronic arrangements found in dianionic ligands, $dhaq^{2-}$ in **1** and CA^{2-} in **4**, are usual i.e., delocalization of π electrons both in $dhaq^{2-}$ and CA^{2-}. The crescent bending nature of $dhaq^{2-}$ in **1** is similar to other ionic/neutral metallacycles possessing this unit.[11, 12b, 14]

2.3.4 Host-guest interactions in solid-state.

The hydrophobic cavity of **1** (width: 6.12 Å excluding the van der Waals radii i.e., distance between two nmiz units and height: 8.7 Å) contains one toluene solvent molecule, which resides deep in the cavity. The cavitand size is similar to cavity size of pillar[6]arene (ca. 6.7 Å) and is bigger than pillar[5]arene cavity (ca. 4.7 Å).[15] All five walls of metallocavitand **1** contact with guest toluene via *face-to-face* π-π stacking interactions and the *edge-to-face* aromatic C-H···π interactions. The benzene

plane of toluene guest is oriented parallel to $dhaq^{2-}$ plane and perpendicular to two nimz planes. The crescent shaped $dhaq^{2-}$ molecule is above the plane of Re···Re with the distance of 0.6 Å. This arrangement may be due to π···π interactions with guest toluene (τ = 7°; d = 3.25-3.77 Å and $d_{av.}$ = 3.45 Å). The $dhaq^{2-}$ and CA^{2-} units are used to make SCC rectangles and other cyclic structures. However, to the best of our knowledge the π···π stacking interactions between the $dhaq^{2-}$/CA^{2-} units and guest aromatic solvent molecule is scarce. The distance of centre of mass (COM) of toluene and COM of nimz ring is 4.8 Å, indicating the strong *edge-to-face* aromatic C-H···π interactions between them. The methyl group of toluene lie at bottom of cavitand and is stabilized by multiple aliphatic C-H···π interactions.

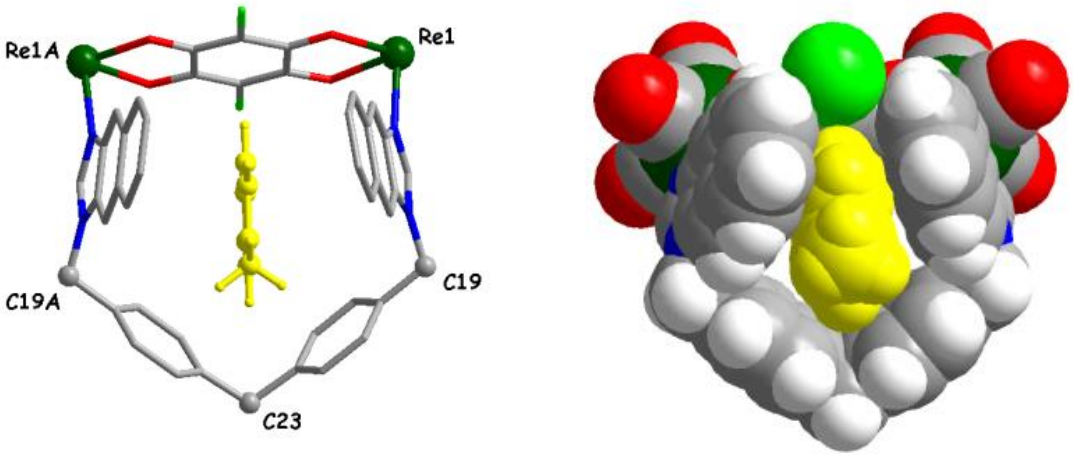

Figure 2.10. Molecular structure of **4** (left: H atoms and six CO units were removed; right: space-filling view of **4**. C = gray, H = white, N = blue, Cl = green, O = red, Re = dark green, toluene = yellow.

The volume of the hydrophobic cavity in **4** is reduced as compared to molecule **1** due to the orientation of two nimz units. In contrary to **1**, the plane of guest toluene is parallel to the two nimz units and perpendicular to the CA^{2-} plane. The distance between two COM of nimz units is 7 Å i.e., diameter is 3.6 Å excluding the van der Waals radii. The distances of benzene unit of toluene and plane of nimz in **4** are 3.35, 3.47, 3.58, 3.84, 3.93 and 4.7 Å, indicates aromatic *edge-to-face* C-H···π interactions. Further, the distance between the one of hydrogen atoms of toluene and chlorine of CA^{2-} is 2.992 Å which is equal to the sum of the van der Waals distance of chlorine (1.80 Å) and hydrogen (1.20 Å), indicates very weak C-H···Cl interaction. In addition,

the methyl group of toluene guest molecule is upward in the cavity and is away from the walls of cyclic framework of **4**.

2.3.5 Photophysical properties.

The photophysical properties of ligands (L^1-L^3) and complexes (**1-4**) were studied in DMSO. The absorption properties of known SCCs possessing [benzimidazolyl-$Re(CO)_3$-dhaq-$Re(CO)_3$-benzimidazolyl] unit are well-studied both experimentally and theoretically by Lu and others.[16] Hence, the assignment of electronic transitions is based on the literature report.[16] The absorption spectra of L^1, L^2, and L^3 display bands in the range of 257-347, 257-283, and 258-285 nm, respectively (Table 1). High energy bands (λ_{abs} = 257, 325, 336, and 350 nm for **1**, 262 nm for **2** and **3**, and 256, 326, 336, and 348 nm for **4**) are assigned to ligand centred π–π^* electronic transitions, whereas low energy bands (at λ_{abs} = 407 nm for **1**, 410 for both **2** and **3**) may correspond to metal-to-ligand charge transfer (MLCT) transitions. In addition, the weak bands (λ_{abs} = 593, 641 nm for **1**, 596, 644 nm for **2**, and 601, 650 nm for **3**) may be attributed to intraligand transition of the $dhaq^{2-}$ moiety. Ligand L^1 shows structured emission in the visible region (345-420nm), whereas L^2 and L^3 show structurelss emission band centred at 294 and 296 nm, respectively. All the complexes show ligand-centred emission in the presence/absence of oxygen at room temperature. No emission was observed in the visible region for all the complexes.

Table 2.1. Absorption and emission spectral data for the ligands and the complexes.

Comp.	λ_{abs} (nm)	λ_{exc} (nm)	λ_{em} (nm)
L^1	257, 318, 332, 347	318	345, 349, 359, 382, 399, 420
L^2	257, 268, 276, 283	257	294
L^3	258, 278, 285	258	296
1	257, 325, 336, 350, 407, 593, 641	325	355, 370, 387
2	262, 410, 596, 644	262	294
3	262, 410, 601, 650	262	303
4	256, 326, 335, 348	328	353, 370, 390, 415

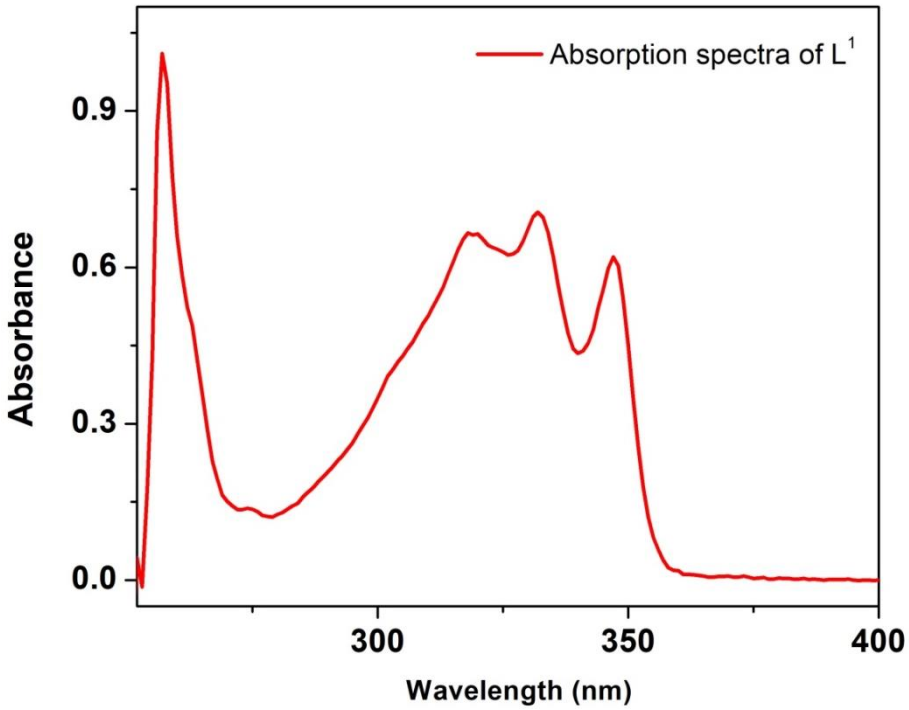

Figure 2.11. UV−Vis spectrum of L^1 in DMSO (0.68×10^{-4} M).

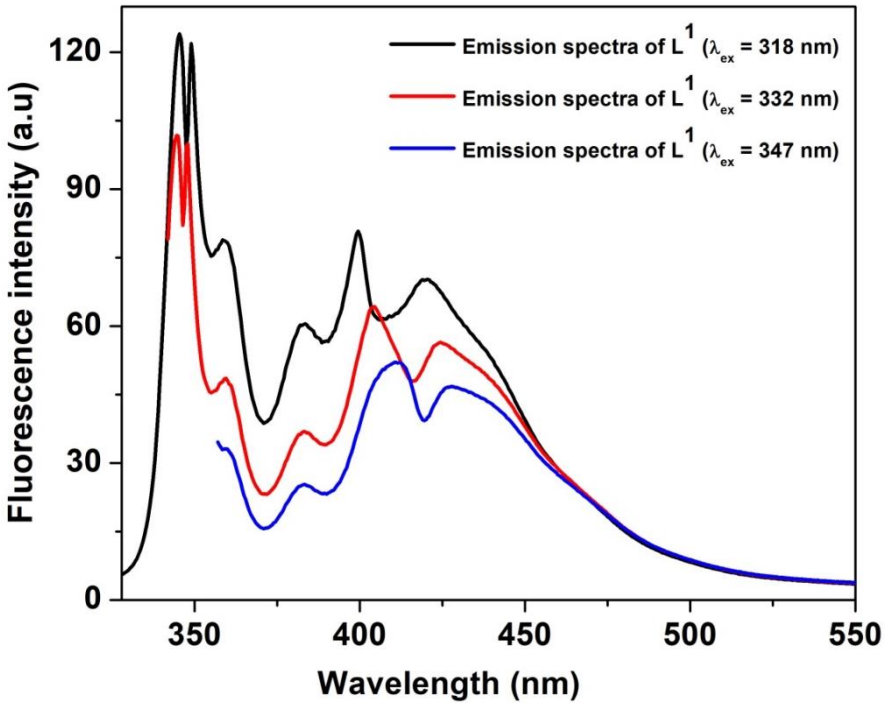

Figure 2.12. Fluorescence spectra of L^1 in DMSO (0.68×10^{-4} M).

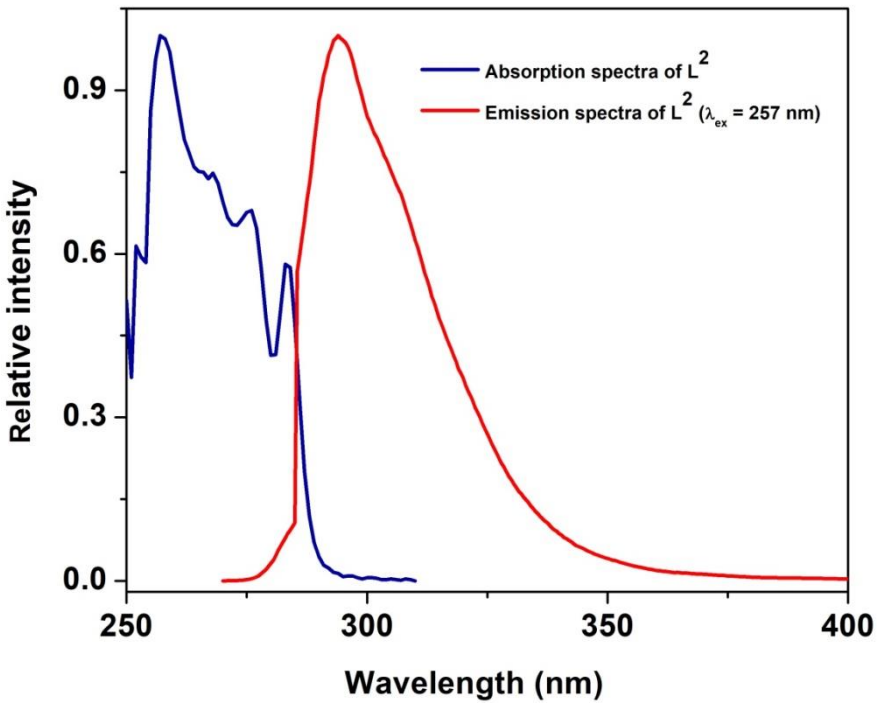

Figure 2.13. UV−Vis and fluorescence spectra of L^2 in DMSO (1×10^{-4} M).

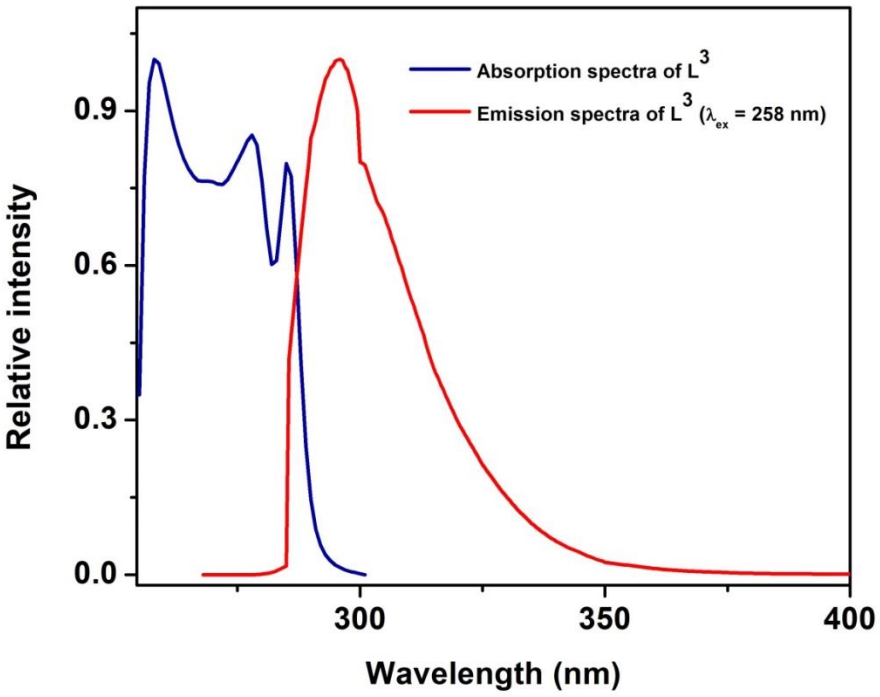

Figure 2.14. UV−Vis and fluorescence spectra of L^3 in DMSO (0.2×10^{-4} M).

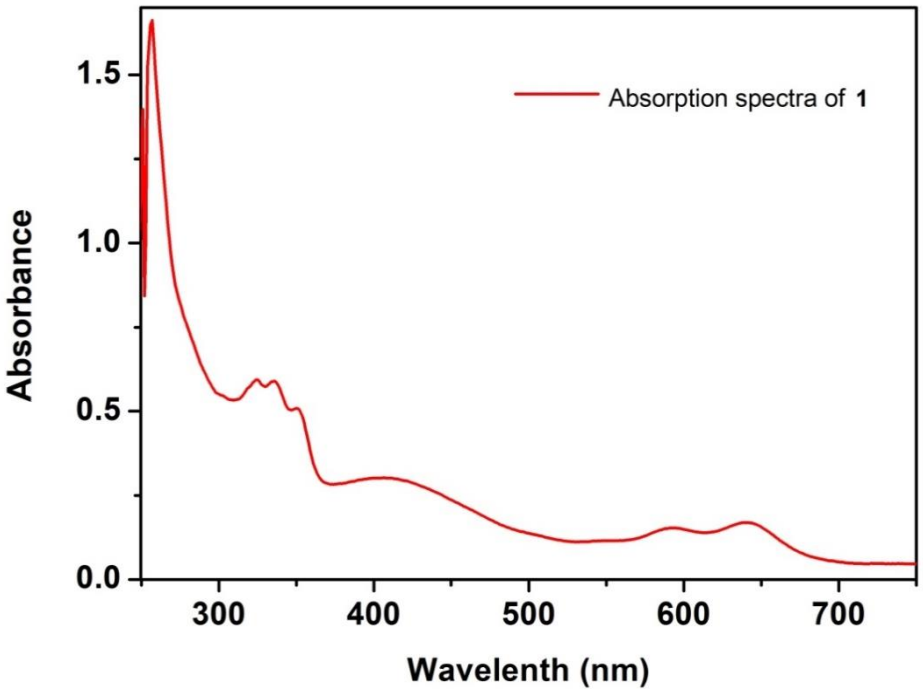

Figure 2.15. UV−Vis spectrum of **1** in DMSO (0.60×10^{-3} M).

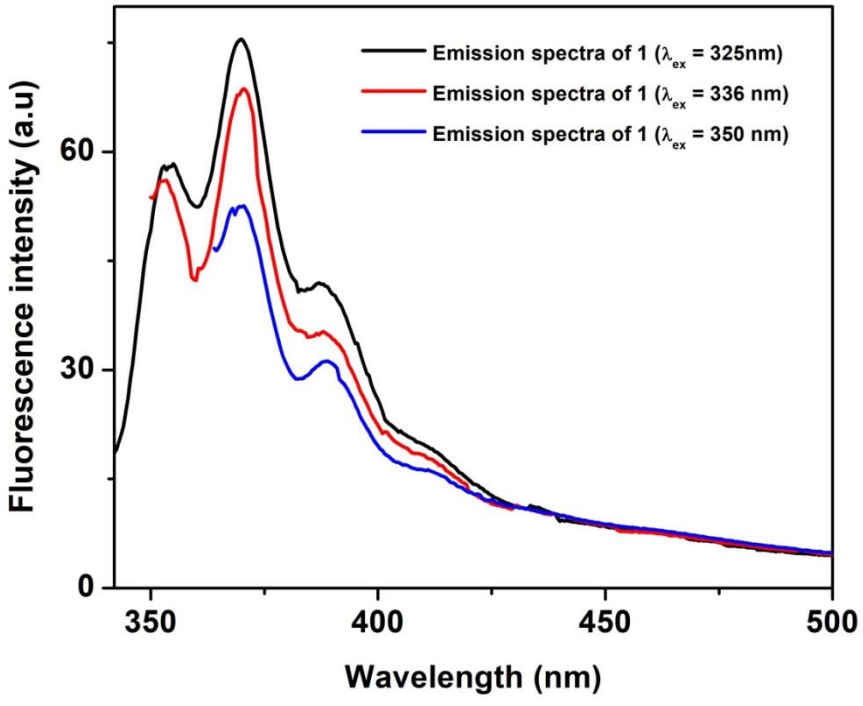

Figure 2.16. Fluorescence spectra of **1** in DMSO (1.92×10^{-4} M).

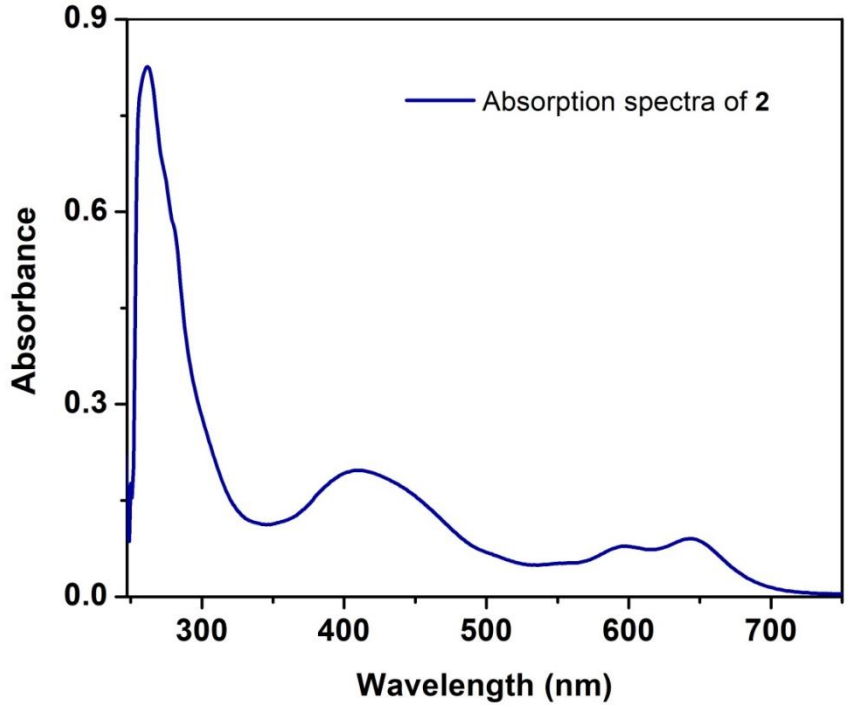

Figure 2.17. UV−Vis spectrum of **2** in DMSO (0.3×10^{-5} M).

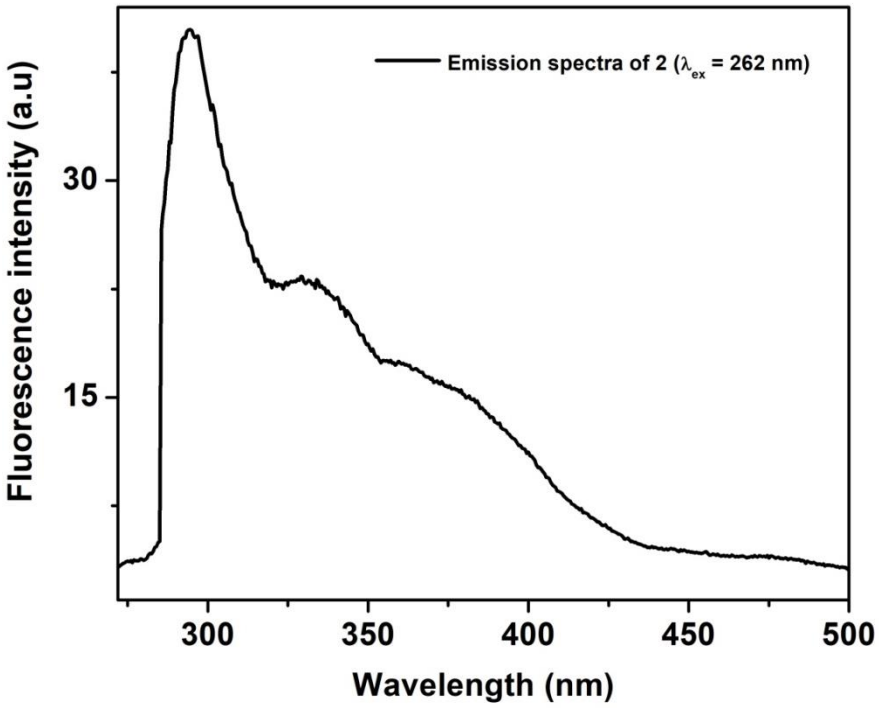

Figure 2.18. Fluorescence spectrum of **2** in DMSO (1×10^{-4} M).

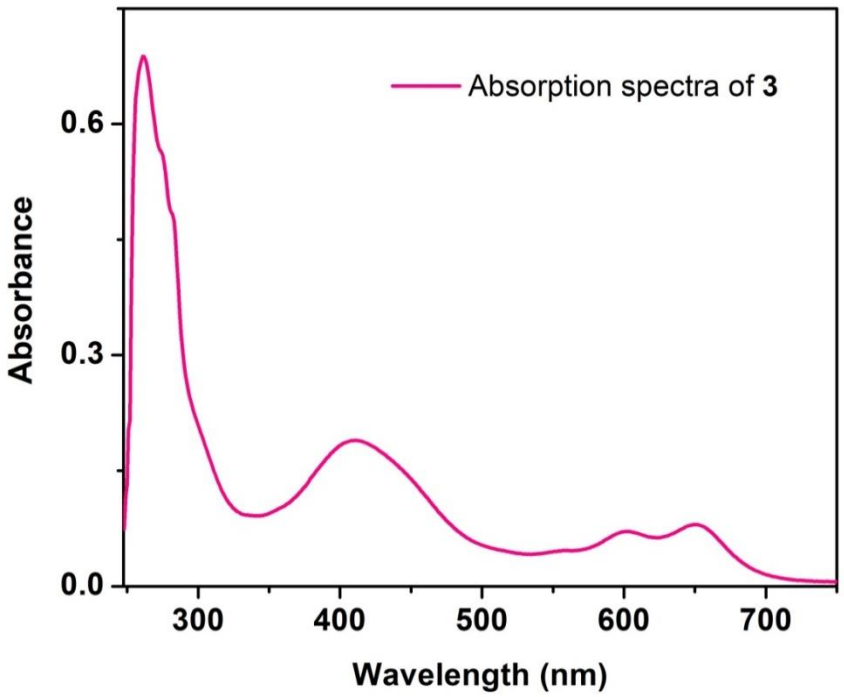

Figure 2.19. UV−Vis spectrum of **3** in DMSO (0.4×10^{-5} M).

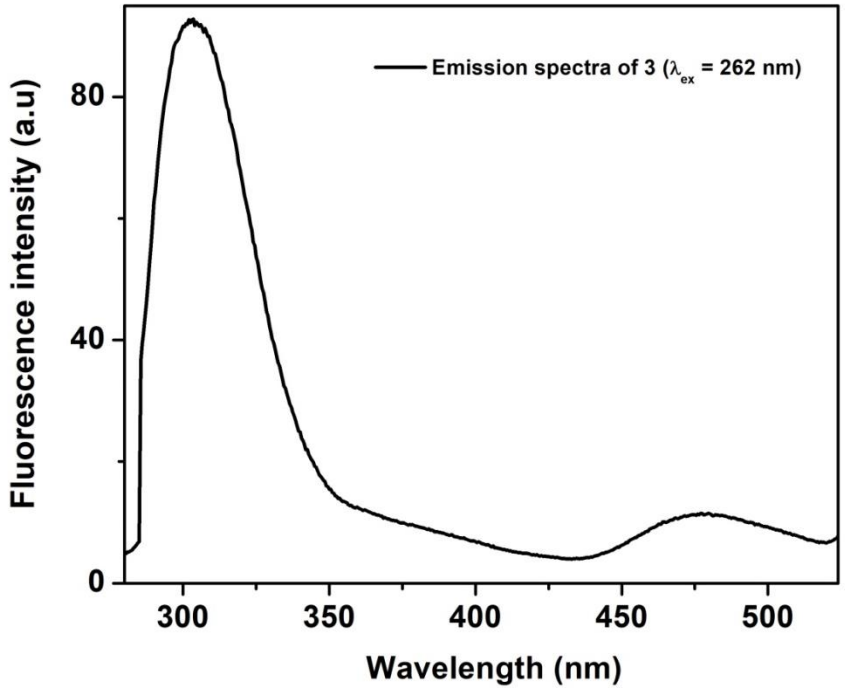

Figure 2.20. Fluorescence spectrum of **3** in DMSO (1×10^{-4} M).

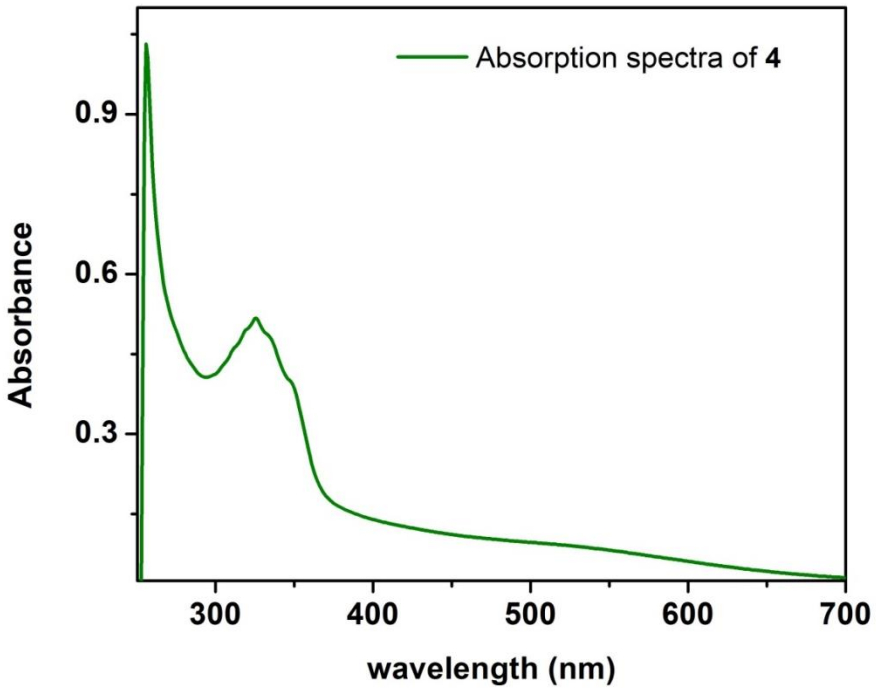

Figure 2.21. UV−Vis spectrum of **4** in DMSO (0.2×10^{-4} M).

2.4 *Binding studies of host 1 with aromatic and nitroaromatic molecule.*

In order to study the host-guest interaction, we selectively chosen nitro substituted aromatic molecules and planar aromatic compounds in DMSO, using emission spectroscopic method (chart 2.1). The study was carried for complex **1** as host. The fluorescence spectrum of **1** exhibits an intense emission at 375 nm upon excitation at 336 nm. Figure 2.22 shows the changes in the fluorescence spectrum upon titrating **1** against nitrobenzene (NB). The fluorescence of **1** is effectively quenched upon addition of NB. Among nitrobenzene, 2-nitrotoluene, 4-nitrotoluene, and 2,4-dinitrotoluene (DNT), DNT display strong fluorescence quenching of **1**. The effective quenching was achieved through electron transfer process from the photo-excited fluorophore (**1**) to the electron deficient nitroaromatic compounds at ground state.[17-19] The fluorescence quenching data was analysed using linear regression plot which indicates the formation of 1:1 host-guest complex. The solid-state structure of **1** shows strong evidence that complex **1** can accommodate one toluene molecule in the cavity. The binding constants (*K*) were calculated on the basis of Benesi–

Hildebrand equation for complexation of **1** with 2,4-DNT, NB, 4-NT and 2-NT and are 2.5×10^3 M^{-1}, 4.7×10^2 M^{-1}, 4.5×10^2 M^{-1}, 1.1×10^3 M^{-1}, respectively.[20] Similarly, the titrations of **1** with various aromatic compounds were carried out by fluorescence method. The fluorescence spectra of **1** with gradual addition of anthracene/naphthalene show hyperchromic shift at 387/322 nm and hypochromic shift at 352/457 nm upon excitation at 336/290 nm. The emission profile of anthracene (An) and naphthalene (Np) are also merging with emission pattern of **1** in the range of 382-508 nm and 300-400 nm, respectively. Hence, we have chosen the emission intensity at 352/457 nm which is not merging with guest emission range, for binding constant calculation using Benesi– Hildebrand equation.[20] Anthracene shows higher binding ability than naphthalene, (K = 1.3×10^4 M^{-1} for An and 1.7×10^3 M^{-1} for Np). In case of benzene and mesitylene with **1**, both fluorescence enhancement and quenching was observed simultaneously. This phenomenon may be due to the process of fast dissociation and association (guest go in/out the cavity) of host-guest complex. The above emission studies indicate that the accessible size of **1** is suitable to accommodate planar aromatic molecules as well as nitroaromatic compounds, which may be stabilized by the effective π···π and C-H···π interactions with host framework wall.

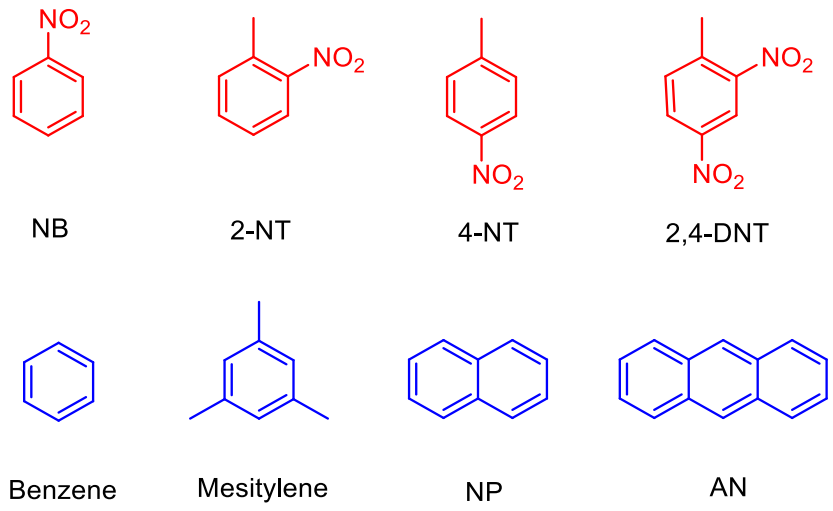

Chart 2.1: Guest molecules used for molecular recognition studies.

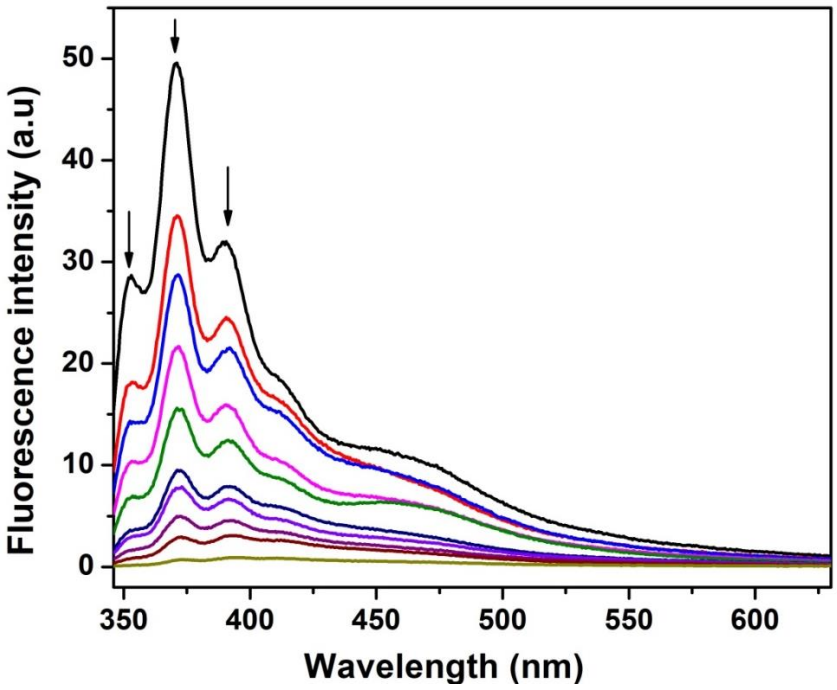

Figure 2.22. Changes in the emission spectra of **1** (3.84×10^{-5} M, λ_{exc} = 336 nm) with the addition of nitro benzene in DMSO. The arrows indicate the changes in the fluorescence intensity by addition of an appropriate aliquot of nitrobenzene.

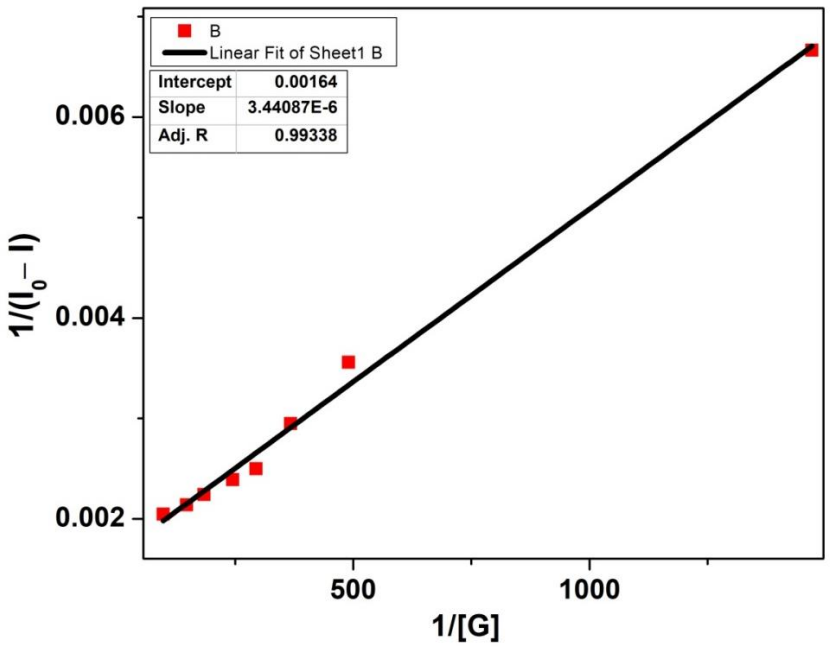

Figure 2.23. Benesi-Hildebrand plot for the emission quenching of host **1** (at 371 nm) with an increase in the concentration of nitrobenzene in DMSO.

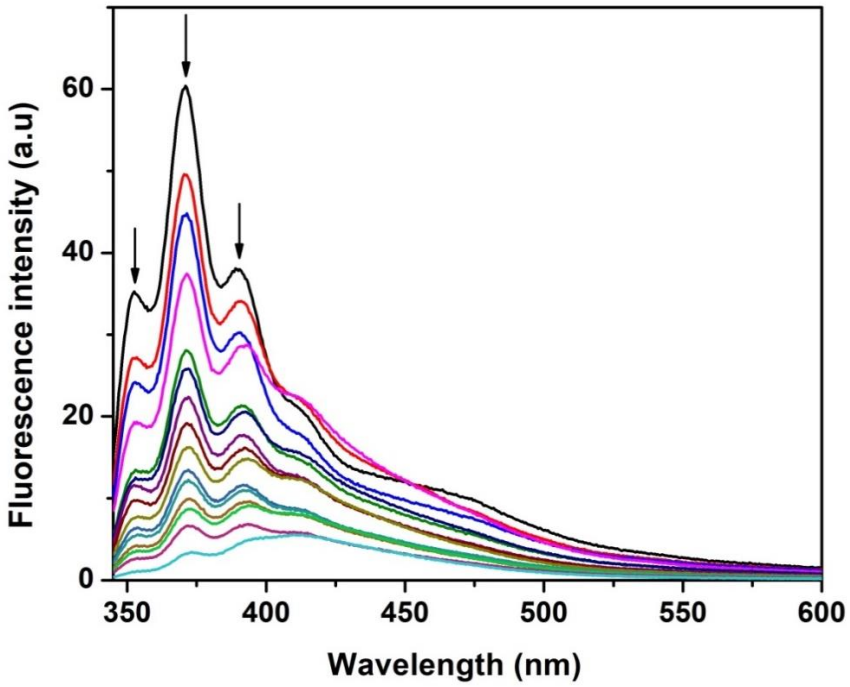

Figure 2.24. Changes in the emission spectra of **1** (3.84×10^{-5} M, λ_{exc} = 336 nm) with the addition of 2-nitrotoluene in DMSO. The arrows indicate the changes in the fluorescence intensity by addition of an appropriate aliquot of 2-nitrotoluene.

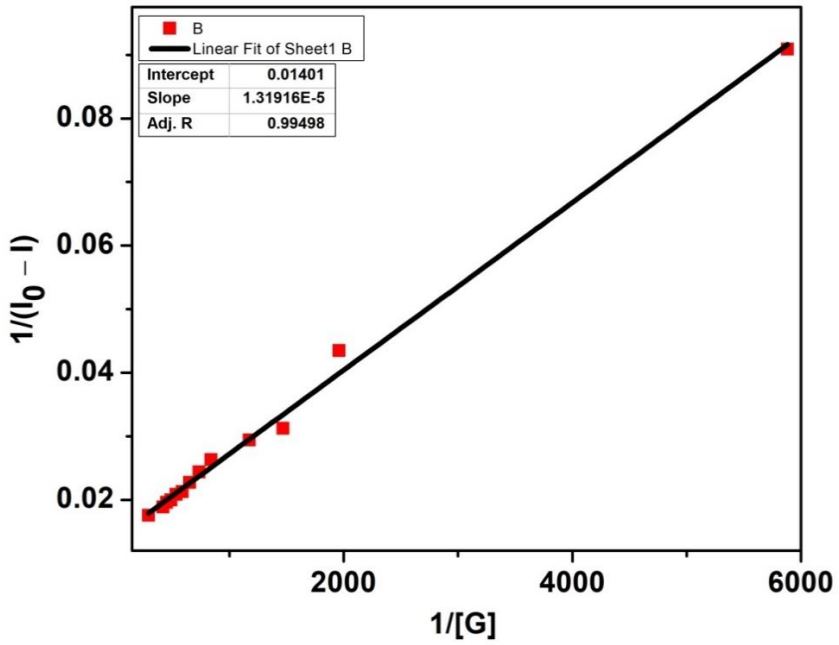

Figure 2.25. Benesi-Hildebrand plot for the emission quenching of host **1** (at 371 nm) with an increase in the concentration of 2-nitrotoluene in DMSO.

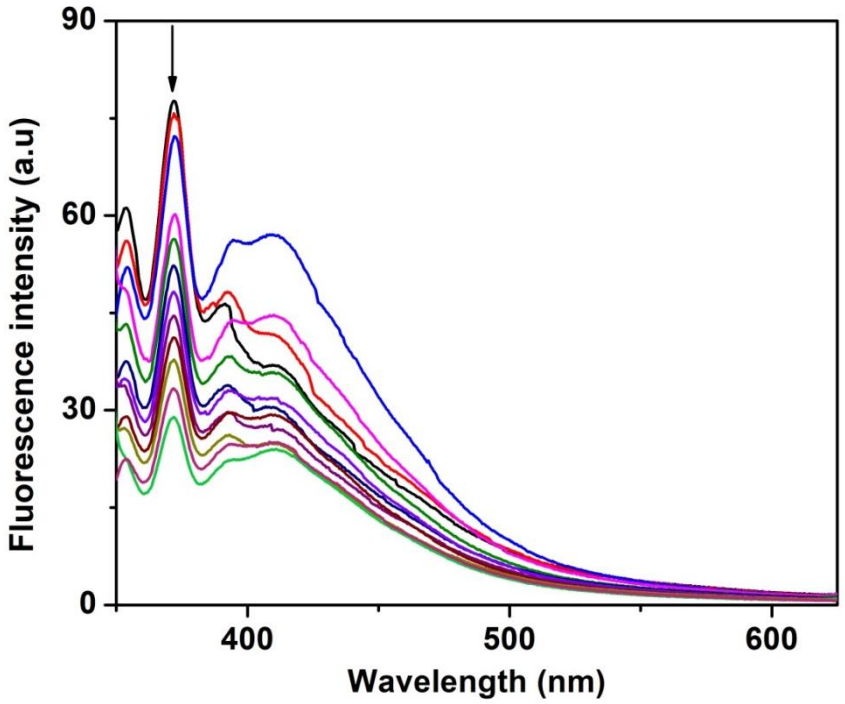

Figure 2.26. Changes in the emission spectra of **1** (3.84×10^{-5} M, λ_{exc} = 336 nm) with the addition of 4-nitrotoluene in DMSO. The arrows indicate the changes in the fluorescence intensity by addition of an appropriate aliquot of 4-nitrotoluene.

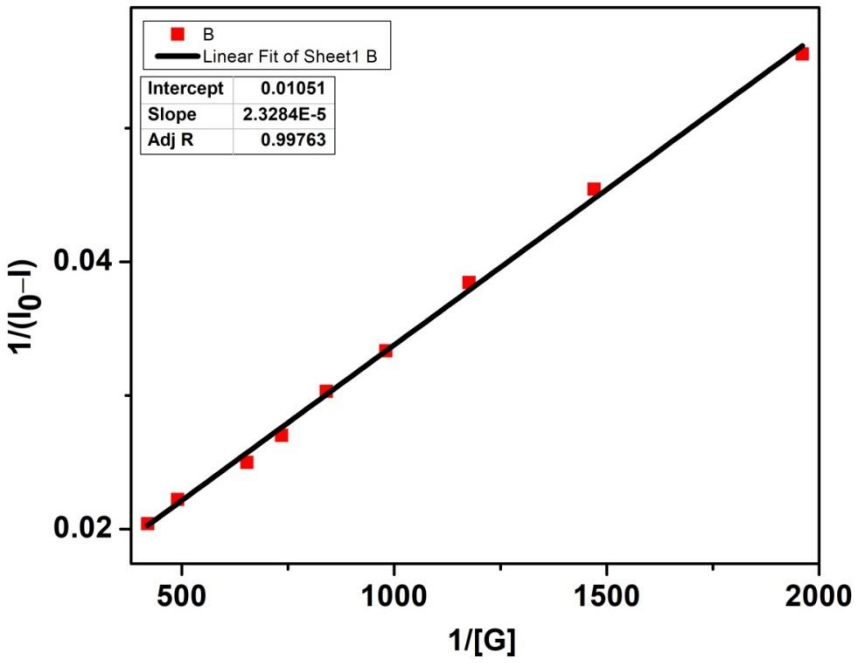

Figure 2.27. Benesi-Hildebrand plot for the emission quenching of host **1** (at 372 nm) with an increase in the concentration of 4-nitrotoluene in DMSO.

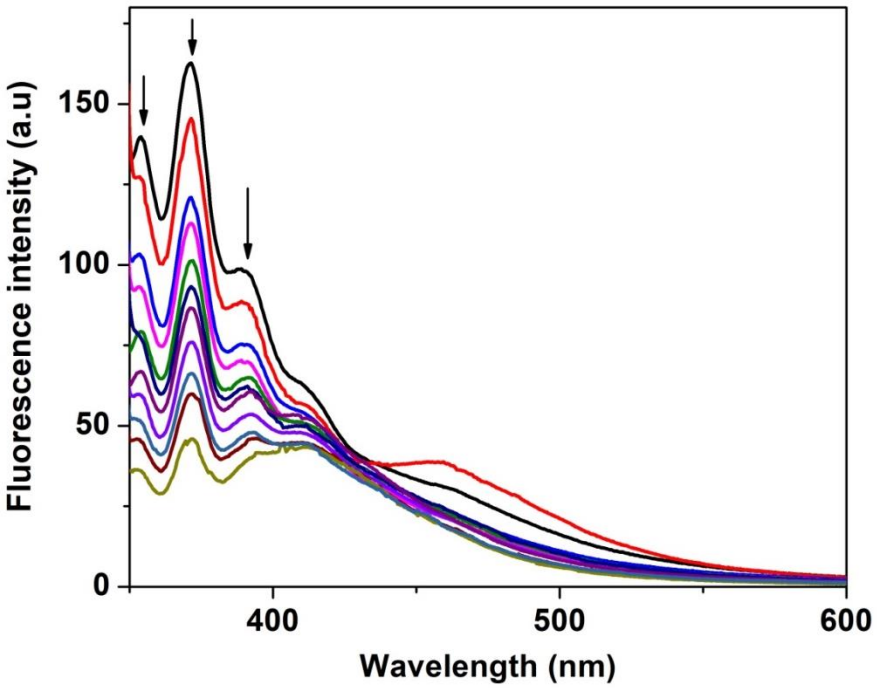

Figure 2.28. Changes in the emission spectra of **1** (3.84×10^{-5} M, λ_{exc} = 336 nm) with the addition of 2,4-dinitrotoluene in DMSO. The arrows indicate the changes in the fluorescence intensity by addition of an appropriate aliquot of 2,4-dinitrotoluene.

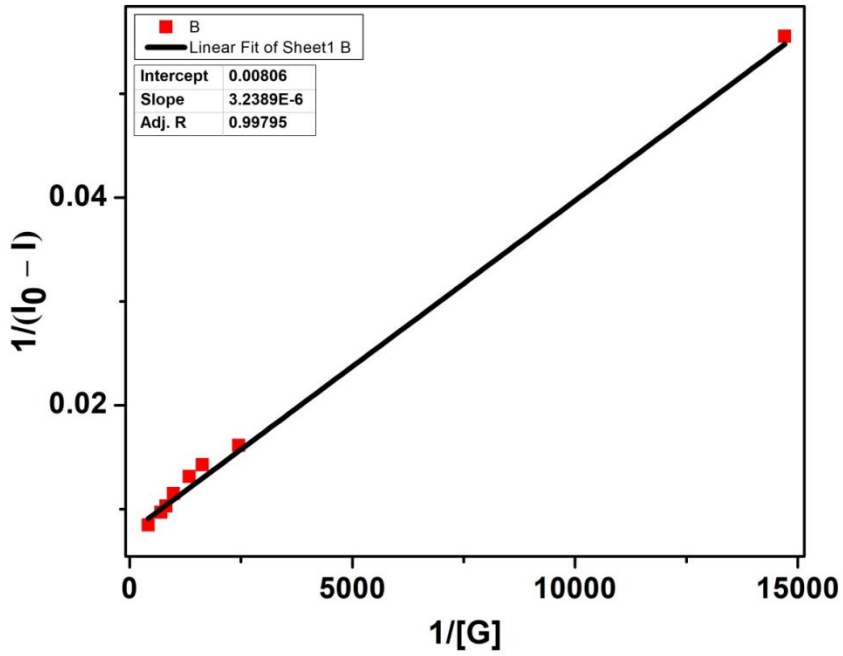

Figure 2.29. Benesi-Hildebrand plot for the emission quenching of host **1** (at 371 nm) with an increase in the concentration of 2,4-dinitrotoluene in DMSO.

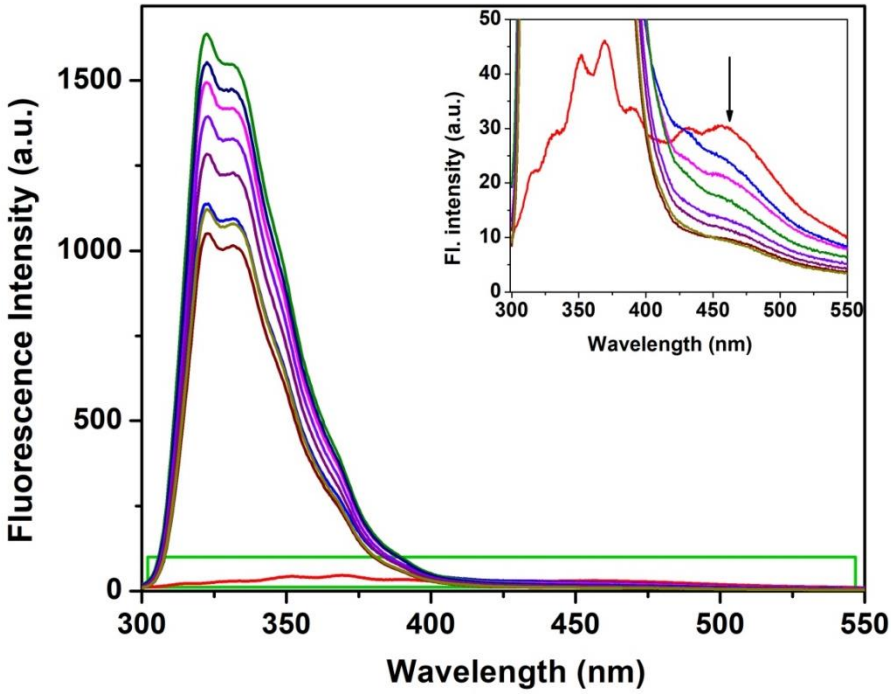

Figure 2.30. Changes in the emission spectra of **1** (4.26×10^{-5} M, λ_{exc} = 290 nm) with the addition of naphthalene in DMSO. The arrow indicates the changes in the fluorescence intensity by addition of an appropriate aliquot of naphthalene.

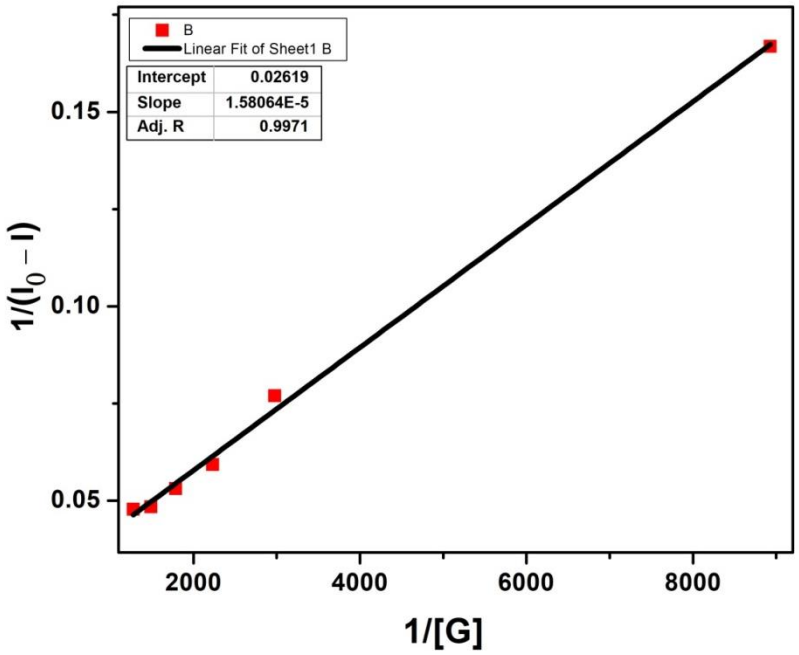

Figure 2.31. Benesi-Hildebrand plot for the emission quenching of host **1** (at 457 nm) with an increase in the concentration of naphthalene in DMSO.

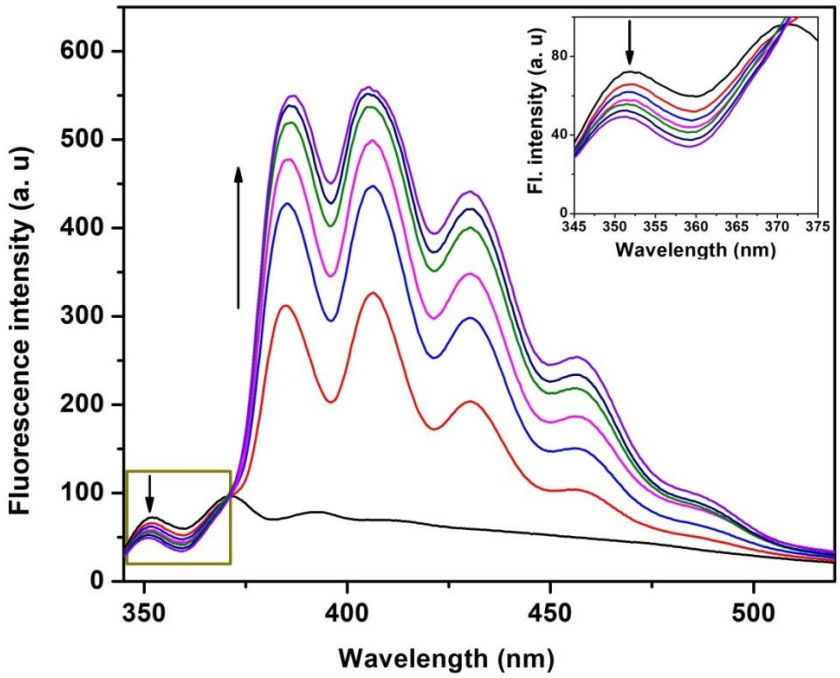

Figure 2.32. Changes in the emission spectra of **1** (3.84×10^{-5} M, λ_{exc} = 336 nm) with the addition of anthracene in DMSO. The arrows indicate the changes in the fluorescence intensity by addition of an appropriate aliquot of anthracene.

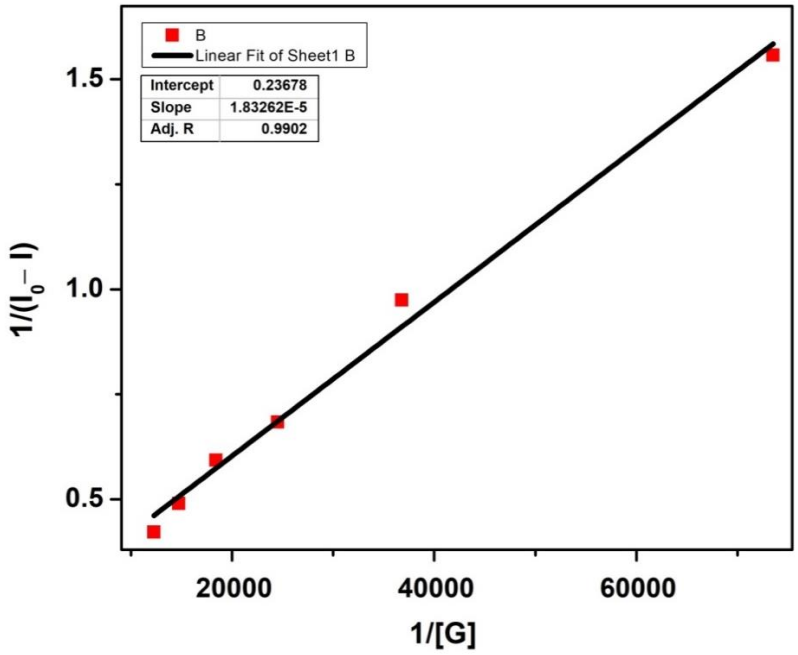

Figure 2.33. Benesi-Hildebrand plot for the emission quenching of host **1** (at 352 nm) with an increase in the concentration of anthracene in DMSO.

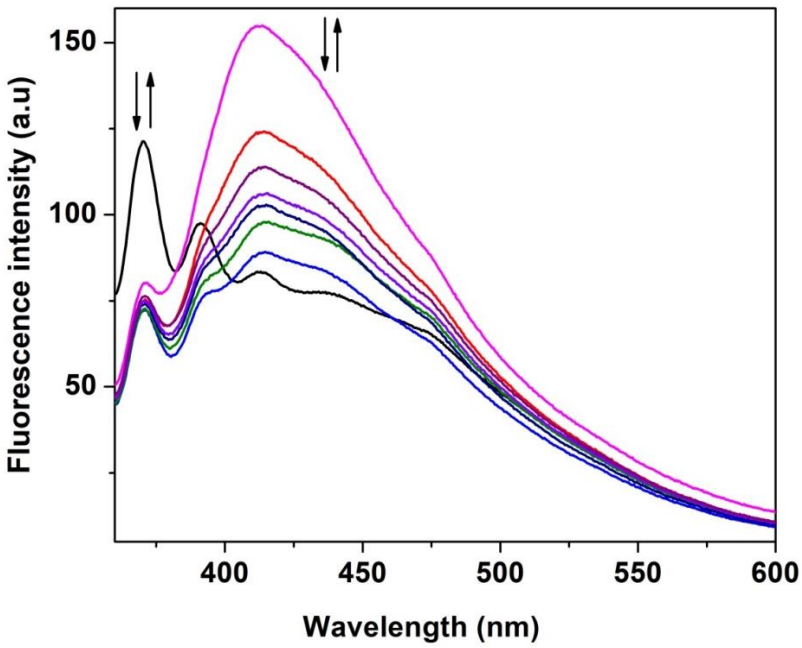

Figure 2.34. Changes in the emission spectra of **1** (3.84×10^{-5} M, λ_{exc} = 350 nm).with the addition of benzene in DMSO. The arrows indicate the arbitrary changes in the fluorescence intensity (not detectable) by addition of an appropriate aliquot of benzene.

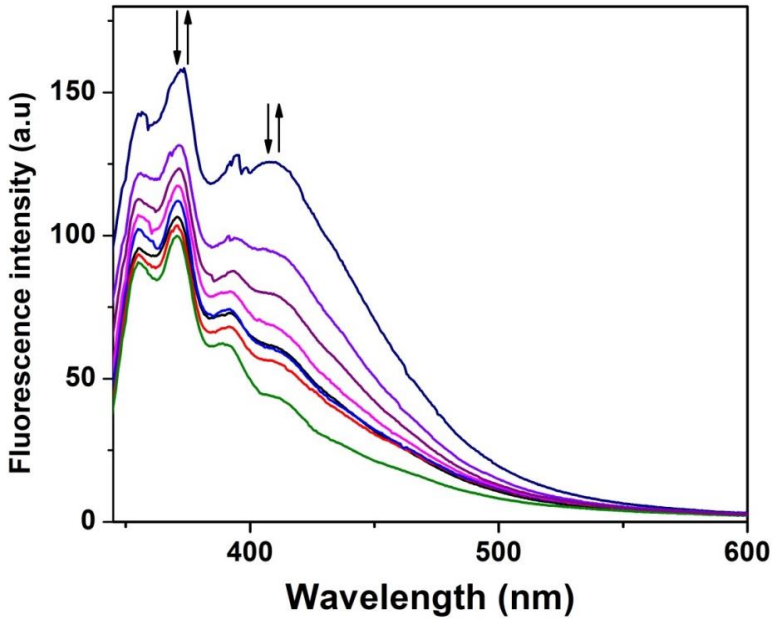

Figure 2.35. Changes in the emission spectra of **1** (3.84×10^{-5} M, λ_{exc} = 325 nm) with the addition of mesitylene in DMSO. The arrows indicate the arbitrary changes in the fluorescence intensity (not detectable) by addition of an appropriate aliquot of mesitylene.

2.5 Conclusion

A new synthetic principle, i.e. treatment of $Re_2(CO)_{10}$, rigid bis-chelating donor, and flexible ditopic nitrogen donor possessing four arene/heteroarene units connected by three methylene bridge via one-pot approach, was developed for making distorted pentagonal shaped metallocavitand. The metallocavitands possess hydrophobic inner cavity is suitable to accommodate molecule like toluene. Molecular recognition studies of **1** indicate that these metallocavitands can act as molecular host for small aromatic guest. The study provides a way to prepare metallocavitands with a tunable cavity and functional group via simple one-pot method.

2.6 References

1. (a) Frischmann, P. D.; MacLachlan, M. J. Metallocavitands: an emerging class of functional multimetallic host molecules. *Chem. Soc. Rev.* **2013**, *42*, 871-890 and references therein. (b) Lippert, B.; Sanz Miguel, P. J. Metallatriangles and metallasquares: the diversity behind structurally characterized examples and the crucial role of ligand symmetry. *Chem. Soc. Rev*. **2011,** *40*, 4475-4487 and references therein. (c) Kulesza, J.; Barros, B. S.; Junior, S. A. Organic–inorganic hybrid materials: Metallacalixarenes. Synthesis and applications. *Coord. Chem. Rev.* **2013**, *257*, 2192-2212. (d) Zhang, Y. Y.; Gao, W. X.; Lin, L.; Jin, G. X. Recent advances in the construction and applications of heterometallic macrocycles and cages. *Coord. Chem. Rev*. **2017**, *344*, 323-344. (e) Han, Y. F.; Jin, G. X. Half-Sandwich Iridium- and Rhodium-based Organometallic Architectures: Rational Design, Synthesis, Characterization, and Applications. *Acc. Chem. Res*., **2014**, *47*, 3571-3579.
2. (a) Zhang, L.; Lin, L.; Liu, D.; Lin, Y. J.; Li, Z. H.; Jin, G. X. Stacking Interactions Induced Selective Conformation of Discrete Aromatic Arrays and Borromean Rings. *J. Am. Chem. Soc.* **2017**, *139*, 1653-1660. (b) Chen, L. J.; Yang, H. B.; Shionoya, M. Chiral metallosupramolecular architectures. *Chem. Soc. Rev*. **2017**, *46*, 2555-2576. (c) Zhang, W. Y.; Lin, Y. J.; Han, Y. F.; Jin, G. X. Facile Separation of Regioisomeric Compounds by a Heteronuclear Organometallic Capsule. *J. Am. Chem. Soc.* **2016**, 1*38*, 10700-10707. (d) Amouri, H.; Desmarets, C.; Moussa, J. Confined Nanospaces in Metallocages: Guest Molecules, Weakly Encapsulated Anions, and Catalyst Sequestration. *Chem. Rev.* **2012**, *112*, 2015-2041. (e) Yoshizawa, M.; Klosterman, J. K.; Fujita, M. Functional Molecular Flasks: New Properties and Reactions within Discrete, Self-Assembled Hosts. *Angew.*

Chem. Int. Ed. **2009**, *48*, 3418-3438. (f) Yoshizawa, M.; Tamura, M.; Fujita, M. Diels-Alderin Aqueous Molecular Hosts: Unusual Regioselectivity and Efficient Catalysis. *Science* **2006**, *312*, 251-254. (g) Vriezema, D. M.; Aragonès, M. C.; Elemans, J. A. A. W.; Cornelissen, J. J. L. M.; Rowan A. E.; Nolte, R. J. M. Self-Assembled Nanoreactors. *Chem. Rev*. **2005**, *105*, 1445-1489.

3. (a) Seidel, S. R.; Stang, P. J. High-Symmetry Coordination Cages via Self-Assembly. *Acc. Chem. Res.* **2002**, *35*, 972-983; (b) Stang, P. J.; Olenyuk, B. Self-Assembly, Symmetry, and Molecular Architecture: Coordination as the Motif in the Rational Design of Supramolecular Metallacyclic Polygons and Polyhedra. *Acc. Chem. Res.* **1998**, *30*, 502-518; (c) Chakrabarty, R.; Mukherjee, P. S.; Stang, P. J. Supramolecular Coordination: Self-Assembly of Finite Two-and Three-Dimensional Ensembles. *Chem. Rev.* **2011**, *111*, 6810-6818. (d) Leininger, S.; Olenyuk. B.; Stang, P. J. Self-Assembly of Discrete Cyclic Nanostructures Mediated by Transition Metals.*Chem. Rev.* **2000**, *100*, 853-908. (e) Cook, T. R.; Vajpayee, V.; Lee, M. H.; Stang, P. S.; Chi, K. W. Biomedical and Biochemical Applications of Self-Assembled Metallacycles and Metallacages. *Acc. Chem. Res*. **2013**, 46, 2464- 2474. (f) Cook, T. R.; Stang, P. S. Recent Developments in the Preparation and Chemistry of Metallacycles and Metallacages via Coordination. *Chem. Rev*. **2015**, *115*, 7001-7045. (g) Han, Y. F.; Jia, W. G.; Yu, W. B.; Jin, G. X.; Stepwise formation of organometallic macrocycles, prisms and boxes from Ir, Rh and Ru-based half-sandwich units. *Chem. Soc. Rev*., **2009**, *38*, 3419- 3434. (h) Han, Y. F.; Li, H.; Jin, G. X. Host–guest chemistry with bi-and tetra-nuclear macrocyclic metallasupramolecules. *Chem. Commun.* **2010**, *46*, 6879-6890. (i) Huang, C. C.; Liu, J. J.; Chen, Y.; Lin, M. J. An electron-deficient metallocavitand with an unusual selectivity towards substituted benzene derivatives during co-crystallizations. *Chem. Commun.* **2013**, *49*, 11512-11514. (j) Liu, J. J.; Guan, Y. F.; Chen, Y.; Lin, M. J.; Huang, C. C.; Dai, W. X. Mixed-metal metallocavitands: a new approach to tune their electrostatic potentials for controllable selectivity towards substituted benzene derivatives. *Dalton Trans*. **2015**, *44*, 9370-9374.
4. (a) MacGillivray, L. R.; Atwood J. L. Structural Classification and General Principles for the Design of Spherical Molecular Hosts. *Angew. Chem. Int. Ed.* **1999**, *38*, 1018-1033 and references therein. (b) Therrien, B. Arene Ruthenium Cages: Boxes Full of Surprises. *Eur. J. Inorg. Chem.* **2009**, 2445-2453. (c) Therrien, B. Transporting and Shielding Photosensitisers by Using Water-Soluble Organometallic Cages: A New Strategy in Drug Delivery and Photodynamic Therapy. *Chem. – Eur. J.* **2013**, *19*, 8378 -8386. (d) Han, Y. F.; Jia, W. G.; Lin, Y. J.; Jin, G. X. Extending Rectangular Metal–Organic Frameworks to

the Third Dimension: Discrete Organometallic Boxes for Reversible Trapping of Halocarbons Occurring with Conservation of the Lattice. *Angew. Chem. Int. Ed.* **2009**, *48*, 6234-6238. (e) Huang,S. L.; Lin,Y. J.; Li, Z. H.; Jin, G. X. Self-Assembly of Molecular Borromean Rings from Bimetallic Coordination Rectangles. *Angew. Chem. Int. Ed.* **2014**, *53*, 11218-11222. (f) Huang, S. L.; Lin, Y. J.; Andy Hor T. S.; Jin, G. X. Cp*Rh-Based Heterometallic Metallarectangles: Size-Dependent Borromean Link Structures and Catalytic Acyl Transfer. *J. Am. Chem. Soc.* **2013**, *135*, 8125-8128.

5. (a) Fondo, M.; Doejo, J.; Garcia-Deibe, A. M.; Matalobos, J. S.; Vicente, R. A. Ni_8 metallacalix[4]arene and a Cu_4 molecular rhomboid: limiting the nuclearity of carboxysalen-like metal complexes. *CrystEngComm*. **2016**, *18*, 6673-6682. (b) Rufino-Felipe, E.; Muñoz-Hernández, M.–Á.; Saucedo-Azpeitiaand, H. F., Cortes-Llamas, S. A.; Calix[4]arenes of Aluminum and Gallium with Benzimidazolyl Ligands: Steric Control of the Conformation via Substitution on the Ligand. *Inorg. Chem*. **2012**, *51*, 12834-12840. (c) Yu, X. Y.; Zhang, X.; Qu, X. S.; Ma, M. S.; Liu, Z. G.; Jin, L.; Yangand, Y. Y.; Luo, Y. N.; A new 3-D Cd(II) coordination polymer with metallacalix[4]arene building blocks based on 2-(pyridin-2-yl)-1H-imidazole-4,5-dicarboxylic acid. *J. Coord. Chem*. **2015**, *68*, 3580-3588. (d) Wang, X.; Hu. H.; Liu, G.; Linand, H.; Tian, A. Self-assembly of nanometre-scale metallacalix[4]arene building blocks and Keggin units to a novel (3,4)-connected 3D self-penetrating framework. *Chem. Commun*. **2010**, *46*, 6485-6487. (e) Li, X.; Wu, B.; Wang, R.; Zhang, H.; Niu, C.; Niu, Y.; Hou, H. Hierarchical Assembly of Extended Coordination Networks Constructed by Novel Metallacalix[4]arenes Building Blocks. *Inorg. Chem*. **2010**, *49*, 2600-2613. (f) Maekawa, M.; Konaka, H.; Minematsu, T.; Kuroda-Sowa, T.; Munakata, M.; Kitagawa, S. Bowl–shaped Cu(I) metallamacrocyclic ethylene and carbonyl adducts as structural analogues of organic calixarenes. *Chem. Commun*. **2007**, 5179-5181. (g) Navarro, J. A. R.; Barea, E.; Salas, J. M.; Masciocchi, N.; Galli, S.; Sironi, A. Structural and Magnetic Properties of Layered Copper(II) Coordination Polymers Intercalating s and f Metal Ions *Inorg. Chem.* **2007**, *46*, 2988-2997. (h) (i) Ene, C. D.; Madalan, A. M.; Maxim, C.; Jurca, B.; Avarvari, N.; Andruh, M. Constructing Robust Channel Structures by Packing Metallacalixarenes: Reversible Single-Crystal-to-Single-Crystal Dehydration. *J. Am. Chem. Soc.* **2009**, *131*, 4586-4587.
6. (a) Sakate, M.; Kashima, A.; Hosoda, H.; Sunatsuki, Y.; Ota, H.; Fuyuhiro, A; Suzuki, T.; Thyminato-bridged cyclic tetranuclear rhodium(III) complexes containing a sodium, calcium or lanthanoid ion as a template metal core. *Inorg. Chim. Acta*. **2016**, *452*, 205-213. (b) Kashima, A.; Sakate, M.; Ota, H.; Fuyuhiro, A.; Sunatsuki, Y.; Suzuki, T.

Thyminate(2−)-bridged cyclic tetranuclear rhodium(iii) complexes formed by a template of a sodium, calcium or lanthanoid ion. *Chem. Commun*. **2015**, *51*, 1889-1892. (c) Galindo, M. A.; Houlton, A.; Clegg, W.; Harrington, R. W.; Dodado, J.; Santoyo-Gonzalez, F.; Linares, F.; Romero, M. A.; Navarro, J. A. R. Electrochemically and photochemically active Palladium(ii) heterotopic metallacalix[3]arenes. *Chem. Commun*. **2008**, *13*, 3735-3737.

7. (a) Velle, A.; Cebollada, A.; Lippert, B.; Sanz Miguel, P. J. Topology of metallacalix[4]arenes with uracil and cytosine ligands: favorable and unfavorable assemblies. *New J. Chem.* **2016**, *40*, 5914 -1519. (b) Khutia, A.; Sanz Miguel, P. J.; Lippert, B."Directed" Assembly of Metallacalix[n]arenes with Pyrimidine Nucleobase Ligands of Low Symmetry: Metallacalix[n]arene Derivatives of cis-$[a_2M(\text{cytosine-}N_3)_2]^{2+}$ ($M=Pt^{II}$, Pd^{II}; n=4 and 6). *Chem. – Eur. J.* **2011**, *17*, 4195-4204. (c) Khutia, A.; Sanz Miguel, P. J.; Lippert, B. Isomerism with Metallacalix[4]arenes of the Nonsymmetrical Pyrimidine Nucleobase Cytosine: How Connectivity and Rotamer State Determine the Topology of Multinuclear Derivatives. *Inorg. Chem.* **2010**, *49*, 7635-7637. (d) Das, N.; Sanz Miguel, P. J.; Khutia, A.; Lazar, M.; Lippert, B. Hybrids between classical and metallacalix[4]arenes based on uracil and cis-$Pt^{II}L_2$ entities (L = $P(Ph)_3$ or L_2 = 2,2′-bipyridine). *Dalton Trans*. **2009**, 9120-9122. (e) Galindo, M. A.; Houlton, A.; Clegg, W.; Harrington, R. W.; Dobado, J.; Santoyo-Gonzalez, F.; Linares, F.; Romero, M. A.; Navarro, J. A. R. Electrochemically and photochemically active Palladium(ii) heterotopic metallacalix[3]arenes. *Chem. Commun*. **2008**, 3735-3737. (f) Galindo, M. A.; Olea, D.; Romero, M. A.; Gomez, J.; del Castillo, P.; Hannon, M. J.; Rodger, A.; Zamora, F.; Navarro, J. A. R. Design and Non-Covalent DNA Binding of Platinum(II) Metallacalix[4]arenes. *Chem. – Eur. J*. **2007**, *13*, 5075-5081. (g) Bardají, E. G.; Freisinger, E.; Costisella, B.; Schalley, C. A.; Bruning, W.; Sabat, M.; Lippert, B. Mixed-Metal (Platinum, Palladium), Mixed-Pyrimidine (Uracil, Cytosine) Self-Assembling Metallacalix[n]arenes: Dynamic Combinatorial Chemistry with Nucleobases and Metal Species. *Chem. – Eur. J*. **2007**, *13*, 6019-6039. (h) Galindo, M. A.; Galli, S., Navarro, J. A. R.; Angustias Romero, M.; Formation of heterotopic metallacalix[n]arenes (n = 3, 4, 6) containing ethylenediaminepalladium(ii) metal fragments and 4,7-phenanthroline and 2-pyrimidinolate bridges. Synthesis, structure and host–guest chemistry. *Dalton Trans*. **2004**, 2780-2785. (i) Barea, E.; Navarro J. A. R.; Salas J. M.; Quiros, M.; Willermann, M.; Lippert, B. Chiral Pyrimidine Metallacalixarenes: Synthesis, Structure and Host–Guest Chemistry. *Chem. – Eur. J*. **2003**, *9*, 4414-4421. (j) Navarro, J. A. R.; Freisinger, E.;

Lippert, B. Self-Assembly of Palladium(II) and Platinum(II) Complexes of 2-Hydroxypyrimidine to Novel Metallacalix[4]arenes. Receptor Properties through Multiple H-Bonding Interactions. *Inorg. Chem*. **2000**, *39*, 2301-2305. (k) Navarro, J. A. R.; Salas, J. M.; A palladium metallacalix[4]arene capped with a gadolinium atom. *Chem. Commun.* **2000**, 235-236. (l) Das, N.; Sanz Miguel, P. J.; Khutia, A.; Lazar, M.; Lippert. B.; Hybrids between classical and metallacalix[4]arenes based on uracil and cis-$Pt^{II}L_2$ entities (L = $P(Ph)_3$ or L_2 = 2,2′-bipyridine). *Dalton Trans*. **2009**, 9120-9122. (m) Bardají, E. G.; Freisinger, E.; Costisella, B.; Schalley, C. A.; Bruning, W.; Sabat, M.; Lippert, B. Mixed-Metal (Platinum, Palladium), Mixed-Pyrimidine (Uracil, Cytosine) Self-Assembling Metallacalix[n]arenes: Dynamic Combinatorial Chemistry with Nucleobases and Metal Species. *Chem. – Eur. J*. **2007**, *13*, 6019-6039. (n) Galindo, M. A.; Navarro, J. A. R.; Romero, M. A.; Quiros, M. Mononucleotide recognition by cyclic trinuclear palladium(ii) complexes containing 4,7-phenanthroline N,N bridges. *Dalton Trans.* **2004**, 1563-1566.

8. (a) Terrett, R.; Cavigliasso, G.; Stranger, R.; Yates, B. F. On the unprecedented level of dinitrogen activation in the calix[4]arene complex of Nb(iii). *Dalton Trans*. **2011**, *40*, 11267-11275. (b) Xu, G. F.; Gamez, P.; Teat, S. J.; Tang, J. Praseodymium(iii)-based bis-metallacalix[4]arene with host–guest behavior. *Dalton Trans*. **2010**, *39*, 4353-4357.
9. (a) Atwood, J. L.; Barbour, L. J.; Heaven, M. W.; Raston, C. L. Controlling van der Waals Contacts in Complexes of Fullerene C60. *Angew. Chem., Int. Ed*., **2003**, *42*, 3254-3257 and reference therein.(b) Atwood, J. L.; Barbour, L. J.; Heaven, M. W.; Raston, C. L. Association and orientation of C70 on complexation with calix[5]arene. *Chem. Commun*., **2003**, 2270-2271.
10. (a) Yasunori, K.; Ryo, S.; Yutaro, Y.; Yuichiro, U.; Takeharu, H.; Induced-Fit Molecular Recognition of Alkyl Chains in p-tert-Butylcalix[5]arene in the Solid State. *Bull. Chem. Soc. Jpn.* **2016**, *89*, 220-225. (b) Brancatelli, G.; Gattuso, G.; Geremia, S.; Notti, A.; Pappalardo, S.; Parisi, M. F.; Pisagatti, I. Probing the Inner Space of Salt-Bridged Calix[5]arene Capsules. *Org. Lett*., **2014**, *16*, 2354-2357.(c) Gargiulli, C.; Gattuso, G.; Liotta, C.; Notti, A.; Parisi, M. F.; Pisagatti, I.; Pappalardo, S. Calix[5]arene-Based Heteroditopic Receptor for 2-Phenylethylamine Hydrochloride. *J. Org. Chem*., **2009**, *74*, 4350-4353.(d) Gattuso, G. Notti, A. Pappalardo, S.; Parisi, M. F.; Pisagatti, I.; Pappalardo, S.; Garozzo, D.; Messina, A.; Cohen, Y.; Slovak, S. Self-Assembly Dynamics of Modular Homoditopic Bis-calix[5]arenes and Long-Chain r,ω Alkanediyldiammonium Components. *J. Org. Chem*., **2008**, *73*, 7280-7289.(e) Garozzo, D.; Gattuso, G.; Kohnke, F. H.; Notti, A.; Pappalardo, S.; Parisi, M. F.; Pisagatti, I.;

White, A. J. P.; Williams, D. J. Inclusion Networks of a Calix[5]arene-Based Exoditopic Receptor and Long-Chain Alkyldiammonium Ions. *Org. Lett*. **2003**, *5*, 4025-4028.

11. (a) Rajakannu, P.; Shankar, B.; Yadav, A.; Shanmugam, R.; Gupta, D.; Hussain, F.; Chang, C. H.; Sathiyendiran, M.; Lu, K. L. Adaptation Toward Restricted Conformational Dynamics: From the Series of Neutral Molecular Rotors. *Organometallics* **2011**, *30*, 3168– 3176. (b) Rajakannu, P.; Mobin, S. M.; Sathiyendiran, M. Thiophene/furan units decorated unsymmetrical dinuclear metallocalix[4]arenes. *J. Organomet. Chem*. **2014**, *771*, 68-77.
12. (a) Elumalai, P.; Kanagaraj, R.; Marimuthu, R.; Shankar, B.; Kalita, A. C.; Sathiyendiran, M. Rhenium(I)-based bridgeless double metallocalix[4]arenes. *Dalton Trans.* **2015**, *44*, 11274–11277. (b) Rajakannu, P.; Elumalai, P.; Shankar, B.; Hussain, F.; Sathiyendiran, M. Rhenium(I) based metallocalix[4]arenes decorated with free functionalized benzimidazolyl units. *Dalton Trans.* **2013**, *42*, 11359-11362. (c) Rajakannu, P.; Elumalai, P.; Mobin, S. M.; Lu, K. L.; Sathiyendiran, M. Hard and soft-donors decorated rhenium based metallocavitands. *J. Organomet. Chem*. **2013**, *743*, 17-23. (d) Rajakannu, P.; Elumalai, P.; Hussain, F.; Sathiyendiran, M. Rhenium-based bicyclic supramolecule with calixarene-shaped bowls. *J. Organomet. Chem*. **2013**, *725*, 1-4.
13. (a) Grober, I.; Smith, V. J.; Bhatt, P. M.; Herbert, S. A.; Barbour, L. J. Tunable Anisotropic Thermal Expansion of a Porous Zinc(II) Metal−Organic Framework. *J. Am. Chem. Soc*. **2013**, *135*, 6411-6441; (b) Halterman, R. L., Pan, X. G., Martyn, D. E., Moore, J. L., Long, A. T. Conformational Interconversions in [2]Catenanes Containing a Wide Rigid Bis(p-benzyl)methyl Spacer. *J. Org. Chem.* **2007**, *72*, 6454– 6458.
14. Bhattacharya, D.; Sathiyendiran, M.; Luo, T. -T.; Chang, C. -H.; Cheng, Y. -H.; Lin, C. -Y.; Lee, G. -H.; Peng, S. -M.; Lu, K. -L. Ground and Excited Electronic States of Quininone-Containing Re(I)-Based Rectangles: a Comprehensive Study of Their Preparation, Electrochemistry, and Photophysics. *Inorg. Chem*. **2009**, *48*, 3731– 3742.
15. Yu, G.; Han, C.; Zhang, Z.; Chen, J.; Yan, X.; Zheng, B.; Lu, S.; Huang, F. Pillar[6]arene-Based Photoresponsive Host−Guest Complexation. *J. Am. Chem. Soc*., **2012**, *134*, 8711-8717.
16. *(a)* Tseng, Y. -H.; Bhattacharya, D.; Lin, S. -M.; Thanasekaran, P.; Wu, J. -Y.; Lee, L. -W.; Sathiyendiran, M.; Ho, M. -L.; Chung, M. -W.; Hsu, K. -C.; Chou, P. -T.; Lu, K. -L. Highly Emissive Cyclometalated Rhenium Metallacycles: Structure−Luminescence Relationship. *Inorg. Chem*. **2010**, *49*, 6805-6807 *(b)* Bhattacharya, D.; Sathiyendiran, M.; Wu, J. -Y.; Chang, C. -H.; Huang, S. -C.; Zeng, Y.- L.; Lin, C. -Y.; Thanasekaran, P.; Lin,

B. -C.; Hsu, C. -P.; Lee, G. -H.; Peng, S. -M.; Lu, K.- L. Quinonoid-Bridged Chair-Shaped Dirhenium(I) Metallacycles: Synthesis, Characterization, and Spectroelectrochemical Studies. *Inorg. Chem.* **2010**, *49*, 10264-10272.

17. (a) Shanmugaraju, S.; Mukherjee, P. S. π-Electron rich small molecule sensors for the recognition of nitroaromatics *Chem. Commun*. **2015**, *51*, 16014 -16032. (b) Salinas, Y.; Manez, R. M.; Marcos, M. D.; Sancenon, F.; Costero, A. M.; Parra, M.; Gil, S. Optical chemosensors and reagents to detect explosives. *Chem. Soc. Rev.* **2012**, *41*, 1261-1296.
18. (a). S. S. Sun and A. J. Lees, Transition metal based supramolecular systems: synthesis, photophysics, photochemistry and their potential applications as luminescent anion chemosensors. *Chem. Soc. Rev*. **2002**, *230*, 171-192.(b) Sathish, V.; Ramdass, A.; Lu, Z. Z.; Velayudham, M.; Thanasekaran, P.; Lu, K. L.; Rajagopal, S. Aggregation-Induced Emission Enhancement in Alkoxy-Bridged Binuclear Rhenium(I) Complexes: Application as Sensor for Explosives and Interaction with Microheterogeneous Media. *J. Phys. Chem. B*. **2013**, *117*, 14358-14366.
19. (a) Zwijnenburg, M. A.; Berardo, E.; Peveler, W. J.; Jelfs, K. M. Amine Molecular Cages as Supramolecular Fluorescent Explosive Sensors: A Computational Perspective. *J. Phys. Chem. B,* **2016**, *120*, 5063-5072. (b) Ghosh, S.; Gole, B.; Bar, A. K.; Mukherjee, P. S. Self-Assembly of Molecular Prisms via Pt_3 Organometallic Acceptors and a Pt_2 Organometallic Clip. *Organometallics.* **2009**, *28*, 4288-4296. (c) Bar, A. K.; Gole, B.; Ghosh, S.; Mukherjee, P. S.; Self-assembly of a Pd^{II} neutral molecular rectangle via a new organometallic Pd^{II}_2 molecular clip and oxygen donor linker *Dalton Trans*. **2009**, 6701-6704.(d) Ghosh, S.; Mukherjee, P. S. Self-Assembly of a Nanoscopic Prism via a New Organometallic Pt_3 Acceptor and Its Fluorescent Detection of Nitroaromatics. *Organometallics* **2008,** *27*, 316-319. (e) Naddo, T.; Che, Y.; Zhang, W.; Balakishnan, K.; Yang, X.; Yen, M.; Zhao, J.; Moore, J. S.; Zang, L. Detection of Explosives with a Fluorescent Nanofibril Film. *J. Am. Chem. Soc*., **2007**, *129*, 6978-6979.
20. (a) Benesi, H. A.; Hildebrand, J. H. A Spectrophotometric Investigation of the Interaction of Iodine with Aromatic Hydrocarbons. *J. Am. Chem. Soc.* **1949**, *71*, 2703 -2707. (b) Murakami, Y.; Kikuchi, J. I.; Suzuki, M.; Matsuura, T. Syntheses of macrocyclic enzyme models. Part 6. Preparation and guest-binding behaviour of octopus cyclophanes. *J. Chem. Soc. Perkin Trans.1* **11988**, 1289 -1299.

Chapter 3

Rhenium(I) Based Heteroleptic Pentagonal Toroid Shaped Metallocavitands: Self-Assembly and Molecular Recognition Studies

Abstract

A family of neutral, heteroleptic, dinuclear M_2LL'-type pentagonal toroid-shaped metallomacrocycles (**1–8**) were synthesized using flexible ditopic N donors (L^n = L^1–L^2), rigid bis-chelating ligands (H_2–L' = H_2–E) and $Re_2(CO)_{10}$ in a one-pot solvothermal self-assembly approach. The ligands and the metallomacrocycles were characterized using ATR-IR, ESI-MS, NMR, UV-Vis, and emission spectroscopic methods. The molecular structures of **1**, **2**, **4**, **6**, and **7** were confirmed by X–ray diffraction study and are similar to those of calix[5]arene. The cyclic inner cavities of the metallomacrocycles accommodate toluene/mesitylene/acetone/chlorobenzene as guest molecules that are stabilized by cumulative C–H···π and π···π interactions with the cyclic framework of metallomacrocycle. The photophysical properties of the ligands and the metallomacrocycles were studied. The host-guest recognition properties of metallocavitands **1**, **2**, **7**, and **8** as a model host with phenol- and nitrobenzene-derivatives as guest molecules were studied by emission spectroscopic methods.

This work has been published in *Inorg. Chem*. **2022**, DOI: 10.1021/acs.inorgchem.2c02061.

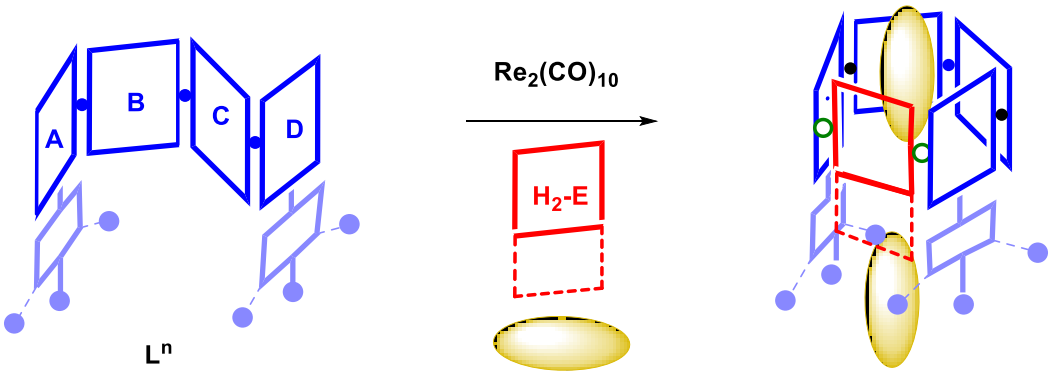

3.1. Introduction

The design and synthesis of metallomacrocycles similar to calixarene-shaped geometry have been attracting significant research interest because of their potential applications in host-guest encapsulation, catalysis, selective reactivity, sensing, and biomimetic structures.[1-5] Naked metal ions and complexes containing partially protected metal ions are employed along with pre-designed organic ligands to self-assemble calixarene-shaped complexes.[6-10] These metallamacrocycles are commonly called as metallocavitands, more specifically metallacalix[n]arenes.[1] Among various metal ions and metal complexes, $Re_2(CO)_{10}$/$[Re(CO)_5X]$, where X = Cl or Br, provide a way to make neutral, heteroleptic metallacalix[n]arenes.[11-15] Up to now, neutral ditopic donors including 4,7-phenanthroline, imidazole, and semi-rigid ditopic N-donor ligands containing phenyl (*–C_6H_4–*) spacer, and rigid bis-chelating ligands are utilized for assembling tunable rhenium tricarbonyl-based metallacalix[3]arenes, and metallacalix[4]arenes.[11,13-14] Recently, the focus in the area has shifted to make functional and cavity tunable metallacalixarenes. To the best of our knowledge, the design approach for making rhenium-core based metallocavitands similar to calix[5]arene are limited.[16] We have recently designed and employed diphenylmethane (*–C_6H_4–CH_2–C_6H_4–*) spacer-based semi-rigid ditopic N-donor ligands along with rigid bis-chelating ligand and $Re_2(CO)_{10}$ to assemble irregular pentagonal-shaped metallocavitands.[16] These metallocavitands adopt tubular structure, accommodate toluene molecule in the solid state and are able to recognize the guest molecules including nitroaromatic compounds and polyaromatic hydrocarbons in the solution. The central cyclic framework i.e., annulus of the metallocavitand, consists of two phenyl motifs, two imidazolyl motifs, and bis-chelating ligand. The size of the cavity thereby the chemistry associated with molecular cavity can be tuned by increasing the fused arenemotif(s) either by modifying the imidazolyl motif or/and by changing the bis-chelating motifs. In continuation of our research in this field, we envision introducing the 4-methoxyphenyl/3,4,5-trimethoxyphenyl motif at the 2-position of benzimidazolyl unit in the ditopic N donor would result in metallocavitands with more extended cavity suitable to accommodate various types of guest molecules. In addition, the solubility of the metallocavitands in general organic solvents would be increased due to the presence of methoxy units at the periphery of the metallocavitands.

Herein, we report two new flexible neutral ditopic nitrogen donors (L^1/L^2) consisting of two terminal 4-methoxyphenyl benzimidazolyl/3,4,5-trimethoxyphenyl benzimidazolyl nitrogen donor and diphenylmethane spacer and eight new neutral heteroleptic dinuclear metallocavitands (**1-8**) in a one-pot approach. The molecular structures of the five metallocavitands (**1**, **2**, **4**, **6** and **7**) are unambiguously determined by a single crystal X-ray diffraction analysis, which reveal that these metallocavitands adopt pentagonal toroid-shaped structure with acetone and mesitylene/toluene/chlorobenzene as guest molecules in their internal cavities. The photophysical properties of the ligands and the complexes were studied in DMSO. The host: guest recognition properties of the metallocavitands **1**, **2**, **7**, and **8** as model hosts were studied with nineteen molecules, phenol, and nitrobenzene-derivatives, as guest molecules using emission spectroscopic methods.

3.2. Experimental

Materials and Methods

3.2.1. Materials

Starting materials such as $Re_2(CO)_{10}$, H_2-dhbq, H_2-CA, H_2-dhaq, H_2-dhnq, 1,2 diaminobenzene, 4-methoxybenzaldehyde, 3,4,5-trimethoxybenzaldehyde, diphenylmethane, phosphoric acid, paraformaldehyde, 30-33% HBr in AcOH, glacial acetic acid, formic acid, and NaH were obtained from commercial sources and used as received. Commercial grade solvents, mesitylene, acetone, and chlorobenzene were used as received without further purification. Bis(4-(bromomethyl) phenyl)methane,[17] 2-(4-methoxyphenyl)-benzimidazole[18] and 2-(3,4,5-trimethoxyphenyl)-benzimidazole[18] were prepared by using the reported procedure. THF, hexane, and toluene were purified and distilled by conventional procedure.

3.2.2. Physical Measurement

ATR-IR spectra were recorded on a Nicolet iS5 ATR- spectrometer. ^{1}H NMR spectra were recorded on a Bruker Avance III 500 MHz spectrometer. HR-MS spectra were recorded on a Bruker maXis mass spectrometer. UV-Vis and emission spectra were recorded on Shimadzu UV-VIS-NIR (UV-3600), and JASCO (V-750) spectrophotometer and JASCO (FP-8500) spectrofluorometer, respectively.

3.2.3. Materials and Methods for Emission Titration Experiments

The solvent (DMSO) used in this study was of spectroscopic grade and used as received. All the guest molecules were obtained from commercial sources and used as received. Quenching experiments of host **1**, **2**, **7**, and **8** were carried out by emission spectroscopic method. Metallocavitand **1** stock solutions (2×10^{-5} M for Phenol; 1.5×10^{-5} M for BA, m-cresol, p-cresol, 3, 4- DMP, 2, 4, 6- TMP, catechol, resorcinol, 2-CP, 4-CP, 2, 4-DCP, 2- NP, 4- NP, 2, 4- DNP, 2, 4, 6-TNP, NB, 2-NT, 4-NT, 2, 4-DNT), metallocavitand **7** stock solutions (2×10^{-5} M for all the guest molecules), metallocavitand **2** and **8** stock solutions (1×10^{-5} M for all the guest molecules) were prepared using DMSO. For host **1**, aromatic guests stock solutions; 1×10^{-2} M for phenol, BA; 1×10^{-3} M for m-cresol, p-cresol, 3, 4- DMP, 2, 4, 6- TMP, catechol, resorcinol, 2-CP, 4-CP, 2, 4-DCP , 2- NP, 2, 4- DNP, 2, 4, 6-TNP, NB, 2-NT, 4-NT, 2, 4-DNT, and 1×10^{-4} M for 4-NP were prepared in DMSO. For host **2**, aromatic guests stock solutions; 1×10^{-2} and 1×10^{-1} M for BA; 1×10^{-3} and 1×10^{-2} M for phenol, 3, 4- DMP, 2, 4, 6- TMP, resorcinol, 2, 4-DCP; 1×10^{-3} M for m-cresol, p-cresol, catechol, 2-CP, 4-CP, 2-NP, 4-NP, 2, 4- DNP, 2-NT, 4-NT, 2, 4-DNT; 1×10^{-4} M and 1×10^{-3} M for 2, 4, 6-TNP and NB were prepared in DMSO. For host **7**, aromatic guests stock solutions; 1×10^{-2} M for phenol, BA; 1×10^{-3} M for m-cresol, p-cresol, 2-CP, 4-CP, 2- NP, 4-NP, 2, 4- DNP, 2, 4, 6-TNP, 2-NT, 4-NT, 2, 4-DNT; 1×10^{-3} M and 1×10^{-2} M for 3, 4- DMP, 2, 4, 6- TMP, catechol, resorcinol, 2, 4-DCP; 1×10^{-4} M and 1×10^{-3} M for NB were prepared in DMSO. For host **8**, aromatic guests stock solutions; 1×10^{-2} for BA, 3, 4- DMP, 2, 4, 6- TMP; 1×10^{-3} and 1×10^{-2} M for catechol, resorcinol, 2, 4-DCP; 1×10^{-3} M for phenol, m-cresol, p-cresol, 2-CP, 4-CP, 2-NP, 4-NP, 2, 4- DNP, 2-NT, 4-NT, 2, 4-DNT; 1×10^{-4} M and 1×10^{-3} M for 2, 4, 6-TNP and 1×10^{-4} M for NB were prepared in DMSO. Test solutions were prepared by the addition of an appropriate aliquot (0.02- 4mL) of each guest stock into 5mL standard volumetric flask followed by placing 0.5 or 1 mL of stock solution of host **1** or **2** or **7** or **8** and then diluting the solution to 5 mL with DMSO. The excitation wavelengths were 283 nm, 285 nm, 276 nm and 275 nm for host **1**, **2**, **7** and **8**, respectively. In all the cases the excitation wavelength was 260 nm for BA. The slit width was 2.5 nm for both the excitation and emission (2.5-5 nm for BA). The binding characteristics of the host molecules with guest molecules were determined by the emission spectroscopic method. The binding constants were calculated based on the Benesi-Hildebrand equation for a 1:1 stoichiometry molar ratio ($1/\Delta I = 1/\Delta I_{max} + (1/ K[G] \Delta I_{max}$). Here, $\Delta I = I–I_{min}$, $\Delta Imax = I_0–I_{min}$, I_0 is the emission intensity of free host molecule, I

is the intensity measured with guest, I_{min} is the intensity measured with an excess of guest, K is the binding constant, and [G] is the concentration of guest molecule.[19]

3.2.4. Crystallography

Single crystal X-ray diffraction data were collected on Rigaku Oxford XtaLAB Synergy or Bruker APEX-II CCD instruments with Mo-Kα radiation (λ = 0.71073 Å). Standard procedures were applied for data reduction, and absorption correction. Structure solutions and refinements were performed with the SHELX program package.[20] Non-H atoms were refined anisotropically.

3.2.5. Synthesis of Ligands

Synthesis of L^1.

A mixture of powdered NaH (0.169 g, 4.24 mmol) and 2-(4-methoxyphenyl)-benzimidazole(0.633 g, 2.82 mmol) in THF (10 mL) was stirred at room temperature for 3 h. Bis(4-(bromomethyl)phenyl)methane (0.5 g, 0.141 mmol) was added to the solution. The reaction mixture was then stirred continuously for 24 h. Half of the solvent was removed by rotavapor. Water (~200 mL) was added to this residue. The resulting pale brown precipitate was filtered, washed several times with water, and air dried. Yield: 88% (1.6 g). ^{1}H NMR (500 MHz, DMSO-d_6): δ 7.68-7.64 (m, 6H, $H^{4, 2', 6'}$), 7.38 (d, J_{HH} = 7.5 Hz, 2H, H^7), 7.23-7.16 (m, 4H, $H^{5, 6}$), 7.10 (d, J_{HH} = 8.1 Hz, 4H, $H^{10, 11}$), 7.05 (d, J_{HH} = 8.7 Hz, 4H, $H^{3',5'}$), 6.89 (d, J_{HH} = 8 Hz, 4H, $H^{9,12}$), 5.49 (s, 4H, H^8, -CH_2-), and 3.80 (s, 8H, H^{13}, -CH_2- , -OCH_3). ^{13}C NMR (500 MHz, DMSO-d_6): δ 160.4, 153.2, 142.7, 140.3, 135.9, 134.7, 130.5, 129.0, 126.2, 122.4, 122.1, 119.0, 114.2, 55.3, 47.2. HRMS- ESI. Calcd for $C_{43}H_{36}N_4O_2$ $[L^1 + H]^+$: *m/z* 641.2917. Found: *m/z* 641.2918.

Synthesis of L^2.

By following the similar approach of L^1, ligand L^2 was synthesized by using NaH (0.06 g, 1.6 mmol), 2-(3,4,5-trimethoxyphenyl)-benzimidazole (0.3 g, 1 mmol), THF (5 mL), and bis(4-(bromomethyl)phenyl)methane (0.187 g, 0.528 mmol). The crude was purified by column chromatography (ethyl acetate/hexane, 8/2, v/v).Yield: 75 % (0.6 g). ^{1}H NMR (500 MHz, DMSO-d_6): δ 7.73 (d, J_{HH} = 7.1 Hz, 2H, H^4), 7.46 (d, J_{HH} = 7.3 Hz, 2H, H^7), 7.26-7.20 (m, 4H, $H^{5, 6}$), 7.11 (d, J_{HH} = 8.1 Hz, 4H, $H^{10, 11}$), 6.96 (d, J_{HH} = 8.1 Hz, 4H, $H^{9,12}$), 6.91 (s, 4H, $H^{2',6'}$), 5.54 (s, 4H, H^8, -CH_2-), 3.82 (s, 2H, H^{13}, -CH_2-), 3.71 (s, 6H, -OCH_3), and 3.58 (s,

12H, -OCH_3). ^{13}C NMR (500 MHz, DMSO-d_6): δ 152.9, 142.5, 140.5, 138.7, 136.3, 135.1, 129.0, 126.0, 125.2, 122.7, 122.2, 119.2, 110.8, 106.3, 60.1, 55.6, 47.4. HRMS-ESI. Calcd for $C_{47}H_{44}N_4O_6$ $[L^2 + H]^+$: *m/z* 761.3339. Found: *m/z* 761.3350.

3.2.6. Synthesis of Complexes

General Synthesis of metallocavitands (1-8).

A mixture of $Re_2(CO)_{10}$, bis-chelating ligand, L^n, and toluene or mesitylene:acetone or chlorobenzene in a Teflon flask was placed in a steel bomb. The bomb was kept in a microprocessor-programmed oven at 160 °C for 48 h and cooled to 30 °C. The product (powder or crystals) obtained in the solvothermal vessel was filtered and washed with distilled hexane.

Synthesis of fac-[{(CO)$_3$Re(μ−dhbq)Re(CO)$_3$}(μ−L^1)] (1).

Brown crystals of **1** were obtained from a mixture of $Re_2(CO)_{10}$ (50 mg, 0.077 mmol), H_2-dhbq (10.7 mg, 0.0766 mmol), L^1 (49 mg, 0.077 mmol), and mesitylene:acetone (6:1 mL). Yield: 54% (55 mg). ^{1}H NMR (500 MHz, DMSO-d_6): δ 8.00 (d, J_{HH} = 7.31 Hz, 1H), 7.84 (d, J_{HH} = 7.72 Hz, 1H), 7.68-7.64 (m, 5H), 7.46 (t, J_{HH} = 7.15 Hz, 1H), 7.39-7.34 (m, 3H), 7.23-7.16 (m, 4H), 7.10 (d, J_{HH} = 8.16 Hz, 3H), 7.06 (d, J_{HH} = 8.76 Hz, 4H), 6.89 (d, J_{HH} = 8 Hz, 3H), 6.54 (s, 2H, H^a, dhbq), 5.79-5.15 (m, 4H, H^8, -CH_2-), 3.80 (s, 6H, -OCH_3), and 3.77-3.73 (m, 2H, H^{13}, -CH_2-). ATR-IR (cm^{-1}): 2012 (C≡O), and 1886 (C≡O). HRMS-ESI. Calcd for $C_{55}H_{38}N_4O_{12}Re_2$ [**1** + H]$^+$: *m/z* 1321.1681. Found: *m/z* 1321.1739.

Synthesis of fac-[{(CO)$_3$Re(μ−dhbq)Re(CO)$_3$}(μ−L^2)] (2).

The clear solution obtained from a mixture of $Re_2(CO)_{10}$ (100 mg, 0.153 mmol), H_2-dhbq (21.4 mg, 0.153 mmol), L^2 (117 mg, 0.153 mmol), and mesitylene:acetone (10:1 mL) was concentrated, washed with hexane and air-dried. Suitable single crystals of **2** for X-ray analysis were obtained from the slow evaporation of the mother liquor at room temperature after ~25 days. Yield: 37% (82 mg). ^{1}H NMR (500 MHz, DMSO-d_6): δ 7.73-7.71 (m, 2H, H^4), 7.50-7.48 (m, 2H, H^7), 7.28-7.22 (m, 4H, H^{5,6}), 7.12 (d, J_{HH} = 8.0 Hz, 4H, H^{10,11}), 6.96 (d, J_{HH} = 8.0 Hz, 4H, H^{9,12}), 6.89 (s, 4H, H$^{2',6'}$), 5.79 (s, 2H, H^a), 5.55 (s, 4H, H^8, -CH_2-), 3.83 (s, 2H, H^{13}, -CH_2-), 3.69 (s, 6H, -OCH_3), and 3.58 (s, 12H, -OCH_3). ATR-IR (cm^{-1}): 2012 (C≡O), 1916 (C≡O), 1879 (C≡O). HRMS-ESI. Calcd for $C_{59}H_{46}N_4O_{16}Re_2$ [**2** + H]$^+$: *m/z* 1441.2099. Found: *m/z* 1441.1906.

Synthesis of fac-[{(CO)$_3$Re(μ−CA)Re(CO)$_3$}(μ−L^1)] (3).

Dark powder was obtained from a mixture of $Re_2(CO)_{10}$ (50 mg, 0.077 mmol), H_2-CA (16 mg, 0.077 mmol), L^1 (49 mg, 0.077 mmol), and toluene:acetone (6:1 mL). Yield: 80% (85 mg).^{1}H NMR (500 MHz, DMSO-d_6): δ 7.80-7.75 (m, 6H, H$^{4,\ 2',\ 6'}$), 7.62 (d, J_{HH} = 7.1 Hz, 2H, H^7), 7.51-7.36 (m, 4H, H$^{5,\ 6}$), 7.17 (d, J_{HH} = 8.6 Hz, 4H, H$^{10,\ 11}$), 7.13 (d, J_{HH} = 8.05 Hz, 4H, H$^{3',5'}$), 7.07- 7.00 (m, 4H, H^{9,12}), 5.61-5.51 (m, 4H, H^8, -CH_2-), and 3.84 (s, 8H, H^{13}, -CH_2- , -OCH_3). ATR-IR (cm^{-1}): 2013 (C≡O), 1888(C≡O). HRMS-ESI. Calcd for $C_{55}H_{36}N_4O_{12}Cl_2Re_2$ [**3** + H]$^+$: *m/z* 1389.0875. Found: *m/z* 1389.0689.

Synthesis of fac-[{(CO)$_3$Re(μ−CA)Re(CO)$_3$}(μ−L^2)] (4).

Clear solution obtained from a mixture of $Re_2(CO)_{10}$ (100 mg, 0.153 mmol), H_2-CA (32 mg, 0.15 mmol), L^2 (117 mg, 0.153 mmol), and mesitylene:acetone (12:2 mL) was concentrated, washed with hexane and air-dried. Suitable single crystals of **4** for X-ray analysis were obtained from the slow evaporation of the mother liquor at room temperature after ~30 days.Yield: 35% (80 mg).^{1}H NMR (500 MHz, DMSO-d_6): δ 7.72 (d, J_{HH} = 8.16 Hz, 2H, H^4), 7.48 (d, J_{HH} = 8.67 Hz, 2H, H^7), 7.27-7.22 (m, 4H, H$^{5,\ 6}$), 7.11 (d, J_{HH} = 8.11 Hz, 4H, H$^{10,\ 11}$), 6.95 (d, J_{HH} = 7.82 Hz, 4H, H^{9,12}), 6.88 (s, 4H, H$^{2',6'}$), 5.54 (s, 4H, H^8, -CH_2-), 3.83 (s, 2H, H^{13}, -CH_2-), 3.69 (s, 6H, -OCH_3), and 3.57 (s, 12H, -OCH_3). ATR-IR (cm^{-1}): 2012 (C≡O), 1913 (C≡O), 1879 (C≡O). HRMS-ESI. Calcd for $C_{59}H_{44}N_4O_{16}Cl_2Re_2$ [**4** + H]$^+$: *m/z* 1509.1313. Found: *m/z* 1509.1170.

Synthesis of fac-[{(CO)$_3$Re(μ−dhaq)Re(CO)$_3$}(μ−L^1)] (5).

Dark colored powder was obtained from a mixture of $Re_2(CO)_{10}$ (50 mg, 0.077 mmol), H_2-dhaq (18.4 mg, 0.0766 mmol), L^1 (49 mg, 0.077 mmol), and mesitylene:acetone (6:1 mL). Yield: 62% (68 mg).^{1}H NMR (500 MHz, DMSO-d_6): δ 8.36-8.34 (m, 2H, H^a), 7.94-7.92 (m, 2H, H^b), 7.69-7.64 (m, 6H, H$^{4,\ 2',\ 6'}$), 7.38 (d, J_{HH} = 8 Hz, 2H, H^7),7.30 (d, 2H, H^c), 7.23-7.16 (m, 4H, H$^{5,\ 6}$), 7.10 (d, J_{HH} = 8.2 Hz, 4H, H$^{10,\ 11}$), 7.06 (d, J_{HH} = 8.9 Hz, 4H, H$^{3',5'}$), 6.90 (d, J_{HH} = 8 Hz, 4H, H^{9,12}), 5.49 (s, 4H, H^8, -CH_2-), and 3.80 (s, 8H, H^{13}, -CH_2- , -OCH_3). ATR-IR (cm^{-1}): 2008 (C≡O), 1902 (C≡O), 1873(C≡O). HRMS-ESI. Calcd for $C_{63}H_{42}N_4O_{12}Re_2$ [**5** + H]$^+$: *m/z* 1421.1996. Found: *m/z* 1421.1831.

Synthesis of fac-[{(CO)$_3$Re(μ−dhaq)Re(CO)$_3$}(μ−L^2)] (6).

Clear solution obtained from a mixture of $Re_2(CO)_{10}$ (50 mg, 0.077 mmol), H_2-dhaq (18.4 mg, 0.0766 mmol), L^2 (58.5 mg, 0.0766 mmol), and toluene (6 mL) was allowed to evaporate at room temperature. The crystals of **6** were obtained from the solution after 30 days at room temperature. Yield: 67% (80 mg).^{1}H NMR (500 MHz, DMSO-d_6): δ 8.31-8.29 (m, 2H, H^a), 8.01-7.99 (m, 2H, H^b), 7.73-7.71 (m, 2H, H^4), 7.48-4.44 (m, 4H, H^7, H^c), 7.27-7.21 (m, 4H, H$^{5,\ 6}$), 7.12 (d, J_{HH} = 8.08 Hz, 4H, H$^{10,\ 11}$), 6.95 (d, J_{HH} = 8.19 Hz, 4H, H^{9,12}), 6.88 (s, 4H, H$^{2',6'}$), 5.54 (s, 4H, H^8, -CH_2-), 3.83 (s, 2H, H^{13}, -CH_2-), 3.69 (s, 6H, -OCH_3), and 3.57 (s, 12H, -OCH_3). ATR-IR (cm^{-1}): 2009 (C≡O), 1899 (C≡O), 1876(C≡O). HRMS-ESI. Calcd for $C_{67}H_{50}N_4O_{16}Re_2$ [**6** + H]$^+$: *m/z* 1541.2419. Found: *m/z* 1541.2327.

Synthesis of fac-[{(CO)$_3$Re(μ−dhnq)Re(CO)$_3$}(μ−L^1)] (7).

Dark colored powder of **7** was obtained from a mixture of $Re_2(CO)_{10}$ (50 mg, 0.077 mmol), H_2-dhnq (22 mg, 0.077 mmol), L^1(49 mg, 0.077 mmol), and mesitylene:acetone (5:1 mL). Suitable single crystals for the X-ray analysis were obtained from the same reaction with chlorobenzene (12mL). Yield: 57% (65 mg).^{1}H NMR (500 MHz, DMSO-d_6): δ 8.42-8.40 (m, 4H, H^a), 7.94-7.92 (m, 4H, H^b), 7.68-7.64 (m, 6H, H$^{4,\ 2',\ 6'}$), 7.38 (d, J_{HH} = 7.4 Hz, 2H, H^7), 7.23-7.16 (m, 4H, H$^{5,\ 6}$), 7.10 (d, J_{HH} = 8 Hz, 4H, H$^{10,\ 11}$), 7.06 (d, J_{HH} = 8.8 Hz, 4H, H$^{3',5'}$), 6.90 (d, J_{HH} = 8.2 Hz, 4H, H^{9,12}), 5.50 (s, 4H, H^8, -CH_2-), and 3.80 (s, 8H, H^{13}, -CH_2- , -OCH_3). ATR-IR (cm^{-1}): 2008 (C≡O), 1874(C≡O). HRMS-ESI. Calcd for $C_{67}H_{44}N_4O_{12}Re_2$ [**7** + H]$^+$: *m/z* 1471.2153. Found: *m/z* 1471.1960.

Synthesis of fac-[{(CO)$_3$Re(μ−dhnq)Re(CO)$_3$}(μ−L^2)] (8).

Dark colored powder was obtained from a mixture of $Re_2(CO)_{10}$ (50 mg, 0.077 mmol), H_2-dhnq (22 mg, 0.077 mmol), L^2 (58.5 mg, 0.0766 mmol), and mesitylene:acetone (5:1 mL). Yield: 51% (62 mg). ^{1}H NMR (500 MHz, DMSO-d_6): δ 8.42-8.40 (m, 4H, H^a), 7.94-7.92 (m, 4H, H^b), 7.73-7.71 (m, 2H, H^4), 7.48-7.46 (m, 2H, H^7), 7.27-7.21 (m, 4H, H$^{5,\ 6}$), 7.12 (d, J_{HH} = 8.1 Hz, 4H, H$^{10,\ 11}$), 6.95 (d, J_{HH} = 8.1 Hz, 4H, H^{9,12}), 6.89 (s, 4H, H$^{2',6'}$), 5.54 (s, 4H, H^8, -CH_2-), 3.83 (s, 2H, H^{13}, -CH_2-), 3.69 (s, 6H, -OCH_3), and 3.57 (s, 12H, -OCH_3). ATR-IR (cm^{-1}): 2008 (C≡O), 1875(C≡O). HRMS- ESI. Calcd for $C_{71}H_{52}N_4O_{16}Re_2$ [8 – 3H + NH_4]$^+$: *m/z* 1605.2607. Found: *m/z* 1605.2667.

3.3. Results and discussion

3.3.1. Synthesis and characterization of ligands L^1- L^2.

Ligands L^1 and L^2 were synthesized from bis(4-bromomethylphenyl)methane, 2-(4-methoxyphenyl)-1H-benzimidazole or 2-(3,4,5-trimethoxyphenyl)-1H-benzimidazole, and NaH in THF (Scheme 3.1). The ligands are air stable and soluble in DMSO, CH_2Cl_2, and $CHCl_3$. The ^1H NMR spectrum of the ligands displayed a single set of chemical resonances, corresponding to the protons of the three methylene (*–CH₂–*) motifs and two methoxyphenylbenzimidazolyl/trimethoxyphenyl benzimidazolyl motifs. Further, the formation of the ligands was confirmed by high resolution ESI-MS analysis, which displayed molecular ion peaks at *m/z,* 641.2918 for $[L^1 + H]^+$ and 761.3350 for $[L^2 + H]^+$. Experimental mass peaks of the ligands match well with the theoretical values.

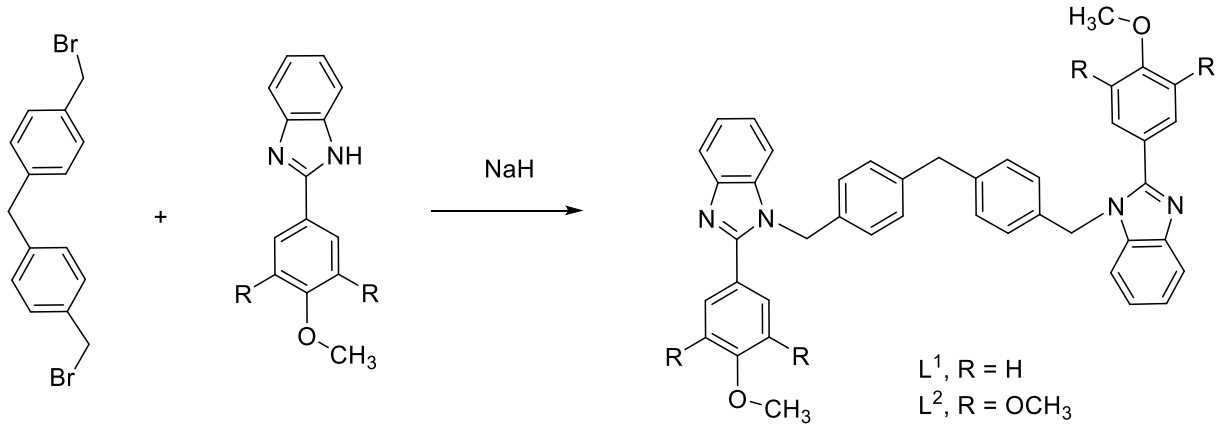

Scheme 3.1. Synthesis of ligands L^1-L^2.

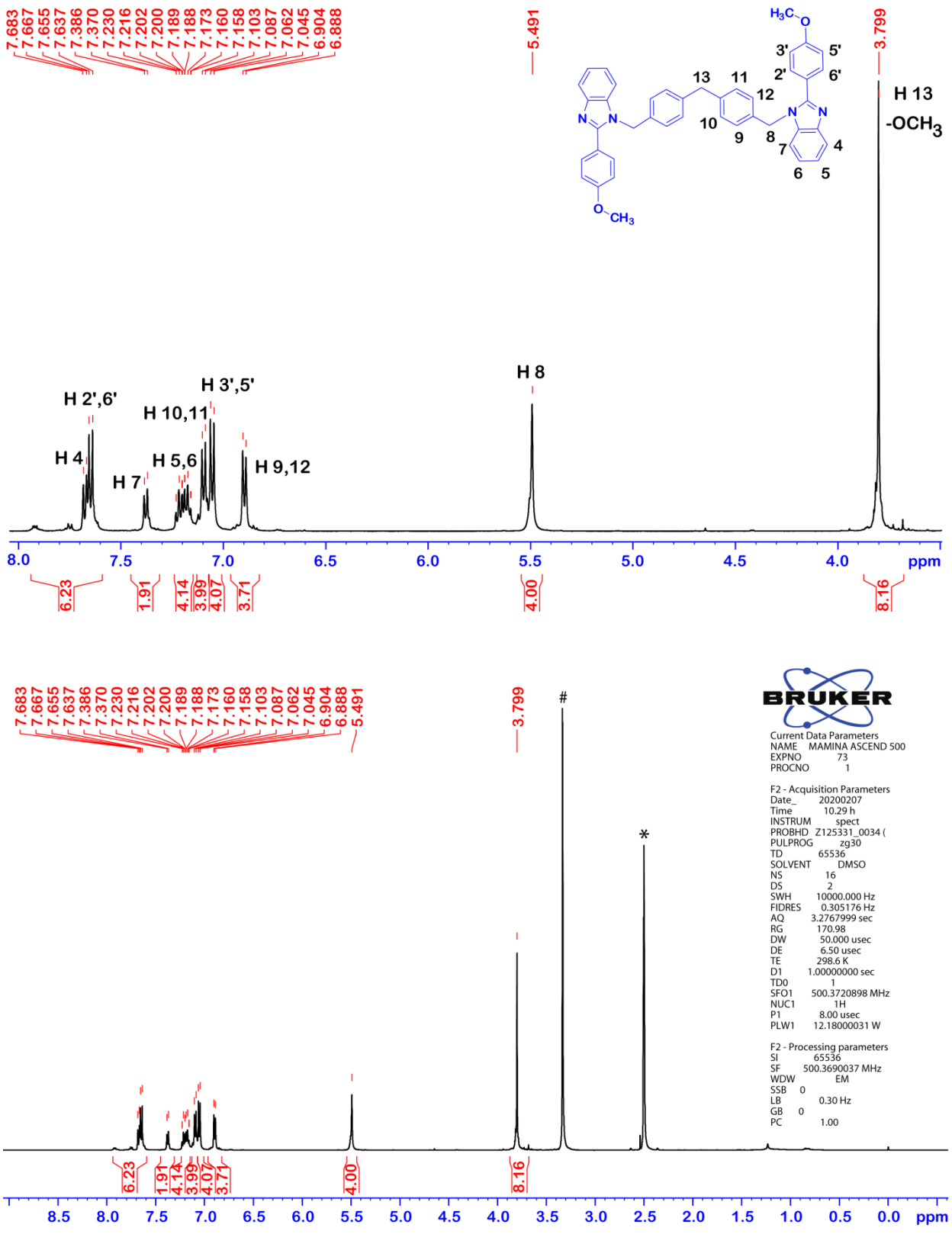

Figure 3.1. ^{1}H NMR (500 MHz) spectrum of L^{1} in d_6-DMSO.

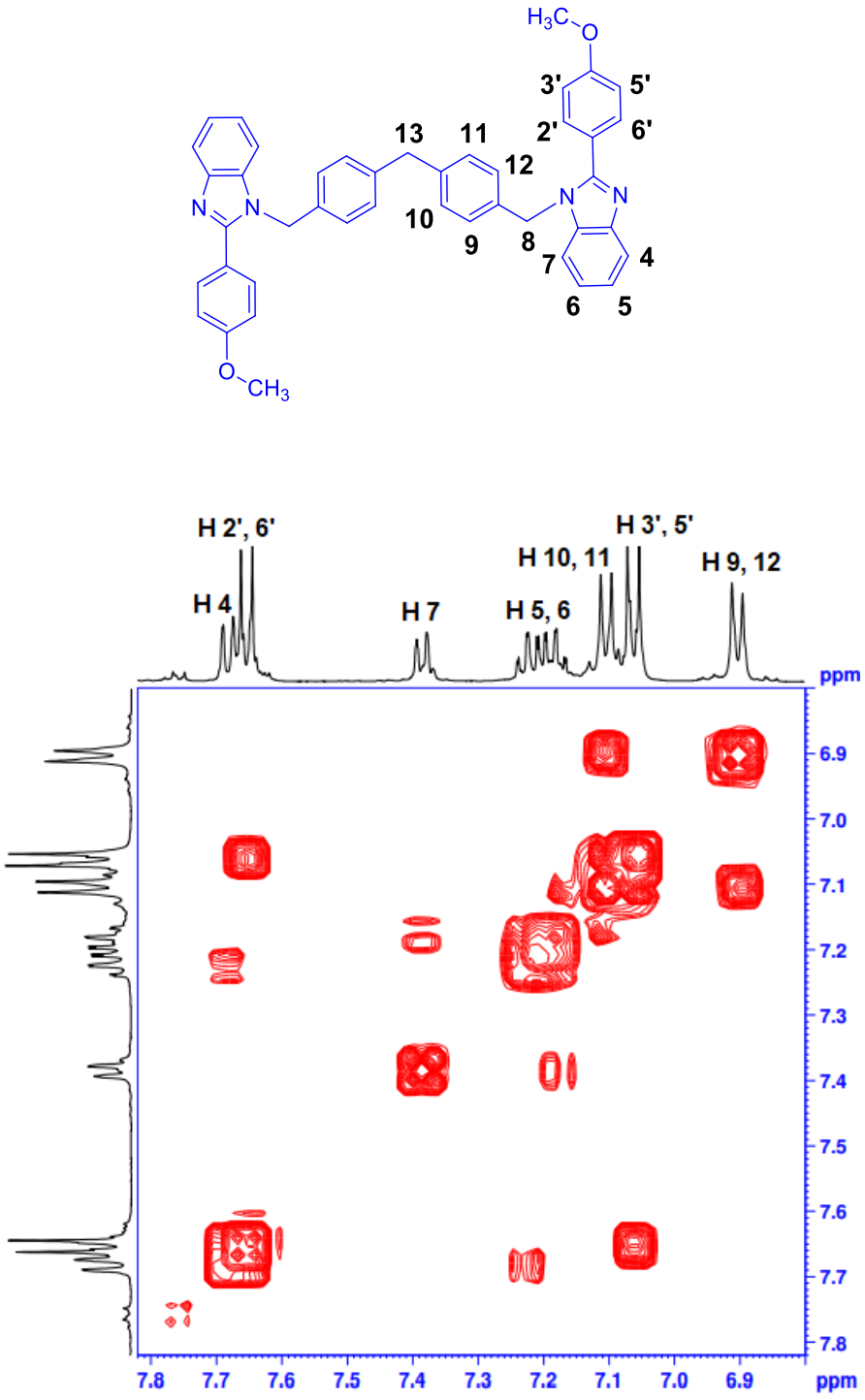

Figure 3.2. Partial ^{1}H-^{1}H COSY NMR (500 MHz) spectrum of L^{1} in d_6-DMSO.

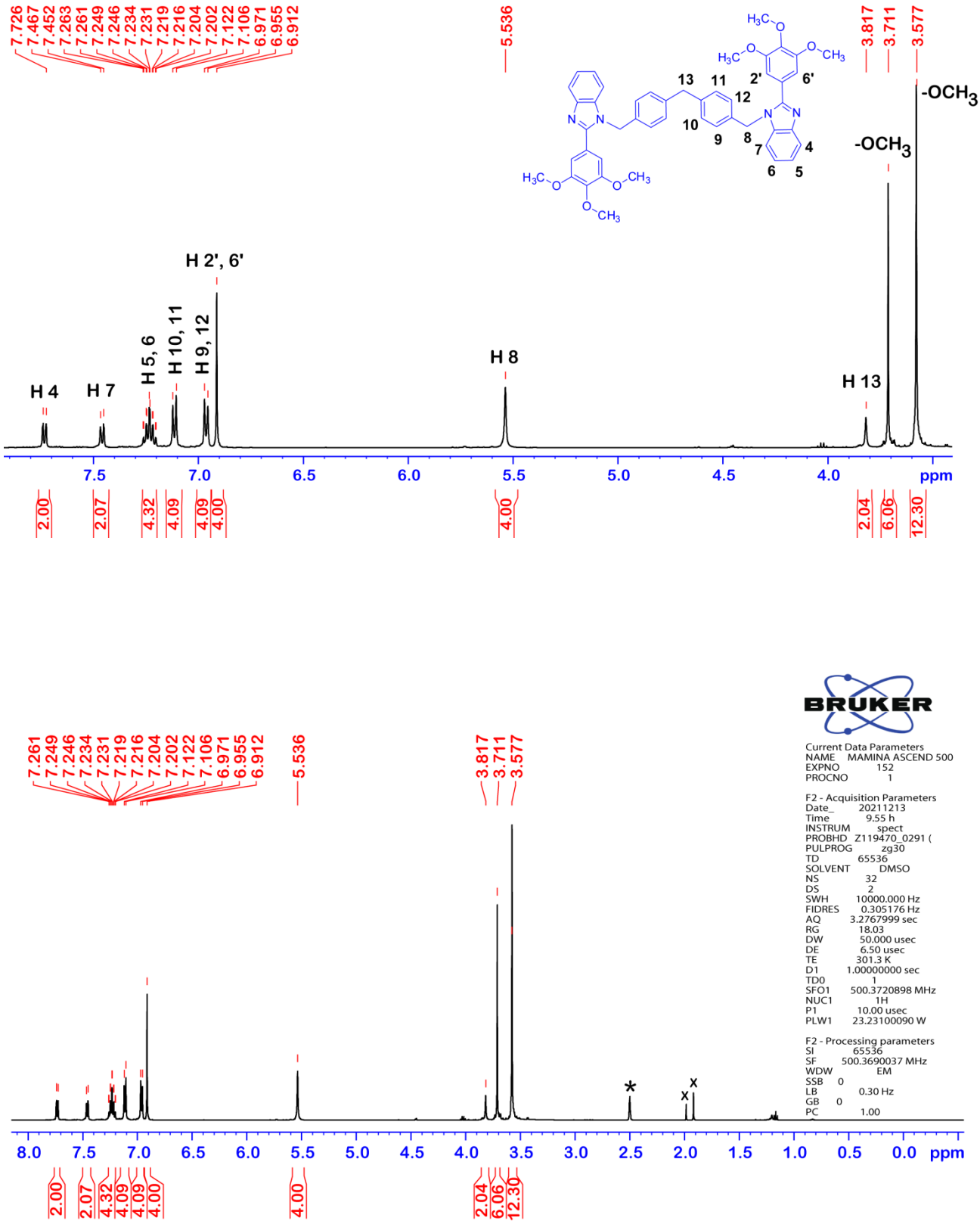

Figure 3.3. ^{1}H NMR (500 MHz) spectrum of L^2 in d_6-DMSO.

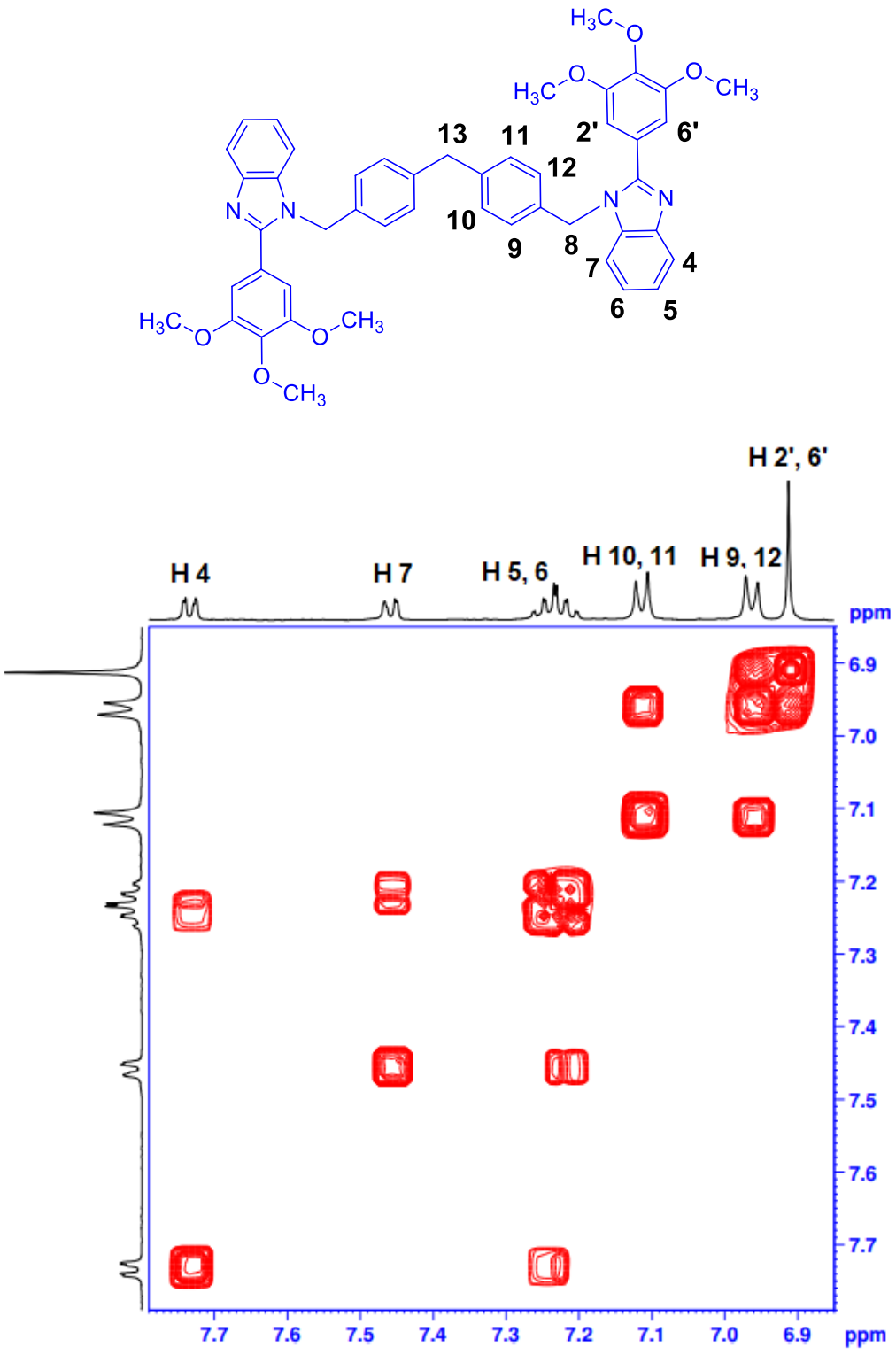

Figure 3.4. Partial ^{1}H-^{1}H COSY NMR (500 MHz) spectrum of L^2 in d_6-DMSO.

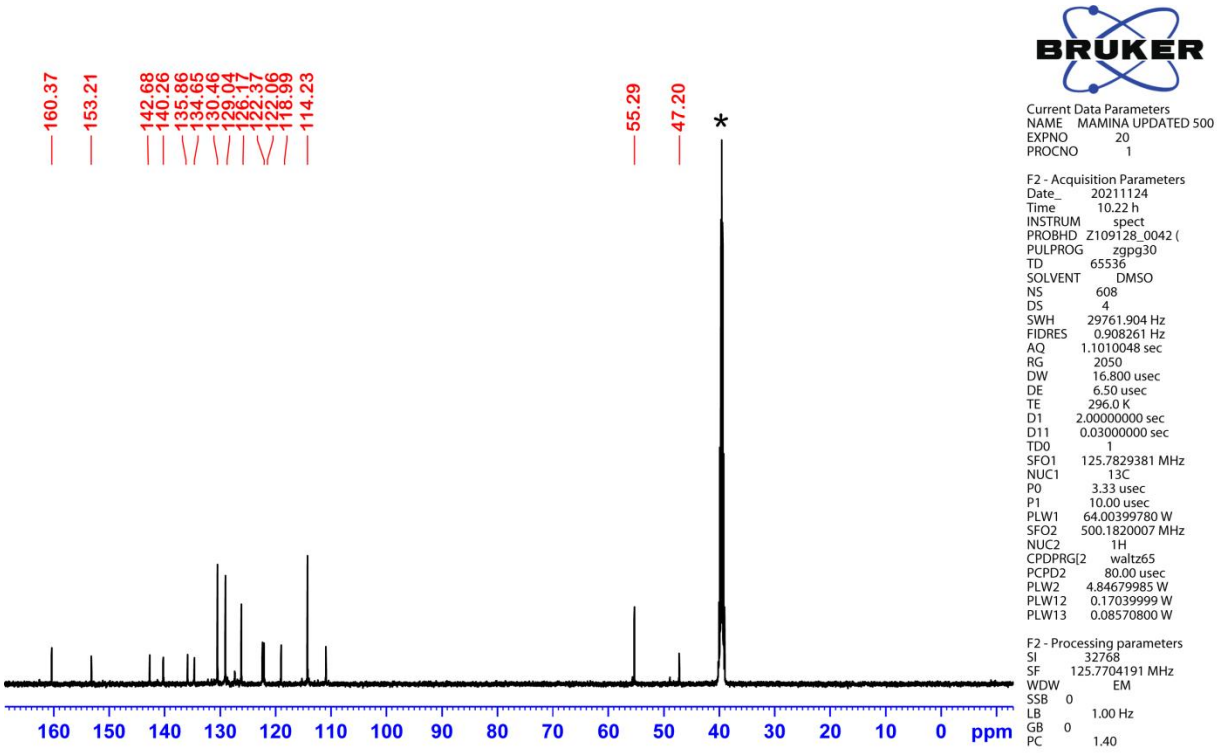

Figure 3.5. ^{13}C-NMR (500 MHz) spectrum of L^1 in d_6-DMSO.

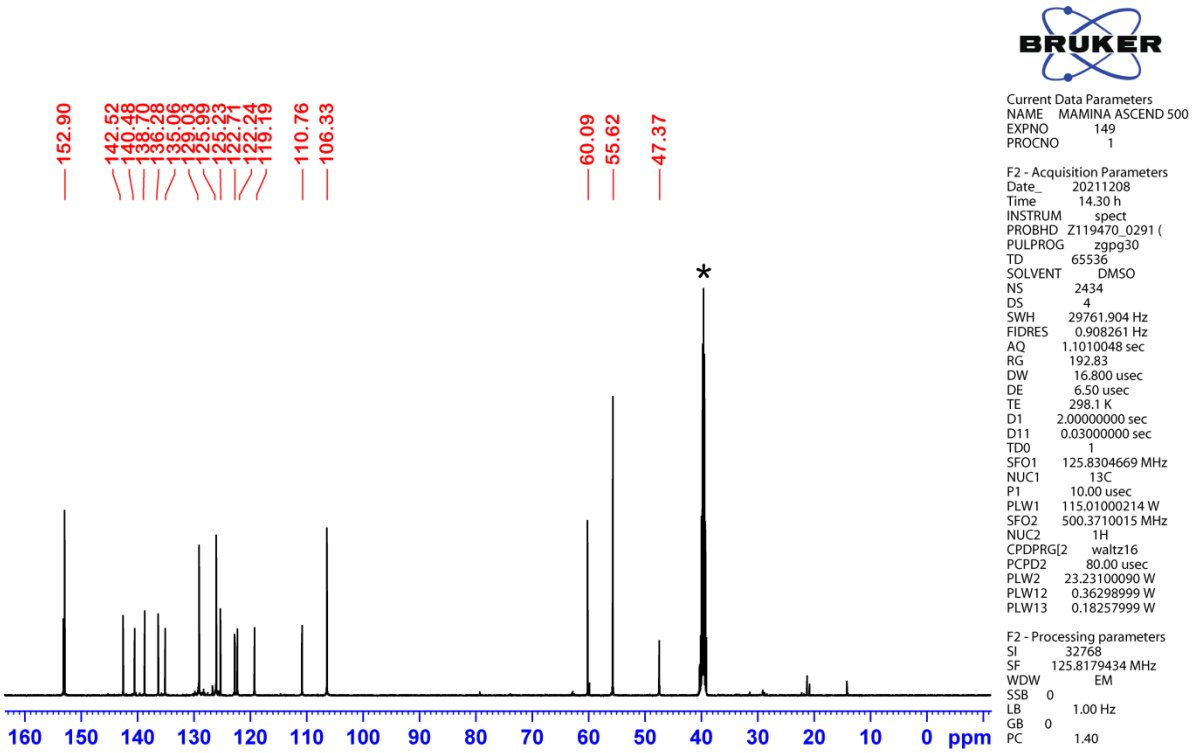

Figure 3.6. ^{13}C-NMR (500 MHz) spectrum of L^2 in d_6-DMSO.

Analysis Info

Analysis Name	D:\Data\2021-data\PROF.MS\OCT\MB4-66.d	Acquisition Date	10/29/2021 4:00:46 PM
Method	tune_low.m	Operator	BDAL
Sample Name	MB4-66	Instrument	maXis 255552.10138
Comment			

Acquisition Parameter

Source Type	ESI	Ion Polarity	Positive	Set Nebulizer	0.3 Bar
Focus	Not active	Set Capillary	3500 V	Set Dry Heater	180 °C
Scan Begin	50 m/z	Set End Plate Offset	-500 V	Set Dry Gas	4.0 l/min
Scan End	2000 m/z	Set Charging Voltage	0 V	Set Divert Valve	Waste
		Set Corona	0 nA	Set APCI Heater	0 °C

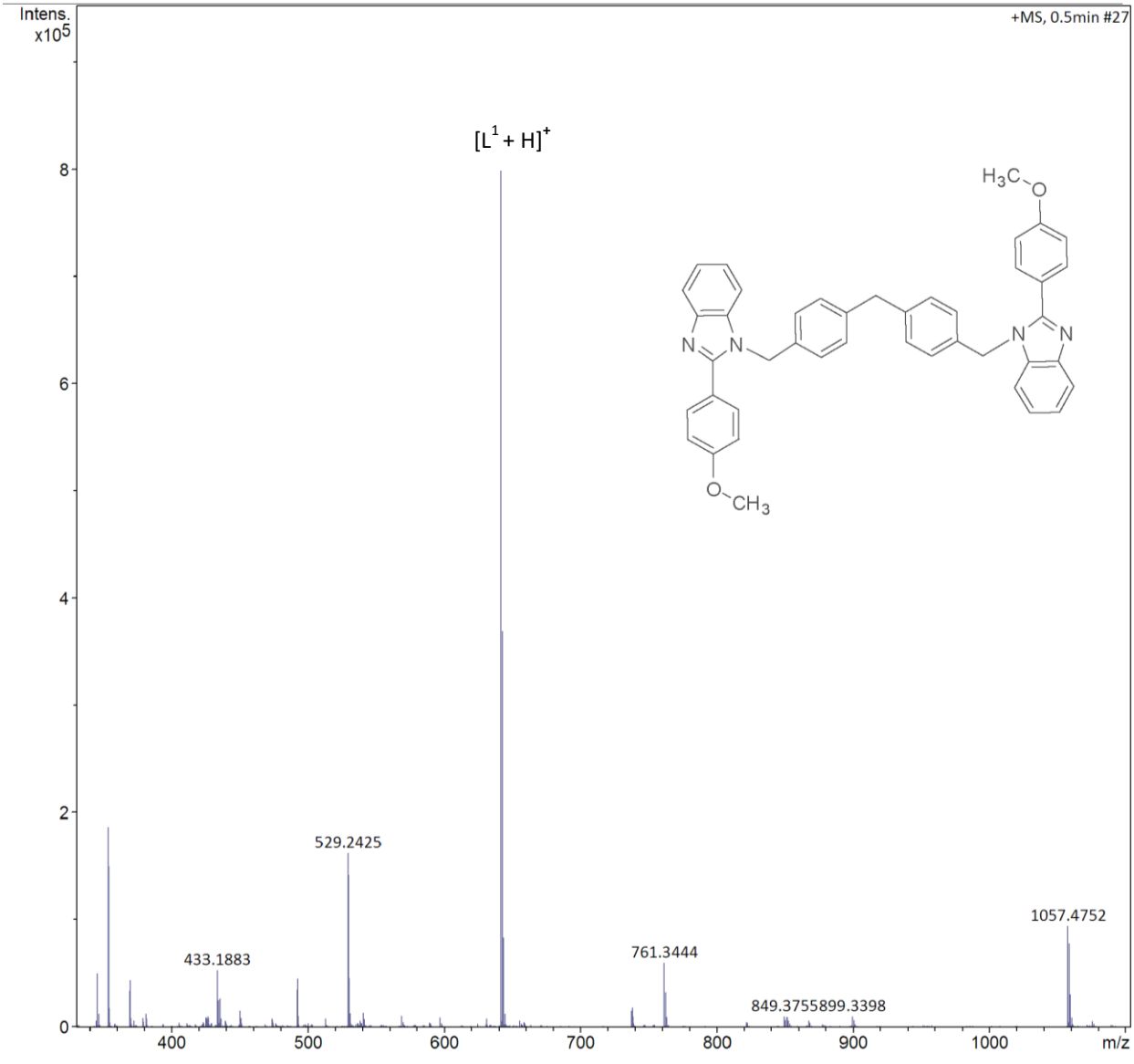

MB4-66.d

Bruker Compass DataAnalysis 4.2 printed: 10/29/2021 5:09:24 PM by: BDAL Page 1 of 1

Figure 3.7. ESI mass spectrum of L^1 in positive ion mode.

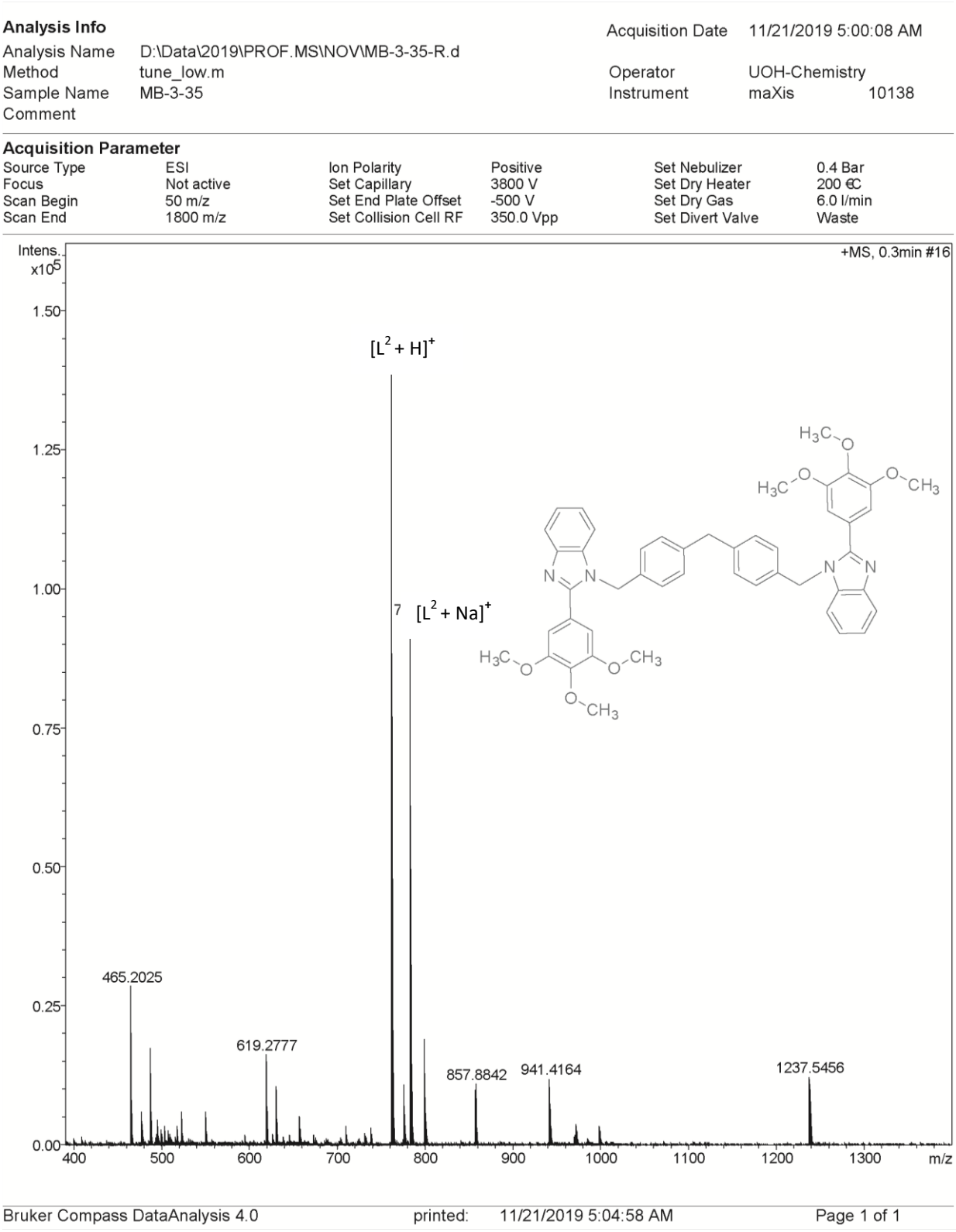

Figure 3.8. ESI mass spectrum of L^2 in positive ion mode.

3.3.2. Synthesis and characterization of metallocavitands 1-8.

Complexes **1-8** were prepared from $Re_2(CO)_{10}$, bis-chelating ligand (H_2-dhbq (2,5-dihydroxy-1,4-benzoquinone) or H_2-CA (chloranilic acid) or H_2-dhaq (1,4-dihydroxyanthraquinone) or H_2-dhnq (6,11-dihydroxy-5,12-naphthacenedione)), L^n, and high boiling aromatic solvents via a one-pot solvothermal procedure (Scheme 3.2- 3.3). The complexes are air- and moisture-stable, and soluble in DMSO, $CHCl_3$, CH_2Cl_2, and CH_3CN. Further, the complexes are sparingly soluble in methanol. The ATR-IR spectra of the complexes showed three strong bands in the 2012-1874 cm^{-1} region, which are characteristic peaks of *fac*-$Re(CO)_3$ core in an asymmetric surrounding.[11,21] The high resolution ESI-MS analysis of the complexes displayed molecular ion peaks (m/z = 1321.1739 for [**1** + H]$^+$, 1441.1906 for [**2** + H]$^+$, 1389.0689 for [**3** + H]$^+$, 1509.1170 for [**4** + H]$^+$, 1421.1831 for [**5** + H]$^+$, 1541.2327 for [**6** + H]$^+$, 1471.1960 for [**7** + H]$^+$, and 1605.2667 for [**8** - 3H + NH4]$^+$) with isotope pattern that match well with the theoretical values.

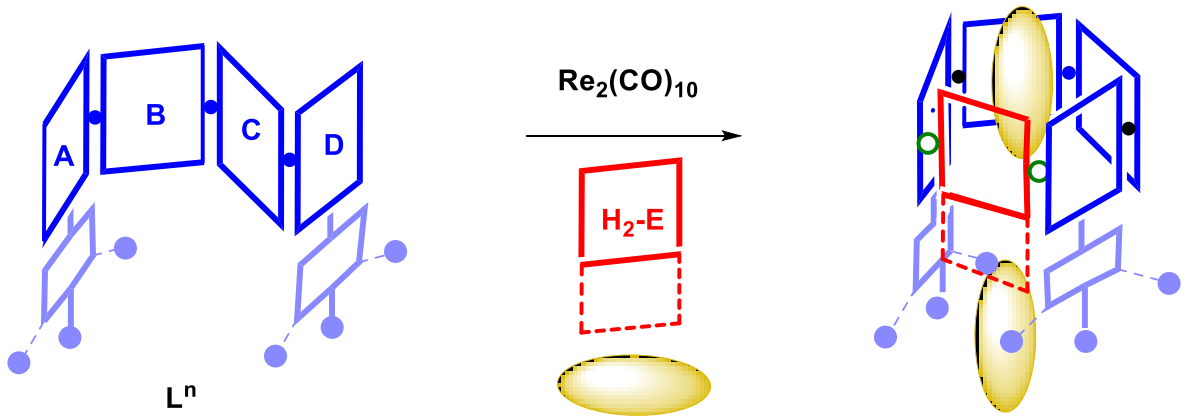

Scheme 3.2. Cartoon representation of synthetic strategy for metallocavitand: A = D = heterocyclic nitrogen donor; B = C = phenylene spacer, H_2E = bis-chelating unit; ● = CH_2; ● = OCH_3; ○ = *fac*-$Re(CO)_3$, guest molecule = ellipsoid motif.

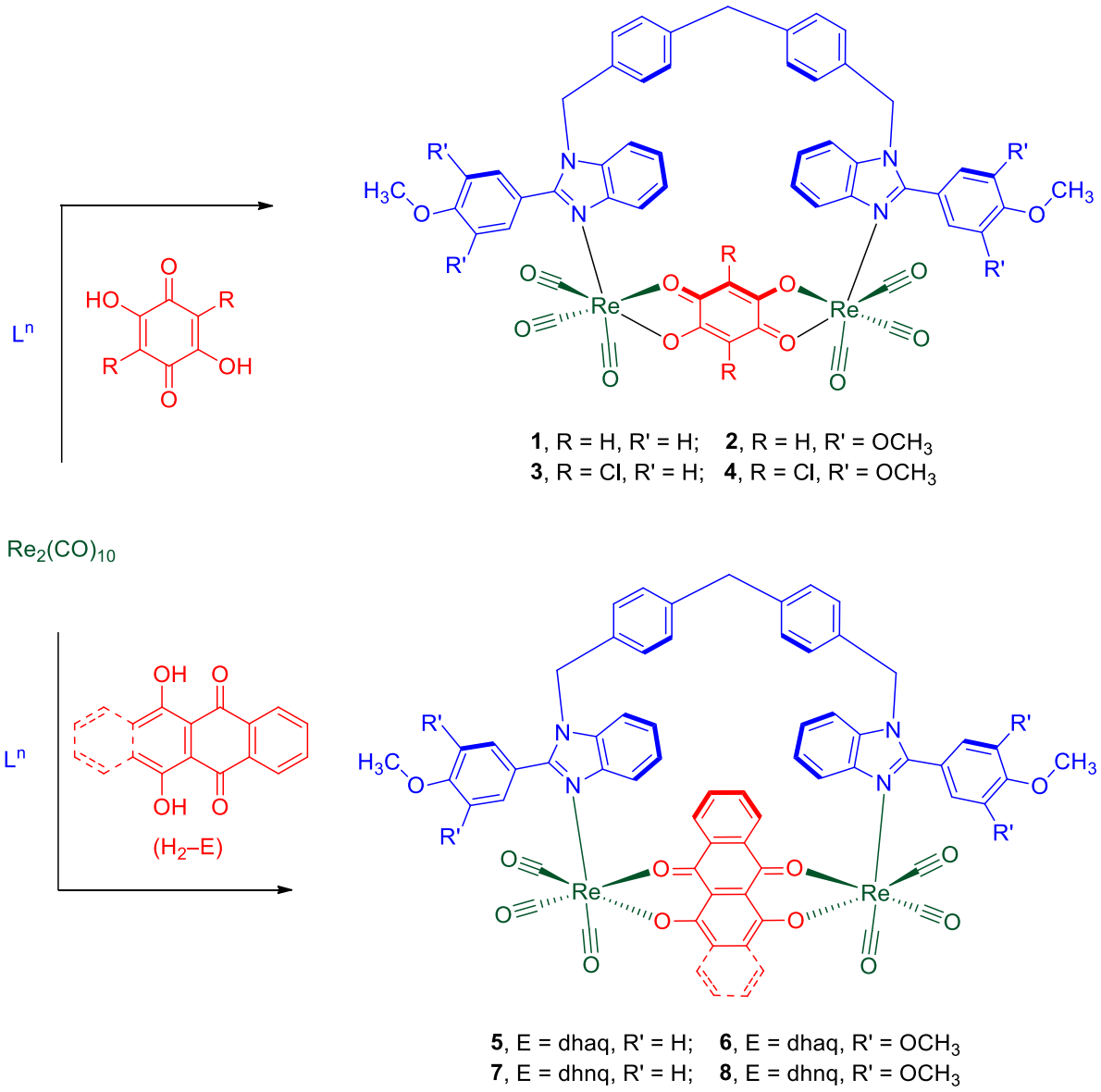

Scheme 3.3. Synthesis of metallocavitands **1-8** (H_2-dhaq = 1,4-dihydroxyanthraquinone; H_2-dhnq = 6,11-dihydroxy-5,12-naphthacenedione).

^{1}H NMR analysis of complexes 1-8.

The ^{1}H NMR spectrum of **1** and **2** displayed the chemical resonances of the protons of L^1/L^2. The proton of dhbq unit of **1** showed singlet and was downfield shifted as compared to free H_2-dhbq ligand. The proton ratio of dhbq:L^1 was 1:1, suggesting the stoichiometry of complex **1**. The H^4, $H^{9,12}$, $H^{2',6'}$, H^8, H^{13} of L^2, and protons of dhbq in **2** were upfield shifted, whereas H^7, $H^{5,6}$, $H^{10,11}$ of L^2 was downfield shifted relative to the free ligand. The proton NMR spectra of **3** and **4** displayed a single set of chemical resonances for all the protons of L^1 and L^2, respectively. All the protons of L^1 in **3** were downfield shifted significantly as compared to the free ligand L^1. In the case of **4**, $H^{2',\ 6'}$ protons were noticeably upfield shifted, whereas the signals of other protons were shifted slightly upfield/downfield in comparison with free ligand L^2. The proton NMR spectra of **5-8** displayed simple pattern with chemical resonances for the protons of L^1/L^2 and dhaq/dhnq. The proton signals of L^1/L^2 in **5-8** are similar to those of the free ligands. In addition to these peaks, two symmetrical multiplets and one single signal corresponding to the dhaq unit were observed for **5** and **6**. The H^a and $H^{b,\ c}$ signals of dhaq in **5** were upfield and downfield shifted respectively. All protons (H^{a-c}) of dhaq in **6** were downfield shifted relative to free H_2-dhaq ligand. In addition to the signals for the protons of L^1/L^2, two symmetrical multiplets (H^a and H^b) for dhnq protons were observed in **7** and **8**. The H^a signal of dhnq in **7** and **8** was downfield shifted relative to free H_2-dhnq. The upfield and downfield shifts of the protons of the ligand framework in the complexes as compared to the free ligands suggest that the cyclic nature of the complexes in solution state.

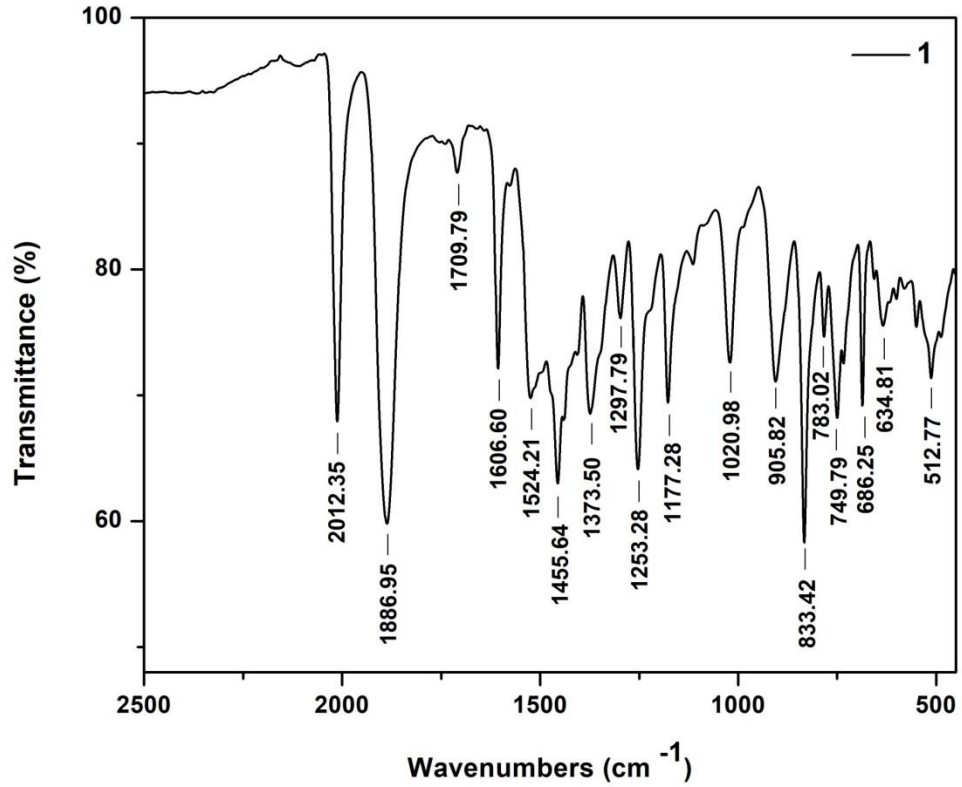

Figure 3.9. ATR-IR spectrum of **1**.

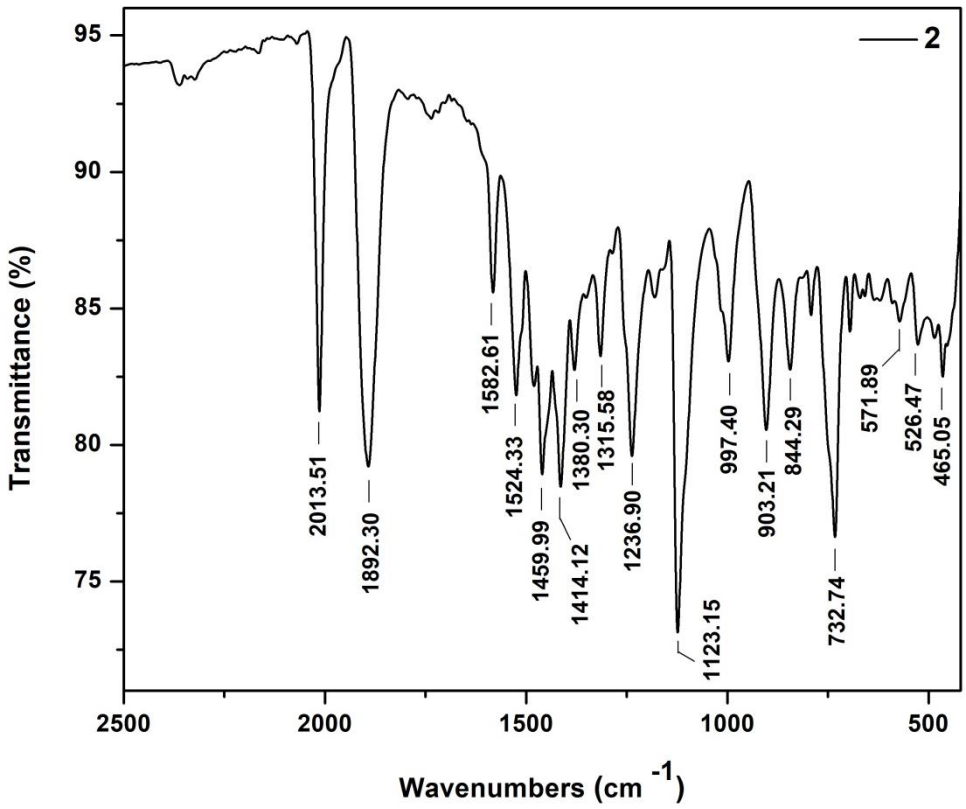

Figure 3.10. ATR-IR spectrum of **2**.

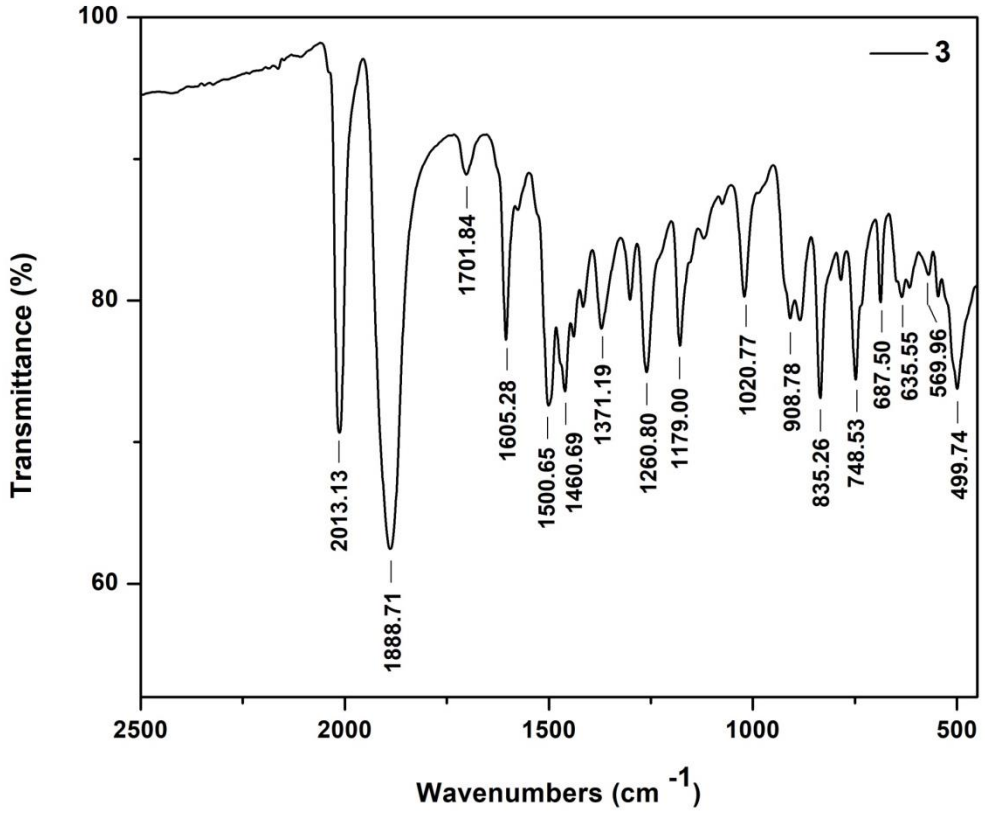

Figure 3.11. ATR-IR spectrum of **3**.

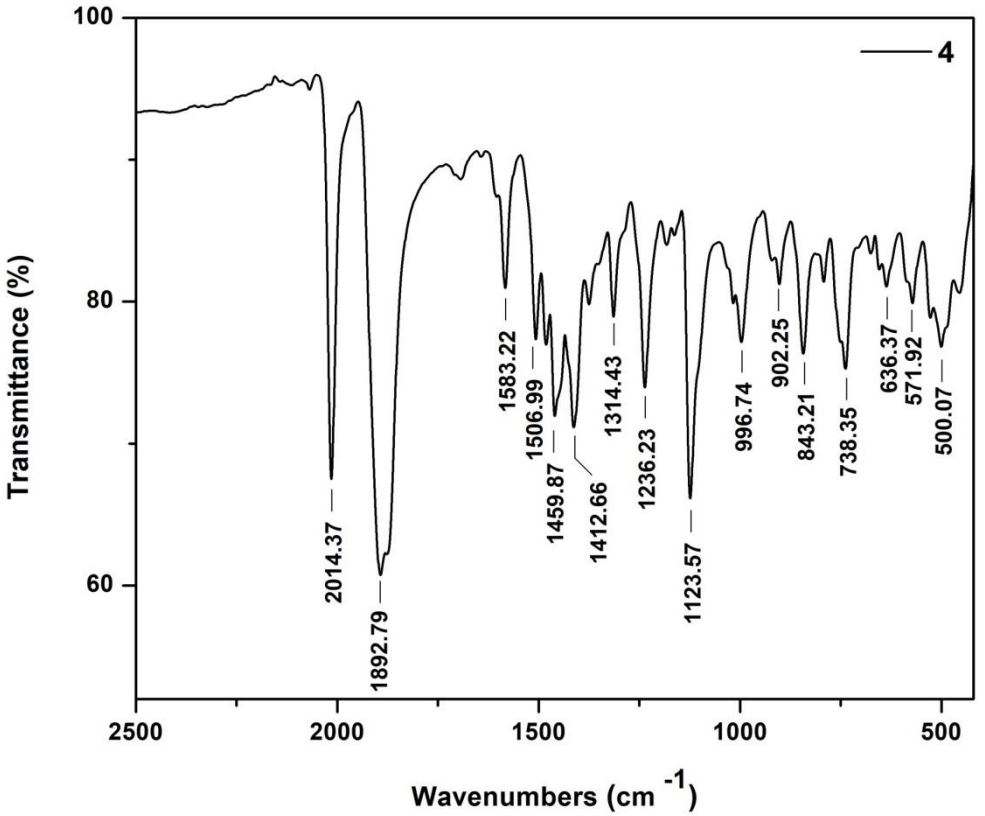

Figure 3.12. ATR-IR spectrum of **4**.

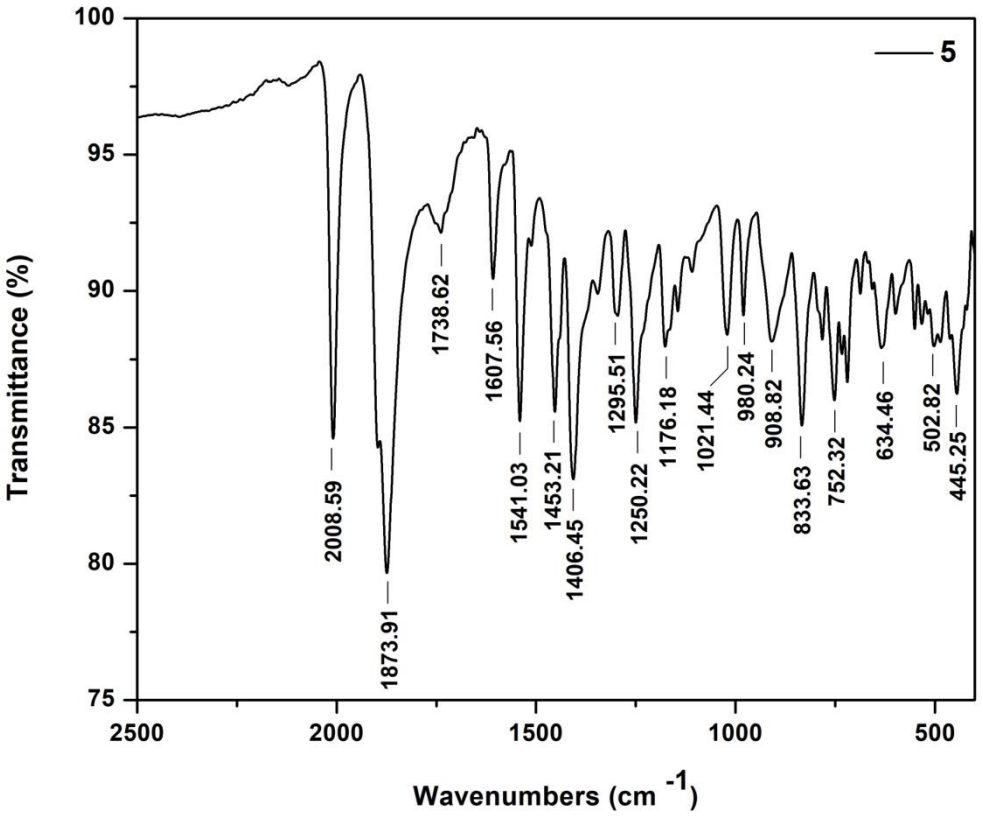

Figure 3.13. ATR-IR spectrum of **5**.

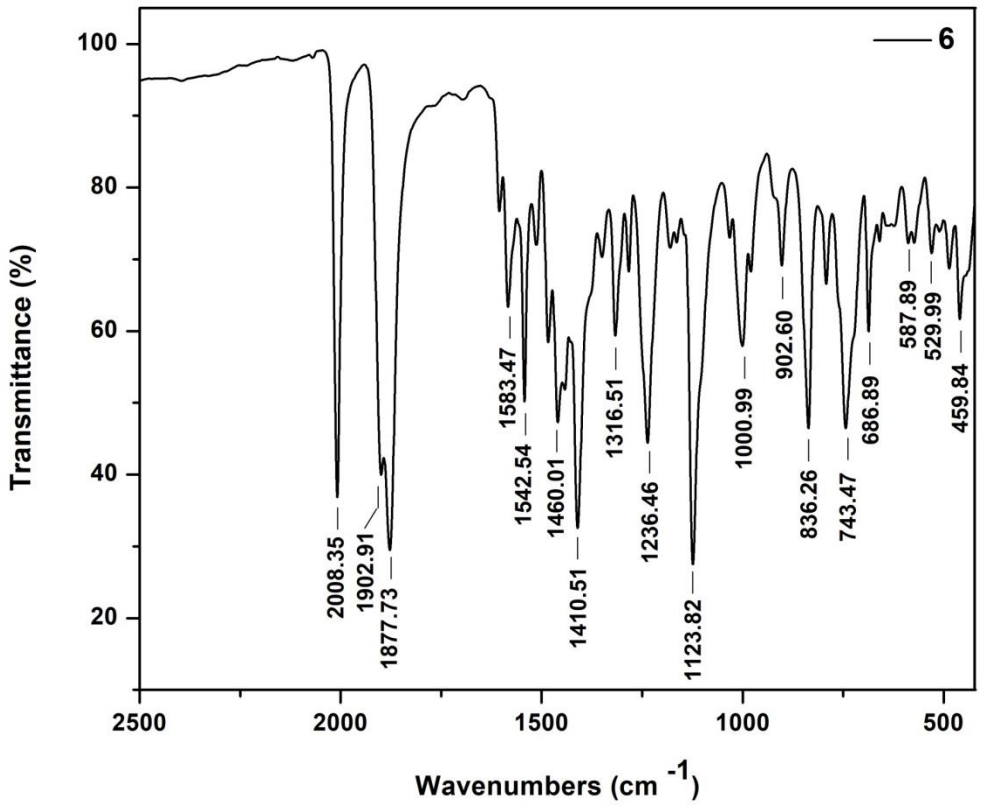

Figure 3.14. ATR-IR spectrum of **6**.

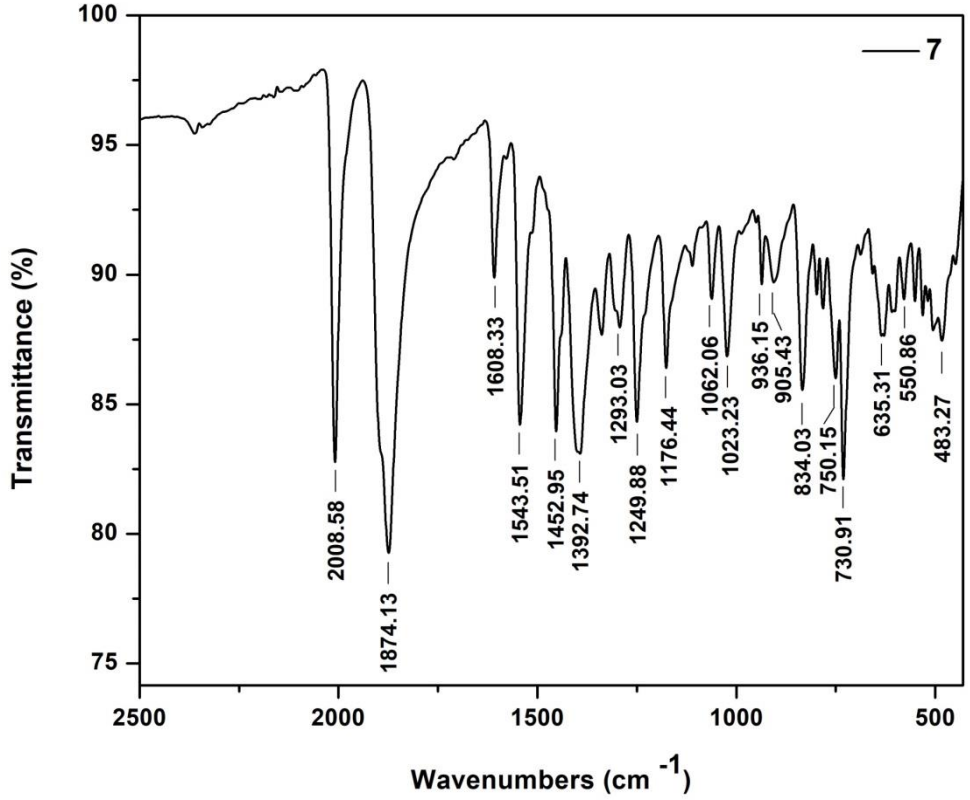

Figure 3.15. ATR-IR spectrum of **7**.

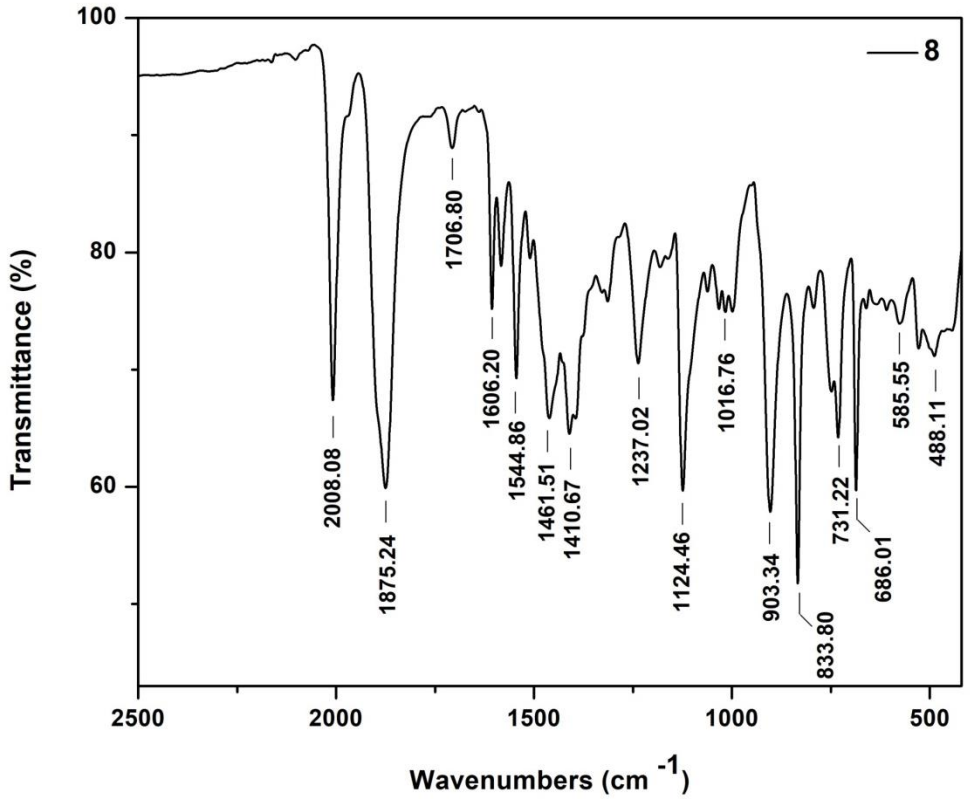

Figure 3.16. ATR-IR spectrum of **8**.

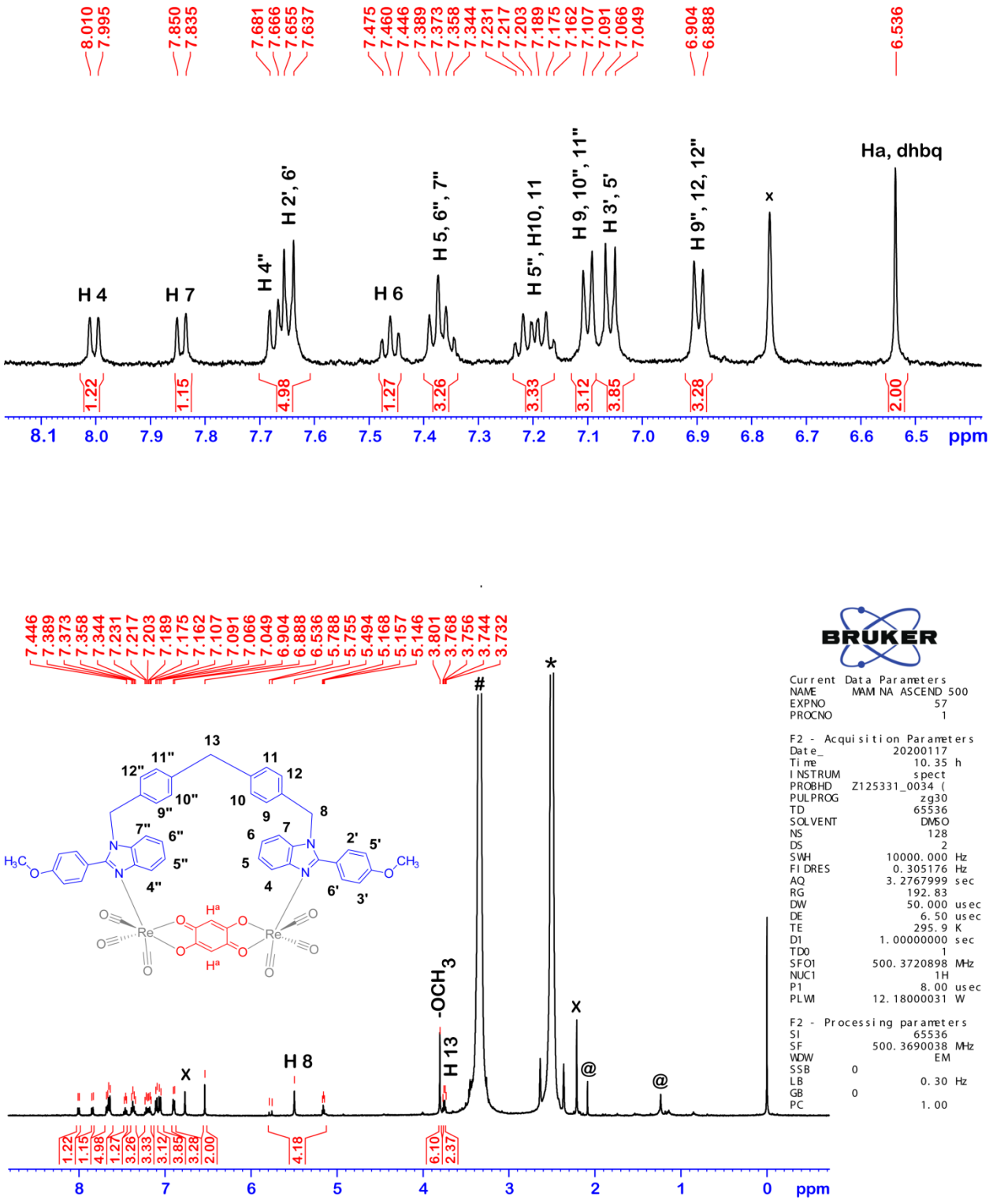

Figure 3.17. ^{1}H NMR (500 MHz) spectrum of **1** in d_6-DMSO.

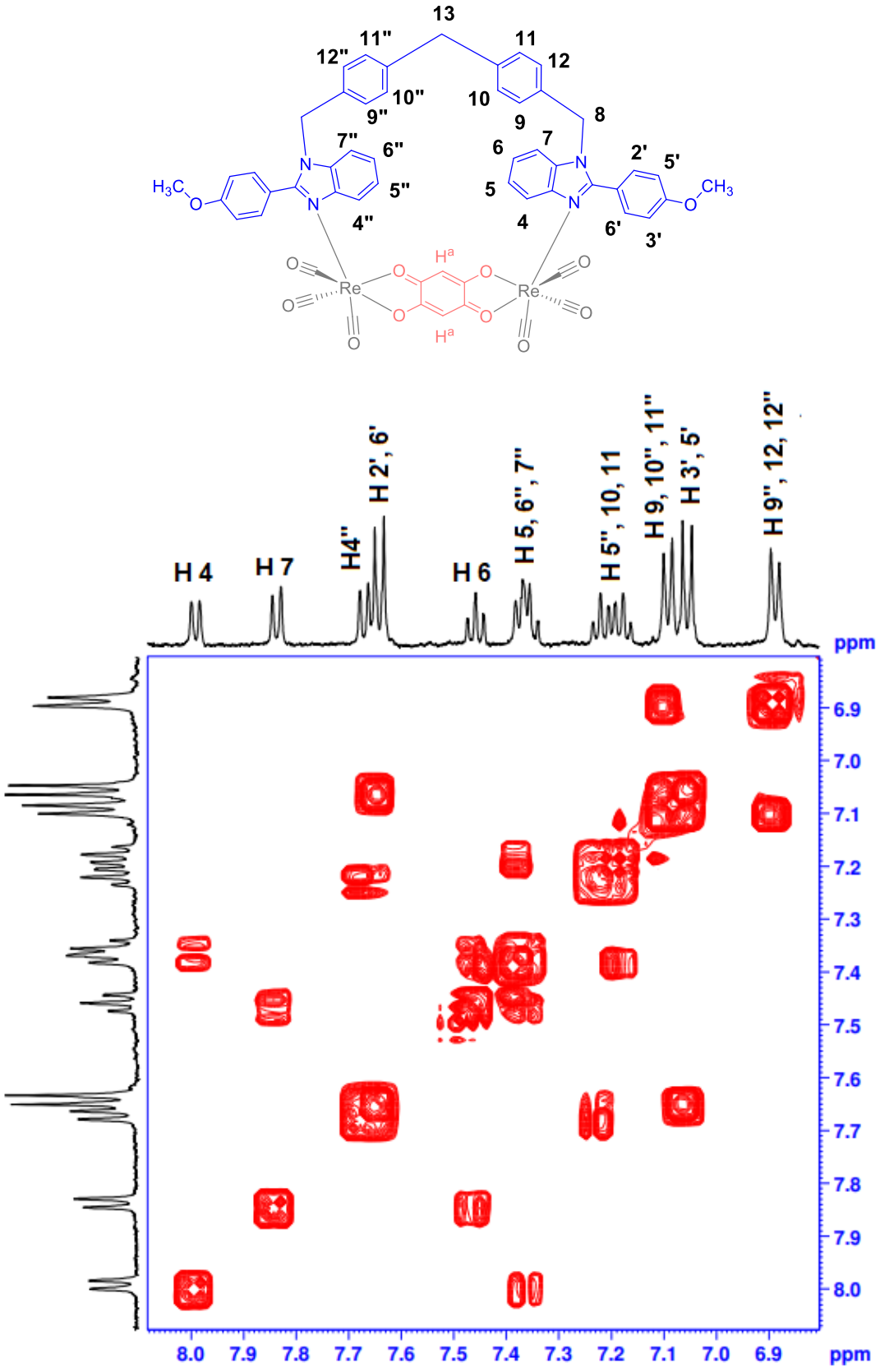

Figure 3.18. Partial ^{1}H-^{1}H COSY NMR (500 MHz) spectrum of **1** in d_6-DMSO.

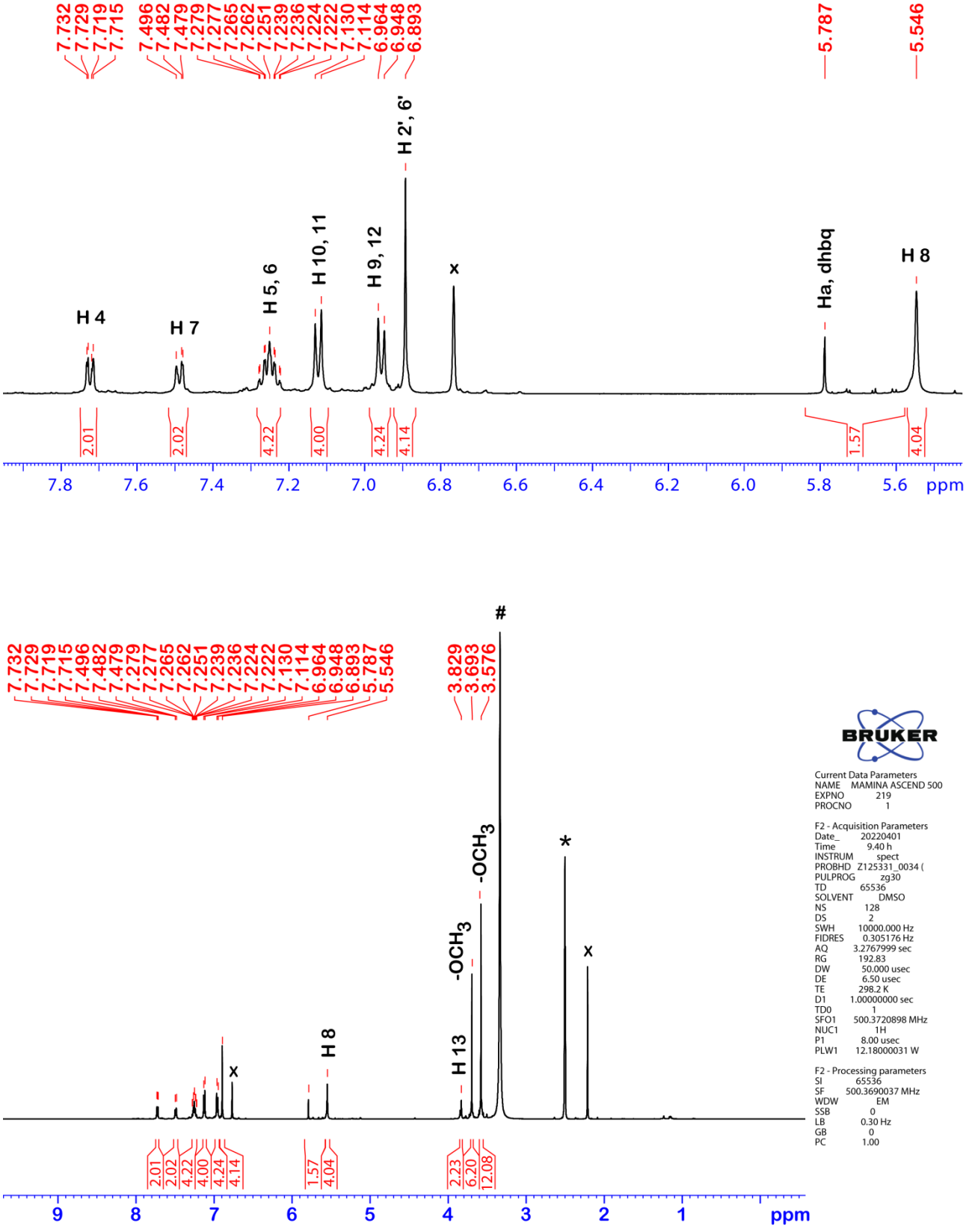

Figure 3.19. ^{1}H NMR (500 MHz) spectrum of **2** in d_6-DMSO.

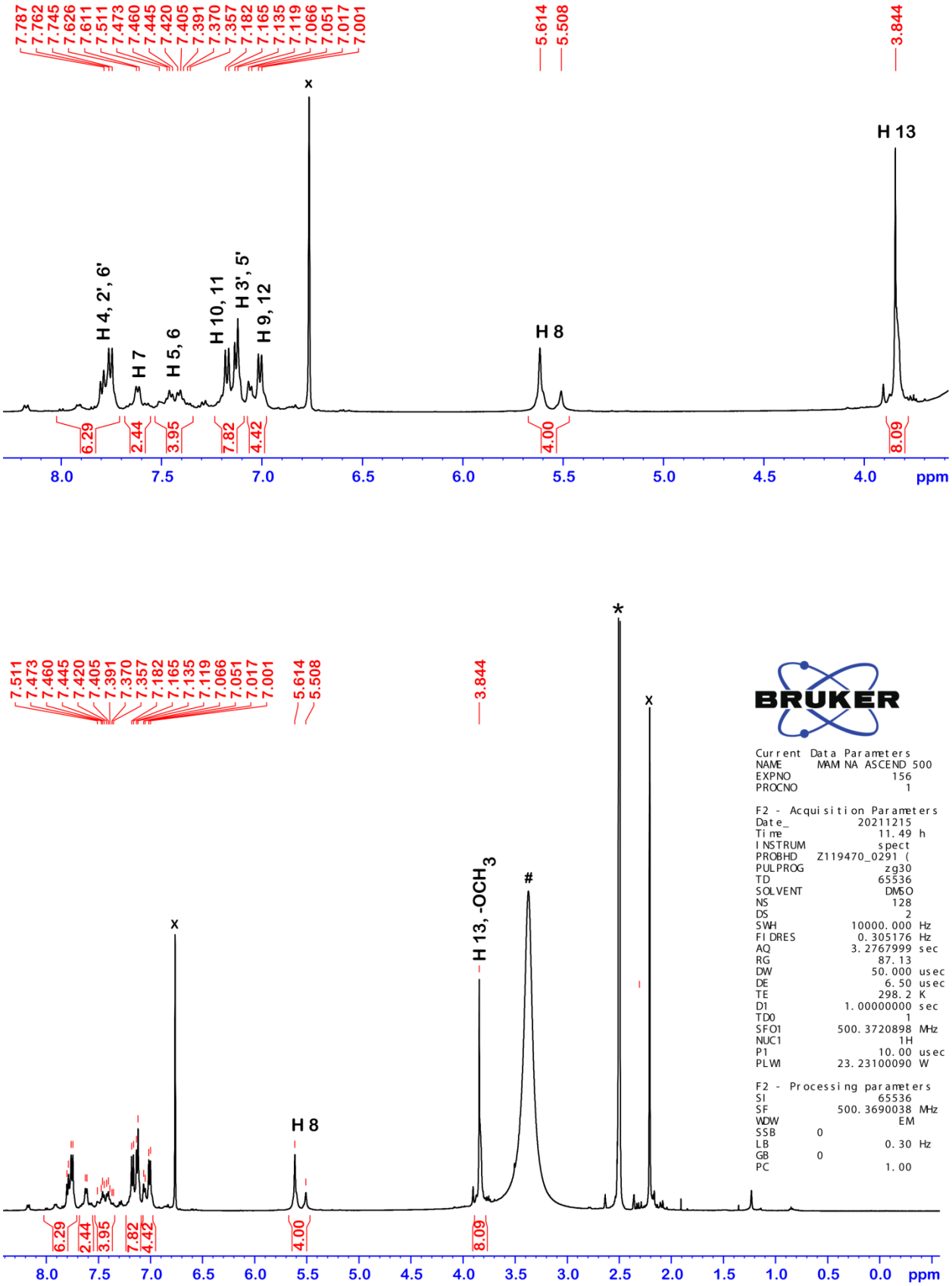

Figure 3.20. ^{1}H NMR (500 MHz) spectrum of **3** in d_6-DMSO.

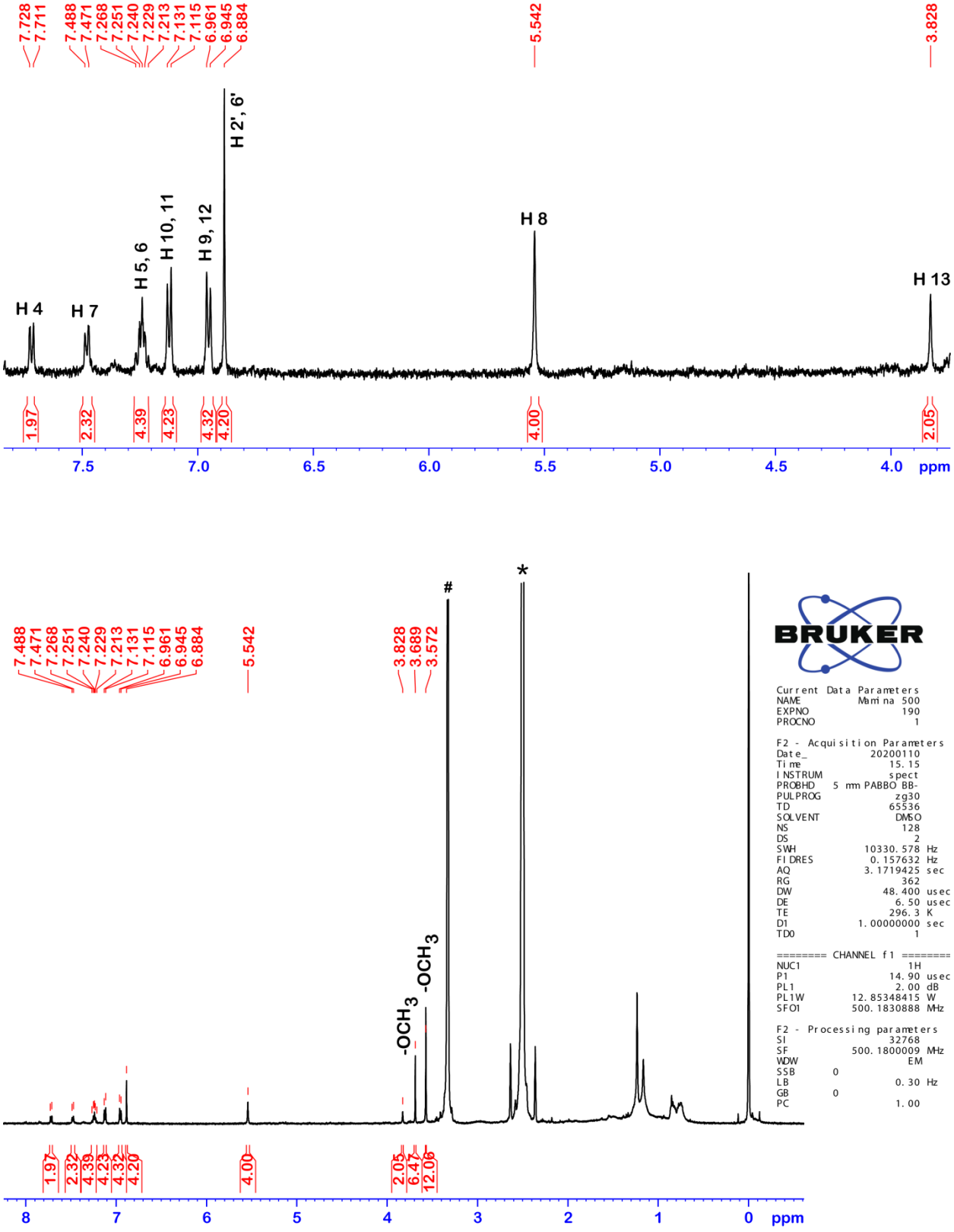

Figure 3.21. ^{1}H NMR (500 MHz) spectrum of **4** in d_6-DMSO.

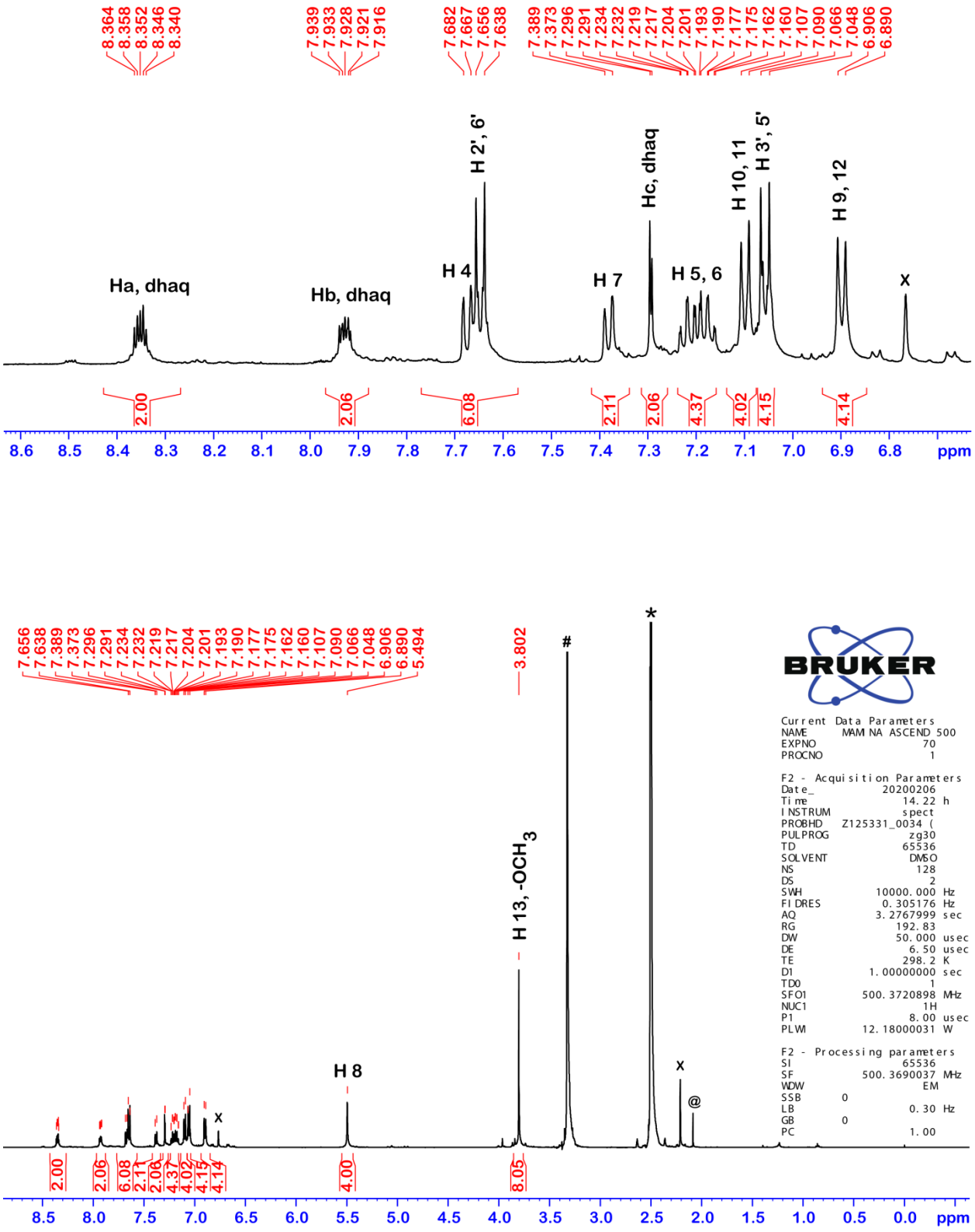

Figure 3.22. ^{1}H NMR (500 MHz) spectrum of **5** in d_6-DMSO.

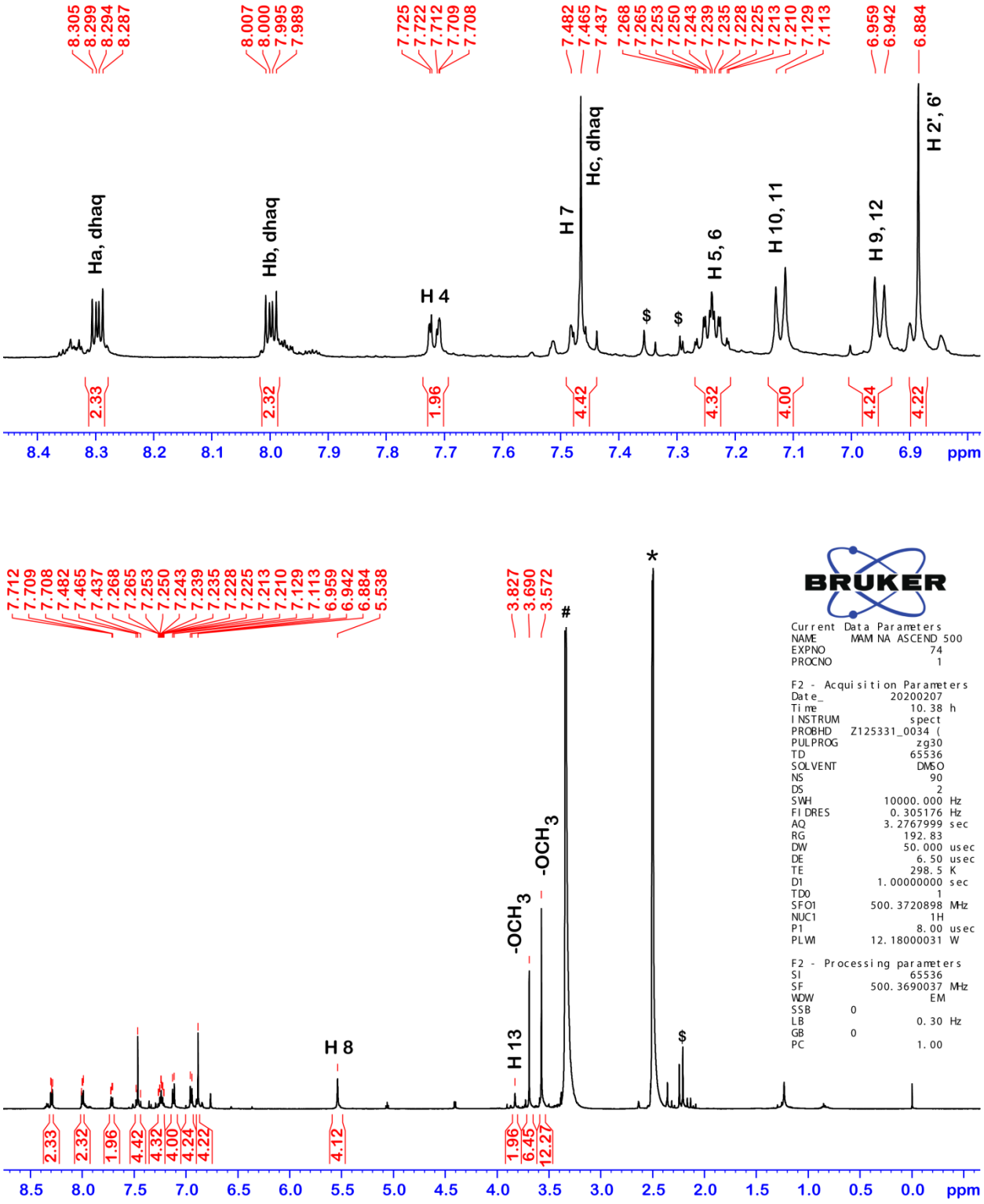

Figure 3.23. ^{1}H NMR (500 MHz) spectrum of **6** in d_6-DMSO.

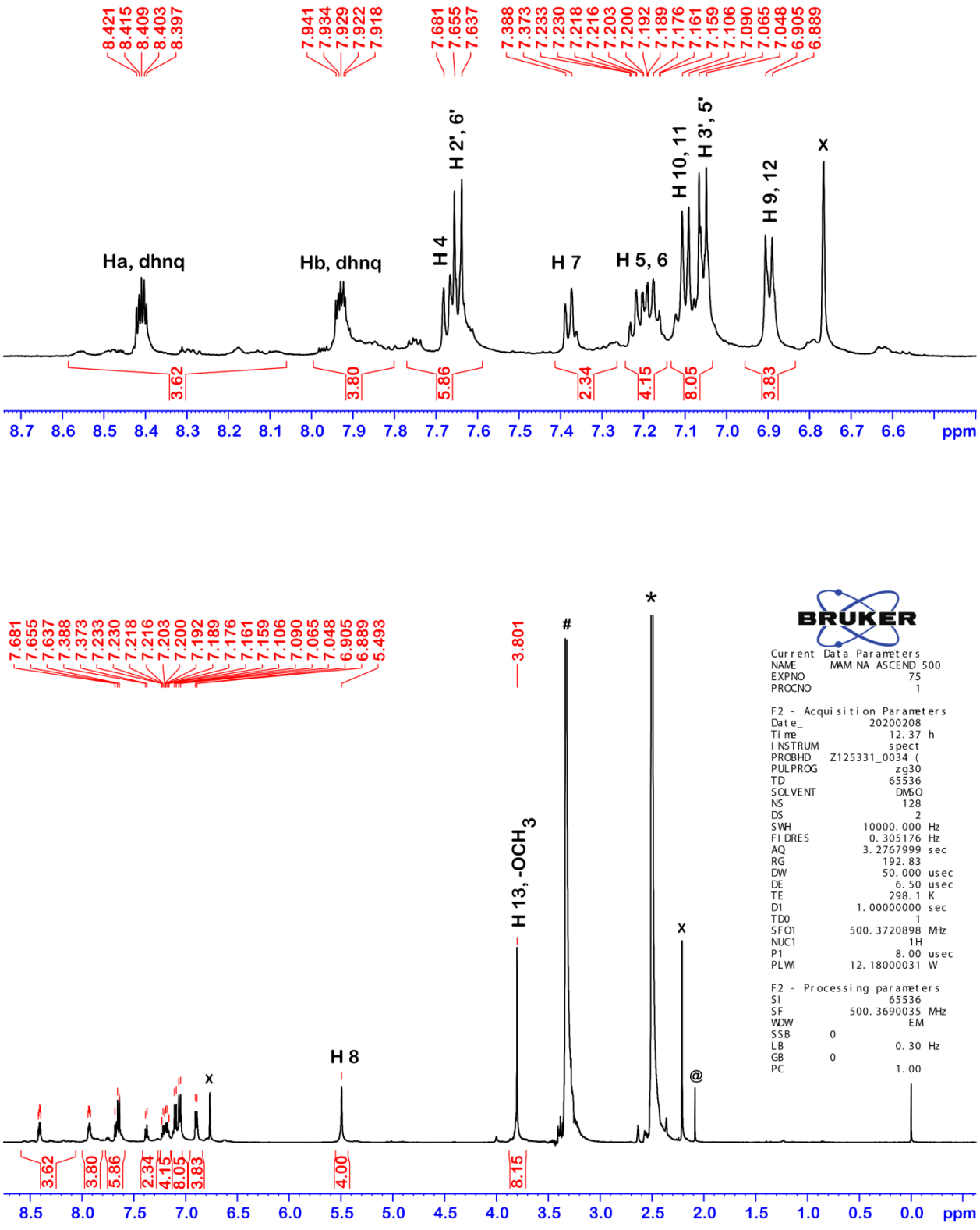

Figure 3.24. ^{1}H NMR (500 MHz) spectrum of **7** in d_6-DMSO.

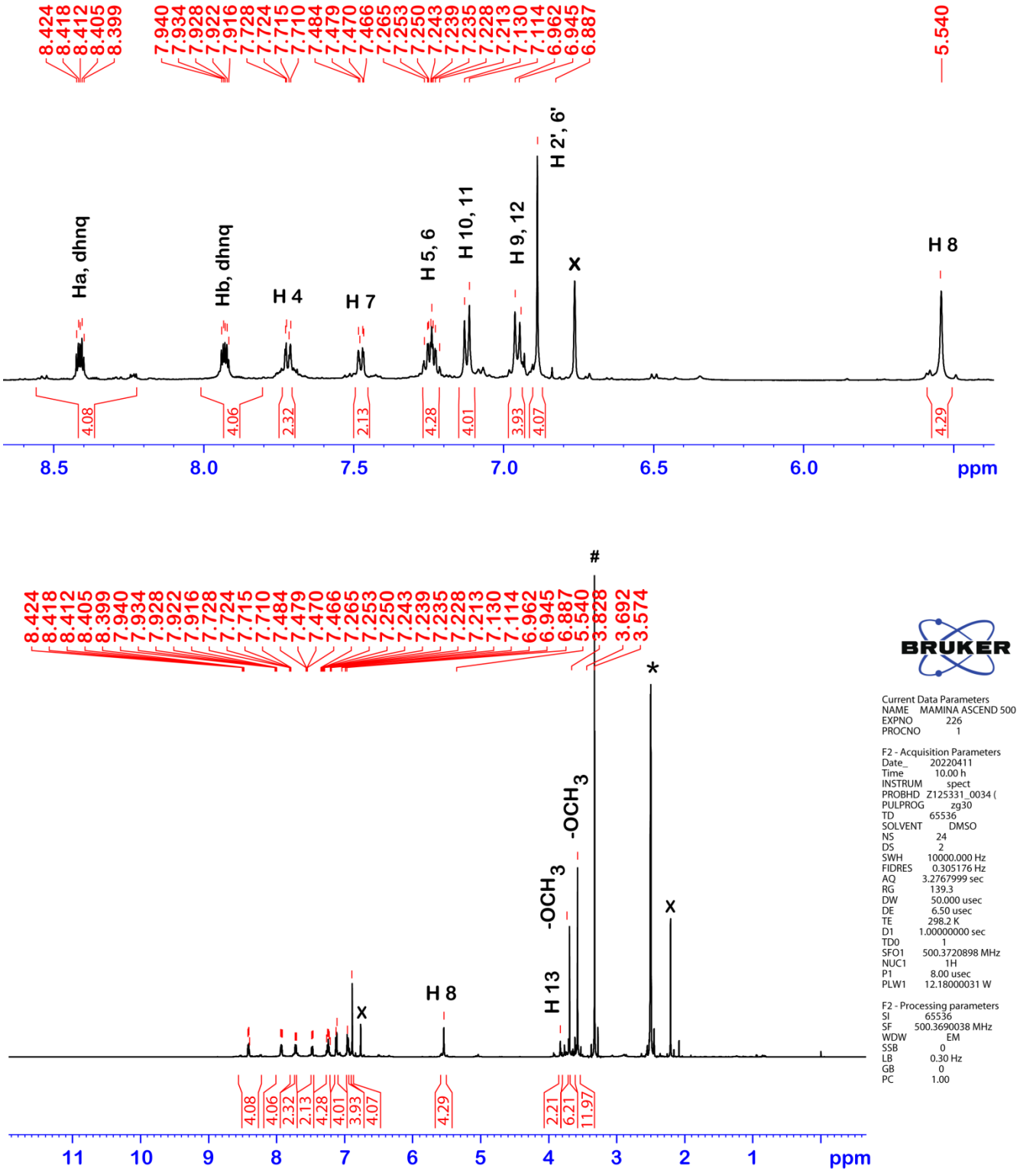

Figure 3.25. ^{1}H NMR (500 MHz) spectrum of **8** in d_6-DMSO.

Display Report

Analysis Info

Analysis Name	D:\Data\2021-data\PROF.MS\NOV\MB-4-73-R2.d	Acquisition Date	11/10/2021 4:33:10 PM
Method	tune_wide_Pos.m	Operator	BDAL
Sample Name	MB-4-73-R2	Instrument	maXis 255552.10138
Comment			

Acquisition Parameter

Source Type	ESI	Ion Polarity	Positive	Set Nebulizer	0.3 Bar
Focus	Not active	Set Capillary	3800 V	Set Dry Heater	180 °C
Scan Begin	200 m/z	Set End Plate Offset	-500 V	Set Dry Gas	4.0 l/min
Scan End	3000 m/z	Set Charging Voltage	0 V	Set Divert Valve	Source
		Set Corona	0 nA	Set APCI Heater	0 °C

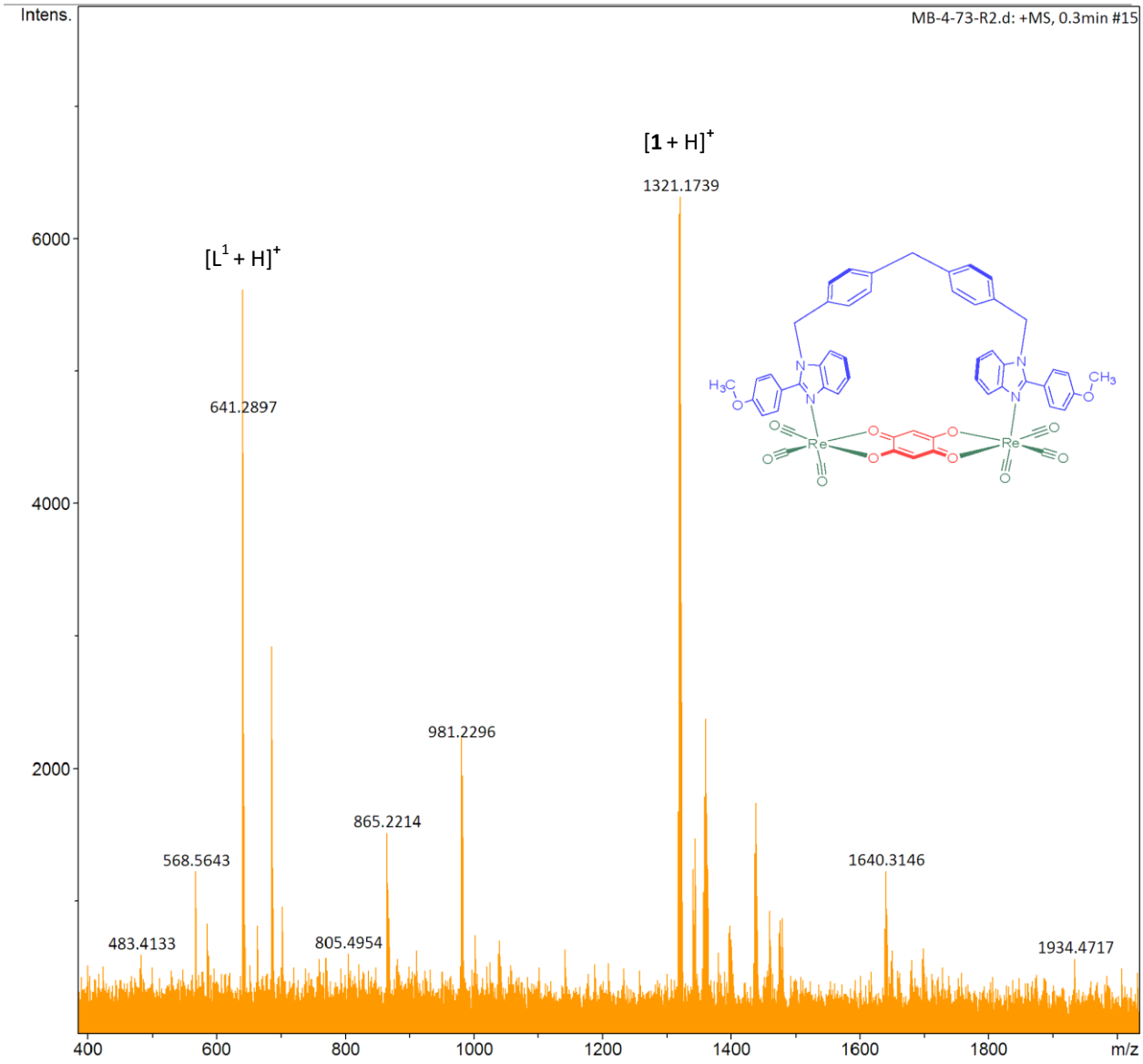

MB-4-73-R2.d

Bruker Compass DataAnalysis 4.2 printed: 11/11/2021 1:02:36 PM by: BDAL Page 1 of 1

Figure 3.26. ESI mass spectrum of **1** in positive ion mode.

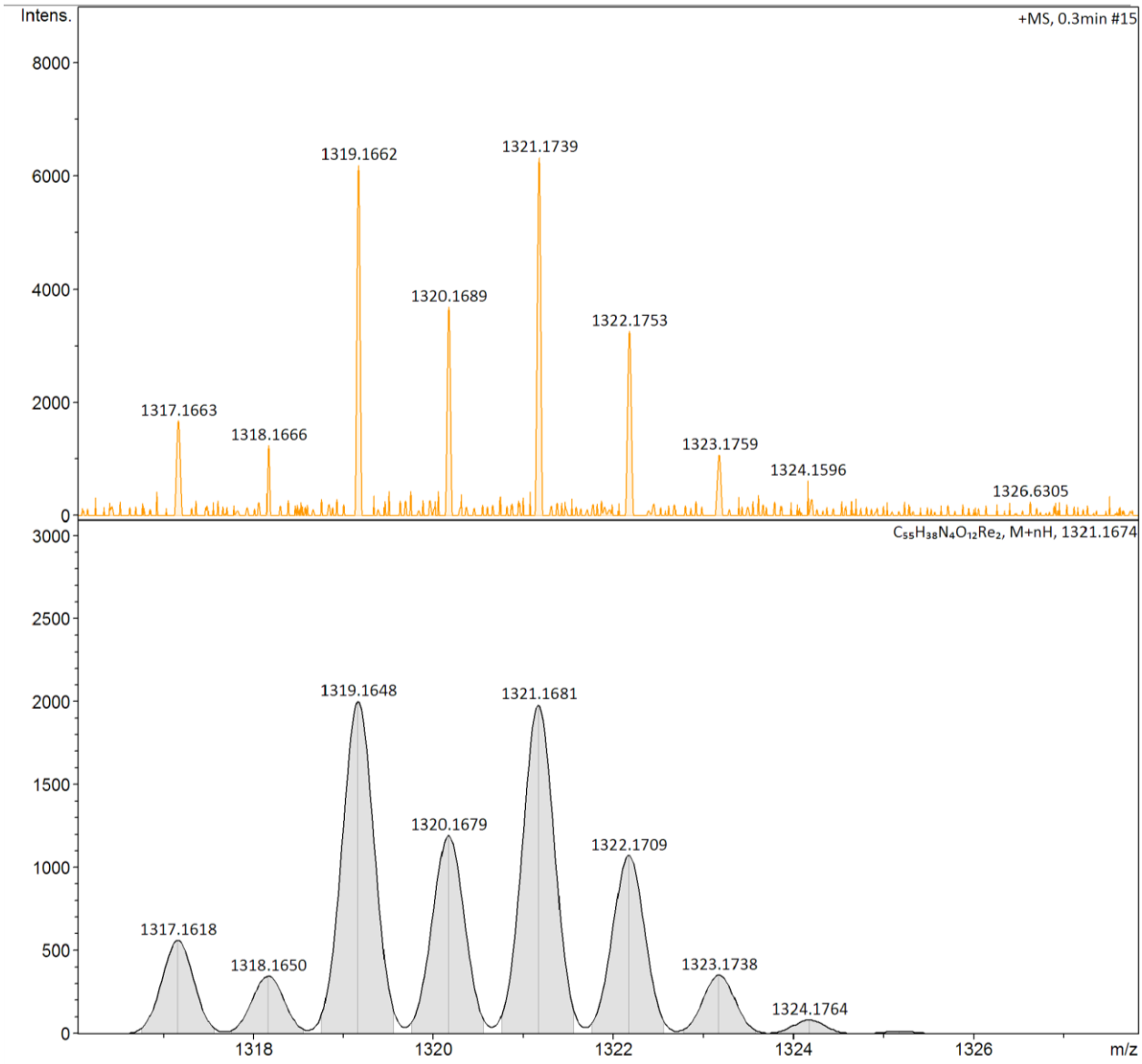

Figure 3.27. Experimental (top) and calculated (below) ESI mass spectrum of **1** in positive ion mode.

Analysis Info

Analysis Name	D:\Data\2019\PROF.MS\NOV\MB-4-48-CRYSTAL-r1.d	Acquisition Date	11/19/2019 4:15:28 AM
Method	tune_wide_PosR.m	Operator	UOH-Chemistry
Sample Name	MB-4-48-CRYSTAL	Instrument	maXis 10138
Comment			

Acquisition Parameter

Source Type	ESI	Ion Polarity	Positive	Set Nebulizer	0.3 Bar
Focus	Not active	Set Capillary	3800 V	Set Dry Heater	180 °C
Scan Begin	50 m/z	Set End Plate Offset	-500 V	Set Dry Gas	4.0 l/min
Scan End	2000 m/z	Set Collision Cell RF	2500.0 Vpp	Set Divert Valve	Source

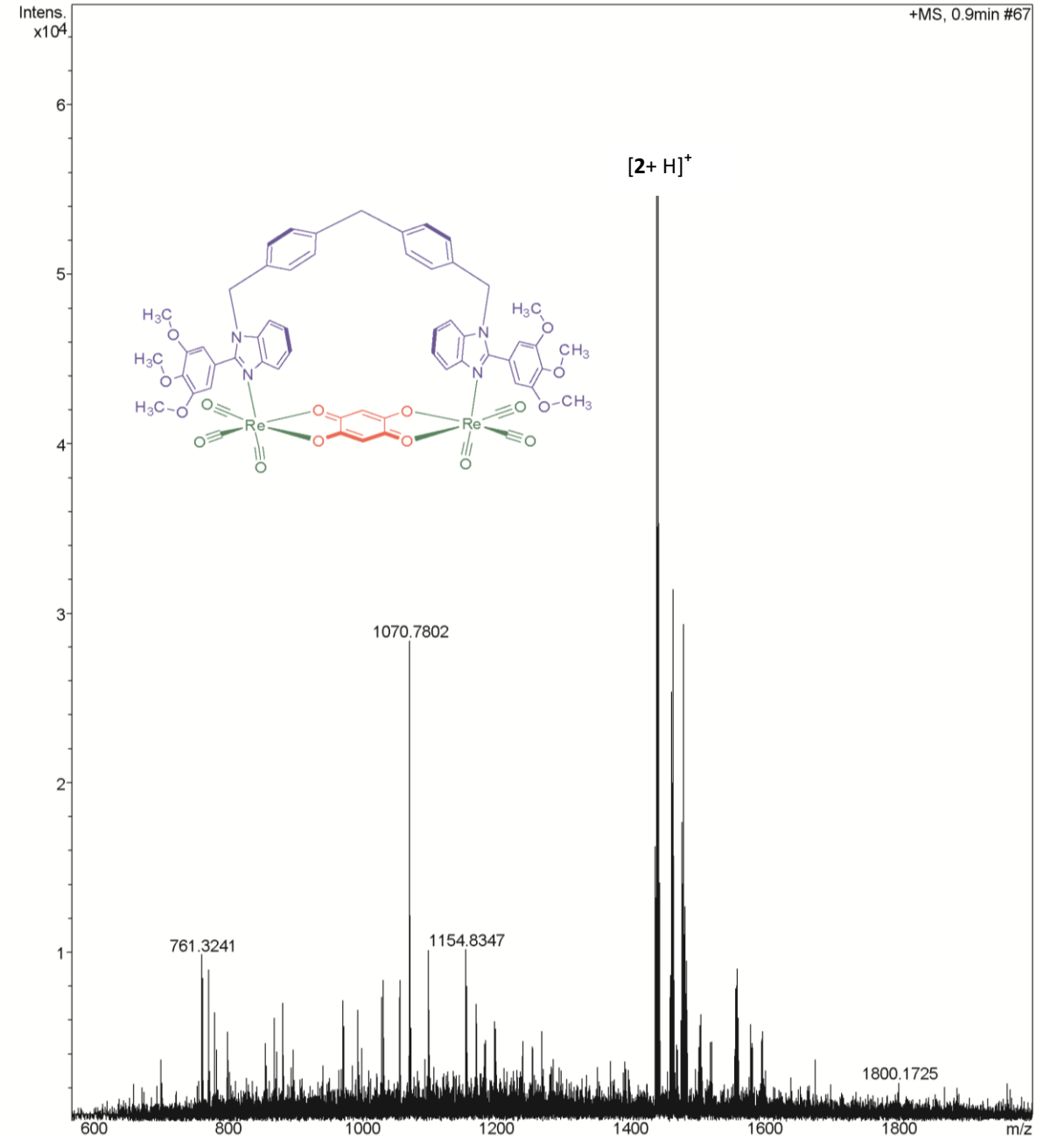

Figure 3.28. ESI mass spectrum of **2** in positive ion mode.

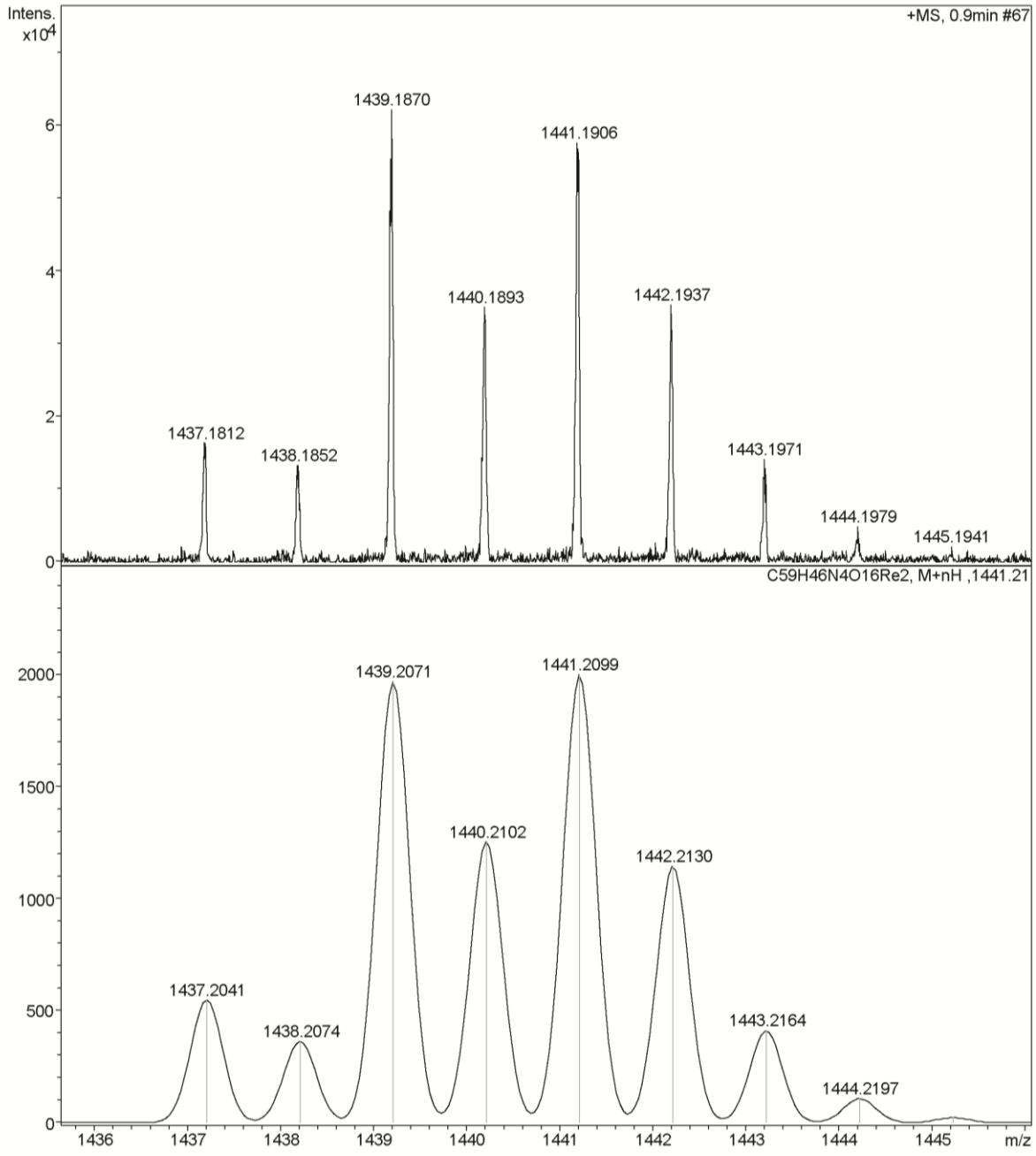

Figure 3.29. Experimental (top) and calculated (below) ESI mass spectrum of **2** in positive ion mode.

Analysis Info

Analysis Name	D:\Data\2021-data\PROF.MS\DEC\MB5-14 R1.d	Acquisition Date	12/2/2021 3:09:03 PM
Method	tune_high_Pos.m	Operator	BDAL
Sample Name	MB5-14 R1	Instrument	maXis 255552.10138
Comment			

Acquisition Parameter

Source Type	ESI	Ion Polarity	Positive	Set Nebulizer	0.3 Bar
Focus	Not active	Set Capillary	3800 V	Set Dry Heater	180 °C
Scan Begin	300 m/z	Set End Plate Offset	-500 V	Set Dry Gas	4.0 l/min
Scan End	3000 m/z	Set Charging Voltage	0 V	Set Divert Valve	Waste
		Set Corona	0 nA	Set APCI Heater	0 °C

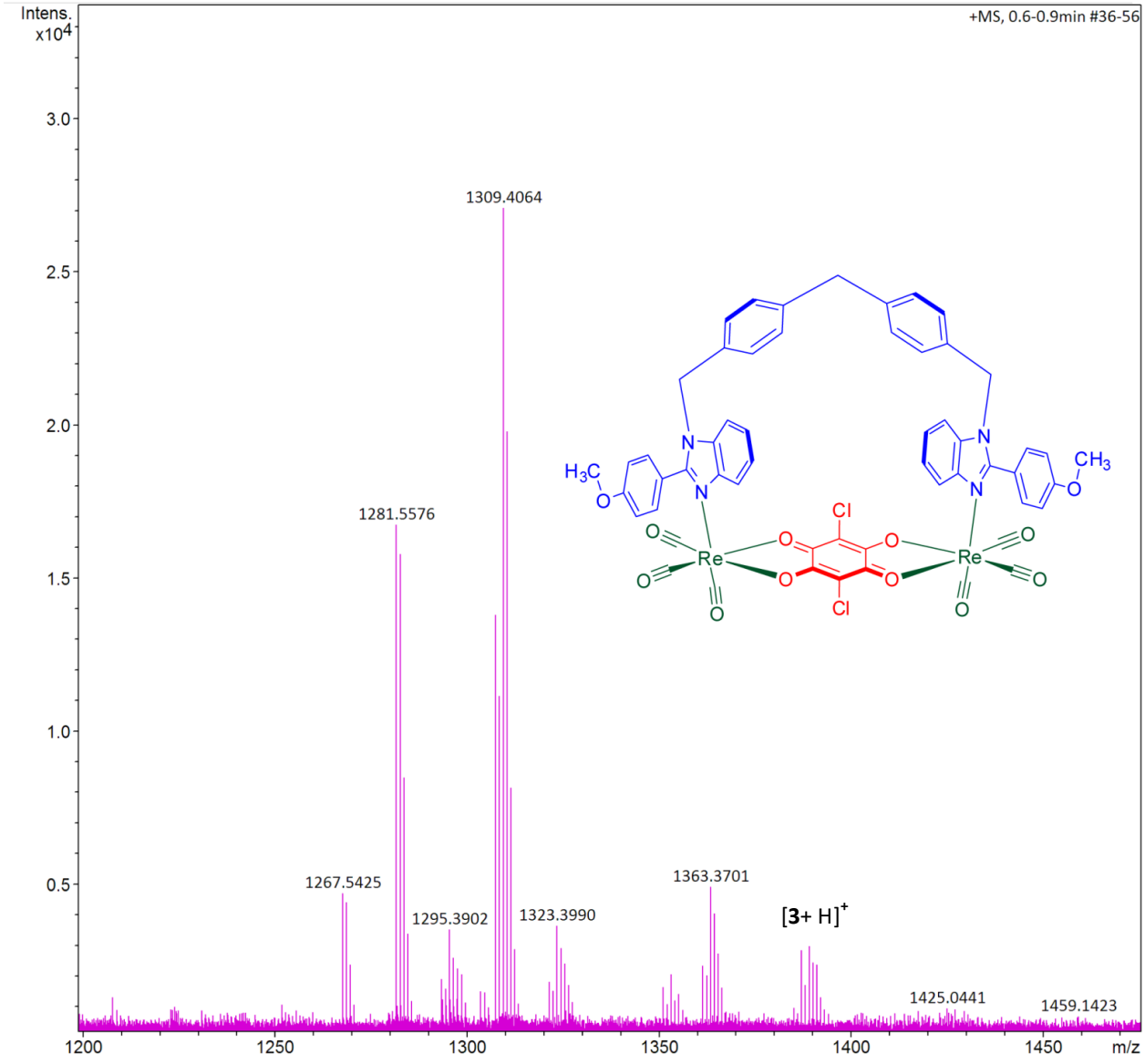

Figure 3.30. ESI mass spectrum of **3** in positive ion mode.

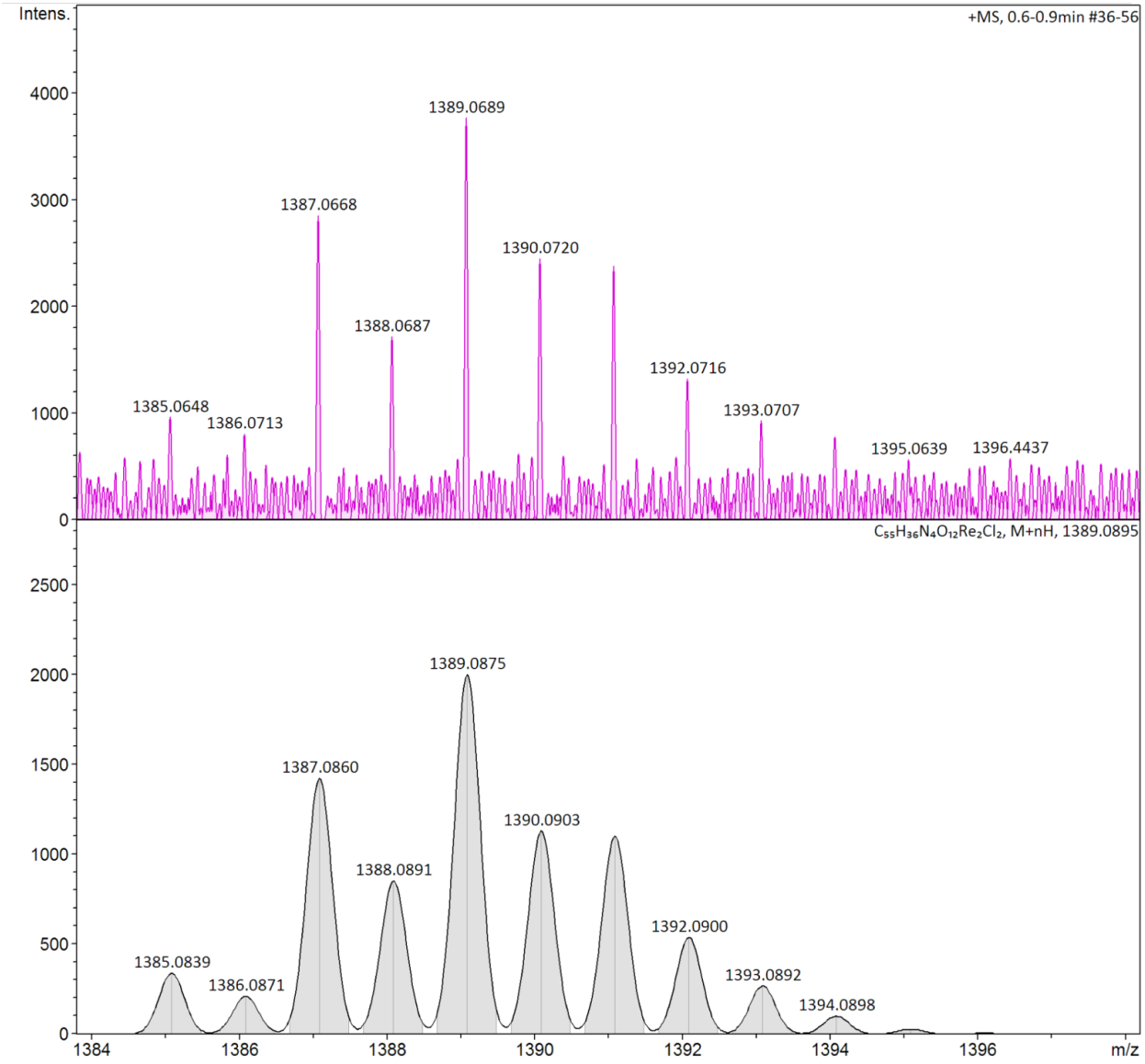

Figure 3.31. Experimental (top) and calculated (below) ESI mass spectrum of **3** in positive ion mode.

Analysis Info

Analysis Name	D:\Data\2019\PROF.MS\NOV\MB-4-47-CRYSTAL-1.d	Acquisition Date	11/13/2019 12:52:08 AM
Method	tune_high_Pos.m	Operator	UOH-Chemistry
Sample Name	MB-4-47-CRYSTAL	Instrument	maXis 10138
Comment			

Acquisition Parameter

Source Type	ESI	Ion Polarity	Positive	Set Nebulizer	0.3 Bar
Focus	Not active	Set Capillary	3800 V	Set Dry Heater	180 °C
Scan Begin	700 m/z	Set End Plate Offset	-500 V	Set Dry Gas	4.0 l/min
Scan End	3000 m/z	Set Collision Cell RF	2500.0 Vpp	Set Divert Valve	Waste

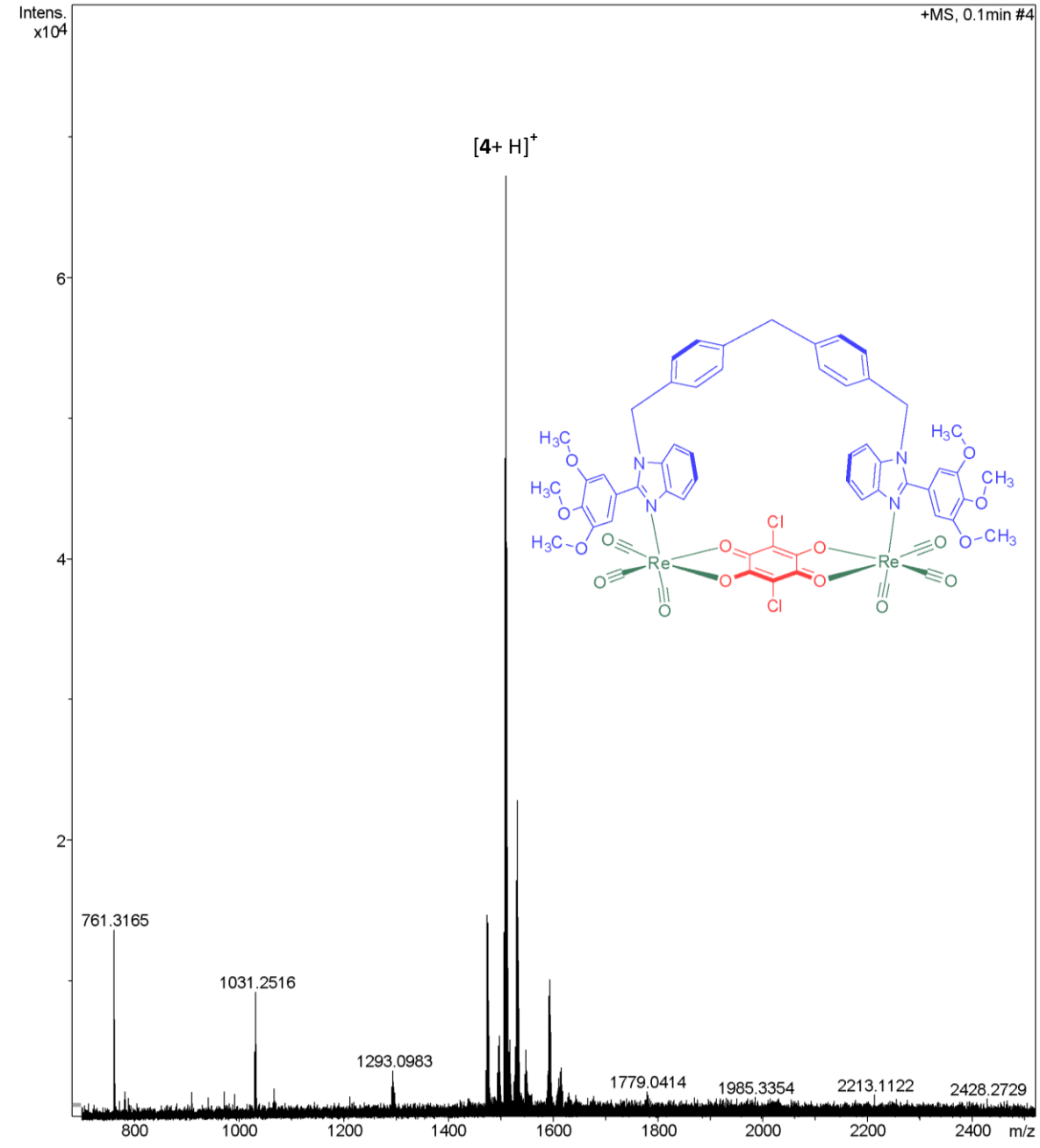

Figure 3.32. ESI mass spectrum of **4** in positive ion mode.

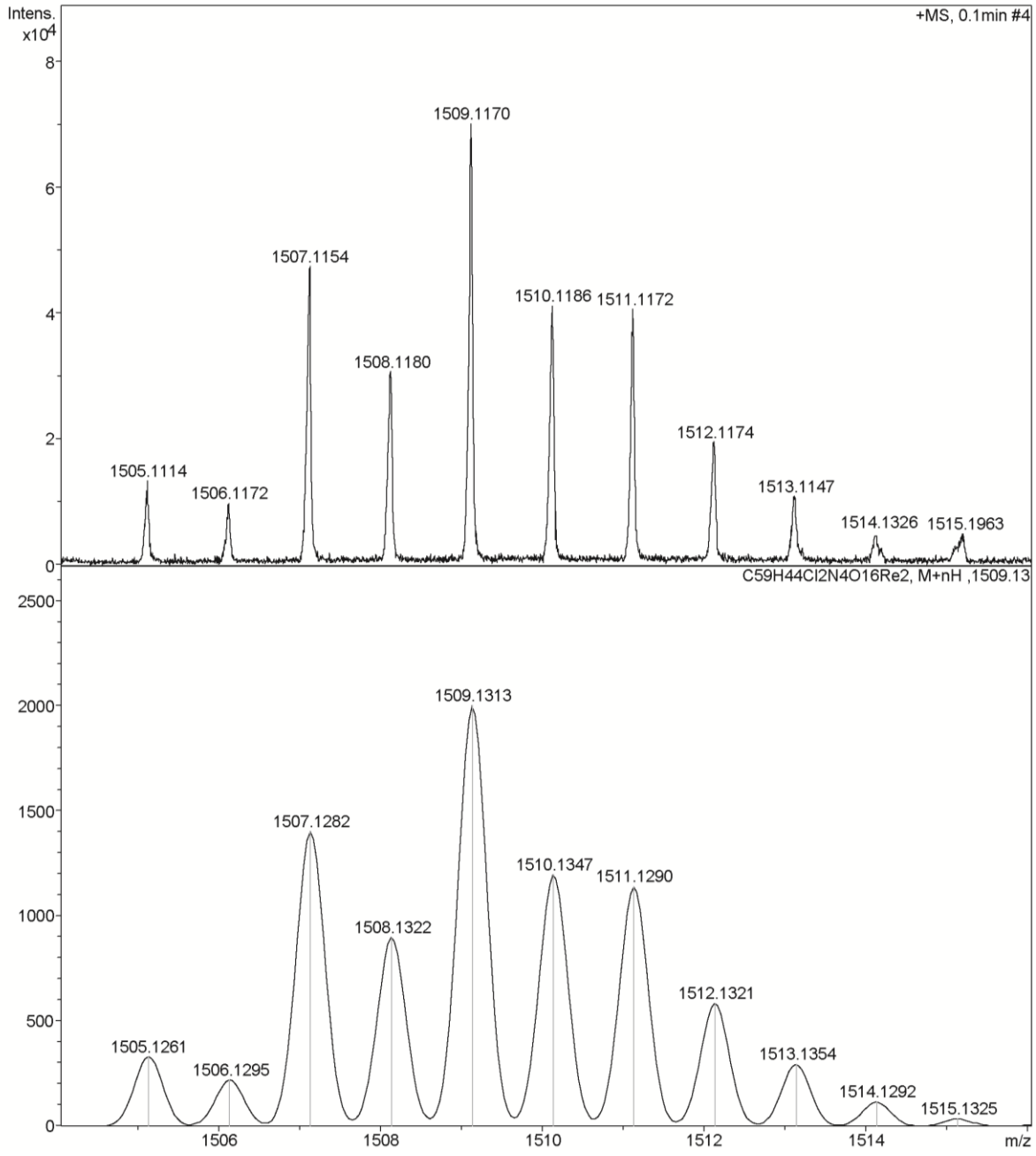

Figure 3.33. Experimental (top) and calculated (below) ESI mass spectrum of **4** in positive ion mode.

Display Report

Analysis Info

Analysis Name	D:\Data\2021-data\PROF.MS\NOV\MB4-68 R4-FA.d	Acquisition Date	11/15/2021 12:48:22 PM
Method	tune_wide_Pos.m	Operator	BDAL
Sample Name	MB4-68 R4-FA	Instrument	maXis 255552.10138
Comment			

Acquisition Parameter

Source Type	ESI	Ion Polarity	Positive	Set Nebulizer	0.3 Bar
Focus	Not active	Set Capillary	3800 V	Set Dry Heater	180 °C
Scan Begin	200 m/z	Set End Plate Offset	-500 V	Set Dry Gas	4.0 l/min
Scan End	3000 m/z	Set Charging Voltage	0 V	Set Divert Valve	Source
		Set Corona	0 nA	Set APCI Heater	0 °C

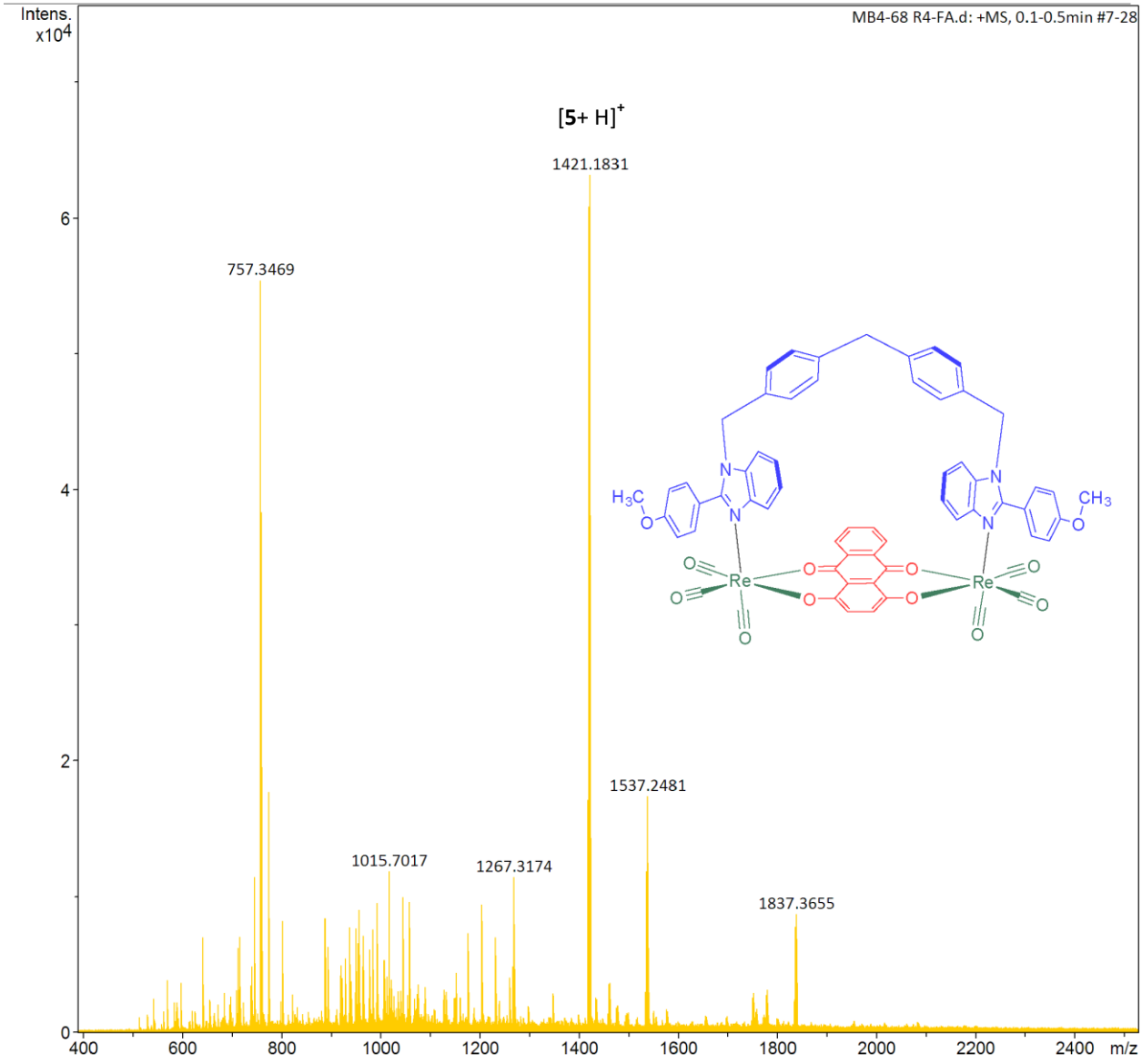

Figure 3.34. ESI mass spectrum of **5** in positive ion mode.

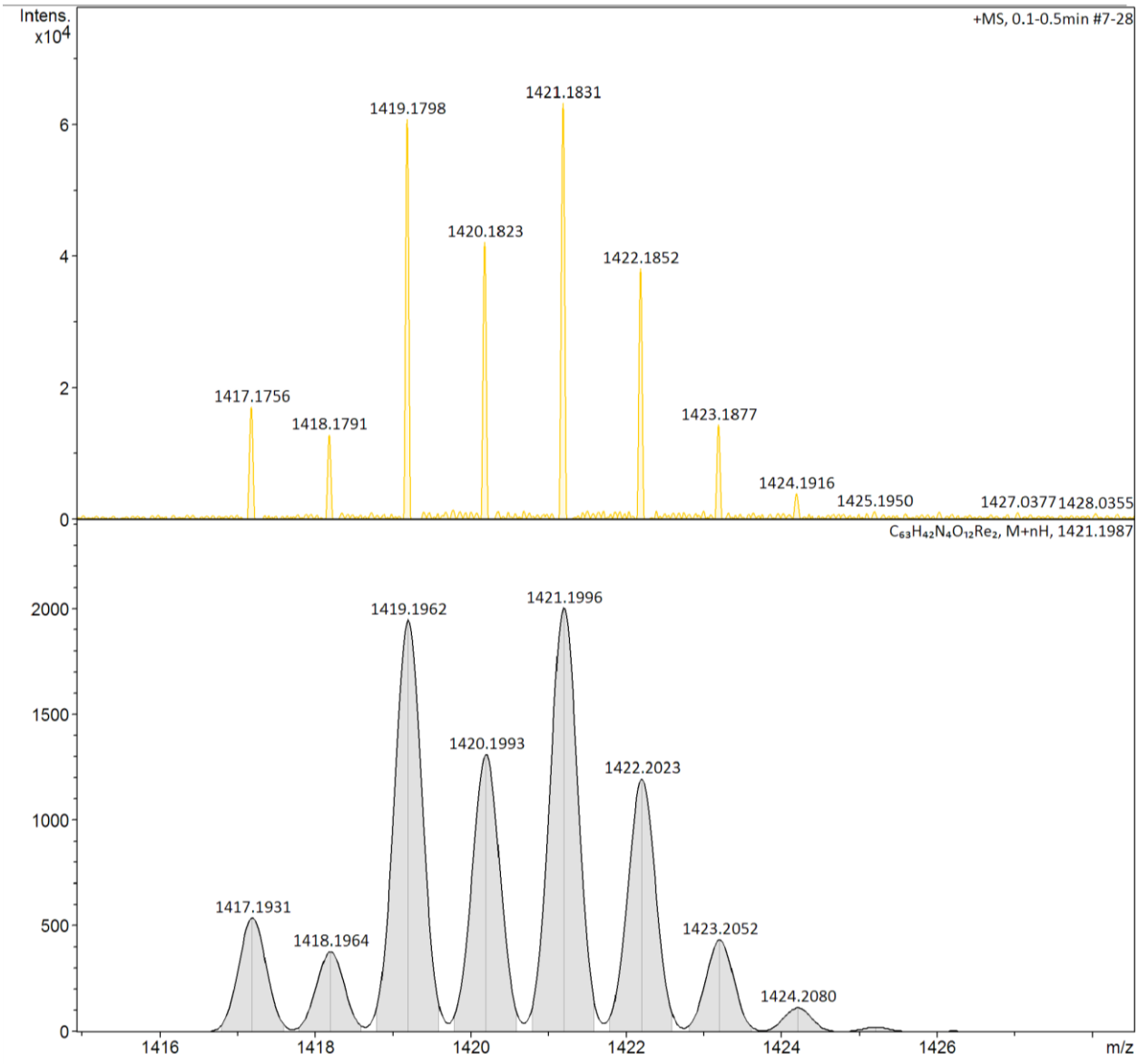

Figure 3.35. Experimental (top) and calculated (below) ESI mass spectrum of **5** in positive ion mode.

Analysis Info

Analysis Name	D:\Data\2021-data\PROF.MS\NOV\MB-4-18R.d	Acquisition Date	11/22/2021 12:54:35 PM
Method	tune_low.m	Operator	BDAL
Sample Name	MB-4--18R	Instrument	maXis 255552.10138
Comment			

Acquisition Parameter

Source Type	ESI	Ion Polarity	Positive	Set Nebulizer	0.3 Bar
Focus	Not active	Set Capillary	4500 V	Set Dry Heater	180 °C
Scan Begin	50 m/z	Set End Plate Offset	-500 V	Set Dry Gas	4.0 l/min
Scan End	2000 m/z	Set Charging Voltage	0 V	Set Divert Valve	Waste
		Set Corona	0 nA	Set APCI Heater	0 °C

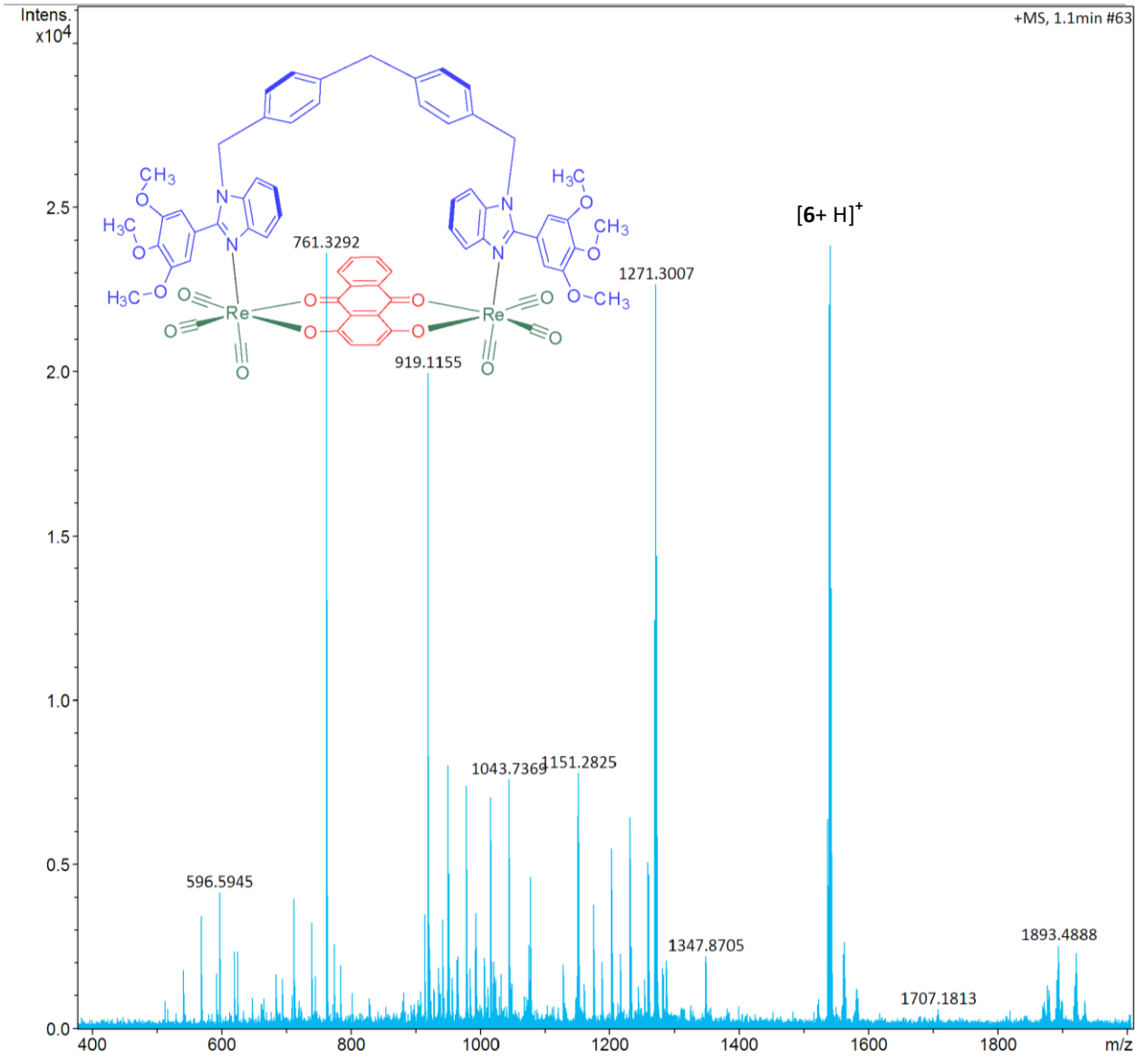

Figure 3.36. ESI mass spectrum of **6** in positive ion mode.

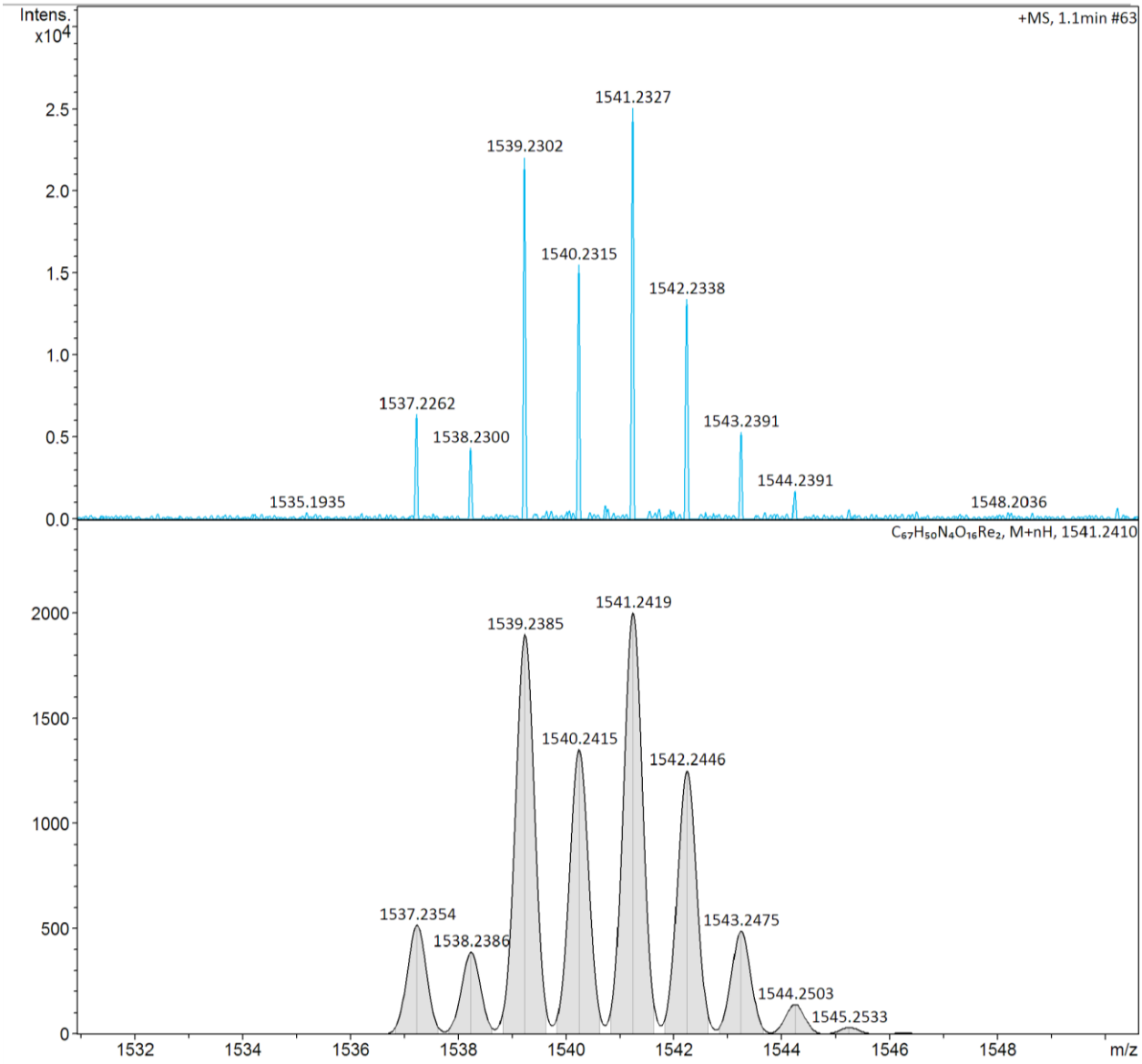

Figure 3.37. Experimental (top) and calculated (below) ESI mass spectrum of **6** in positive ion mode.

Analysis Info

Analysis Name	D:\Data\2021-data\PROF.MS\NOV\MB-4-81-R.d	Acquisition Date	11/29/2021 12:49:54 PM
Method	tune_low.m	Operator	BDAL
Sample Name	MB-4-81	Instrument	maXis 255552.10138
Comment			

Acquisition Parameter

Source Type	ESI	Ion Polarity	Positive	Set Nebulizer	0.3 Bar
Focus	Not active	Set Capillary	4500 V	Set Dry Heater	180 °C
Scan Begin	50 m/z	Set End Plate Offset	-500 V	Set Dry Gas	4.0 l/min
Scan End	2000 m/z	Set Charging Voltage	0 V	Set Divert Valve	Waste
		Set Corona	0 nA	Set APCI Heater	0 °C

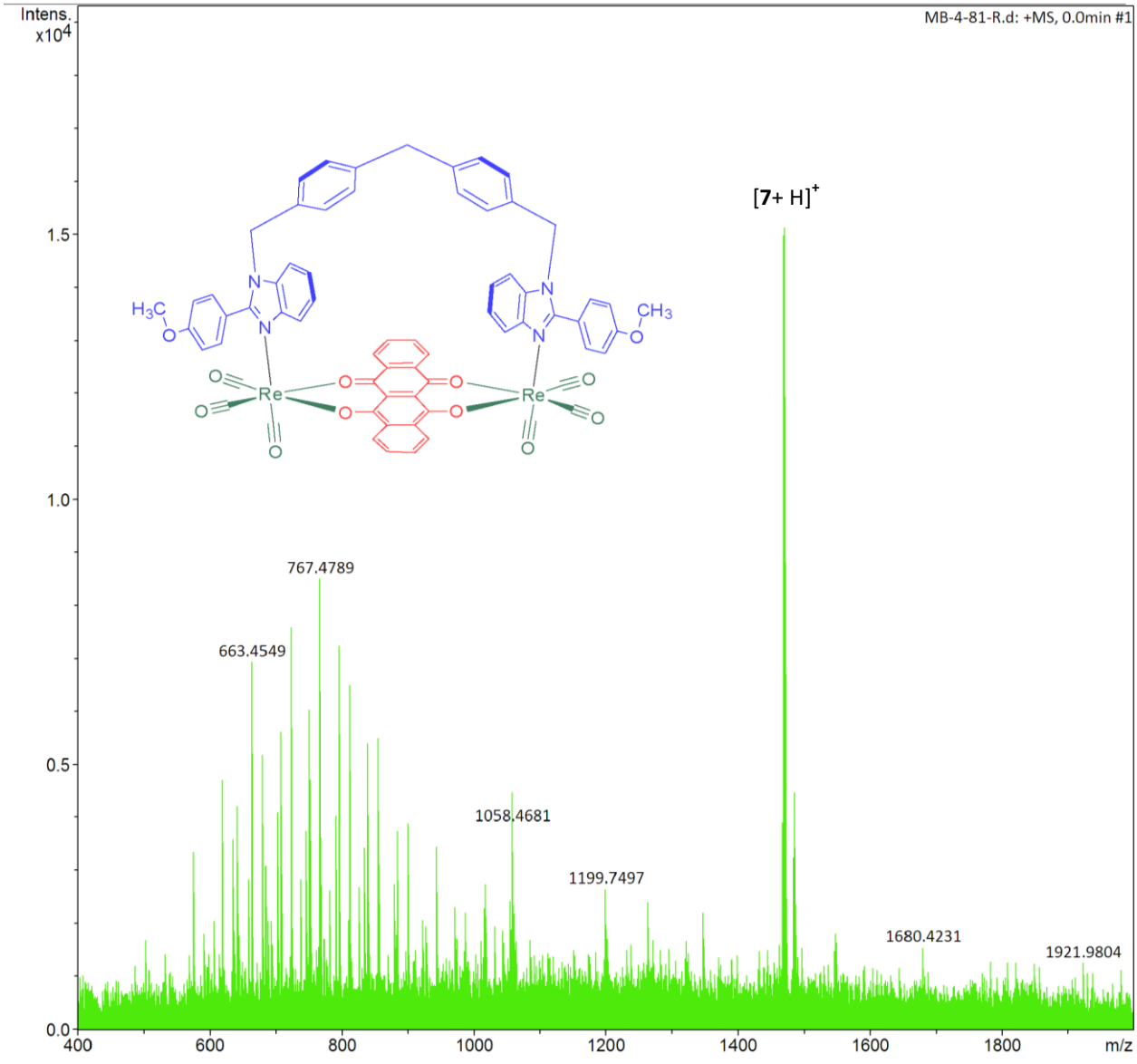

Figure 3.38. ESI mass spectrum of **7** in positive ion mode.

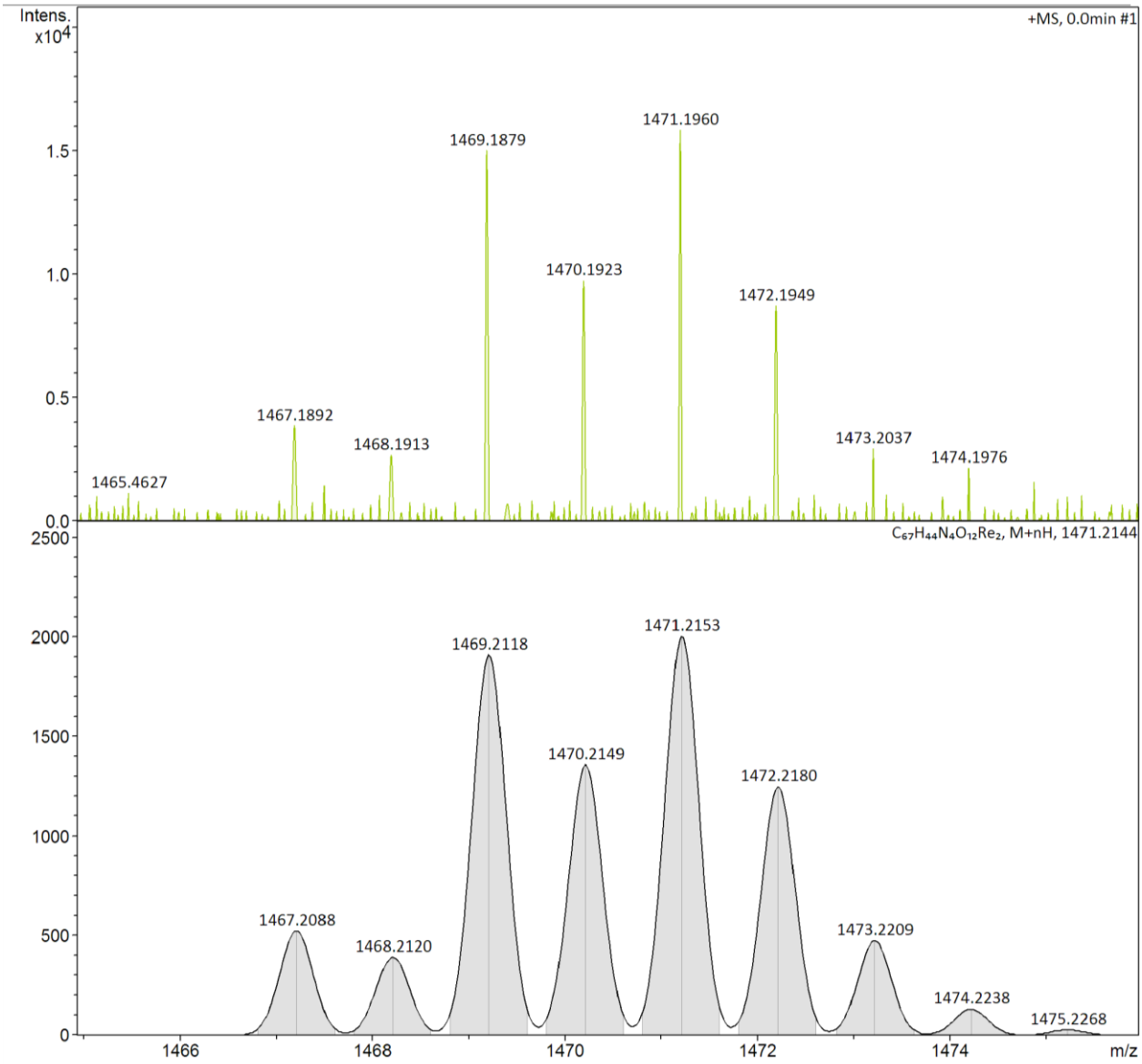

Figure 3.39. Experimental (top) and calculated (below) ESI mass spectrum of **7** in positive ion mode.

Analysis Info

Analysis Name	D:\Data\2021-data\PROF.MS\DEC\MB4-82 R3.d	Acquisition Date	12/7/2021 4:01:12 PM
Method	tune_wide_Pos.m	Operator	BDAL
Sample Name	MB4-82 R3	Instrument	maXis 255552.10138
Comment			

Acquisition Parameter

Source Type	ESI	Ion Polarity	Positive	Set Nebulizer	0.3 Bar
Focus	Not active	Set Capillary	3800 V	Set Dry Heater	180 °C
Scan Begin	200 m/z	Set End Plate Offset	-500 V	Set Dry Gas	4.0 l/min
Scan End	3000 m/z	Set Charging Voltage	0 V	Set Divert Valve	Source
		Set Corona	0 nA	Set APCI Heater	0 °C

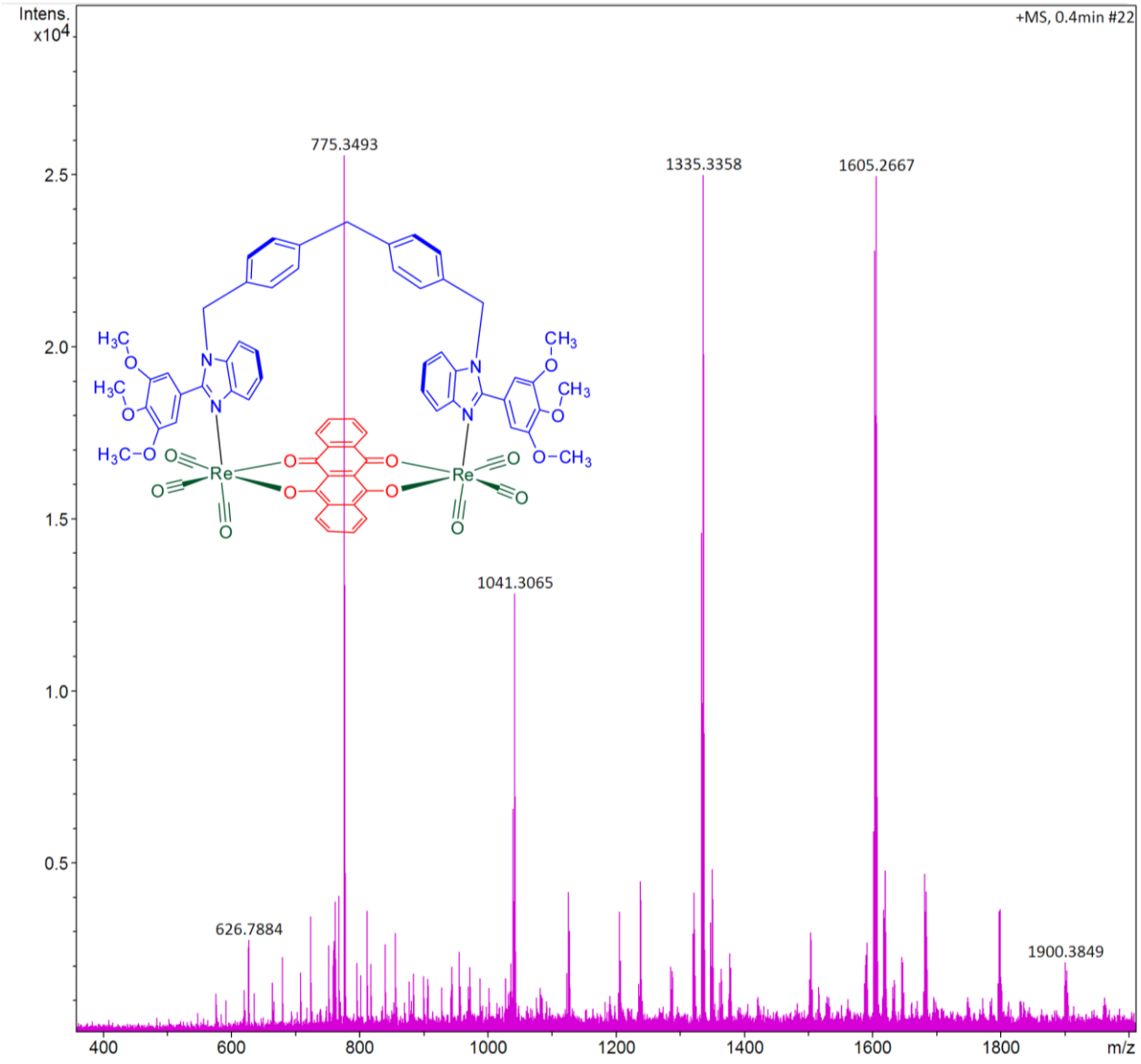

Figure 3.40. ESI mass spectrum of **8** in positive ion mode.

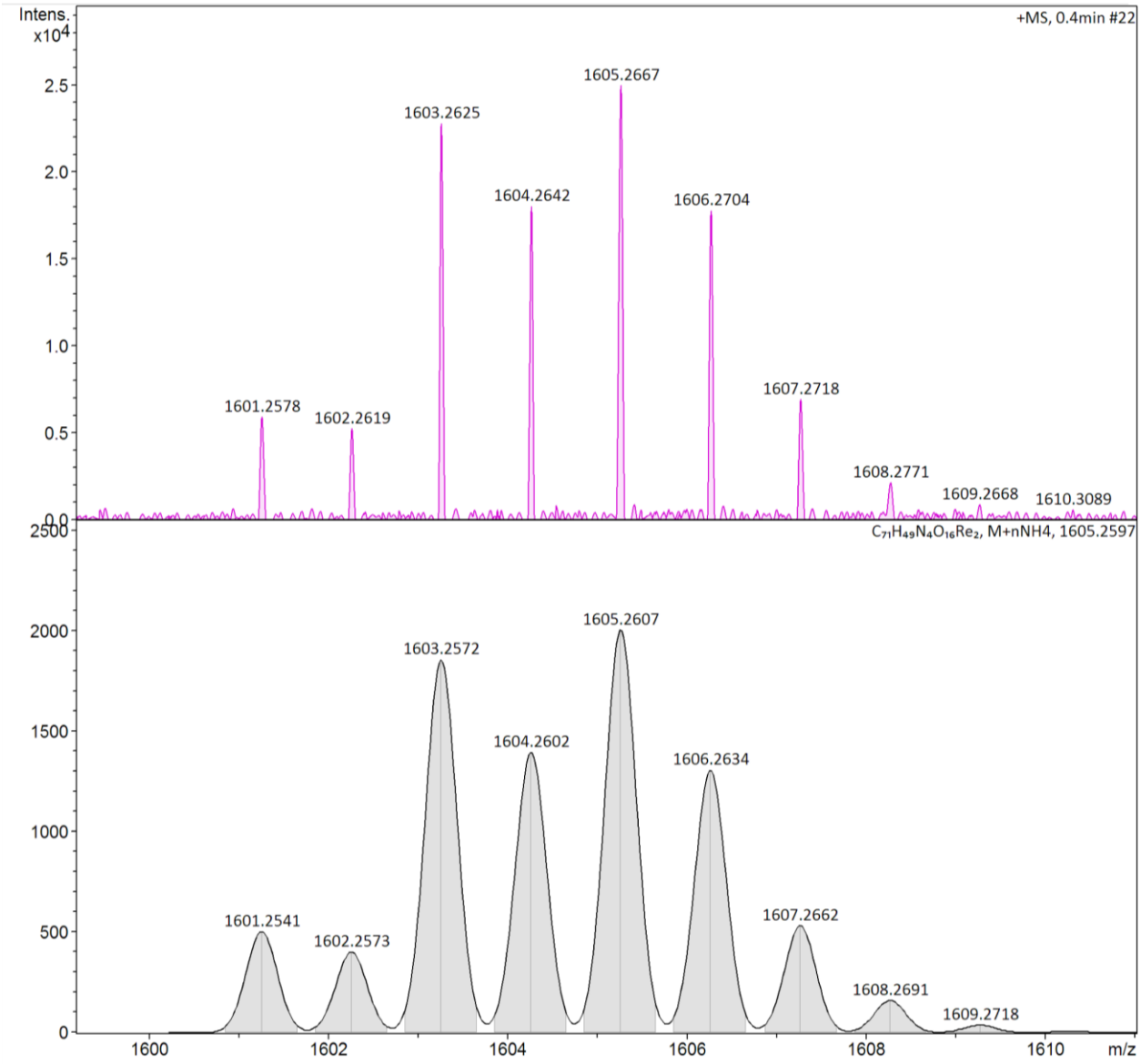

Figure 3.41. Experimental (top) and calculated (below) ESI mass spectrum of **8** in positive ion mode.

3.3.3. Crystal structures of metallocavitands.

Crystals of **1**, **2**, **4**, **6**, and **7** were obtained by either directly from the solvothermal reactions or by slow evaporation of the solution obtained from the solvothermal reactions at room temperature. The structures of the complexes were confirmed by the single-crystal X-ray diffraction method. All the complexes adopt an M_2LL'-type metallomacrocyclic structure and consist of two *fac*-$Re(CO)_3$ cores, one $dhbq^{2-}/CA^{2-}/dhaq^{2-}/dhnq^{2-}$ (E^{2-}) motif, and one L^1/L^2 motif (Figure 3.42- 3.43). The rigid E^{2-} motif binds two rhenium ions using its four oxygen atoms in a symmetrical bis-chelating manner resulting in (2+1) assembly of *fac*–$[(CO)_3Re(\mu–E)Re(CO)_3]$. Ligand L^1/L^2 acts as an arc-type bidentate clip and binds two rhenium ions of the binuclear assembly using the benzimidazolyl nitrogen atom, leading to the distorted pentagonal tubular architecture. Therefore, the complexes can be considered as metallacalix[5]arene in which the hetero(arene) units (two benzimidazolyl-, and two *p*-phenylene-motifs), E^{2-} motif, three methylene (–CH_2–) groups and two rhenium ions in the metallomacrocycle are related to the five *p*-phenylene frames, three methylene (–CH_2–) groups, and two methylene (–CH_2–) cores of calix[5]arene, respectively. To the best of our knowledge, these complexes are the second examples of heteroleptic *fac*-$Re(CO)_3$-based metallacalix[5]arene.[16] Important parameters describing the metallomacrocyclic structures are given in Table 3.1. The size of the cyclic framework of the compounds is described on the basis of the two adjacent connectors (Re···Re, Re···CH_2, CH_2···CH_2, CH_2···CH_2, and CH_2···Re) of hetero(arene)/E^{2-} motifs. Among the two *p*-phenylene units of L^1/L^2 in the metallomacrocycles, one unit is twisted with respect to the other unit presumably either to have effective non-covalent interactions with the guest molecule residing in the cyclic cavity and/or to avoid steric interactions between the two *o*-hydrogen atoms of the two *p*-phenylene motifs. The two substituents, 4-methoxyphenyl or 3,4,5-trimethoxyphenyl motifs, decorated at the lower rim of the metallomacrocycles are parallel to each other and perpendicular to the benzimidazolyl motif. The two *p*-methoxy units in **1** and **7** are directed away from each other, resulting in an extended hydrophobic cavity containing molecular tubes. In the case of **2**, **4**, and **6**, the two *m*-methoxy units are directed towards each other, resulting in a pentagonal cylindrical bowl.

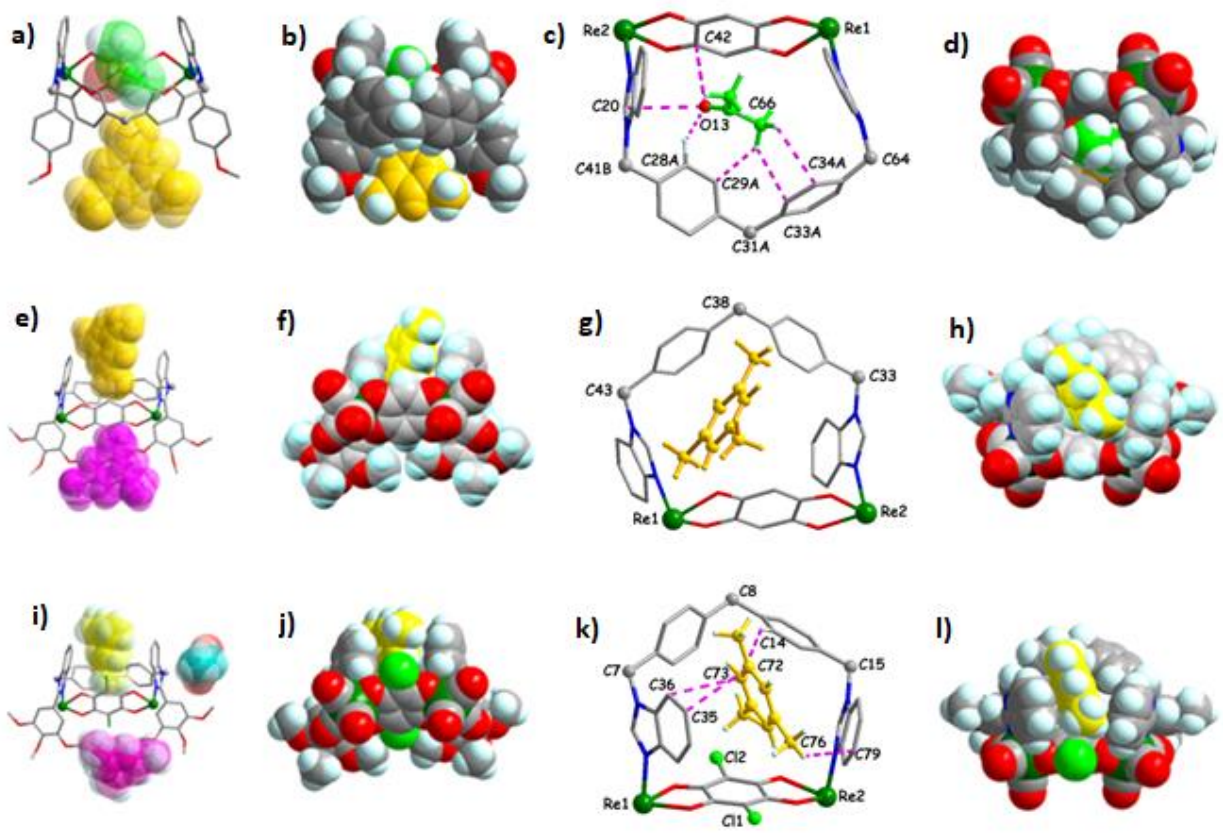

Figure 3.42. Various views of molecular structures of **1** (a-d), **2** (e-h), and **4** (i-l) with guest molecules (H atoms of metallocavitand are removed for clarity in a, c, e, g, i, and k; CO units and methoxyphenyl units are omitted to show the metallocavitand framework clearly in c, g, and k; C = gray, H= pale blue, Cl = pale green, N = blue, O= red, Re= green, guest acetone = green and red, guest mesitylene = yellow, lattice mesitylene = pink, lattice acetone = sky and orange.

All the metallomacrocycles crystallize with one or more solvent molecules and accommodate one solvent molecule as a guest in their cyclic hydrophobic internal cavity. For example, compound **1** crystallizes with one acetone and one mesitylene. Among the two guest molecules, acetone occupies the center of the internal cavity of the complex. The plane of the acetone is parallel to the dhbq plane and perpendicular to the two benzimidazolyl planes. Cumulative C–H$^{\cdots}\pi$, C–H$^{\cdots}$O and lone pair-π interactions were found between the acetone and the framework of the host. The mesitylene solvent almost occupies the cavity present at the lower rim and the extended cavity available between the two phenoxy units.

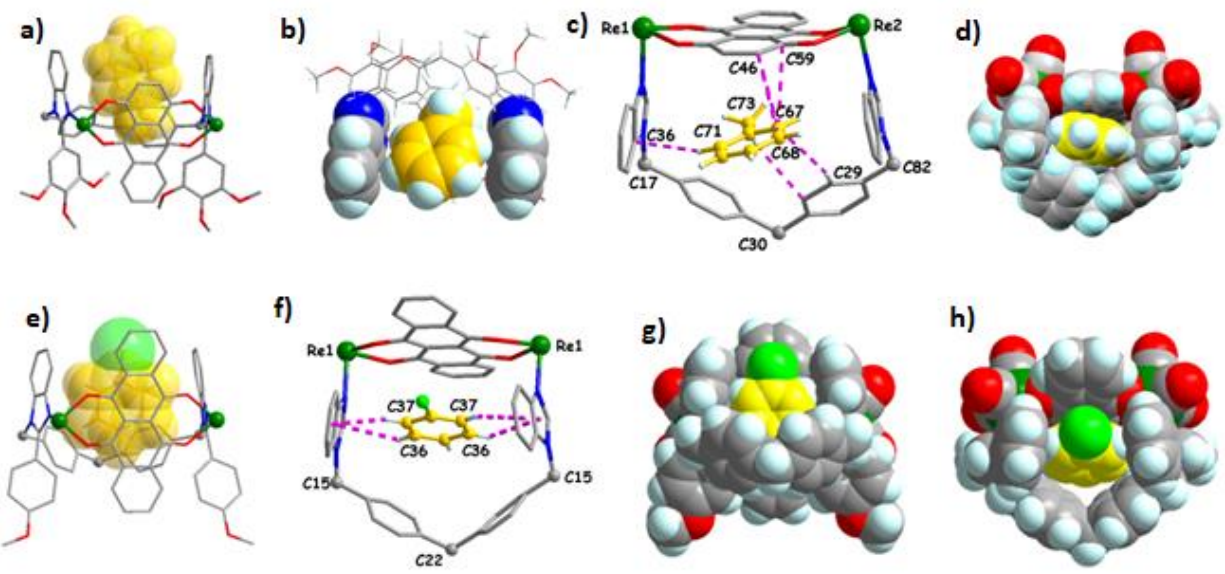

Figure 3.43. Various views of molecular structures of **6** (a-d), and **7** (e-h) with guest molecules (H atoms of metallocavitand are removed for clarity in a, c, e, and f; CO units and methoxyphenyl units are omitted to show the metallocavitand framework clearly in c, and f; C = gray, H= pale blue, Cl = pale green, N = blue, O= red, Re= green, toluene = yellow, chlorobenzene = yellow and green.

Table 3.1. Structural parameters of the metallocavitands.

complex	*perimeters of molecular pentagons:* ~*d*, Å: Re···Re, Re···CH_2, CH_2···CH_2, CH_2···CH_2, CH_2···Re (Å)	~τ° (benz)[a] and ~H···H (Å)[b] (benz)	τ° (phenyl)[c]	Guest(s)
1	8.08, 5.72, 5.75, 5.85, 5.71	35 and 6.69, 7.72	67	acetone mesitylene
2	8.09, 5.71, 5.82, 5.82, 5.75	27 and 7.14, 8.08	77	mesitylene
4	8.10, 5.70, 5.80, 5.83, 5.71	27 and 7.51, 6.74	81	mesitylene
6	8.49, 5.75, 5.84, 5.83, 5.75	16 and 10.35, 9.82	65	toluene
7	8.62, 5.70, 5.78, 5.78, 5.73	23 and 7.87, 7.83	48, 73	chlorobenzene

[a]dihedral angle between two benzimidazolyl motifs; [b]non-bonding distances between the H atoms of the oppositely arranged benzimidazolyl motifs; [c]dihedral angle between two *p*-phenylene motifs.

The molecular pentagons **2**, **4**, **6**, and **7** accommodate mesitylene, toluene, and chlorobenzene, respectively, in the hydrophobic internal cavity. Multiple non-covalent contacts (C–H$^{\cdots}\pi$ or/and $\pi^{\cdots}\pi$ interactions) were found between the guest and the cyclic framework of the host. A portion of the mesitylene molecule resides in the internal cavity of **2** and **4**, whereas a full molecule of toluene/chlorobenzene occupies the cavity of **6** and **7**. The different arrangement of the guest molecules in the cavity of the complexes correlates with the different sizes and electronic environment of the cyclic framework due to varying the bridging motifs (E^{2-}). The results further indicate that the molecular pentagons **6** and **7** are the most suitable host for mono-substituted benzene molecules.

The crystal structures of the metallamacrocycles were stabilized by various types of non-covalent interactions. Metallomacrocycles **1** arrange to form a tubular structure (Figure 3.44). Solvent molecules reside only in the non-covalent tubes in **1**. Metallamacrocycles **4** also forms a tubular structure (Figure 3.45). In addition, two one-dimensional voids are present that is perpendicular to the tubular structure of **4**. Both lattice acetone and lattice mesitylene molecules occupy the void space in **4**. Complex **6** packs in such a way that solvent mesitylene molecule resides in the lattice cavity created by four neighboring molecules which contacts each other through various non-covalent interactions (Figure 3.46). Each macrocycle **7** interacts with two neighboring macrocycles along the tubular axis (Figure 3.47).

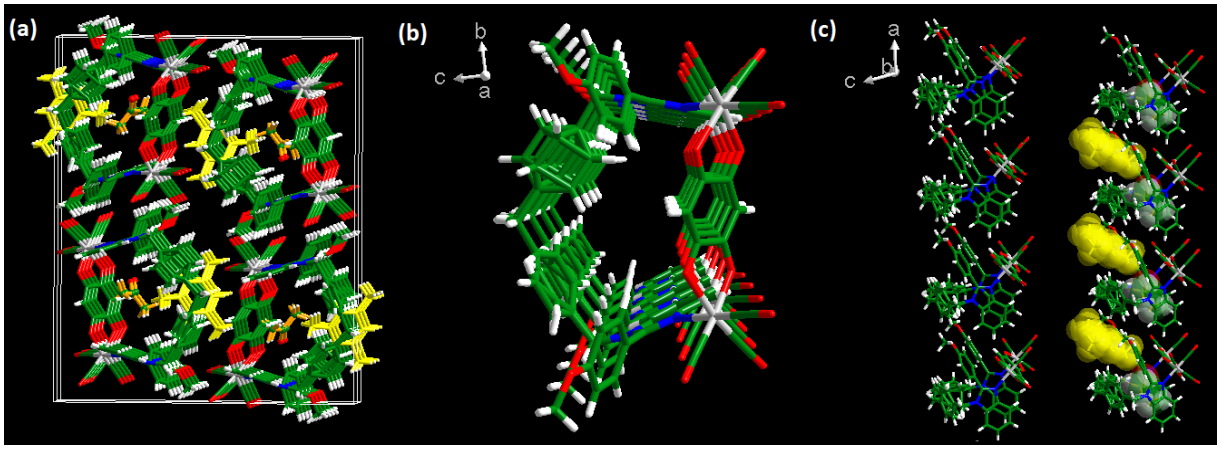

Figure 3.44 (a) Partial packing diagram of **1** showing the tubular arrangement of neighboring metallocavitands with guest acetone molecules (green and red) and lattice mesitylene molecules (yellow, stick representation) (b) One set of tubular framework of "a" without guest molecules. (c) Side view of "b" with and without guest molecules.

The space (cavity) below the lower rim of one molecule is occupied by the portion of dhnq unit of the neighboring molecule. Mesityelene is not sterically possible to fit completely in the hydrophobic cavity of metallomacrocycles **1**, **2**, and **4** due to the overall size, whereas toluene and chlorobenzene are fully occupied in the hydrophobic cavity of metallomacrocycles **6** and **7**.

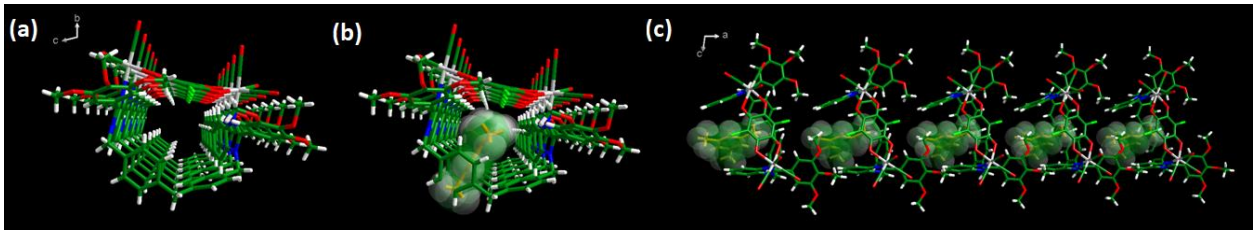

Figure 3.45. (a-b) Partial packing diagram of **4** showing the tubular arrangement of neighboring metallocavitands without and with guest mesitylene molecules (green and white) (c) side view of "b".

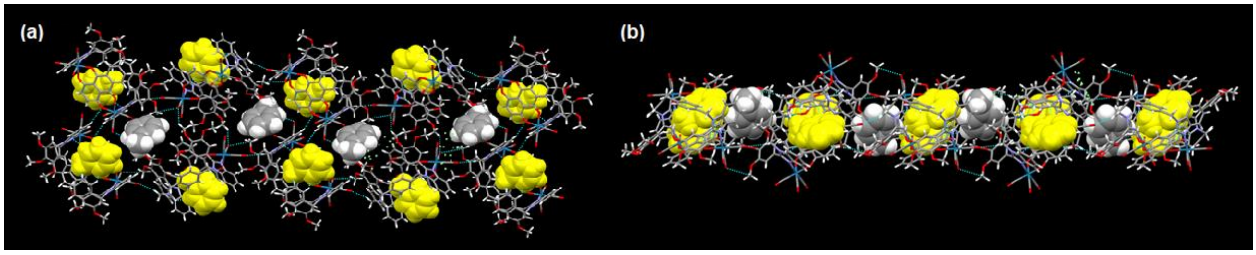

Figure 3.46. Two different views of partial packing diagram of metallocavitand **6** (stick representation) with guest toluene (yellow), and lattice toluene (gray and white).

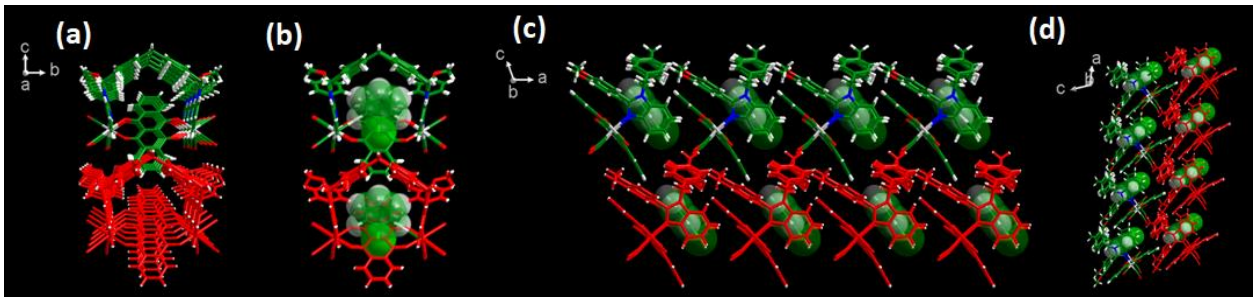

Figure 3.47. (a-b) Partial packing diagram of **7** showing the tubular arrangement of neighboring metallocavitands without and with guest chlorobenzene molecules (green and white) (c-d) two different side views of "b".

3.3.4. Photophysical properties of the ligands and the complexes.

The UV-Vis absorption spectra of L^1 and L^2 show strong absorption bands with maxima *ca*~296 nm in DMSO (Table 3.2). The bands are attributed to spin-allowed π–π* electronic transitions of the aromatic motifs of the ligands. Complexes **1**–**4** displayed intense absorption bands in the UV-region similar to that of the ligands in DMSO. In addition, complexes **1**–**4** show moderate broad absorption bands in the range of 400-650 nm (λ_{max}, nm = ~493 for **1**, ~489 for **2**, ~505 for **3** and **4**). These bands may be assigned to metal-to-ligand charge transfer (MLCT) transitions from rhenium core to the bis-chelating framework (Re → dhbq/CA) and intra-ligand charge transfer (ILCT) transitions of quinonoid motif (dhbq/CA→ dhbq/CA) in the complexes.[12e,22] Complexes **5-8** show strong absorption bands at high energy region, medium broad absorption bands in the range of ~350-540 nm, and structured weak absorption bands in the range of 550-700 nm. The absorption spectra of **5**–**8** are similar to previously reported metallocycles (*fac*-[{$(CO)_3Re(\mu-E)Re(CO)_3$}(μ−L)]**I**–**II**, where E = dhaq for **I**, E = dhnq for **II**, and L = 1,4-bis(5,6-dimethylbenzimidazol-1-ylmethyl)naphthalene) containing almost similar chromophoric unit *fac*-[{$(CO)_3Re(\mu-E)Re(CO)_3$}(benzimidazolyl)].[23] The absorption bands around 400 nm may be ascribed to both MLCT- (Re → dhaq/dhnq)and LLCT-charge transfer transitions. The low energy absorptions of the complexes are ascribed to intra-ligand charge transfer (ILCT) transitions (dhaq/dhnq → dhaq/dhnq) mainly centered on $dhaq^{2-}$/$dhnq^{2-}$ motifs in the complexes.

Both the ligands display broad emission at ~363 nm in DMSO at room temperature (Table 3.2). The complexes containing monomethoxyphenyl-bezimidazolyl-based ligand framework (**1**, **3**, **5**, and **7**) and trimethoxyphenyl-bezimidazolyl-based ligand framework (**2**, **4**, **6**, and **8**) displayed structured emission around ~337, ~352, ~368 nm, and structureless emission around ~360 or ~363 nm, respectively. The emission of complexes **5** and **7** are blue shifted as compared to the free ligand. No emission was observed while exciting at other absorption bands for **5** and **7**. Complex **6** shows two different emission bands while exciting at two different absorption maxima. Similar to the other complexes, complex **6** displayed emission at ~360 nm when excited at ~285 nm. All the results show the origins of emission around ~363 nm are from the excited state of nitrogen donor motifs. In addition, the emission at the visible region ($\lambda_{em\ (max)}$ = 567 nm) was observed while exciting at 458 nm for compound **6**.

Table 3.2. Absorption and Emission Spectral Data for L^1, L^2, and 1–8 in DMSO at 298 K.

compounds	absorption	emission	
	λ_{max} (nm)	$\lambda_{exc,\ max}$ (nm)	$\lambda_{em,\ max}$ (nm)
L^1	296	296	363
L^2	296	296	363
1	283, 493	283	337, 352, 368
2	285, 489	285	363
3	285, 505	285	338, 352, 367
4	277, 505	277	364
5	262, 292, 405, 583, 626	292	337, 352, 369
6	260, 285, 458, 581, 626	285 458	360 567
7	276, 381, 551, 593	276	337, 353, 368
8	275, 383, 559, 591	275	360

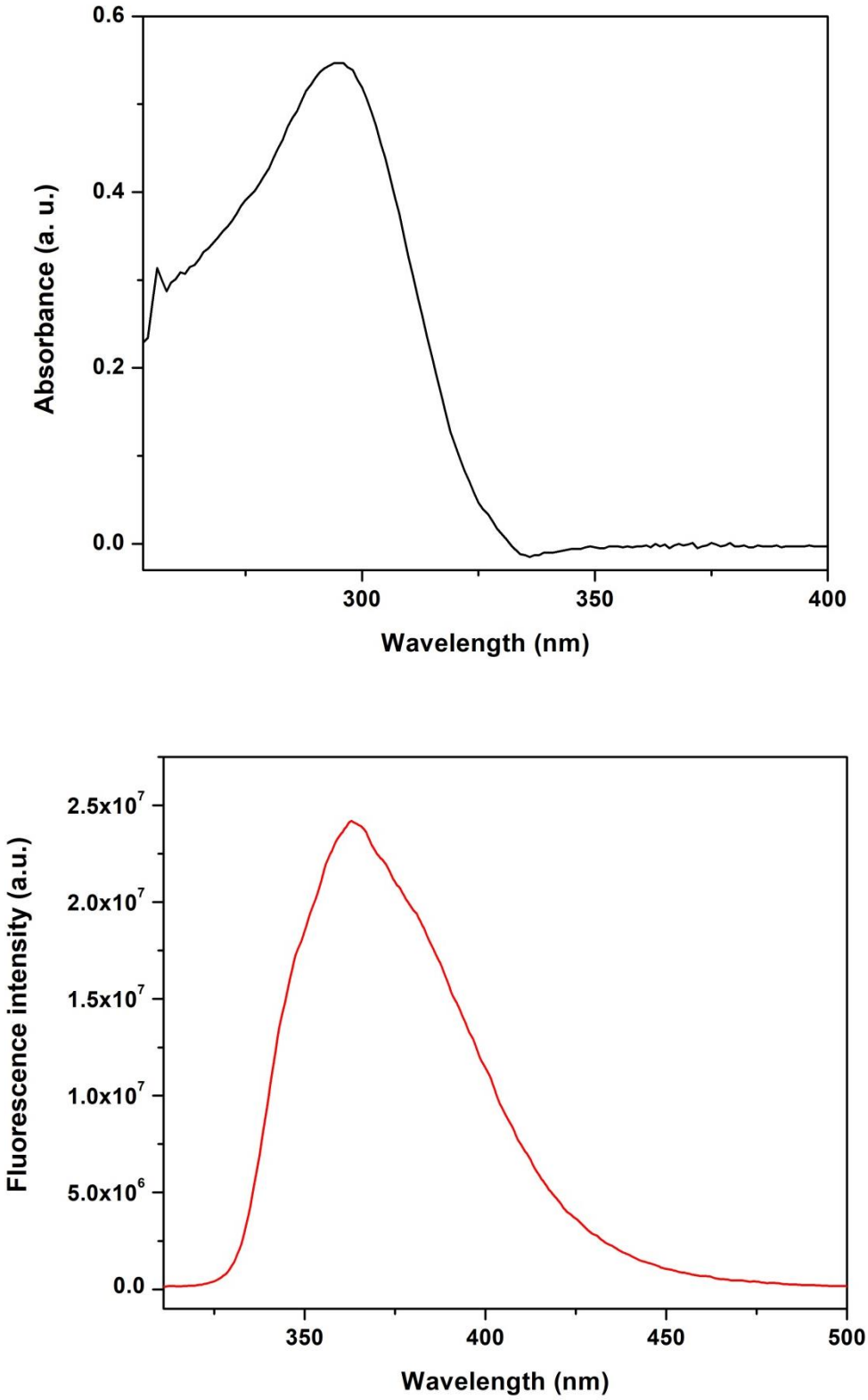

Figure 3.48. Absorption (top) and emission (bottom) spectra of L^1 in DMSO (0.2×10^{-4} M, λ_{exc} = 296 nm).

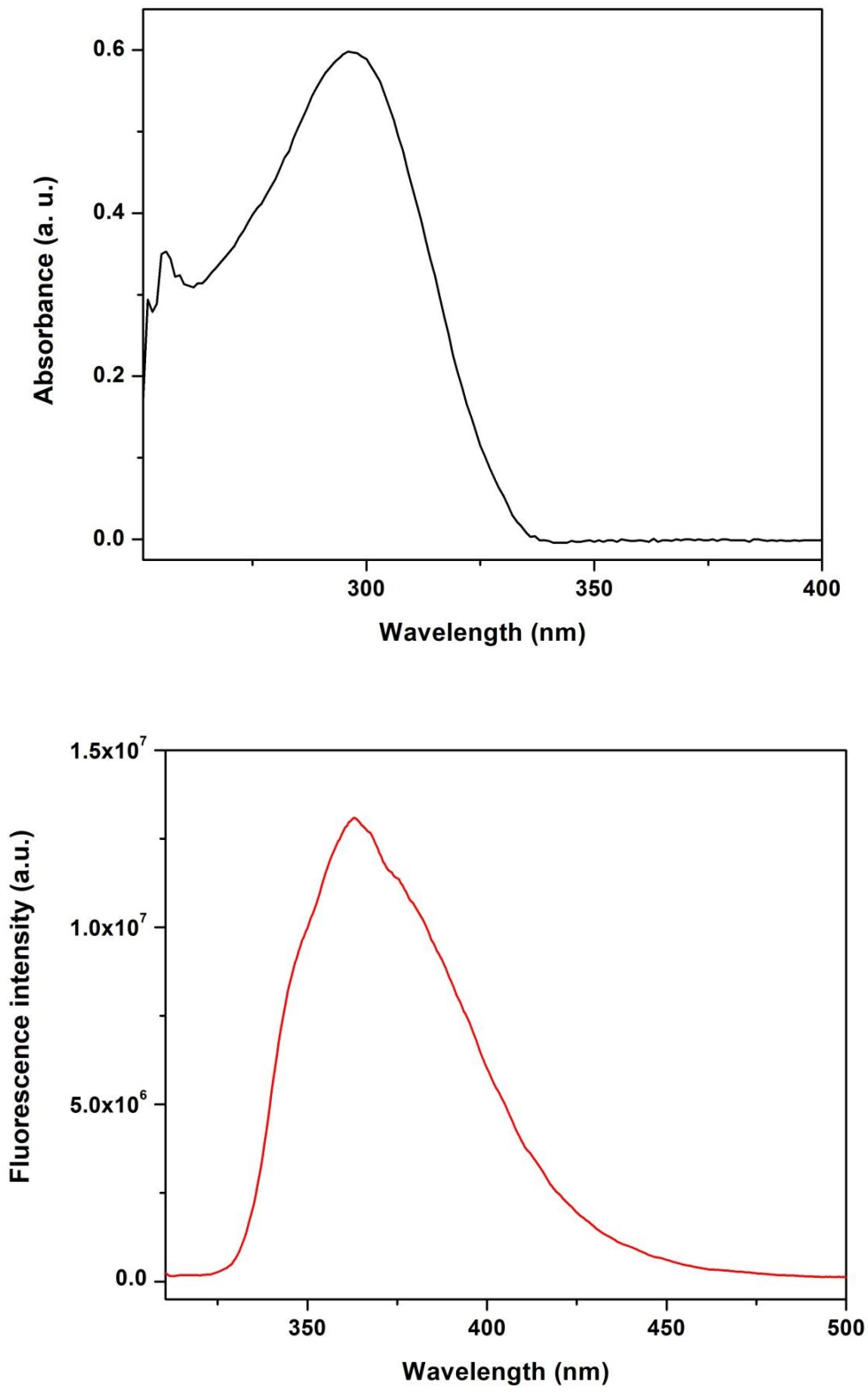

Figure 3.49. Absorption (top) and emission (bottom) spectra of L^2 in DMSO (0.2×10^{-4} M, λ_{exc} = 296 nm).

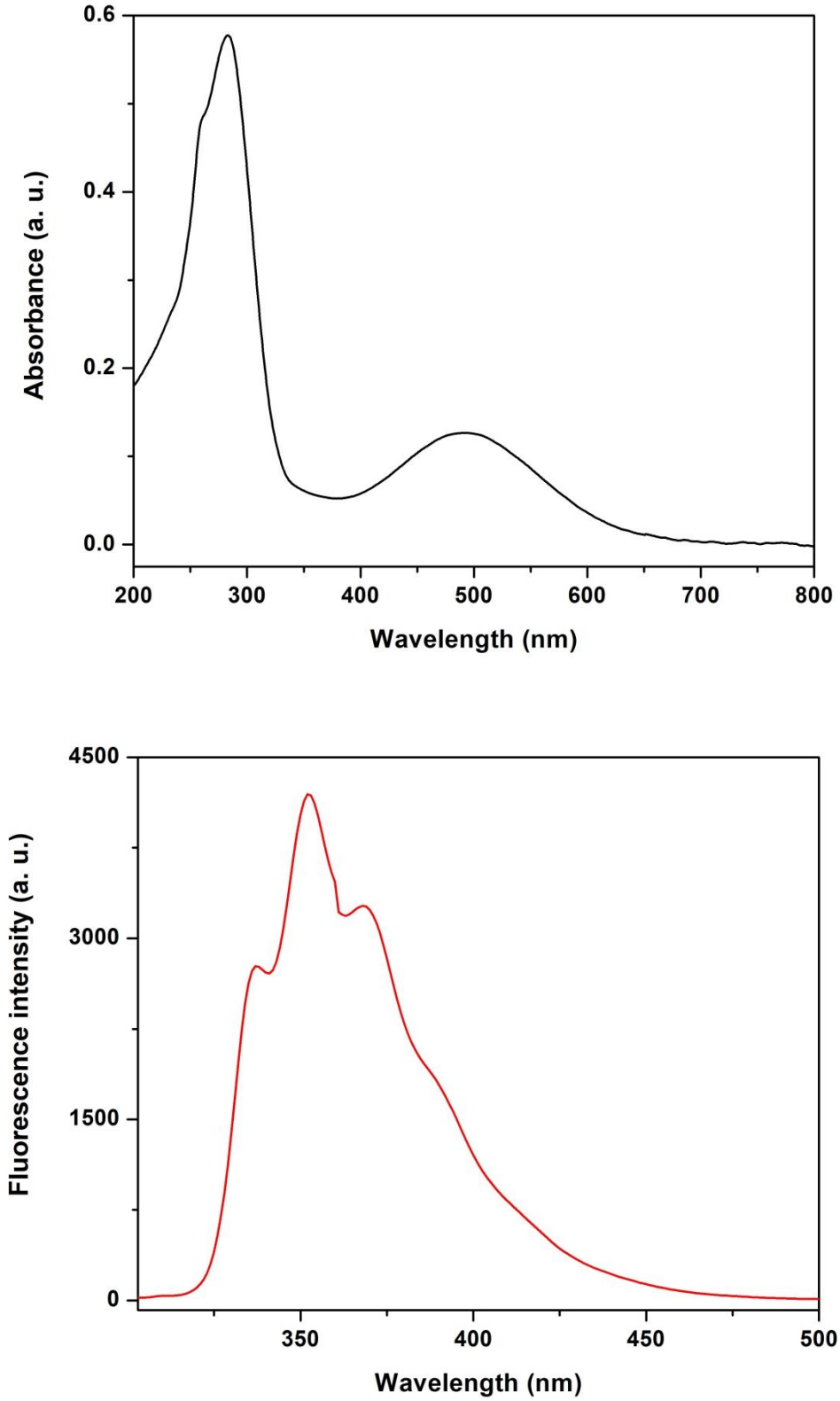

Figure 3.50. Absorption (top) and emission (bottom) spectra of **1** in DMSO (0.2×10^{-4} M, λ_{exc} = 283 nm).

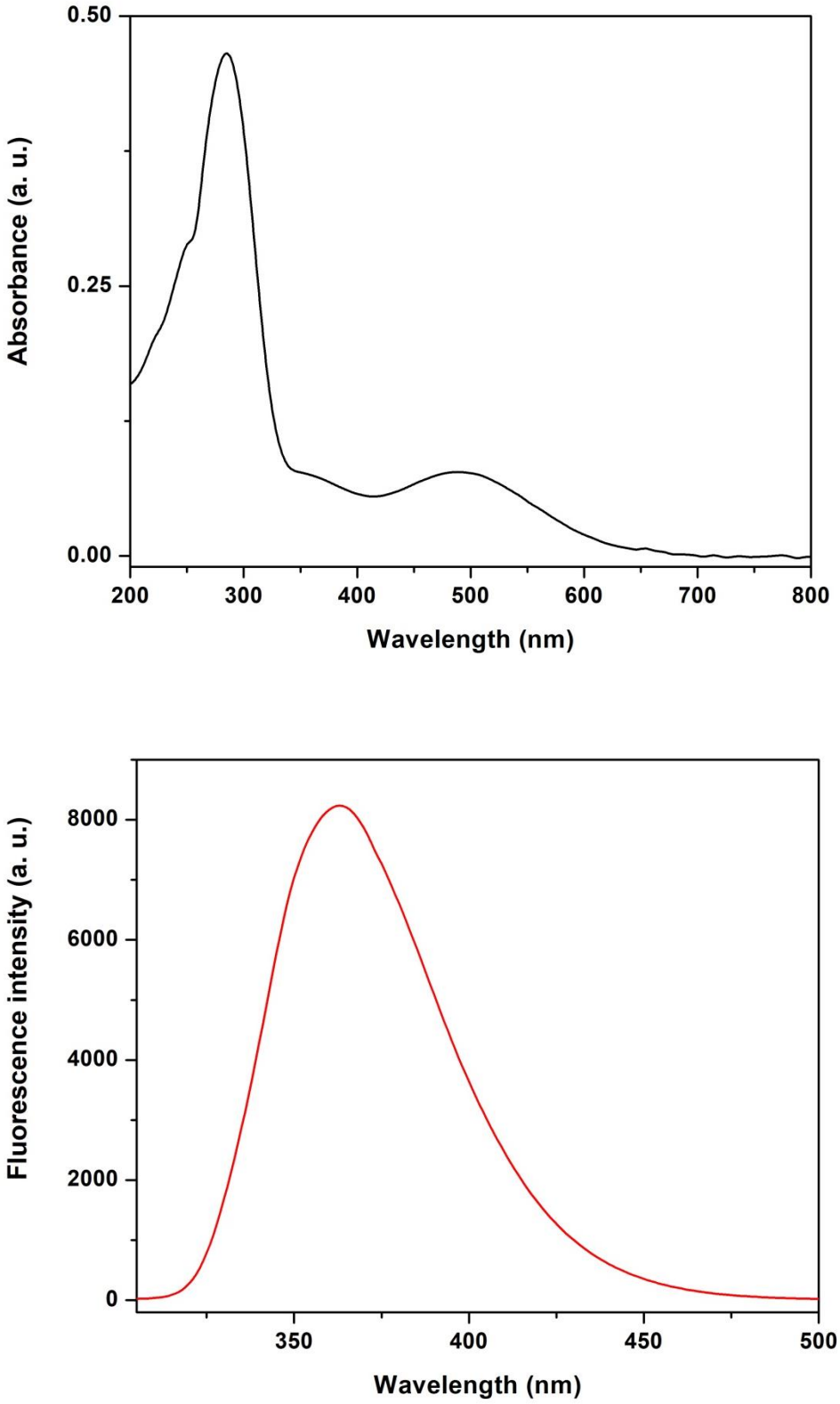

Figure 3.51. Absorption (top) and emission (bottom) spectra of **2** in DMSO (0.3×10^{-4} M, λ_{exc} = 285 nm).

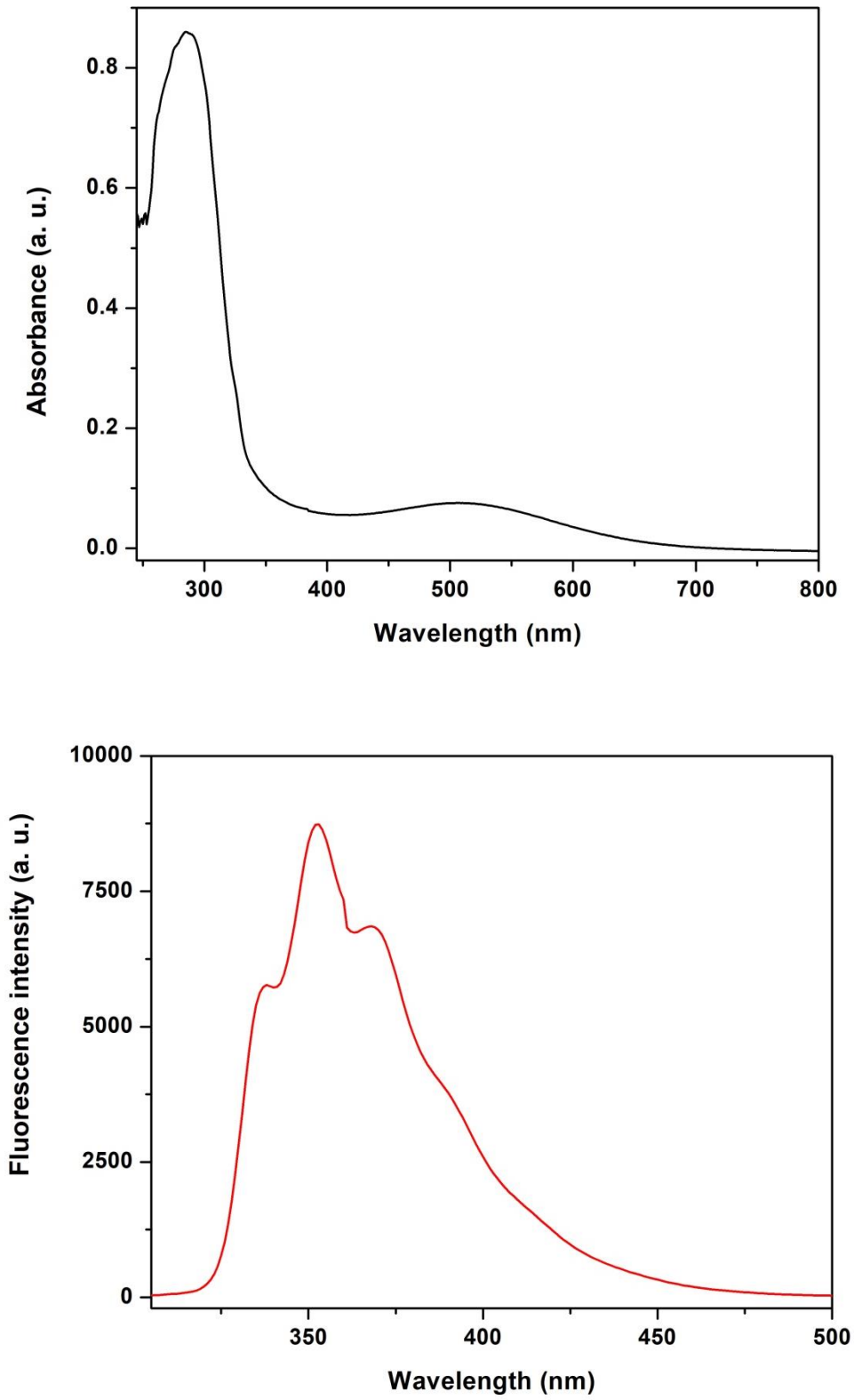

Figure 3.52. Absorption (top) and emission (bottom) spectra of **3** in DMSO (0.3×10^{-3} M, λ_{exc} = 285 nm).

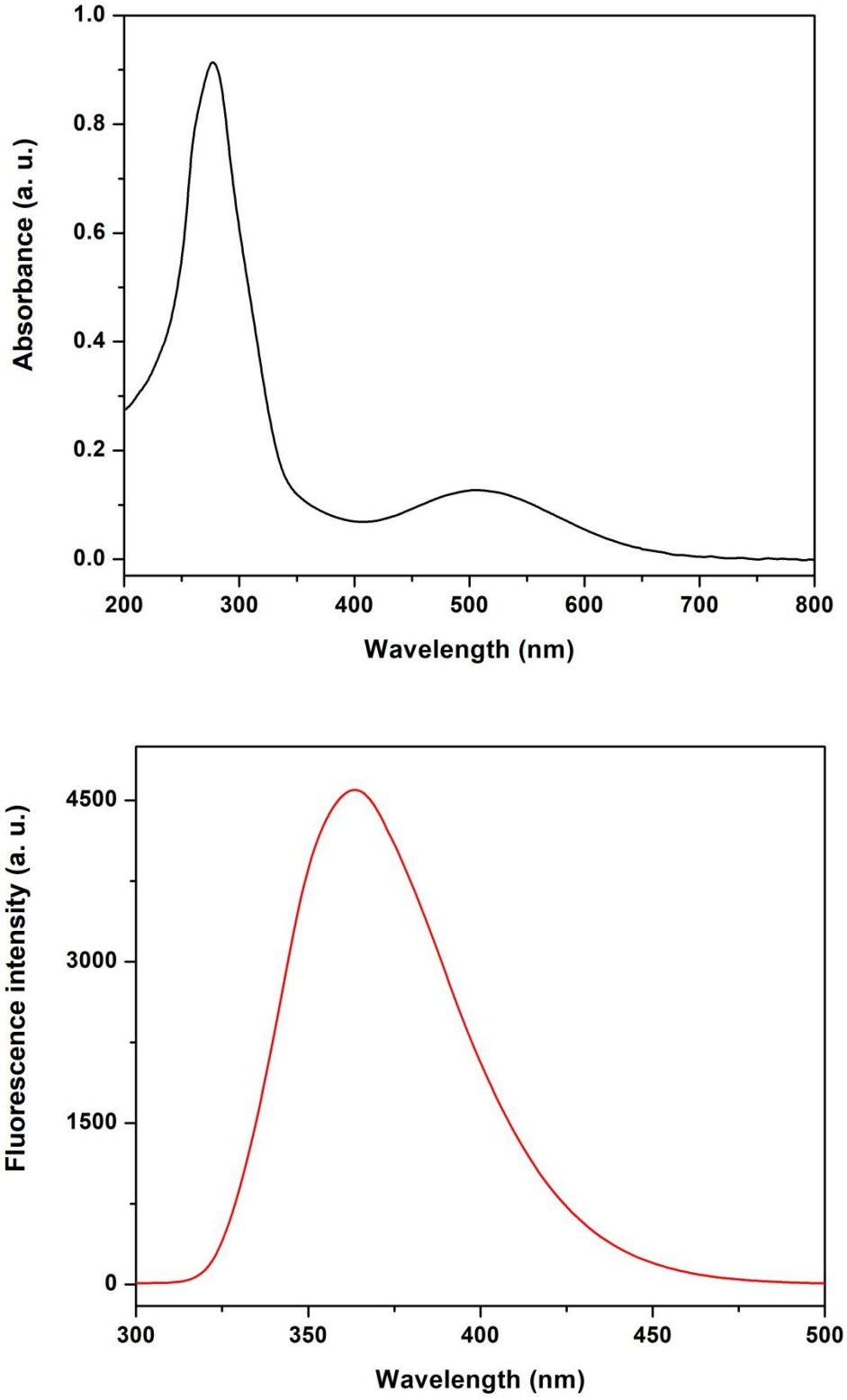

Figure 3.53. Absorption (top) and emission (bottom) spectra of **4** in DMSO (0.55×10^{-6} M, λ_{exc} = 277 nm).

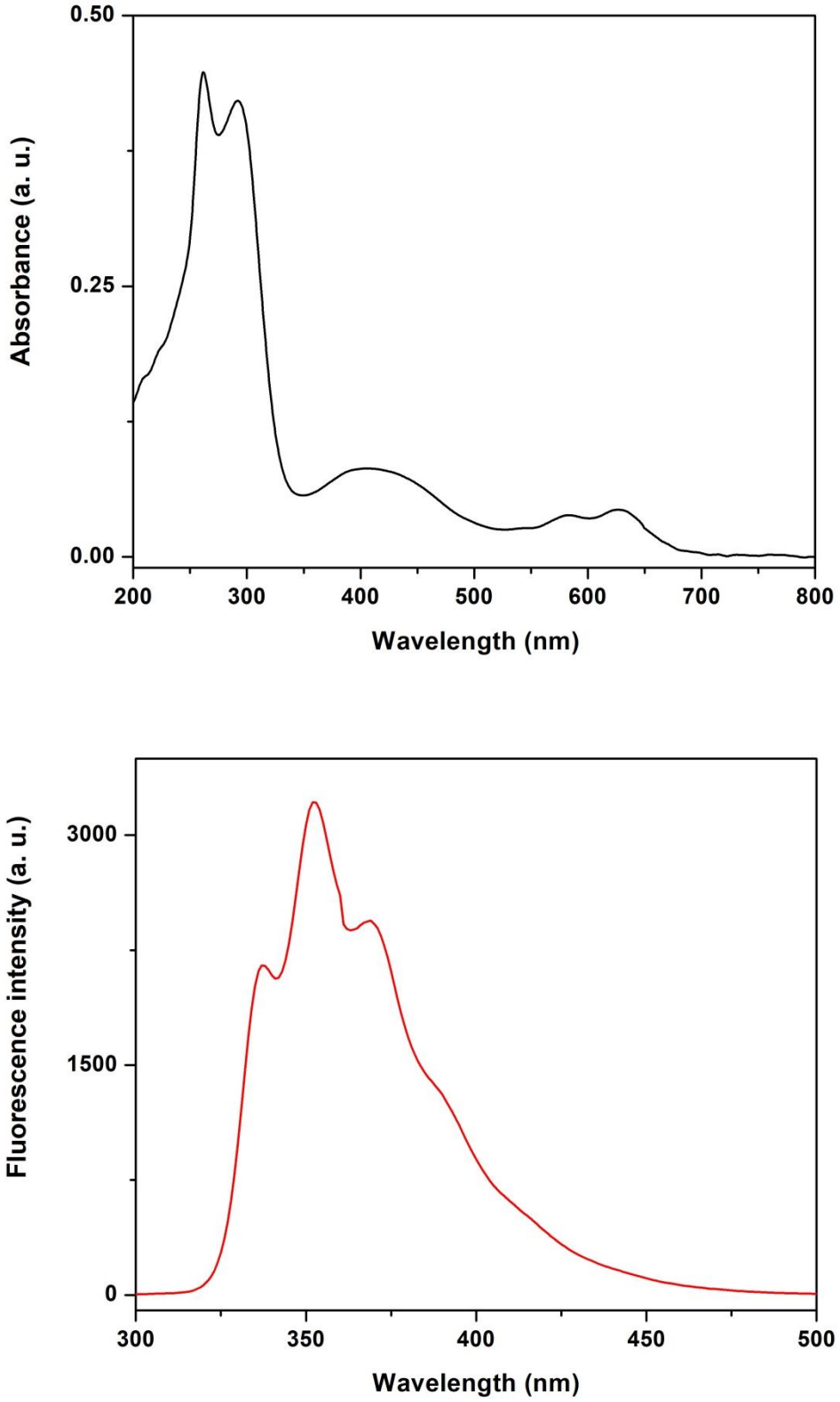

Figure 3.54. Absorption (top) and emission (bottom) spectra of **5** in DMSO (0.67×10^{-5} M, λ_{exc} = 292 nm).

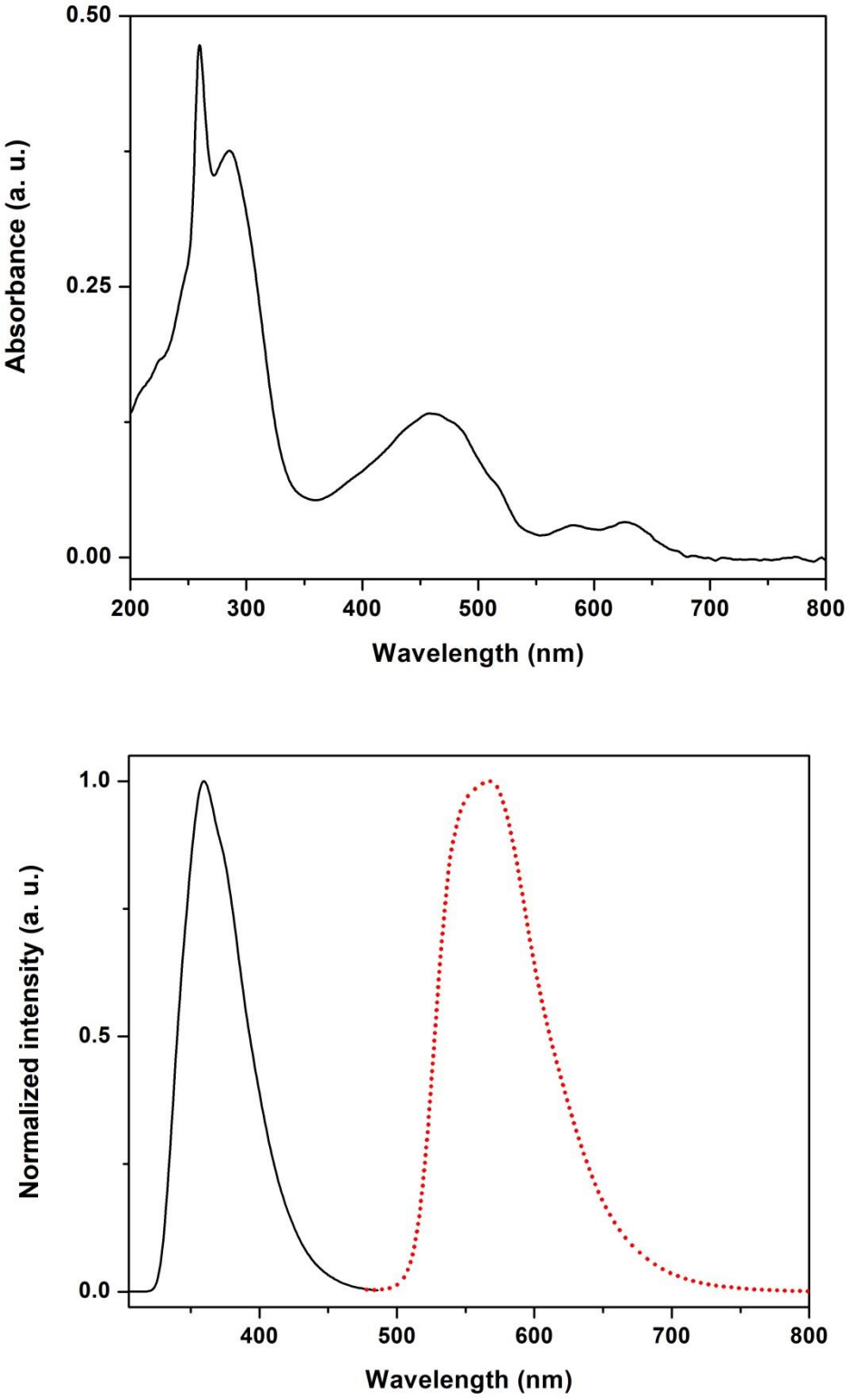

Figure 3.55. Absorption (top) and emission (bottom) spectra of **6** in DMSO (0.5×10^{-4} M, $\lambda_{exc1} = 285$ nm, $\lambda_{exc2} = 458$ nm).

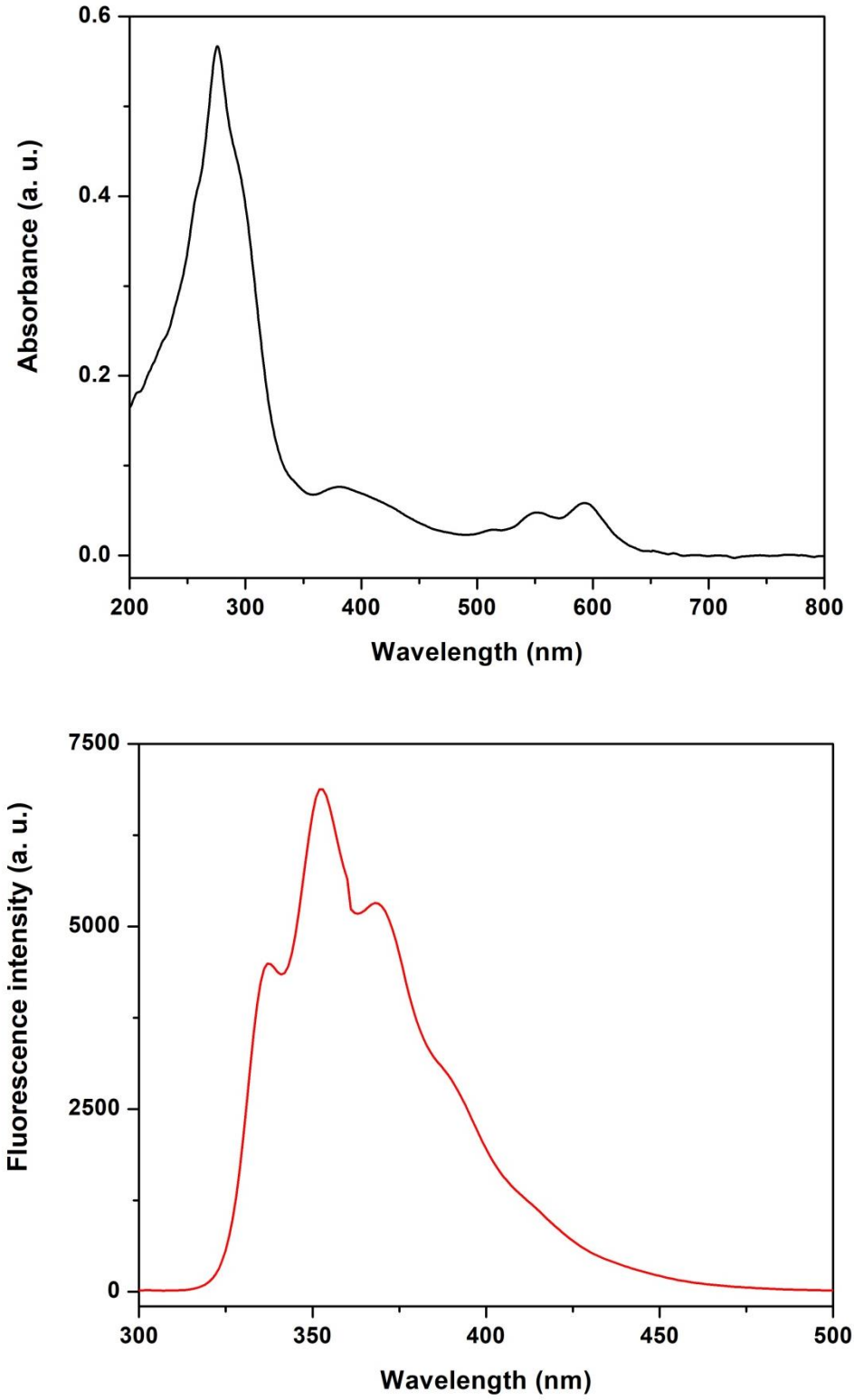

Figure 3.56. Absorption (top) and emission (bottom) spectra of **7** in DMSO (0.32×10^{-5} M, λ_{exc} = 276 nm).

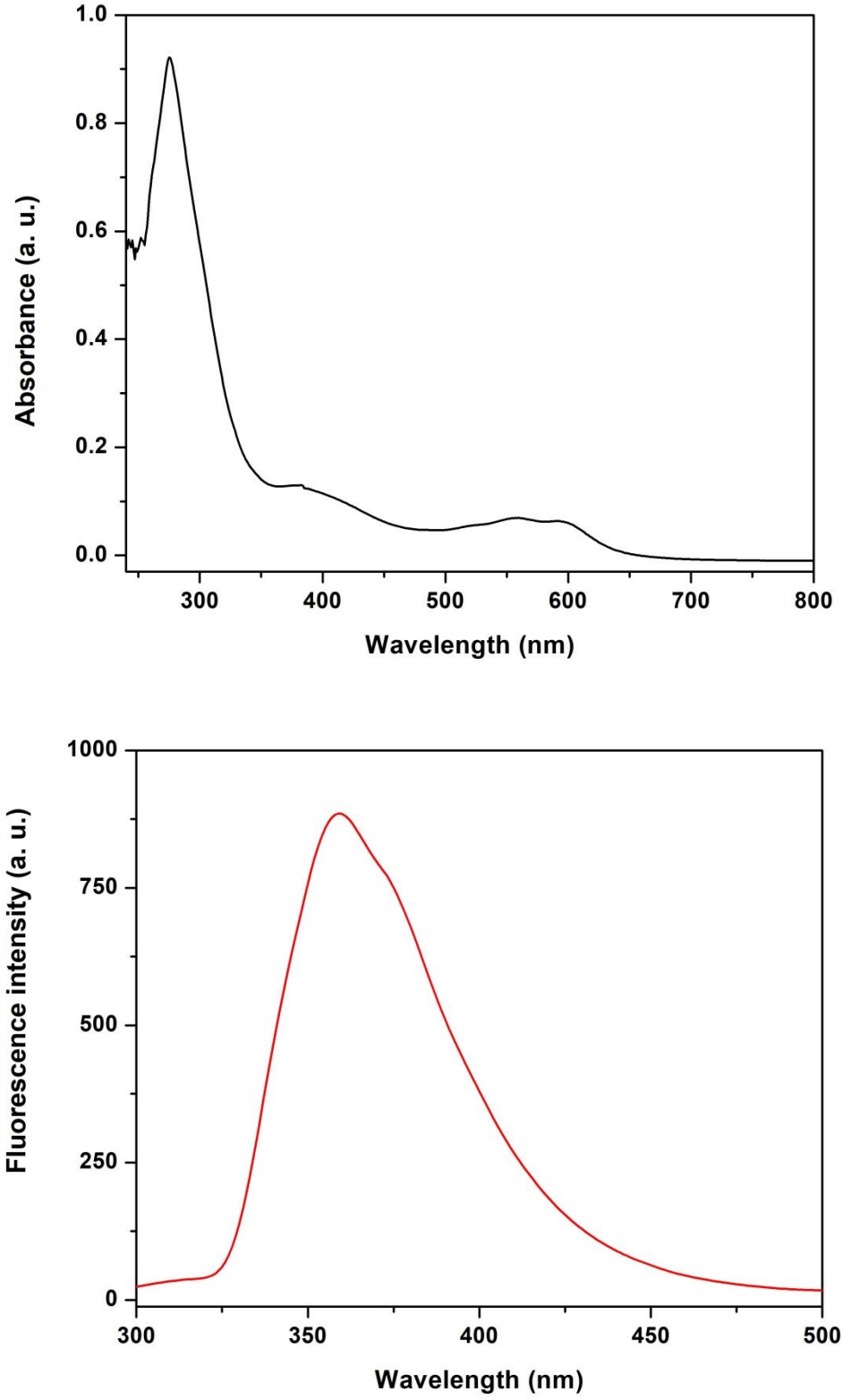

Figure 3.57. Absorption (top) and emission (bottom) spectra of **8** in DMSO (0.16×10^{-3} M, λ_{exc} = 275 nm).

3.4. Binding studies of host 1, 2, 7, and 8 with substituted phenol and nitrobenzene based guest molecules.

The crystal structures of the metallocavitands reveal that these molecules can act as molecular hosts for substituted benzene guest molecules. Host-guest binding studies of **1**, **2**, **7**, and **8** with nineteen phenol- and nitrobenzene- substituted guest molecules were performed using the emission feature of these metallocavitands in DMSO (Chart 1, Table 3.3). Upon titrating with the guest molecules, the emission pattern of metallocavitands **1** and **7** is quenched effectively with a slight blueshift of 2- 4 nm at 337/352 nm and a slight redshift of 3-5 nm at 368 nm. On the other hand, the emission pattern of **2** and **8** is quenched smoothly with a considerable blue shift of 2-10 nm, whereas on titrating with 2-NP and 4-NP, the quenching was observed with a significant redshift of 18-20 nm. Further, the analysis of the titration studies of metallocavitands **1**, **2**, **7**, and **8** with guest molecules using the Benesi-Hildebrand relationship reveals the formation of a 1:1 host:guest system.[19] Binding measurements reveal that $dhnq^{2-}$ and 4-methoxyphenyl benzimidazolyl N-donor substituted metallocavitand **7** is a more effective host, and shows better binding constant with guest molecules than metallocavitand **1**. This may be due to the presence of $dhnq^{2-}$ motif in **7**, which increases the hydrophobic cavity size [(~d, Å: Re···Re, 8.62 (for **7**) 8.08 (for **1**)] and the higher π-surface of $dhnq^{2-}$ motif leads to have better non-covalent interactions between the host-guest system. Metallocavitand **8** shows a significantly higher binding constant for phenol, BA, NB, resorcinol, and 2,4-DNT, whereas a slightly higher or a similar association constant was observed for m-Cresol, 2-CP, 2-NT, 4-NT, and 2,4,6-TNP in comparison with metallocavitand **2**. The possible reason can be the compact cavity size of host **8** due to the presence of $dhnq^{2-}$ motifs and 3,4,5-trimethoxyphenyl benzimidazolyl motif on N-donor ligand, which maximizes the non-covalent interactions between the host framework and guest molecules effectively. For all other guest molecules, host **2** shows a higher binding constant than **8**, which can be due to the slight rigid nature of the cyclic framework of **2** in the presence of $dhbq^{2-}$ motif, which accommodates the guest molecules with better interaction than metallocavitand **8**. In general, for all the host molecules, substituted nitrobenzene molecules bind more effectively than the other selected guest molecules. The emission quenching of these metallocavitands may be due to the electron transfer process from the metallocavitands to the electron-deficient guest molecules at the ground state.[24-25] Introducing H_2-dhnq motif as bis-chelating ligand and 4-methoxyphenyl/3,4,5-trimethoxyphenyl motif at the 2-position of benzimidazolyl unit in the ditopic N donor resulted in metallocavitands with

a more extended higher dimensional hydrophobic cavity as compared to the irregular pentagonal-shaped metallocavitands synthesized in our previous paper.[16] The 4-methoxyphenyl/3,4,5-trimethoxyphenyl motif provides additional hydrogen bonding and C–H···π interactions to stabilize the host-guest system. The binding constant measurements for nitro-substituted guest molecules reveal that hosts **1**, **2**, **7**, and **8** with larger hydrophobic cavities have higher binding constants than the previously reported complex (Table 3.4).[16]

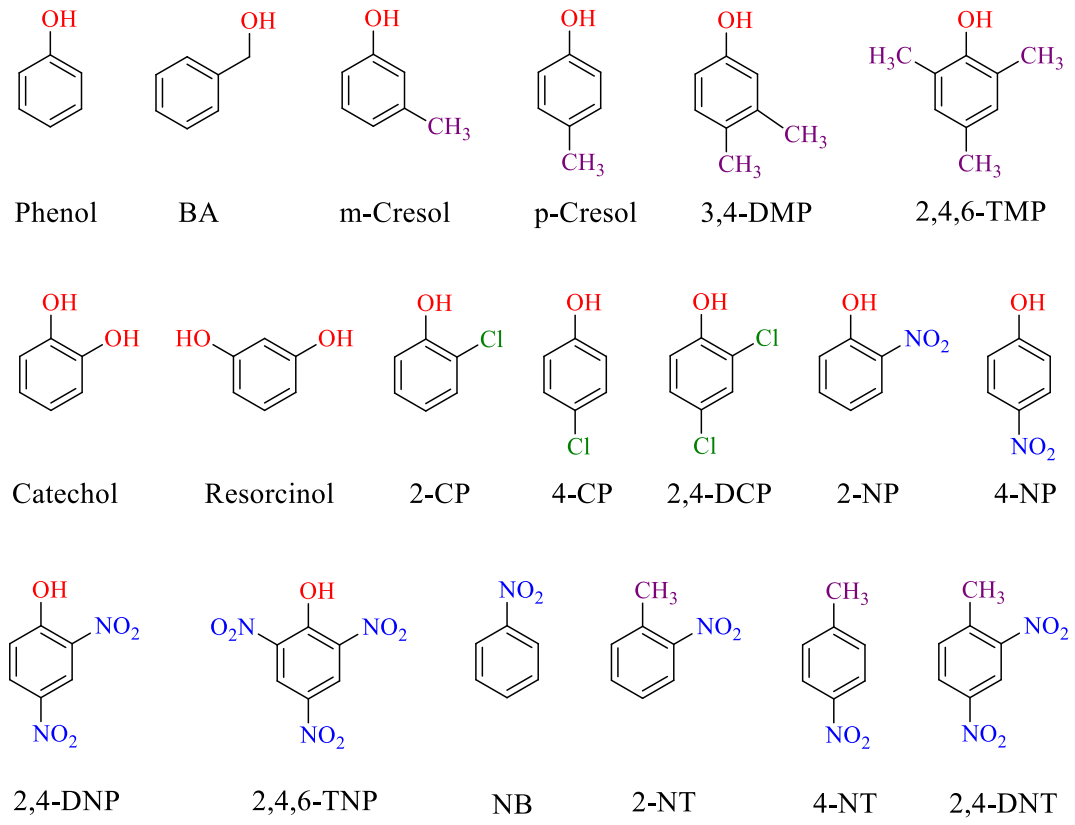

Chart 3.1. Guest molecules used in the current work.

Table 3.3. Binding Constants K_a (M^{-1}) of Metallocavitands 1, 2, 7, and 8 towards Various Guest Molecules Calculated by Emission Titration in DMSO at 298K.

guest molecules	**1** (K_a, M^{-1})	**2** (K_a, M^{-1})	**7** (K_a, M^{-1})	**8** (K_a, M^{-1})
Phenol	2.8×10^3	3.6×10^3	7.0×10^3	1.0×10^4
Benzyl alcohol (BA)	1.2×10^2	4.3×10^2	7.3×10^2	7.2×10^2
m-Cresol	1.9×10^3	1.2×10^4	5.5×10^3	1.4×10^4
p-Cresol	1.5×10^3	9.8×10^3	4.5×10^3	2.6×10^3
3,4-Dimethylphenol	8.1×10^2	2.5×10^3	2.1×10^3	1.6×10^3
2,4,6-Trimethylphenol	1.2×10^2	1.8×10^3	2.6×10^3	1.2×10^3
Catechol	3.3×10^3	4.1×10^3	3.5×10^3	2.6×10^3
Resorcinol	1.0×10^3	1.1×10^3	2.1×10^3	3.2×10^3
2-Chlorophenol	6.0×10^3	1.2×10^4	2.1×10^4	1.0×10^4
4-Chlorophenol	1.4×10^3	8.9×10^3	7.0×10^3	5.6×10^3
2,4-Dichlorophenol	2.4×10^3	4.0×10^3	1.4×10^3	2.0×10^3
2-Nitrophenol	9.8×10^3	8.5×10^3	1.3×10^4	7.8×10^3
4-Nitrophenol	1.4×10^5	2.1×10^4	2.2×10^4	9.6×10^3
2,4-Dinitrophenol	2.1×10^4	2.0×10^4	2.0×10^4	1.5×10^4
2,4,6-Trinitrophenol	2.2×10^4	4.6×10^4	4.0×10^4	5.0×10^4
Nitrobenzene	1.4×10^4	2.4×10^4	8.3×10^4	6.2×10^4
2-Nitrotoluene	1.1×10^4	1.8×10^4	2.8×10^4	2.0×10^4
4-Nitrotoluene	1.7×10^4	1.6×10^4	2.3×10^4	1.5×10^4
2,4-Dinitrotoluene	1.5×10^4	8.5×10^3	1.7×10^4	1.9×10^4

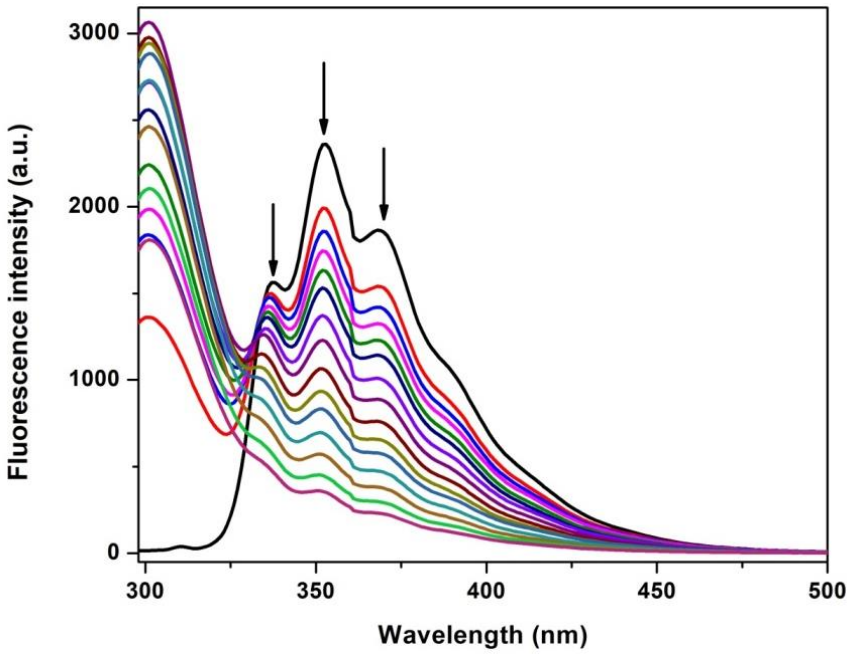

Figure 3.58. Changes in the emission spectra of **1** (4×10^{-6} M, λ_{exc} = 283 nm) with the addition of phenol in DMSO. The arrow indicates the quenching of the fluorescence intensity by addition of an appropriate aliquot of phenol.

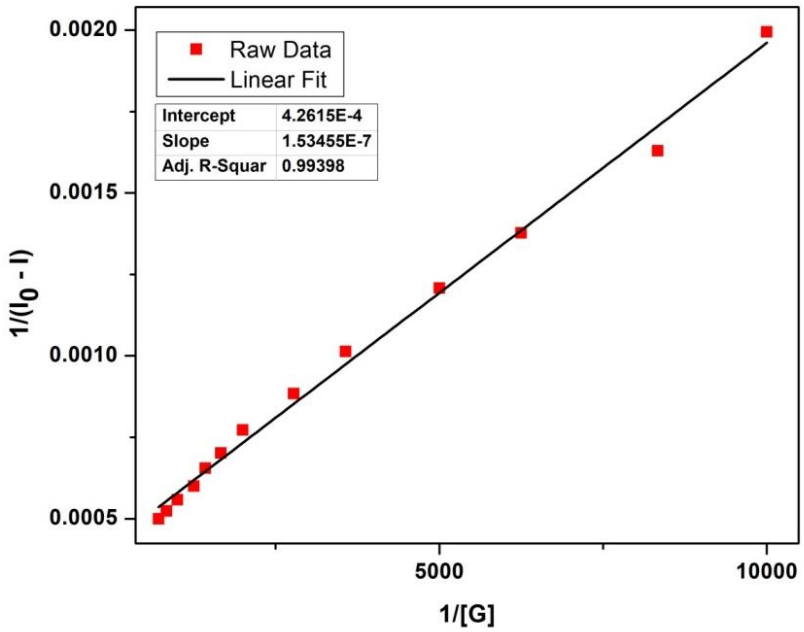

Figure 3.59. Benesi-Hildebrand plot for the emission quenching of host **1** (at 352 nm) with an increase in the concentration of phenol in DMSO.

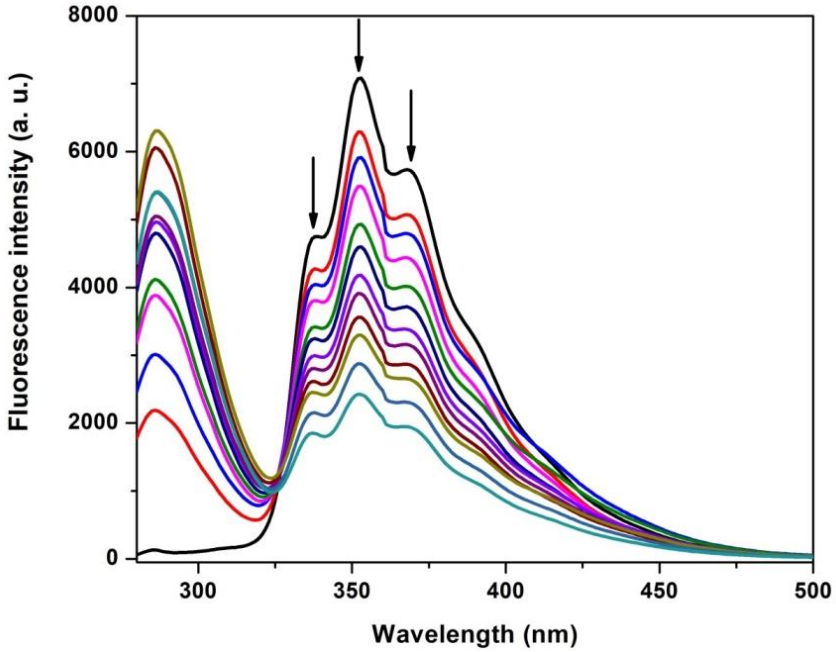

Figure 3.60. Changes in the emission spectra of **1** (3×10^{-6} M, λ_{exc} = 260 nm) with the addition of BA in DMSO. The arrow indicates the quenching of the fluorescence intensity by addition of an appropriate aliquot of BA.

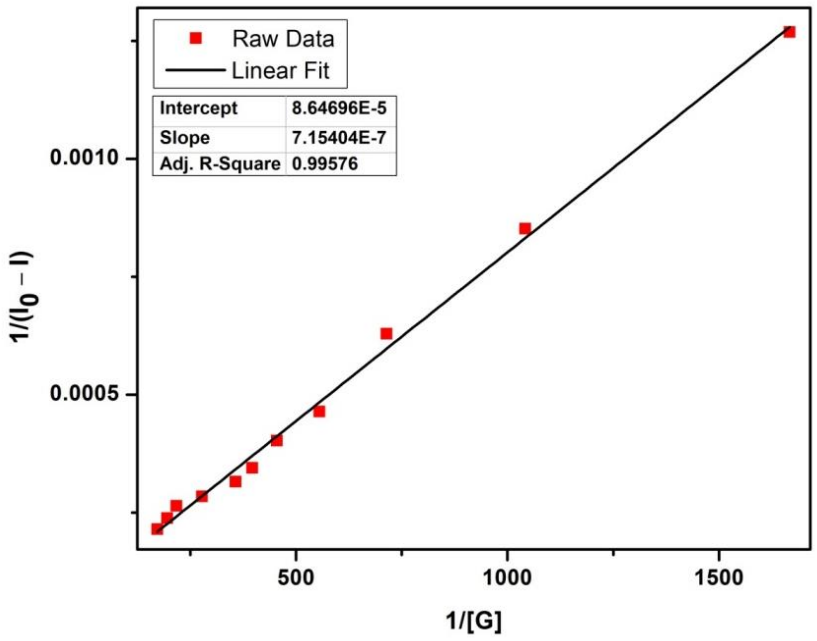

Figure 3.61. Benesi-Hildebrand plot for the emission quenching of host **1** (at 352 nm) with an increase in the concentration of BA in DMSO.

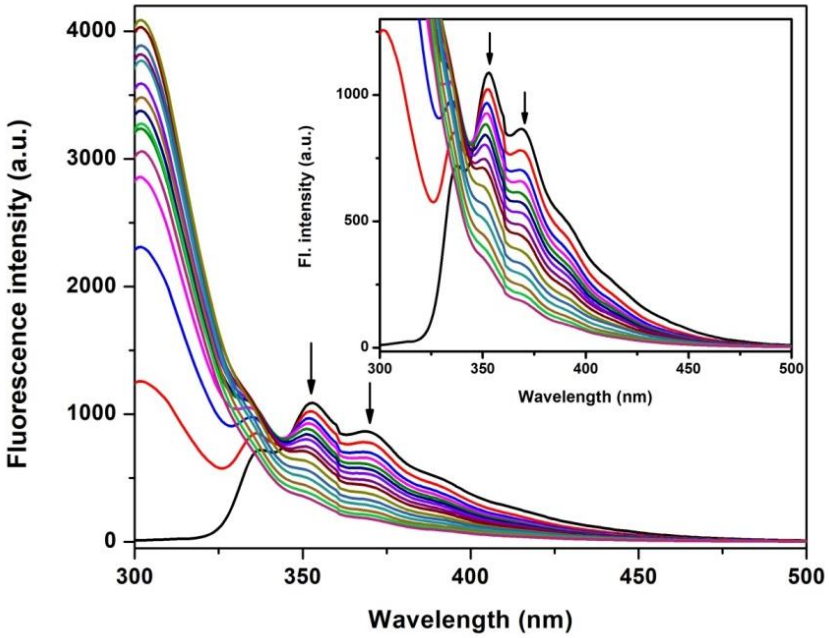

Figure 3.62. Changes in the emission spectra of **1** (1.5×10^{-6} M, λ_{exc} = 283 nm) with the addition of m-cresol in DMSO. The arrow indicates the quenching of the fluorescence intensity by addition of an appropriate aliquot of m-cresol.

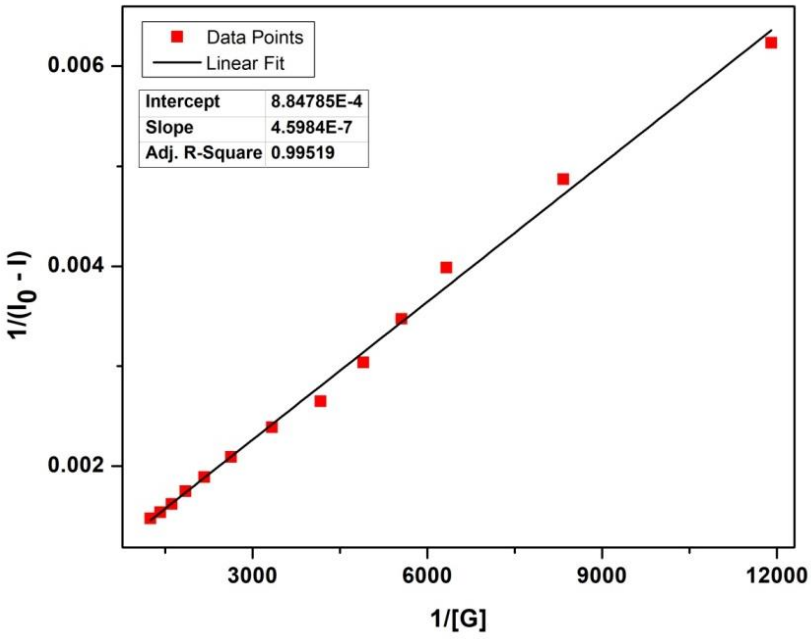

Figure 3.63. Benesi-Hildebrand plot for the emission quenching of host **1** (at 368 nm) with an increase in the concentration of m-cresol in DMSO.

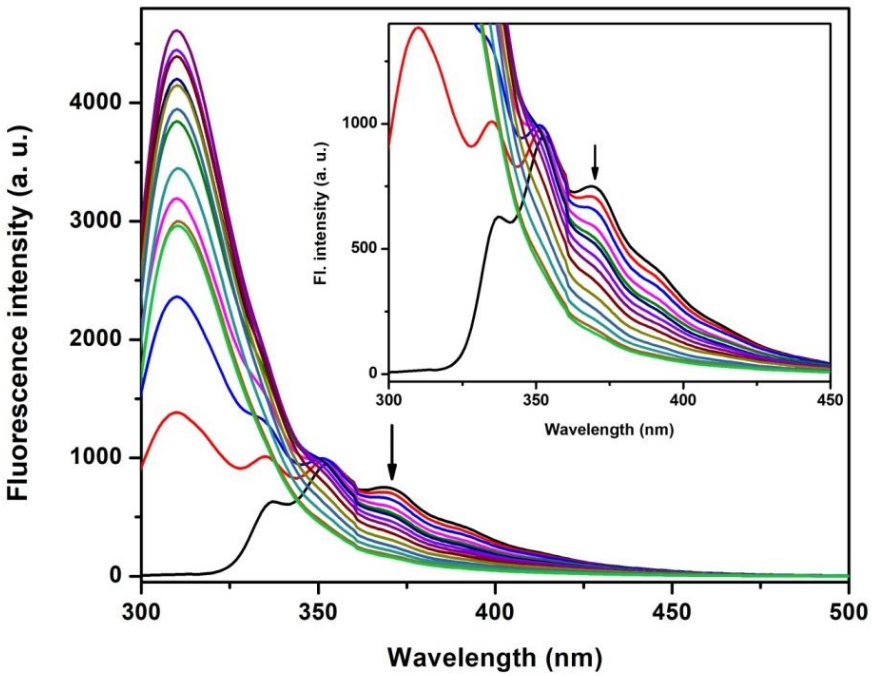

Figure 3.64. Changes in the emission spectra of **1** (1.5×10^{-6} M, λ_{exc} = 283 nm) with the addition of p-cresol in DMSO. The arrow indicates the quenching of the fluorescence intensity by addition of an appropriate aliquot of p-cresol.

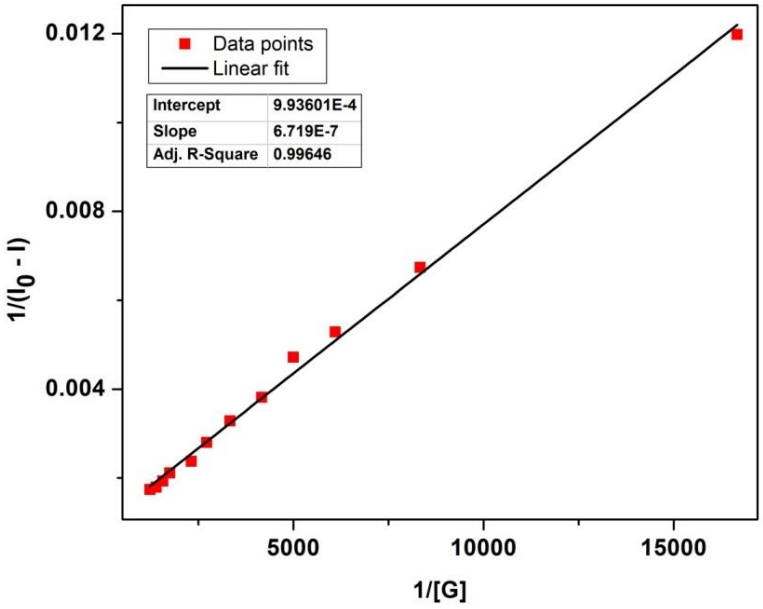

Figure 3.65. Benesi-Hildebrand plot for the emission quenching of host **1** (at 368 nm) with an increase in the concentration of p-cresol in DMSO.

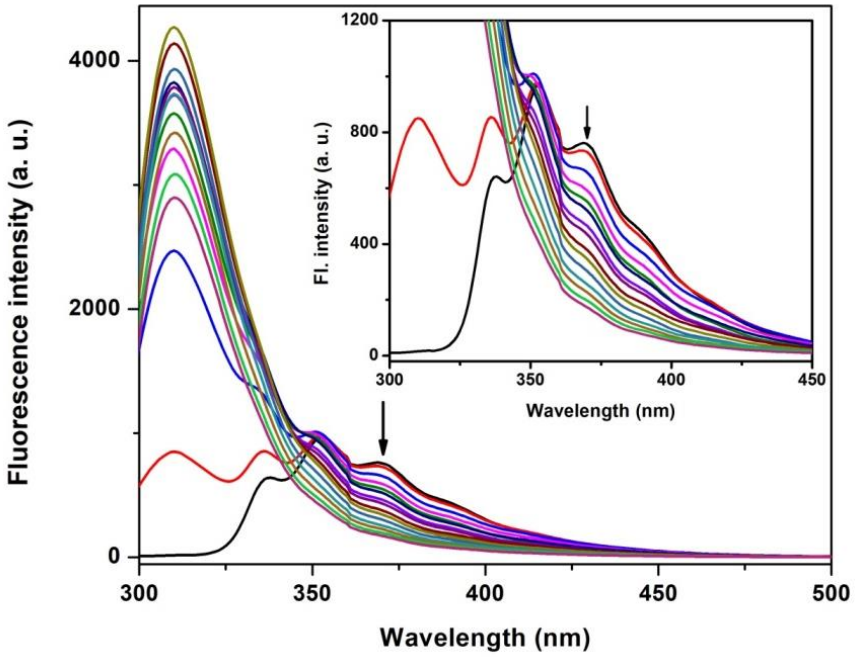

Figure 3.66. Changes in the emission spectra of **1** (1.5×10^{-6} M, λ_{exc} = 283 nm) with the addition of 3, 4- DMP in DMSO. The arrow indicates the quenching of the fluorescence intensity by addition of an appropriate aliquot of 3, 4- DMP

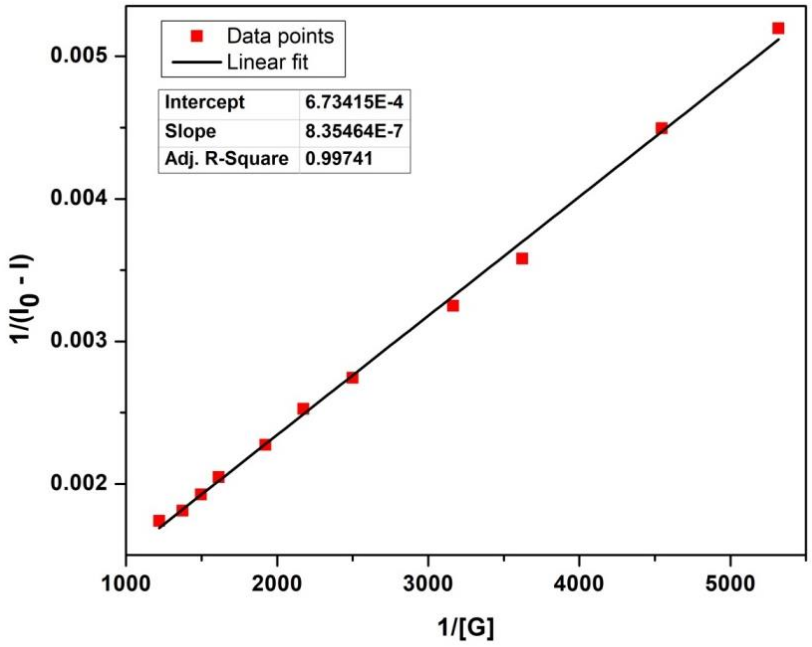

Figure 3.67. Benesi-Hildebrand plot for the emission quenching of host **1** (at 368 nm) with an increase in the concentration of 3, 4- DMP in DMSO.

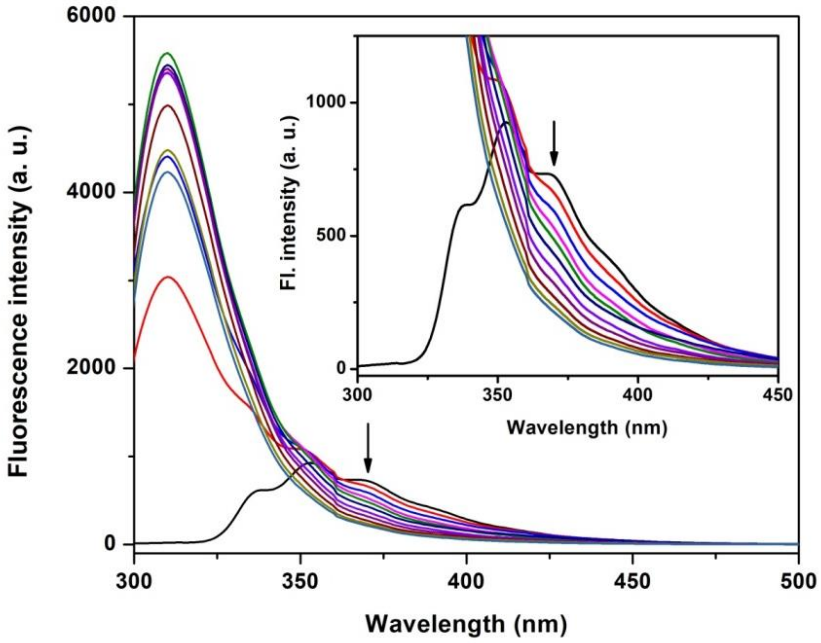

Figure 3.68. Changes in the emission spectra of **1** (1.5×10^{-6} M, λ_{exc} = 283 nm) with the addition of 2, 4, 6- TMP in DMSO. The arrow indicates the quenching of the fluorescence intensity by addition of an appropriate aliquot of 2, 4, 6- TMP.

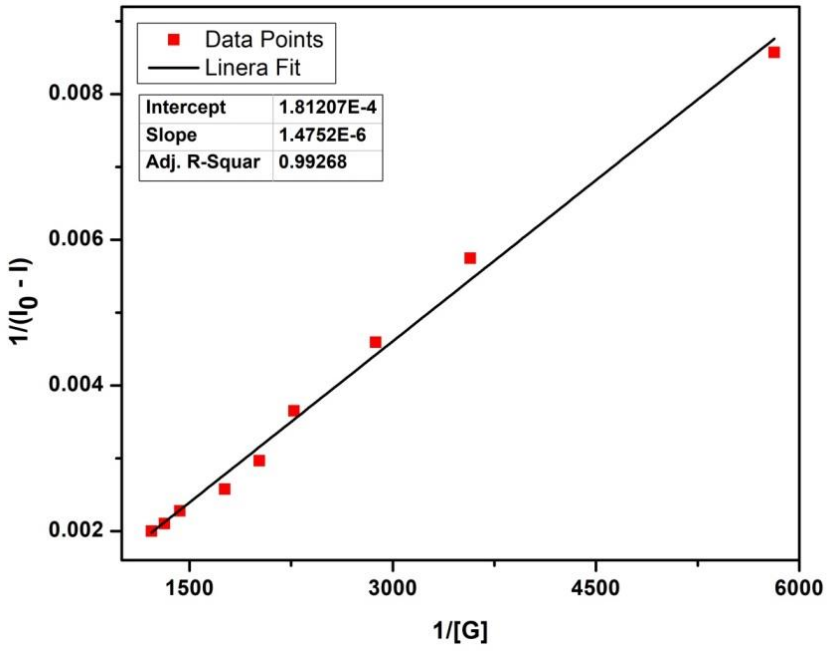

Figure 3.69. Benesi-Hildebrand plot for the emission quenching of host **1** (at 368 nm) with an increase in the concentration of 2, 4, 6- TMP in DMSO.

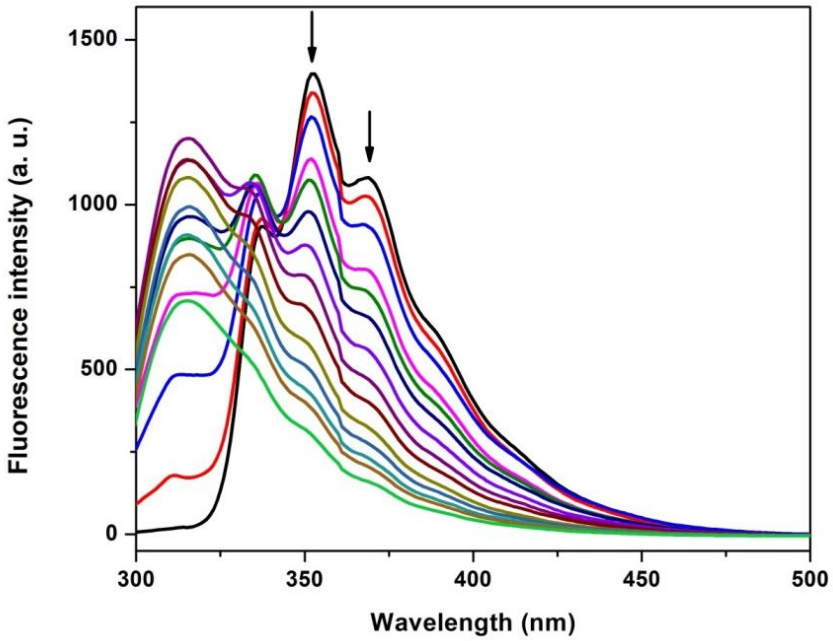

Figure 3.70. Changes in the emission spectra of **1** (3×10^{-6} M, λ_{exc} = 283 nm) with the addition of catechol in DMSO. The arrow indicates the quenching of the fluorescence intensity by addition of an appropriate aliquot of catechol.

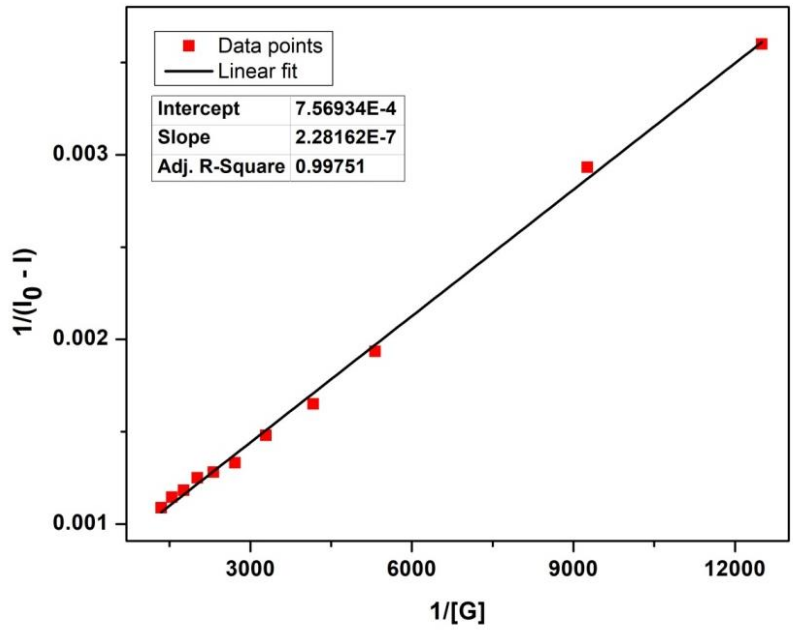

Figure 3.71. Benesi-Hildebrand plot for the emission quenching of host **1** (at 368 nm) with an increase in the concentration of catechol in DMSO.

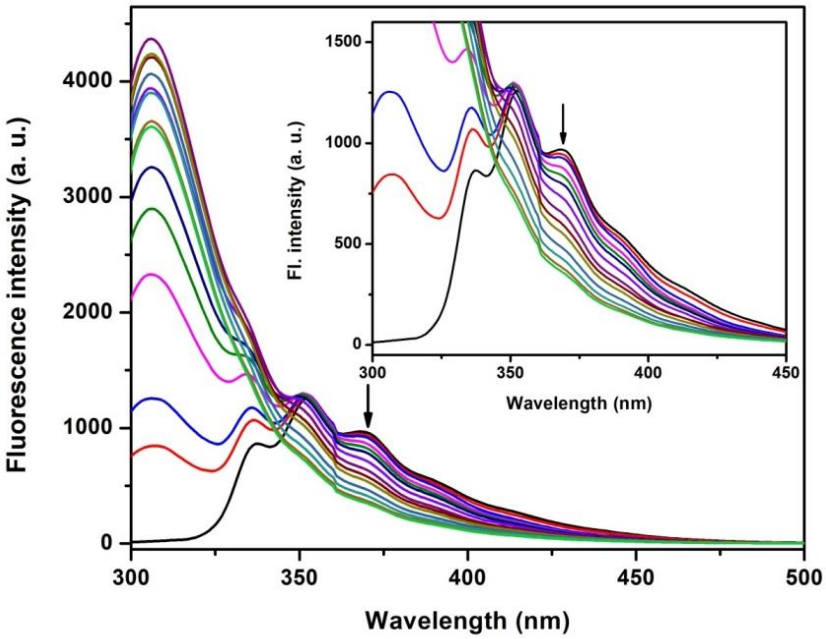

Figure 3.72. Changes in the emission spectra of **1** (3×10^{-6} M, λ_{exc} = 283 nm) with the addition of resorcinol in DMSO. The arrow indicates the quenching of the fluorescence intensity by addition of an appropriate aliquot of resorcinol.

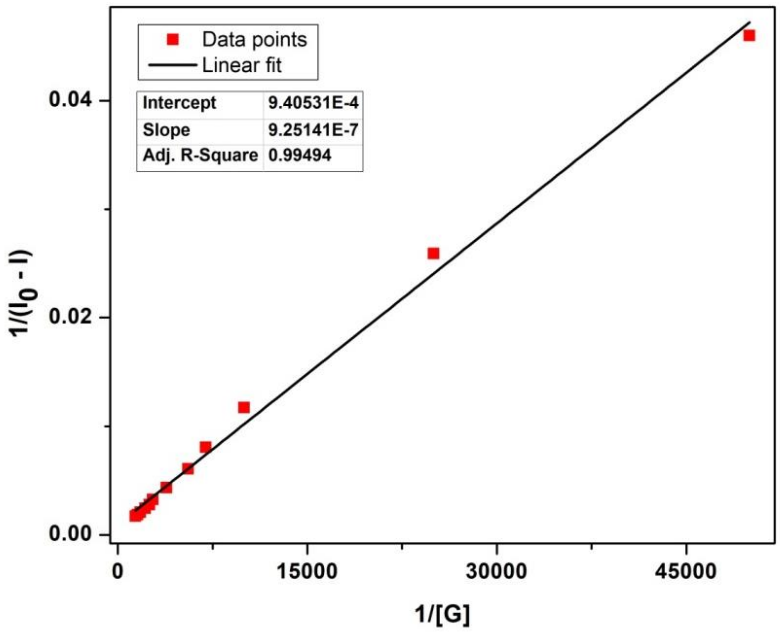

Figure 3.73. Benesi-Hildebrand plot for the emission quenching of host **1** (at 368 nm) with an increase in the concentration of resorcinol in DMSO.

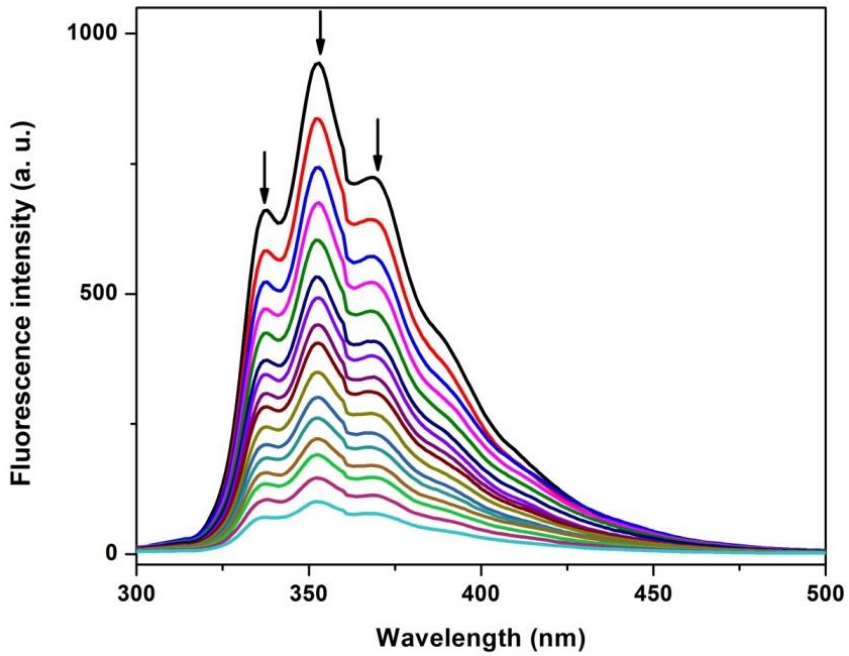

Figure 3.74. Changes in the emission spectra of **1** (1.5×10^{-6} M, λ_{exc} = 283 nm) with the addition of 2-CP in DMSO. The arrow indicates the quenching of the fluorescence intensity by addition of an appropriate aliquot of 2-CP.

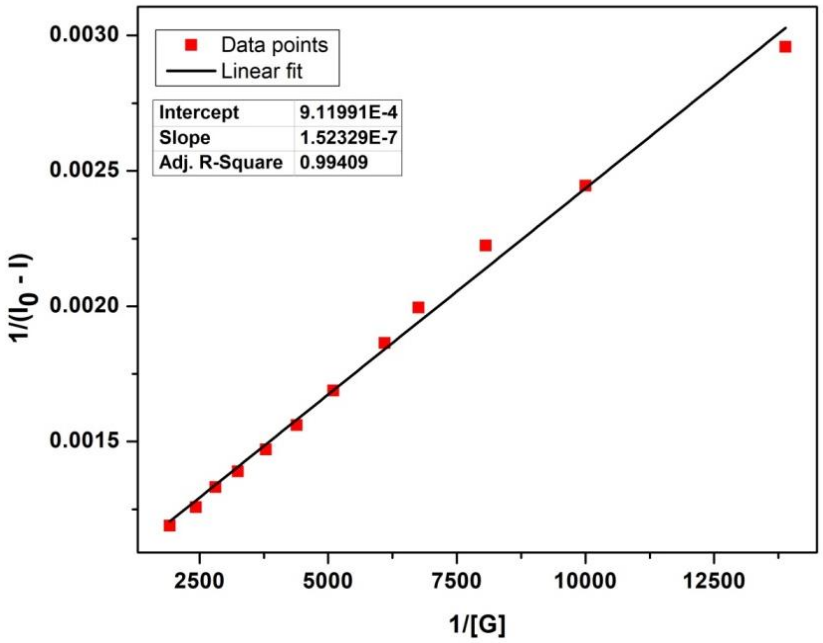

Figure 3.75. Benesi-Hildebrand plot for the emission quenching of host **1** (at 352 nm) with an increase in the concentration of 2-CP in DMSO.

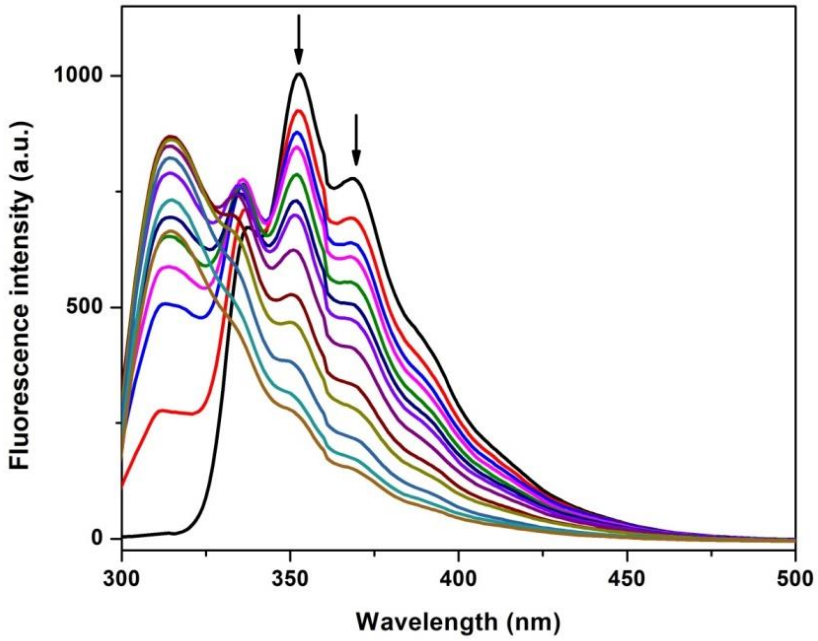

Figure 3.76. Changes in the emission spectra of **1** (1.5×10^{-6} M, λ_{exc} = 283 nm) with the addition of 4-chlorophenol in DMSO. The arrow indicates the quenching of the fluorescence intensity by addition of an appropriate aliquot of 4-CP.

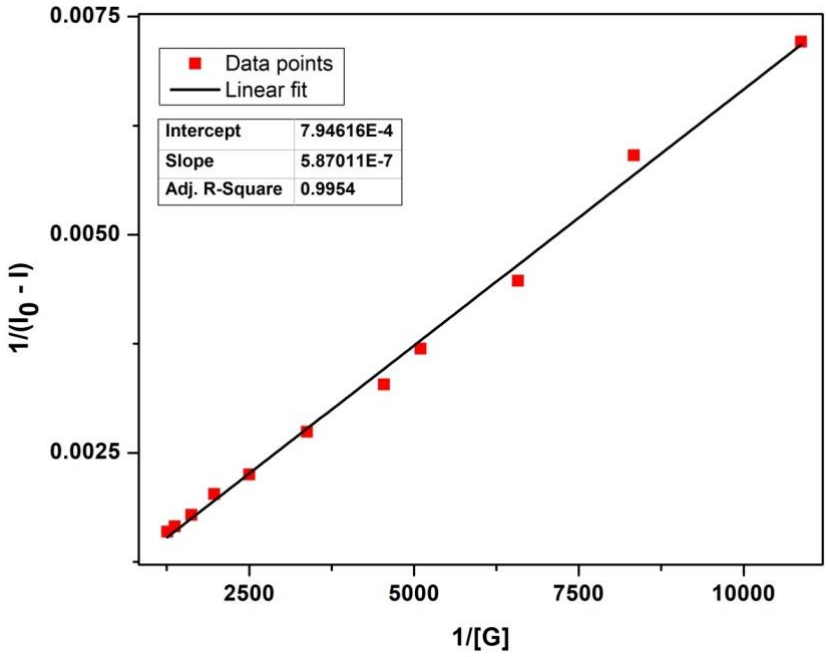

Figure 3.77. Benesi-Hildebrand plot for the emission quenching of host **1** (at 368 nm) with an increase in the concentration of 4-CP in DMSO.

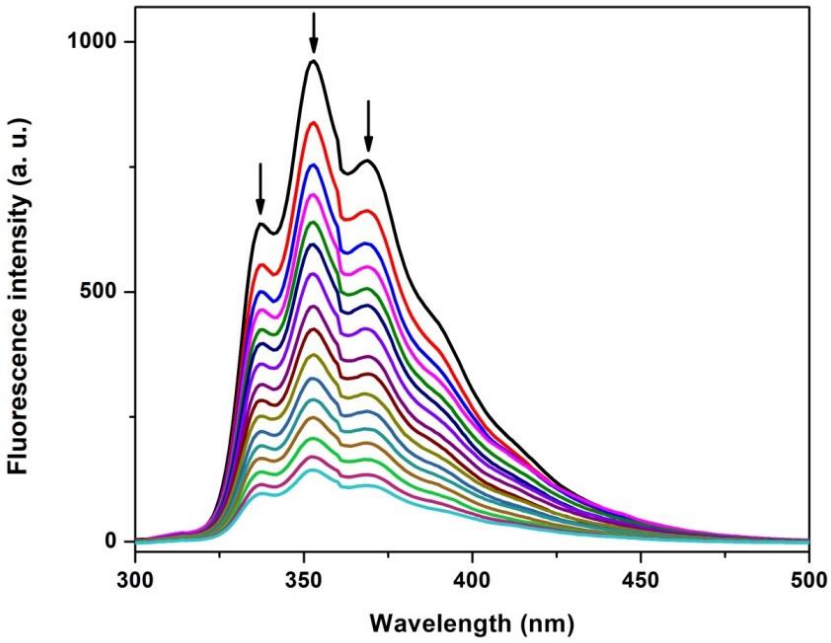

Figure 3.78. Changes in the emission spectra of **1** (1.5×10^{-6} M, λ_{exc} = 283 nm) with the addition of 2, 4-DCP in DMSO. The arrow indicates the quenching of the fluorescence intensity by addition of an appropriate aliquot of 2, 4-DCP.

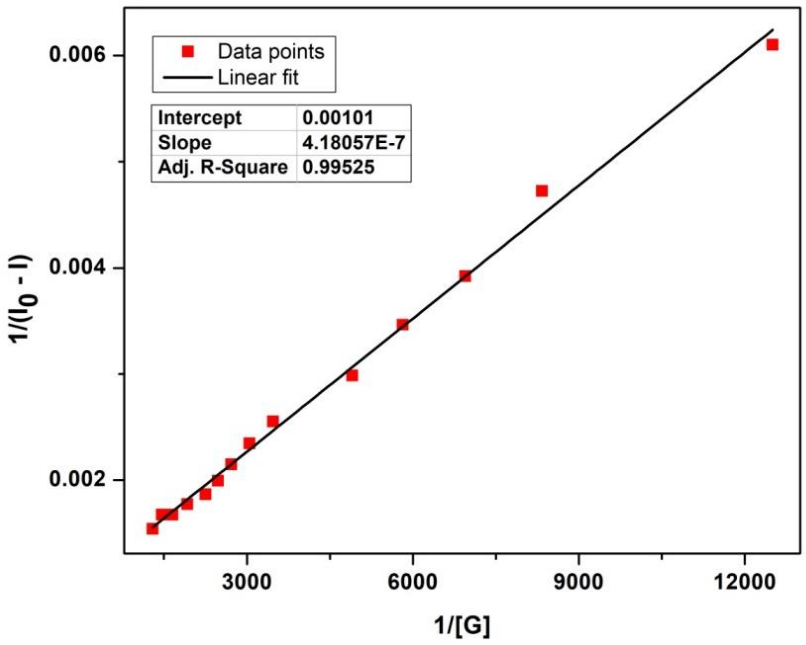

Figure 3.79. Benesi-Hildebrand plot for the emission quenching of host **1** (at 368 nm) with an increase in the concentration of 2, 4-DCP in DMSO.

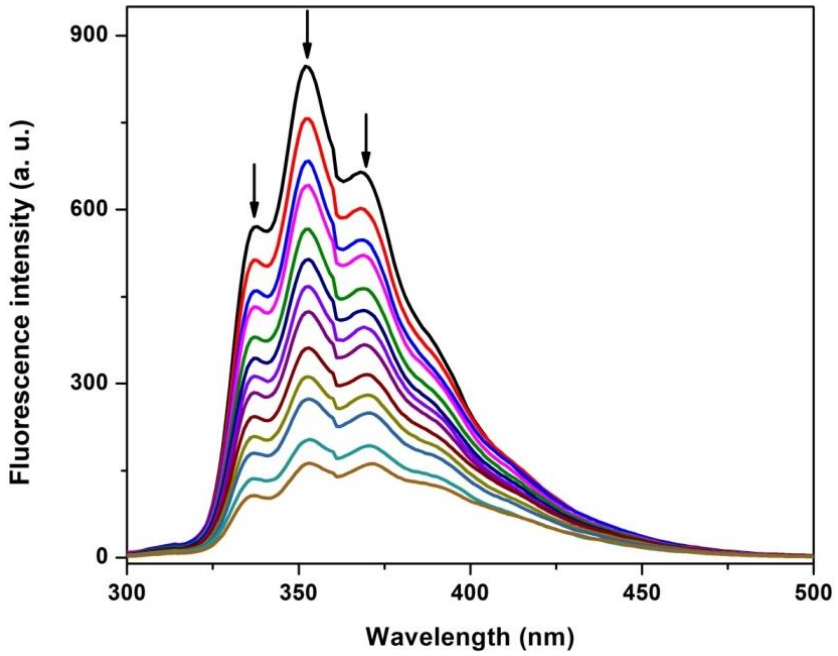

Figure 3.80. Changes in the emission spectra of **1** (3×10^{-6} M, λ_{exc} = 283 nm) with the addition of 2- NP in DMSO. The arrow indicates the quenching of the fluorescence intensity by addition of an appropriate aliquot of 2-NP.

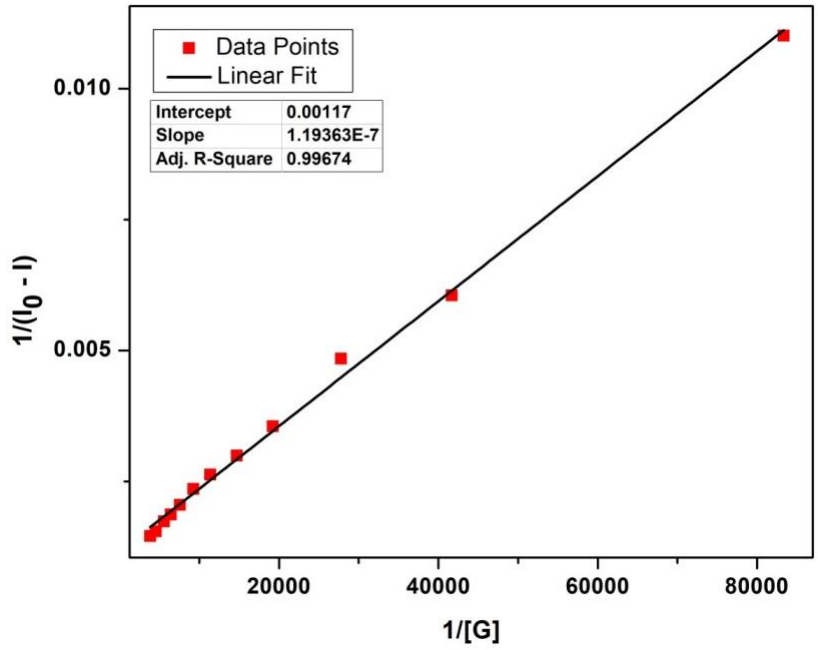

Figure 3.81. Benesi-Hildebrand plot for the emission quenching of host **1** (at 352 nm) with an increase in the concentration of 2-NP in DMSO.

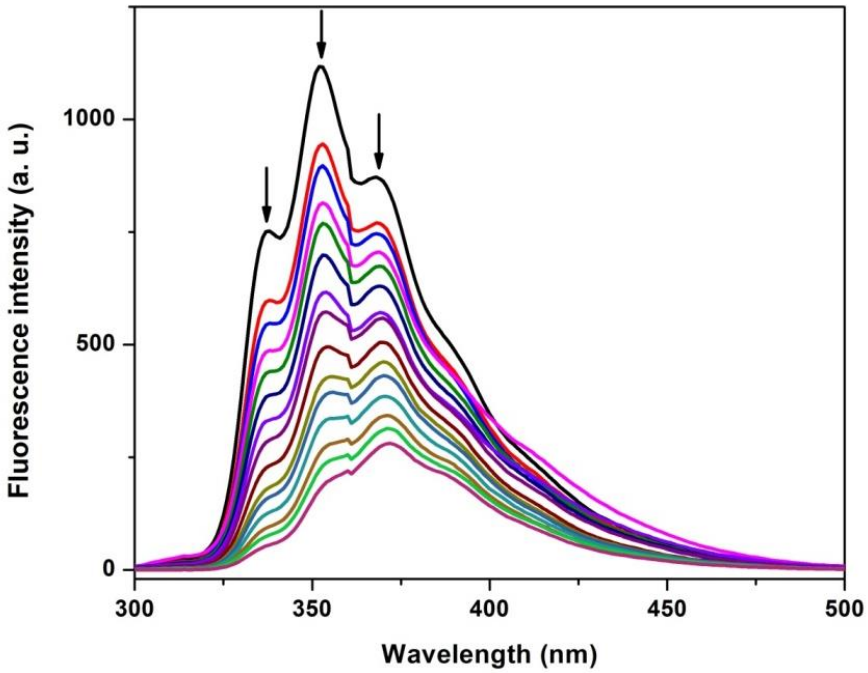

Figure 3.82. Changes in the emission spectra of **1** (3×10^{-6} M, λ_{exc} = 283 nm) with the addition of 4- NP in DMSO. The arrow indicates the quenching of the fluorescence intensity by addition of an appropriate aliquot of 4-NP.

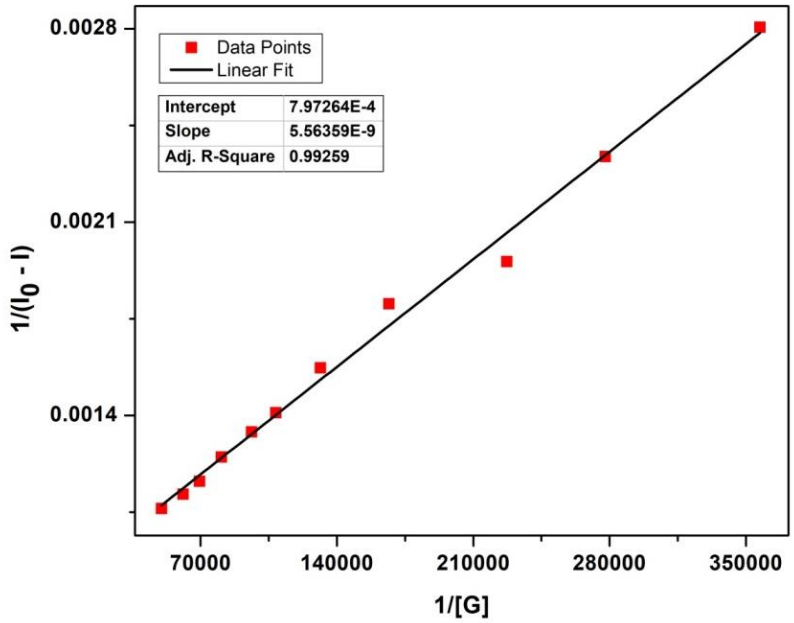

Figure 3.83. Benesi-Hildebrand plot for the emission quenching of host **1** (at 352 nm) with an increase in the concentration of 4-NP in DMSO.

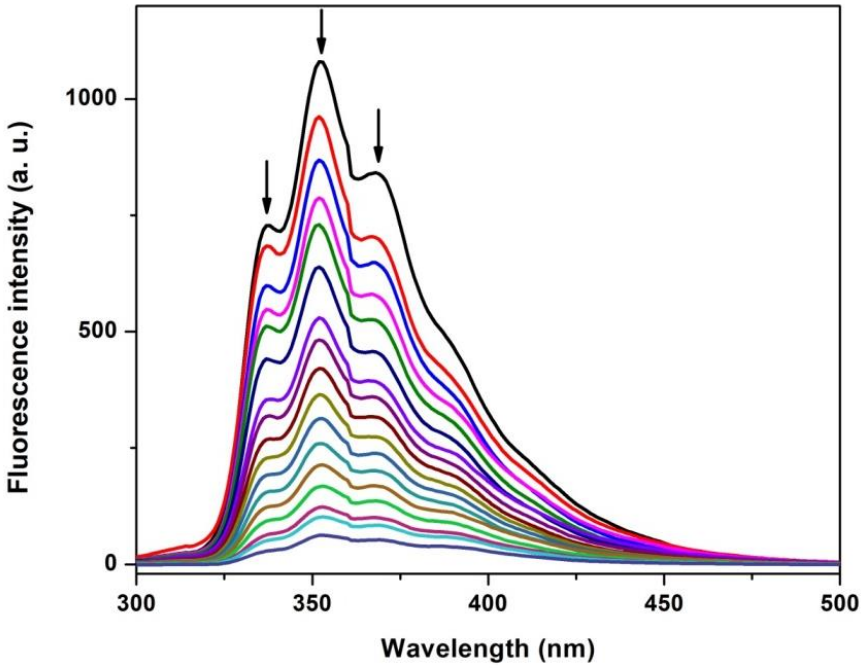

Figure 3.84. Changes in the emission spectra of **1** (3×10^{-6} M, λ_{exc} = 283 nm) with the addition of 2, 4- DNP in DMSO. The arrow indicates the quenching of the fluorescence intensity by addition of an appropriate aliquot of 2, 4- DNP.

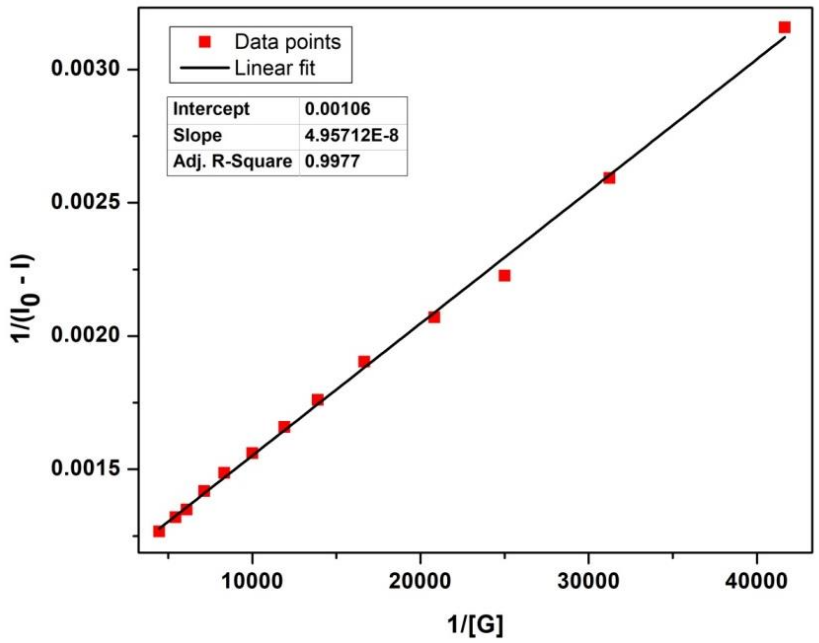

Figure 3.85. Benesi-Hildebrand plot for the emission quenching of host **1** (at 368 nm) with an increase in the concentration of 2, 4- DNP in DMSO.

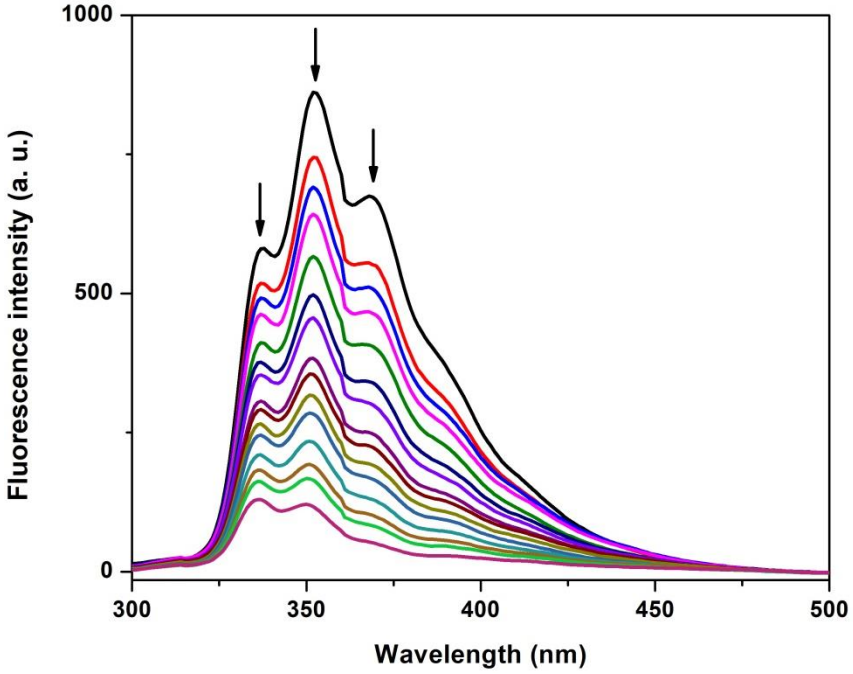

Figure 3.86. Changes in the emission spectra of **1** (3×10^{-6} M, λ_{exc} = 283 nm) with the addition of 2, 4, 6- TNP/ picric acid in DMSO. The arrow indicates the quenching of the fluorescence intensity by addition of an appropriate aliquot of picric acid.

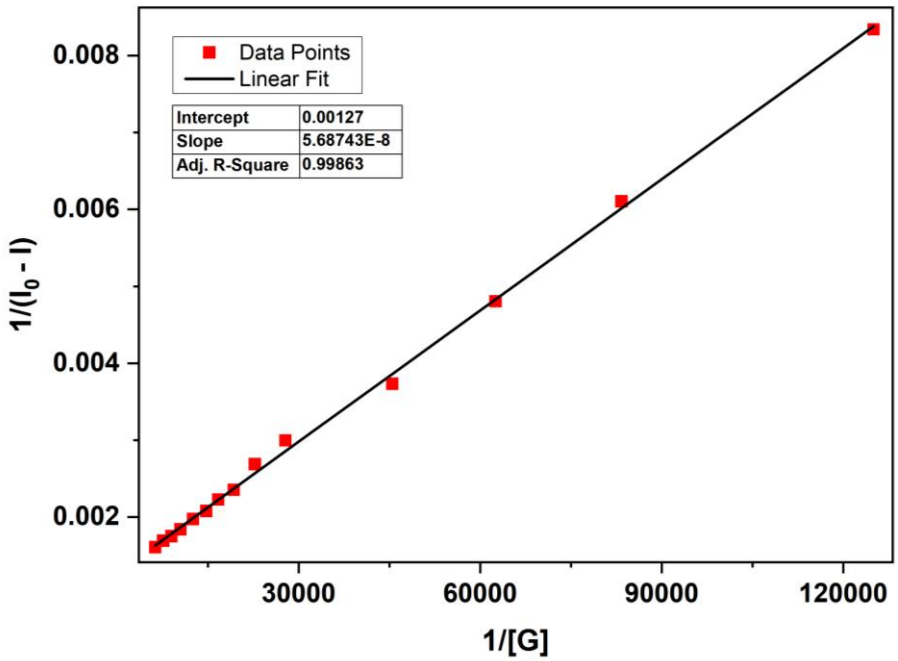

Figure 3.87. Benesi-Hildebrand plot for the emission quenching of host **1** (at 368 nm) with an increase in the concentration of 2, 4, 6- TNP in DMSO.

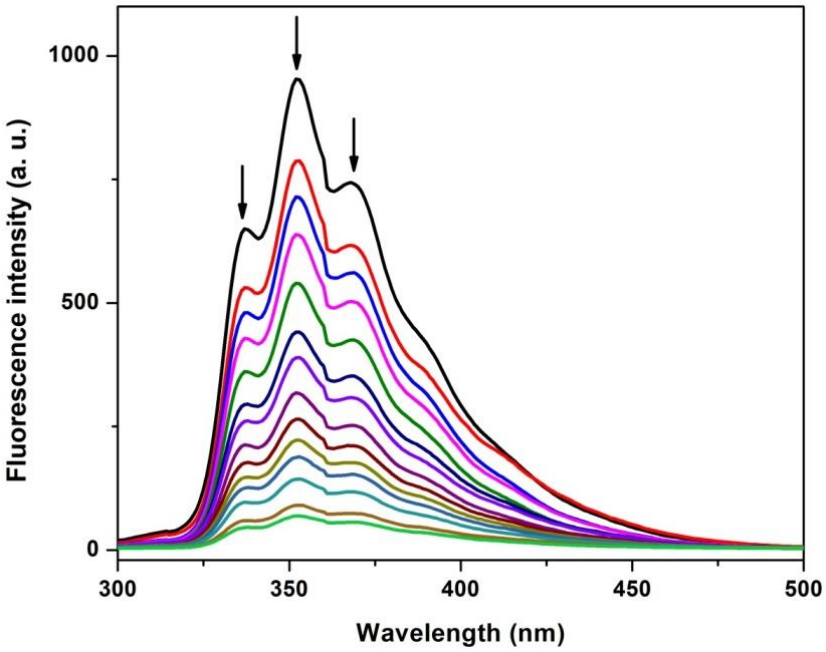

Figure 3.88. Changes in the emission spectra of **1** (3×10^{-6} M, λ_{exc} = 283 nm) with the addition of NB in DMSO. The arrow indicates the quenching of the fluorescence intensity by addition of an appropriate aliquot of NB.

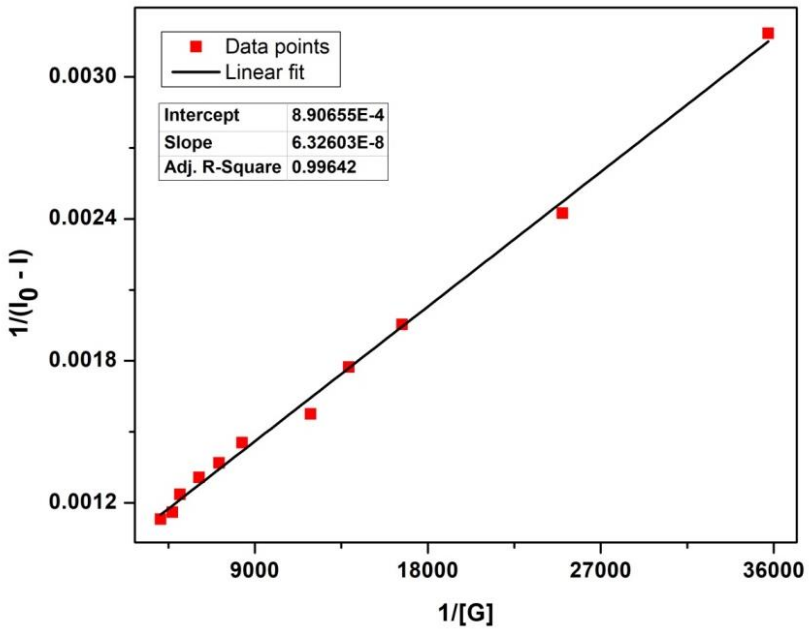

Figure 3.89. Benesi-Hildebrand plot for the emission quenching of host **1** (at 352 nm) with an increase in the concentration of NB in DMSO.

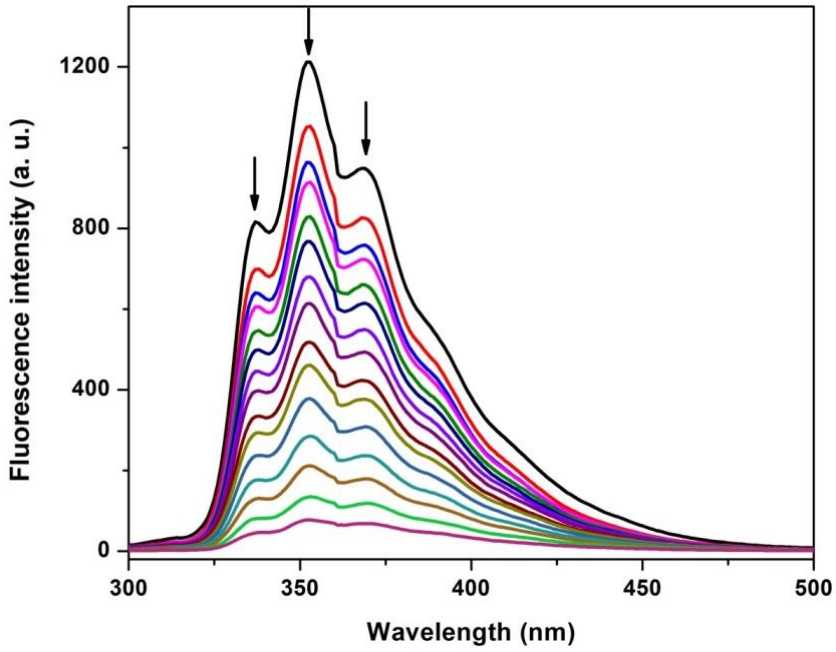

Figure 3.90. Changes in the emission spectra of **1** (3×10^{-6} M, λ_{exc} = 283 nm) with the addition of 2-NT in DMSO. The arrow indicates the quenching of the fluorescence intensity by addition of an appropriate aliquot of 2-NT.

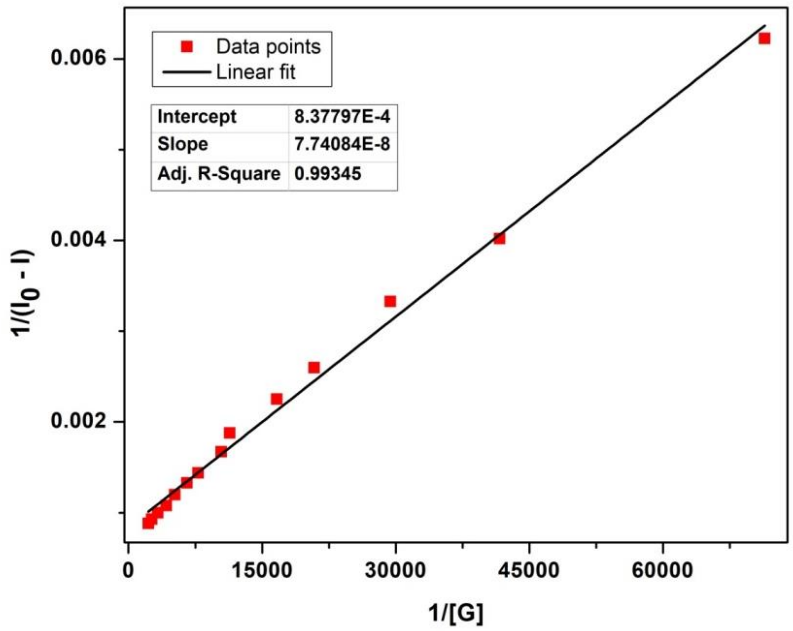

Figure 3.91. Benesi-Hildebrand plot for the emission quenching of host **1** (at 352 nm) with an increase in the concentration of 2-NT in DMSO.

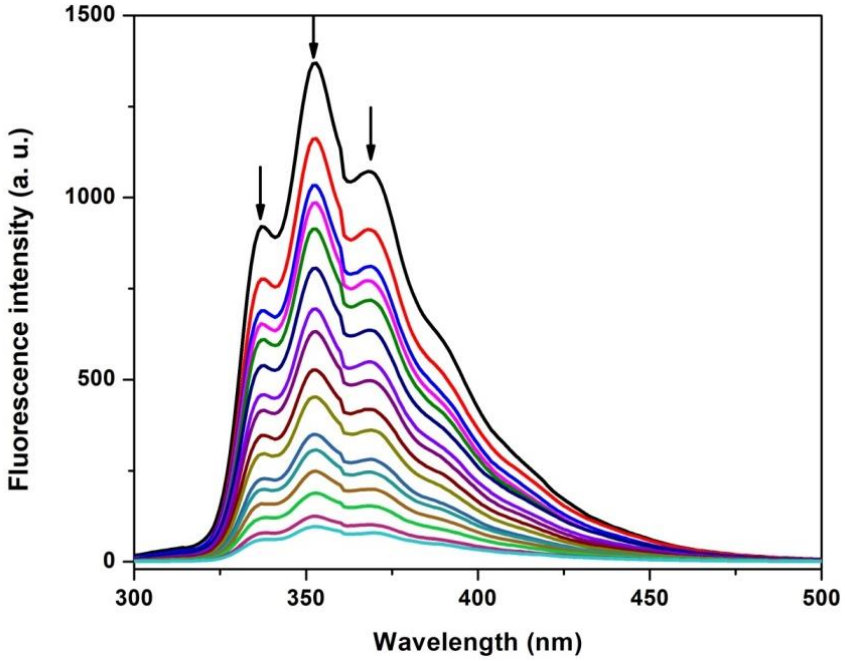

Figure 3.92. Changes in the emission spectra of **1** (3×10^{-6} M, λ_{exc} = 283 nm) with the addition of 4-NT in DMSO. The arrow indicates the quenching of the fluorescence intensity by addition of an appropriate aliquot of 4-NT.

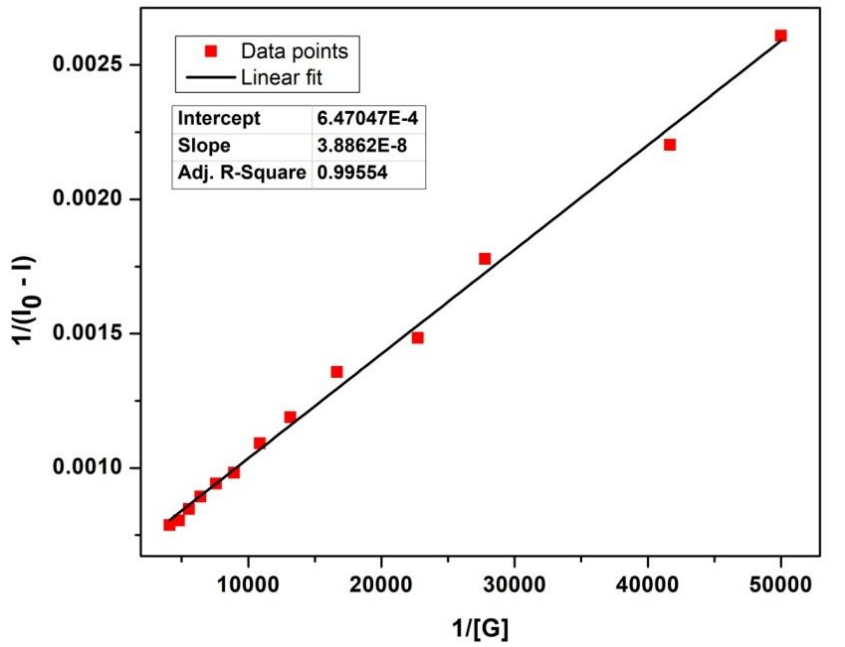

Figure 3.93. Benesi-Hildebrand plot for the emission quenching of host **1** (at 352 nm) with an increase in the concentration of 4-NT in DMSO.

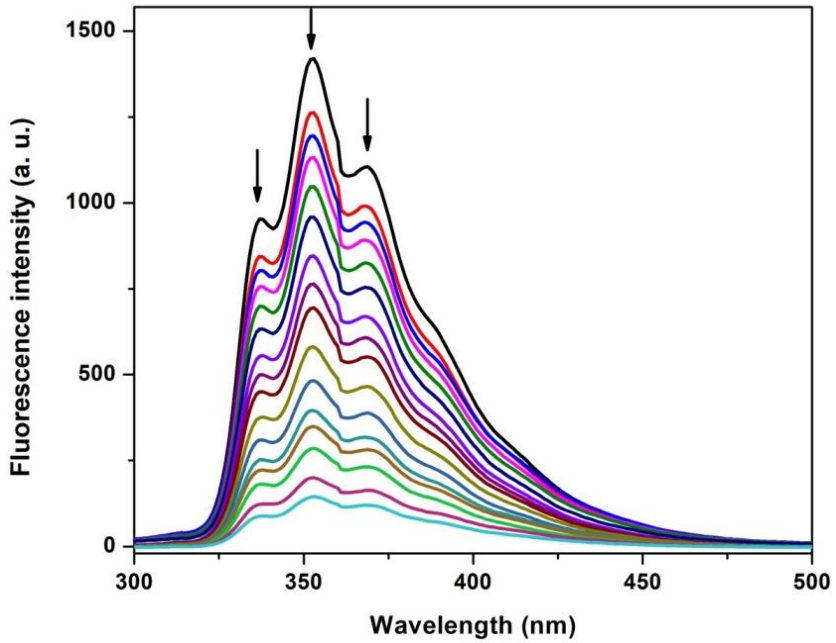

Figure 3.94. Changes in the emission spectra of **1** (3×10^{-6} M, λ_{exc} = 283 nm) with the addition of 2, 4-DNT in DMSO. The arrow indicates the quenching of the fluorescence intensity by addition of an appropriate aliquot of 2, 4-DNT.

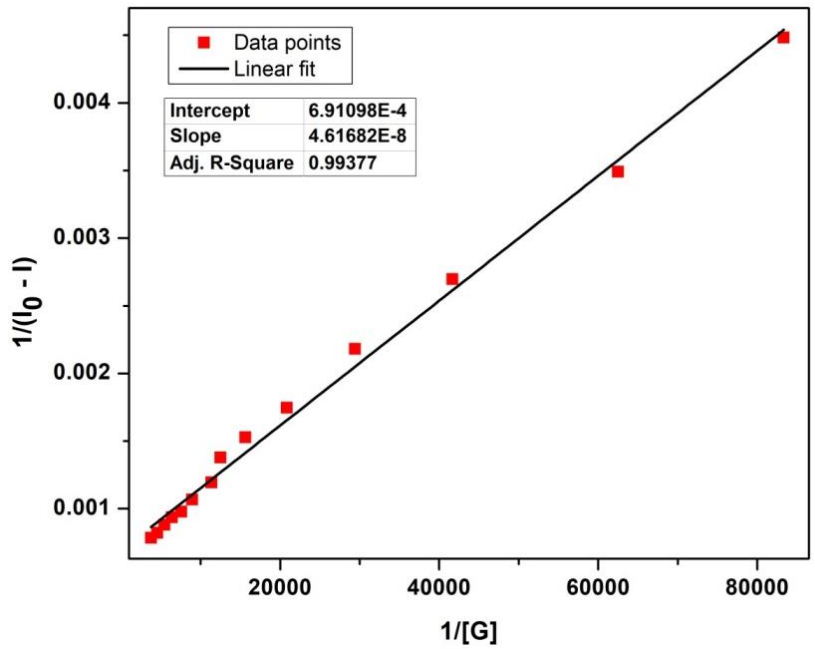

Figure 3.95. Benesi-Hildebrand plot for the emission quenching of host **1** (at 352 nm) with an increase in the concentration of 2, 4-DNT in DMSO.

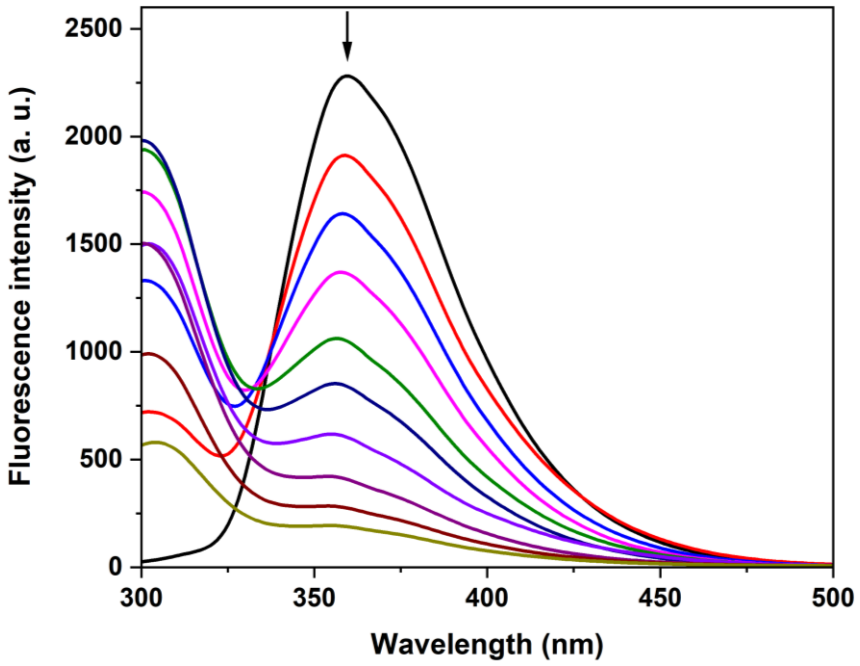

Figure 3.96. Changes in the emission spectra of **2** (1×10^{-6} M, λ_{exc} = 285 nm) with the addition of phenol in DMSO. The arrow indicates the quenching of the fluorescence intensity by addition of an appropriate aliquot of phenol.

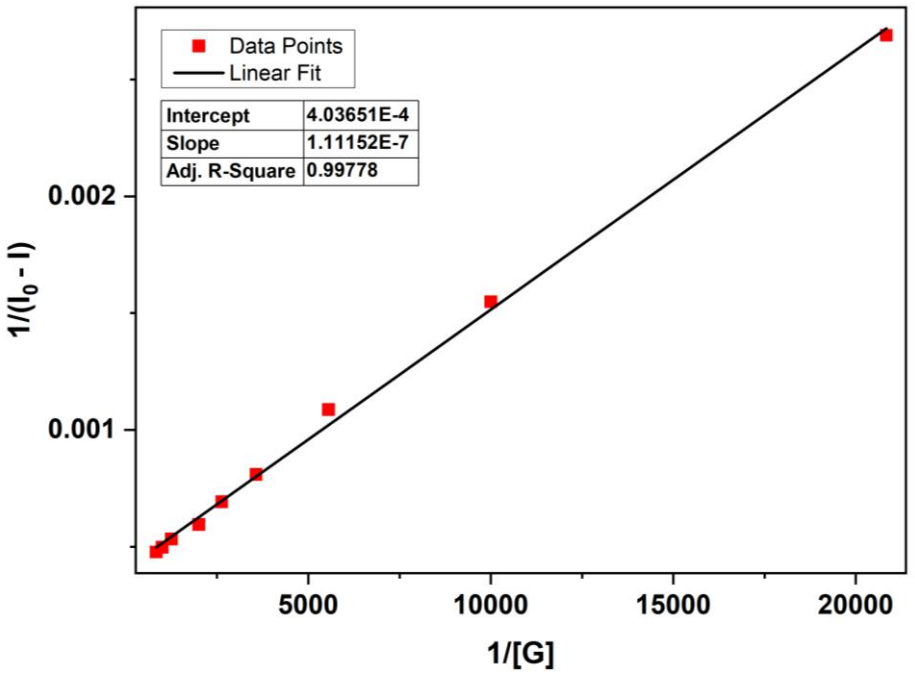

Figure 3.97. Benesi-Hildebrand plot for the emission quenching of host **2** (at 360 nm) with an increase in the concentration of phenol in DMSO.

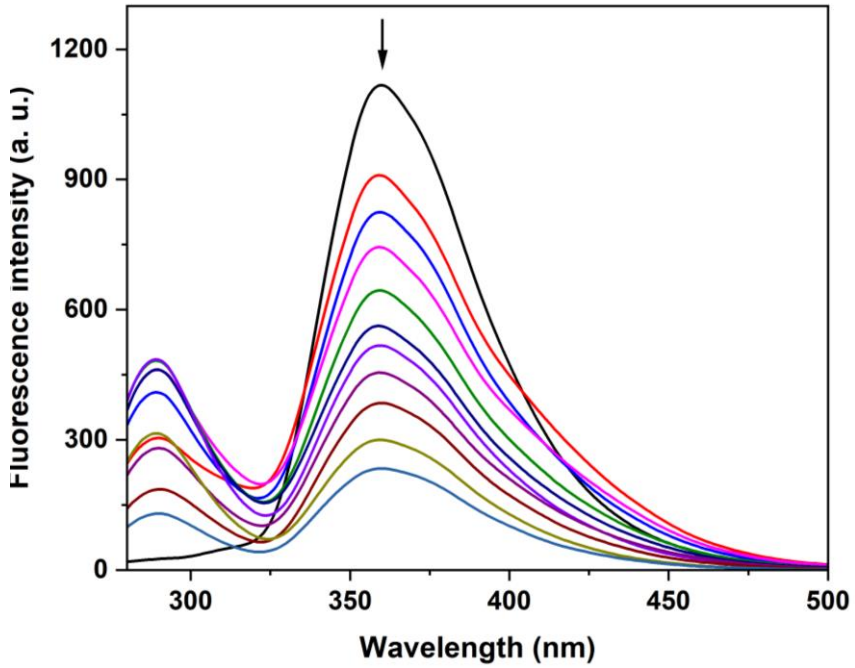

Figure 3.98. Changes in the emission spectra of **2** (1×10^{-6} M, λ_{exc} = 260 nm) with the addition of BA in DMSO. The arrow indicates the quenching of the fluorescence intensity by addition of an appropriate aliquot of BA.

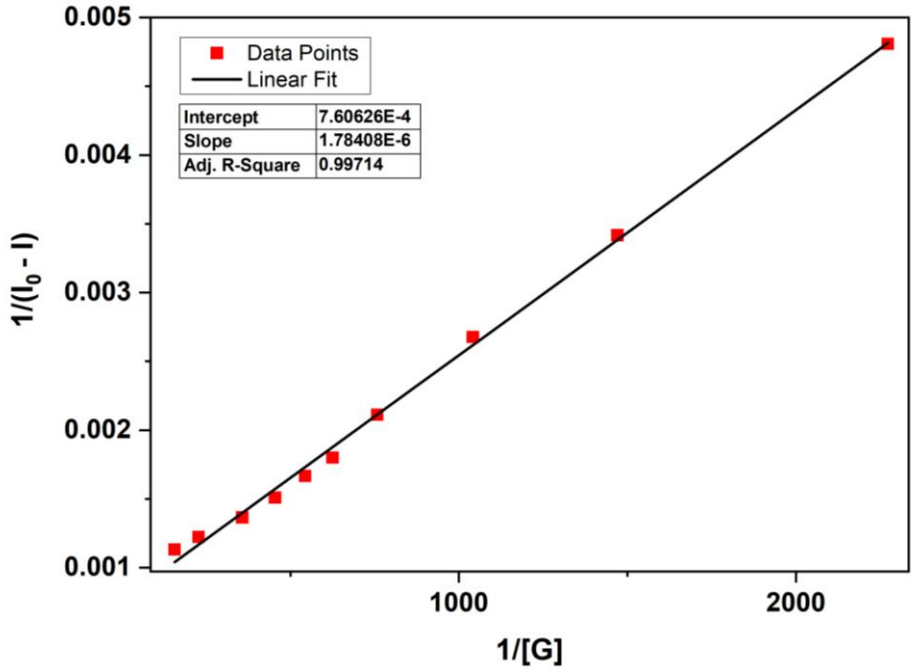

Figure 3.99. Benesi-Hildebrand plot for the emission quenching of host **2** (at 360 nm) with an increase in the concentration of BA in DMSO.

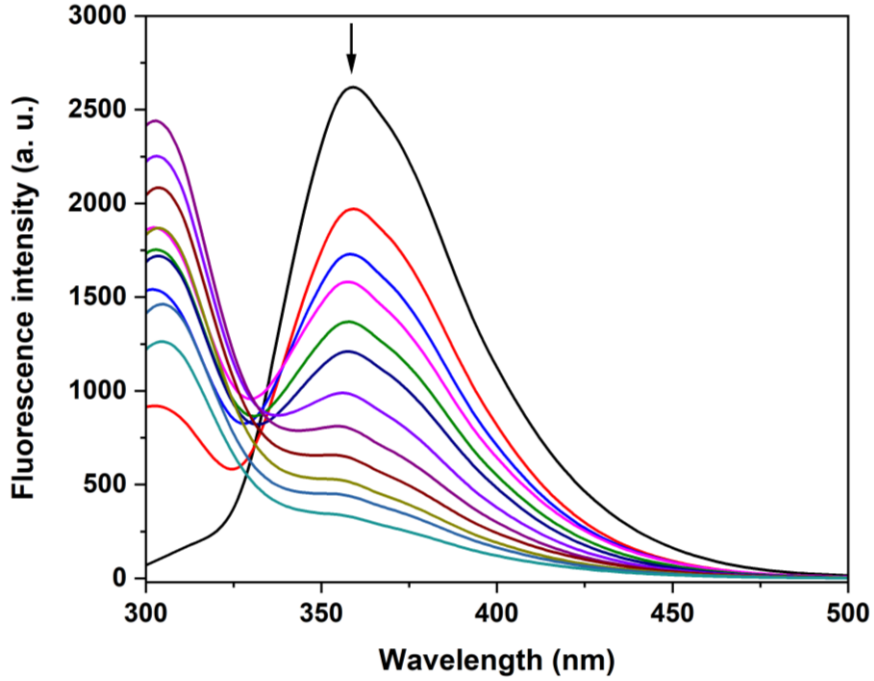

Figure 3.100. Changes in the emission spectra of **2** (1×10^{-6} M, λ_{exc} = 285 nm) with the addition of m-cresol in DMSO. The arrow indicates the quenching of the fluorescence intensity by addition of an appropriate aliquot of m-cresol.

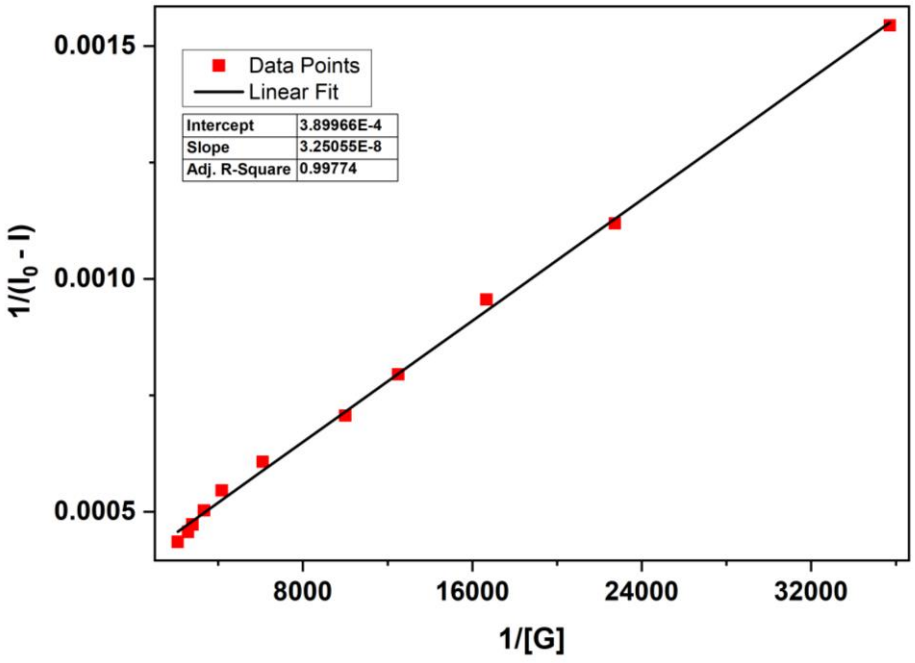

Figure 3.101. Benesi-Hildebrand plot for the emission quenching of host **2** (at 360 nm) with an increase in the concentration of m-cresol in DMSO.

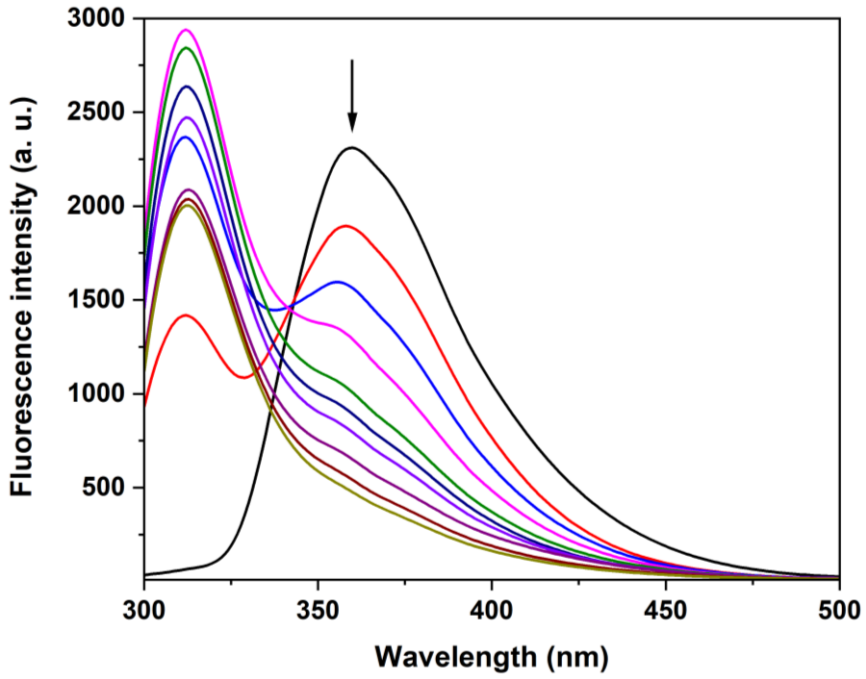

Figure 3.102. Changes in the emission spectra of **2** (1×10^{-6} M, λ_{exc} = 285 nm) with the addition of p-cresol in DMSO. The arrow indicates the quenching of the fluorescence intensity by addition of an appropriate aliquot of p-cresol.

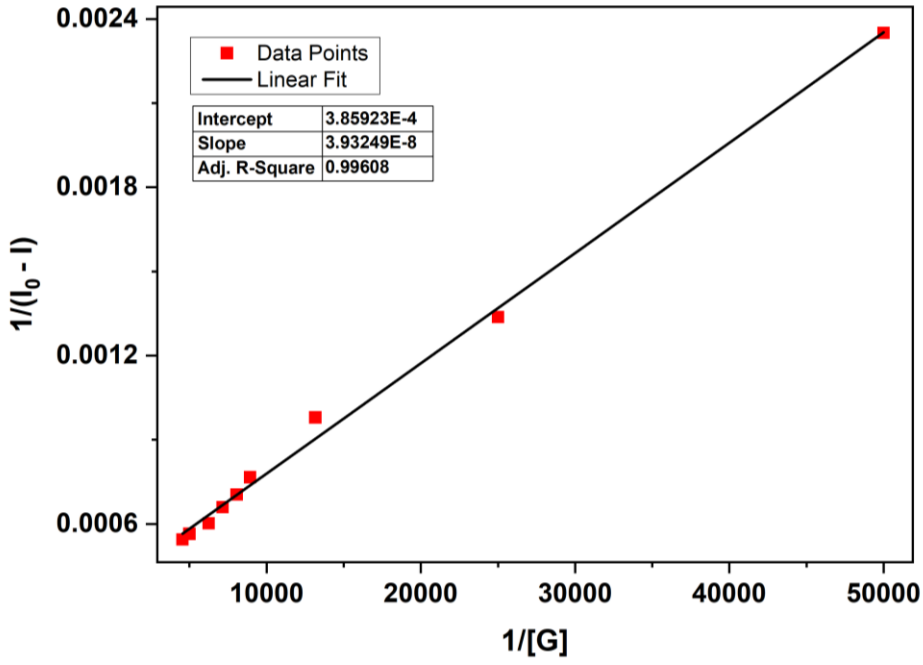

Figure 3.103. Benesi-Hildebrand plot for the emission quenching of host **2** (at 360 nm) with an increase in the concentration of p-cresol in DMSO.

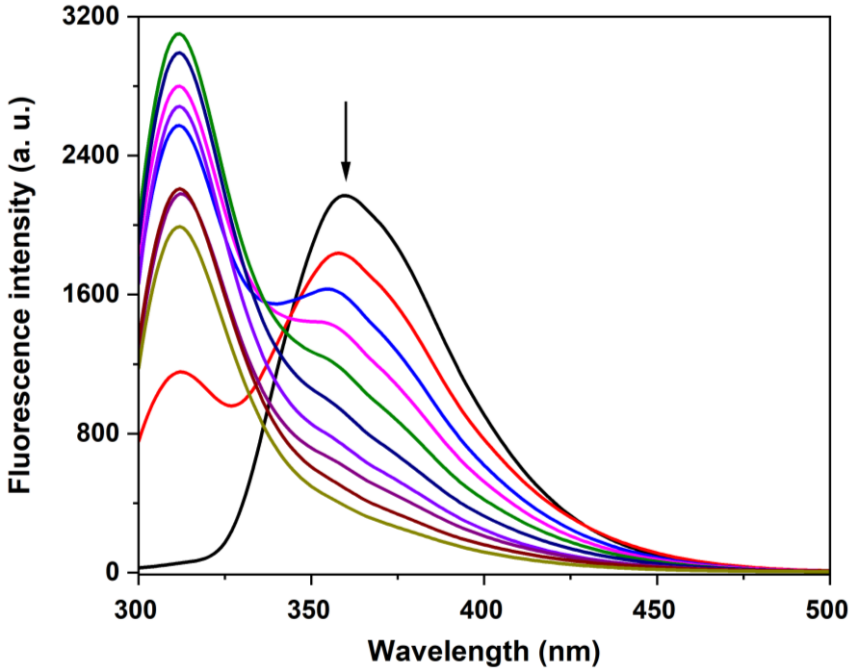

Figure 3.104. Changes in the emission spectra of **2** (1×10^{-6} M, λ_{exc} = 285 nm) with the addition of 3, 4- DMP in DMSO. The arrow indicates the quenching of the fluorescence intensity by addition of an appropriate aliquot of 3, 4- DMP.

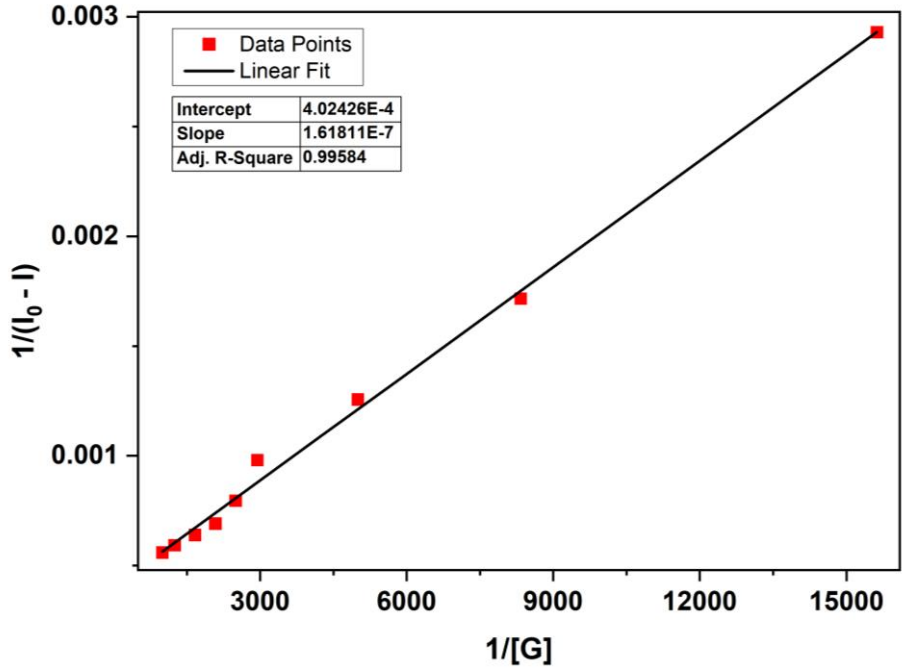

Figure 3.105. Benesi-Hildebrand plot for the emission quenching of host **2** (at 360 nm) with an increase in the concentration of 3, 4- DMP in DMSO.

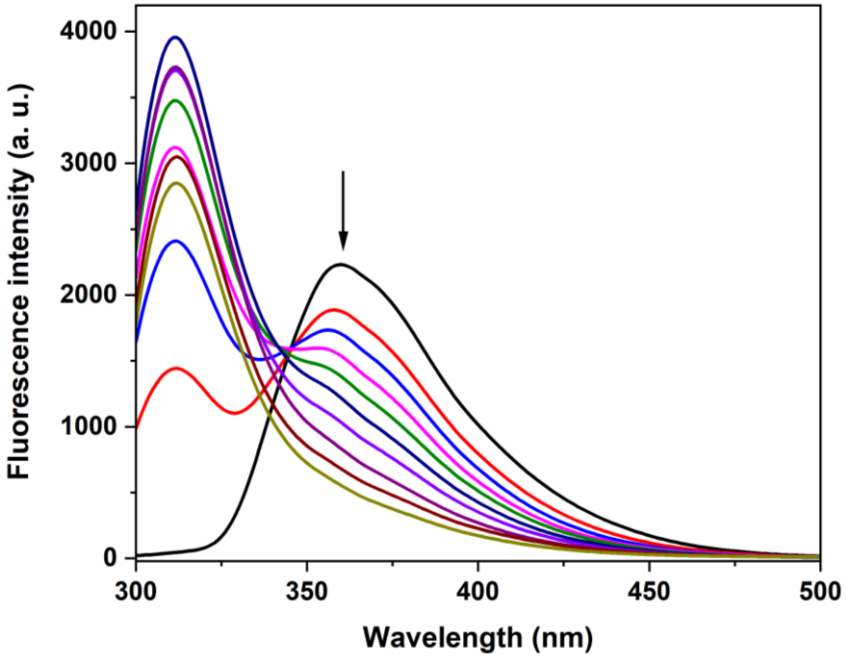

Figure 3.106. Changes in the emission spectra of **2** (1×10^{-6} M, λ_{exc} = 285 nm) with the addition of 2, 4, 6- TMP in DMSO. The arrow indicates the quenching of the fluorescence intensity by addition of an appropriate aliquot of 2, 4, 6- TMP.

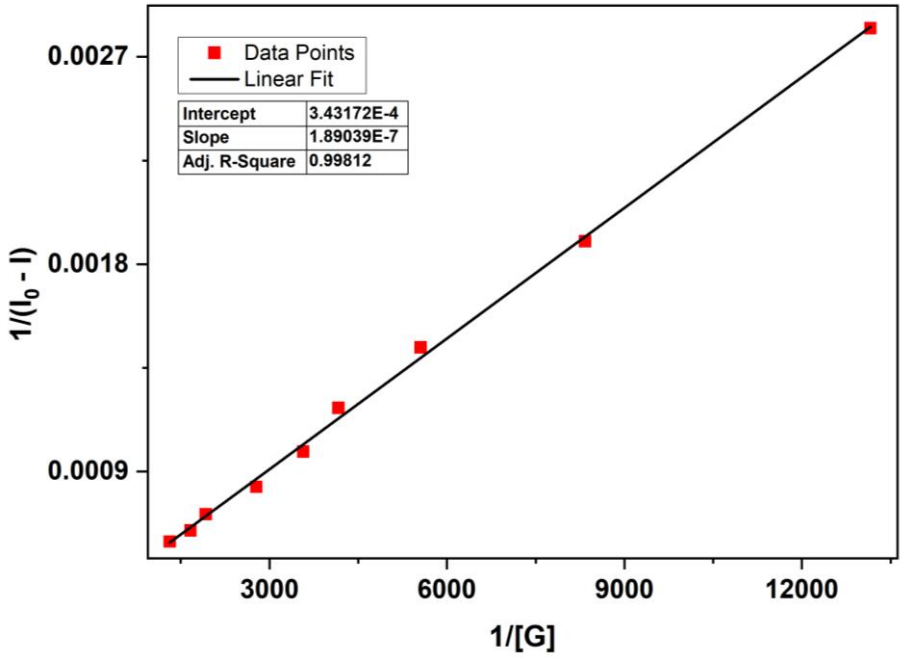

Figure 3.107. Benesi-Hildebrand plot for the emission quenching of host **2** (at 360 nm) with an increase in the concentration of 2, 4, 6- TMP in DMSO.

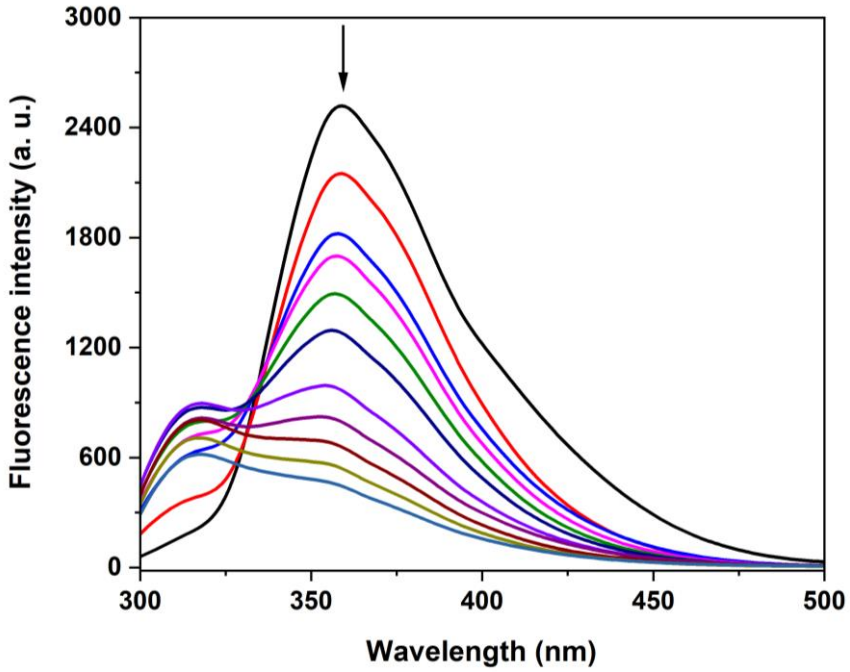

Figure 3.108. Changes in the emission spectra of **2** (1×10^{-6} M, λ_{exc} = 285 nm) with the addition of catechol in DMSO. The arrow indicates the quenching of the fluorescence intensity by addition of an appropriate aliquot of catechol.

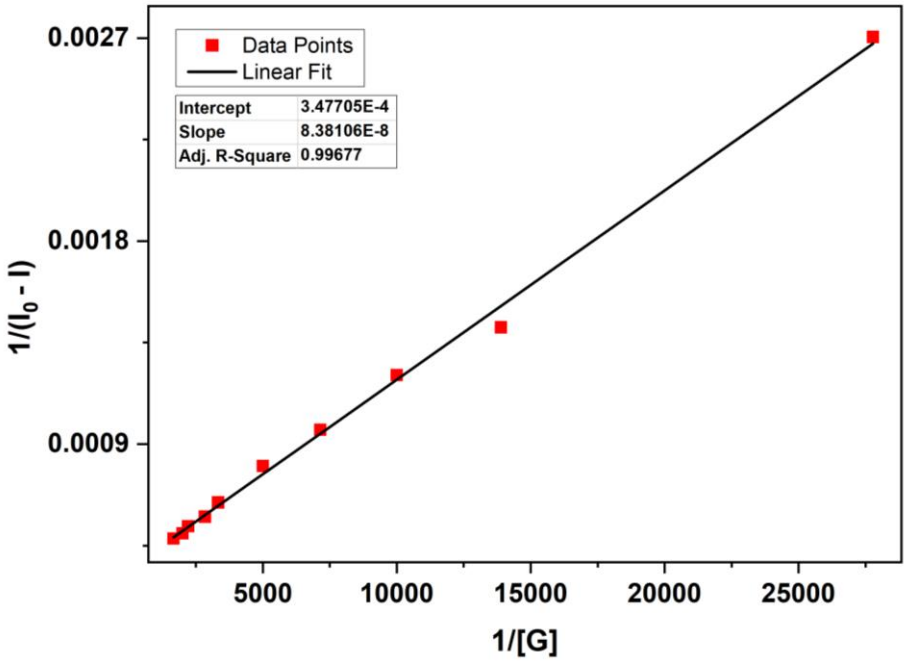

Figure 3.109. Benesi-Hildebrand plot for the emission quenching of host **2** (at 360 nm) with an increase in the concentration of catechol in DMSO.

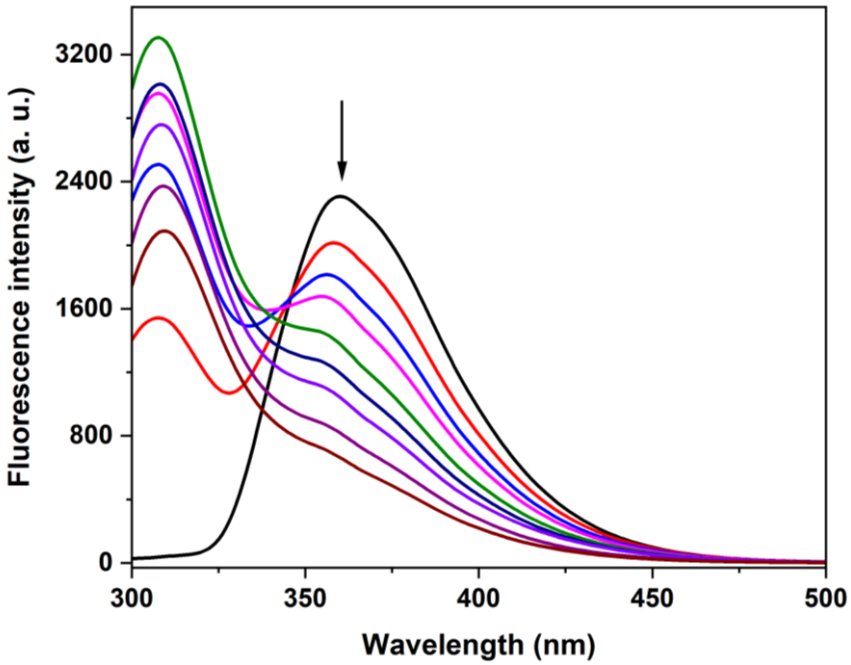

Figure 3.110. Changes in the emission spectra of **2** (1×10^{-6} M, λ_{exc} = 285 nm) with the addition of resorcinol in DMSO. The arrow indicates the quenching of the fluorescence intensity by addition of an appropriate aliquot of resorcinol.

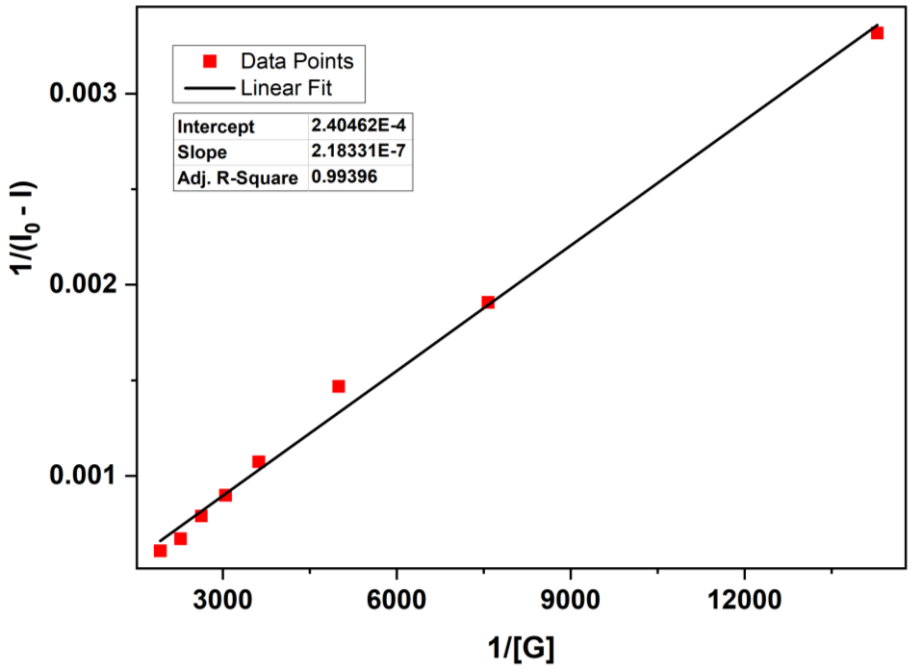

Figure 3.111. Benesi-Hildebrand plot for the emission quenching of host **2** (at 360 nm) with an increase in the concentration of resorcinol in DMSO.

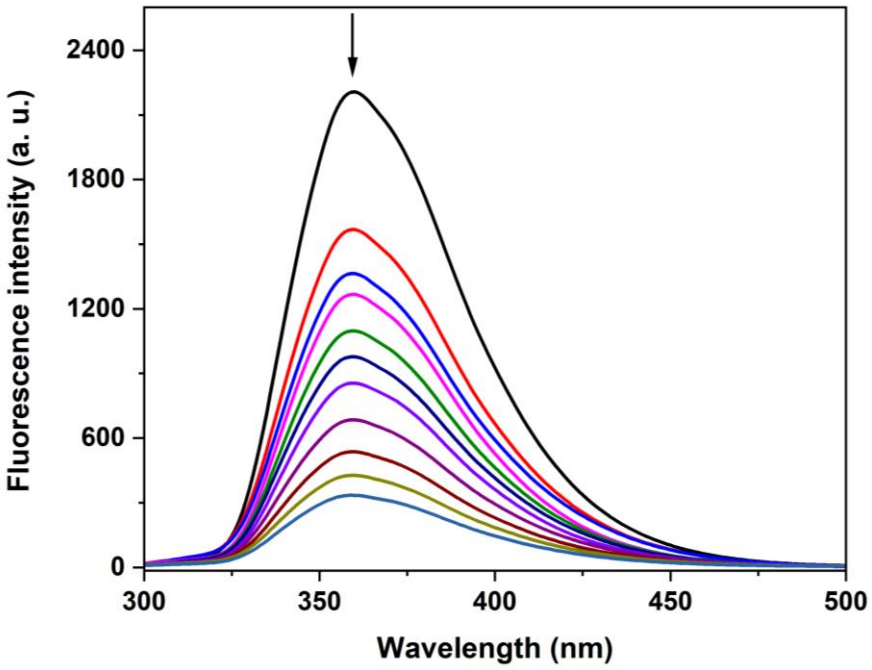

Figure 3.112. Changes in the emission spectra of **2** (1×10^{-6} M, λ_{exc} = 285 nm) with the addition of 2-CP in DMSO. The arrow indicates the quenching of the fluorescence intensity by addition of an appropriate aliquot of 2-CP.

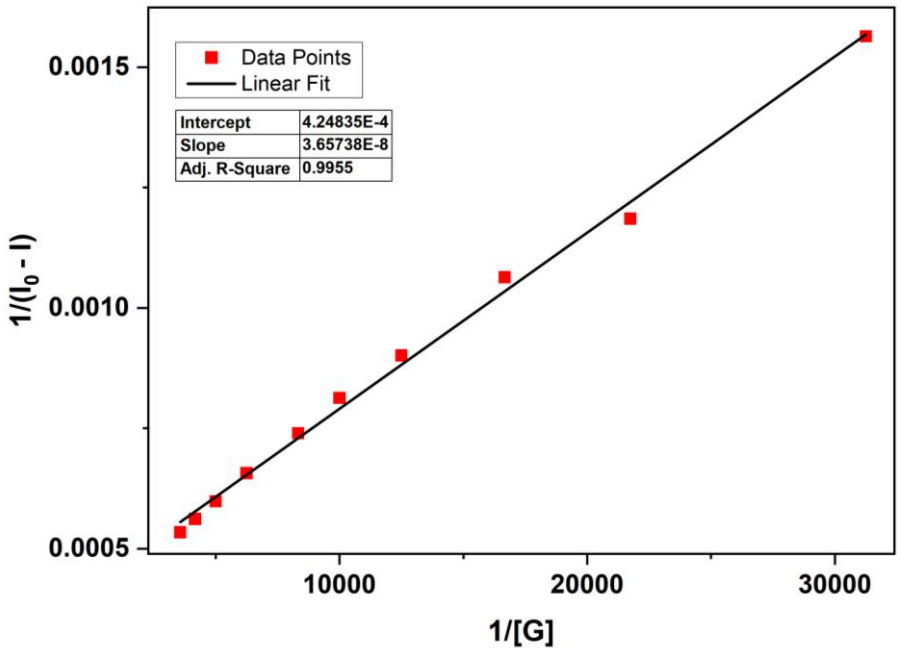

Figure 3.113. Benesi-Hildebrand plot for the emission quenching of host **2** (at 360 nm) with an increase in the concentration of 2-CP in DMSO.

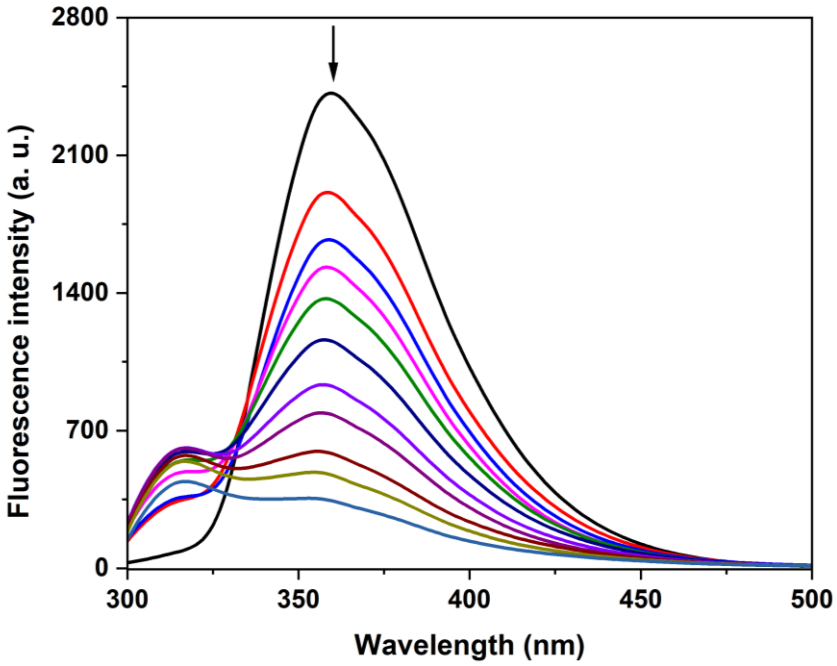

Figure 3.114. Changes in the emission spectra of **2** (1×10^{-6} M, λ_{exc} = 285 nm) with the addition of 4-chlorophenol in DMSO. The arrow indicates the quenching of the fluorescence intensity by addition of an appropriate aliquot of 4-CP.

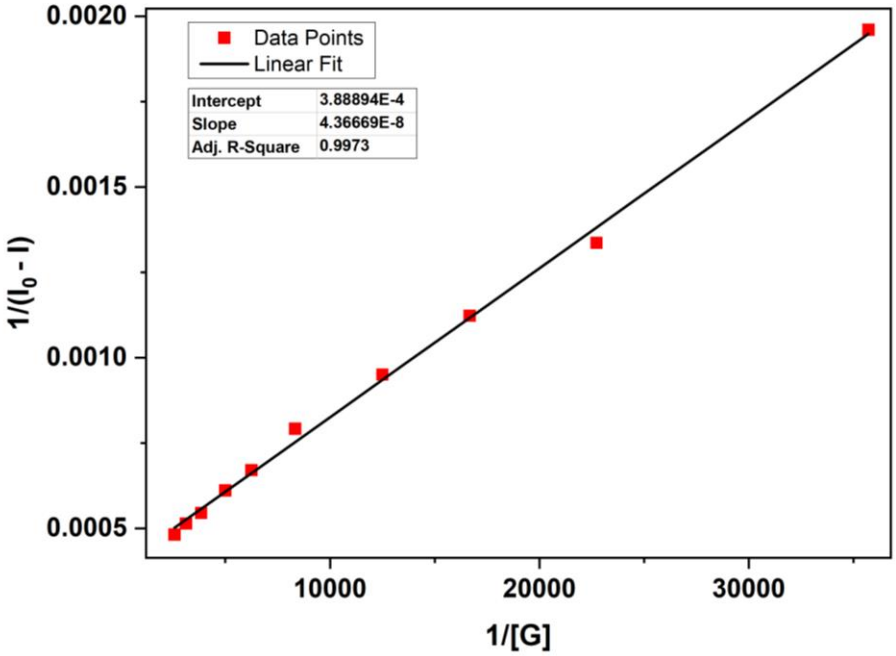

Figure 3.115. Benesi-Hildebrand plot for the emission quenching of host **2** (at 360 nm) with an increase in the concentration of 4-CP in DMSO.

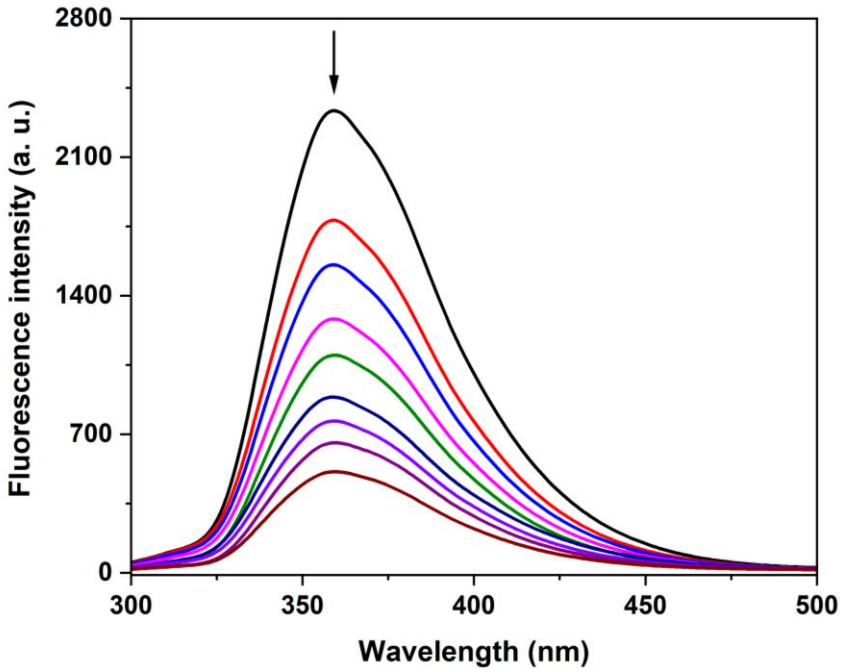

Figure 3.116. Changes in the emission spectra of **2** (1×10^{-6} M, λ_{exc} = 285 nm) with the addition of 2, 4-DCP in DMSO. The arrow indicates the quenching of the fluorescence intensity by addition of an appropriate aliquot of 2, 4-DCP.

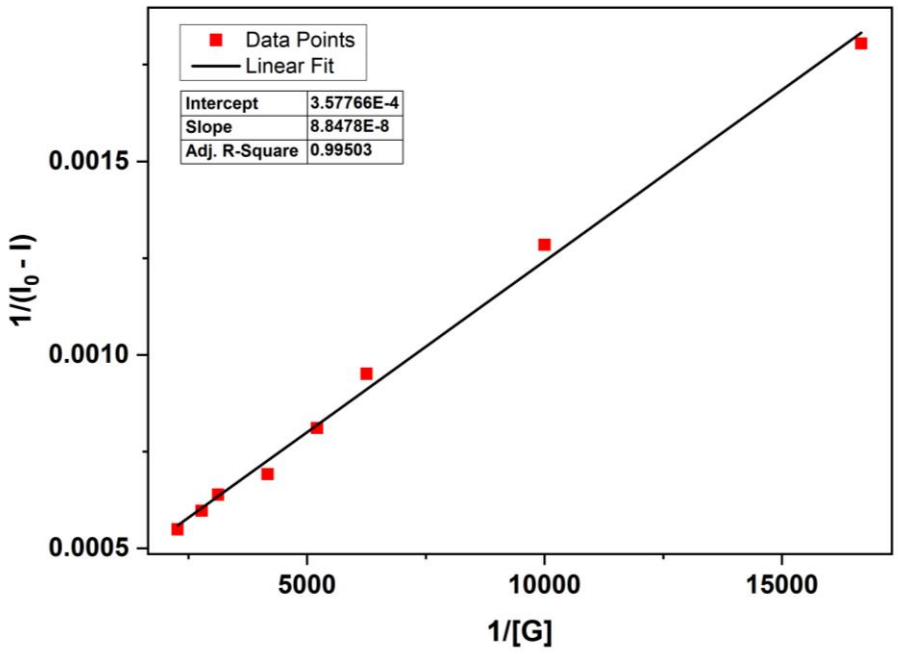

Figure 3.117. Benesi-Hildebrand plot for the emission quenching of host **2** (at 360 nm) with an increase in the concentration of 2, 4-DCP in DMSO.

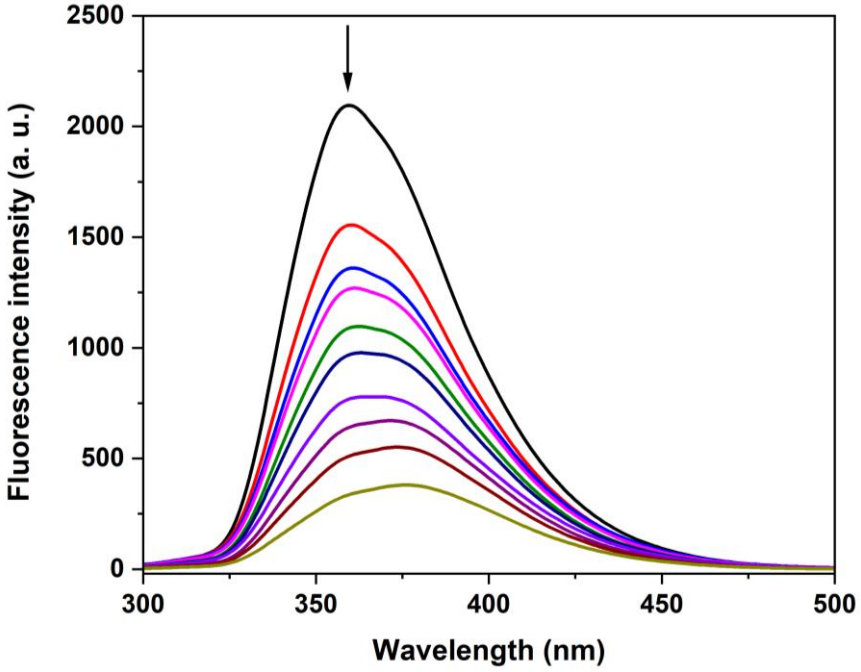

Figure 3.118. Changes in the emission spectra of **2** (1×10^{-6} M, λ_{exc} = 285 nm) with the addition of 2- NP in DMSO. The arrow indicates the quenching of the fluorescence intensity by addition of an appropriate aliquot of 2-NP.

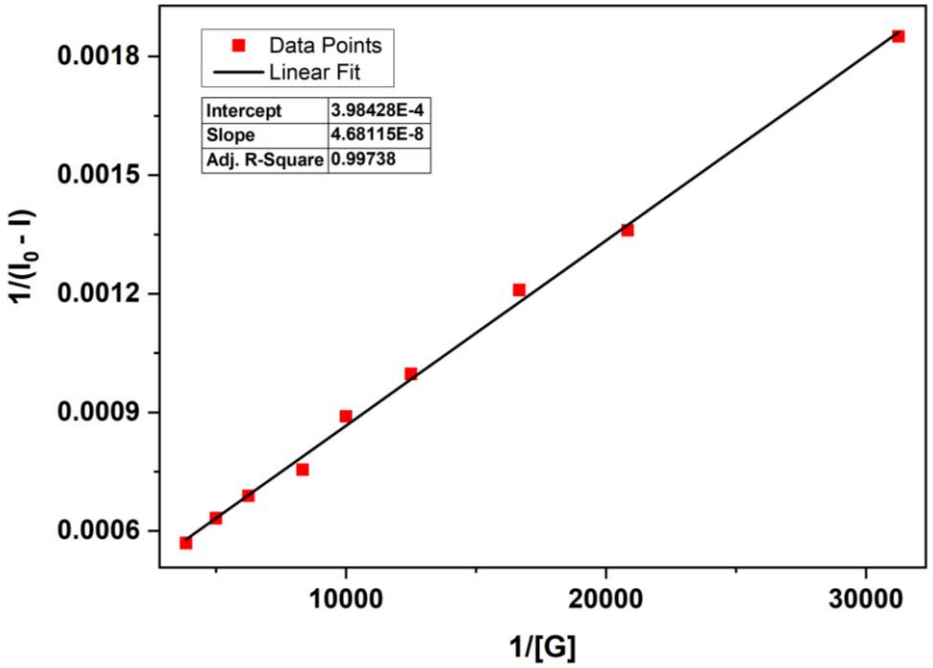

Figure 3.119. Benesi-Hildebrand plot for the emission quenching of host **2** (at 360 nm) with an increase in the concentration of 2-NP in DMSO.

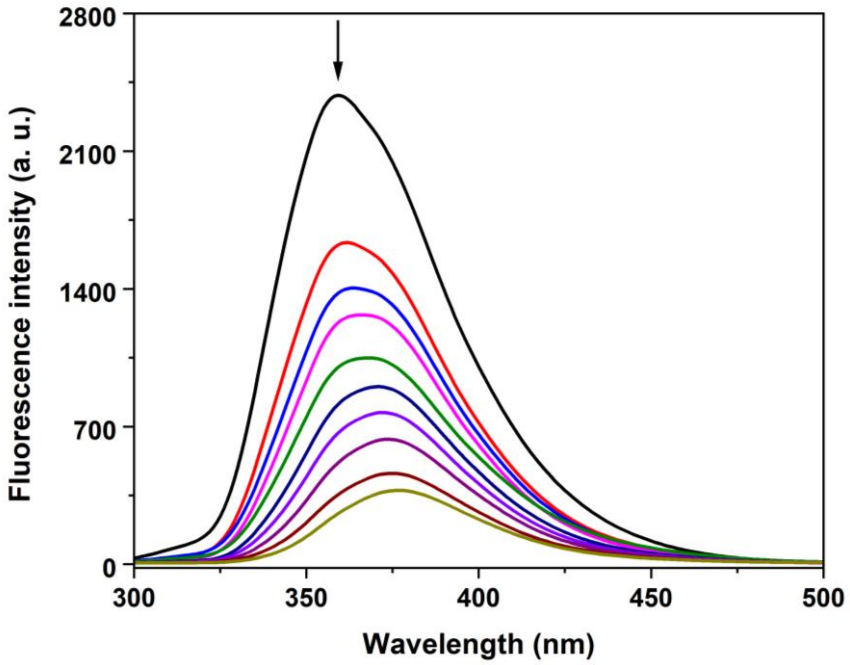

Figure 3.120. Changes in the emission spectra of **2** (1×10^{-6} M, λ_{exc} = 285 nm) with the addition of 4- NP in DMSO. The arrow indicates the quenching of the fluorescence intensity by addition of an appropriate aliquot of 4-NP.

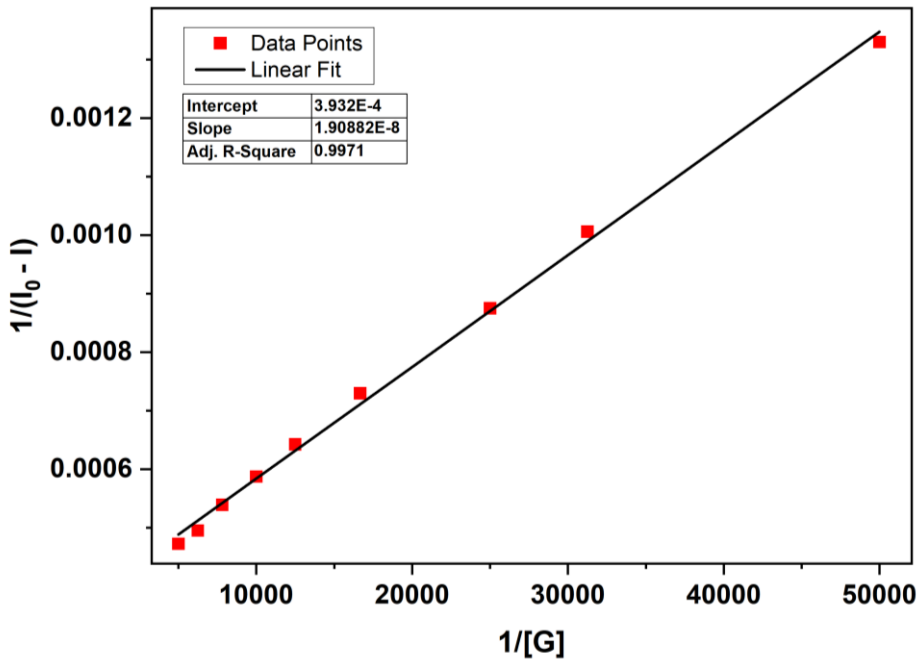

Figure 3.121. Benesi-Hildebrand plot for the emission quenching of host **2** (at 360 nm) with an increase in the concentration of 4-NP in DMSO.

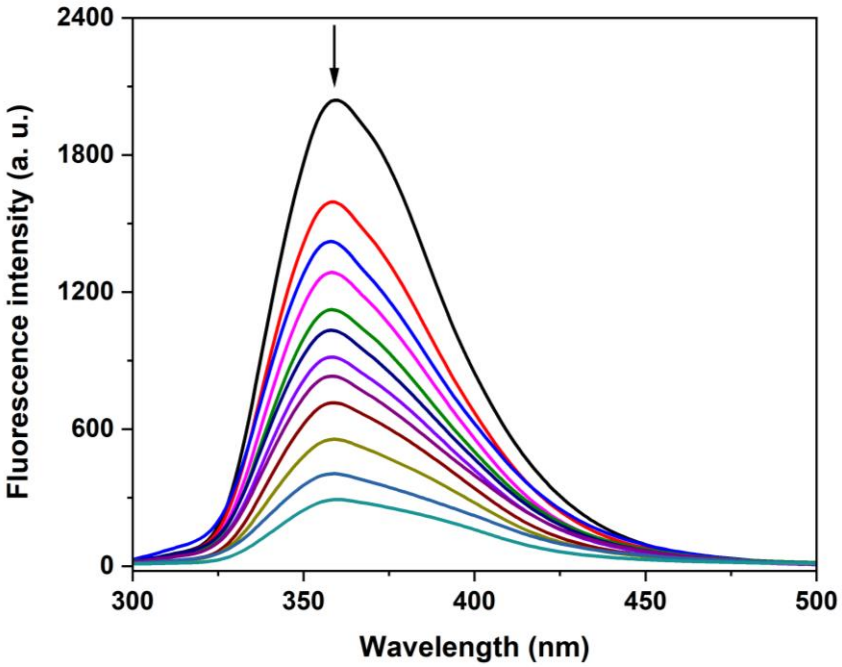

Figure 3.122. Changes in the emission spectra of **2** (1×10^{-6} M, λ_{exc} = 285 nm) with the addition of 2, 4- DNP in DMSO. The arrow indicates the quenching of the fluorescence intensity by addition of an appropriate aliquot of 2, 4- DNP.

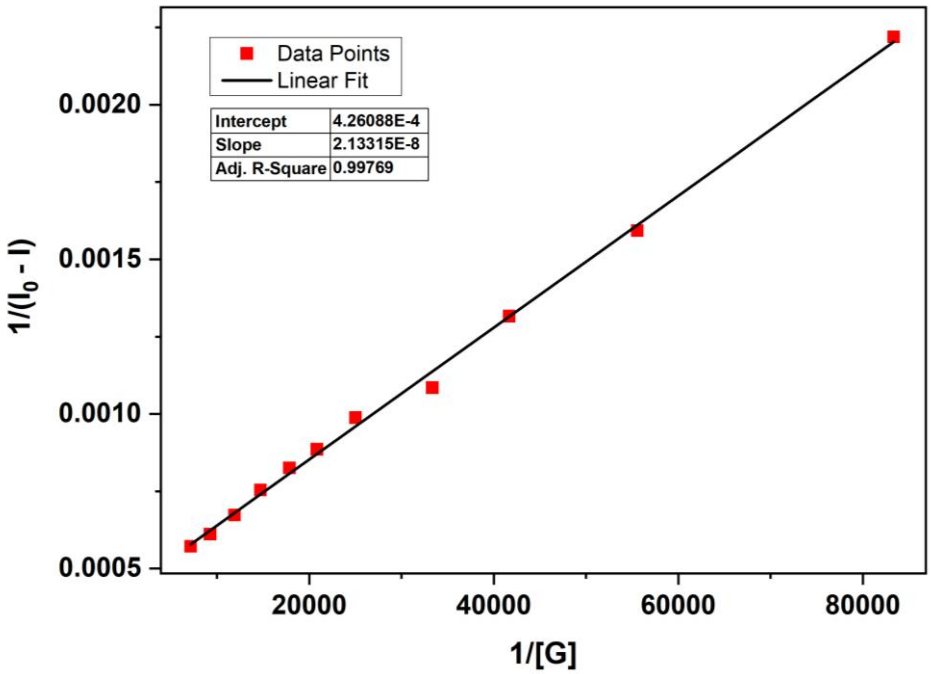

Figure 3.123. Benesi-Hildebrand plot for the emission quenching of host **2** (at 360 nm) with an increase in the concentration of 2, 4- DNP in DMSO.

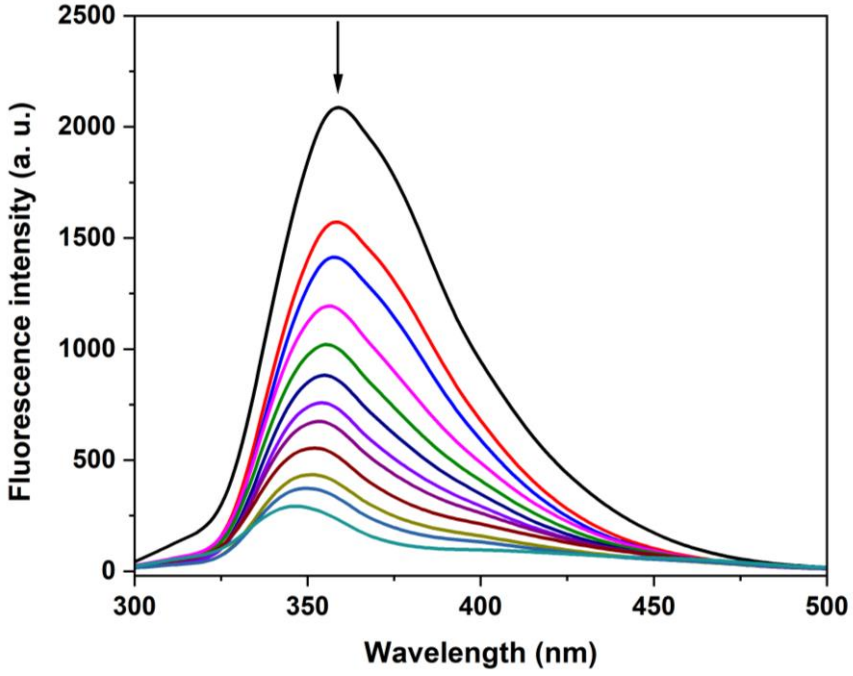

Figure 3.124. Changes in the emission spectra of **2** (1×10^{-6} M, λ_{exc} = 285 nm) with the addition of 2, 4, 6- TNP/ picric acid in DMSO. The arrow indicates the quenching of the fluorescence intensity by addition of an appropriate aliquot of picric acid.

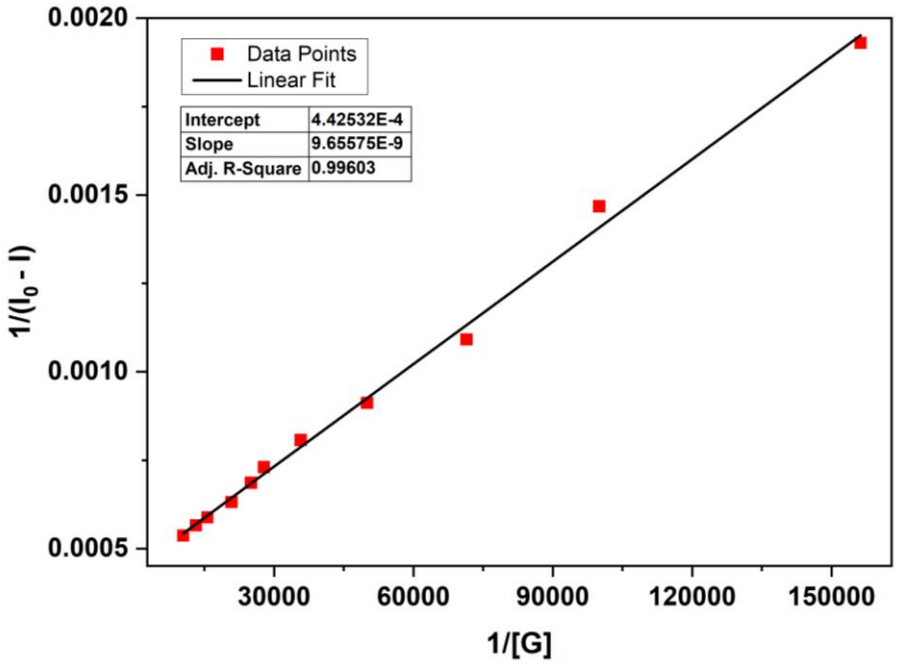

Figure 3.125. Benesi-Hildebrand plot for the emission quenching of host **2** (at 360 nm) with an increase in the concentration of 2, 4, 6- TNP in DMSO.

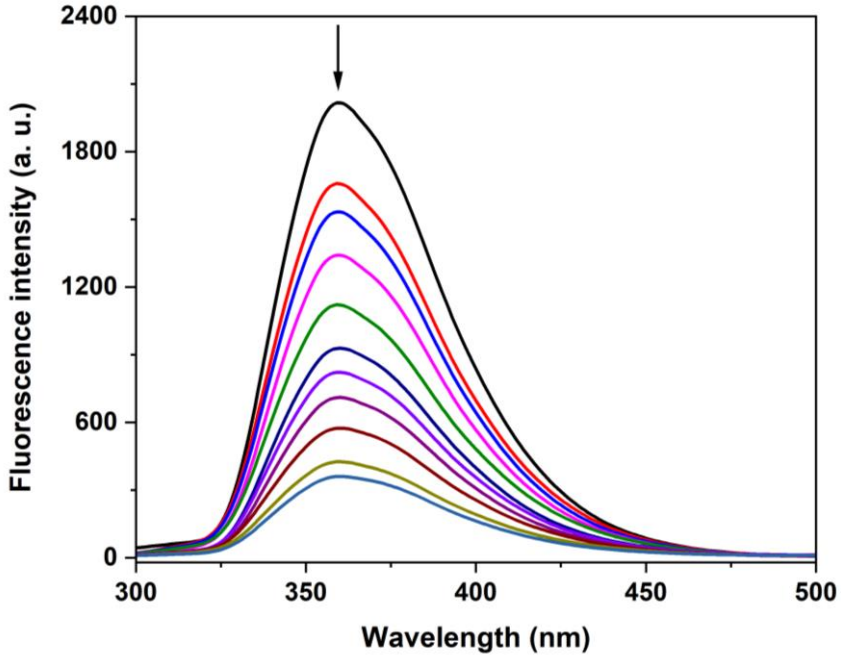

Figure 3.126. Changes in the emission spectra of **2** (1×10^{-6} M, λ_{exc} = 285 nm) with the addition of NB in DMSO. The arrow indicates the quenching of the fluorescence intensity by addition of an appropriate aliquot of NB.

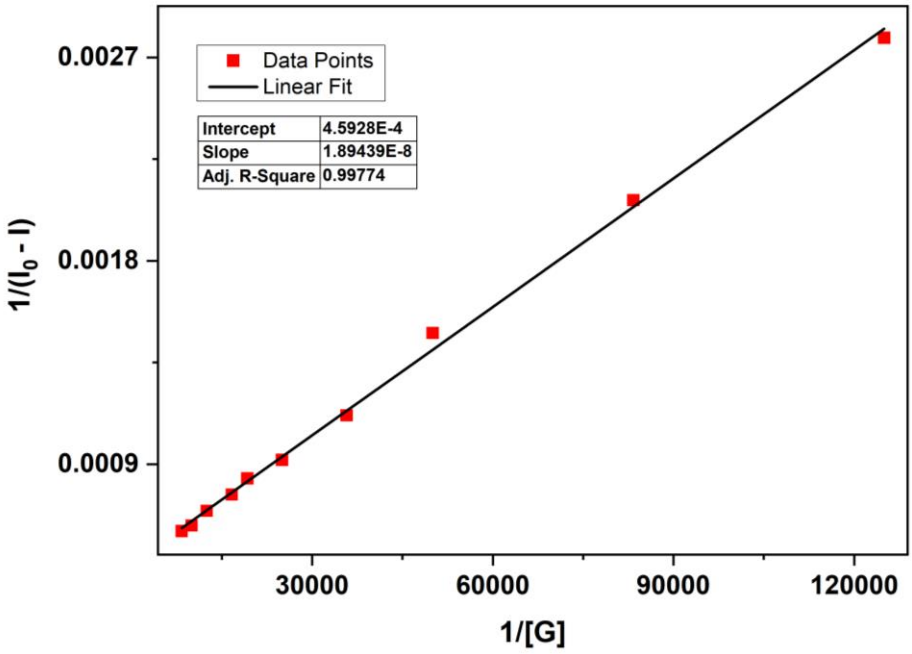

Figure 3.127. Benesi-Hildebrand plot for the emission quenching of host **2** (at 360 nm) with an increase in the concentration of NB in DMSO.

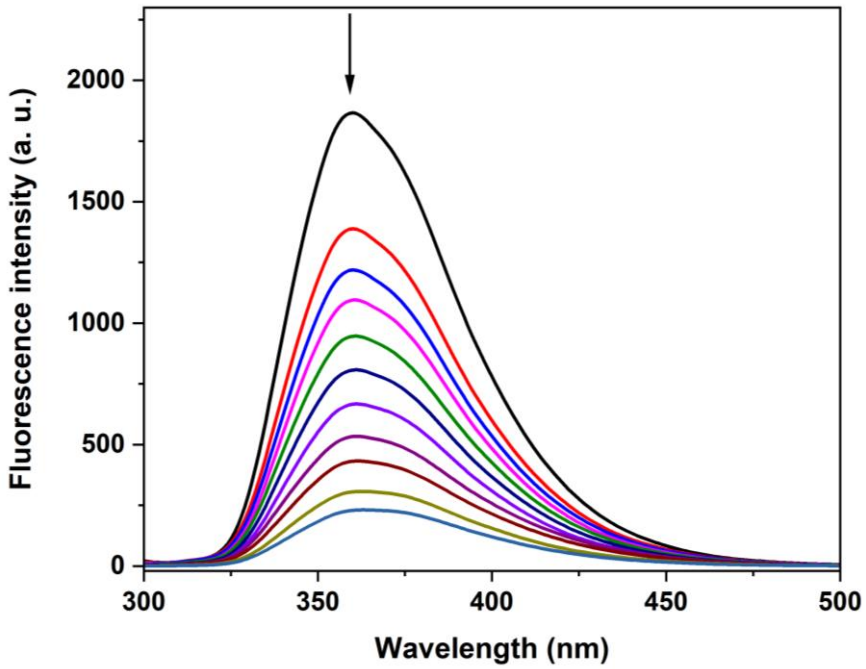

Figure 3.128. Changes in the emission spectra of **2** (1×10^{-6} M, λ_{exc} = 285 nm) with the addition of 2-NT in DMSO. The arrow indicates the quenching of the fluorescence intensity by addition of an appropriate aliquot of 2-NT.

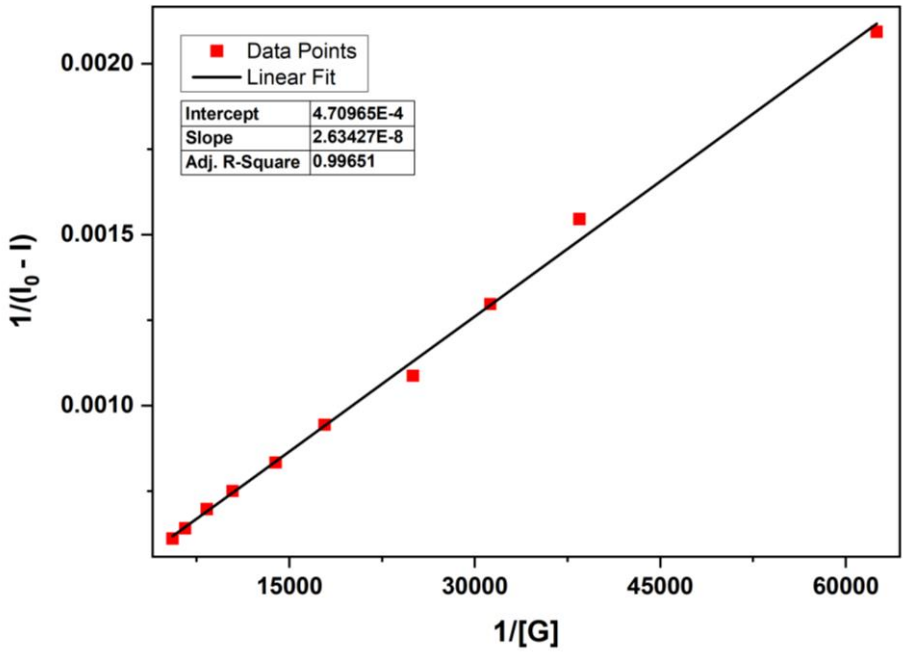

Figure 3.129. Benesi-Hildebrand plot for the emission quenching of host **2** (at 360 nm) with an increase in the concentration of 2-NT in DMSO.

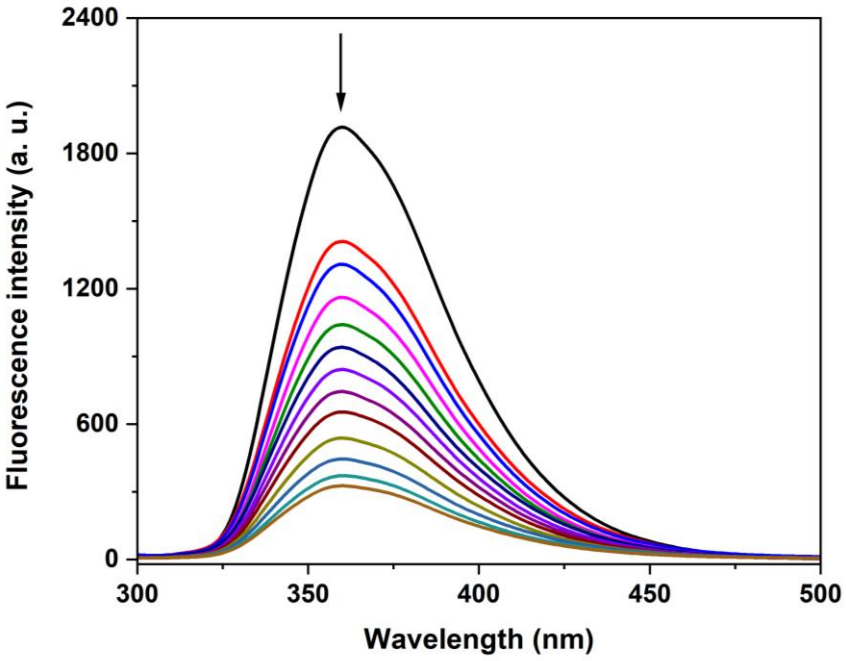

Figure 3.130. Changes in the emission spectra of **2** (1×10^{-6} M, λ_{exc} = 285 nm) with the addition of 4-NT in DMSO. The arrow indicates the quenching of the fluorescence intensity by addition of an appropriate aliquot of 4-NT.

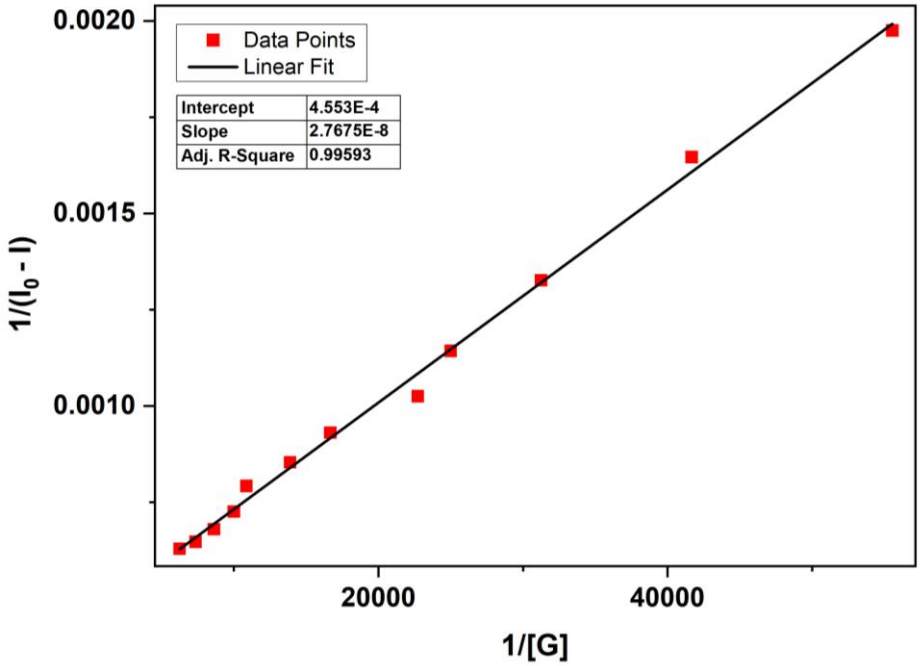

Figure 3.131. Benesi-Hildebrand plot for the emission quenching of host **2** (at 360 nm) with an increase in the concentration of 4-NT in DMSO.

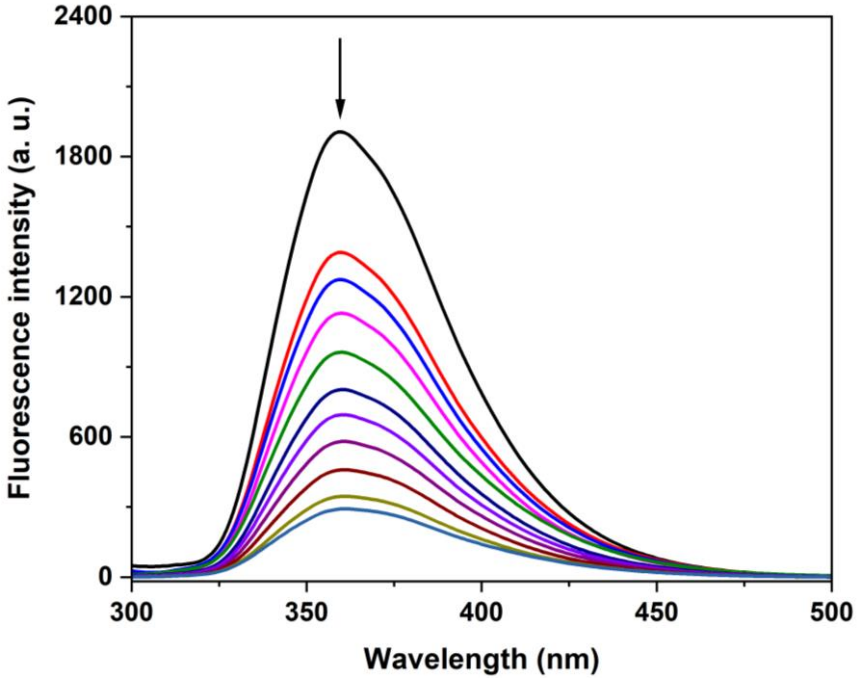

Figure 3.132. Changes in the emission spectra of **2** (1×10^{-6} M, λ_{exc} = 285 nm) with the addition of 2, 4-DNT in DMSO. The arrow indicates the quenching of the fluorescence intensity by addition of an appropriate aliquot of 2, 4-DNT.

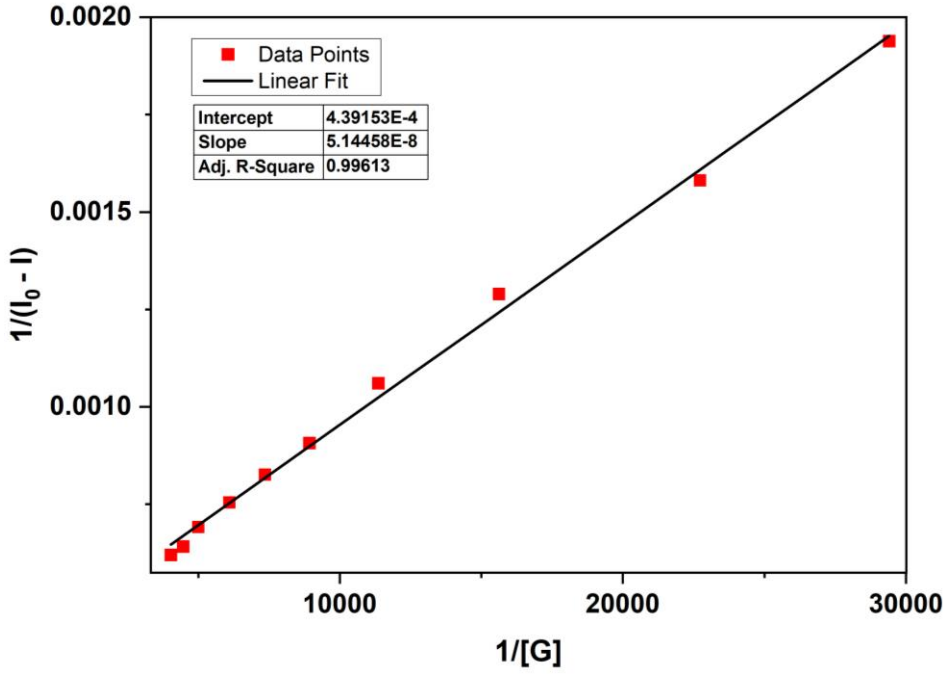

Figure 3.133. Benesi-Hildebrand plot for the emission quenching of host **2** (at 360 nm) with an increase in the concentration of 2, 4-DNT in DMSO.

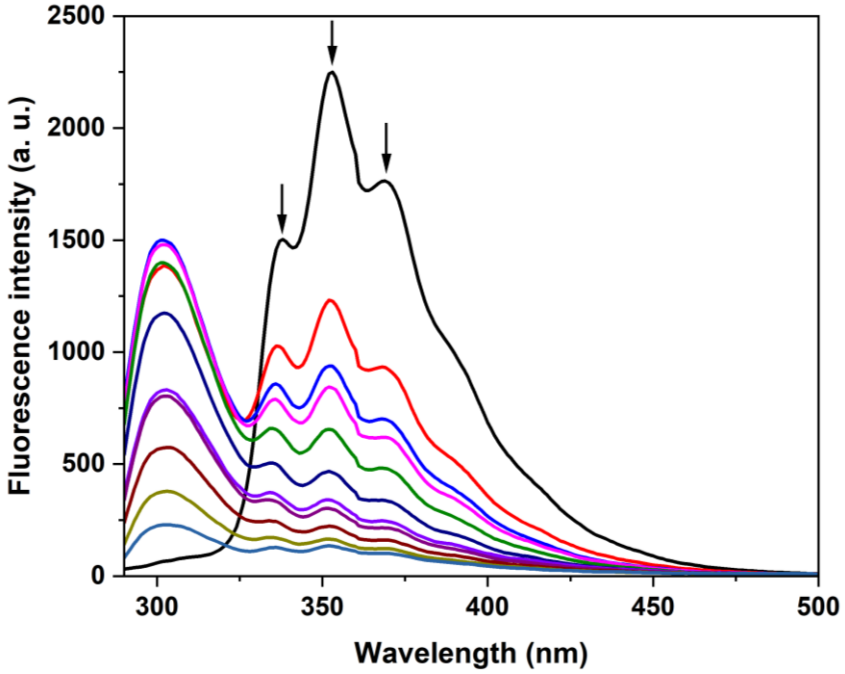

Figure 3.134. Changes in the emission spectra of **7** (4×10^{-6} M, λ_{exc} = 276 nm) with the addition of phenol in DMSO. The arrow indicates the quenching of the fluorescence intensity by addition of an appropriate aliquot of phenol.

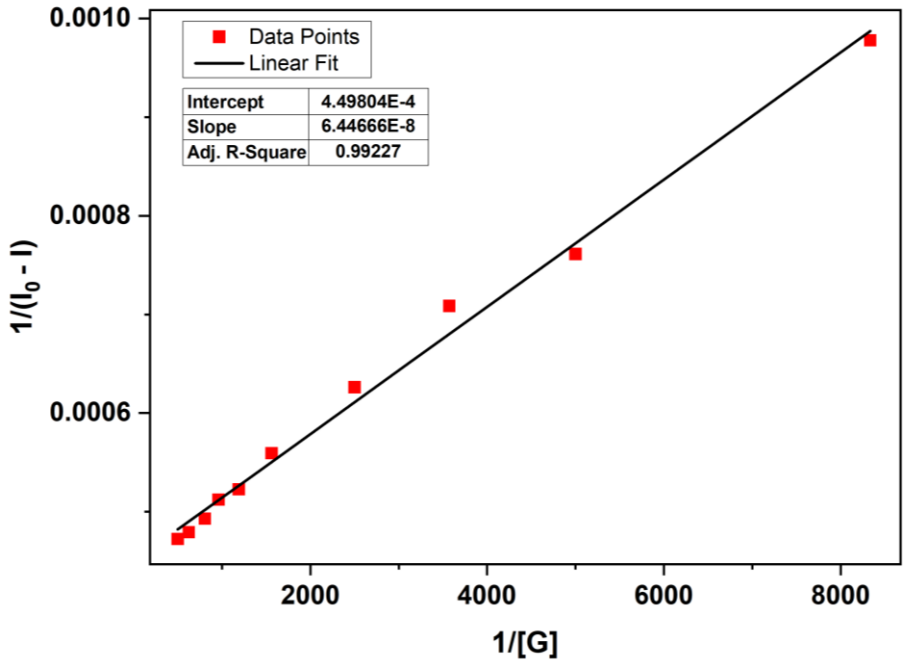

Figure 3.135. Benesi-Hildebrand plot for the emission quenching of host **7** (at 353 nm) with an increase in the concentration of phenol in DMSO.

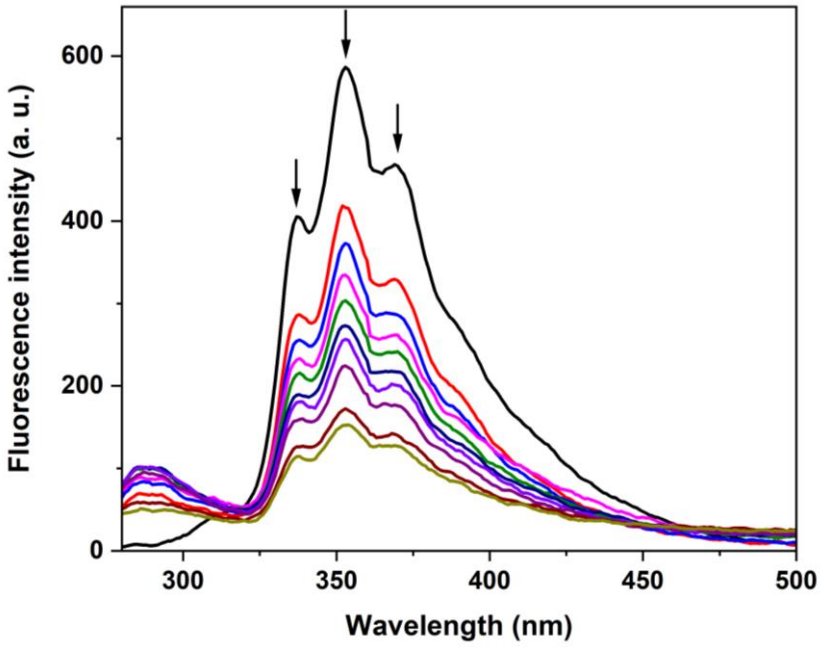

Figure 3.136. Changes in the emission spectra of **7** (4×10^{-6} M, λ_{exc} = 260 nm) with the addition of BA in DMSO. The arrow indicates the quenching of the fluorescence intensity by addition of an appropriate aliquot of BA.

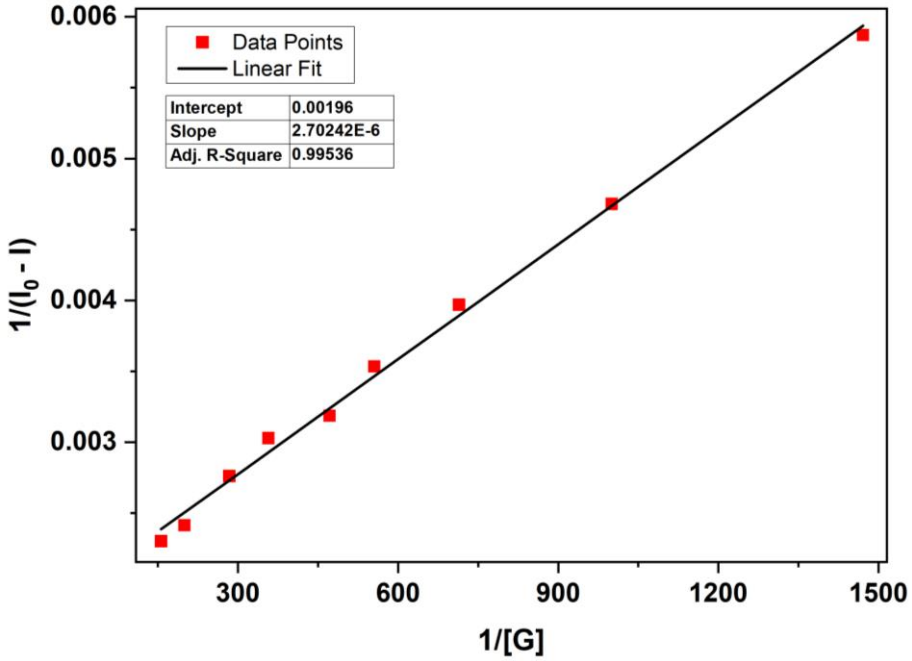

Figure 3.137. Benesi-Hildebrand plot for the emission quenching of host **7** (at 353 nm) with an increase in the concentration of BA in DMSO.

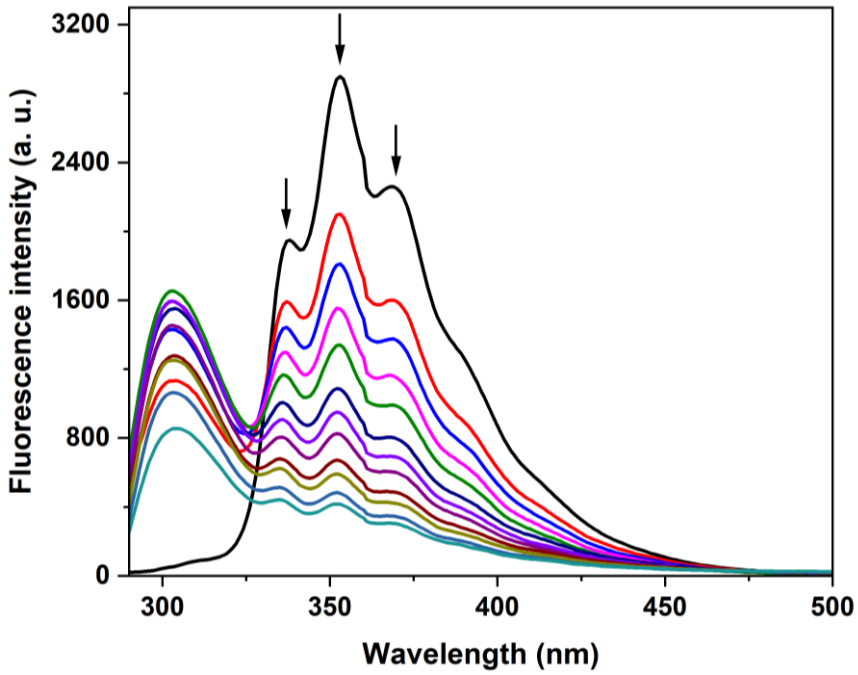

Figure 3.138. Changes in the emission spectra of **7** (4×10^{-6} M, λ_{exc} = 276 nm) with the addition of m-cresol in DMSO. The arrow indicates the quenching of the fluorescence intensity by addition of an appropriate aliquot of m-cresol.

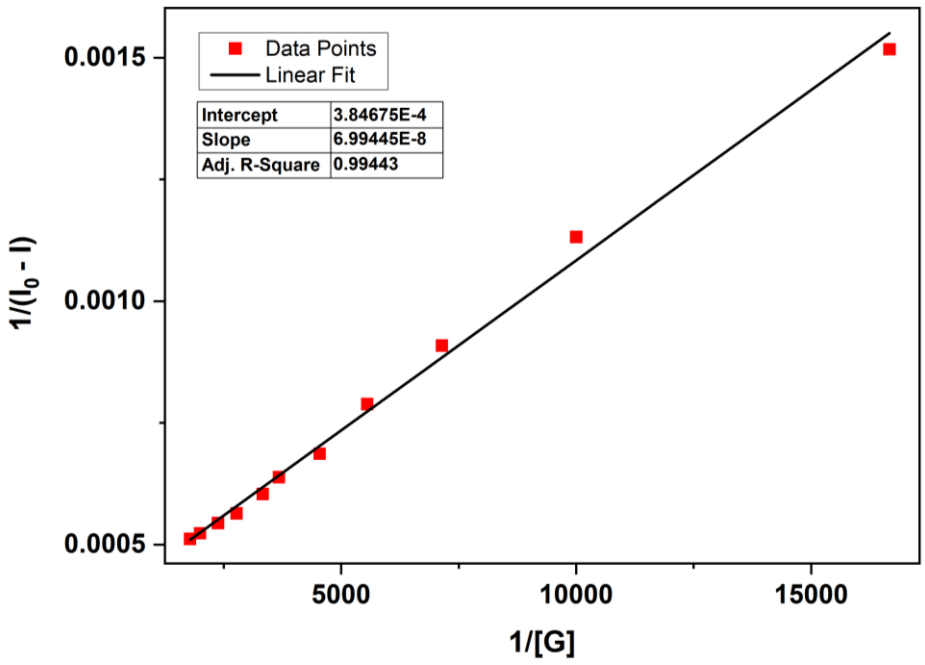

Figure 3.139. Benesi-Hildebrand plot for the emission quenching of host **7** (at 369 nm) with an increase in the concentration of m-cresol in DMSO.

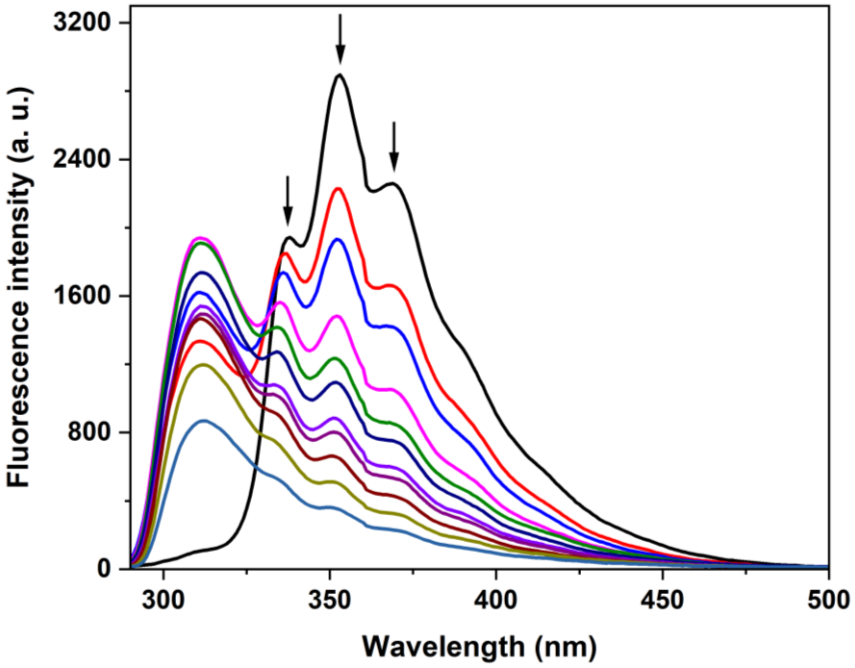

Figure 3.140. Changes in the emission spectra of **7** (4×10^{-6} M, λ_{exc} = 276 nm) with the addition of p-cresol in DMSO. The arrow indicates the quenching of the fluorescence intensity by addition of an appropriate aliquot of p-cresol

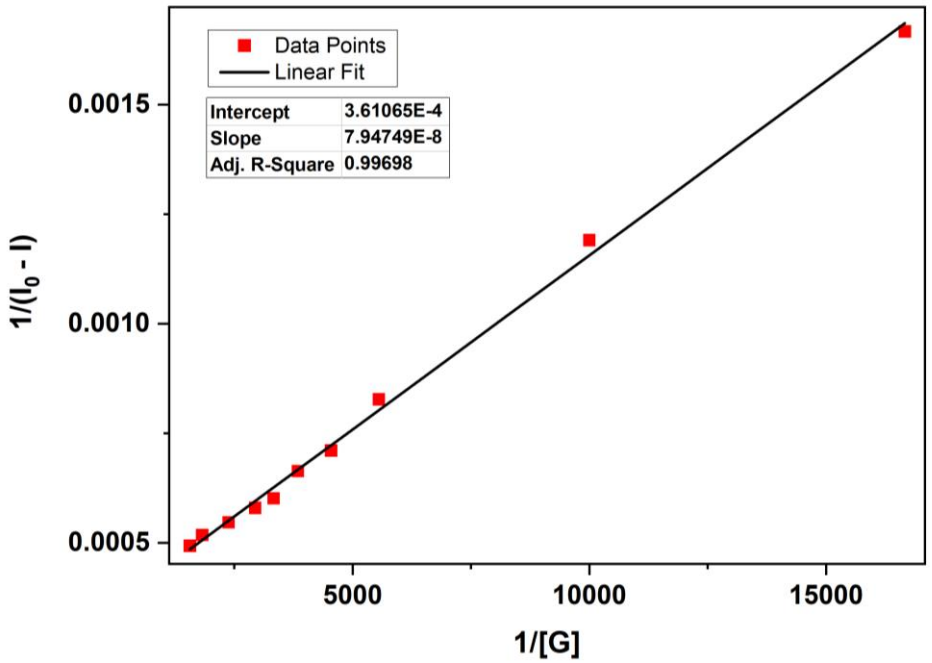

Figure 3.141. Benesi-Hildebrand plot for the emission quenching of host **7** (at 369 nm) with an increase in the concentration of p-cresol in DMSO.

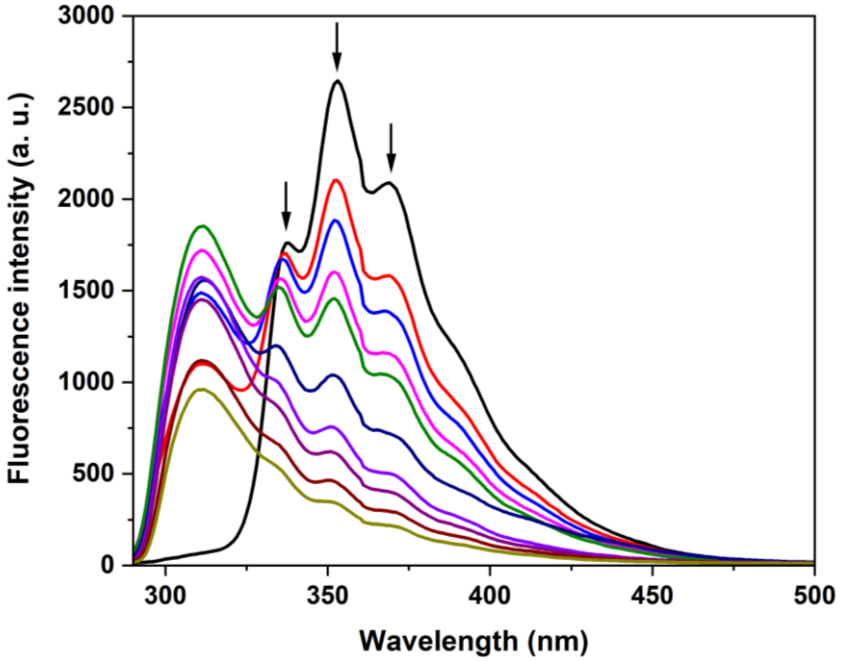

Figure 3.142. Changes in the emission spectra of **7** (4×10^{-6} M, λ_{exc} = 276 nm) with the addition of 3, 4- DMP in DMSO. The arrow indicates the quenching of the fluorescence intensity by addition of an appropriate aliquot of 3, 4- DMP.

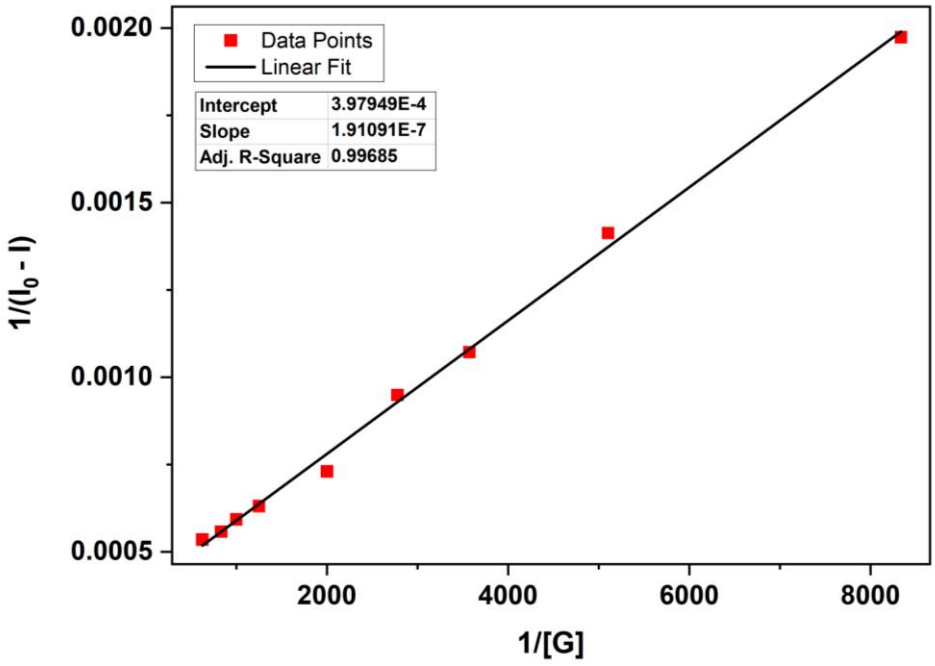

Figure 3.143. Benesi-Hildebrand plot for the emission quenching of host **7** (at 369 nm) with an increase in the concentration of 3, 4- DMP in DMSO.

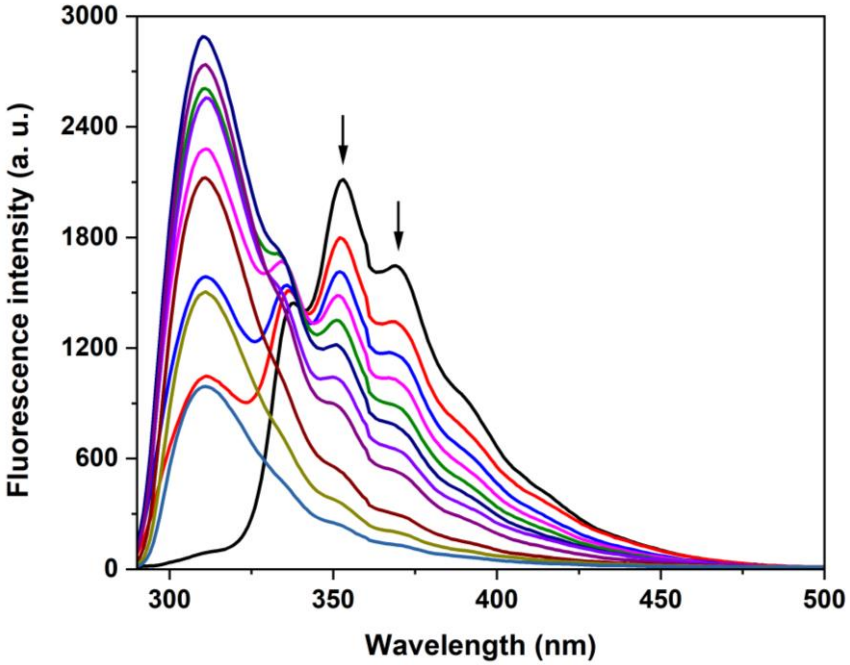

Figure 3.144. Changes in the emission spectra of **7** (2×10^{-6} M, λ_{exc} = 276 nm) with the addition of 2, 4, 6- TMP in DMSO. The arrow indicates the quenching of the fluorescence intensity by addition of an appropriate aliquot of 2, 4, 6- TMP.

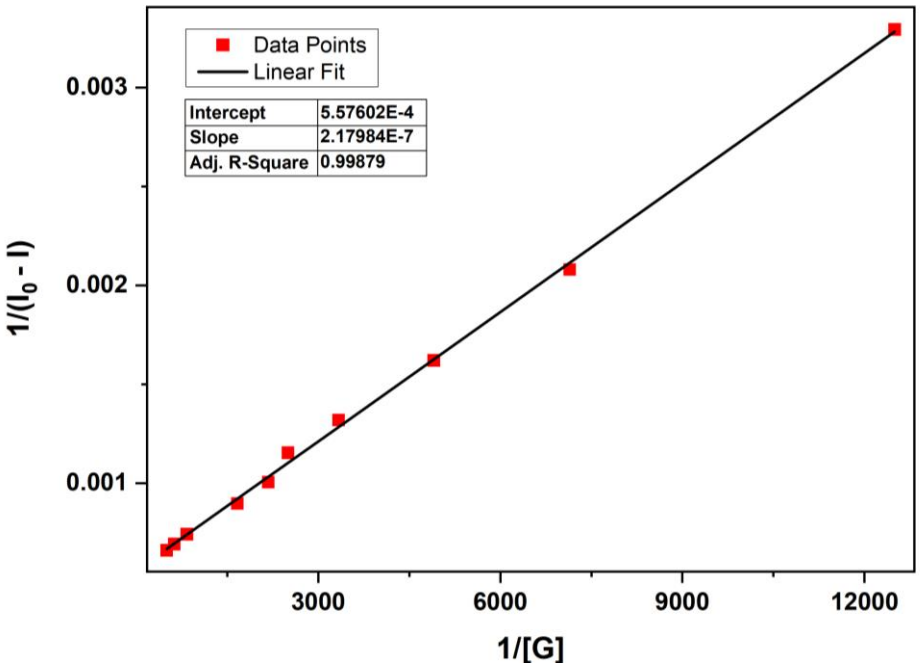

Figure 3.145. Benesi-Hildebrand plot for the emission quenching of host **7** (at 369 nm) with an increase in the concentration of 2, 4, 6- TMP in DMSO.

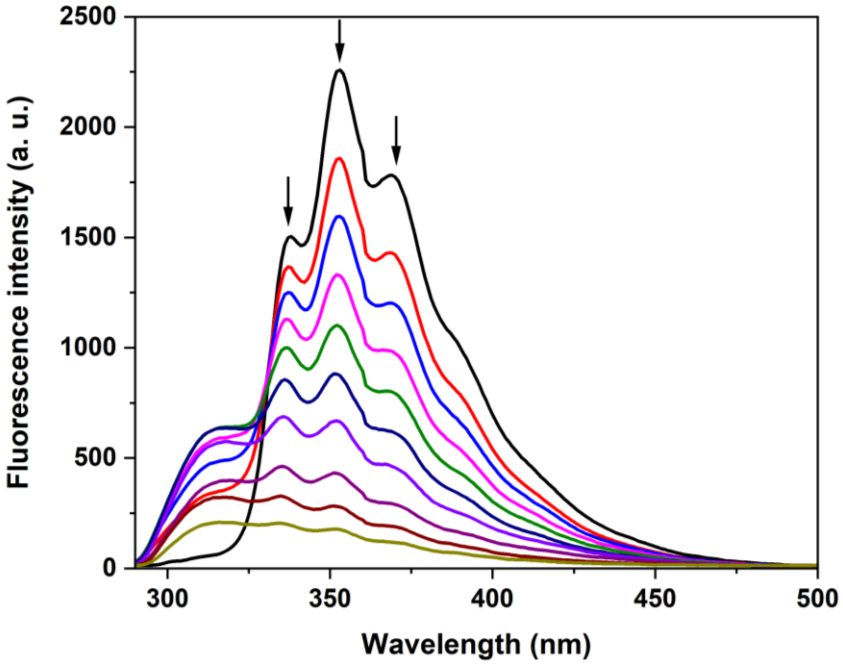

Figure 3.146. Changes in the emission spectra of **7** (2×10^{-6} M, λ_{exc} = 276 nm) with the addition of catechol in DMSO. The arrow indicates the quenching of the fluorescence intensity by addition of an appropriate aliquot of catechol.

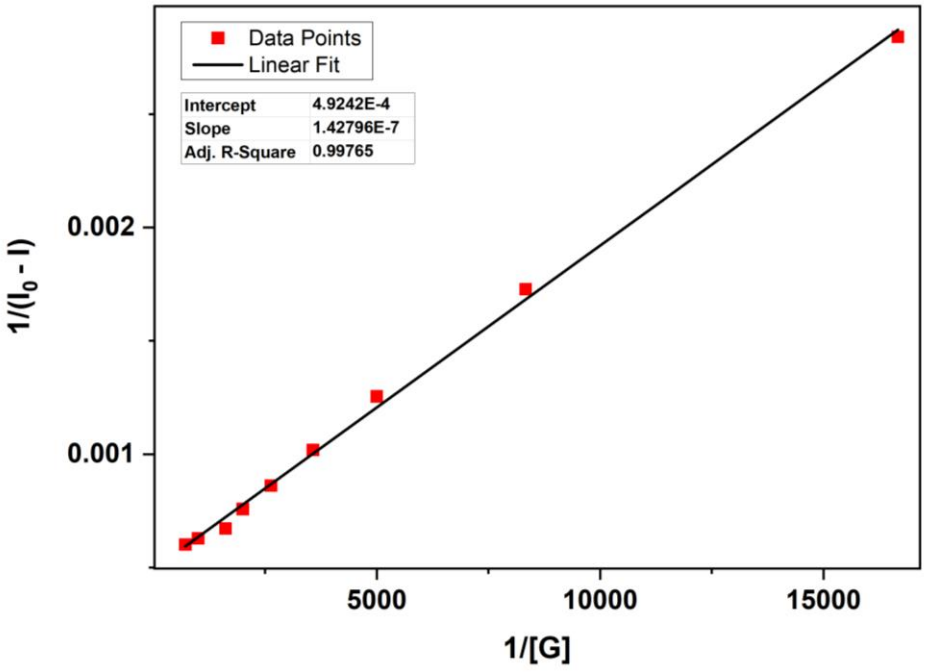

Figure 3.147. Benesi-Hildebrand plot for the emission quenching of host **7** (at 369 nm) with an increase in the concentration of catechol in DMSO.

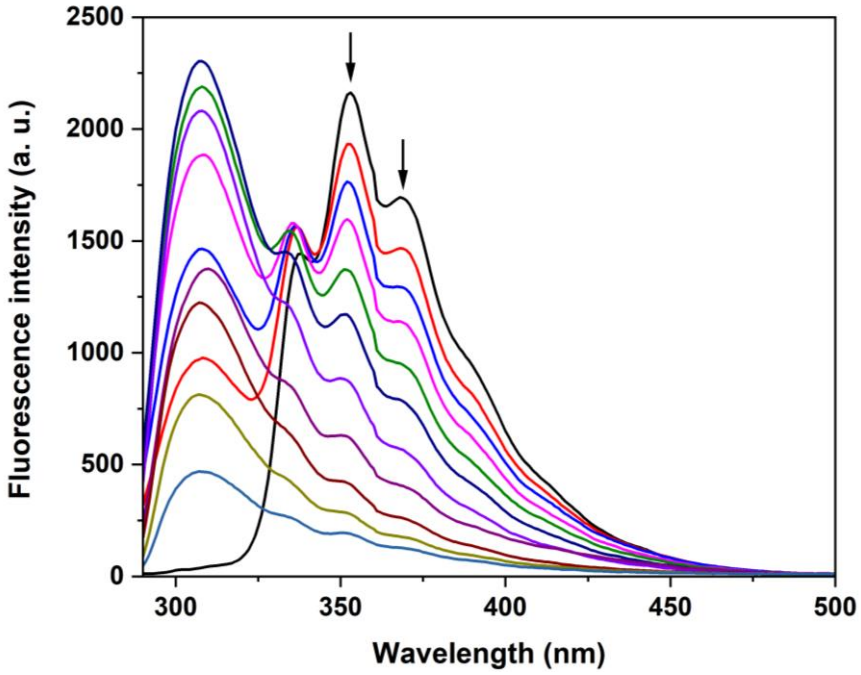

Figure 3.148. Changes in the emission spectra of **7** (2×10^{-6} M, λ_{exc} = 276 nm) with the addition of resorcinol in DMSO. The arrow indicates the quenching of the fluorescence intensity by addition of an appropriate aliquot of resorcinol.

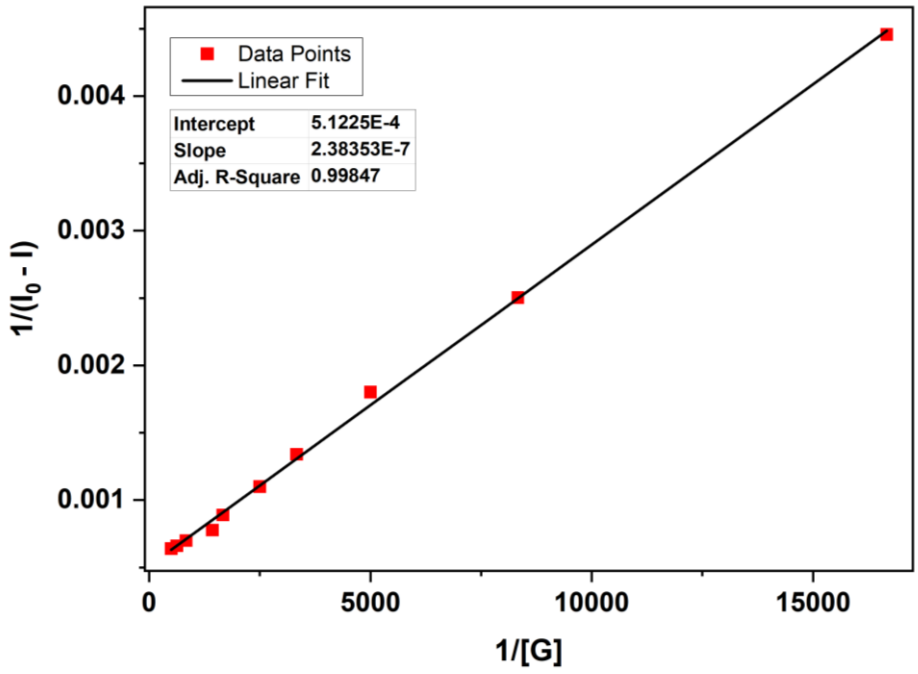

Figure 3.149. Benesi-Hildebrand plot for the emission quenching of host **7** (at 369 nm) with an increase in the concentration of resorcinol in DMSO.

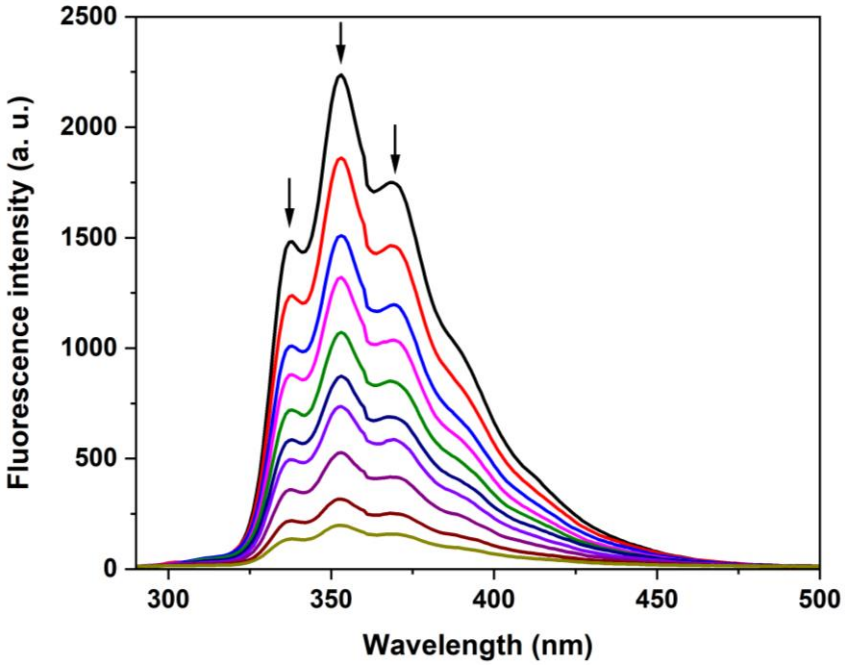

Figure 3.150. Changes in the emission spectra of **7** (2×10^{-6} M, λ_{exc} = 276 nm) with the addition of 2-CP in DMSO. The arrow indicates the quenching of the fluorescence intensity by addition of an appropriate aliquot of 2-CP.

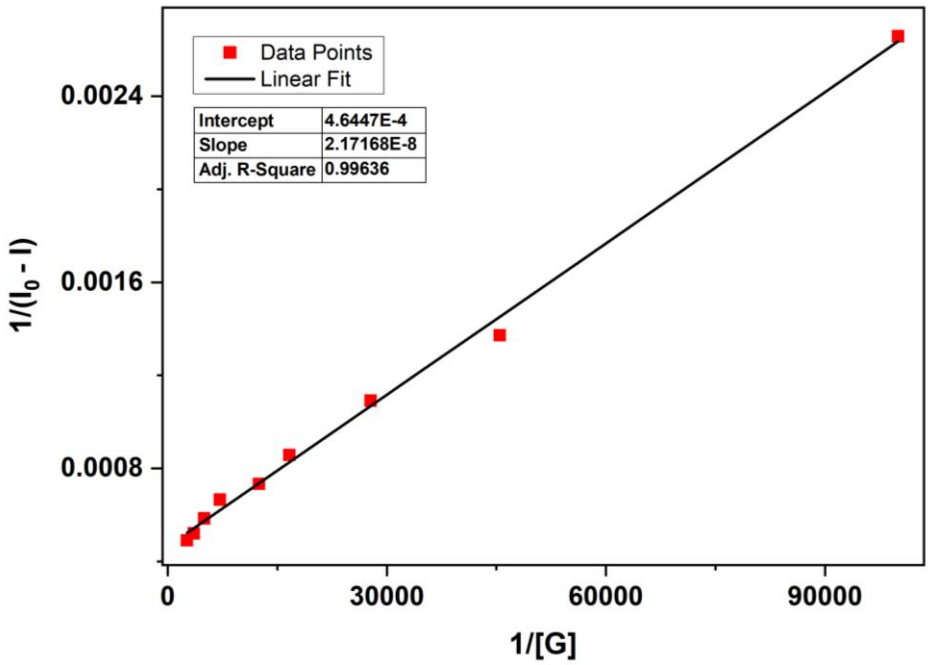

Figure 3.151. Benesi-Hildebrand plot for the emission quenching of host **7** (at 353 nm) with an increase in the concentration of 2-CP in DMSO.

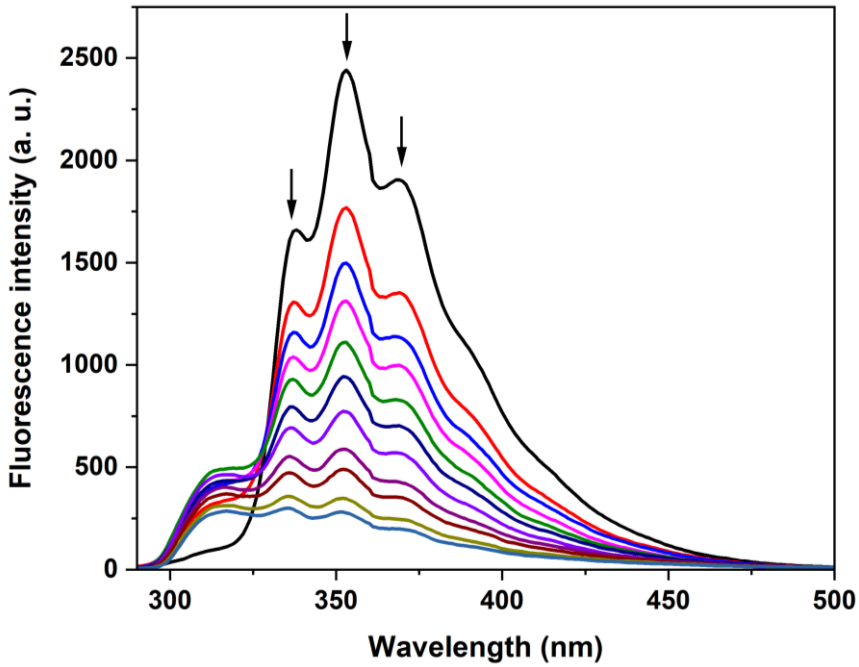

Figure 3.152. Changes in the emission spectra of **7** (2×10^{-6} M, λ_{exc} = 276 nm) with the addition of 4-chlorophenol in DMSO. The arrow indicates the quenching of the fluorescence intensity by addition of an appropriate aliquot of 4-CP.

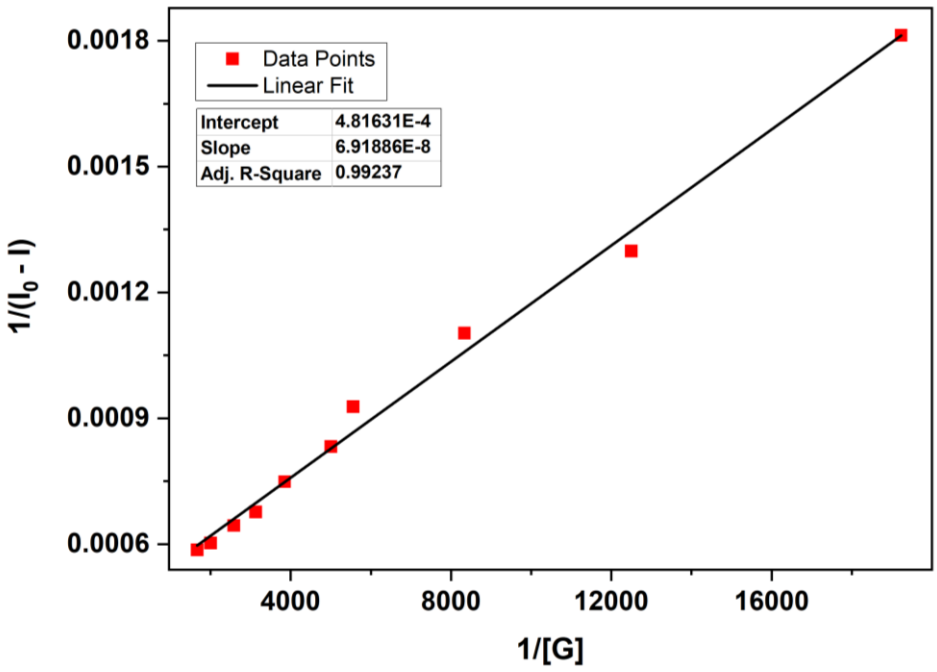

Figure 3.153. Benesi-Hildebrand plot for the emission quenching of host **7** (at 369 nm) with an increase in the concentration of 4-CP in DMSO.

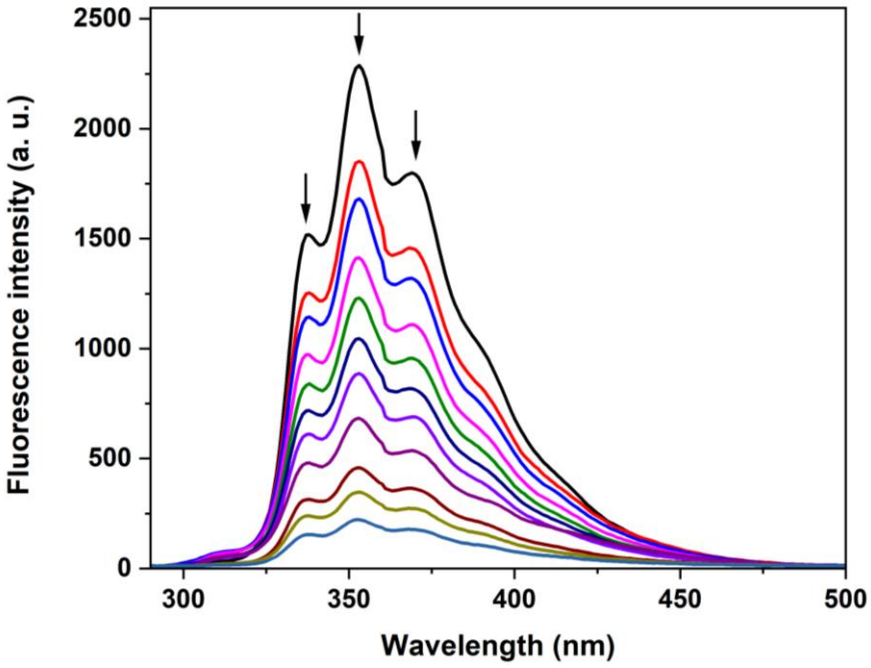

Figure 3.154. Changes in the emission spectra of **7** (2×10^{-6} M, λ_{exc} = 276 nm) with the addition of 2, 4-DCP in DMSO. The arrow indicates the quenching of the fluorescence intensity by addition of an appropriate aliquot of 2, 4-DCP.

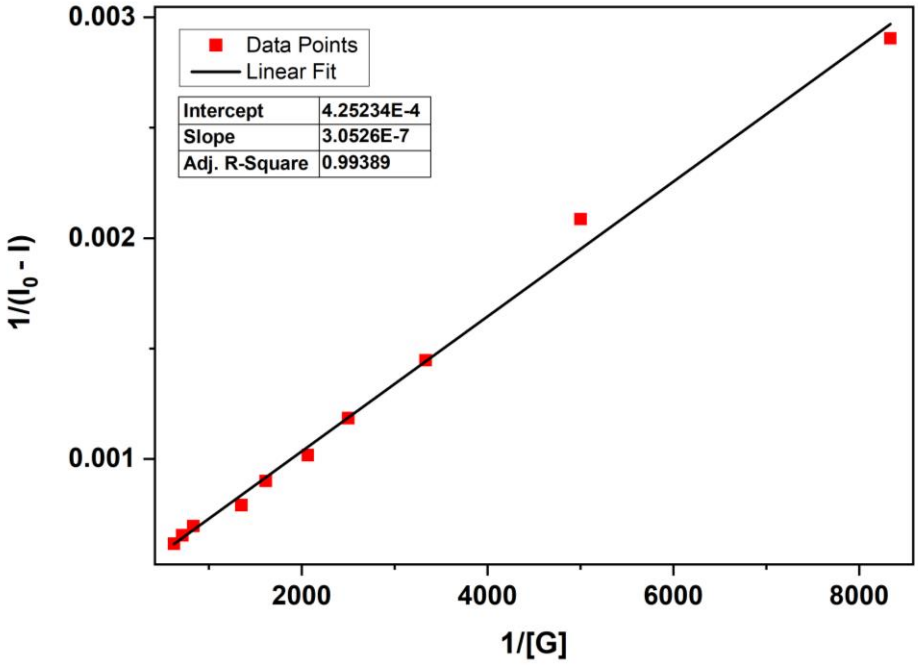

Figure 3.155. Benesi-Hildebrand plot for the emission quenching of host **7** (at 369 nm) with an increase in the concentration of 2, 4-DCP in DMSO.

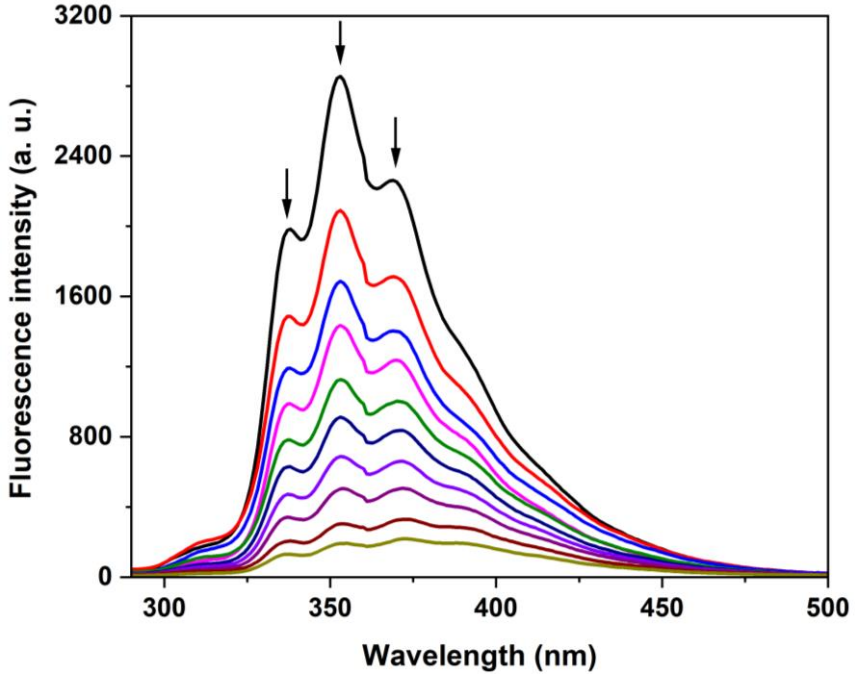

Figure 3.156. Changes in the emission spectra of **7** (4×10^{-6} M, λ_{exc} = 276 nm) with the addition of 2- NP in DMSO. The arrow indicates the quenching of the fluorescence intensity by addition of an appropriate aliquot of 2-NP.

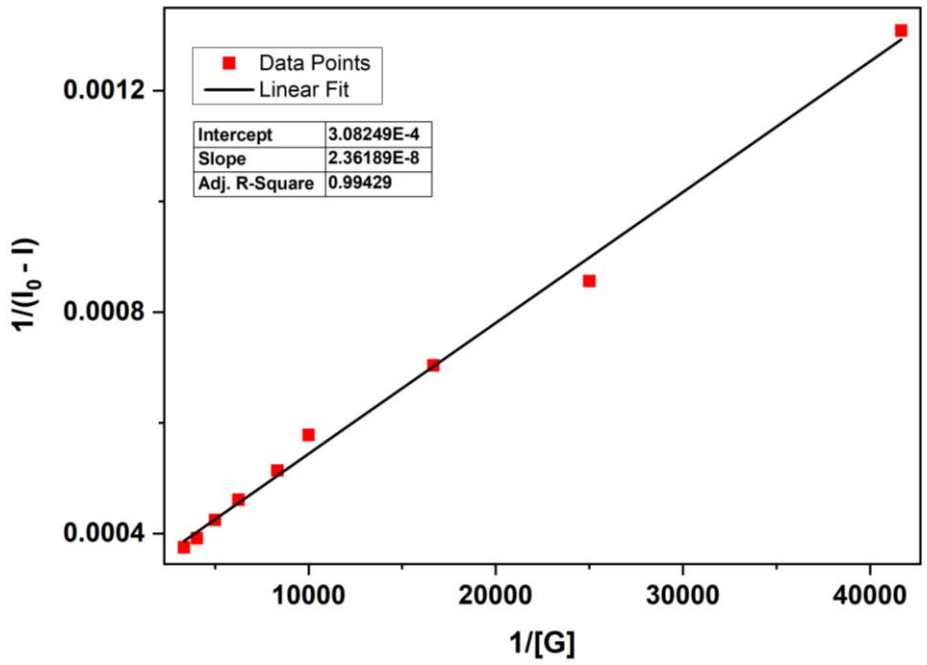

Figure 3.157. Benesi-Hildebrand plot for the emission quenching of host **7** (at 353 nm) with an increase in the concentration of 2-NP in DMSO.

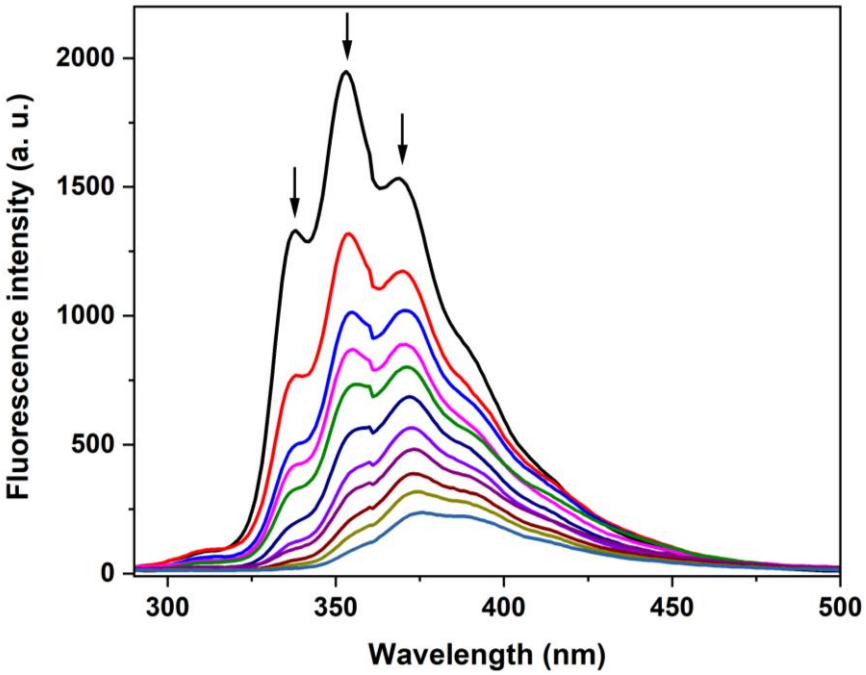

Figure 3.158. Changes in the emission spectra of **7** (2×10^{-6} M, λ_{exc} = 276 nm) with the addition of 4- NP in DMSO. The arrow indicates the quenching of the fluorescence intensity by addition of an appropriate aliquot of 4-NP.

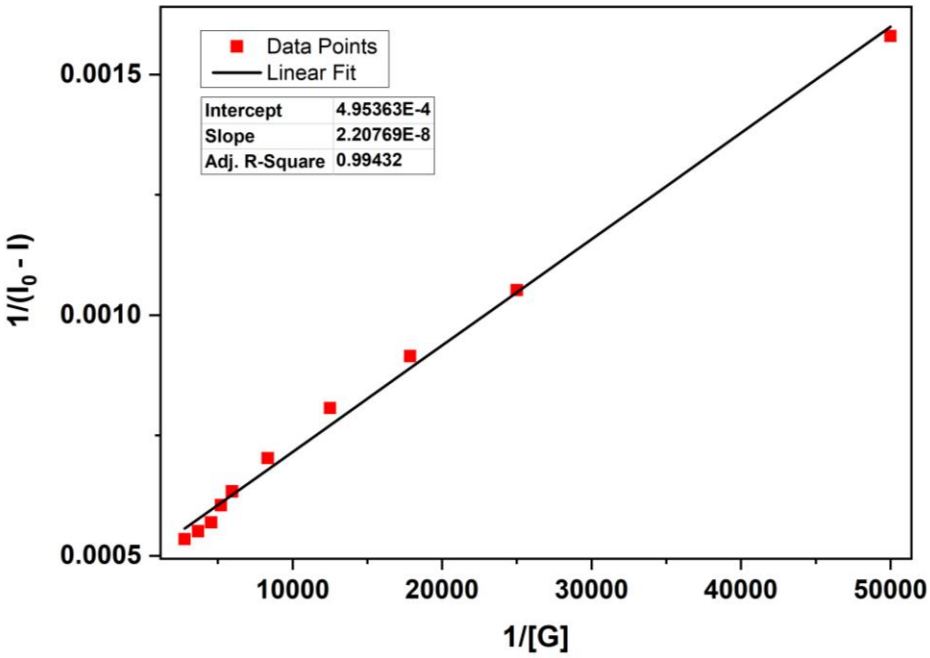

Figure 3.159. Benesi-Hildebrand plot for the emission quenching of host **7** (at 353 nm) with an increase in the concentration of 4-NP in DMSO.

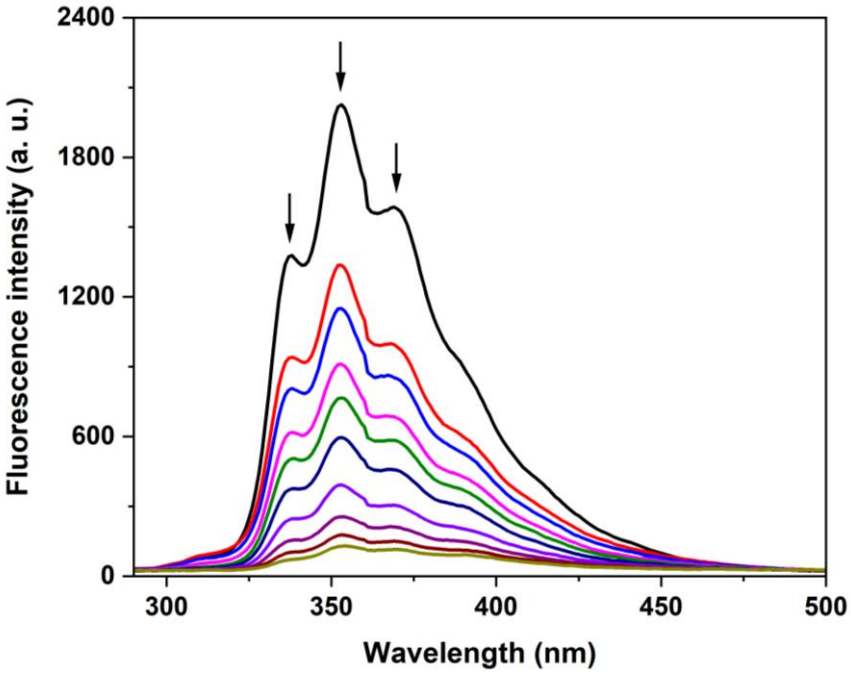

Figure 3.160. Changes in the emission spectra of **7** (2×10^{-6} M, λ_{exc} = 276 nm) with the addition of 2, 4- DNP in DMSO. The arrow indicates the quenching of the fluorescence intensity by addition of an appropriate aliquot of 2, 4- DNP.

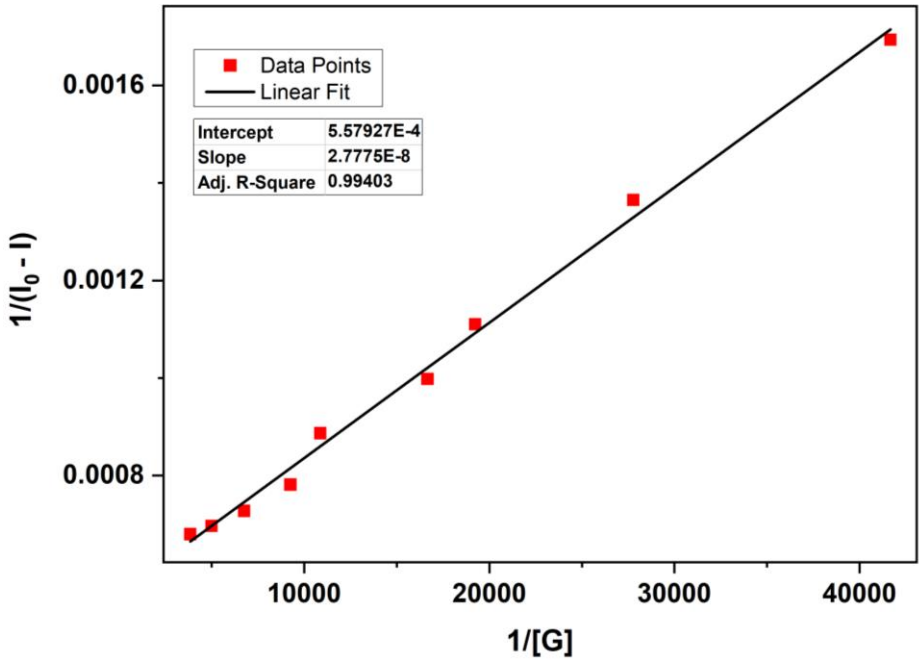

Figure 3.161. Benesi-Hildebrand plot for the emission quenching of host **7** (at 369 nm) with an increase in the concentration of 2, 4- DNP in DMSO.

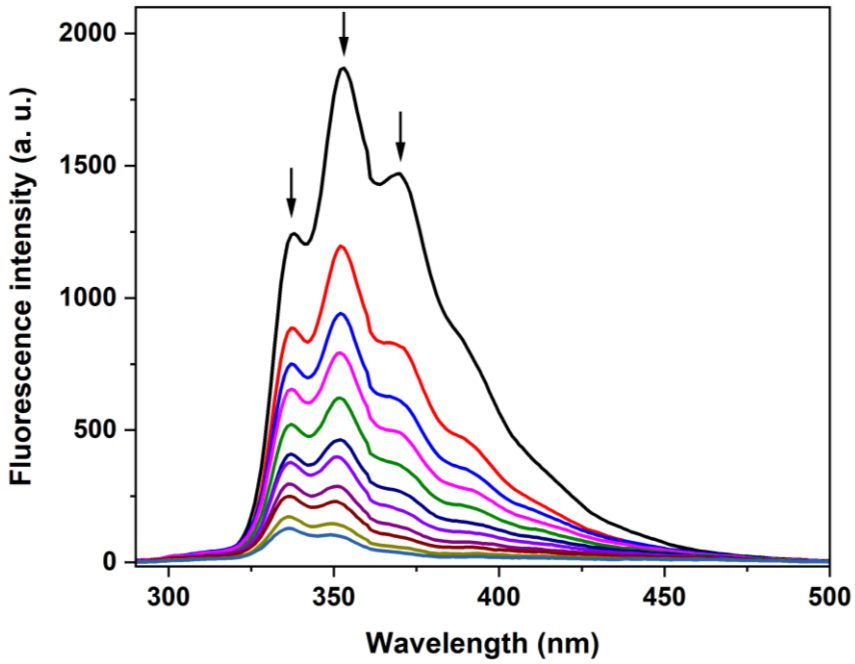

Figure 3.162. Changes in the emission spectra of **7** (2×10^{-6} M, λ_{exc} = 276 nm) with the addition of 2, 4, 6- TNP/ picric acid in DMSO. The arrow indicates the quenching of the fluorescence intensity by addition of an appropriate aliquot of picric acid.

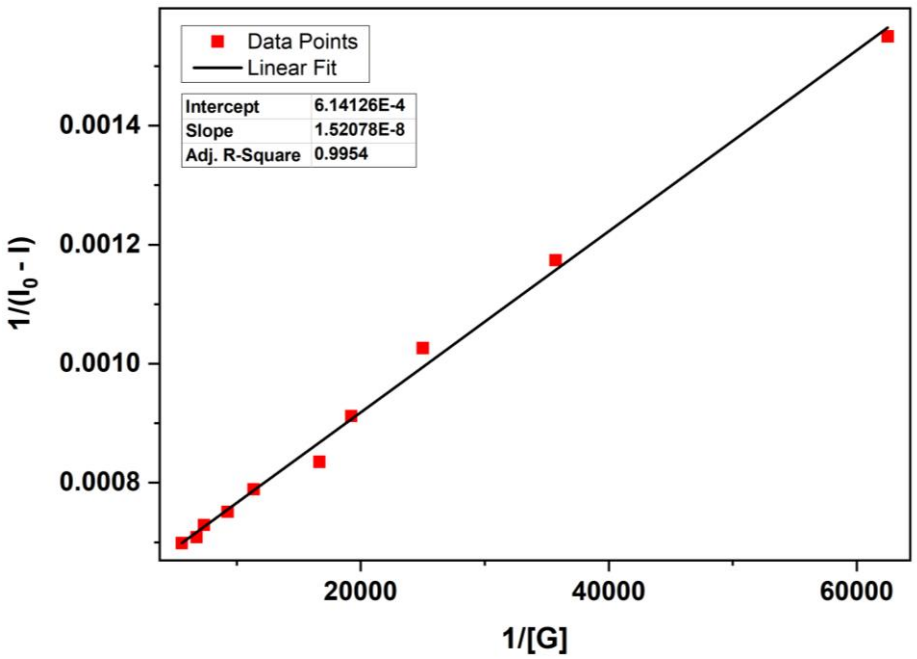

Figure 3.163. Benesi-Hildebrand plot for the emission quenching of host **7** (at 369 nm) with an increase in the concentration of 2, 4, 6- TNP in DMSO.

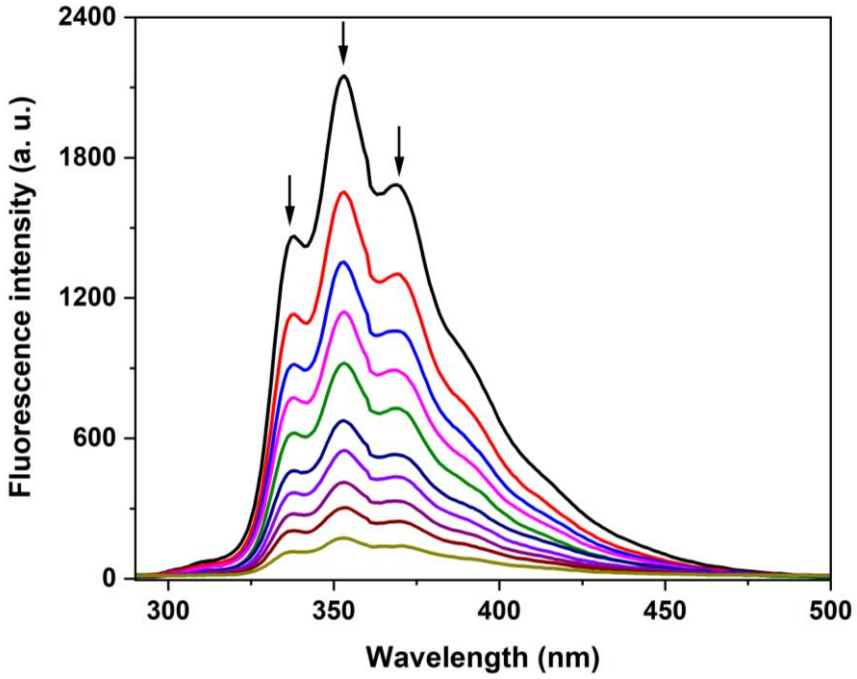

Figure 3.164. Changes in the emission spectra of **7** (2×10^{-6} M, λ_{exc} = 276 nm) with the addition of NB in DMSO. The arrow indicates the quenching of the fluorescence intensity by addition of an appropriate aliquot of NB.

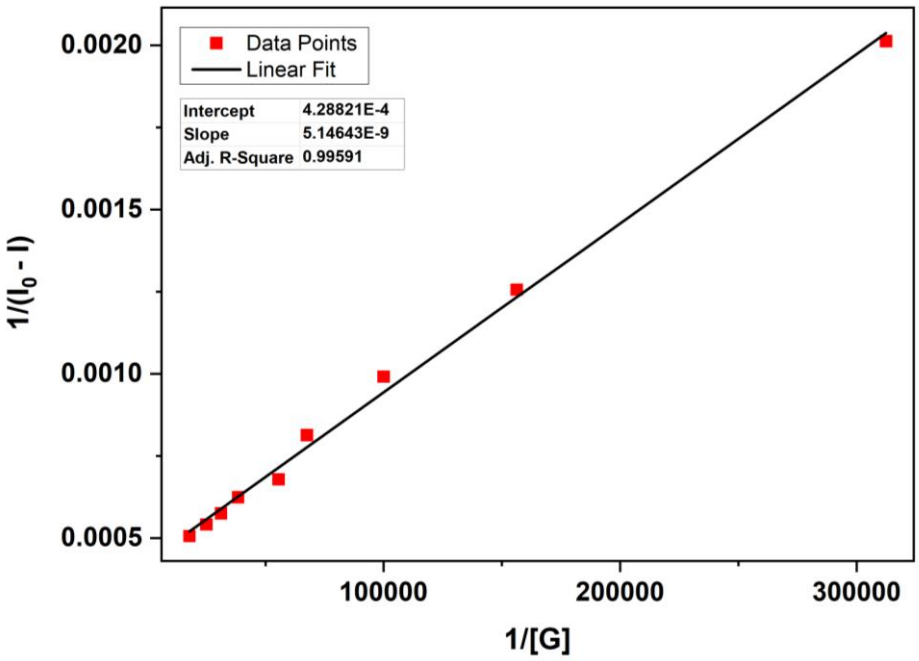

Figure 3.165. Benesi-Hildebrand plot for the emission quenching of host **7** (at 353 nm) with an increase in the concentration of NB in DMSO.

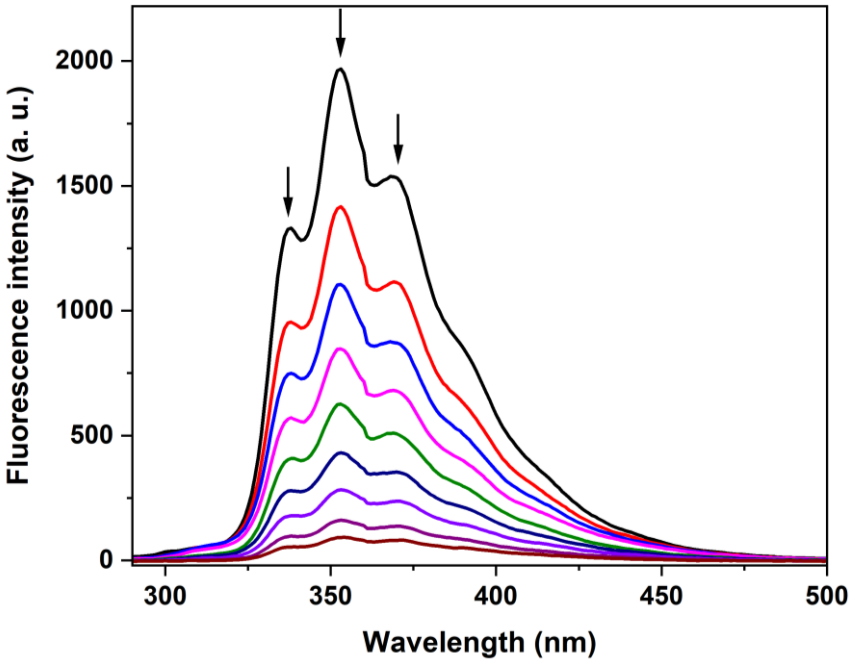

Figure 3.166. Changes in the emission spectra of **7** (2×10^{-6} M, λ_{exc} = 276 nm) with the addition of 2-NT in DMSO. The arrow indicates the quenching of the fluorescence intensity by addition of an appropriate aliquot of 2-NT.

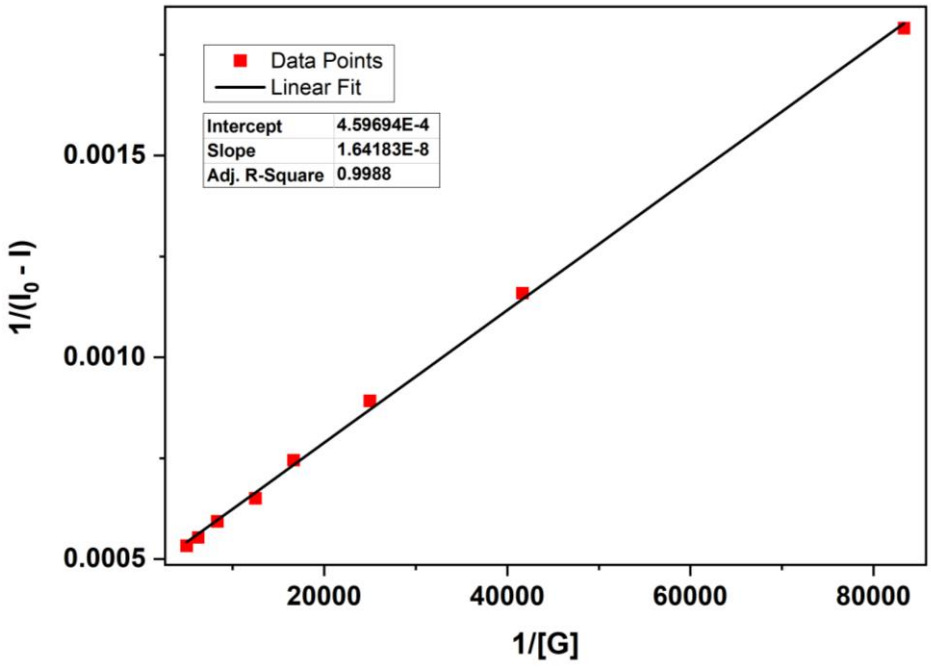

Figure 3.167. Benesi-Hildebrand plot for the emission quenching of host **7** (at 353 nm) with an increase in the concentration of 2-NT in DMSO.

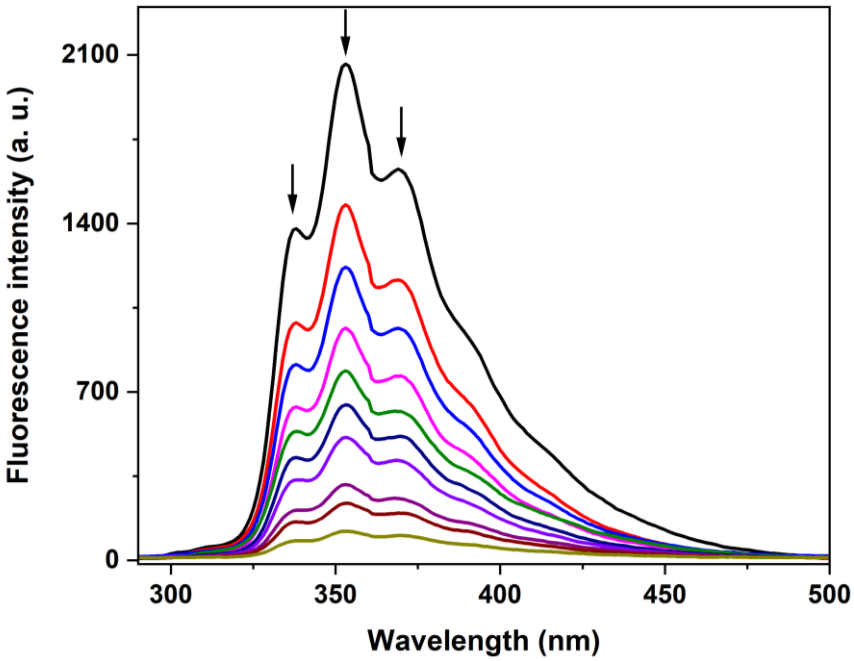

Figure 3.168. Changes in the emission spectra of **7** (2×10^{-6} M, λ_{exc} = 276 nm) with the addition of 4-NT in DMSO. The arrow indicates the quenching of the fluorescence intensity by addition of an appropriate aliquot of 4-NT.

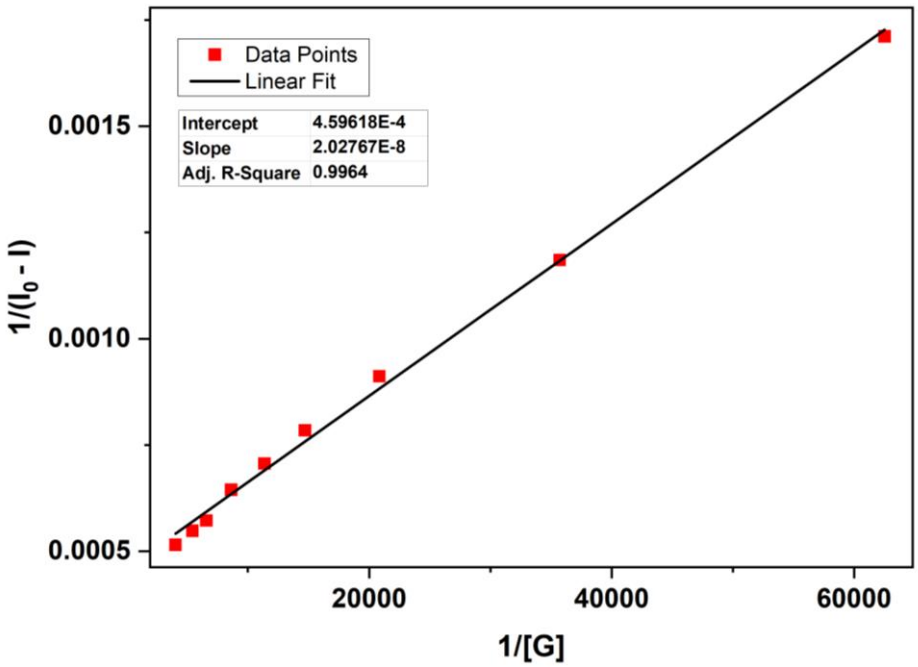

Figure 3.169. Benesi-Hildebrand plot for the emission quenching of host **7** (at 353 nm) with an increase in the concentration of 4-NT in DMSO.

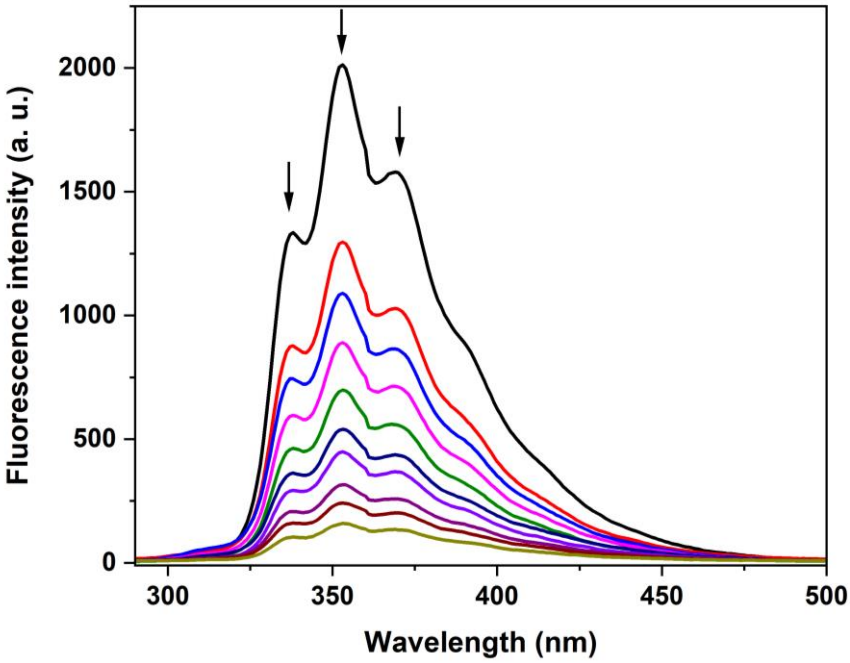

Figure 3.170. Changes in the emission spectra of **7** (2×10^{-6} M, λ_{exc} = 276 nm) with the addition of 2, 4-DNT in DMSO. The arrow indicates the quenching of the fluorescence intensity by addition of an appropriate aliquot of 2, 4-DNT.

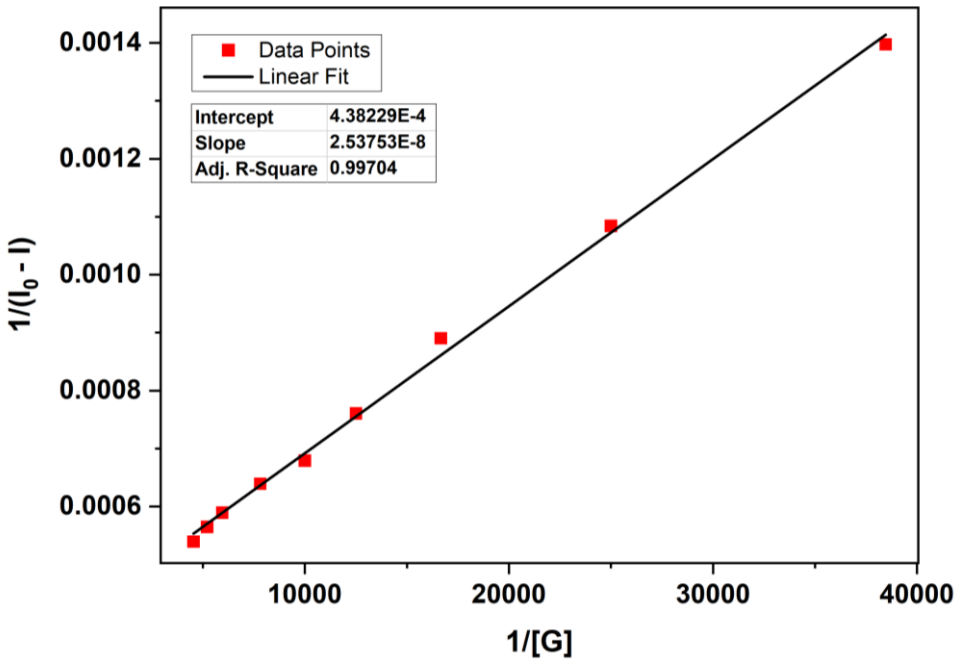

Figure 3.171. Benesi-Hildebrand plot for the emission quenching of host **7** (at 353 nm) with an increase in the concentration of 2, 4-DNT in DMSO.

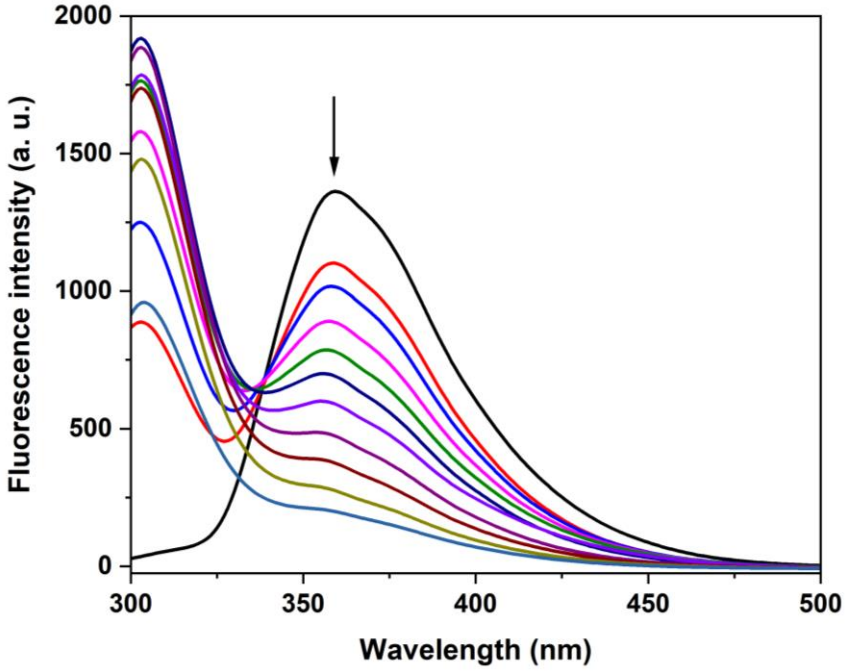

Figure 3.172. Changes in the emission spectra of **8** (1×10^{-6} M, λ_{exc} = 275 nm) with the addition of phenol in DMSO. The arrow indicates the quenching of the fluorescence intensity by addition of an appropriate aliquot of phenol.

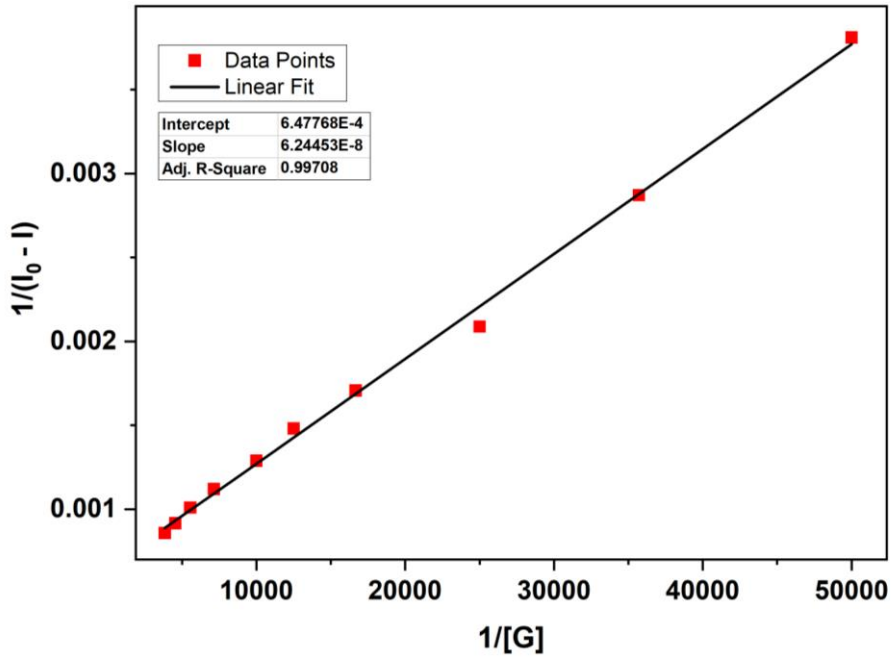

Figure 3.173. Benesi-Hildebrand plot for the emission quenching of host **8** (at 360 nm) with an increase in the concentration of phenol in DMSO.

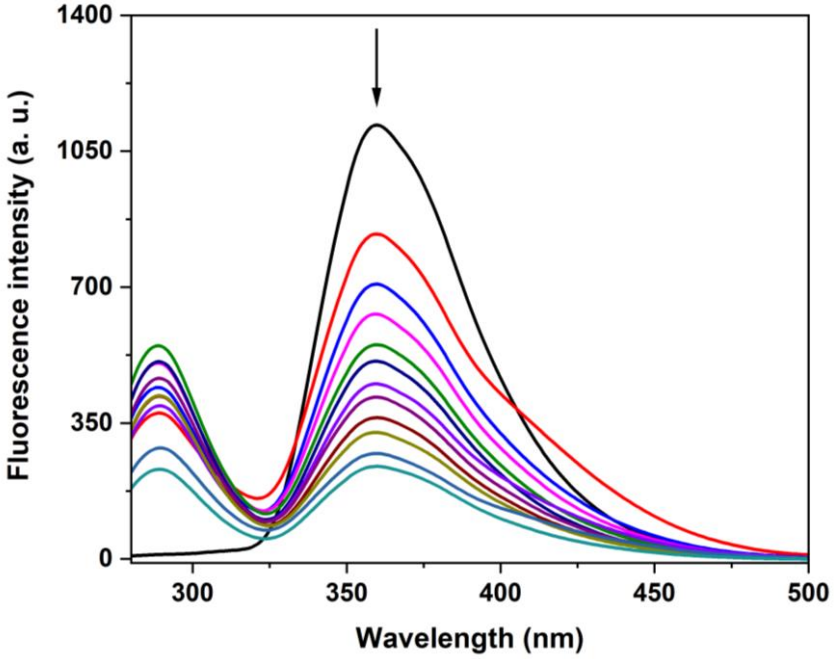

Figure 3.174. Changes in the emission spectra of **8** (1×10^{-6} M, λ_{exc} = 260 nm) with the addition of BA in DMSO. The arrow indicates the quenching of the fluorescence intensity by addition of an appropriate aliquot of BA.

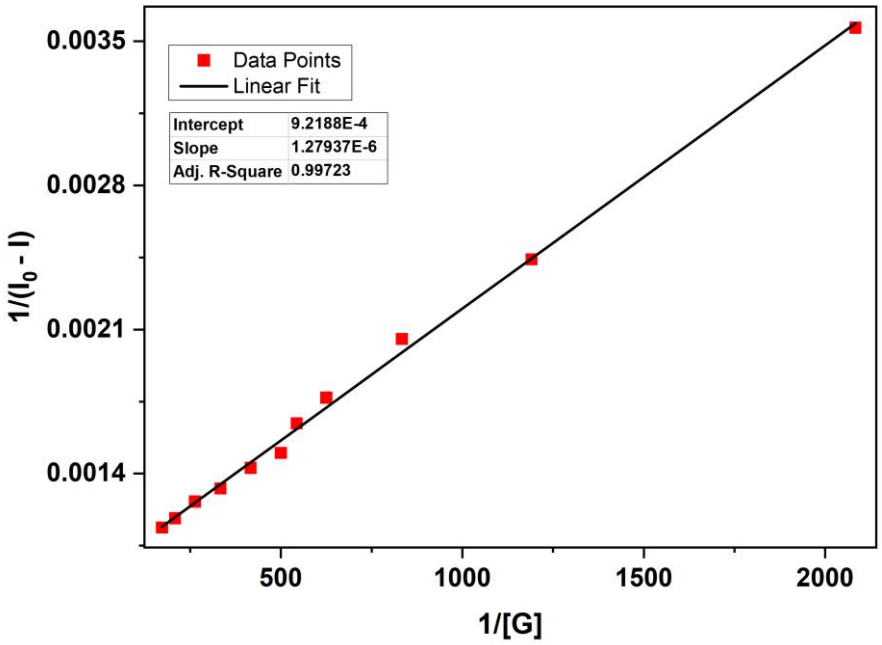

Figure 3.175. Benesi-Hildebrand plot for the emission quenching of host **8** (at 360 nm) with an increase in the concentration of BA in DMSO.

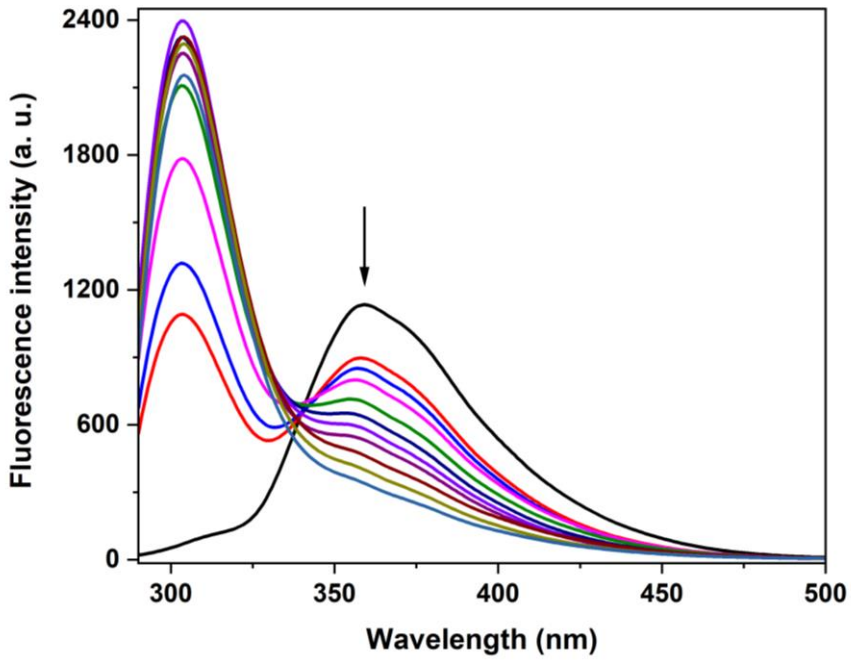

Figure 3.176. Changes in the emission spectra of **8** (1×10^{-6} M, λ_{exc} = 275 nm) with the addition of m-cresol in DMSO. The arrow indicates the quenching of the fluorescence intensity by addition of an appropriate aliquot of m-cresol.

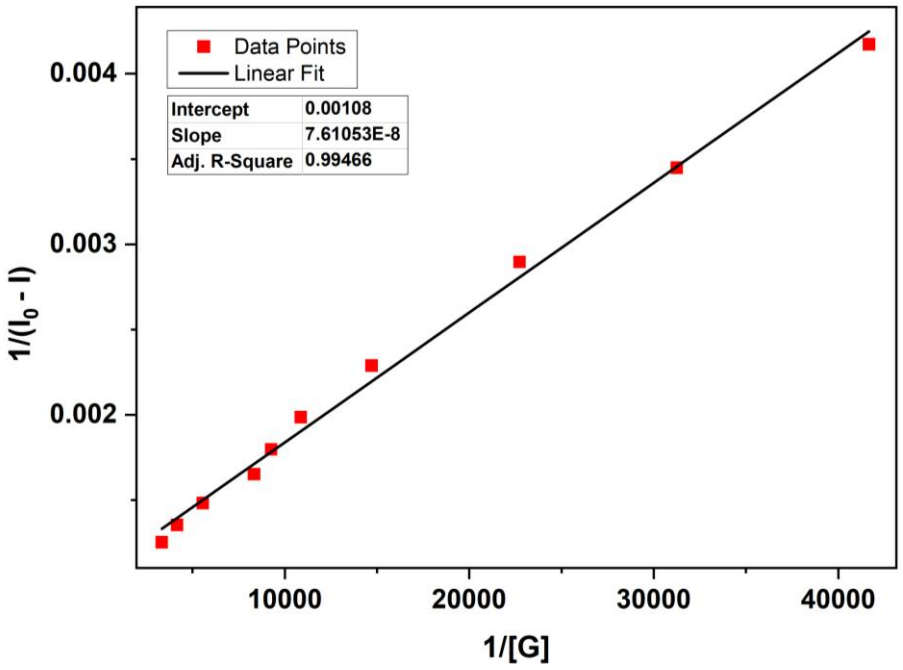

Figure 3.177. Benesi-Hildebrand plot for the emission quenching of host **8** (at 360 nm) with an increase in the concentration of m-cresol in DMSO.

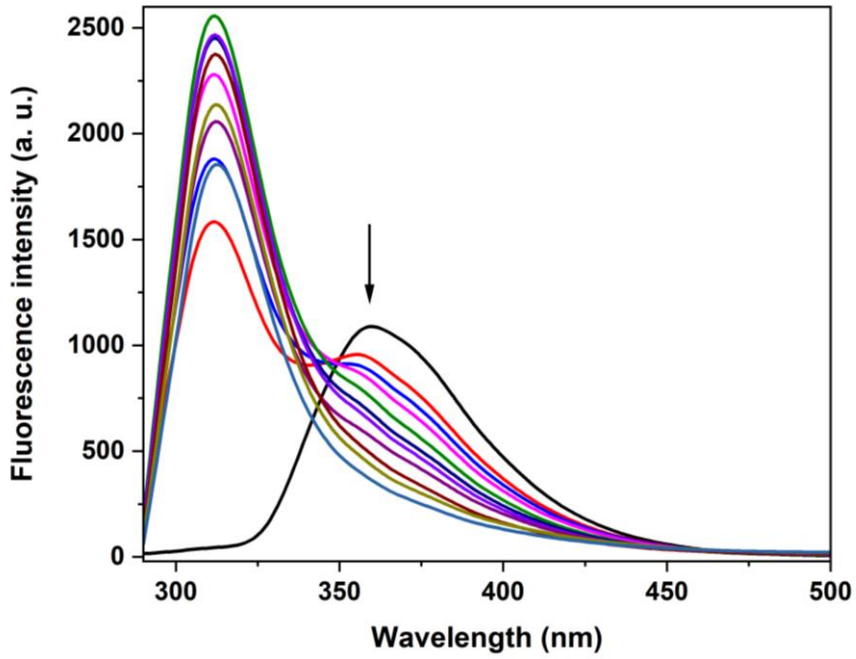

Figure 3.178. Changes in the emission spectra of **8** (1×10^{-6} M, λ_{exc} = 275 nm) with the addition of p-cresol in DMSO. The arrow indicates the quenching of the fluorescence intensity by addition of an appropriate aliquot of p-cresol.

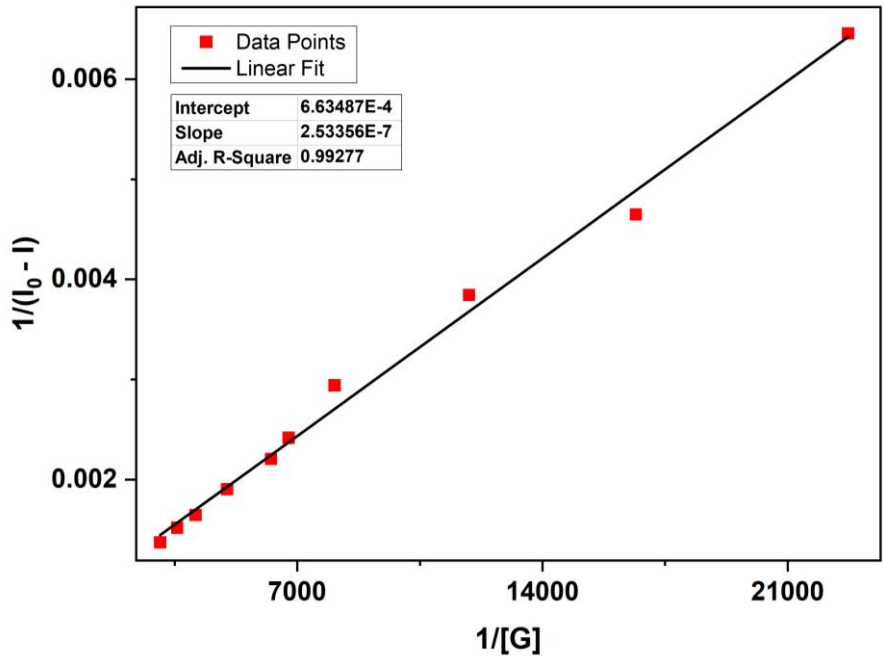

Figure 3.179. Benesi-Hildebrand plot for the emission quenching of host **8** (at 360 nm) with an increase in the concentration of p-cresol in DMSO.

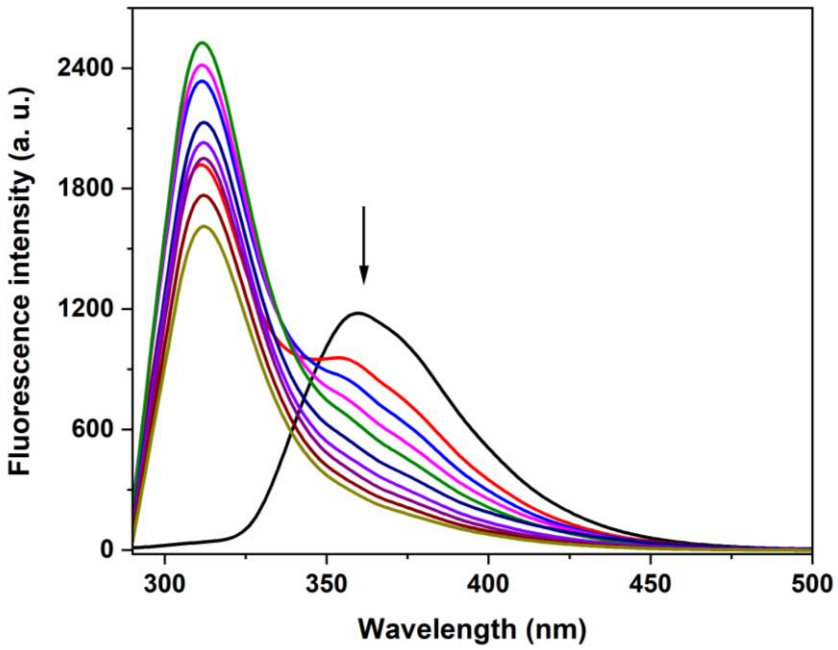

Figure 3.180. Changes in the emission spectra of **8** (1×10^{-6} M, λ_{exc} = 275 nm) with the addition of 3, 4- DMP in DMSO. The arrow indicates the quenching of the fluorescence intensity by addition of an appropriate aliquot of 3, 4- DMP.

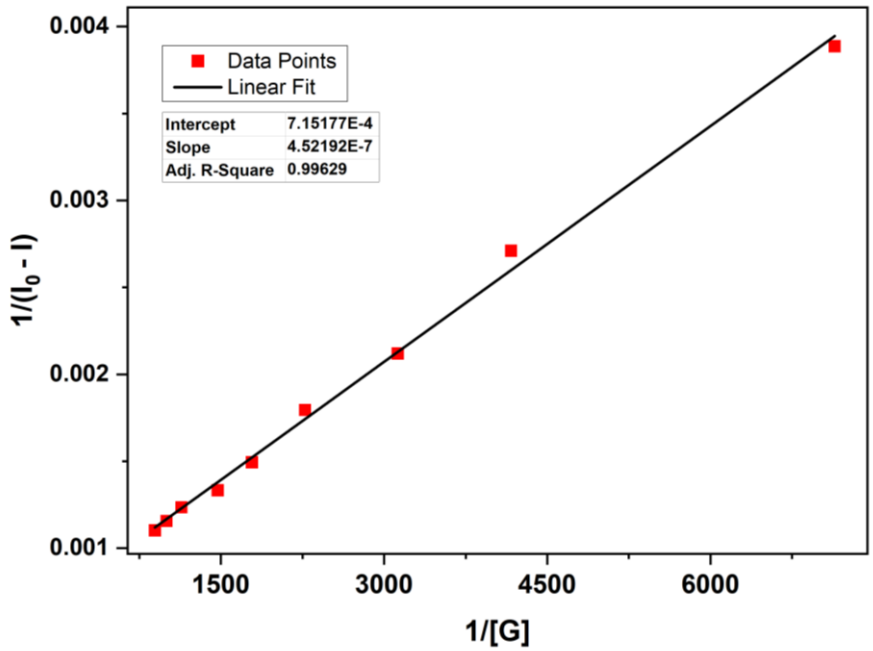

Figure 3.181. Benesi-Hildebrand plot for the emission quenching of host **8** (at 360 nm) with an increase in the concentration of 3, 4- DMP in DMSO.

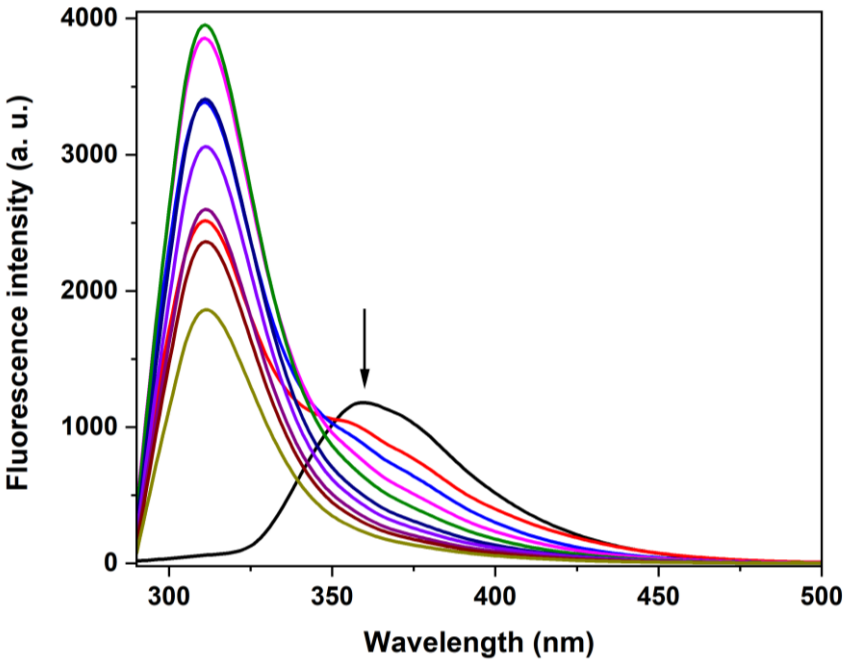

Figure 3.182 Changes in the emission spectra of **8** (1×10^{-6} M, λ_{exc} = 275 nm) with the addition of 2, 4, 6- TMP in DMSO. The arrow indicates the quenching of the fluorescence intensity by addition of an appropriate aliquot of 2, 4, 6- TMP.

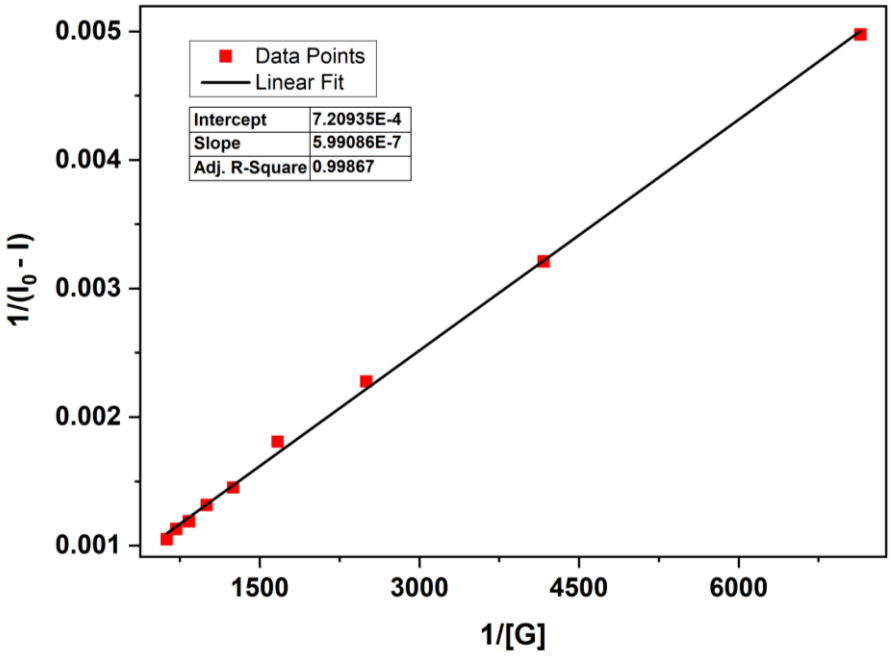

Figure 3.183 Benesi-Hildebrand plot for the emission quenching of host **8** (at 360 nm) with an increase in the concentration of 2, 4, 6- TMP in DMSO.

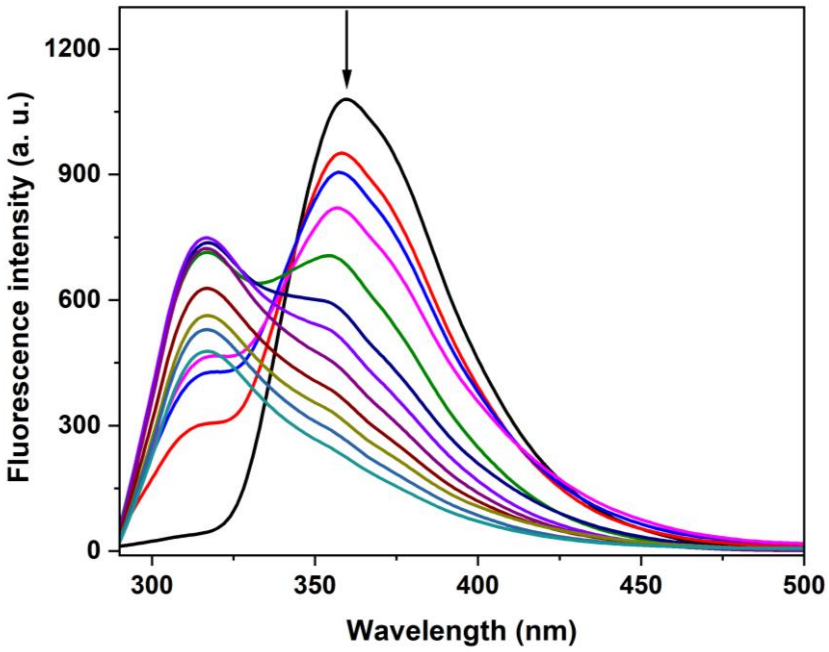

Figure 3.184 Changes in the emission spectra of **8** (1×10^{-6} M, λ_{exc} = 275 nm) with the addition of catechol in DMSO. The arrow indicates the quenching of the fluorescence intensity by addition of an appropriate aliquot of catechol.

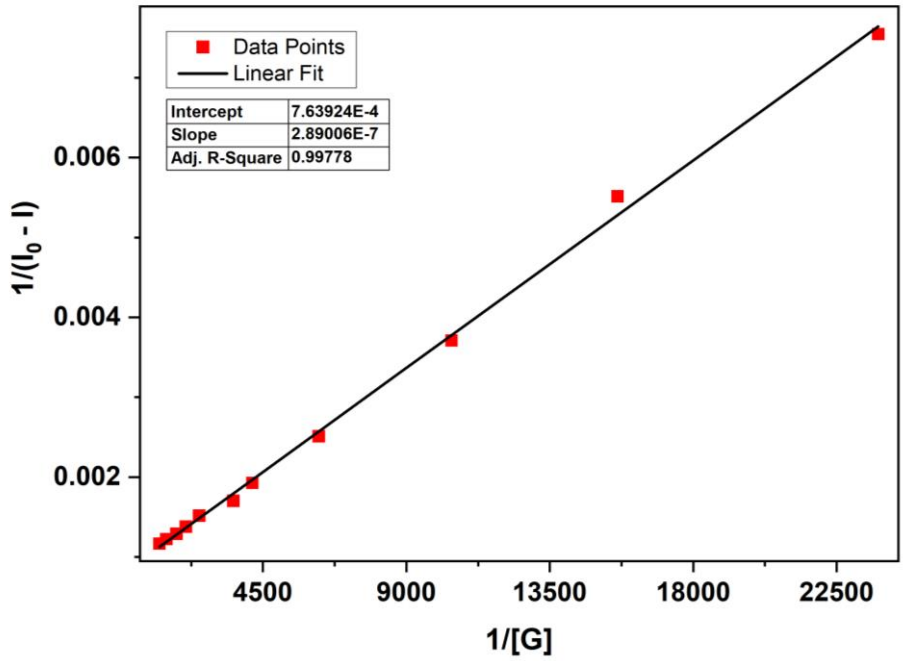

Figure 3.185. Benesi-Hildebrand plot for the emission quenching of host **8** (at 360 nm) with an increase in the concentration of catechol in DMSO.

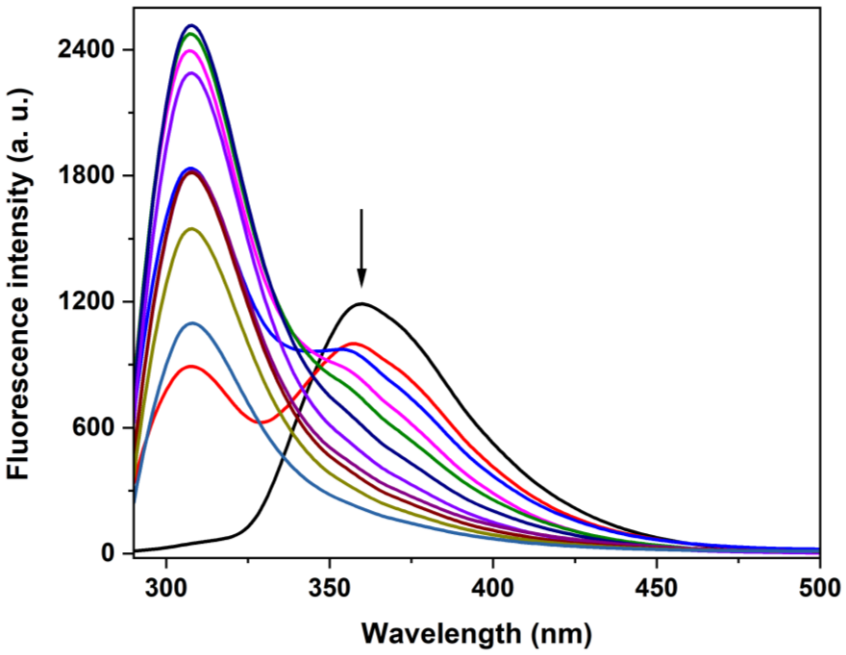

Figure 3.186. Changes in the emission spectra of **8** (1×10^{-6} M, λ_{exc} = 275 nm) with the addition of resorcinol in DMSO. The arrow indicates the quenching of the fluorescence intensity by addition of an appropriate aliquot of resorcinol.

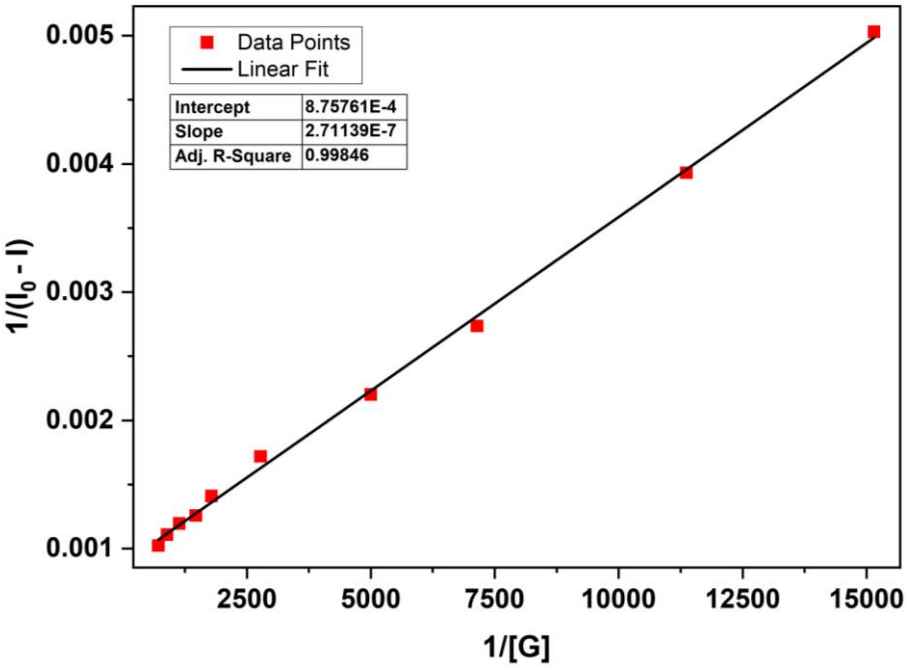

Figure3.187. Benesi-Hildebrand plot for the emission quenching of host **8** (at 360 nm) with an increase in the concentration of resorcinol in DMSO.

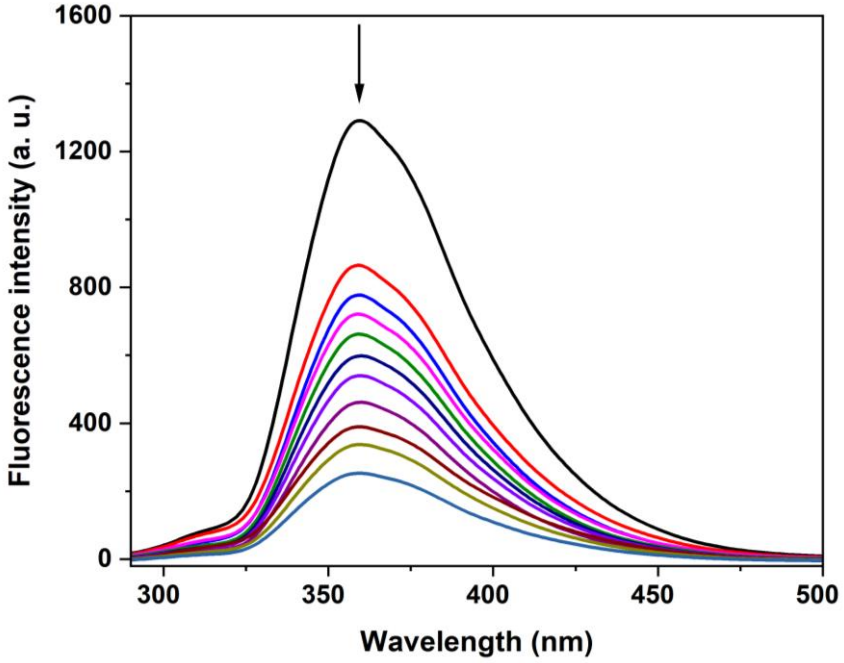

Figure 3.188. Changes in the emission spectra of **8** (1×10^{-6} M, λ_{exc} = 275 nm) with the addition of 2-CP in DMSO. The arrow indicates the quenching of the fluorescence intensity by addition of an appropriate aliquot of 2-CP.

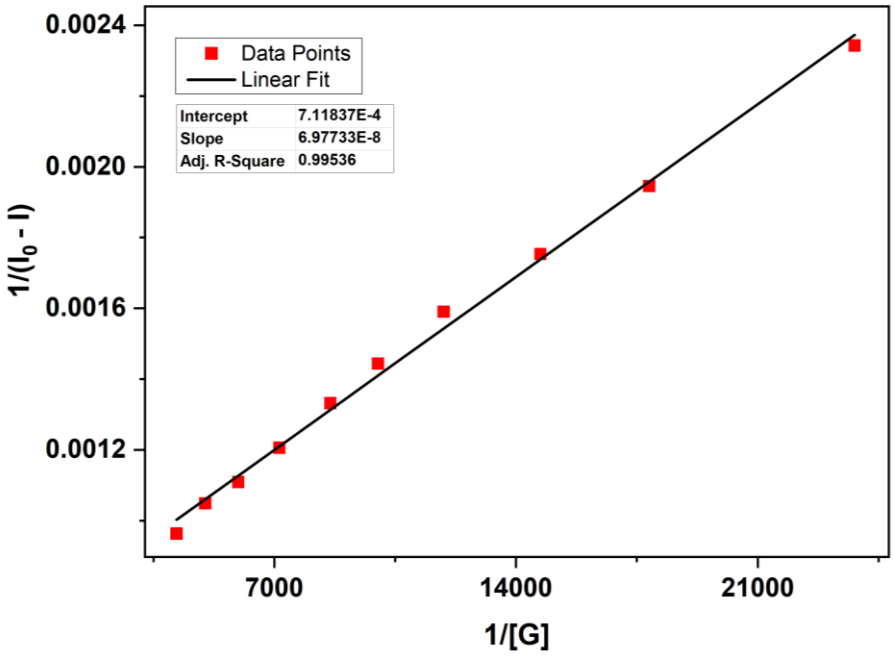

Figure 3.189. Benesi-Hildebrand plot for the emission quenching of host **8** (at 360 nm) with an increase in the concentration of 2-CP in DMSO.

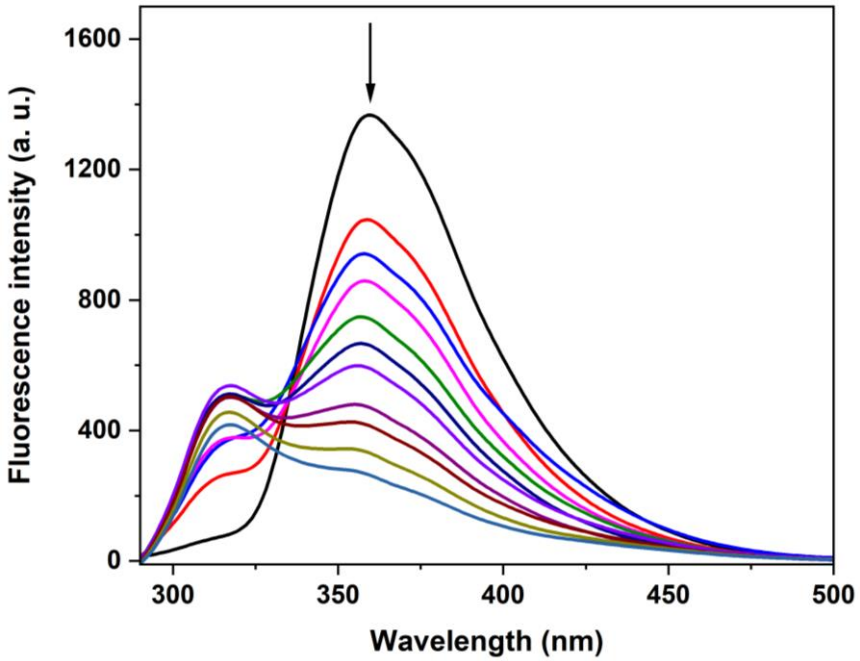

Figure 3.190. Changes in the emission spectra of **8** (1×10^{-6} M, λ_{exc} = 275 nm) with the addition of 4-chlorophenol in DMSO. The arrow indicates the quenching of the fluorescence intensity by addition of an appropriate aliquot of 4-CP.

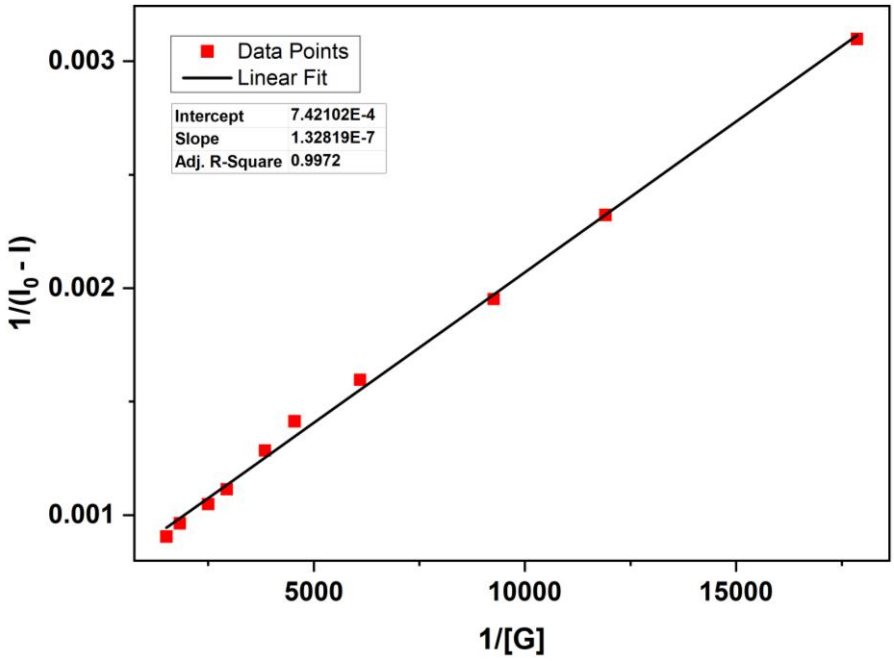

Figure 3.191. Benesi-Hildebrand plot for the emission quenching of host **8** (at 360 nm) with an increase in the concentration of 4-CP in DMSO.

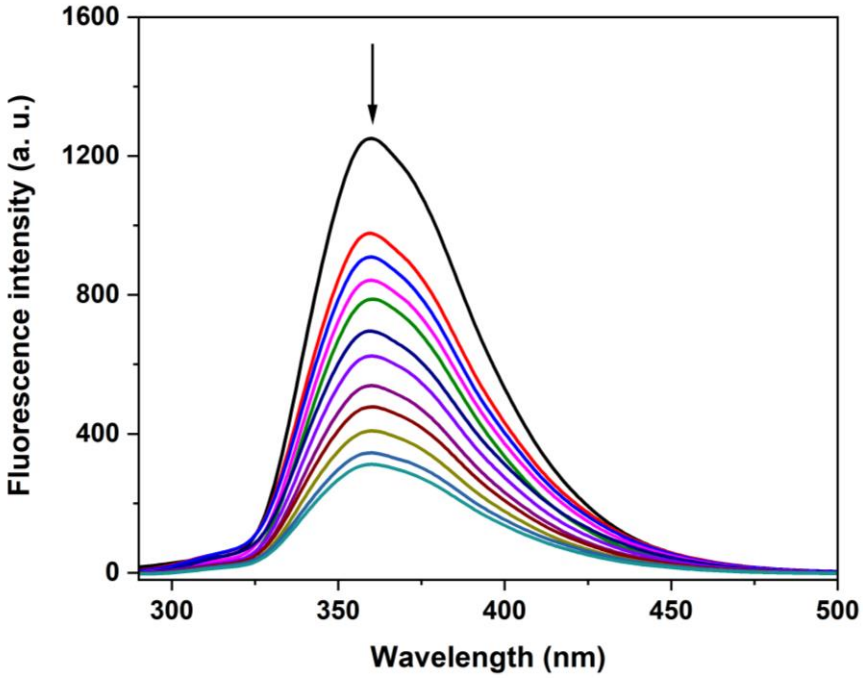

Figure 3.192. Changes in the emission spectra of **8** (1×10^{-6} M, λ_{exc} = 275 nm) with the addition of 2, 4-DCP in DMSO. The arrow indicates the quenching of the fluorescence intensity by addition of an appropriate aliquot of 2, 4-DCP.

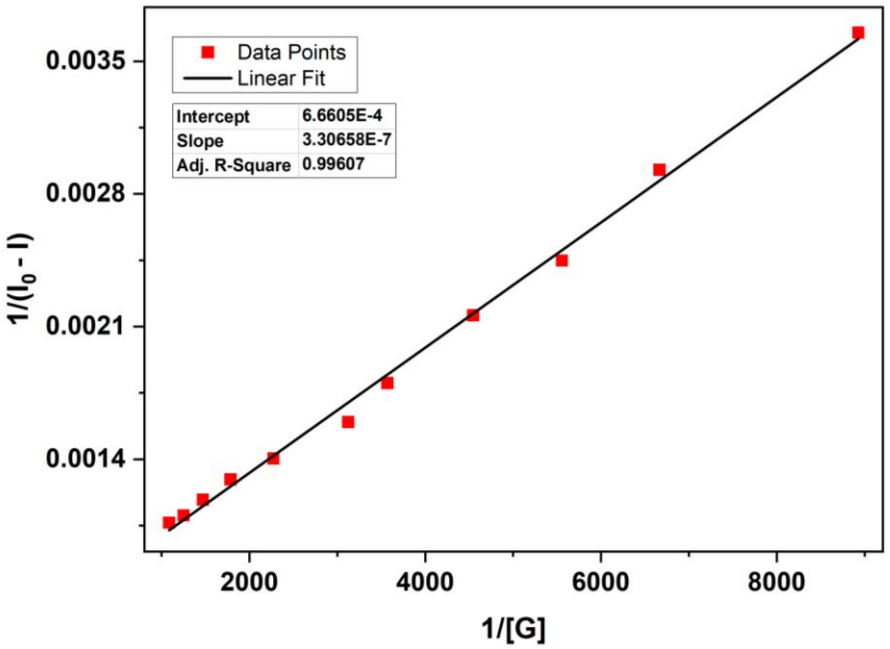

Figure 3.193. Benesi-Hildebrand plot for the emission quenching of host **8** (at 360 nm) with an increase in the concentration of 2, 4-DCP in DMSO.

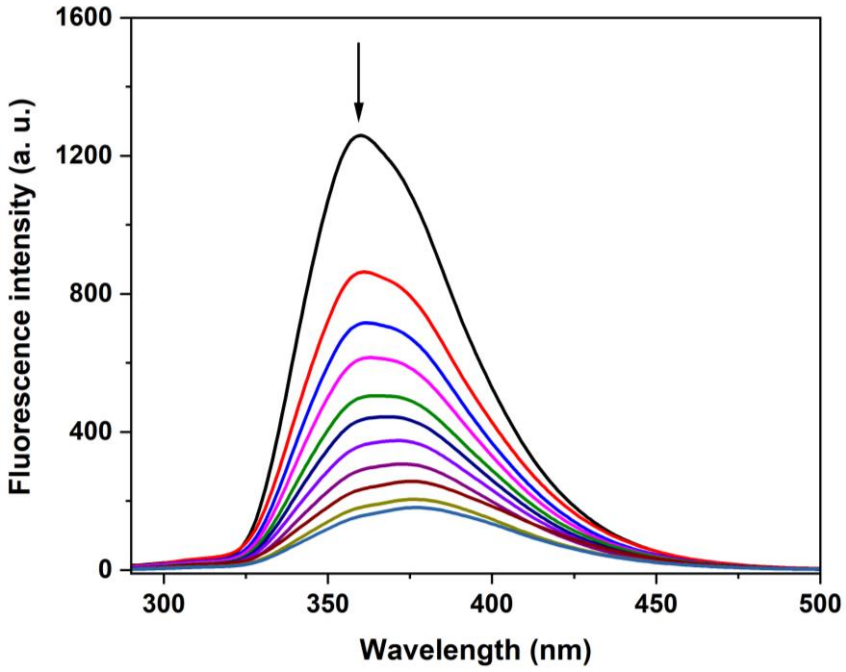

Figure 3.194. Changes in the emission spectra of **8** (1×10^{-6} M, λ_{exc} = 275 nm) with the addition of 2- NP in DMSO. The arrow indicates the quenching of the fluorescence intensity by addition of an appropriate aliquot of 2-NP.

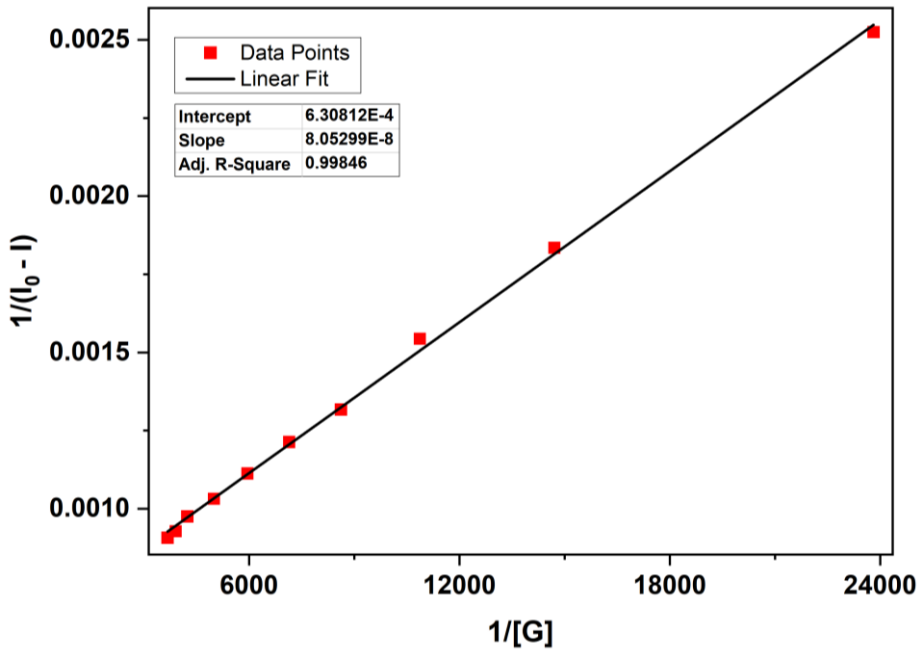

Figure 3.195. Benesi-Hildebrand plot for the emission quenching of host **8** (at 360 nm) with an increase in the concentration of 2-NP in DMSO.

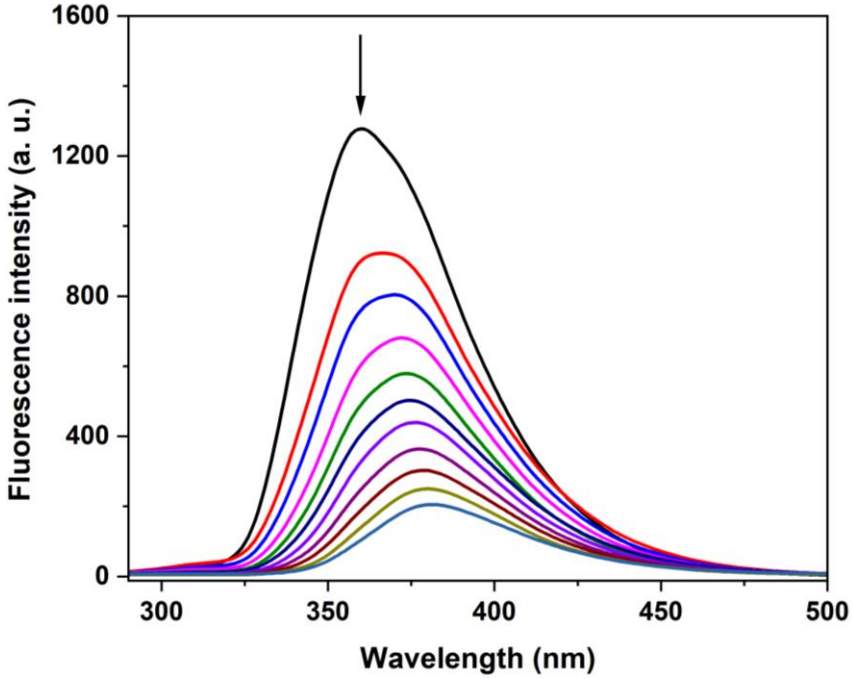

Figure 3.196. Changes in the emission spectra of **8** (1×10^{-6} M, λ_{exc} = 275 nm) with the addition of 4- NP in DMSO. The arrow indicates the quenching of the fluorescence intensity by addition of an appropriate aliquot of 4-NP.

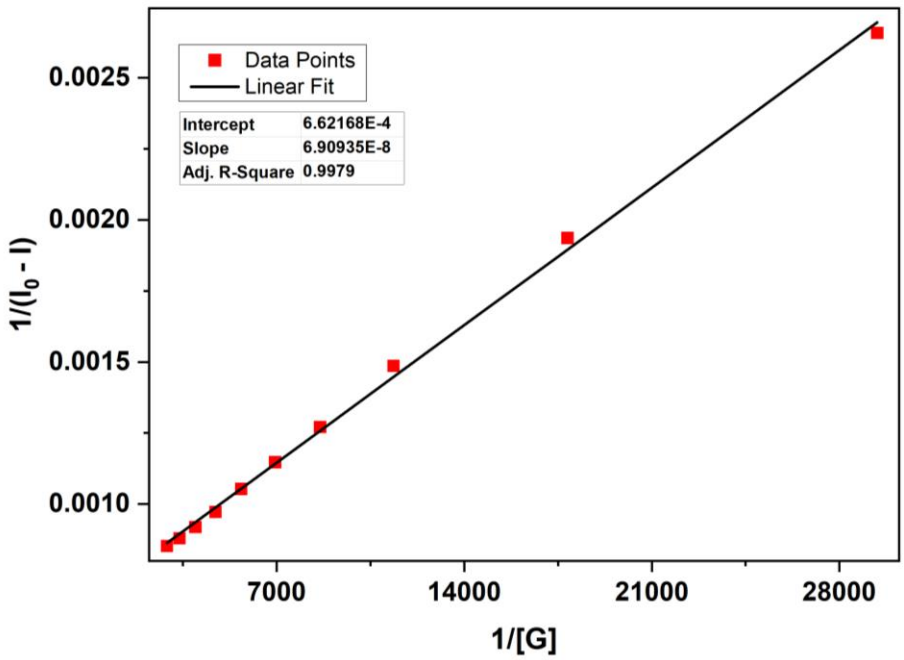

Figure 3.197. Benesi-Hildebrand plot for the emission quenching of host **8** (at 360 nm) with an increase in the concentration of 4-NP in DMSO.

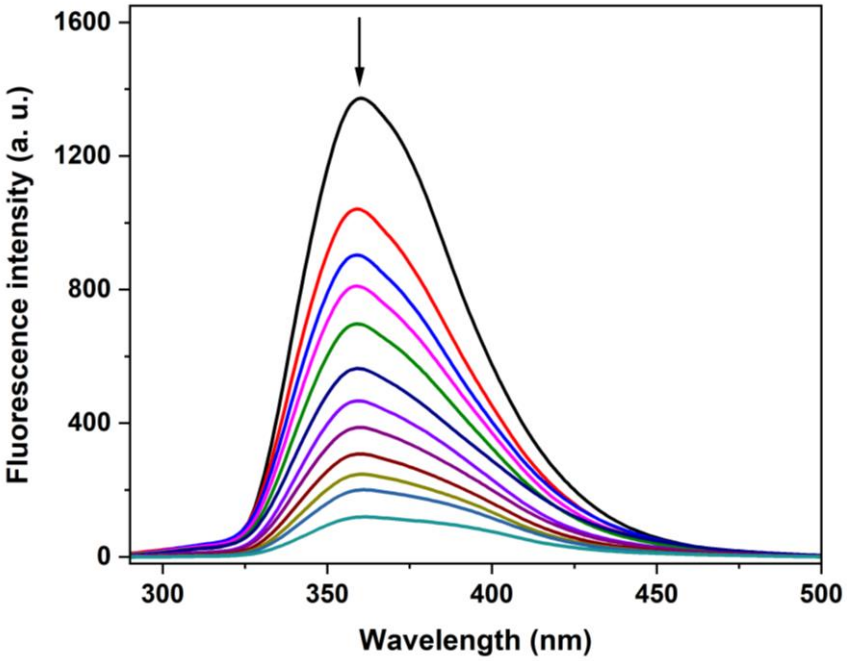

Figure 3.198. Changes in the emission spectra of **8** (1×10^{-6} M, λ_{exc} = 275 nm) with the addition of 2, 4- DNP in DMSO. The arrow indicates the quenching of the fluorescence intensity by addition of an appropriate aliquot of 2, 4- DNP.

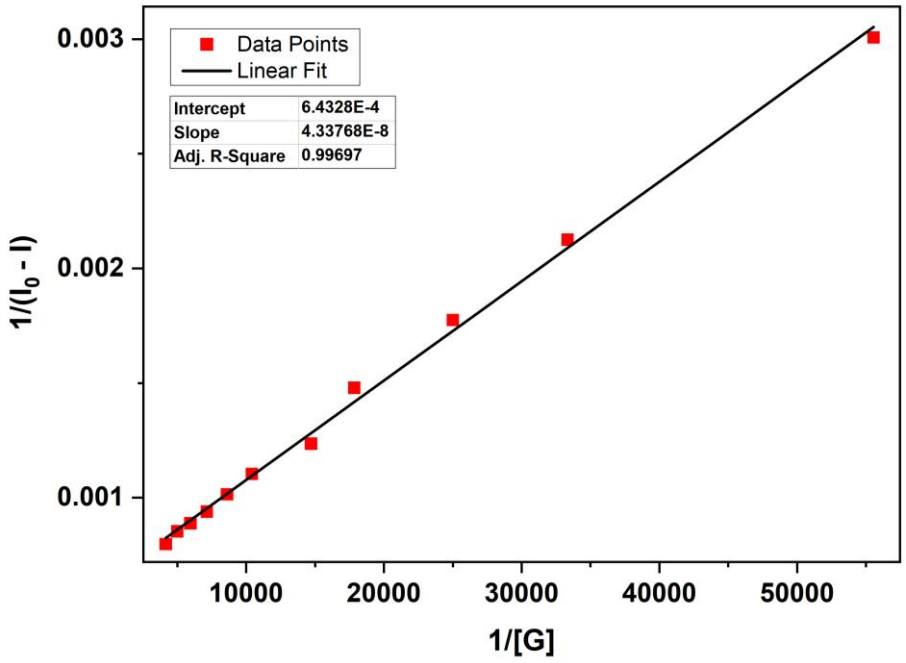

Figure 3.199. Benesi-Hildebrand plot for the emission quenching of host **8** (at 360 nm) with an increase in the concentration of 2, 4- DNP in DMSO.

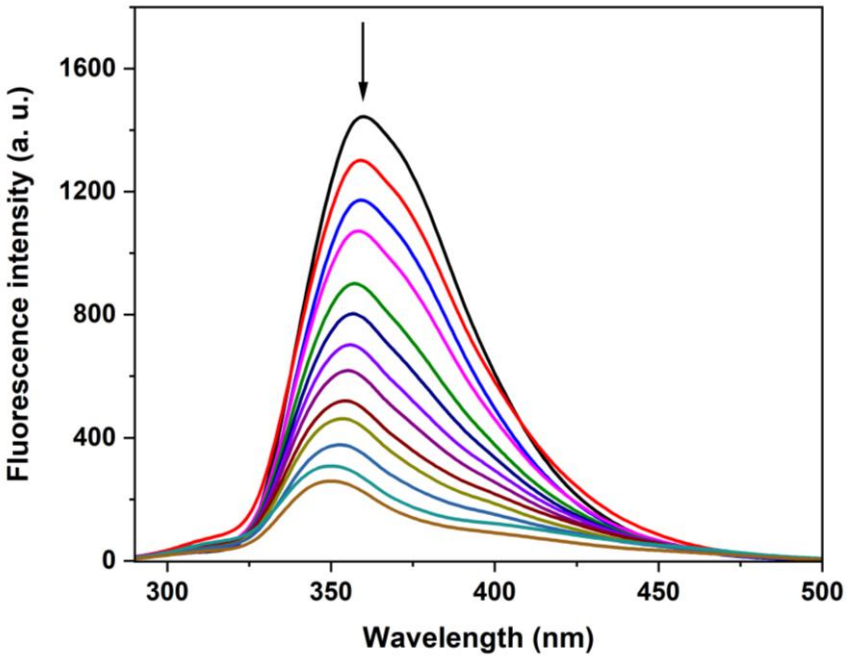

Figure 3.200. Changes in the emission spectra of **8** (1×10^{-6} M, λ_{exc} = 275 nm) with the addition of 2, 4, 6- TNP/ picric acid in DMSO. The arrow indicates the quenching of the fluorescence intensity by addition of an appropriate aliquot of picric acid.

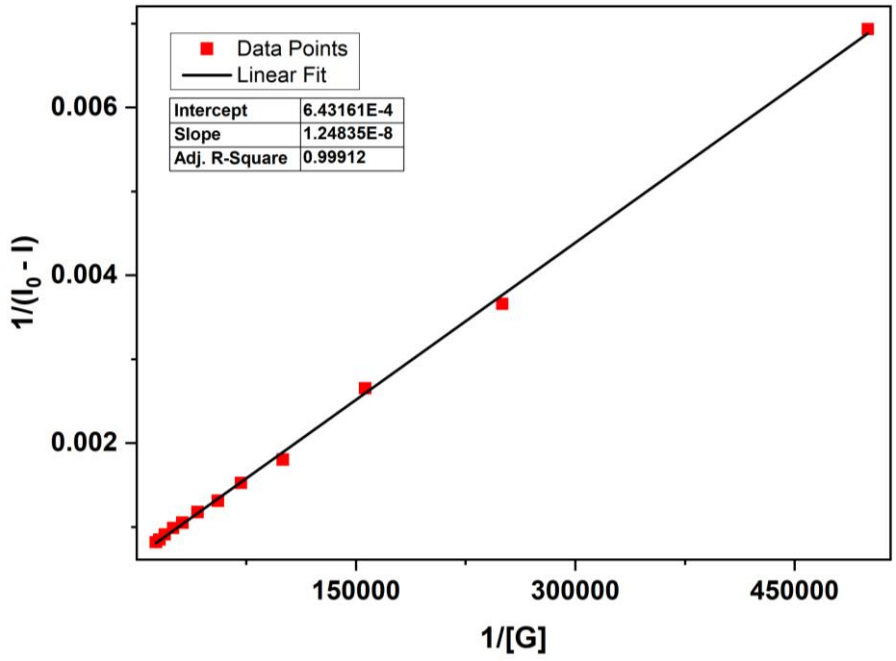

Figure 3.201. Benesi-Hildebrand plot for the emission quenching of host **8** (at 360 nm) with an increase in the concentration of 2, 4, 6- TNP in DMSO.

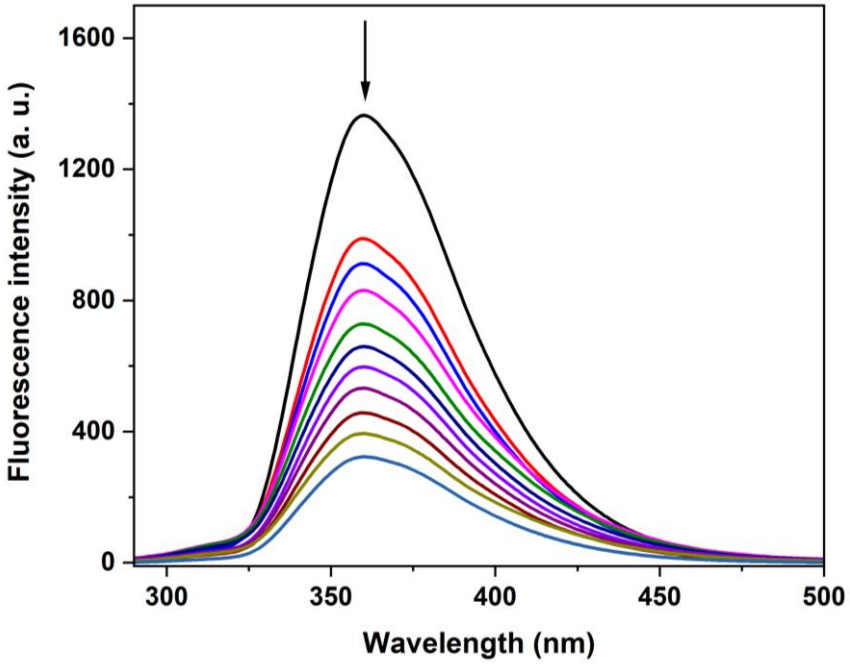

Figure 3.202. Changes in the emission spectra of **8** (1×10^{-6} M, λ_{exc} = 275 nm) with the addition of NB in DMSO. The arrow indicates the quenching of the fluorescence intensity by addition of an appropriate aliquot of NB.

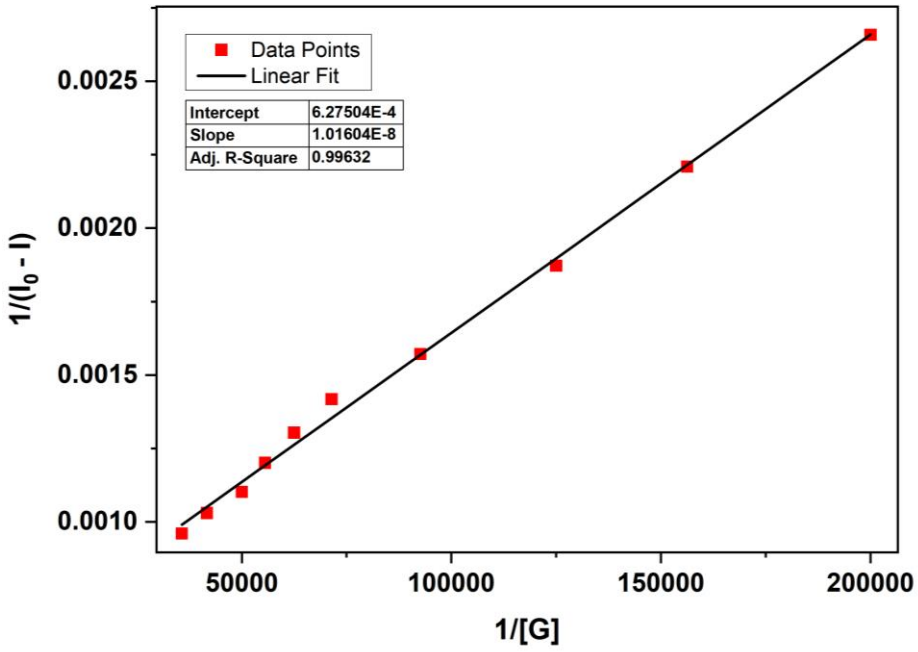

Figure 3.203. Benesi-Hildebrand plot for the emission quenching of host **8** (at 360 nm) with an increase in the concentration of NB in DMSO.

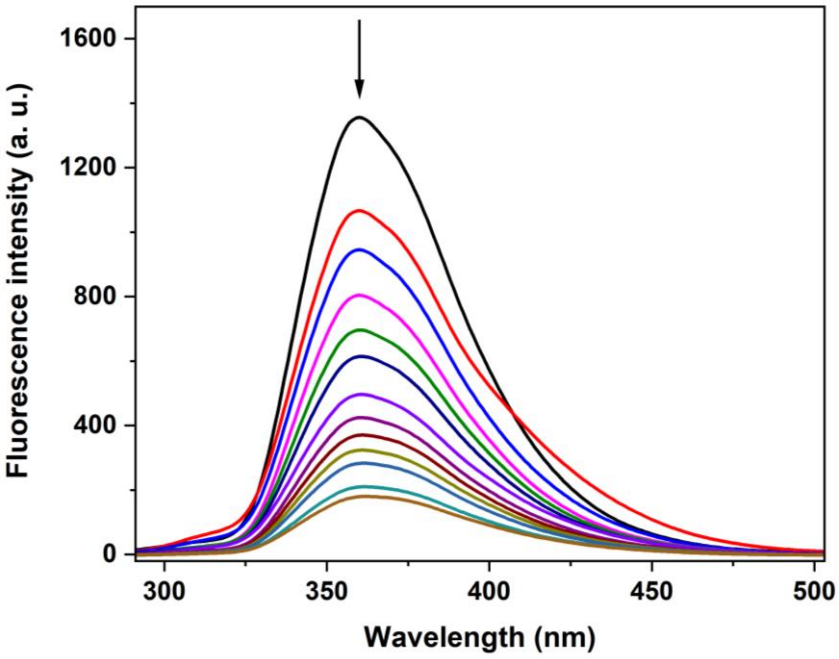

Figure 3.204. Changes in the emission spectra of **8** (1×10^{-6} M, λ_{exc} = 275 nm) with the addition of 2-NT in DMSO. The arrow indicates the quenching of the fluorescence intensity by addition of an appropriate aliquot of 2-NT.

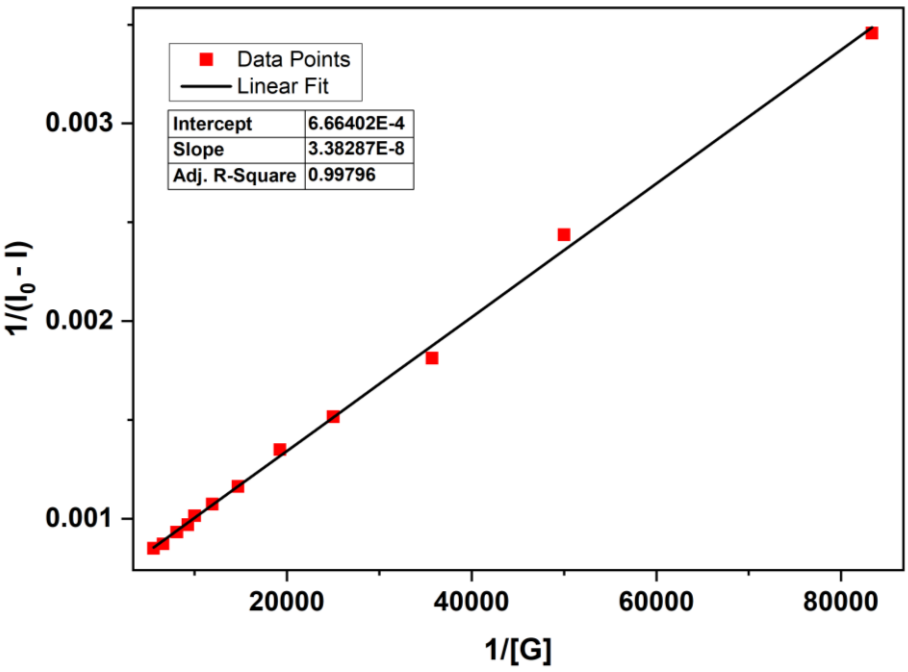

Figure 3.205. Benesi-Hildebrand plot for the emission quenching of host **8** (at 360 nm) with an increase in the concentration of 2-NT in DMSO.

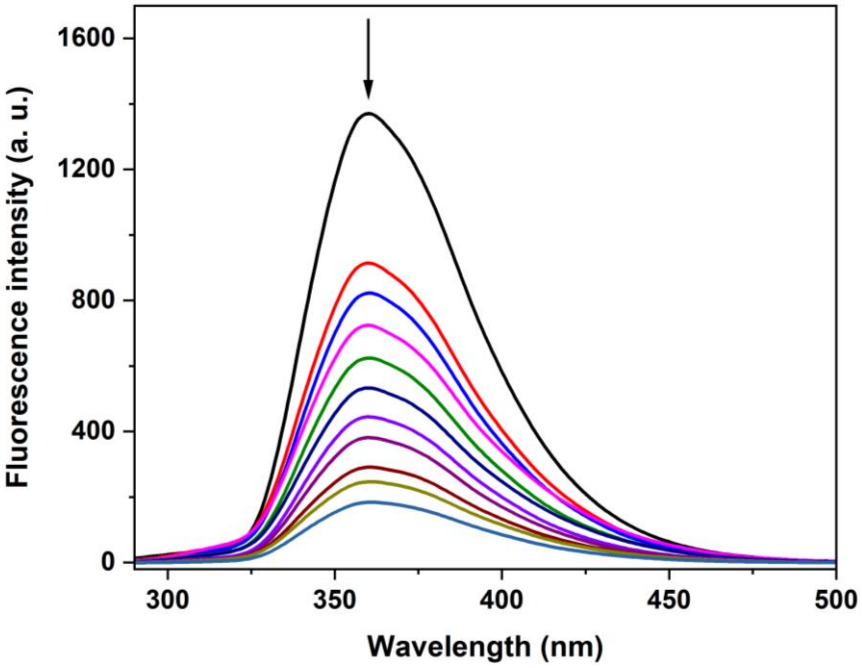

Figure 3.206. Changes in the emission spectra of **8** (1×10^{-6} M, λ_{exc} = 275 nm) with the addition of 4-NT in DMSO. The arrow indicates the quenching of the fluorescence intensity by addition of an appropriate aliquot of 4-NT.

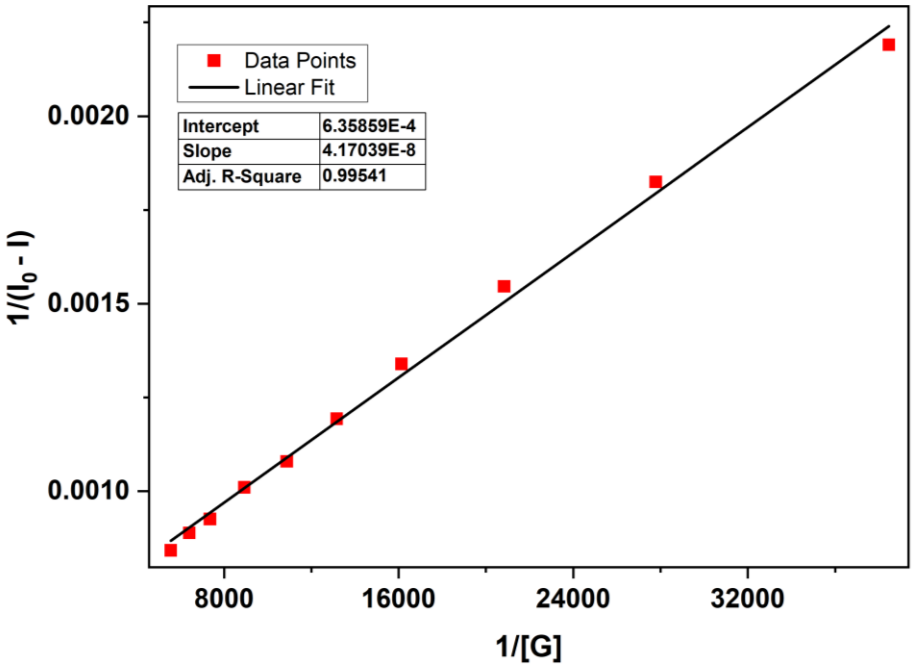

Figure 3.207. Benesi-Hildebrand plot for the emission quenching of host **8** (at 360 nm) with an increase in the concentration of 4-NT in DMSO.

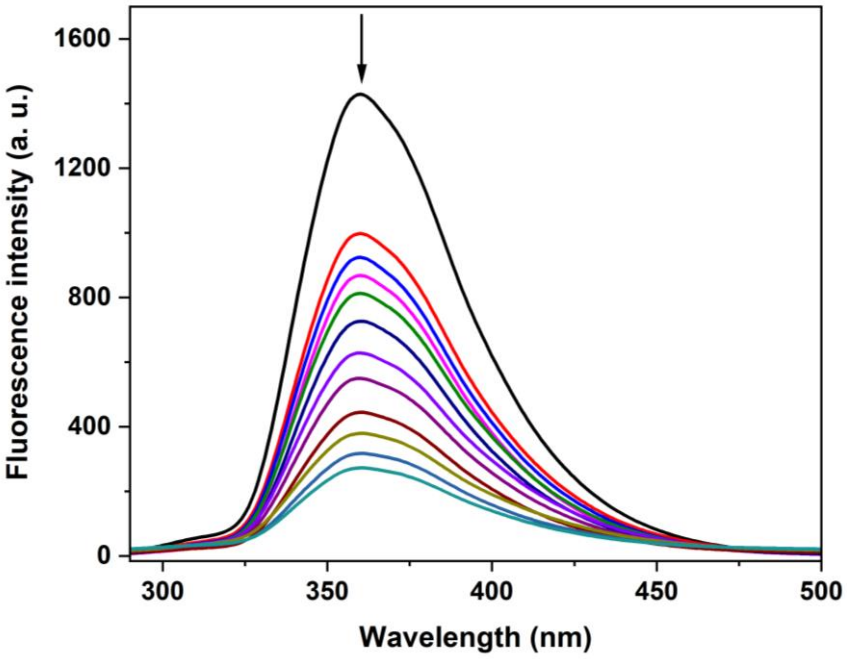

Figure 3.208. Changes in the emission spectra of **8** (1×10^{-6} M, λ_{exc} = 275 nm) with the addition of 2, 4-DNT in DMSO. The arrow indicates the quenching of the fluorescence intensity by addition of an appropriate aliquot of 2, 4-DNT.

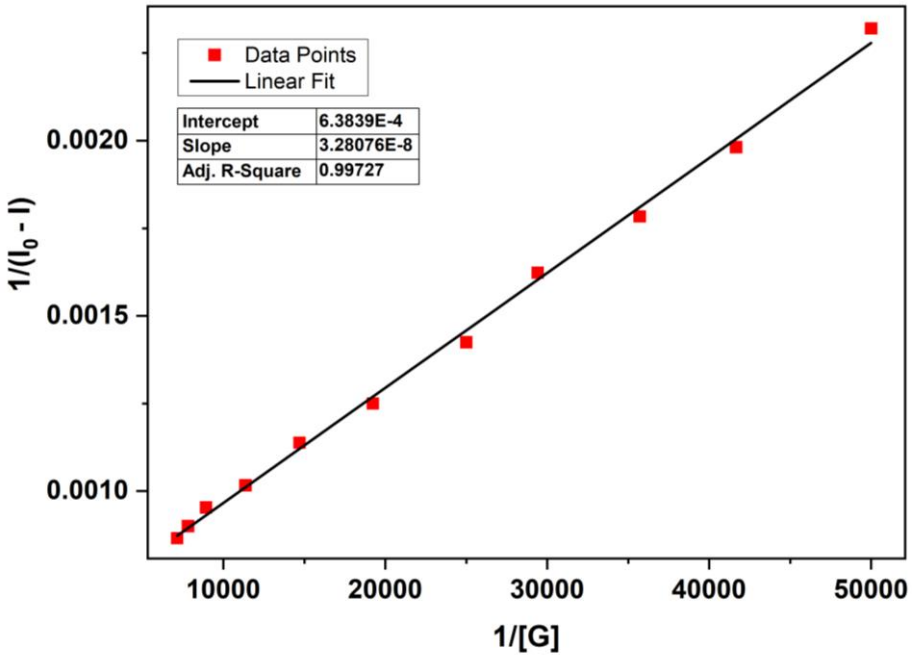

Figure 3.209. Benesi-Hildebrand plot for the emission quenching of host **8** (at 360 nm) with an increase in the concentration of 2, 4-DNT in DMSO.

Table 3.4. Comparison of Binding Constants K_a (M^{-1}) of previously reported complex (C**1**),[16] and Metallocavitands **1**, **2**, **7**, and **8** towards Nitro-substituted Guest Molecules Calculated by Emission Titration in DMSO at 298K.

guest molecule,	**C1**	**1**	**2**	**7**	**8**
Nitrobenzene	4.7×10^2	1.4×10^4	2.4×10^4	8.3×10^4	6.2×10^4
2-Nitrotoluene	1.1×10^3	1.1×10^4	1.8×10^4	2.8×10^4	2.0×10^4
4-Nitrotoluene	4.5×10^2	1.7×10^4	1.6×10^4	2.3×10^4	1.5×10^4
2,4-Dinitrotoluene	2.5×10^3	1.5×10^4	8.5×10^3	1.7×10^4	1.9×10^4

3.5 Conclusion

Eight neutral, heteroleptic *fac*-[$Re(CO)_3$] core-based metallocavitands (**1**-**8**) analogous to calix[5]arene were self-assembled using two new neutral, flexible ditopic nitrogen donors (L^1-L^2), bis-chelating ligands and $Re_2(CO)_{10}$ *via* one-pot approach. The inner cavity of the metallocavitands is tuneable by modulating the bis-chelating framework motifs. The solid-state structures of the metallocavitands confirm that their inner cavity is suitable to accommodate acetone, mesitylene, toluene and chlorobenzene. The host-guest recognition studies of metallocavitands **1**, **2**, **7** and **8** with a family of substituted phenol and nitrobenzene as guest molecules have suggested that the metallocavitands may act as hosts for substituted benzene core-based molecules. This study provides an easy synthetic approach for assembling neutral, heteroleptic pentagonal toroid-shaped host molecules. Further research to increase the width, tuning functional groups at the periphery as well as to make calix[n]arene (n = 6, 7)-shaped *fac*-[$Re(CO)_3$]-core based metallocavitands are currently under process in our laboratory.

3.6 References

1. (a) Frischmann, P. D.; MacLachlan, M. J. Metallocavitands: an emerging class of functional multimetallic host molecules. *Chem. Soc. Rev.* **2013**, *42*, 871-890. (b) Lippert, B.; Sanz Miguel, P. J. Metallatriangles and metallasquares: the diversity behind structurally characterized examples and the crucial role of ligand symmetry. *Chem. Soc. Rev*. **2011,** *40*, 4475-4487. (c) Kulesza, J.; Barros, B. S.; Junior, S. A. Organic–inorganic hybrid materials: Metallacalixarenes. Synthesis and applications. *Coord. Chem. Rev.* **2013**, *257*, 2192-2212. (d) Díaz-Ramírez, M. L.; Huggins, H.; Donnadieu, B.; Lopez, N.; Muñoz-Hernández, M. -Á. The Quest for Large Group 13 Metallacalixarenes Based on Benzymidazolyl Ligands and Al and Ga Alkyls. *Eur. J. Inorg. Chem.* **2021**, 3896-3902 and references therein.
2. (a) Zhang, Y. Y.; Gao, W. X.; Lin, L.; Jin, G. X. Recent advances in the construction and applications of heterometallic macrocycles and cages. *Coord. Chem. Rev*. **2017**, *344*, 323-344. (b) Zhang, L.; Lin, L.; Liu, D.; Lin, Y. J.; Li, Z. H.; Jin, G. X. Stacking Interactions Induced Selective Conformation of Discrete Aromatic Arrays and Borromean Rings. *J. Am. Chem. Soc.* **2017**, *139*, 1653-1660.(c) Zhang, W. Y.; Lin, Y. J.; Han, Y. F.; Jin, G. X. Facile Separation of Regioisomeric Compounds by a Heteronuclear Organometallic Capsule. *J. Am. Chem. Soc.* **2016**, 1*38*, 10700-10707. (d) Chen, L. J.; Yang, H. B.; Shionoya, M. Chiral metallosupramolecular architectures. *Chem. Soc. Rev*. **2017**, *46*, 2555-2576. (e) Amouri, H.; Desmarets, C.; Moussa, J. Confined Nanospaces in Metallocages: Guest Molecules, Weakly Encapsulated Anions, and Catalyst Sequestration. *Chem. Rev.* **2012**, *112*, 2015-2041. (f) Yoshizawa, M.; Klosterman, J. K.; Fujita, M. Functional Molecular Flasks: New Properties and Reactions within Discrete, Self-Assembled Hosts. *Angew. Chem. Int. Ed.* **2009**, *48*, 3418-3438. (g) Yoshizawa, M.; Tamura, M.; Fujita, M. Diels-Alderin Aqueous Molecular Hosts:Unusual Regioselectivity and Efficient Catalysis. *Science* **2006**, *312*, 251-254.
3. (a) Chakrabarty, R.; Mukherjee, P. S.; Stang, P. J. Supramolecular Coordination:Self-Assembly of Finite Two-and Three-Dimensional Ensembles. *Chem. Rev.* **2011**, *111*, 6810-6818. (b) Cook, T. R.; Stang, P. S. Recent Developments in the Preparation and Chemistry of Metallacycles and Metallacages via Coordination. *Chem. Rev.* **2015**, *115*, 7001–7045. (c) Cook, T. R.; Vajpayee, V.; Lee, M. H.; Stang, P. S.; Chi, K. W.

Biomedical and Biochemical Applications of Self-Assembled Metallacycles and Metallacages. *Acc. Chem. Res*. **2013**, 46, 2464– 2474. (d) Casini, A.; Woods, B.; Wenzel, M. The Promise of Self-Assembled 3D Supramolecular Coordination Complexes for Biomedical Applications. *Inorg. Chem.* **2017**, 56, 14715–14729. (e) Therrien, B. Drug Delivery by Water-soluble Organometallic Cages. *Top. Curr. Chem*. **2012**, *319*, 35– 55. (f) Han, Y. F.; Li, H.; Jin, G. X. Host–guest chemistry with bi-and tetra-nuclear macrocyclic metallasupramolecules. *Chem. Commun.* **2010**, *46*, 6879-6890. (g) Huang, C. C.; Liu, J. J.; Chen, Y.; Lin, M. J. An electron-deficient metallocavitand with an unusual selectivity towards substituted benzene derivatives during co-crystallizations. *Chem. Commun.* **2013**, *49*, 11512-11514.

4. (a) Bhat, I. A.; Zangrando, E.; Mukherjee, P. S. Coordination-Driven Self-Assembly of Discrete Molecular Nanotubular Architectures. *Inorg. Chem*. **2019**, *58*, 11172– 11179. (b) Bhattacharyya, S.; Venkateswarulu, M.; Sahoo, J.; Zangrando, E.; De, M.; Mukherjee, P. S. Self-Assembled $Pt^{II}8$ Metallosupramolecular Tubular Cage as Dual Warhead Antibacterial Agent in Water. *Inorg. Chem* **2020**, *59*, 12690– 12699. (c) Purba, P. C.; Maity, M.; Bhattacharyya, S.; Mukherjee, P. S. A Self-Assembled Palladium(II) Barrel for Binding of Fullerenes and Photosensitization Ability of the Fullerene-Encapsulated Barrel. *Angew. Chem. Int. Ed.* **2021**, *60*, 14109– 14116. (d) Ramakrishna, B.; Nagarajaprakash, R.; Veena, V.; Sakthivel, N.; Manimaran, B. Self-assembly of Oxamidato Bridged Ester Functionalised Dirhenium Metallastirrups: Synthesis, Characterisation and Cytotoxicity Studies. *Dalton. Trans*. **2015**, *44*, 17629– 17638. (e) Ashok Kumar, C.; Divya, D.; Nagarajaprakash, R.; Veena, V.; Vidhyapriya, P.; Sakthivel, N.; Manimaran, B. Self-assembly of Manganese(I) and Rhenium(I) Based Semi-rigid Ester Functionalized M_2L_2-type Metallacyclophanes: Synthesis, Characterization and Cytotoxicity Evaluation. *J. Organomet. Chem*. **2017**, *846*, 152– 160. (f) Botana, E.; Silva, E. D.; Benet-Buchholz, J.; Ballester, P.; de Mendoza, J. Inclusion of Cavitands and Calix[4]arenes into a Metallobridged para-(1H-imidazo[4,5-f][3,8]phenanthrolin-2-yl)-expanded Calix[4]arene. *Angew. Chem. Int. Ed.* **2007**, *46*, 198–201. (g) Samantray, S., Krishnaswamy, S. & Chand, D. K. Self-assembled conjoined-cages. *Nat. Commun.* **2020**, *11*, 880 1-11. (h) Bardhan, D.; Chand, D. K. Palladium(II)-Based Self-Assembled Heteroleptic Coordination Architectures: A Growing Family. *Chem. Eur. J.* **2019**, *25*, 12241 – 12269.
5. (a) MacGillivray, L. R.; Atwood J. L. Structural Classification and General Principles for the Design of Spherical Molecular Hosts. *Angew. Chem. Int. Ed.* **1999**, *38*, 1018-1033. (b)

Therrien, B. Arene Ruthenium Cages: Boxes Full of Surprises. *Eur. J. Inorg. Chem.* **2009**, 2445-2453. (c) Therrien, B. Transporting and Shielding Photosensitisers by Using Water-Soluble Organometallic Cages: A New Strategy in Drug Delivery and Photodynamic Therapy. *Chem. – Eur. J.* **2013**, *19*, 8378 -8386. (d) Han, Y. F.; Jia, W. G.; Lin, Y. J.; Jin, G. X. Extending Rectangular Metal–Organic Frameworks to the Third Dimension: Discrete Organometallic Boxes for Reversible Trapping of Halocarbons Occurring with Conservation of the Lattice. *Angew. Chem. Int. Ed.* **2009**, *48*, 6234-6238.(e) Huang,S. L.; Lin,Y. J.; Li, Z. H.; Jin, G. X. Self-Assembly of Molecular Borromean Rings from Bimetallic Coordination Rectangles. *Angew. Chem. Int. Ed.* **2014**, *53*, 11218-11222. (f) Huang, S. L.; Lin, Y. J.; Andy Hor T. S.; Jin, G. X. Cp*Rh-Based Heterometallic Metallarectangles: Size-Dependent Borromean Link Structures and Catalytic Acyl Transfer. *J. Am. Chem. Soc.* **2013**, *135*, 8125-8128 (g) Lu, Y.; Deng. Y. X.; Lin, Y. J.; Han, Y. F.; Weng. L. H.; Li. Z. H.; Jin, G. X.; Molecular Borromean Rings Based on Dihalogenated Ligands. *Chem*. **2017**, *3*, 110-121.

6. (a) Fondo, M.; Doejo, J.; Garcia-Deibe, A. M.; Matalobos, J. S.; Vicente, R. A. Ni_8 metallacalix[4]arene and a Cu_4 molecular rhomboid: limiting the nuclearity of carboxysalen-like metal complexes. *CrystEngComm*. **2016**, *18*, 6673-6682. (b) Lopez, N.; Rufino-Felipe, E.; Muñoz-Hernández, M. –Á. 1,3-alternate conformation of a gallium calix[4]arene based on a benzimidazolyl ligand. *Inorg. Chem. Commun*. **2016**, *64*, 50-52. (c) Rufino-Felipe, E.; Muñoz-Hernández, M. –Á.; Saucedo-Azpeitiaand, H. F., Cortes-Llamas, S. A.; Calix[4]arenes of Aluminum and Gallium with Benzimidazolyl Ligands: Steric Control of the Conformation via Substitution on the Ligand. *Inorg. Chem*. **2012**, *51*, 12834-12840. (d) Yu, X. Y.; Zhang, X.; Qu, X. S.; Ma, M. S.; Liu, Z. G.; Jin, L.; Yangand, Y. Y.; Luo, Y. N.; A new 3-D Cd(II) coordination polymer with metallacalix[4]arene building blocks based on 2-(pyridin-2-yl)-1H-imidazole-4,5-dicarboxylic acid. *J. Coord. Chem*. **2015**, *68*, 3580-3588.
7. (a) Wang, X.; Hu. H.; Liu, G.; Linand, H.; Tian, A. Self-assembly of nanometre-scale metallacalix[4]arene building blocks and Keggin units to a novel (3,4)-connected 3D self-penetrating framework. *Chem. Commun*. **2010**, *46*, 6485-6487. (b) Li, X.; Wu, B.; Wang, R.; Zhang, H.; Niu, C.; Niu, Y.; Hou, H. Hierarchical Assembly of Extended Coordination Networks Constructed by Novel Metallacalix[4]arenes Building Blocks. *Inorg. Chem*. **2010**, *49*, 2600-2613. (c) Maekawa, M.; Konaka, H.; Minematsu, T.; Kuroda-Sowa, T.; Munakata, M.; Kitagawa, S. Bowl–shaped Cu(i) metallamacrocyclic ethylene and carbonyl adducts as structural analogues of organic calixarenes. *Chem.*

Commun. **2007**, 5179-5181. (d) Navarro, J. A. R.; Barea, E.; Salas, J. M.; Masciocchi, N.; Galli, S.; Sironi, A. Structural and Magnetic Properties of Layered Copper(II) Coordination Polymers Intercalating s and f Metal Ions *Inorg. Chem.* **2007**, *46*, 2988-2997. (e) Ene, C. D.; Madalan, A. M.; Maxim, C.; Jurca, B.; Avarvari, N.; Andruh, M. Constructing Robust Channel Structures by Packing Metallacalixarenes: Reversible Single-Crystal-to-Single-Crystal Dehydration. *J. Am. Chem. Soc.* **2009**, *131*, 4586-4587.

8. (a) Sakate, M.; Kashima, A.; Hosoda, H.; Sunatsuki, Y.; Ota, H.; Fuyuhiro, A; Suzuki, T.; Thyminato-bridged cyclic tetranuclear rhodium(III) complexes containing a sodium, calcium or lanthanoid ion as a template metal core. *Inorg. Chim. Acta*. **2016**, *452*, 205-213. (b) Terrett, R.; Cavigliasso, G.; Stranger, R.; Yates, B. F. On the unprecedented level of dinitrogen activation in the calix[4]arene complex of Nb(iii). *Dalton Trans*. **2011**, *40*, 11267-11275. (c) Kashima, A.; Sakate, M.; Ota, H.; Fuyuhiro, A.; Sunatsuki, Y.; Suzuki, T. Thyminate(2−)-bridged cyclic tetranuclear rhodium(iii) complexes formed by a template of a sodium, calcium or lanthanoid ion. *Chem. Commun*. **2015**, *51*, 1889-1892. (d) Galindo, M. A.; Houlton, A.; Clegg, W.; Harrington, R. W.; Dodado, J.; Santoyo-Gonzalez, F.; Linares, F.; Romero, M. A.; Navarro, J. A. R. Electrochemically and photochemically active Palladium(ii) heterotopic metallacalix[3]arenes. *Chem. Commun*. **2008**, *13*, 3735-3737. (e) Xu, G. F.; Gamez, P.; Teat, S. J.; Tang, J. Praseodymium(iii)-based bis-metallacalix[4]arene with host–guest behavior. *Dalton Trans*. **2010**, *39*, 4353-4357.

9. (a) Velle, A.; Cebollada, A.; Lippert, B.; Sanz Miguel, P. J. Topology of metallacalix[4]arenes with uracil and cytosine ligands: favorable and unfavorable assemblies. *New J. Chem.* **2016**, *40*, 5914 -1519. (b) Khutia, A.; Sanz Miguel, P. J.; Lippert, B."Directed" Assembly of Metallacalix[n]arenes with Pyrimidine Nucleobase Ligands of Low Symmetry: Metallacalix[n]arene Derivatives of cis-$[a_2M(\text{cytosine-}N_3)_2]^{2+}$ ($M=Pt^{II}$, Pd^{II}; n=4 and 6). *Chem. – Eur. J.* **2011**, *17*, 4195-4204. (c) Khutia, A.; Sanz Miguel, P. J.; Lippert, B. Isomerism with Metallacalix[4]arenes of the Nonsymmetrical Pyrimidine Nucleobase Cytosine: How Connectivity and Rotamer State Determine the Topology of Multinuclear Derivatives. *Inorg. Chem.* **2010**, *49*, 7635-7637 (d) Das, N.; Sanz Miguel, P. J.; Khutia, A.; Lazar, M.; Lippert, B. Hybrids between classical and metallacalix[4]arenes based on uracil and cis-$Pt^{II}L_2$ entities (L = $P(Ph)_3$ or L_2 = 2,2′-bipyridine). *Dalton Trans*. **2009**, 9120-9122. (e) Galindo, M. A.; Houlton, A.; Clegg, W.; Harrington, R. W.; Dobado, J.; Santoyo-Gonzalez, F.; Linares, F.; Romero, M. A.; Navarro, J. A. R. Electrochemically and photochemically active Palladium(ii) heterotopic

metallacalix[3]arenes. *Chem. Commun*. **2008**, 3735-3737 (f) Galindo, M. A.; Olea, D.; Romero, M. A.; Gomez, J.; del Castillo, P.; Hannon, M. J.; Rodger, A.; Zamora, F.; Navarro, J. A. R. Design and Non-Covalent DNA Binding of Platinum(II) Metallacalix[4]arenes. *Chem. – Eur. J*. **2007**, *13*, 5075-5081 (g) Bardají, E. G.; Freisinger, E.; Costisella, B.; Schalley, C. A.; Bruning, W.; Sabat, M.; Lippert, B. Mixed-Metal (Platinum, Palladium), Mixed-Pyrimidine (Uracil, Cytosine) Self-Assembling Metallacalix[n]arenes: Dynamic Combinatorial Chemistry with Nucleobases and Metal Species. *Chem. – Eur. J*. **2007**, *13*, 6019-6039.

10. (a) Galindo, M. A.; Galli, S., Navarro, J. A. R.; Angustias Romero, M.; Formation of heterotopic metallacalix[n]arenes (n = 3, 4, 6) containing ethylenediaminepalladium(ii) metal fragments and 4,7-phenanthroline and 2-pyrimidinolate bridges. Synthesis, structure and host–guest chemistry. *Dalton Trans*. **2004**, 2780-2785. (b) Barea, E.; Navarro J. A. R.; Salas J. M.; Quiros, M.; Willermann, M.; Lippert, B. Chiral Pyrimidine Metallacalixarenes: Synthesis, Structure and Host–Guest Chemistry. *Chem. – Eur. J*. **2003**, *9*, 4414-4421. (c) Navarro, J. A. R.; Freisinger, E.; Lippert, B. Self-Assembly of Palladium(II) and Platinum(II) Complexes of 2-Hydroxypyrimidine to Novel Metallacalix[4]arenes. Receptor Properties through Multiple H-Bonding Interactions. *Inorg. Chem*. **2000**, *39*, 2301-2305. (d) Navarro, J. A. R.; Salas, J. M.; A palladium metallacalix[4]arene capped with a gadolinium atom. *Chem. Commun.* **2000**, 235-236. (e) Das, N.; Sanz Miguel, P. J.; Khutia, A.; Lazar, M.; Lippert. B.; Hybrids between classical and metallacalix[4]arenes based on uracil and cis-$Pt^{II}L_2$ entities (L = $P(Ph)_3$ or L_2 = 2,2′-bipyridine). *Dalton Trans*. **2009**, 9120-9122 (f) Galindo, M. A.; Navarro, J. A. R.; Romero, M. A.; Quiros, M. Mononucleotide recognition by cyclic trinuclear palladium(ii) complexes containing 4,7-phenanthroline N,N bridges. *Dalton Trans.* **2004**, 1563-1566.
11. (a) Rajakannu, P.; Elumalai, P.; Shankar, B.; Hussain, F.; Sathiyendiran, M. Rhenium(I) based metallocalix[4]arenes decorated with free functionalized benzimidazolyl units. *Dalton Trans.* **2013**, *42*, 11359-11362. (b) Elumalai, P.; Kanagaraj, R.; Marimuthu, R.; Shankar, B.; Kalita, A. C.; Sathiyendiran, M. Rhenium(I)-based bridgeless double metallocalix[4]arenes. *Dalton Trans.* **2015**, *44*, 11274–11277. (c) Rajakannu, P.; Shankar, B.; Sathiyendiran, M. fac-$Re(CO)_3$-based organometallic supramolecular coordination complexes using thiophene motif decorated flexible ditopic benzimidazolyl donor. *J. Organomet. Chem*. **2018**, *866*, 243-250. (d) Rajakannu, P.; Elumalai, P.; Hussain, F.; Sathiyendiran, M. Rhenium-based bicyclic supramolecule with calixarene-shaped bowls. *J. Organomet. Chem*. **2013**, *725*, 1-4. (e) Rajakannu, P.; Mobin, S. M.; Sathiyendiran, M.

Thiophene/furan units decorated unsymmetrical dinuclear metallocalix[4]arenes. *J. Organomet. Chem*. **2014**, *771*, 68-77. (f) Rajakannu, P.; Elumalai, P.; Mobin, S. M.; Lu, K. L.; Sathiyendiran, M. Hard and soft-donors decorated rhenium based metallocavitands. *J. Organomet. Chem*. **2013**, *743*, 17-23.

12. (a) Karges, J.; Seo, H.; M. Cohen, S. Synthesis of tetranuclear rhenium(I) tricarbonyl metallacycles. *Dalton Trans*. **2021**, *50*, 16147- 16155 and references there in. (b) Liao, R. -T.; Yang, W. -C.; Thanasekaran, P.; Tsai, C. -C.; Sathiyendiran, M.; Liu, Y. -H.; Rajendran, T.; Lin, H. -M.; Tseng, T. -W.; Lu, K. -L. Rhenium-based molecular rectangular boxes with large inner cavity and high shape selectivity towards benzene molecule. *Chem. Commun*. **2008**, 3175-3177. (c) Sathiyendiran, M.; Liao, R. T.; Thanasekaran, P.; Luo, T. T.; Venkataramanan, N. S.; Lee, G. H.; Peng, S. M.; Lu, K. L. Gondola-Shaped Luminescent Tetrarhenium Metallacycles with Crown-Ether-like Multiple Recognition Sites. *Inorg. Chem*. **2006**, *45*, 10052–10054. (d) Gupta, D.; Sathiyendiran, M. Rhenium-Carbonyl-Based Supramolecular Coordination Complexes: Synthesis, Structure and Properties. *ChemistrySelect* **2018**, *3*, 7439 – 7458 and references there in. (e) Thanasekaran, P.; Lee, C. C.; Lu, K. L. One-Step Orthogonal-Bonding Approach to the Self-Assembly of Neutral Rhenium-Based Metallacycles: Synthesis, Structures, Photophysics, and Sensing Applications. *Acc. Chem. Res*. **2012**, *45*, 1403–1418.
13. (a) Coogan, M. P.; Fernández-Moreira, V.; Kariuki, B. M.; Pope, S. J. A.; Thorp-Greenwood, F. L. A Rhenium Tricarbonyl 4′-Oxo-terpy Trimer as a Luminescent Molecular Vessel with a Removable Silver Stopper. *Angew. Chem. Int. Ed.* **2009**, *48*, 4965-4968. (b) Wright, P. J.; Muzzioli, S.; Skelton, B. W.; Raiteri, P.; Lee, J.; Koutsantonis, G.; Silvester, D. S.; Stangi, S.; Massi, M. One-step Assembly of Re(I) tricarbonyl 2-pyridyltetrazolato Metallacalix[3]arene with Aqua Emission and Reversible Three-electron Oxidation. *Dalton Trans.* **2013**, *42*, 8188– 8191. (c) Lin, S. M.; Velayudham, M.; Tsai, C. H.; Chang, C. H.; Lee, C. C.; Luo, T. T.; Thanasekaran, P.; Lu, K. L. A Molecular Triangle as a Precursor Toward the Assembly of a Jar-Shaped Metallasupramolecule. *Organometallics* **2014**, *33*, 40-44.
14. (a) Kedia, M.; Priyatharsini, M.; Sathiyashivan, S. D.; Shankar, B.; Krishnakumar, R. V.; Sathiyendiran, M. Prototype rhenium metallocavitand with four exocyclic cavities for small molecules. *J. Organomet. Chem*. **2022**, *959*, 122123. (b) Shankar, B.; Elumalai, P.; Deval Sathiyashivan, S.; Sathiyendiran, M. Spheroid Metallocavitands with Eight Calixarene-Shaped Receptors on the Surface. *Inorg. Chem*. **2014**, *53*, 10018– 10020. (c)

Shankar, B.; Hussain, F.; Sathiyendiran, M. Synthesis of rhenium-based M_3L_3L'-type metallacycle from benzimidazole and flexible tri(benzimidazole) ligands. *J. Organomet. Chem*. **2012**, *719*, 26-29.

15. (a) Sathiyendiran, M.; Tsai, C. -C.; Thanasekaran, P.; Luo, T. -T.; Yang, C. -I.; Lee, G. -H.; Peng, S. -M.; Lu, K. -L. Organometallic Calixarenes: Syceelike Tetrarhenium(I) Cavitands with Tunable Size, Color, Functionality, and Coin–Slot Complexation. *Chem. Eur. J.* **2011**, *17*, 3343-3346. (b) Huang, G. G.; Lee, C. J.; Yang, J.; Lu, Z. Z.; Sathiyendiran, M.; Huang, C. Y.; Kao, Y. C.; Lee, G. H.; Lu, K. L. Cavity-containing rhenium metallacycle treated evanescent wave infrared chemical sensors for the selective determination of odorous amines in the atmosphere. *Sens. Actuators B: Chem*. **2018**, *254*, 424-430.
16. Bhol, M.; Shankar, B.; Sathiyendiran, M. Rhenium(I) based irregular pentagonal-shaped metallacavitands. *Dalton Trans*. **2018**, *47*, 4494– 4500.
17. Halterman, R. L., Pan, X. G., Martyn, D. E., Moore, J. L., Long, A. T. Conformational Interconversions in [2]Catenanes Containing a Wide Rigid Bis(p-benzyl)methyl Spacer. *J. Org. Chem.* **2007**, *72*, 6454– 6458.
18. Han, X., Ma, H. Wang, Y. A simple and efficient synthesis of 2-aryl-substituted benzimidazoles. *Russ. J. Org. Chem.* **2008**, *44*, 863.
19. (a) Benesi, H. A.; Hildebrand, J. H. A Spectrophotometric Investigation of the Interaction of Iodine with Aromatic Hydrocarbons. *J. Am. Chem. Soc.* **1949**, *71*, 2703 -2707. (b) Murakami, Y.; Kikuchi, J. I.; Suzuki, M.; Matsuura, T. Syntheses of macrocyclic enzyme models. Part 6. Preparation and guest-binding behaviour of octopus cyclophanes. *J. Chem. Soc. Perkin Trans.1* **11988**, 1289 -1299.
20. (a) Sheldrick, G. M. A short history of SHELX. *Acta Crystallogr., Sect. A: Found. Crystallogr.* **2008**, *64*, 112– 122. (b) Sheldrick, G. M. Crystal structure refinement with SHELXL. *Acta Crystallogr., Sect. C: Struct. Chem*. **2015**, *71*, 3–8.
21. Jr, A. V. Ultrafast Excited-State Processes in Re(I) Carbonyl-Diimine Complexes: From Excitation to Photochemistry. *Top. Organomet. Chem.* **2010**, *29*, 73–114.
22. Tseng, Y. -H.; Bhattacharya, D.; Lin, S. -M.; Thanasekaran, P.; Wu, J. -Y.; Lee, L. -W.; Sathiyendiran, M.; Ho, M. -L.; Chung, M. -W.; Hsu, K. -C.; Chou, P. -T.; Lu, K. -L. Highly Emissive Cyclometalated Rhenium Metallacycles: Structure−Luminescence Relationship. *Inorg. Chem*. **2010**, *49*, 6805-6807.
23. (a) Bhattacharya, D.; Sathiyendiran, M.; Wu, J. -Y.; Chang, C. -H.; Huang, S. -C.; Zeng, Y.- L.; Lin, C. -Y.; Thanasekaran, P.; Lin, B. -C.; Hsu, C. -P.; Lee, G. -H.; Peng, S. -M.;

Lu, K.- L. Quinonoid-Bridged Chair-Shaped Dirhenium(I) Metallacycles: Synthesis, Characterization, and Spectroelectrochemical Studies. *Inorg. Chem.* **2010**, *49*, 10264-10272. (b) Bhattacharya, D.; Sathiyendiran, M.; Luo, T. -T.; Chang, C. -H.; Cheng, Y. -H.; Lin, C. -Y.; Lee, G. -H.; Peng, S. -M.; Lu, K. -L. Ground and Excited Electronic States of Quininone-Containing Re(I)-Based Rectangles: a Comprehensive Study of Their Preparation, Electrochemistry, and Photophysics. *Inorg. Chem.* **2009**, *48*, 3731– 3742.

24. (a) Sun, S. S.; Lees, A. J.; Transition metal based supramolecular systems: synthesis, photophysics, photochemistry and their potential applications as luminescent anion chemosensors. *Coord. Chem. Rev*. **2002**, *230*, 171-192. (b) Sathish, V.; Ramdass, A.; Lu, Z. Z.; Velayudham, M.; Thanasekaran, P.; Lu, K. L.; Rajagopal, S. Aggregation-Induced Emission Enhancement in Alkoxy-Bridged Binuclear Rhenium(I) Complexes: Application as Sensor for Explosives and Interaction with Microheterogeneous Media. *J. Phys. Chem. B.* **2013**, *117*, 14358-14366. (c) Zwijnenburg, M. A.; Berardo, E.; Peveler, W. J.; Jelfs, K. M. Amine Molecular Cages as Supramolecular Fluorescent Explosive Sensors: A Computational Perspective. *J. Phys. Chem. B,* **2016**, *120*, 5063-5072.

25. (a) Shanmugaraju, S.; Mukherjee, P. S. π-Electron rich small molecule sensors for the recognition of nitroaromatics *Chem. Commun*. **2015**, *51*, 16014 -16032. (b) Salinas, Y.; Manez, R. M.; Marcos, M. D.; Sancenon, F.; Costero, A. M.; Parra, M.; Gil, S. Optical chemosensors and reagents to detect explosives. *Chem. Soc. Rev.* **2012**, *41*, 1261-1296. (c) Ghosh, S.; Gole, B.; Bar, A. K.; Mukherjee, P. S. Self-Assembly of Molecular Prisms via Pt_3 Organometallic Acceptors and a Pt_2 Organometallic Clip. *Organometallics.* **2009**, *28*, 4288-4296.

Chapter 4

Calix[4]arene-Analogous Technetium and Rhenium Core-based Supramolecules

Abstract

Calix[4]arene-analogous technetium supramolecules (**1**-**2**) were assembled using $(NBu_4)[Tc_2(\mu\text{-}Cl)_3(CO)_6]$ and neutral flexible bidentate nitrogen donor ligands (L^1 and L^2) consisting of four arene units covalently joined *via* methylene units. The neutral homoleptic technetium macrocycles adopt a partial cone/cone-shaped conformation in the solid-state. These supramolecules are the first example of *fac*-$[Tc(CO)_3]^+$ core-based metallacalix[4]arenes and second example of *fac*-$[Tc(CO)_3]^+$ core-based metallomacrocycles. Structurally similar *fac*-$[Re(CO)_3]^+$ core-based macrocycles (**3**-**4**) were also prepared using $[Re(CO)_5X]$ (where X = Cl or Br) and L^1 or L^2. The products were characterized spectroscopically and by X-ray analysis. The molecular recognition studies of rhenium macrocycles were studied with PAHs and imidazole derivatives using by emission spectroscopic methods

This work has been published in *Inorg. Chem*. **2022**, *61*, 5173−5177.

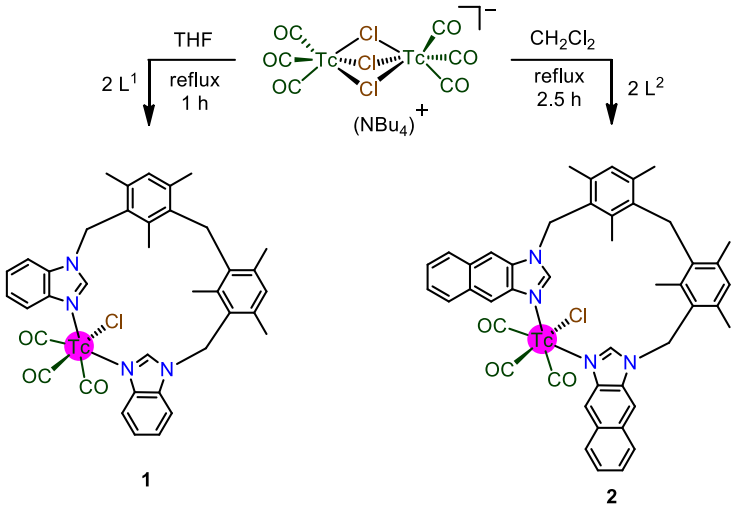

$$[Re(CO)_5X] + L^n \xrightarrow[\text{reflux}\\ \text{10 h or 24 h}]{C_7H_8 \text{ or } CHCl_3} \textit{fac}\text{–}[Re(CO)_3XL^n] \quad (1)$$

3a, $L^n = L^1$; X = Cl
3b, $L^n = L^1$; X = Br
4, $L^n = L^2$; X = Br

4.1. Introduction

The design and synthesis of stable and kinetically inert *fac*-$[M(CO)_3]^+$ (M = ^{99m}Tc/ $^{186/188}$Re) core-based complexes have been gaining continuous research interest for the development of new radiopharmaceuticals as diagnostic and therapeutic agents.[1-17] ^{99m}Tc is still the workhorse of nuclear diagnostics due to its ideal nuclear decay properties ($t_{1/2}$ = 6.02 h, pure γ emitter, Eγ = 140 keV, 89%), whereas the beta-emitting rhenium nuclides ^{188}Re ($t_{1/2}$ = 17 h, E_β = 2.12 MeV) and ^{186}Re ($t_{1/2}$ = 89.3 h, E_β = 1.07 MeV) possess potential for therapy.[2] Iso-structural technetium and rhenium complexes are good candidates for nuclear medical theranostics and there exist procedures for the synthesis of the aqua complexes [^{99m}Tc/^{188}Re$(CO)_3(H_2O)_3]^+$ as appropriate precursor molecules.[1c, 2b, 4, 6] Several attempts have been made towards the synthesis of organometallic technetium complexes using various types of heterocyclic ligands due to their importance in medicinal fields.[1-17] Recently, efforts have been directed towards the design and synthesis of *fac*-$[Re(CO)_3]^+$ core-based metal-organic macrocycles, i.e., supramolecular coordination complexes or metallomacrocycles, due to their potential applications as bio-imaging and anti-cancer agents.[18-20]

We envision that the synthesis of *fac*-$[Tc(CO)_3]^+$ core-based macrocycles may result in a new class of supramolecules that may find potential utility in the medicinal fields due to the combined properties of the technetium(I) tricarbonyl core and discrete 2D/3D supramolecular structures. In general, the known synthetic approaches for making *fac*-$[Re(CO)_3]^+$ core-based discrete supramolecules can be applied to create structurally analogous *fac*-$[Tc(CO)_3]^+$ core-based supramolecules.[20-22] To the best of our knowledge, *fac*-$[\{Tc(CO)_3Cl\}_2(ptc)_2]$ (ptc = 4-pyridyl-thiosemicarbazone = C_6H_5N-$C(CH_3)$=N-NH-C(S)-NH_2), is the only known example for a metallomacrocycle based on the *fac*-$[Tc(CO)_3]^+$ core.[15] Here, we report the fac-$[Tc(CO)_3Cl]$ core-based supramolecules analogous to calix[4]arenes and isostructural rhenium macrocycles.

4.2. Experimental

4.2.1. Radiation Precautions

Caution: ^{99}Tc is a long-lived weak β^- emitter (E_{max} = 0.292 MeV). Normal glassware provides sufficient protection against the weak beta radiation when milligram amounts are used. Secondary X-rays (bremsstrahlung) play a significant role only when larger amounts of ^{99}Tc compounds are handled. All manipulations were performed in a laboratory approved for the handling of radioactive materials.

Materials and Methods

4.2.2. Materials

All chemicals and solvents were reagent grade and used as received without further purification. The starting materials, $(NBu_4)[TcOCl_4]$,[23] $(NBu_4)[Tc_2(\mu\text{-}Cl)_3(CO)_6]$,[24] $Re(CO)_5Br$,[25] $Re(CO)_5Cl$,[26] naphtho[2,3-*d*]imidazole,[27] bis-(mesityl)methane,[28] and bis(3-(bromomethyl-2,4,6-trimethylphenyl)methane,[29] have been synthesized by the following previously published procedures. Solvents including toluene, $CHCl_3$, CH_2Cl_2 and THF were purified and distilled by conventional procedures.

4.2.3. Physical Measurement

FT-IR spectra of ^{99}Tc complexes were recorded on a Shimadzu FTIR spectrometer as KBr pellets. All other IR spectra were measured on a Nicolet iS10 and iS5 ATR- IR spectrometers. NMR spectra were recorded on a JEOL 400 MHz multinuclear spectrometer or a Bruker Avance III 500 MHz spectrometer. ^{1}H chemical shifts are reported relative to residual solvent protons as a reference (7.26 ppm for $CDCl_3$, 5.30 for CD_2Cl_2). For the ^{99}Tc chemical shifts, $KTcO_4$ in D_2O was used as the external reference. ESI-HR-MS spectra were collected on a Bruker maXis mass spectrometer.

4.2.4. Materials and Methods for Emission Titration Experiments

Emission spectra were recorded on a JASCO (FP-8500) spectrofluorometer. All the experiments were done in HPLC and spectroscopy grade dichloromethane and used as received from FINAR. Metallacalix[4]arene **3a** stock solutions (1×10^{-4} M for benzene, anthracene and benzimidazole; 1×10^{-5} M for naphthalene, imidazole) were prepared using CH_2Cl_2. Aromatic guests stock solutions (1×10^{-2} M for naphthalene; 1×10^{-3} M and

1×10^{-4} M for anthracene, and 1×10^{-1} M for benzene, imidazole and benzimidazole) were prepared in CH_2Cl_2. Metallacalix[4]arene **4** stock solutions (1×10^{-5} M for benzene, naphthalene and anthracene; 1×10^{-6} M for imidazole and 1×10^{-4} M for benzimidazole) were prepared using CH_2Cl_2. Aromatic guests stock solutions (1×10^{-1} M for benzene and naphthalene; 1×10^{-3} M for anthracene; 3×10^{-1} M for imidazole and 5×10^{-2} M for benzimidazole) were prepared in CH_2Cl_2. Test solutions were prepared by the addition of an appropriate aliquot (0.04- 3.5 mL) of each guest stock into 5mL standard volumetric flask followed by placing 1 mL of stock solution of host **3a /4** and then diluting the solution to 5 mL with CH_2Cl_2. The excitation wavelength was 231 nm and 240 nm for **3a** and **4** respectively. The slit bandwidth was 5 nm for both the excitation and emission. The binding characteristics of host **3a** and **4** with guest molecules were determined by the emission spectroscopic method. The binding constants were calculated on the basis of the Benesi-Hildebrand equation for a 1:1 stoichiometry molar ratio ($1/\Delta I = 1/\Delta I_{max} + (1/ K[G]\ \Delta I_{max})$. Here, $\Delta I = I - I_{min}$, $\Delta I_{max} = I_0 - I_{min}$, I_0 is the emission intensity of free host **3a** or **4**, I is the intensity measured with guest, I_{min} is the intensity measured with an excess of guest, *K* is the binding constant, and [G] is the concentration of guest molecule**.**

4.2.5. Crystallography

Single crystal X-ray diffraction data were collected on STOE IPDS 2T, Bruker D8 Quest diffractometer or Rigaku Oxford XtaLAB Synergy instruments with Mo-Kα radiation (λ = 0.71073 Å). Standard procedures were applied for data reduction, and absorption correction. Structure solutions and refinements were performed with the SHELX program package.[30] Non-H atoms were refined anisotropically.

4.2.6. Synthesis of Ligands

Bis(3-(benzimidazol-1-ylmethyl)-2,4,6-trimethylphenyl)methane (L^1):

A mixture of powdered KOH (125 mg, 2.11 mmol) and benzimidazole (250 mg, 2.11 mmol) was stirred in DMF (8 mL) at room temperature for 2.5 h. Bis(3-(bromomethyl)-2,4,6-trimethylphenyl)methane (463 mg, 1.05 mmol) was added to the colourless solution and stirred for further 32 h at room temperature under N_2 atmosphere. The reaction was quenched by adding ice water (200 mL). The resulting colourless powder was collected by filtration, washed several times with water, and air-dried. Yield: 61% (331 mg). ^{1}H NMR (500 MHz,

$CDCl_3$): δ 7.81 - 7.79 (m, 2H, H^7), 7.44 - 7.43 (m, 2H, H^4), 7.35 (s, 2H, H^2), 7.32 - 7.29 (m, 4H, H^{5-6}), 6.94 (s, 2H, H^9), 5.21 (s, 4H, H^8 –CH_2–), 4.12 (s, 2H, H^{10} –CH_2–), 2.26 (s, 6H, –CH_3), 2.19 (s, 6H, –CH_3) and 1.92 (s, 6H, –CH_3). ^{13}C NMR (500 MHz, $CDCl_3$): δ 144.0, 141.7, 137.8, 137.1, 136.8, 135.5, 134.2, 131.4, 128.4, 123.0, 122.4, 120.4, 109.7, 43.9, 32.3, 21.3, 19.8, 16.4. ESI-HRMS (*m/z*): $[L^1 + H]^+$ calcd. for $C_{37}H_{28}N_4$, 513.3018; found, 513.3031.

Bis((3-(naphtho[2,3-d]imidazol-1-yl)methyl)-2,4,6-trimethylphenyl)methane (L^2):

A mixture of powdered KOH (117 mg, 2.081 mmol) and naphtho[2,3-*d*]imidazole (350 mg, 2.081 mmol) in DMF (10 mL) was stirred at room temperature for 2.5 h. Bis(3-(bromomethyl)-2,4,6-trimethylphenyl)methane (456 mg, 1.041 mmol) was added to the greyish colored solution, and the reaction mixture was stirred for another 32 h. The reaction was quenched by adding water (200 mL), and the resulting grey precipitate was filtered off, washed several times with water, and air-dried. Yield: 78% (500 mg). ^{1}H NMR (500 MHz, $CDCl_3$): δ 8.28 (s, 2H, H^2), 8.03 - 8.01 (d, J = 7.26 Hz, 2H, H^8), 7.97 - 7.95 (d, J = 7.54 Hz, 2H, H^5), 7.82 (s, 2H, H^9), 7.53 (s, 2H, H^4), 7.45 - 7.34 (m, 4H, H^{6-7}), 6.96 (s, 2H, H^{11}), 5.25 (s, 4H, H^{10} –CH_2–), 4.13 (s, 2H, H^{12} –CH_2–), 2.29 (s, 6H, –CH_3), 2.22 (s, 6H, –CH_3) and 1.93 (s, 6H, –CH_3). ^{13}C NMR (500 MHz, $CDCl_3$): δ 145.7, 144.2, 137.9, 137.2, 136.9, 135.5, 134.8, 131.5, 130.6, 130.4, 128.7, 128.5, 127.6, 124.7, 123.7, 117.5, 105.5, 44.0, 32.4, 21.4, 19.8, 16.4. ESI-HRMS (*m/z*): $[L^2 + H]^+$ calcd. for $C_{43}H_{40}N_4$, 613.3331; found, 613.3331.

4.2.7. Synthesis of Technetium and Rhenium Complexes

Synthesis of fac-[Tc(CO)$_3$Cl(L^1)] (1):

$(NBu_4)[Tc_2(\mu\text{-}Cl)_3(CO)_6]$ (9 mg, 0.0126 mmol) was dissolved in THF (0.5 mL) and L^1 (13 mg, 0.0254 mmol) in THF (2 mL) was added. The mixture was heated under reflux for 1 h. The clear solution was filtered. Colorless single crystals were obtained by the slow evaporation of a THF/hexane solution. Yield: 11 mg (0.015 mmol, 60%). ^{99}Tc NMR ($CDCl_3$, ppm): -1172 ($\nu_{1/2}$ = 788 Hz). ^{1}H NMR (400 MHz, $CDCl_3$): δ 8.52 (s, 1H, $H^{2'}$), 8.21 (s, 1H, H^2) 7.54 - 7.46 (d, 3H, $H^{4'\text{-}5',7'}$), 6.94 (s, 4H, $H^{4,6',9,9'}$), 6.79 (s, 3H, H^{5-7}), 5.49-5.38 (dd, J = 16 Hz, 2H, $H^{8'}$ -CH_2-), 5.08-5.04 (d, J =16 Hz, 1H, H^{8a}, –CH_2–), 4.74-4.72 (d, J = 8 Hz, 1H, H^{8b}, -CH_2-), 4.10-3.84 (dd, J = 16 -20 Hz, 2H, H^{10} –CH_2–), 2.58 (s, 3H, –CH_3), 2.40 (s, 6H, –CH_3), 2.00 (s, 3H, –CH_3), 1.43 (s, 3H, –CH_3).and 0.81 (s, 3H, –CH_3). FT-IR (KBr, cm^{-1}): 2029 (C≡O), 1923 (C≡O), 1896 (C≡O).

Synthesis of fac-[Tc(CO)$_3$Cl(L^2)] (2):

$(NBu_4)[Tc_2(\mu\text{-}Cl)_3(CO)_6]$ (9 mg, 0.0126 mmol) was dissolved in CH_2Cl_2 (0.5 mL) and L^2 (16 mg, 0.0261 mmol) in CH_2Cl_2 (2 mL) was added. The mixture was heated on reflux for 2.5 h. The clear brown solution was filtered. Yellow single crystals deposited by slow evaporation of CH_2Cl_2/methanol solution. The crystals were filtered off and washed with hexane. Yield: 10 mg (0.012 mmol, 46%).^{99}Tc NMR (CD_2Cl_2, ppm): -1165 ($\nu_{1/2}$ = 1378 Hz). ^{1}H NMR (400 MHz, CD_2Cl_2): δ 8.74 (s, 2H, H$^{2',2}$), 8.25-8.01 (m, 4H, H$^{4'\text{-}5',8'\text{-}9'}$), 7.70 - 7.56 (m, 4H, H$^{4,9,6',7'}$), 7.31 - 7.01 (m, 6H, H$^{5\text{-}8,11,11'}$), 5.54-5.09 (m, 4H, H$^{10',10}$ –CH_2–), 4.10-3.82 (dd, J =18 Hz, 2H, H^{12} –CH_2–), 2.44 (s, 6H, –CH_3), 2.06 (s, 3H, –CH_3), 1.26 (s, 3H, –CH_3), 0.88 (s, 3H, –CH_3).and 0.60 (s, 3H, –CH_3). FT-IR (KBr, cm^{-1}): 2027(C≡O), 1924 (C≡O), 1894 (C≡O).

Synthesis of fac-[Re(CO)$_3$Cl(L^1)] (3a):

A mixture of $Re(CO)_5Cl$ (30 mg, 0.083 mmol) and L^1 (43 mg, 0.083 mmol) was dissolved in toluene (10 mL) and heated on reflux for 10 h under an argon atmosphere. Colourless single crystals deposited after slow evaporation of the solvent. Yield: 35 mg (0.043 mmol, 52%). ^{1}H NMR (500 MHz, $CDCl_3$): δ 8.83 (s, 1H, H$^{2'}$), 8.30 (s, 1H, H^2) 7.60 - 7.50 (d, 3H, H$^{4'\text{-}5',7'}$), 7.06 -6.92 (m, 4H, H$^{4,6',9,9'}$), 6.72 - 6.61 (d, 3H, H$^{5\text{-}7}$), 5.53 - 5.42 (dd, J = 15 Hz, 2H, H$^{8'}$ –CH_2–), 5.06-5.03 (d, J = 14 Hz, 1H, H^{8a}, –CH_2–), 4.68-4.66 (d, J = 10 Hz, 1H, H^{8b}, –CH_2–), 4.12 - 3.85 (dd, J = 18 Hz, 2H, H^{10} –CH_2–), 2.65 (s, 3H, –CH_3), 2.41 (s, 6H, –CH_3), 1.94 (s, 3H, -CH_3), 1.40 (s, 3H, –CH_3) and 0.80 (s, 3H, –CH_3). ^{13}C NMR (500 MHz, $CDCl_3$): δ 196.3, 196.0, 192.8, (1:1:1, CO), 148.7, 143.1, 141.5, 137.3, 137.1, 136.7, 136.1, 134.1, 133.1, 132.3, 131.8, 131.0, 126.3, 124.8, 124.6, 124.0, 123.6, 120.4, 118.2, 111.8, 110.4, 46.0, 43.9, 32.6, 22.1, 21.6, 20.6, 19.2. ATR-IR (ν, cm^{-1}): 2015 (C≡O), 1901(C≡O), 1878(C≡O). ESI-HRMS (*m/z*): [**3a** + Na]$^+$ calcd for $C_{38}H_{36}ClN_4O_3Re$, 841.1931; found, 841.1932.

Synthesis of fac-[Re(CO)$_3$Br(L^1)] (3b):

A mixture of $Re(CO)_5Br$ (50 mg, 0.123 mmol) and L^1 (63 mg, 0.123 mmol) was dissolved in toluene (10 mL) and heated on reflux for 10 h under an inert atmosphere. Colourless single crystals are obtained from the vapour diffusion of acetonitrile and hexane solvents. Yield: 57 mg (0.066 mmol, 54%). ^{1}H NMR (500 MHz, $CDCl_3$): δ 8.83 (s, 1H, H$^{2'}$), 8.30 (s, 1H, H^2)

7.60 - 7.50 (d, 3H, $H^{4'\text{-}5',7'}$), 7.06 -6.92 (m, 4H, $H^{4,6',9,9'}$), 6.72 - 6.61 (d, 3H, $H^{5\text{-}7}$), 5.52 - 5.42 (dd, *J* = 15 Hz, 2H, $H^{8'}$ –CH_2–), 5.06-5.03 (d, *J* = 14 Hz, 1H, H^{8a}, –CH_2–), 4.68-4.66 (d, *J* = 10 Hz, 1H, H^{8b}, –CH_2–), 4.11 - 3.85 (dd, *J* = 18 Hz, 2H, H^{10} –CH_2–), 2.65 (s, 3H, –CH_3), 2.41 (s, 6H, –CH_3), 1.93 (s, 3H, –CH_3), 1.39 (s, 3H, –CH_3) and 0.80 (s, 3H, –CH_3). ^{13}C NMR (500 MHz, $CDCl_3$): *δ* 195.9, 195.7,192.1 (1:1:1, CO), 150.1, 145.9, 141.6, 137.3, 137.2, 136.7, 136.0, 134.1, 133.0, 132.3, 131.8, 131.0, 126.3, 124.9, 124.6, 124.0, 123.6, 120.5, 118.4, 111.9, 110.4, 46.1, 43.9, 32.6, 22.2, 21.6, 20.6, 19.2. ATR-IR (ν, cm^{-1}): 2012 (C≡O), 1901(C≡O), 1874 (C≡O). ESI-HRMS (*m/z*): [**3b** + Na]$^+$ calcd for $C_{38}H_{36}BrN_4O_3Re$, 885.1426; found, 885.1425.

Synthesis of fac-[Re(CO)$_3$Br(L^2)] (4):

A mixture of $Re(CO)_5Br$ (30 mg, 0.074 mmol) and L^2 (45 mg, 0.074 mmol) was dissolved in $CHCl_3$ (20 mL) and heated on reflux for 24 h under an inert atmosphere. The solution was filtered and the solvent was removed under vacuum. The residue was dissolved in CH_2Cl_2 and layered with methanol. Suitable single crystals were obtained for X-ray diffraction. Yield: 52 mg (0.054 mmol, 73%).^{1}H NMR (500 MHz, DMSO-d_6): *δ* 9.39 (s, 1H, $H^{2'}$), 8.72 (s, 1H, H^2), 8.36-7.89 (m, 4H, $H^{4'\text{-}5',8'\text{-}9'}$), 7.62 (s, merged, 4H, $H^{4,9,6',7'}$), 7.28 – 6.65 (m, 6H, $H^{5\text{-}8,11,11'}$), 6.00-4.53 (m, 4H, $H^{10',10}$ –CH_2–), 4.01-3.72 (dd, *J* =17.5 Hz, 2H, H^{12} –CH_2–), 2.37-1.84 (s, merged, 12H, –CH_3), 1.33 (s, 3H, –CH_3) and 1.21 (s, 3H, –CH_3).^{13}C NMR (500 MHz, DMSO-d_6): *δ*196.1, 192.0 (2:1, CO). ATR IR (ν, cm^{-1}): 2014 (C≡O), 1904 (C≡O), 1875 (C≡O). ESI-HRMS (*m/z*): [**4** - H]$^+$ calcd for $C_{46}H_{40}BrN_4O_3Re$, 961.1763; found, 961.2436.

4.3. Results and discussion

4.3.1. Synthesis and characterization of ligands L^1- L^2.

Ligands L^1 and L^2 were designed as single building units for assembling mononuclear calix-shaped supramolecules because of two reasons: (i) the ligands contain four hetero(arene) units that are linked *via* three methylene (–CH_2–) groups alternatively as (heteroarene)–CH_2–(*meta*-phenylene)–CH_2–(*meta*-phenylene)–CH_2–(heteroarene), which is almost the basic structural units in the ring of calix[4]arene, and (ii) the ligands are flexible and have ability to chelate one metal ion using their two terminal heteroarene motifs, thus chelating to metal ion could result in bowl-shaped macrocycles. The ligands were obtained by the reactions of benzimidazole/naphtho[2,3-*d*]imidazole, bis(3-(bromomethyl)-2,4,6-

trimethylphenyl)methane and KOH in DMF (scheme 4.1).[22] The formation of the ligands was confirmed by ^{1}H NMR spectroscopy. The spectra display single sets of well-resolved resonances. High resolution mass spectra of the ligands show the molecular ion peaks (*m/z* = 513.3031 for $[L^1 + H]^+$ and 613.3331 for $[L^2 + H]^+$), which match well with the theoretical values.

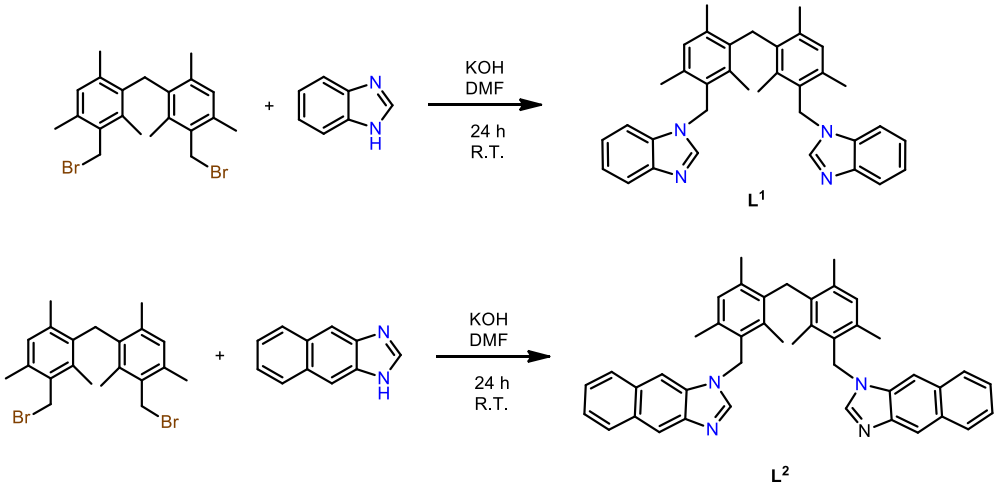

Scheme 4.1. Synthesis of ligands L^1-L^2

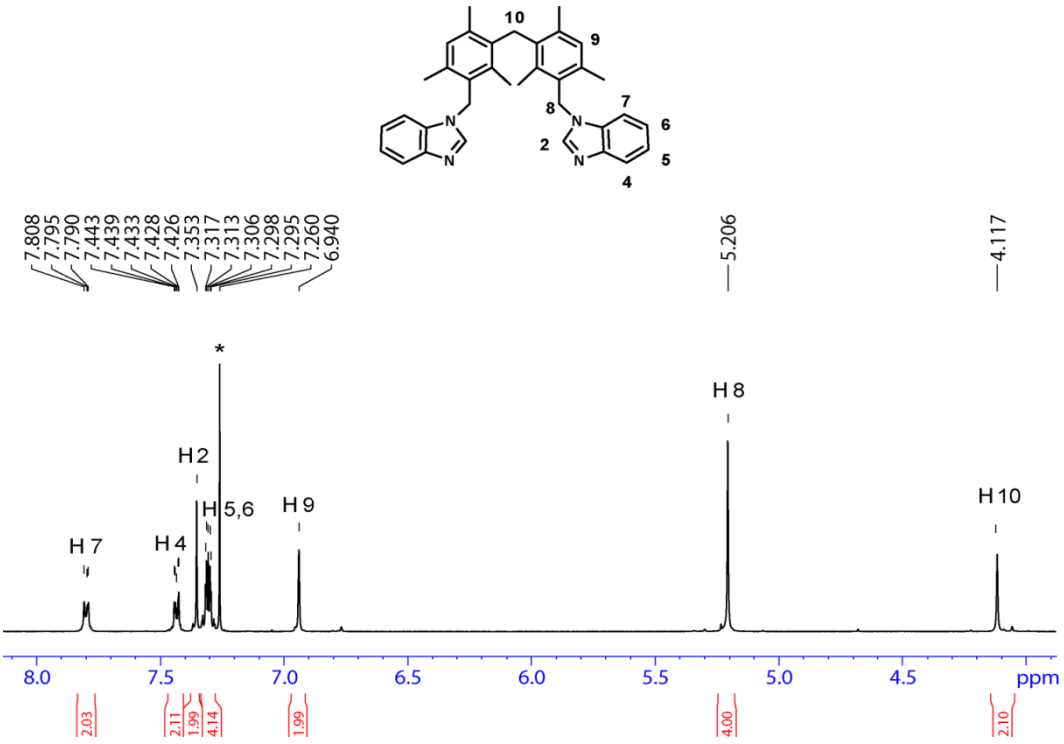

Figure 4.1. Partial ^{1}H NMR spectrum of L^1 in $CDCl_3$.

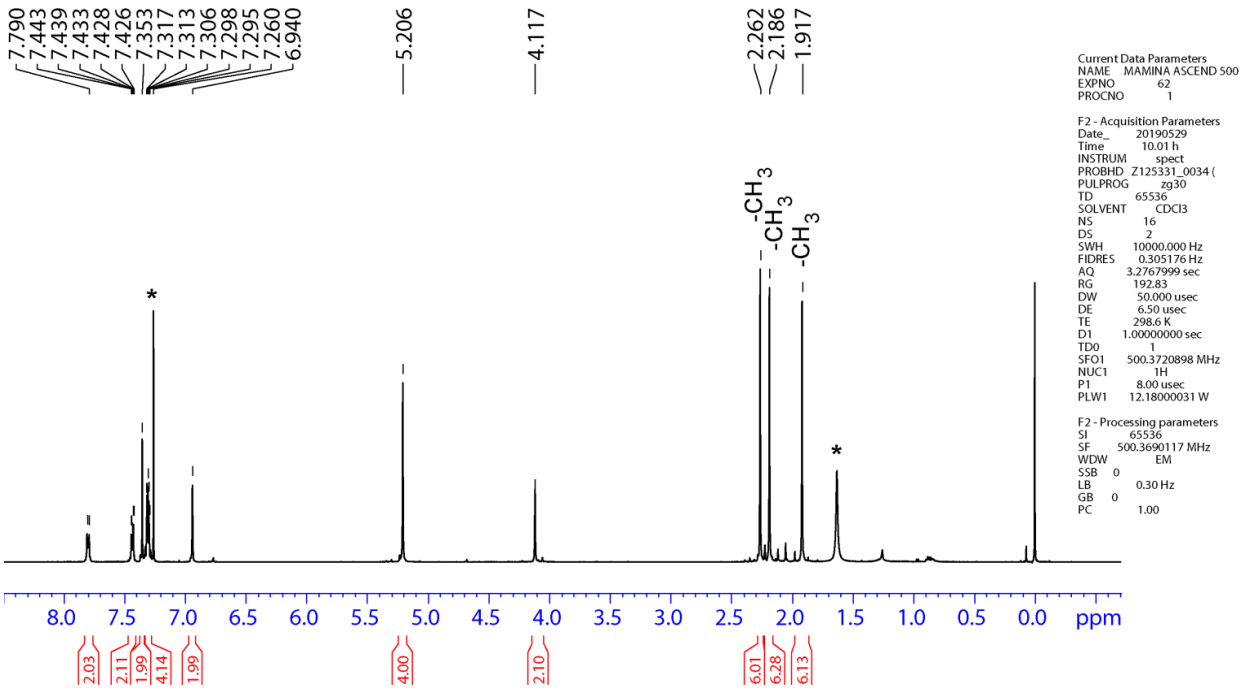

Figure 4.2. ^{1}H NMR spectrum of L^{1} in $CDCl_3$.

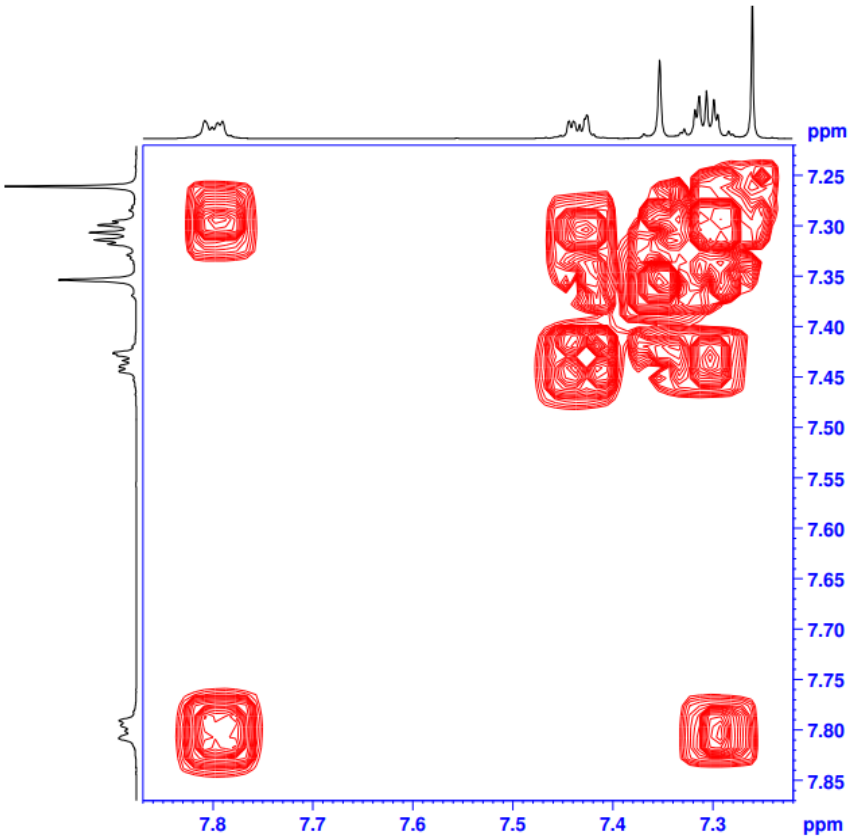

Figure 4.3. Partial ^{1}H-^{1}H COSY NMR spectrum of L^{1} in $CDCl_3$.

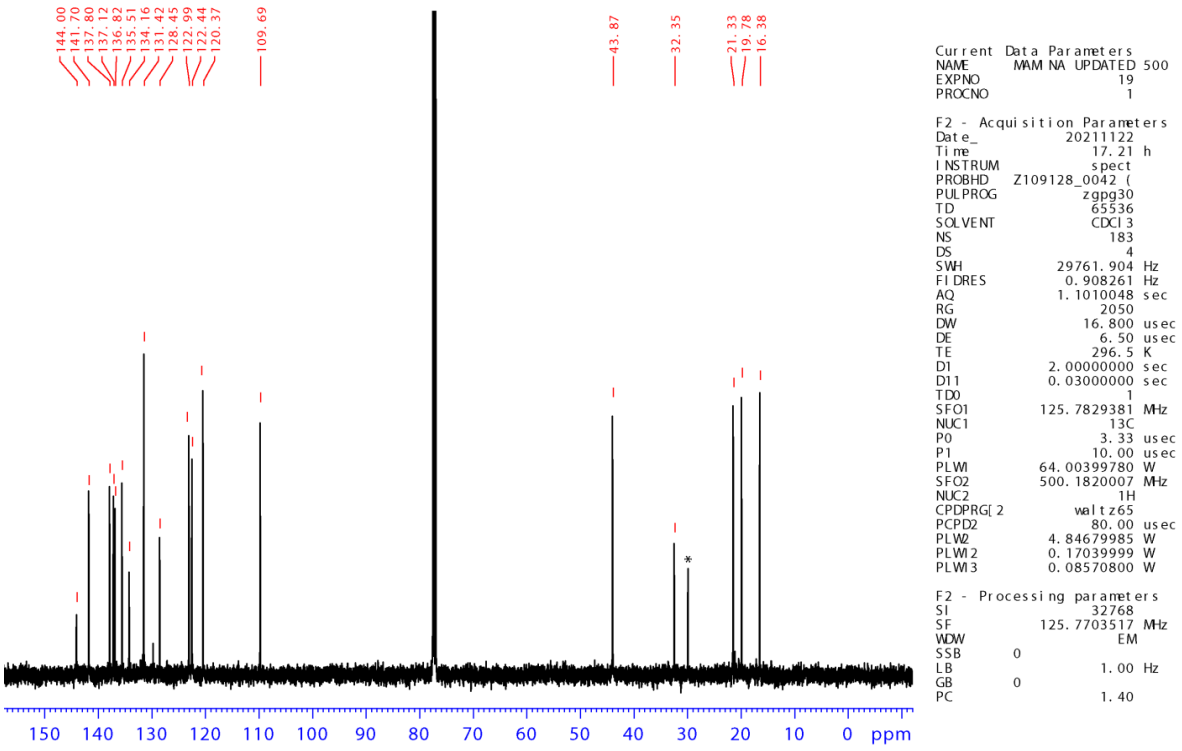

Figure 4.4. ^{13}C NMR spectrum of L^1 in $CDCl_3$.

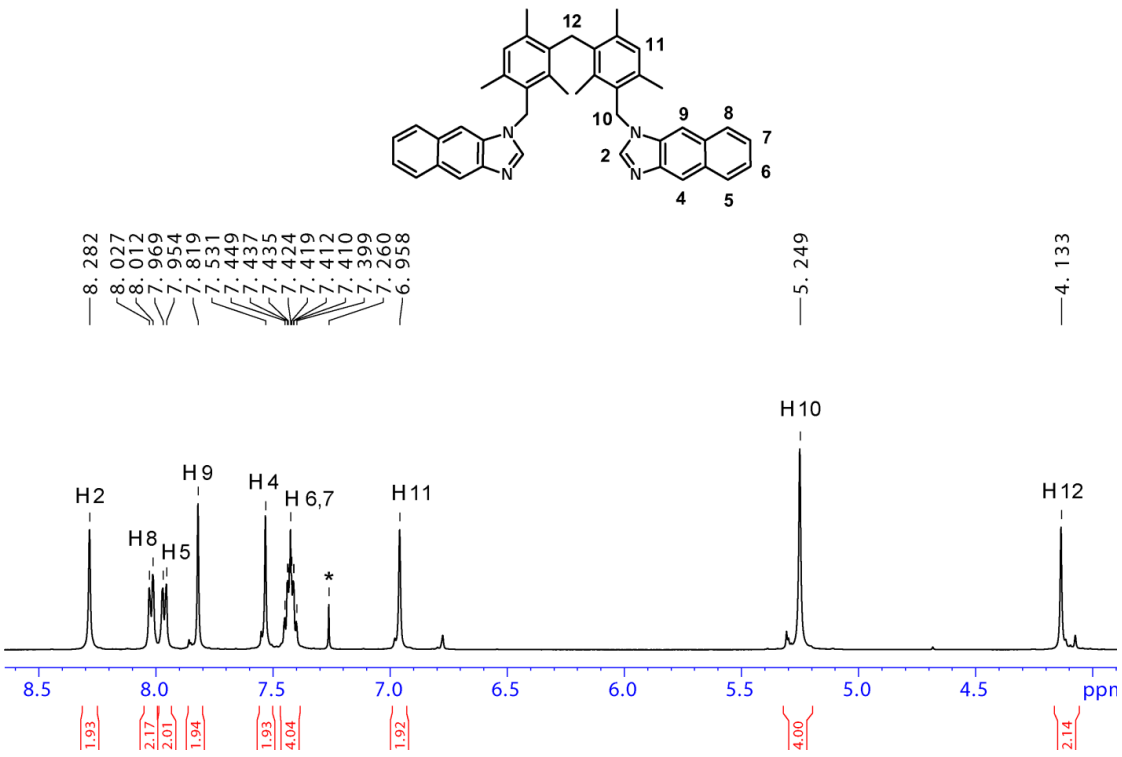

Figure 4.5. Partial ^1H NMR spectrum of L^2 in $CDCl_3$.

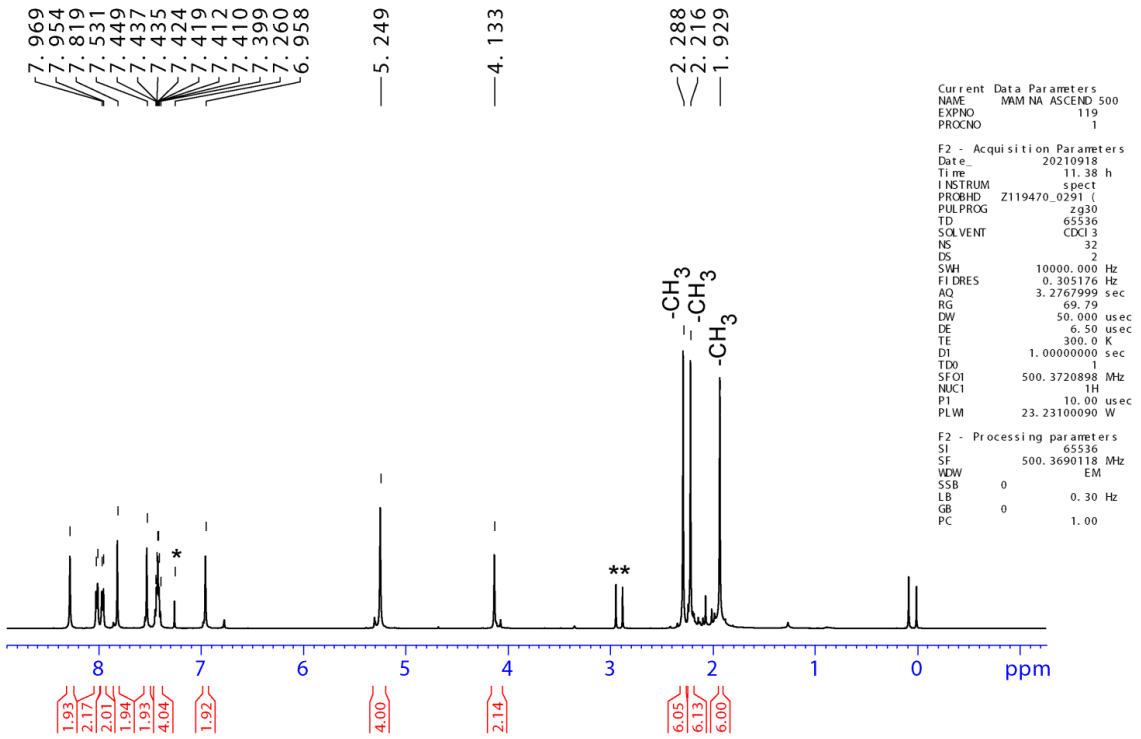

Figure 4.6. ^{1}H NMR spectrum of L^2 in $CDCl_3$.

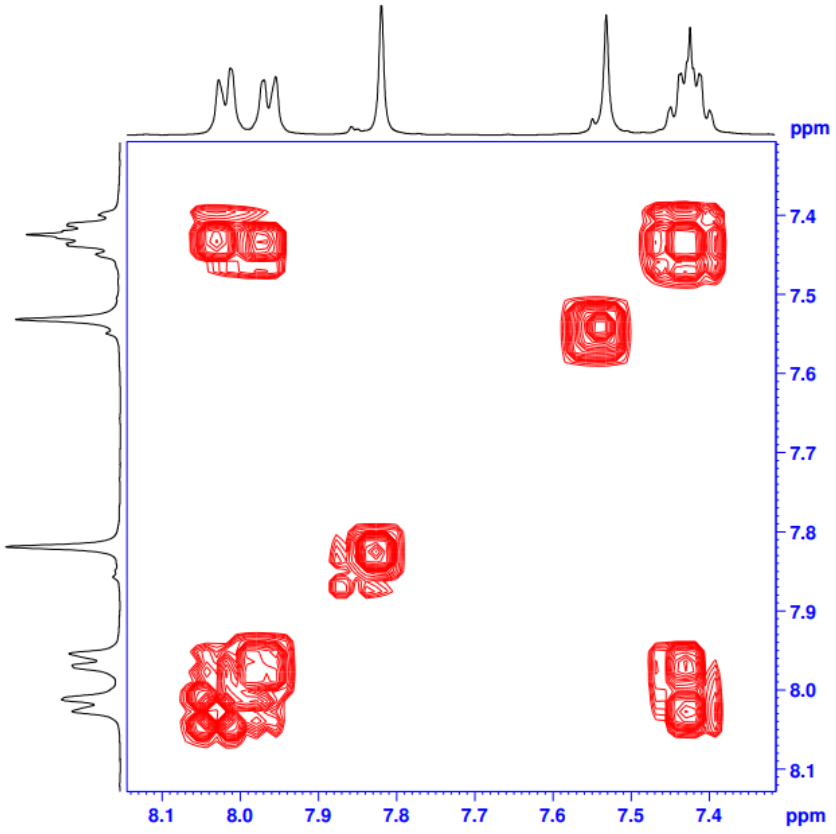

Figure 4.7. Partial ^{1}H-^{1}H COSY NMR spectrum of L^2 in $CDCl_3$.

Display Report

Analysis Info

Analysis Name	D:\Data\2021-data\PROF.MS\SEPT\MB-33.d	Acquisition Date	9/24/2021 11:35:44 AM
Method	tune_low.m	Operator	BDAL
Sample Name	MB-33	Instrument	maXis 255552.10138
Comment			

Acquisition Parameter

Source Type	ESI	Ion Polarity	Positive	Set Nebulizer	0.3 Bar
Focus	Not active	Set Capillary	4500 V	Set Dry Heater	180 °C
Scan Begin	100 m/z	Set End Plate Offset	-500 V	Set Dry Gas	4.0 l/min
Scan End	2900 m/z	Set Charging Voltage	0 V	Set Divert Valve	Waste
		Set Corona	0 nA	Set APCI Heater	0 °C

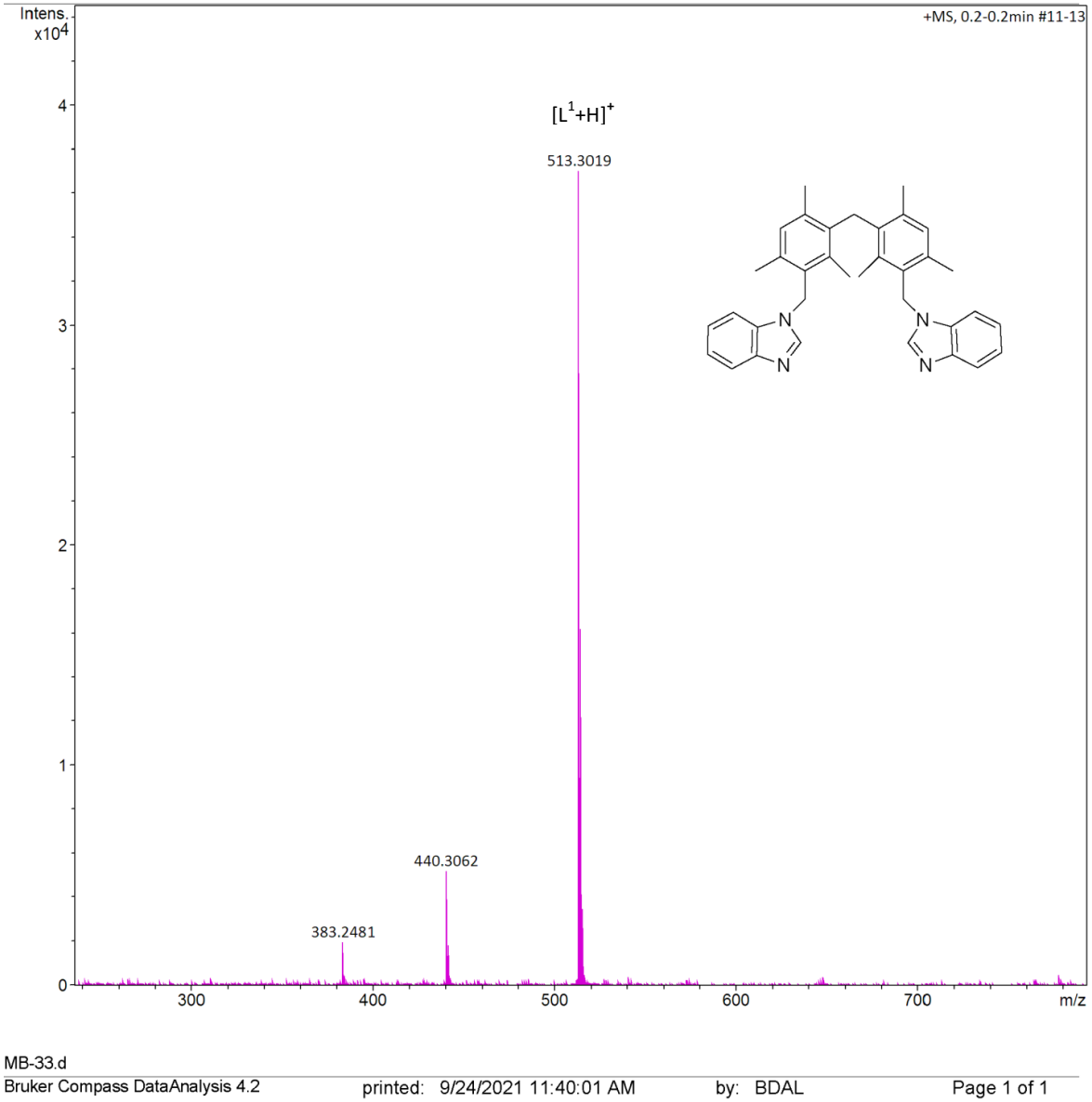

MB-33.d

Bruker Compass DataAnalysis 4.2 printed: 9/24/2021 11:40:01 AM by: BDAL Page 1 of 1

Figure 4.8. ESI mass spectrum of L^1 in positive ion mode.

Display Report

Analysis Info

Analysis Name	D:\Data\2021-data\PROF.MS\SEPT\MB2-75.d	Acquisition Date	9/23/2021 4:44:03 PM
Method	tune_low.m	Operator	BDAL
Sample Name	MB2-75	Instrument	maXis 255552.10138
Comment			

Acquisition Parameter

Source Type	ESI	Ion Polarity	Positive	Set Nebulizer	0.3 Bar
Focus	Not active	Set Capillary	4000 V	Set Dry Heater	180 °C
Scan Begin	100 m/z	Set End Plate Offset	-500 V	Set Dry Gas	4.0 l/min
Scan End	2900 m/z	Set Charging Voltage	0 V	Set Divert Valve	Waste
		Set Corona	0 nA	Set APCI Heater	0 °C

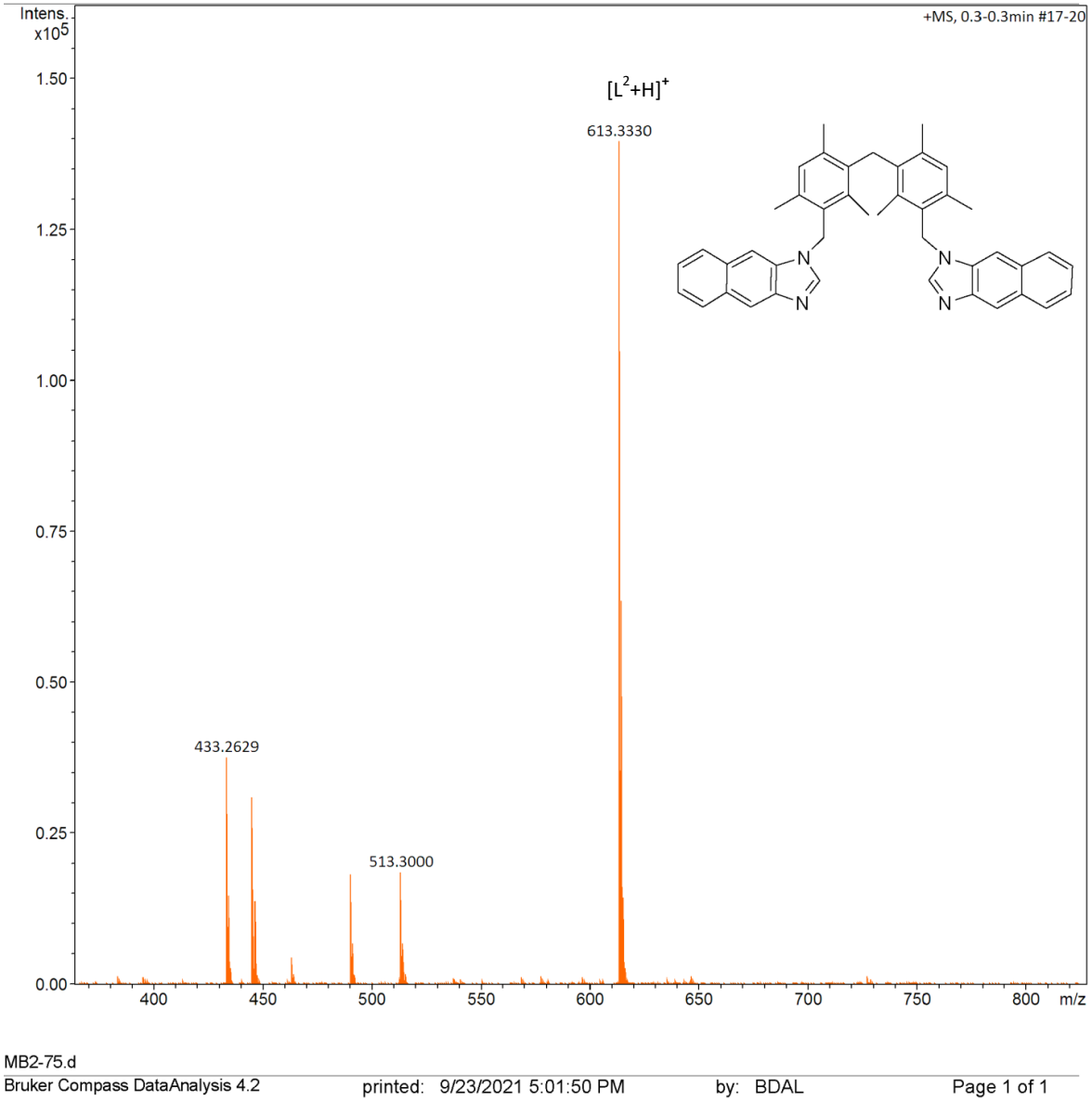

MB2-75.d

Bruker Compass DataAnalysis 4.2 printed: 9/23/2021 5:01:50 PM by: BDAL Page 1 of 1

Figure 4.9. ESI mass spectrum of L^2 in positive ion mode.

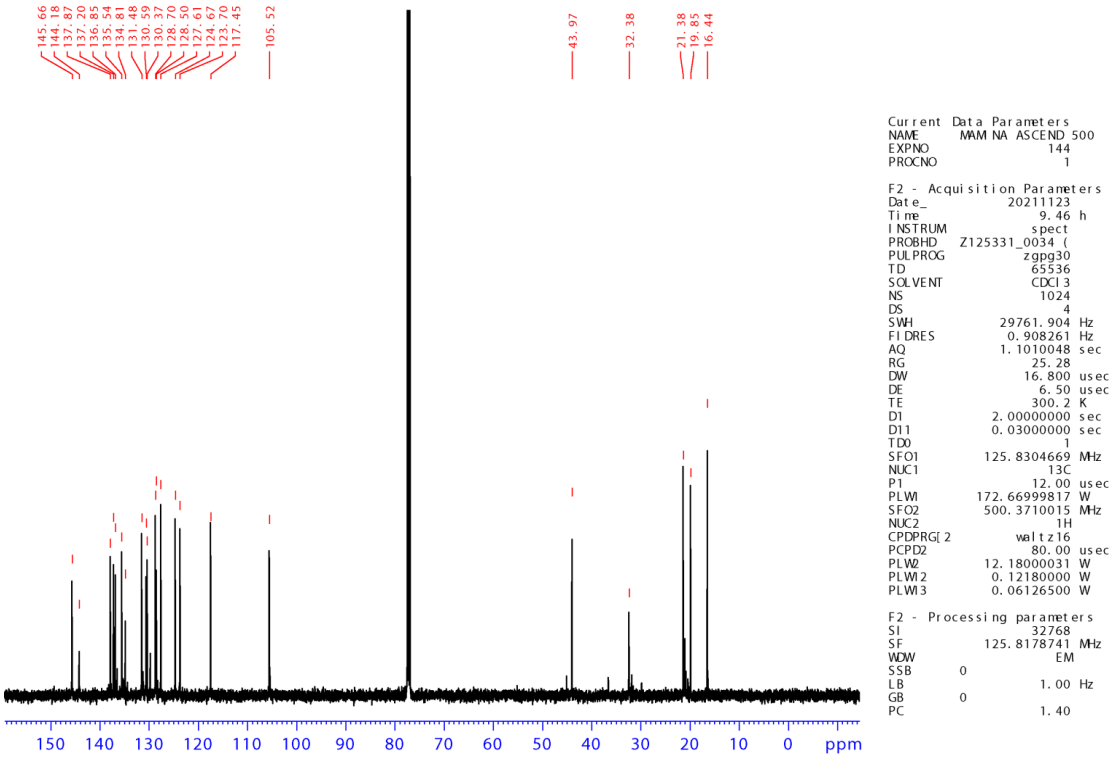

Figure 4.10. ^{13}C NMR spectrum of L^2 in $CDCl_3$.

4.3.2. Synthesis and characterization of metallocycles 1-4.

The self-assembly of technetium macrocycles **1** and **2** was achieved by treating $(NBu_4)[Tc_2(\mu\text{-}Cl)_3(CO)_6]$ with ligand L^1 or L^2 respectively in THF/CH_2Cl_2 (Scheme 4.2). The metallomacrocycles *fac*-$[Tc(CO)_3Cl(L^n)]$ (**1** and **2**) were self-assembled via reaction between $(NBu_4)[Tc_2(\mu\text{-}Cl)_3(CO)_6]$ and the neutral flexible bidentate nitrogen donors (L^1 for **1** and L^2 for **2**), see Scheme 4.2. Isostructural rhenium macrocycles *fac*-$[Re(CO)_3X(L^n)]$ (**3a, 3b** and **4**) were assembled using $[Re(CO)_5X]$ and the nitrogen donor ligands of Scheme 4.2 (X = Cl, $L^n = L^1$ for **3a,** X = Br, $L^n = L^1$ for **3b** and X = Br, $L^n = L^2$ for **4**).

The IR spectra of the products display three strong bands in the range ~2029–1894 cm^{-1}, which are characteristic of the *fac*-$[Tc(CO)_3]^+$ unit (2029 or 2027 cm^{-1} for symmetric in-phase CO vibration, 1923 or 1924 cm^{-1} for asymmetric equatorial CO vibration, and 1896 or 1894 cm^{-1} for symmetric out of-phase CO vibration).[16, 31] The ^{99}Tc-NMR spectra of the macrocycles show intense upfield signals (–1172 ppm, $\Delta\nu_{1/2}$ = 788 Hz for **1**, -1165 ppm, $\Delta\nu_{1/2}$ = 1378 Hz for **2**), compared to the resonance of the starting material $(NBu_4)[Tc_2(\mu\text{-}Cl)_3(CO)_6]$ at –947 ppm.

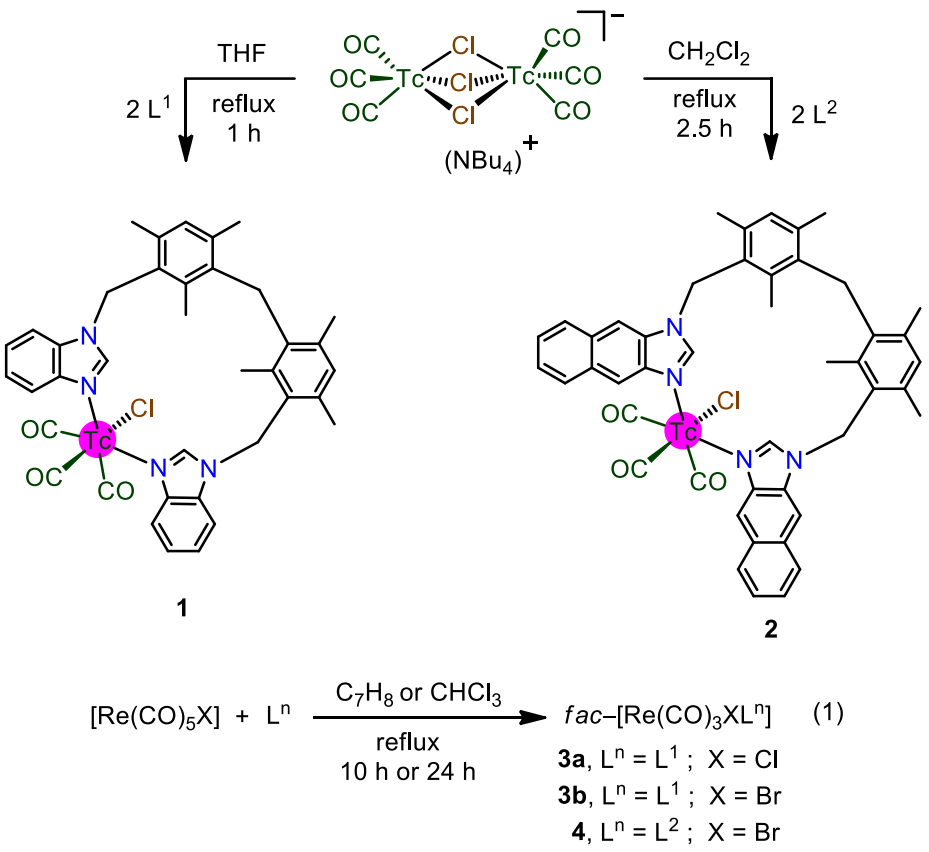

Scheme 4.2. Synthesis of technetium and rhenium core-based supramolecules.

This is typical for the coordination of N donor ligands to the Tc core.[17] The ^{1}H NMR spectrum of **1** in $CDCl_3$ displays well-separated slightly broad, but not well-resolved resonances for all arene protons, whereas the ^{1}H resonances of the arene and heteroarene motifs of complex **2** are broad resulting in a merged pattern. On the other hand, the protons of the methylene motifs (C-C*H*$_2$-C) show two well-resolved doublets with a coupling constant of 16-19 Hz, while the resonance of the N-bound methylene group (N-C*H*$_2$-C) appears as four doublets. The data suggest that the complexes adopt cyclic structures and the aromatic frameworks are flexible (moving back and forth) in solution. Further, it indicates the asymmetrical arrangement of all four arene motifs that causes a duplication of the proton signals as compared to the free ligands. The *fac*-[Re(CO)$_3$X] core-based macrocycles **3a, 3b** and **4** were assembled by the reactions of [Re(CO)$_5$X] (**3a**, X = Cl; **3b**, X = Br and **4**, X = Br) with L^1 or L^2 in toluene (C_7H_8) or $CHCl_3$ (Equation 1). The complexes are air and moisture stable and soluble in polar organic solvents. The ^{1}H NMR patterns of **3** and **4** are similar to those of **1** and **2**. The arene framework in complex **4** exhibits the highest degree of

fluxionality among all other complexes of this study. The ESI-MS spectra of the Re macrocycles display their respective molecular ion peaks (*m/z* = 841.1932 for [**3a** + Na]$^+$, *m/z* = 885.1425 for [**3b** + Na]$^+$, *m/z* = 961.2436 for [**4** - H]$^+$) with experimental isotopic distribution patterns that match well with the theoretical values.

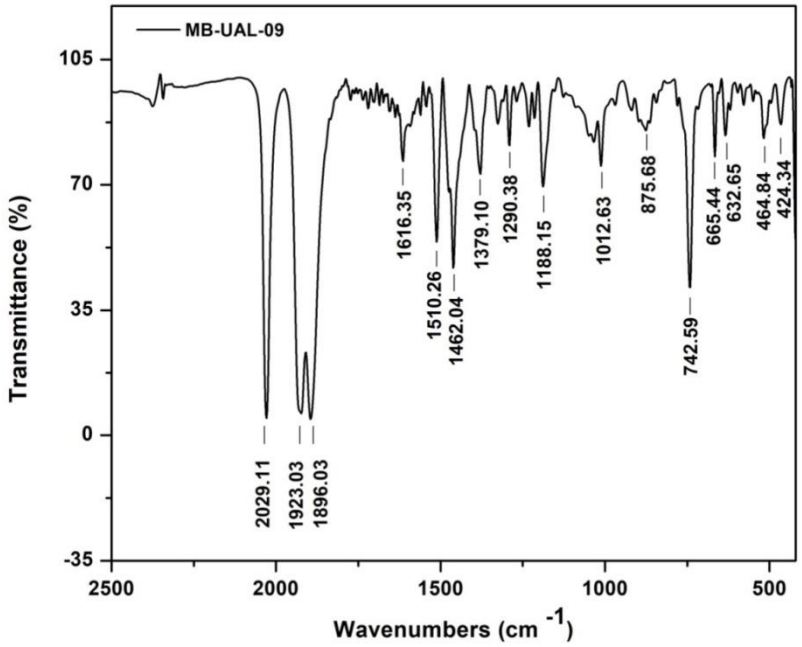

Figure 4.11. FT-IR (KBr) spectrum of **1**.

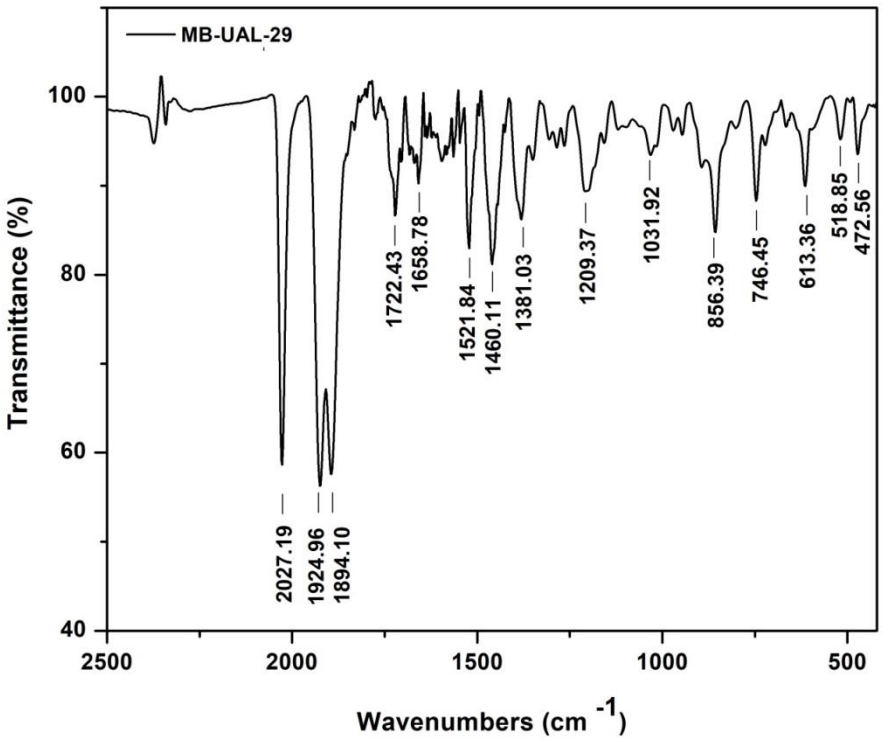

Figure 4.12. FT-IR (KBr) spectrum of **2**.

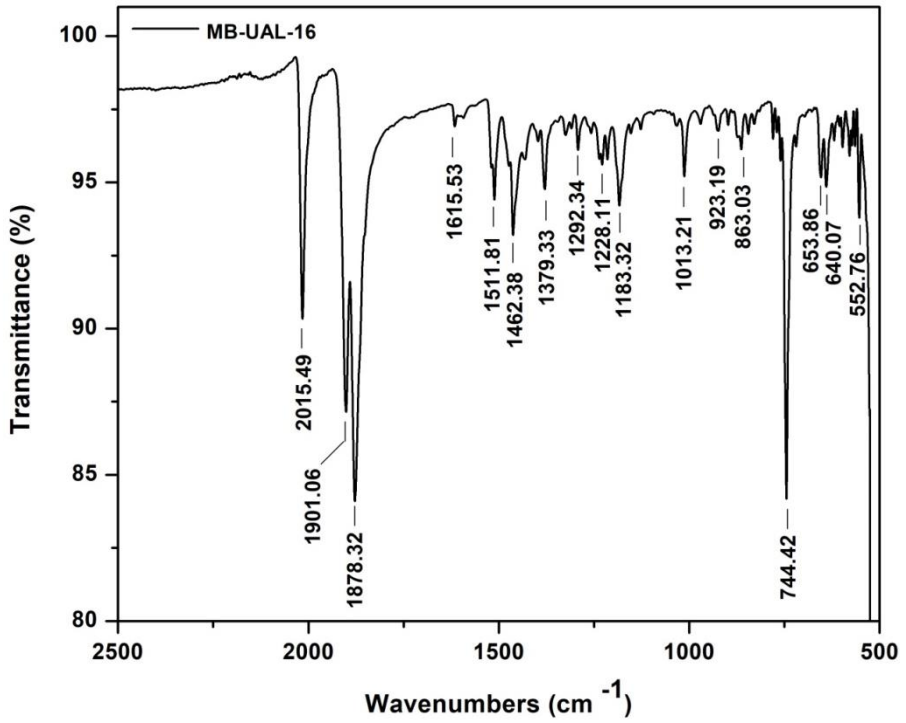

Figure 4.13. ATR-IR spectrum of **3a.**

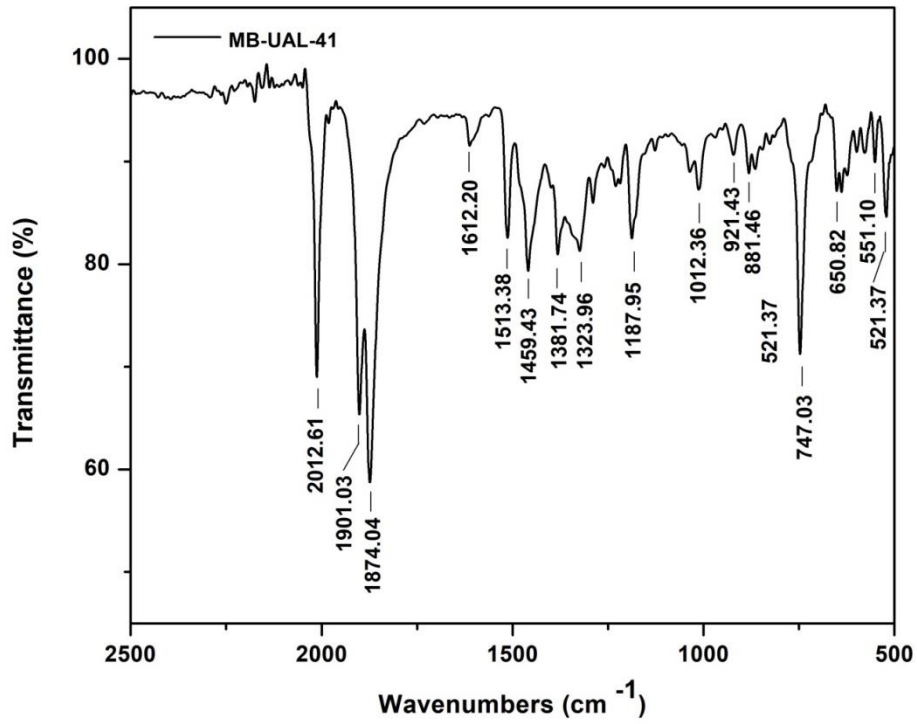

Figure 4.14. ATR-IR spectrum of **3b.**

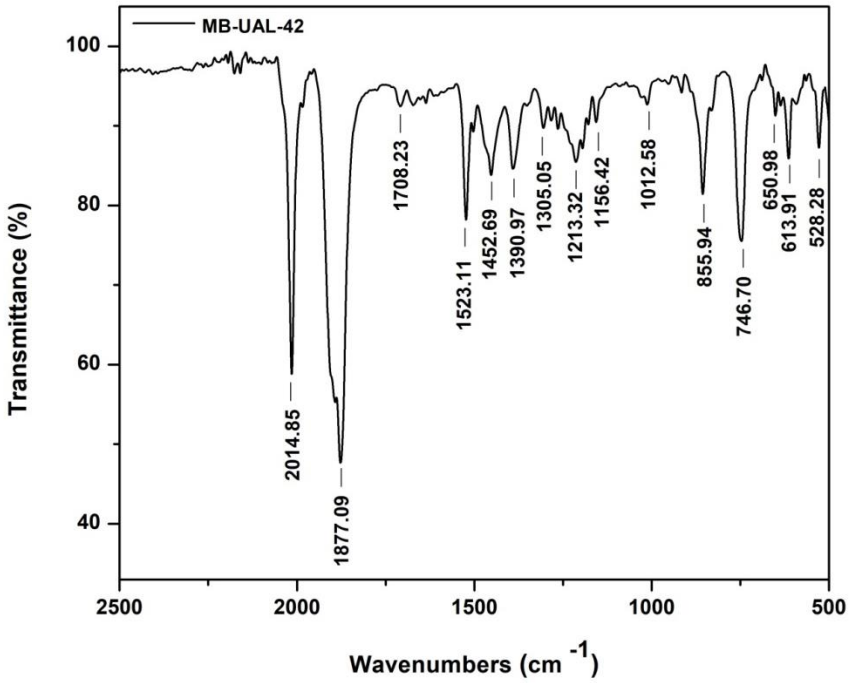

Figure 4.15. ATR-IR spectrum of **4.**

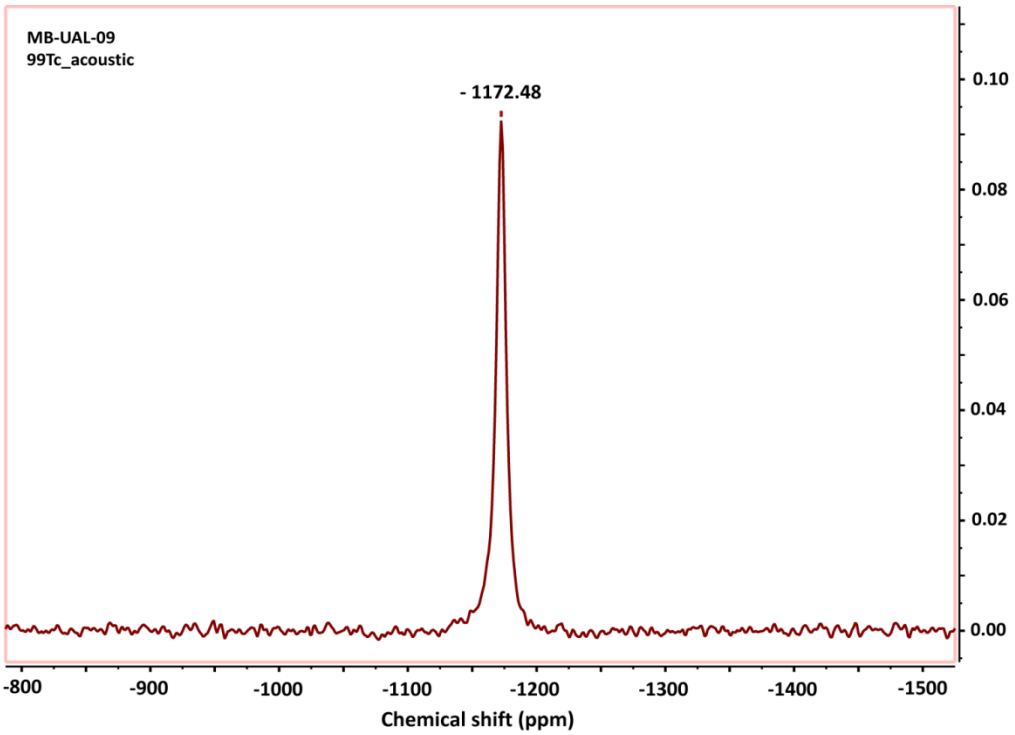

Figure 4.16. ^{99}Tc NMR spectrum of **1** in $CDCl_3$.

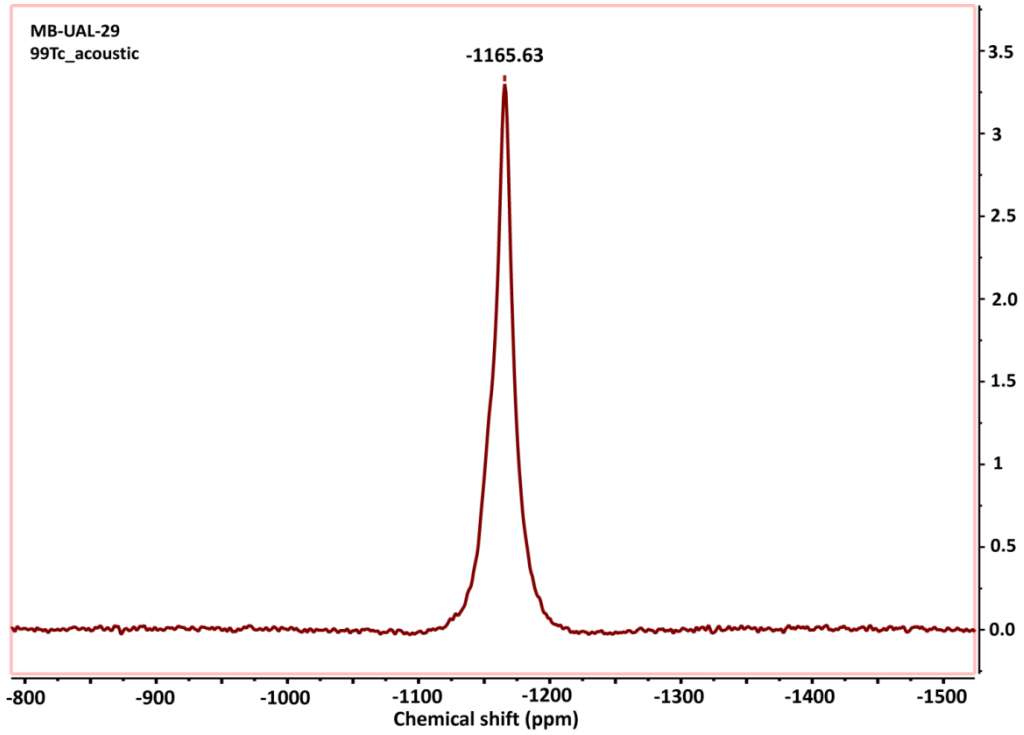

Figure 4.17. ^{99}Tc NMR spectrum of **2** in CD_2Cl_2.

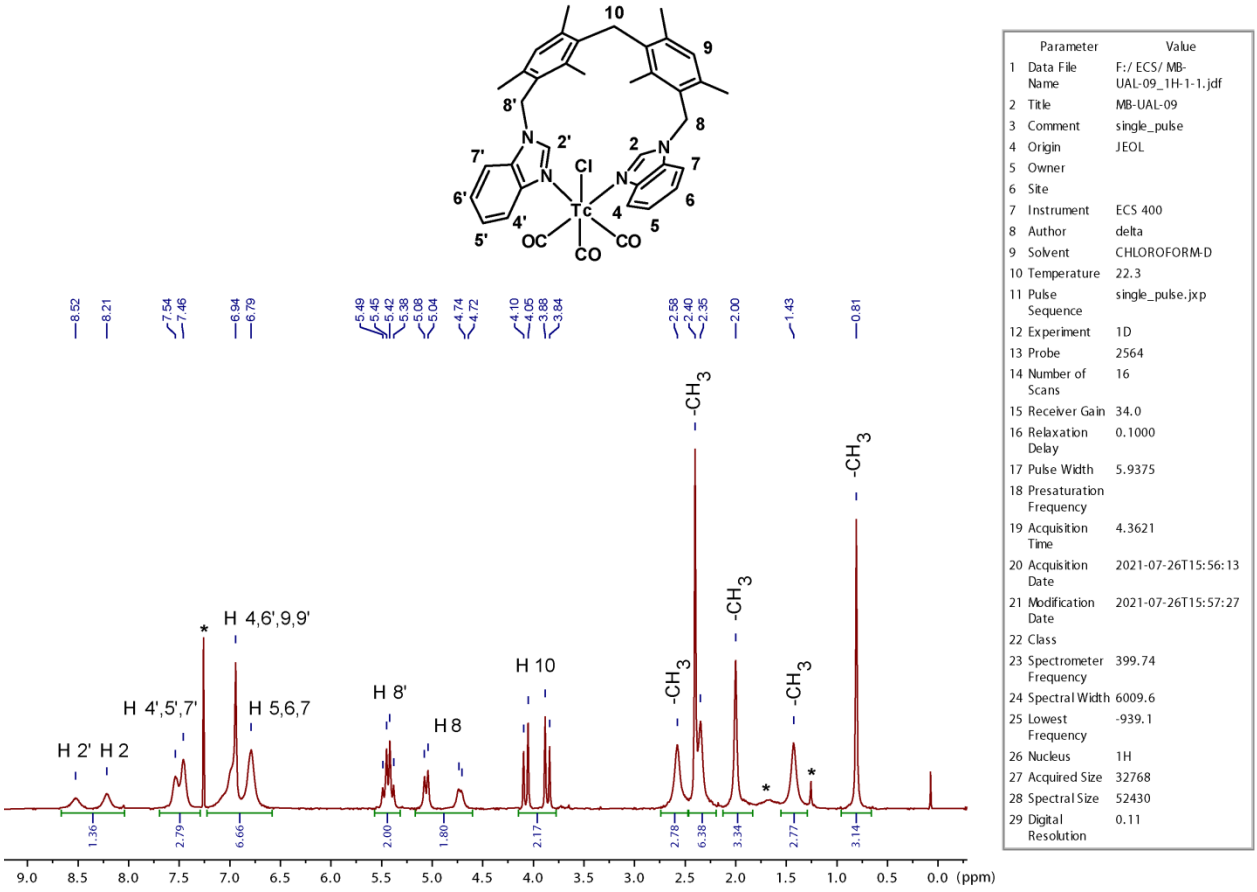

Figure 4.18. ^{1}H NMR spectrum of **1** in $CDCl_3$.

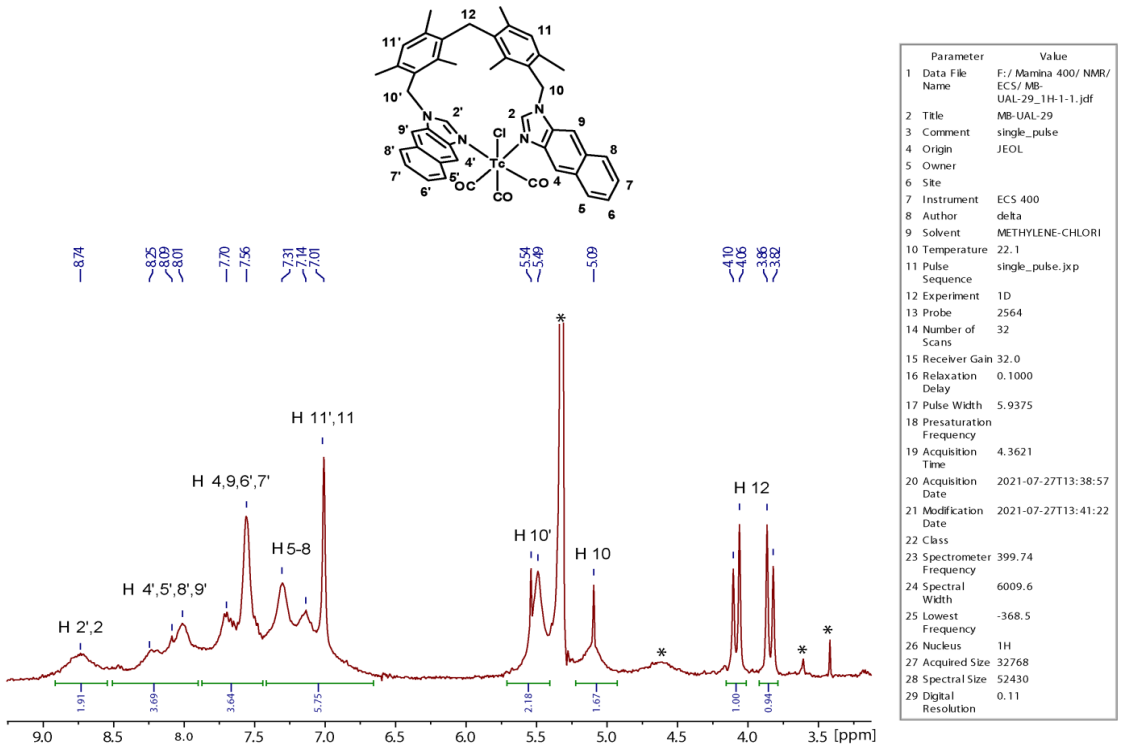

	Parameter	Value
1	Data File Name	F:/ Mamina 400/ NMR/ ECS/ MB-UAL-29_1H-1-1.jdf
2	Title	MB-UAL-29
3	Comment	single_pulse
4	Origin	JEOL
5	Owner	
6	Site	
7	Instrument	ECS 400
8	Author	delta
9	Solvent	METHYLENE-CHLORI
10	Temperature	22.1
11	Pulse Sequence	single_pulse.jxp
12	Experiment	1D
13	Probe	2564
14	Number of Scans	32
15	Receiver Gain	32.0
16	Relaxation Delay	0.1000
17	Pulse Width	5.9375
18	Presaturation Frequency	
19	Acquisition Time	4.3621
20	Acquisition Date	2021-07-27T13:38:57
21	Modification Date	2021-07-27T13:41:22
22	Class	
23	Spectrometer Frequency	399.74
24	Spectral Width	6009.6
25	Lowest Frequency	-368.5
26	Nucleus	1H
27	Acquired Size	32768
28	Spectral Size	52430
29	Digital Resolution	0.11

Figure 4.19. Partial ^{1}H NMR spectrum of **2** in CD_2Cl_2.

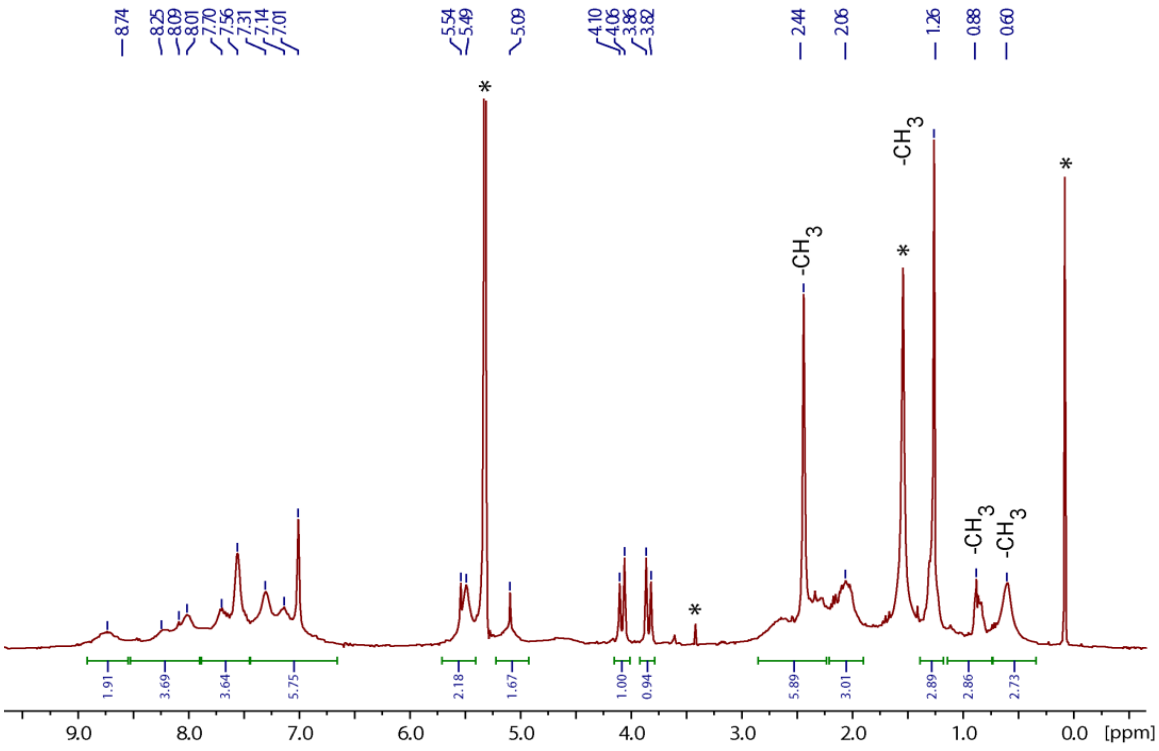

Figure 4.20. ^{1}H NMR spectrum of **2** in CD_2Cl_2.

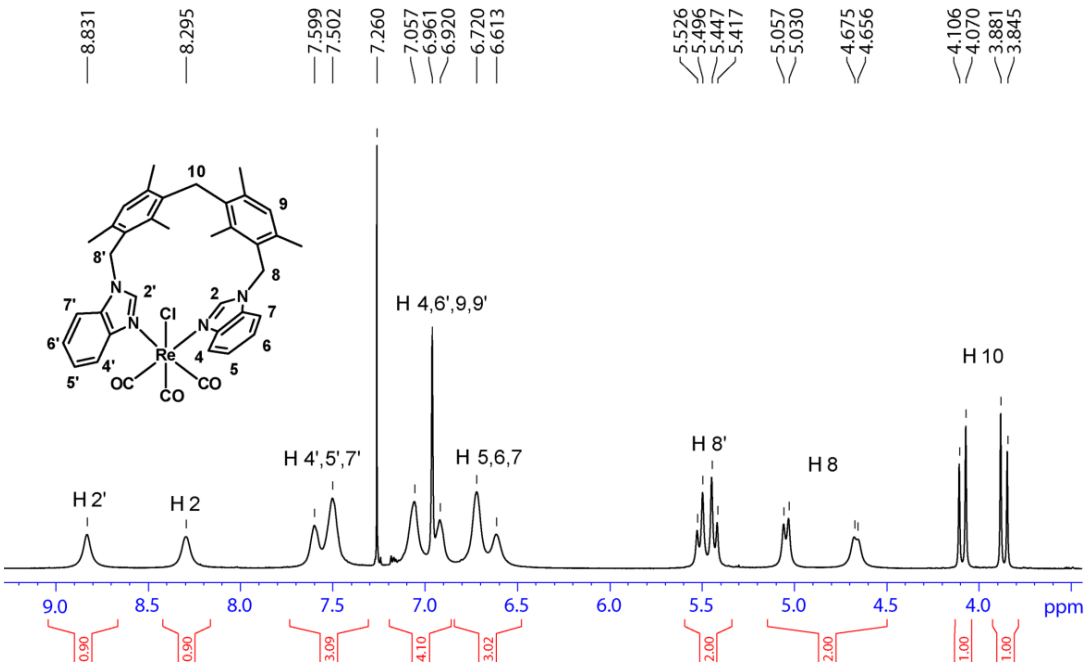

Figure 4.21. Partial ^{1}H NMR spectrum of **3a** in $CDCl_3$.

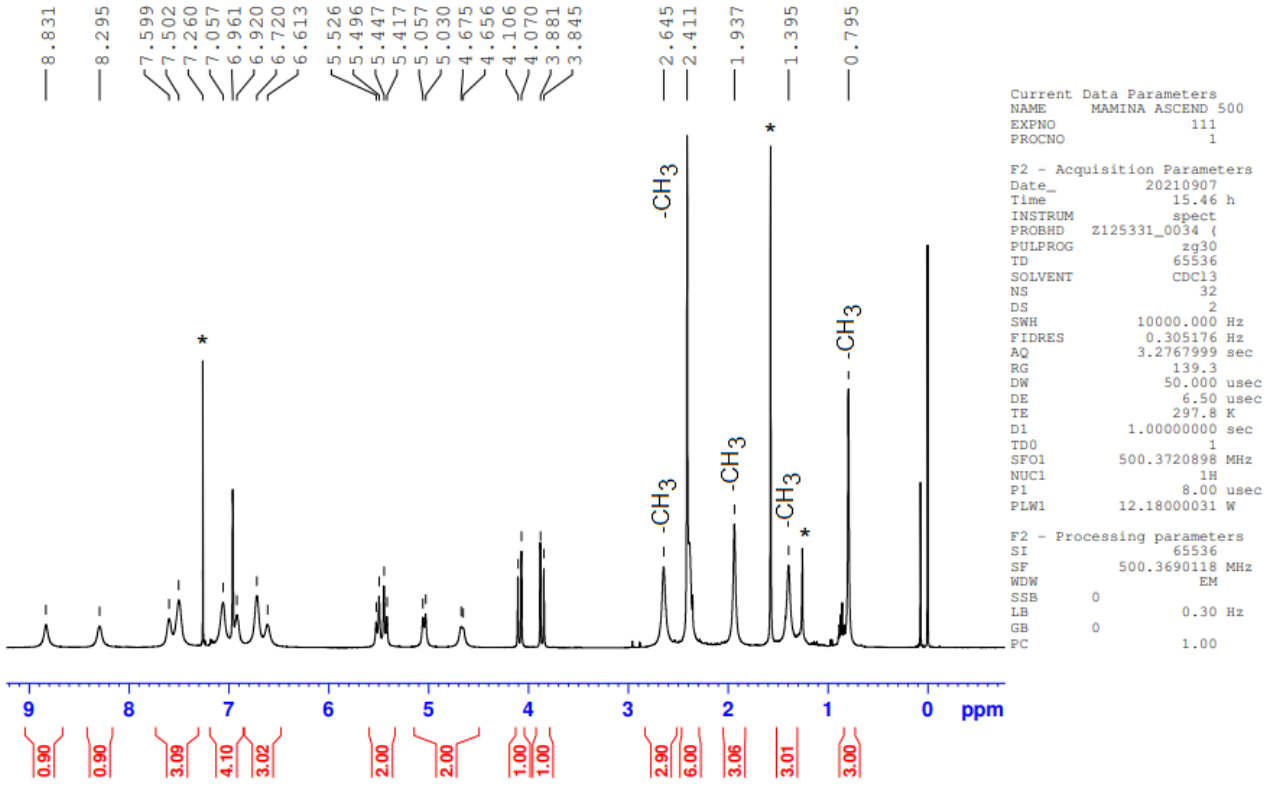

Figure 4.22. ^{1}H NMR spectrum of **3a** in $CDCl_3$.

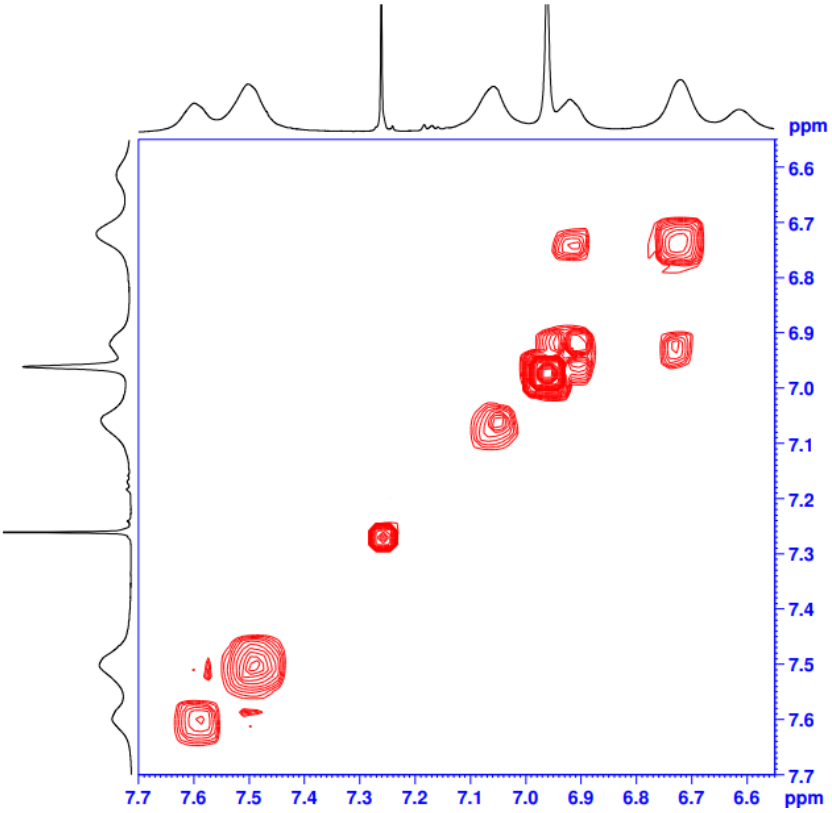

Figure 4.23. Partial ^{1}H-^{1}H COSY NMR spectrum of **3a** in $CDCl_3$.

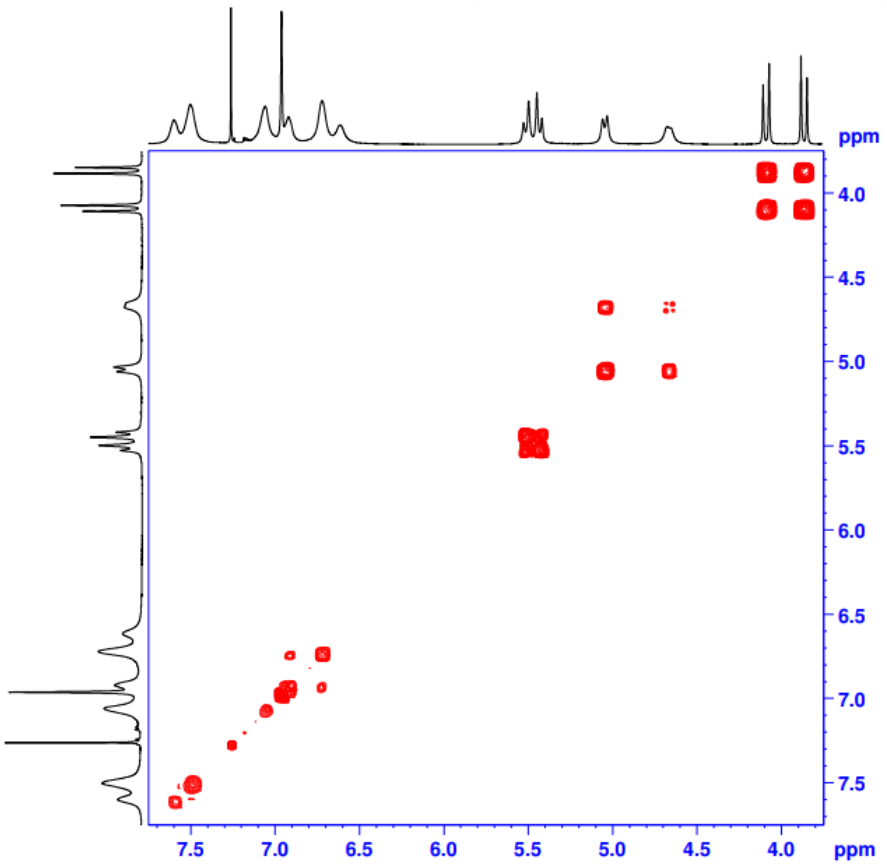

Figure 4.24. Partial ^{1}H-^{1}H COSY NMR spectrum of **3a** in $CDCl_3$.

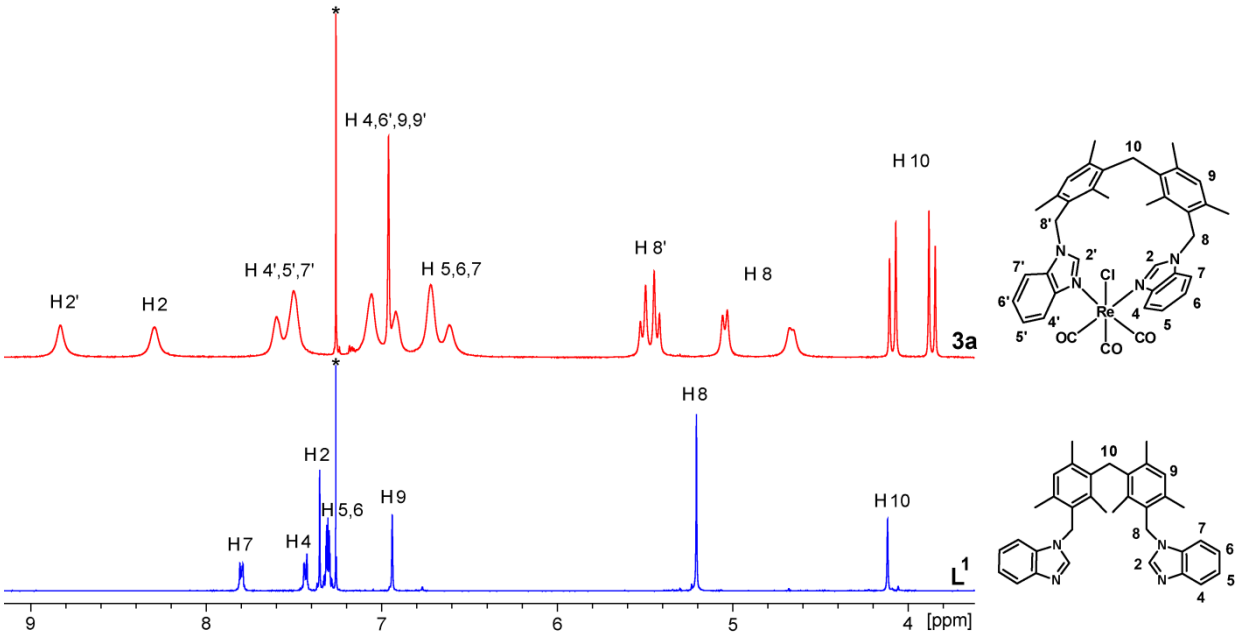

Figure 4.25. Partial ^{1}H NMR spectra of free ligand L^{1}, and **3a** in $CDCl_3$.

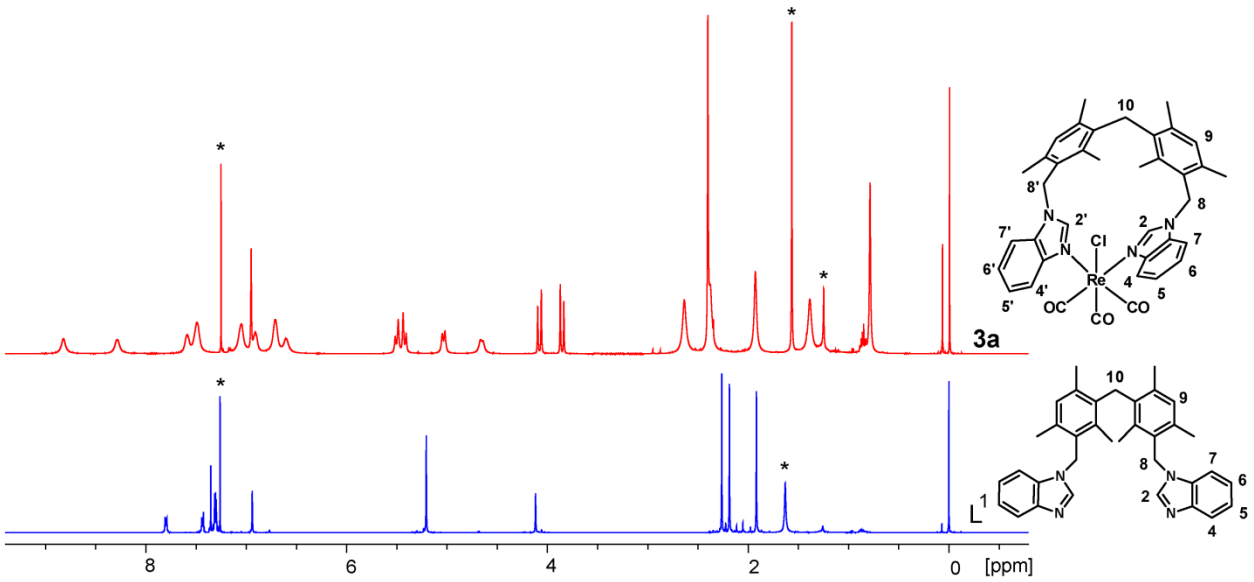

Figure 4.26. ^{1}H NMR spectra of free ligand L^{1}, and **3a** in $CDCl_3$.

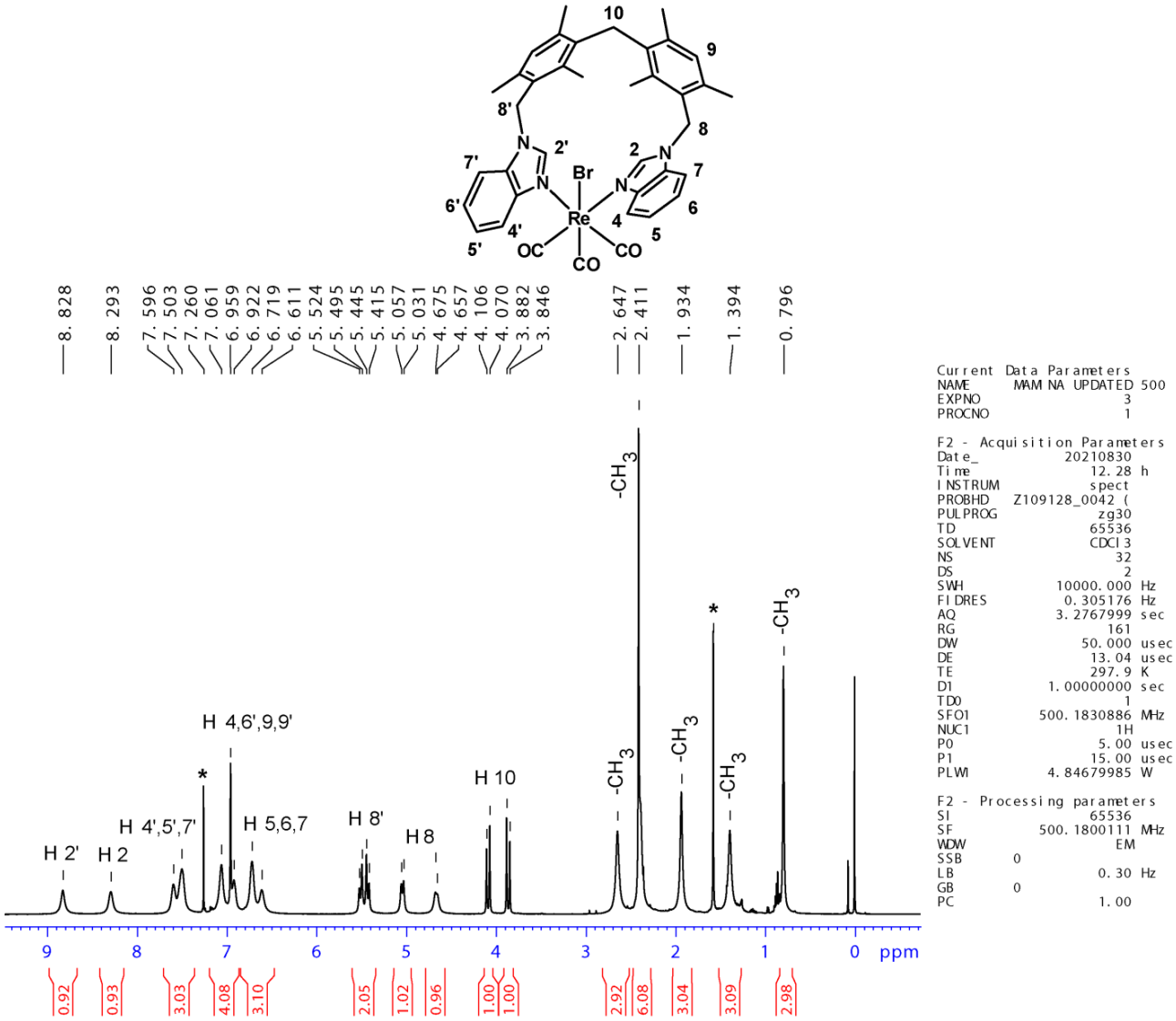

Figure 4.27. ^{1}H NMR spectrum of **3b** in $CDCl_3$.

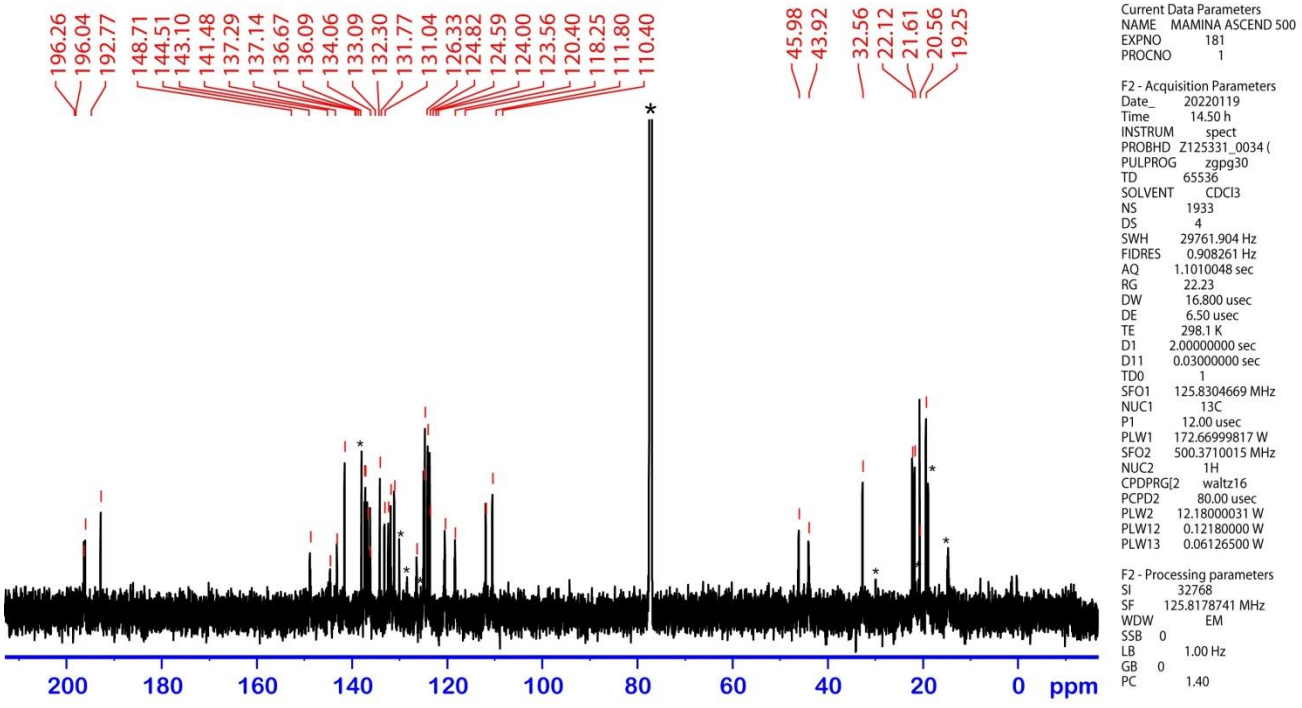

Figure 4.28. ^{13}C NMR spectrum of **3a** in $CDCl_3$.

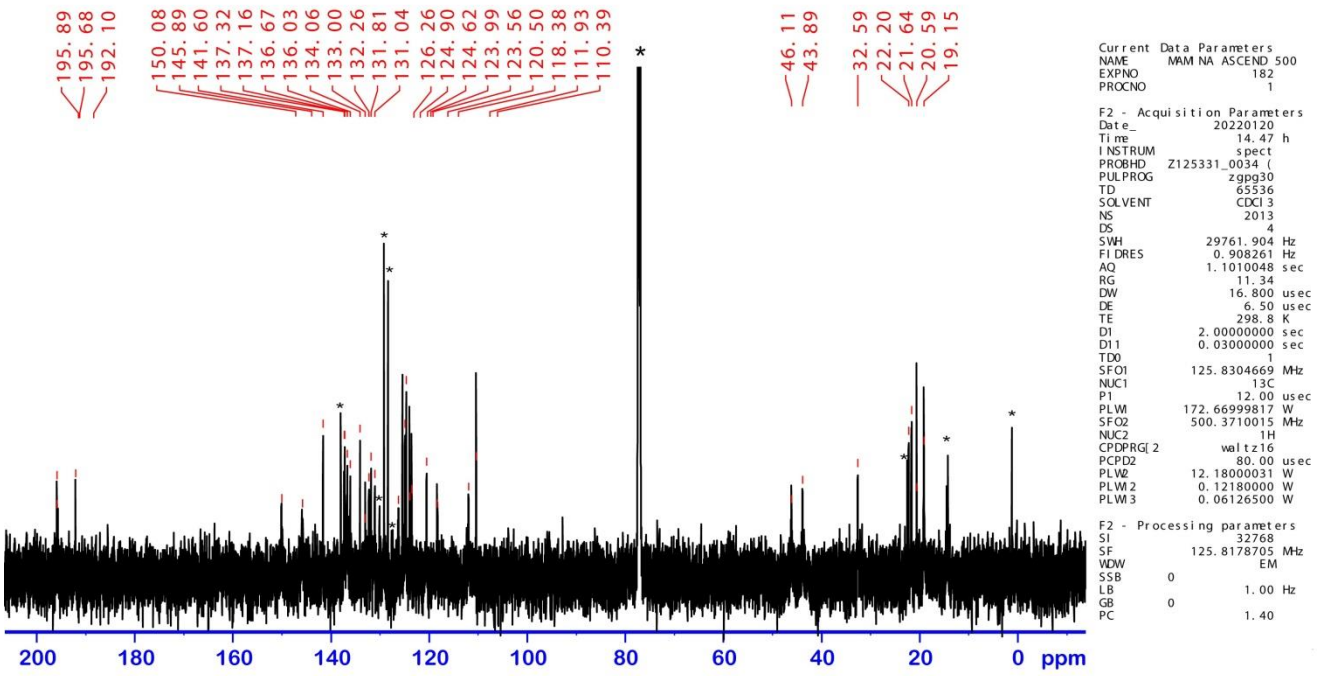

Figure 4.29. ^{13}C NMR spectrum of **3b** in $CDCl_3$.

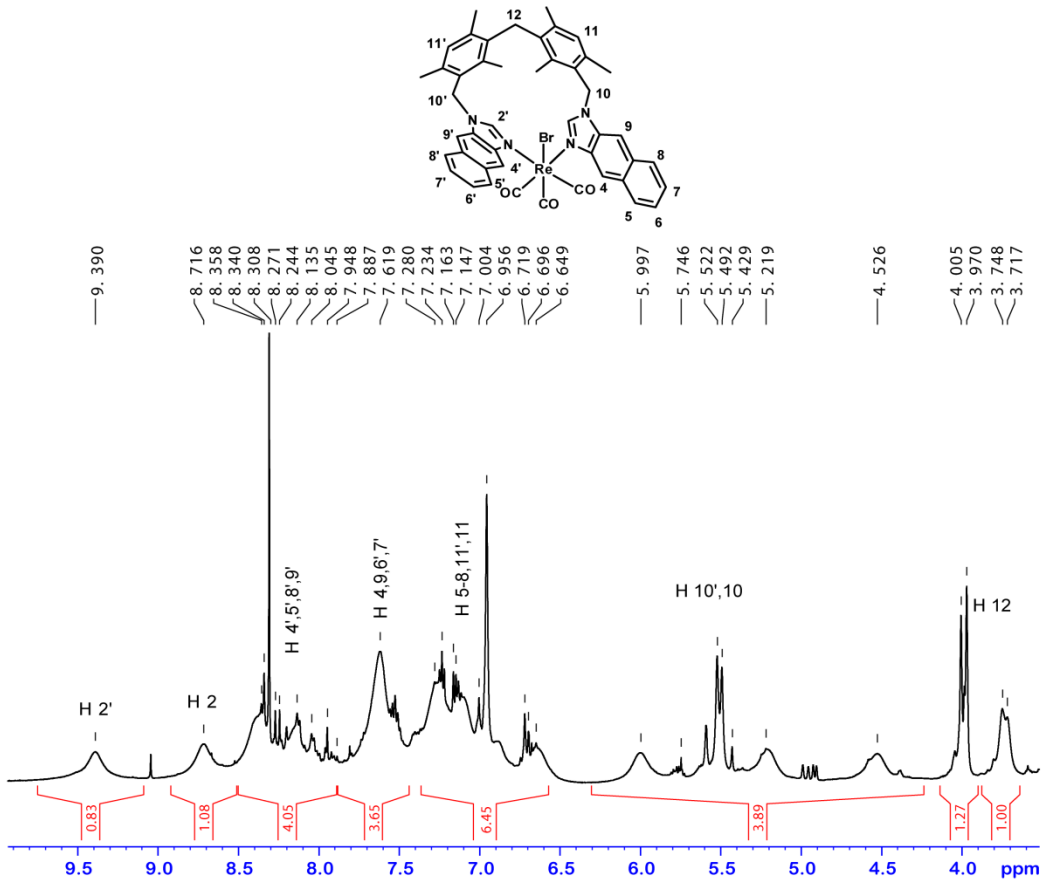

Figure 4.30. Partial ^{1}H NMR spectrum of **4** in DMSO-d_6.

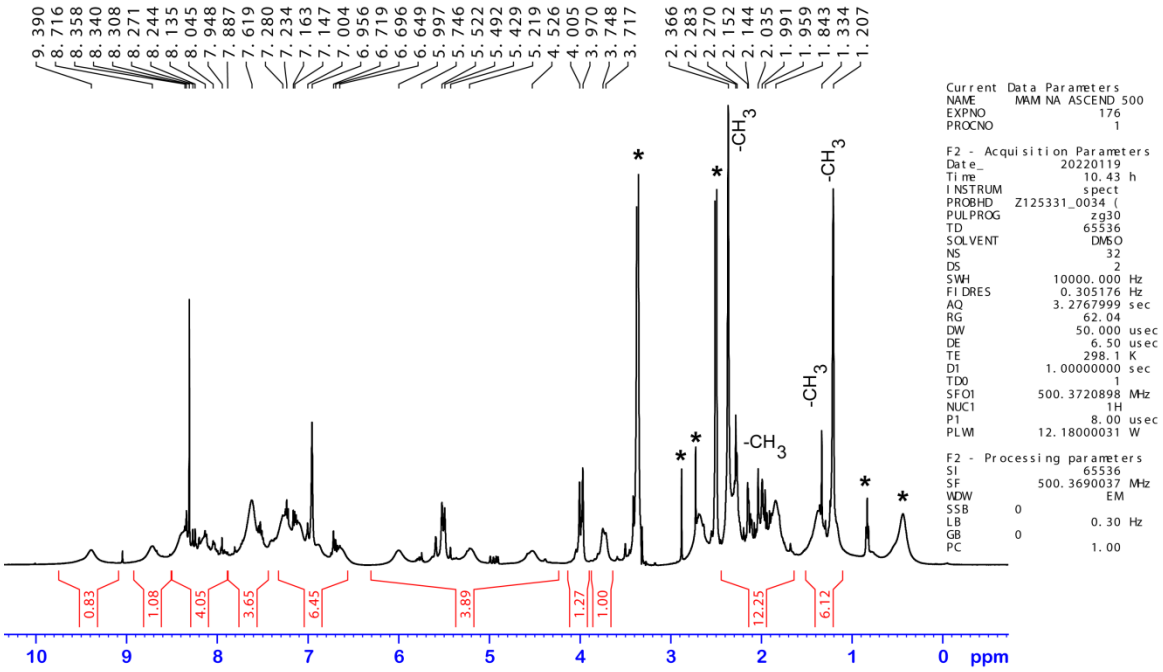

Figure 4.31. ^{1}H NMR spectrum of **4** in DMSO-d_6.

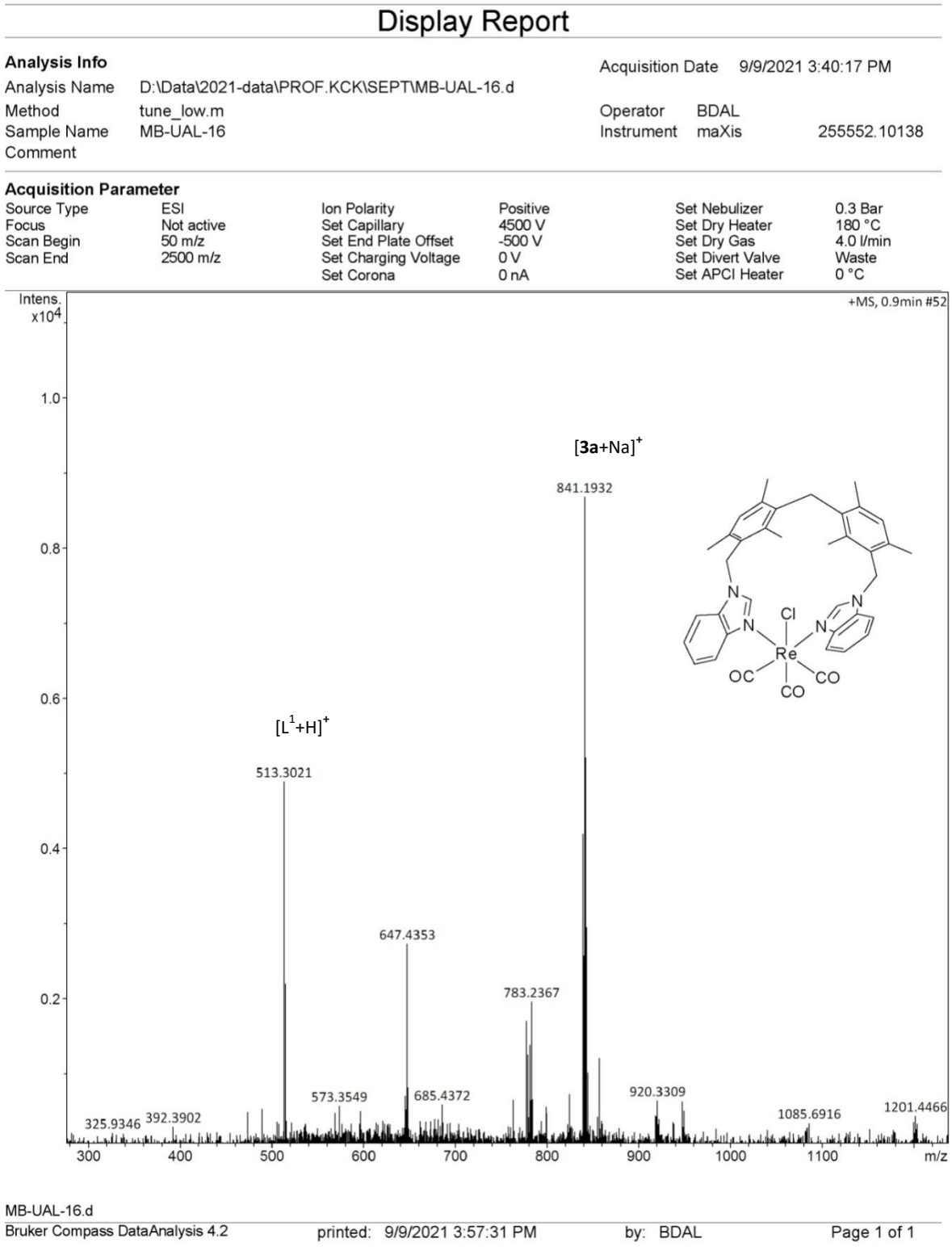

Figure 4.32. ESI mass spectrum of **3a** in positive ion mode.

Display Report

Analysis Info

Analysis Name	D:\Data\2021-data\PROF.KCK\SEPT\MB-UAL-16.d	Acquisition Date	9/9/2021 3:40:17 PM
Method	tune_low.m	Operator	BDAL
Sample Name	MB-UAL-16	Instrument	maXis 255552.10138
Comment			

Acquisition Parameter

Source Type	ESI	Ion Polarity	Positive	Set Nebulizer	0.3 Bar
Focus	Not active	Set Capillary	4500 V	Set Dry Heater	180 °C
Scan Begin	50 m/z	Set End Plate Offset	-500 V	Set Dry Gas	4.0 l/min
Scan End	2500 m/z	Set Charging Voltage	0 V	Set Divert Valve	Waste
		Set Corona	0 nA	Set APCI Heater	0 °C

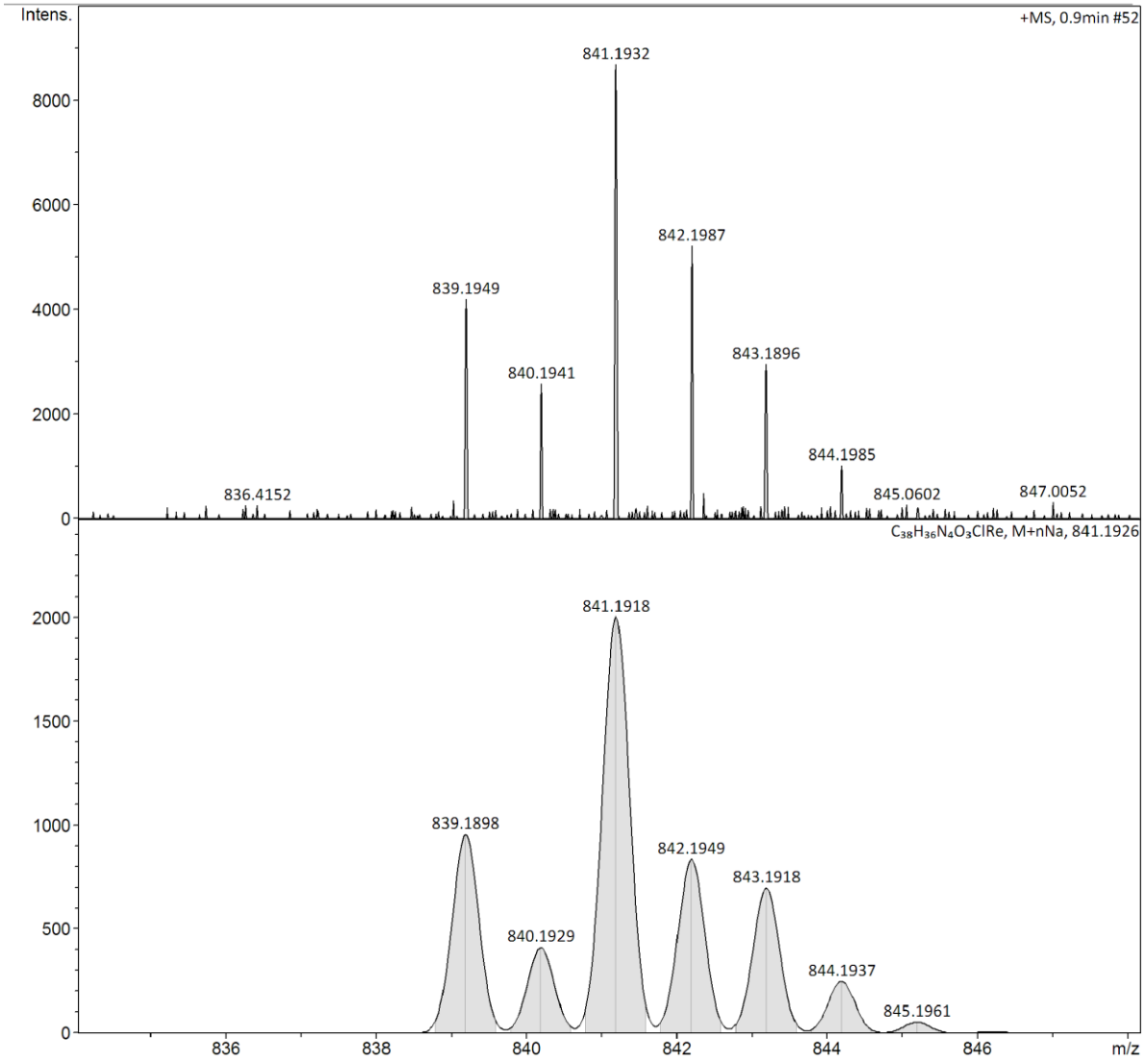

MB-UAL-16.d

Bruker Compass DataAnalysis 4.2 printed: 9/9/2021 3:55:04 PM by: BDAL Page 1 of 1

Figure 4.33. Experimental (top) and calculated (bottom) ESI mass spectra of [**3a** + Na]$^+$ in positive ion mode.

Display Report

Analysis Info

Analysis Name	D:\Data\2021-data\PROF.MS\NOV\MB-UAL-41R.d	Acquisition Date	11/24/2021 4:05:18 PM
Method	tune_low.m	Operator	BDAL
Sample Name	MB-UAL-41R	Instrument	maXis 255552.10138
Comment			

Acquisition Parameter

Source Type	ESI	Ion Polarity	Positive	Set Nebulizer	0.3 Bar
Focus	Not active	Set Capillary	3000 V	Set Dry Heater	180 °C
Scan Begin	50 m/z	Set End Plate Offset	-500 V	Set Dry Gas	4.0 l/min
Scan End	2000 m/z	Set Charging Voltage	0 V	Set Divert Valve	Waste
		Set Corona	0 nA	Set APCI Heater	0 °C

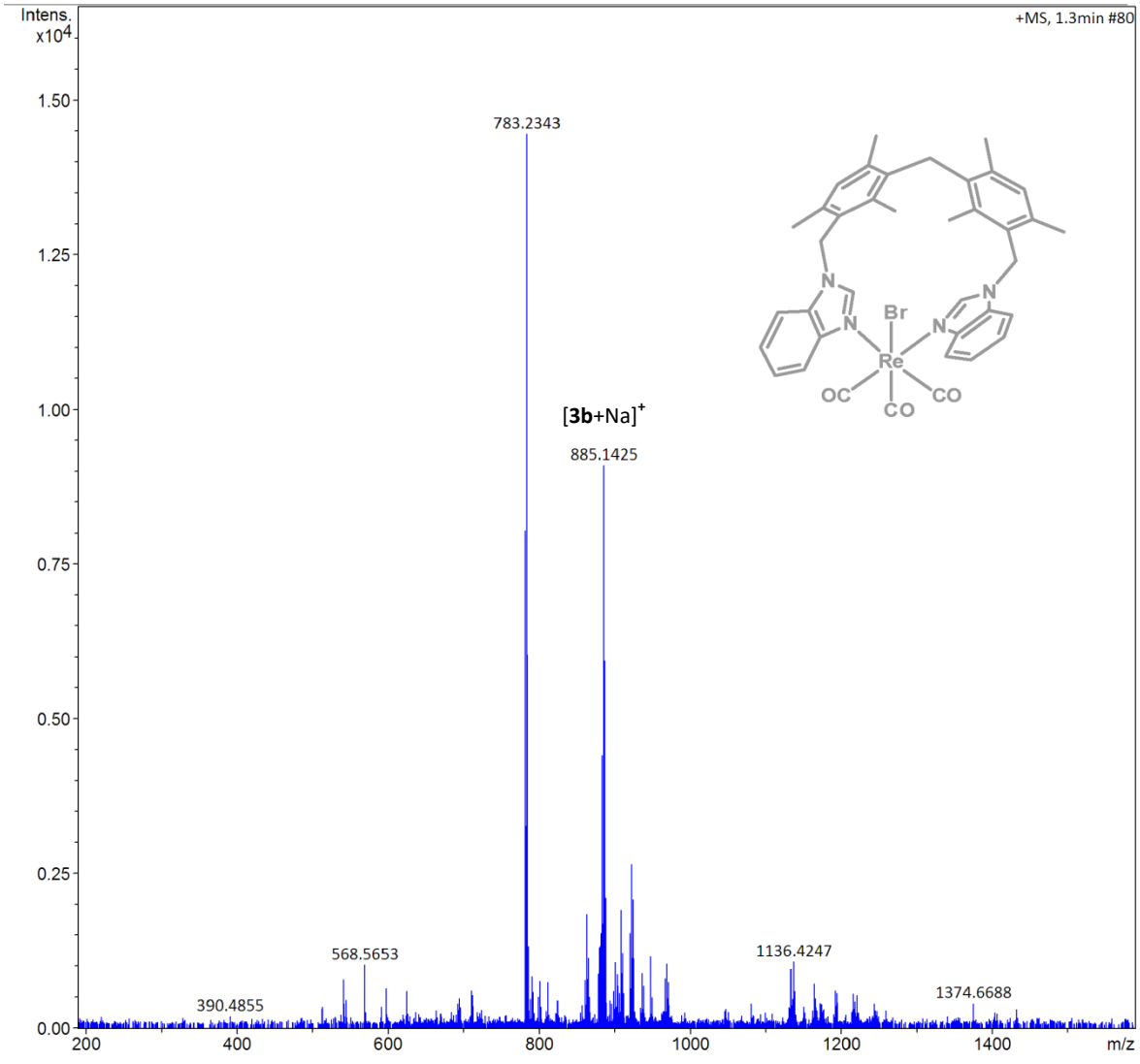

MB-UAL-41R.d

Bruker Compass DataAnalysis 4.2 printed: 11/24/2021 4:11:40 PM by: BDAL Page 1 of 1

Figure 4.34. ESI mass spectrum of **3b** in positive ion mode.

Display Report

Analysis Info

Analysis Name	D:\Data\2021-data\PROF.MS\NOV\MB-UAL-41R.d	Acquisition Date	11/24/2021 4:05:18 PM
Method	tune_low.m	Operator	BDAL
Sample Name	MB-UAL-41R	Instrument	maXis 255552.10138
Comment			

Acquisition Parameter

Source Type	ESI	Ion Polarity	Positive	Set Nebulizer	0.3 Bar
Focus	Not active	Set Capillary	3000 V	Set Dry Heater	180 °C
Scan Begin	50 m/z	Set End Plate Offset	-500 V	Set Dry Gas	4.0 l/min
Scan End	2000 m/z	Set Charging Voltage	0 V	Set Divert Valve	Waste
		Set Corona	0 nA	Set APCI Heater	0 °C

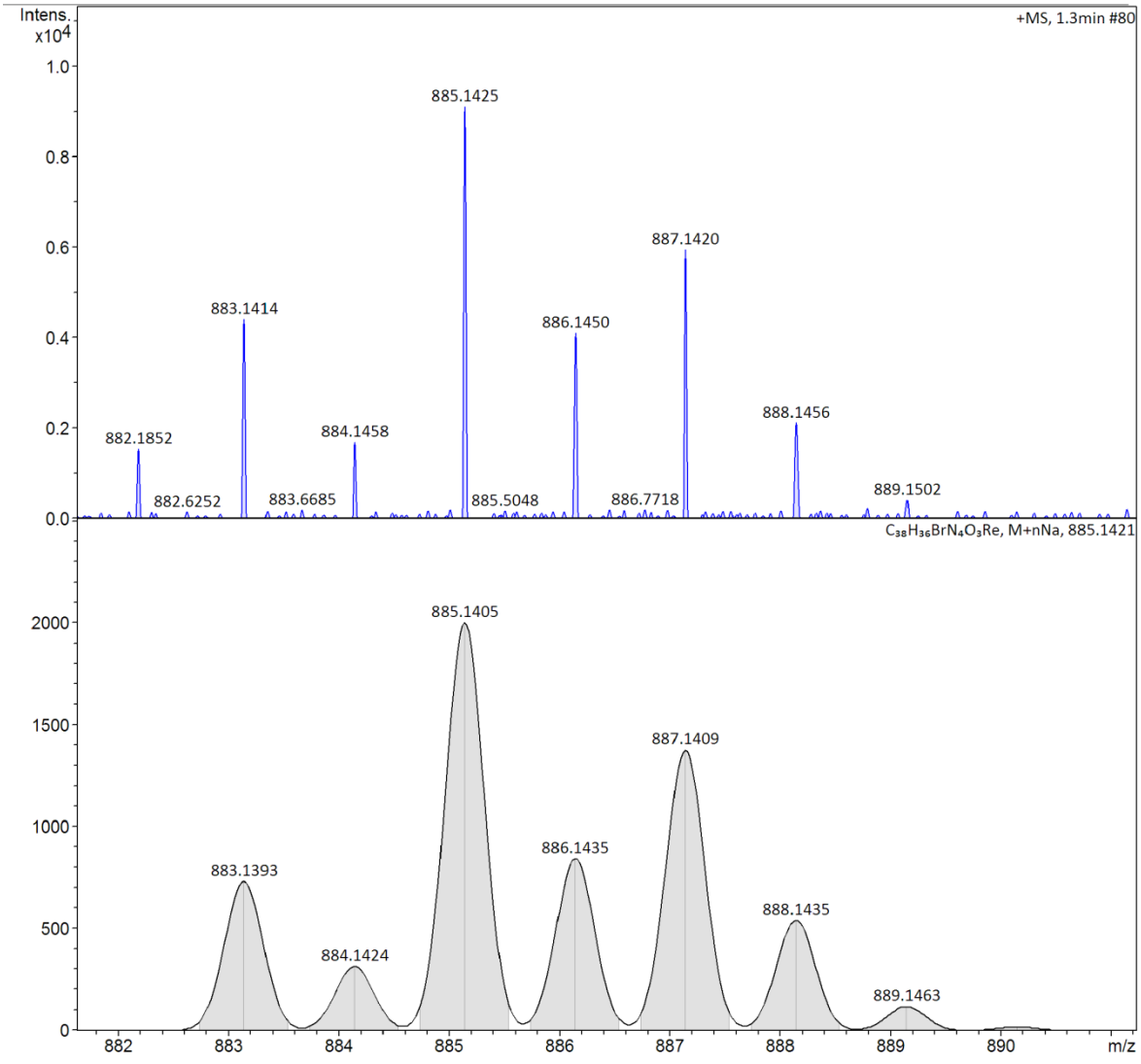

MB-UAL-41R.d

Bruker Compass DataAnalysis 4.2 printed: 11/24/2021 4:09:53 PM by: BDAL Page 1 of 1

Figure 4.35. Experimental (top) and calculated (bottom) ESI mass spectra of [**3b** + Na]$^+$ in positive ion mode.

Display Report

Analysis Info

Analysis Name	D:\Data\2021-data\PROF.MS\SEPT\MB-UAL-42-R.d	Acquisition Date	9/17/2021 4:13:53 PM
Method	tune_low.m	Operator	BDAL
Sample Name	MB-UAL-42-R	Instrument	maXis 255552.10138
Comment			

Acquisition Parameter

Source Type	ESI	Ion Polarity	Positive	Set Nebulizer	0.3 Bar
Focus	Not active	Set Capillary	4500 V	Set Dry Heater	180 °C
Scan Begin	50 m/z	Set End Plate Offset	-500 V	Set Dry Gas	4.0 l/min
Scan End	1500 m/z	Set Charging Voltage	0 V	Set Divert Valve	Waste
		Set Corona	0 nA	Set APCI Heater	0 °C

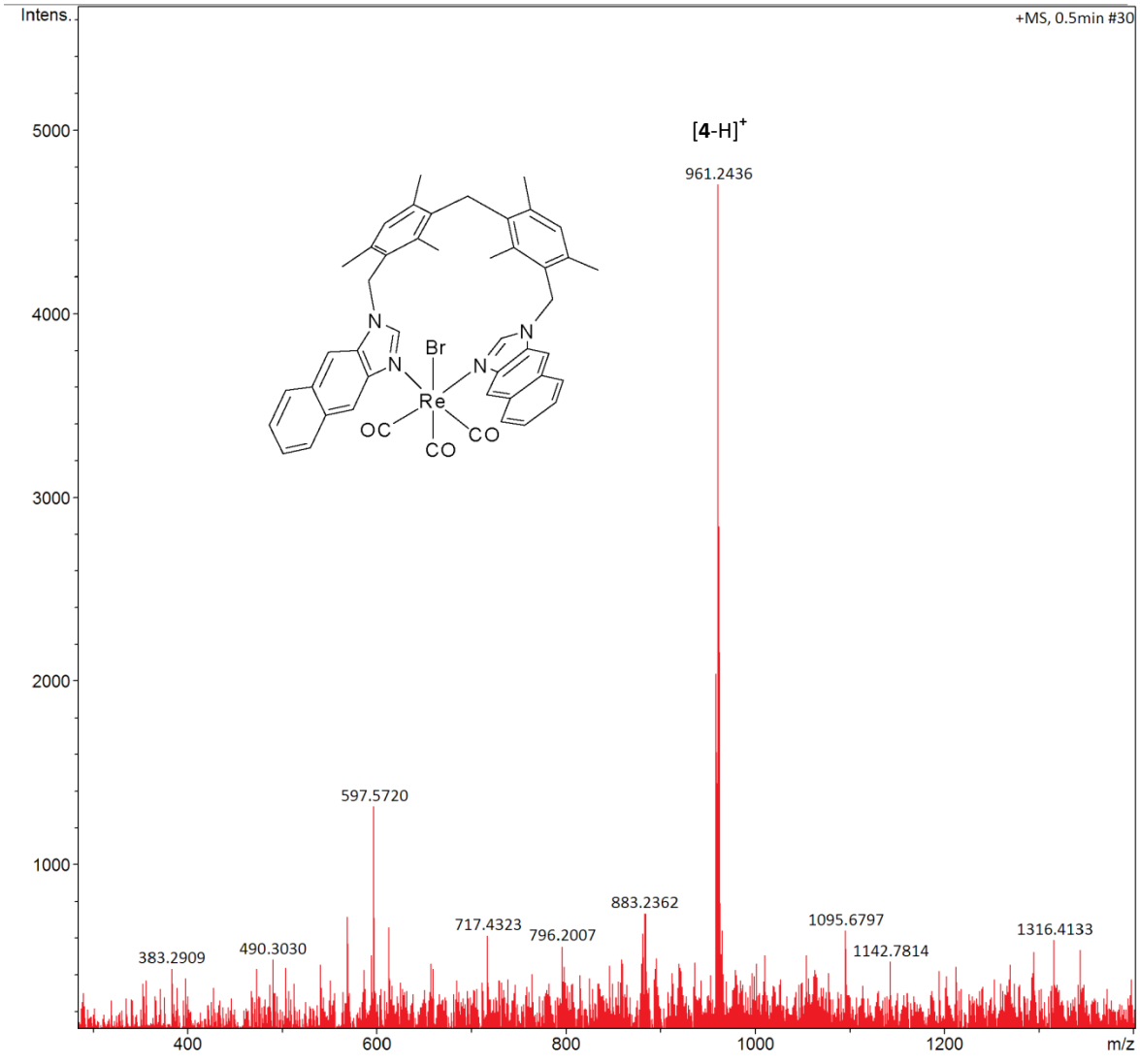

MB-UAL-42-R.d

Bruker Compass DataAnalysis 4.2 printed: 10/8/2021 4:11:53 PM by: BDAL Page 1 of 1

Figure 4.36. ESI mass spectrum of **4** in positive ion mode.

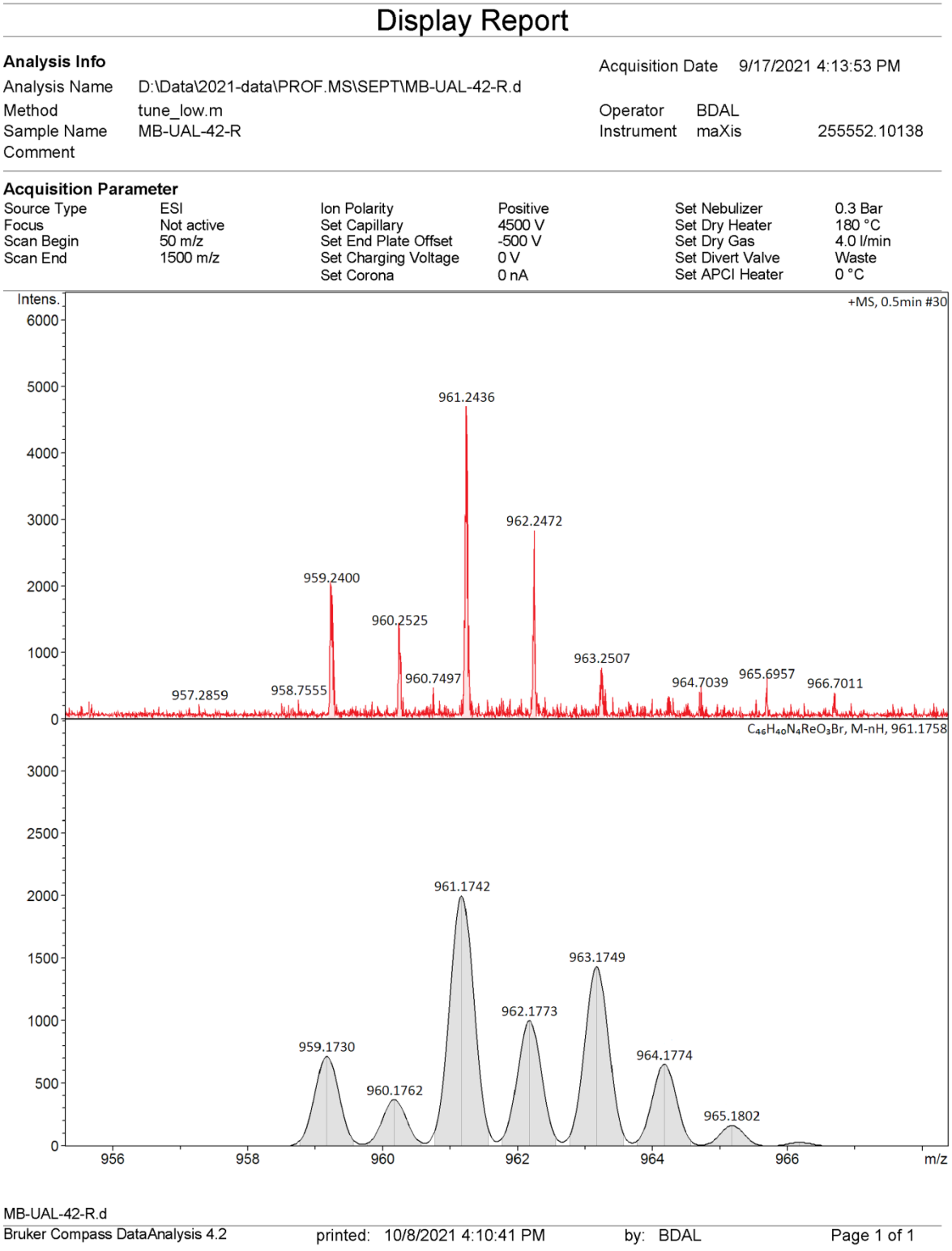

Figure 4.37. Experimental (top) and calculated (bottom) ESI mass spectra of [**4** - H]$^+$ in positive ion mode.

4.3.3. Molecular structure of metallacycles 1-4.

The molecular structures of **1** and **2** are unambiguously confirmed by X-ray diffraction analysis and adopt a bowl-shaped structure similar to calix[4]arene (Figure 4.38).[32] In the calix-like cyclic structure, the technetium atom can be considered as one of the methylene units. Due to the syn, syn, anti, syn/syn, syn, syn, syn arrangement of four arene units with respect to each other, **1** adopts a partial-cone conformation, whereas **2** takes a cone conformation. One of the mesitylene motifs in **1** is arranged in such a way that two methyl units are directed below the plane, generated by the four corner atoms of the cycle, i.e., Tc1···C28···C18···C8.

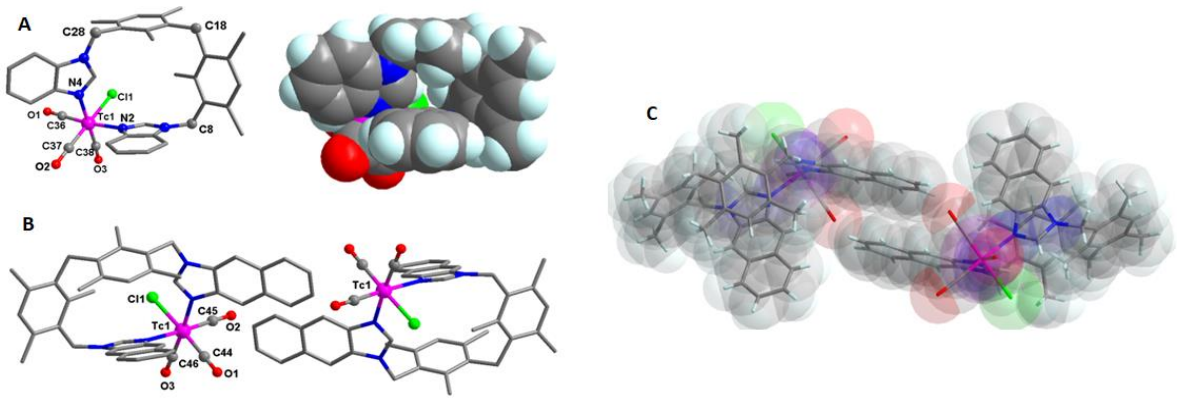

Figure 4.38. Molecular structures of technetium supramolecules. A: Stick and space-filling representations of **1**. B and C: Arrangement of two neighboring molecules in the crystal structure of **2**. Hydrogen atoms and solvent molecules are removed for clarity in stick representation.

The oppositely arranged pair of arene motifs, i.e., benzimidazolyl and mesitylene, is almost parallel (dihedral angle = 12.6°), and another arene and heteroarene pair is arranged away from each other (dihedral angle = 74° or 106°). Similar to **1**, one of the oppositely arranged arene pairs in **2** come close to each other (dihedral angle = 31°), whereas the other pair is flattened with respect to each other (dihedral angle = 45° or 135°). The crystal structures of **1** and **2** are stabilized by various types of intermolecular non-covalent interactions [(C–H···π, N–CH_2–C/phenylene(H)···Cl–Tc, (–CH_3)H···N–Tc for **1**, C–H···π, π···π, $CHCl_3$(H)···O≡C–Re

for **2**)]. Particularly in the solid-state crystal structure of **2**, two neighbouring molecules partially occupy each other's internal cavity using their naphthoimidazolyl arm to form a non-covalent dimer, which is stabilized by offset parallel displaced π···π interactions (~3.385 Å) between parallelly arranged naphthoimidazolyl motifs. The CH_2Cl_2 solvent molecules occupy the lattice voids in the crystal structure of **2**.

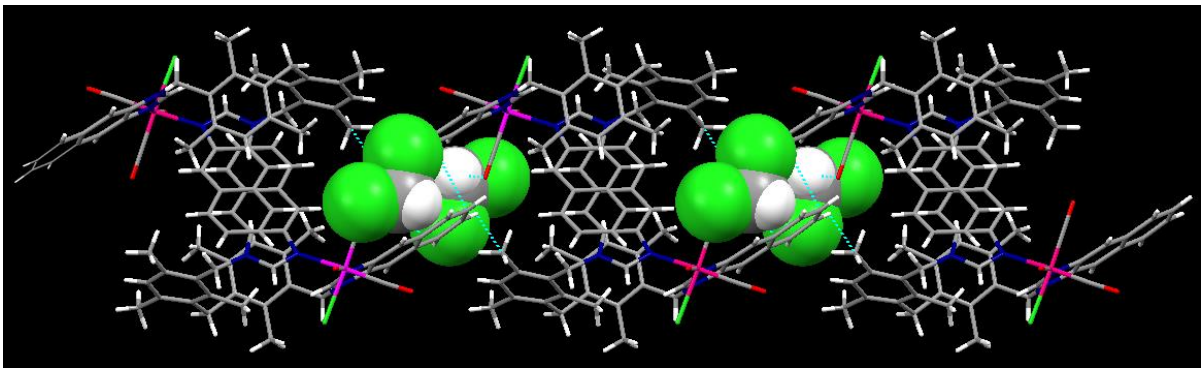

Figure 4.39. Partial packing diagram of **2** (capped stick representation) with CH_2Cl_2 solvent molecules (space-filling model) along b-axis.

The molecular structures of the rhenium-based macrocycles **3a, 3b** and **4** are similar to those of **1** and **2**, respectively. Complex **3a** crystallized with solvent toluene molecules. In the solid-state structure of **3a,** the macrocycles interact with each other *via* various types of intermolecular non-covalent interactions, which result in a three-dimensional network structure with a one-dimensional channel along the a axis. In particular, four of the macrocycles interact with each other through non-classical H-bonding interactions (C(H)···O≡C–Re; 3.432, Å, θ = 160°, 3.304 Å, θ = 128°) resulting in a lattice cavity, in which the disordered toluene sits perfectly. The disordered toluene molecules are arranged in a helical structure that is stabilized through *edge-to-face* C–H···π interactions. The toluene molecules reside in the 1D column and interact with the metallocycle *via* non-classical hydrogen bonding interactions C–H···O≡C–Re (~2.580 Å, θ = 135°) (Figure 4.40). Single crystals of **3b** were obtained from acetonitrile. The molecular structure of **3b** is similar to that of **3a**. In the crystal structure, each molecule of **3b** is surrounded by two CH_3CN molecules that are in contact with the outside wall of the cyclic framework *via* H-bonding interactions (C35–H···N6, ~2.586 Å, θ~130°, C28–H···N6, ~2.731 Å, θ ~135°, and C39–H···O2, ~2.704 Å, θ ~119°).

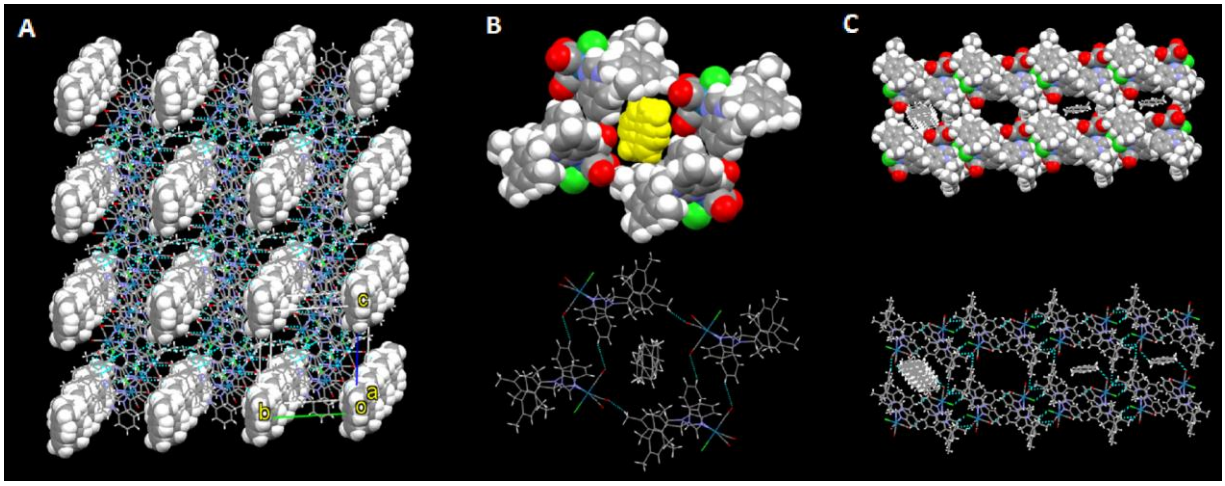

Figure 4.40. (A) Partial packing diagram of **3a** showing a 3D network structure with a one-dimensional cavity, which is occupied by toluene solvent molecules (space-filling view). (B) Space filling and wireframe structures showing how the disordered toluene sits perfectly in the lattice cavity, created by four adjacent molecules in "A" (C) Packing of one layered structure of macrocycles in "A" showing four intermolecular cavities with and without solvent molecules (space filling and wireframe view).

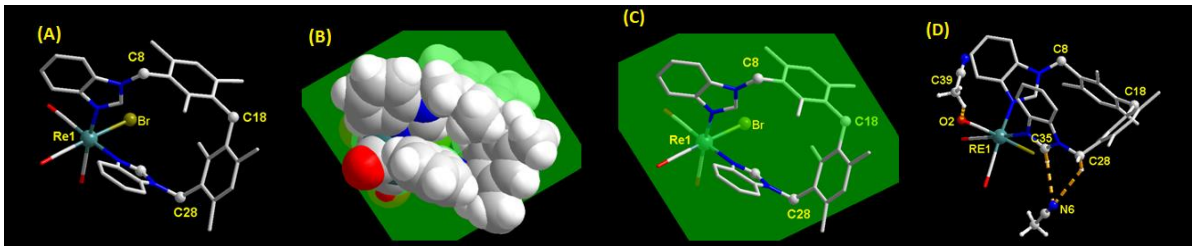

Figure 4.41. (A) Molecular structure of **3b** without hydrogen atoms and solvent molecules. (B-C) Space-filling and stick views of **3b** showing plane (green) generated through four corner atoms Re1···C8···C18···C28. (D) Two CH_3CN solvent molecules contact with framework of **3b** (C35–H···N6, ~2.586 Å, θ~130°, C28–H···N6, ~2.731 Å, θ ~135°, and C39–H···O2, ~2.704 Å, θ ~119°).

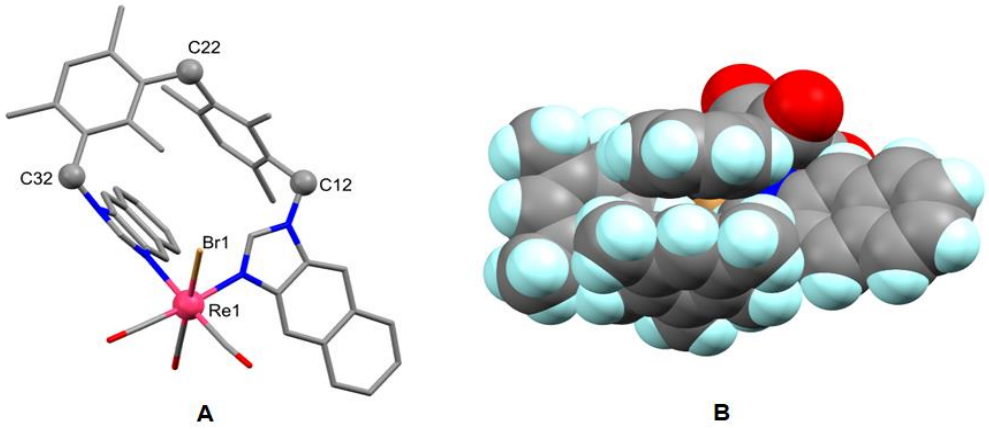

Figure 4.42. Molecular structure of **4**, A: Capped stick representation (Hydrogen atoms and solvent molecules are removed for clarity), B: Space-filling model (C= grey, N = blue, O = red, Br = brown, H = light blue, Re = deep pink).

4.4. Binding studies of metallacalix[4]arenes 3a and 4 with polyaromatic hydrocarbons and imidazole derivative guest molecules.

In order to study the host guest interaction, preliminary experiments were performed on host **3a** with the potential guest molecules benzene, naphthalene, anthracene, imidazole, and benzimidazole. In the absence of guest molecule, complex **3a** displayed a structured emission (λ_{max} = 333, 344, and 400 nm) upon excitation at 231 nm in CH_2Cl_2 at room temperature. The emission maxima of **3a** quenched upon the addition of an appropriate aliquot of the guest molecules, which suggests host-guest interactions between **3a** and the guest molecules. The emission pattern of guest molecules is partially overlapping with the emission profile of **3a** in the range of 300-375 nm for naphthalene, and 375-500 nm for both anthracene and imidazole. Therefore, the emission intensities at 400 nm for naphthalene and 333 nm for both anthracene and imidazole were chosen for the determination of the binding constant. In contrast, the emission maxima of **3a** are randomly quenched and enhanced during the addition of benzimidazole guest molecule, suggesting a dynamic association and dissociation of the formed host-guest complex. The binding constant (*K*) were calculated using Benesi-Hildebrand method, and a linear fit plot of $1/(\Delta I)$ vs $[G]^{-1}$ indicates the formation of 1:1 host:guest complex.[33] The corresponding binding constant is 8.7×10^1 M^{-1} for benzene, 6.7×10^3 M^{-1} for naphthalene, 1.35×10^4 M^{-1} for athracene, and 7.5×10^1 M^{-1} for imidazole.

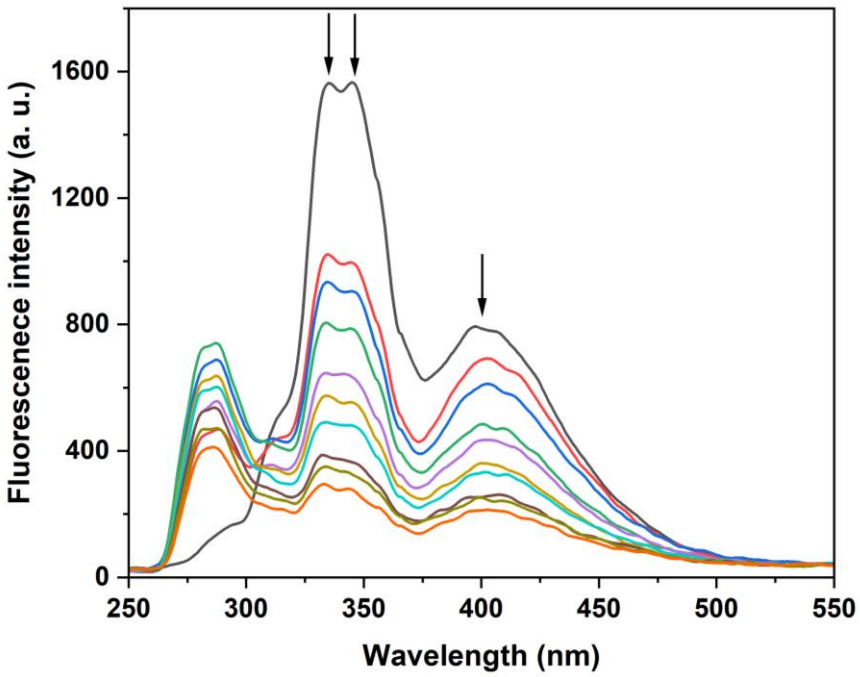

Figure 4.43. Changes in the emission spectra of **3a** (2×10^{-5} M, λ_{exc} = 231 nm) with the addition of benzene in DCM. The arrow indicates the quenching of the emission intensity by addition of an appropriate aliquot of benzene.

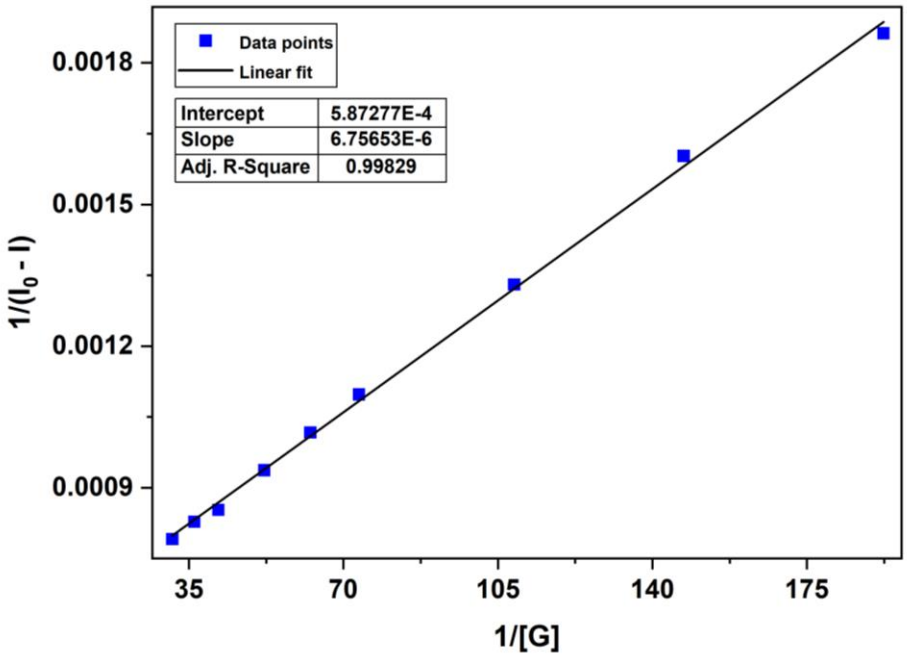

Figure 4.44. Benesi-Hildebrand plot for the emission quenching of host **3a** (at 334 nm) with an increase in the concentration of benzene in DCM.

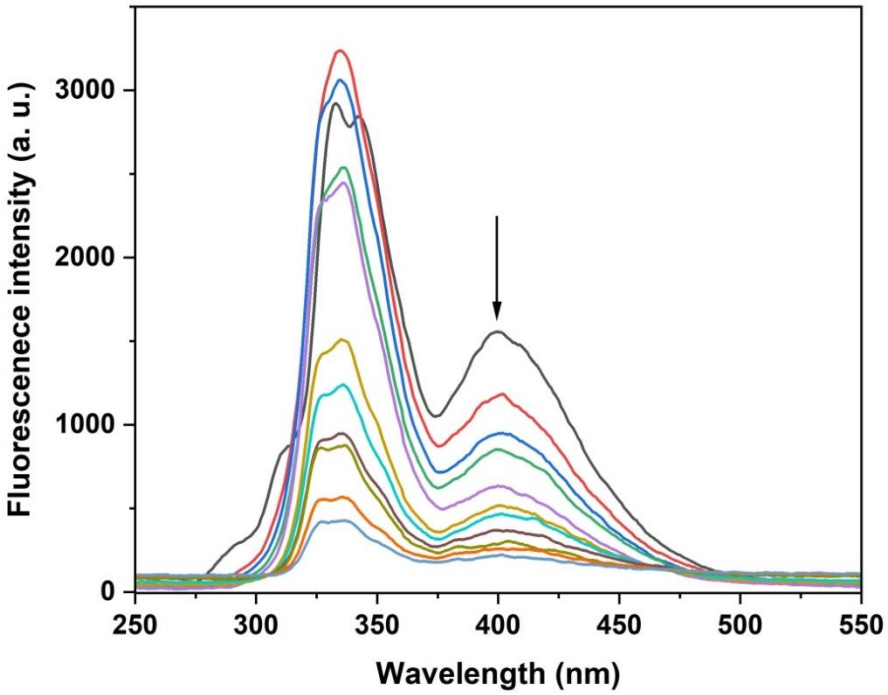

Figure 4.45. Changes in the emission spectra of **3a** (2×10^{-6} M, λ_{exc} = 231 nm) with the addition of naphthalene in DCM. The arrow indicates the quenching of the emission intensity by addition of an appropriate aliquot of naphthalene.

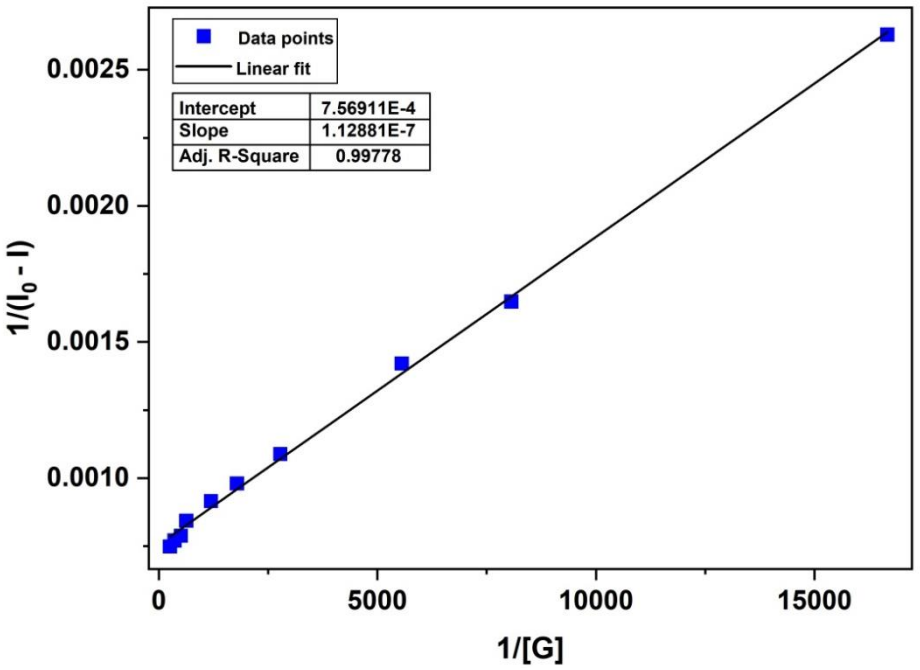

Figure 4.46. Benesi-Hildebrand plot for the emission quenching of host **3a** (at 400 nm) with an increase in the concentration of naphthalene in DCM.

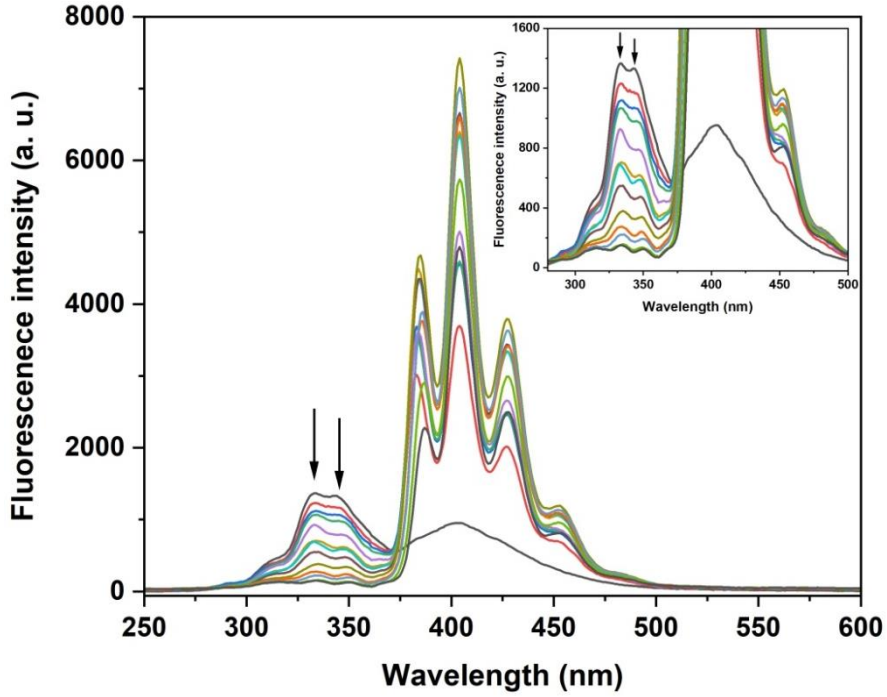

Figure 4.47. Changes in the emission spectra of **3a** (2×10^{-5} M, λ_{exc} = 231 nm) with the addition of anthracene in DCM. The arrows indicate the quenching of the emission intensity by addition of an appropriate aliquot of anthracene.

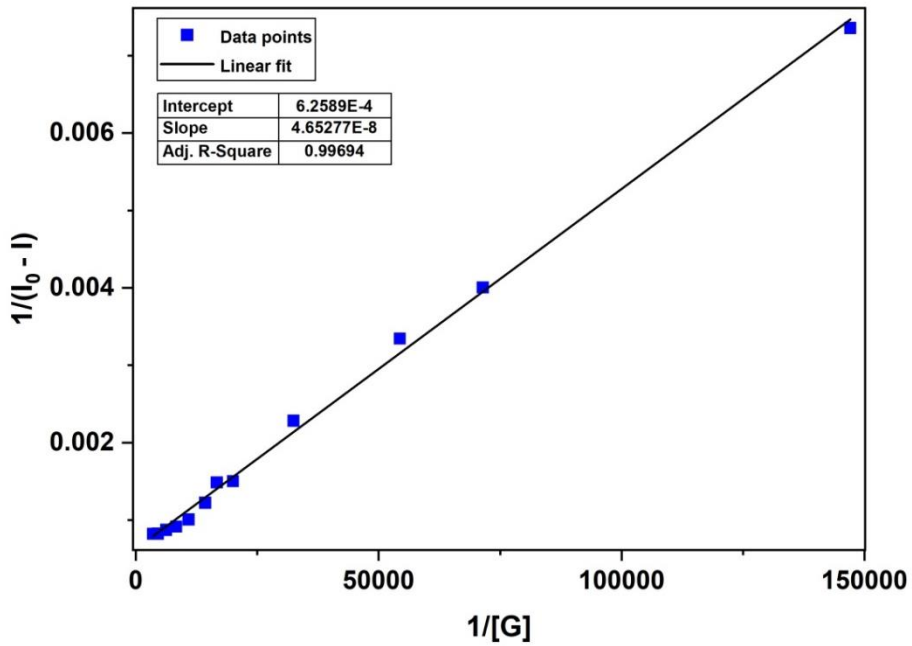

Figure 4.48. Benesi-Hildebrand plot for the emission quenching of host **3a** (at 333 nm) with an increase in the concentration of anthracene in DCM.

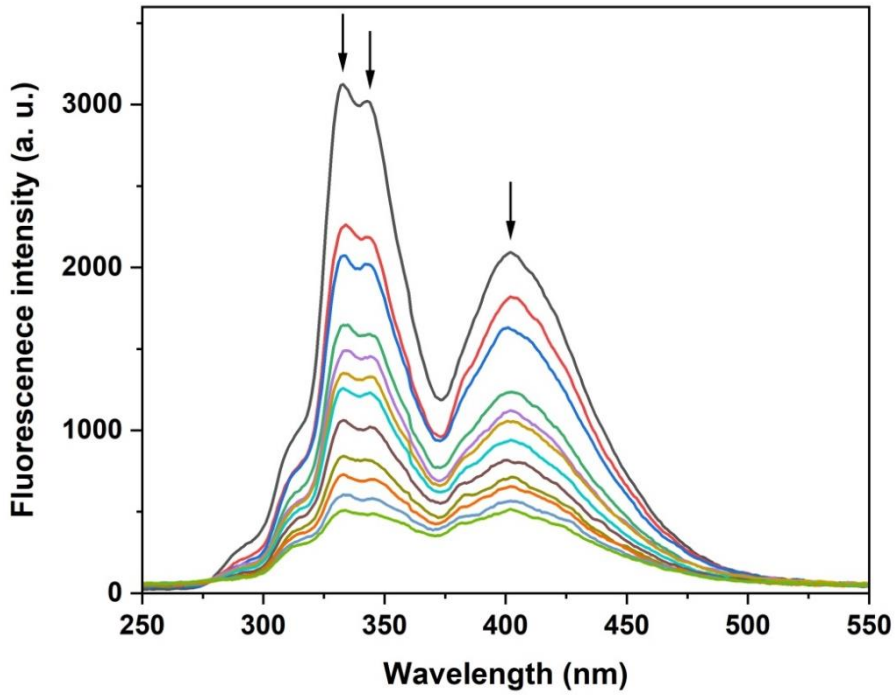

Figure 4.49. Changes in the emission spectra of **3a** (2×10^{-6} M, λ_{exc} = 231 nm) with the addition of imidazole in DCM. The arrows indicate the quenching of the emission intensity by addition of an appropriate aliquot of imidazole.

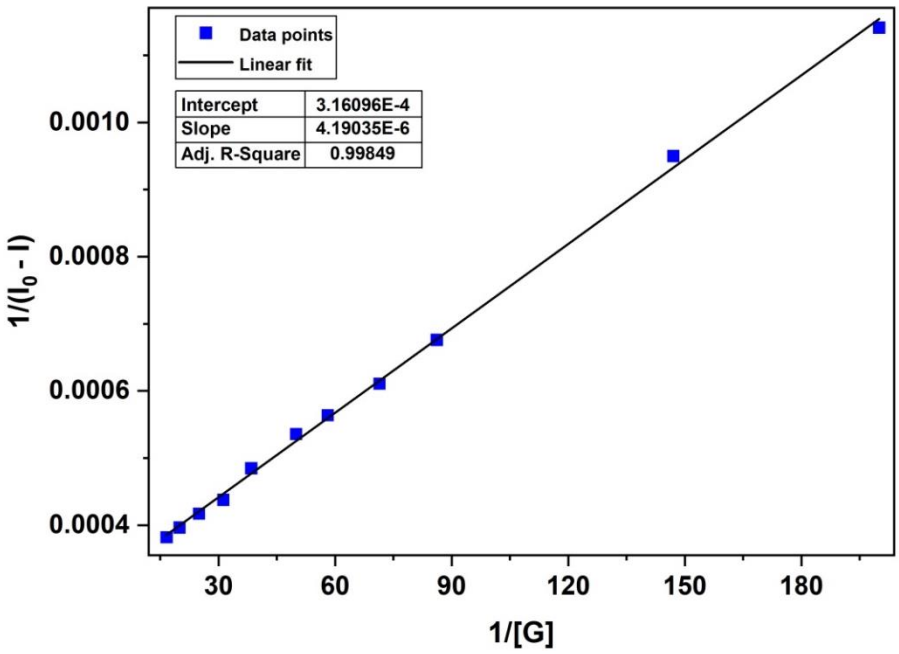

Figure 4.50. Benesi-Hildebrand plot for the emission quenching of host **3a** (at 333 nm) with an increase in the concentration of imidazole in DCM.

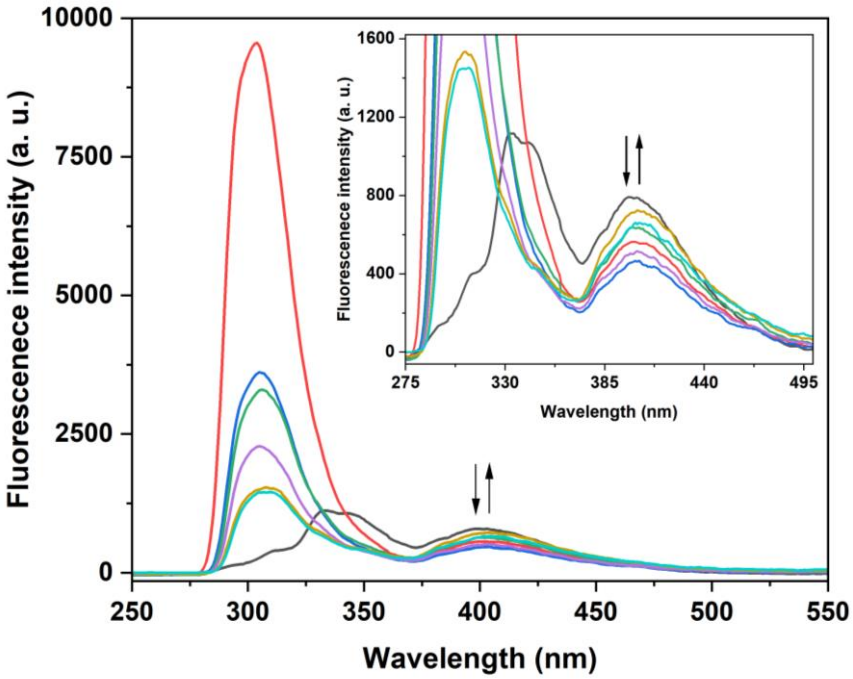

Figure 4.51. Changes in the emission spectra of **3a** (2×10^{-5} M, λ_{exc} = 231 nm) with the addition of benzimidazole in DCM. The arrows indicate the quenching and enhancement of the emission intensity randomly by addition of an appropriate aliquot of benzimidazole.

The host–guest behaviour of **3a** with naphthalene and anthracene were studied using ^{1}H NMR studies in $CDCl_3$ to understand how the guests interact with the macrocycle. The protons of naphthalene were shifted upfield, whereas the protons of the aromatic unit and part of the aliphatic protons of **3a** were shifted downfield relative to those of the free naphthalene and the free macrocycle. No additional peaks for either the naphthalene or the complex were observed. This data suggests that the cavity of macrocycle **3a** is suitable for accommodating naphthalene guest. However, there was dynamic equilibrium between **3a** and naphthalene i.e., the host–guest complex assembles and disassembles in the solution, on the NMR time scale.[34] In the case of anthracene, the protons of **3a** were shifted upfield noticeably, whereas the protons of the anthracene remain unaffected. These data suggest that the anthracene contacts with the macrocycle by sitting on the top of the rim of the macrocycle.[35] The higher binding constant of anthracene with macrocycle **3a** may be due to the cooperative C–H$\cdots\pi$ contacts between these molecules. The host-guest binding studies of **4** with benzene (K = 1.0 $\times$ 10^1 M^{-1}), naphthalene (K = 7.4 $\times$ 10^2 M^{-1}), anthracene (K = 1.9 $\times$ 10^4 M^{-1}), imidazole (K = 0.3 $\times$ 10^1 M^{-1}), and benzimidazole (K = 0.4 $\times$ 10^1 M^{-1}) were studied by using the emission titration method. The higher binding constant of **3a** with naphthalene than **4** with naphthalene

may be due to the compact cavity of **3a**, which maximizes the non-covalent interactions between the host-guest systems effectively.

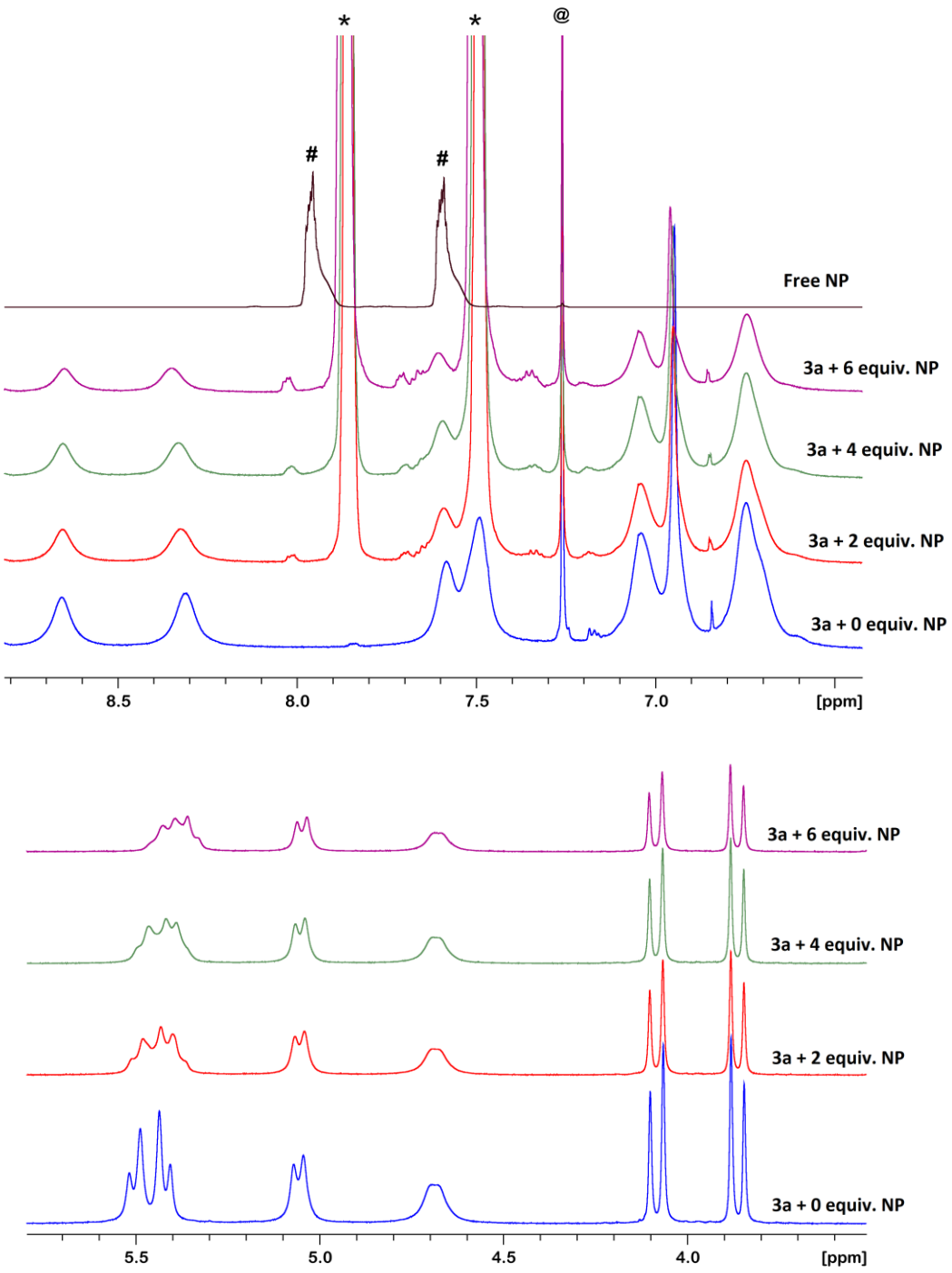

Figure 4.52. Partial ^{1}H NMR spectra from the titration of **3a** with naphthalene (top = aromatic; bottom = aliphatic region) in $CDCl_3$ (# = free naphthalene; *= bound naphthalene; @ = $CDCl_3$).

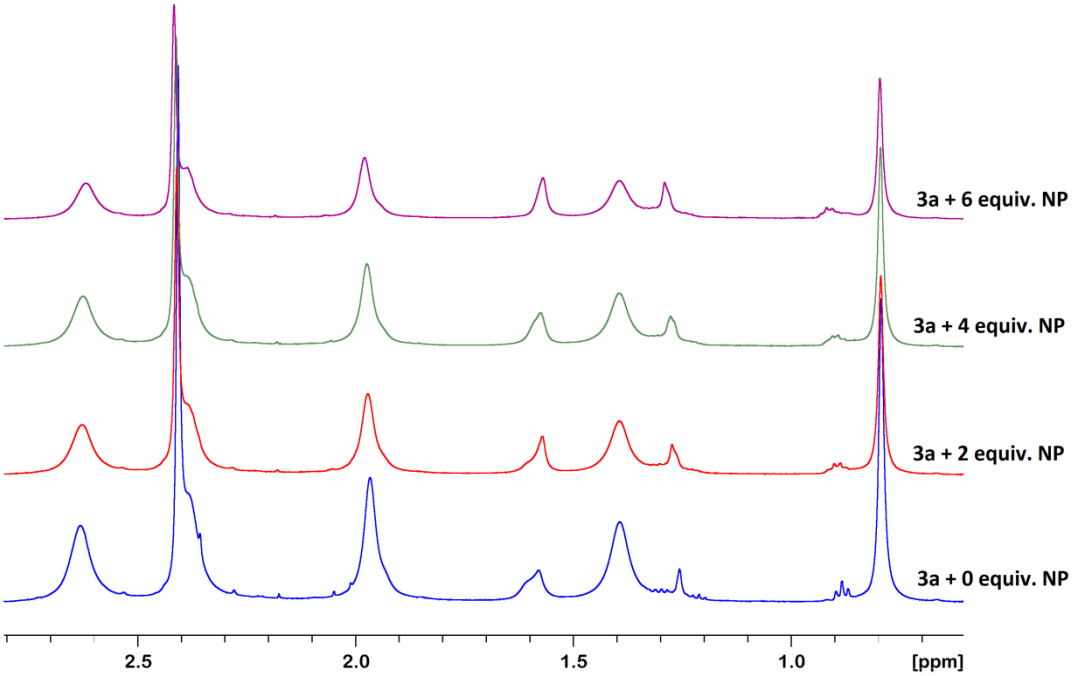

Figure 4.53. Partial ^{1}H NMR spectra (aliphatic region) from the titration of **3a** with naphthalene in $CDCl_3$.

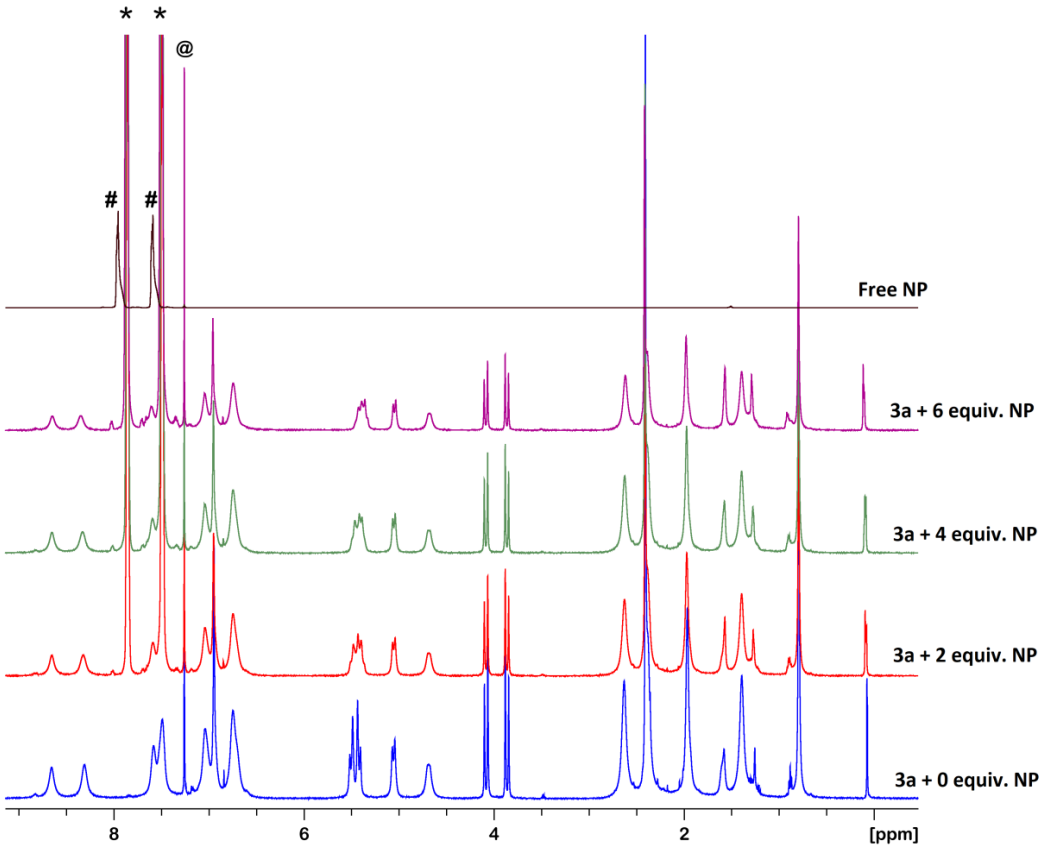

Figure 4.54. ^{1}H NMR spectra from the titration of **3a** with naphthalene in $CDCl_3$ (# = free naphthalene; *= bound naphthalene; @ = $CDCl_3$).

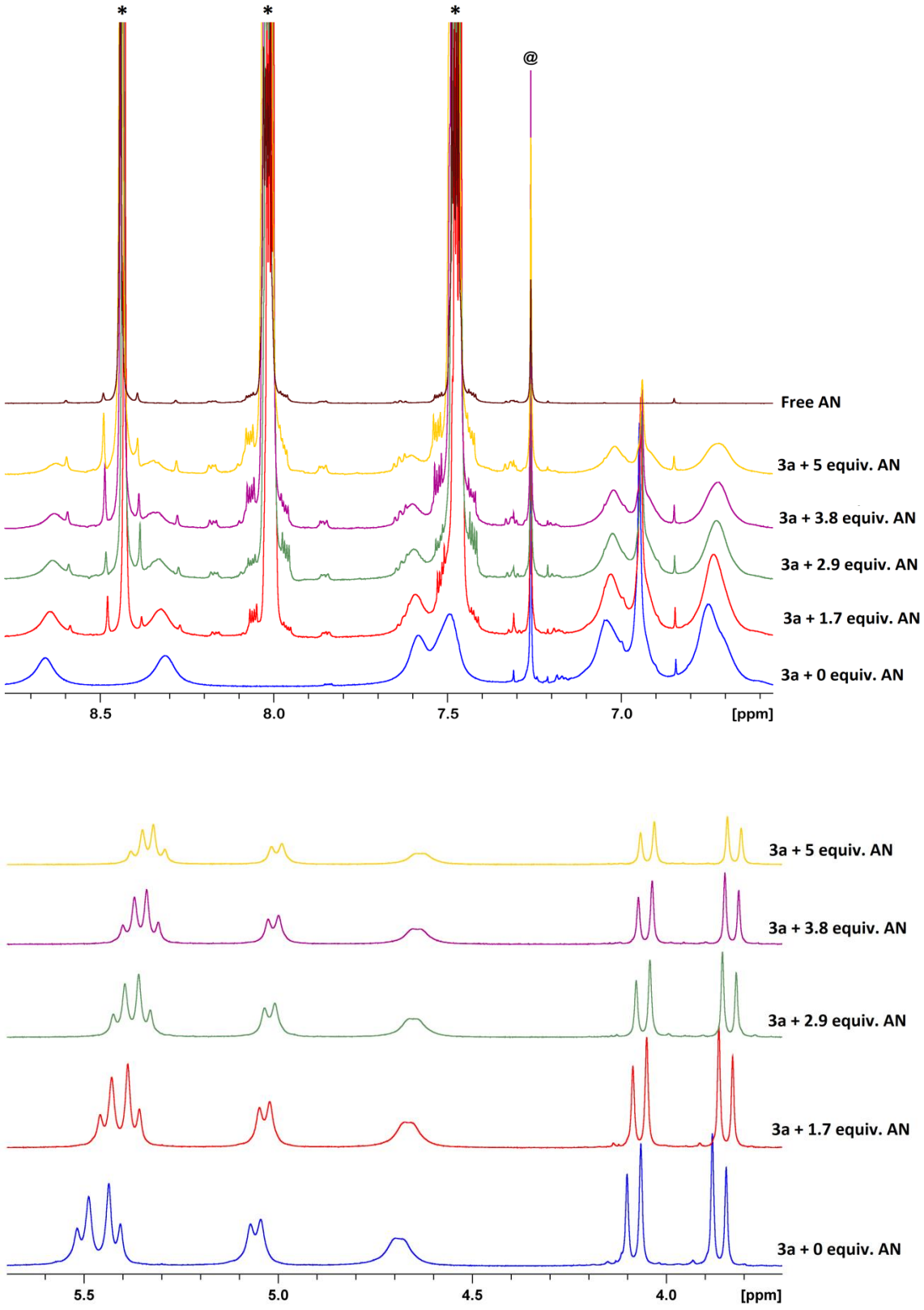

Figure 4.55. Partial ^{1}H NMR spectra from the titration of **3a** with anthracene (top = aromatic; bottom = aliphatic region) in $CDCl_3$ (*= anthracene; @ = $CDCl_3$). The minor peak signals are from the free anthracene.

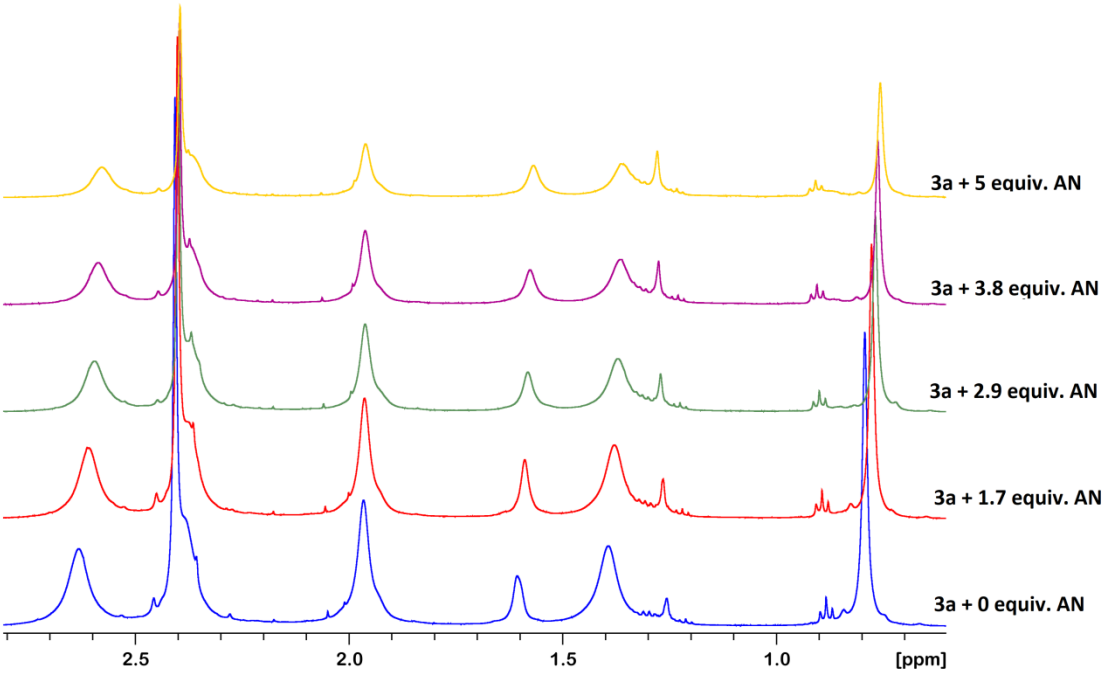

Figure 4.56. Partial ^{1}H NMR spectra (aliphatic region) from the titration of **3a** with anthracene in $CDCl_3$.

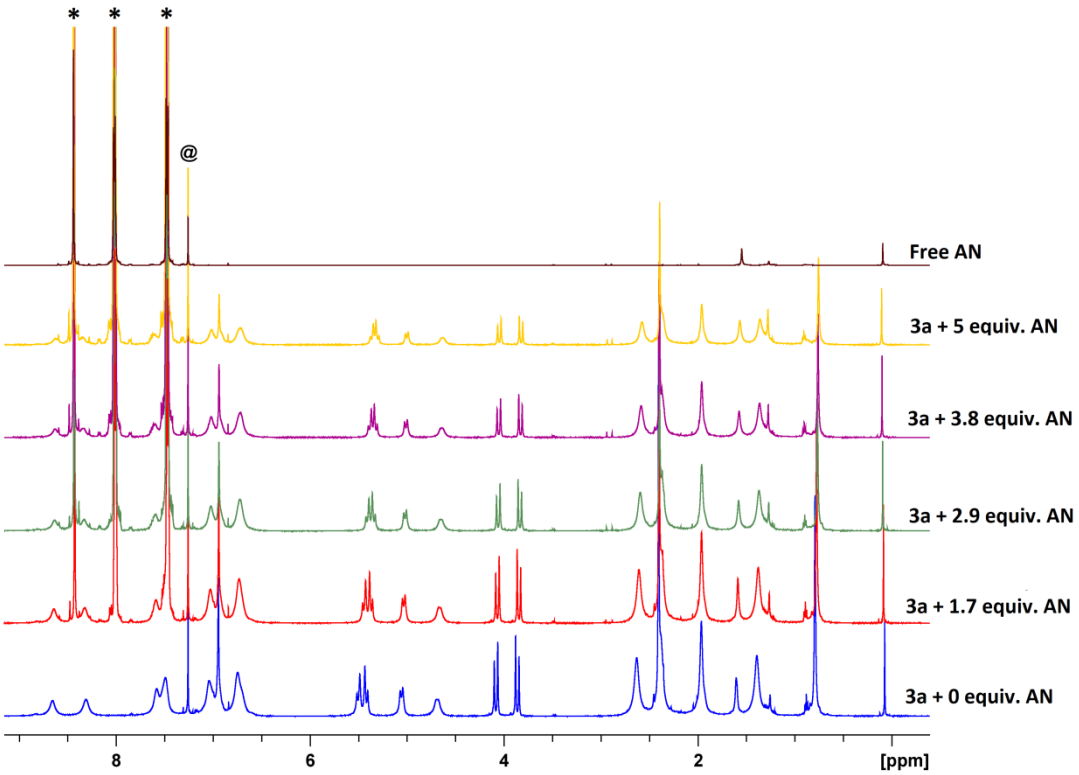

Figure 4.57. ^{1}H NMR spectra from the titration of **3a** with anthracene in $CDCl_3$ (*= anthracene; @ = $CDCl_3$).

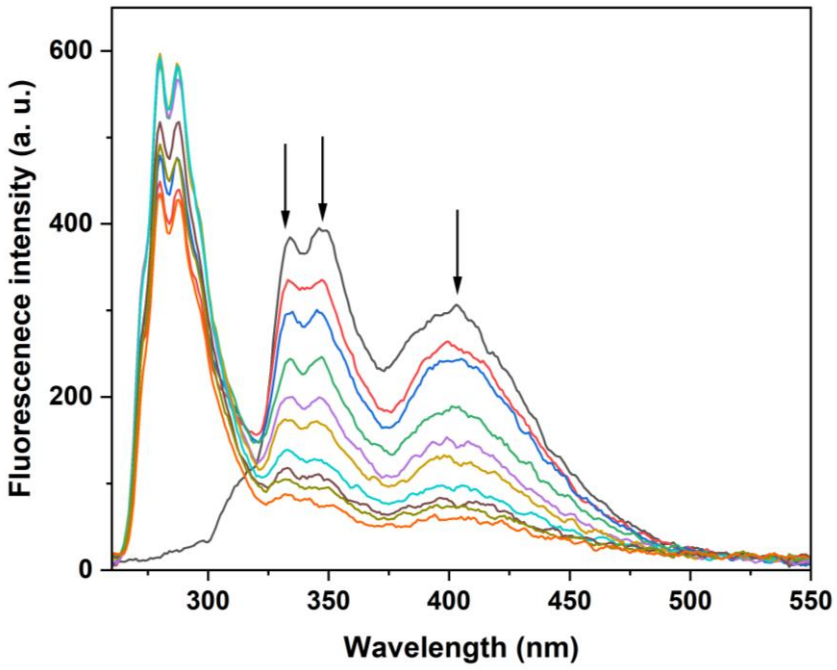

Figure 4.58. Changes in the emission spectra of **4** (2×10^{-6} M, λ_{exc} = 240 nm) with the addition of benzene in DCM. The arrow indicates the quenching of the emission intensity by addition of an appropriate aliquot of benzene.

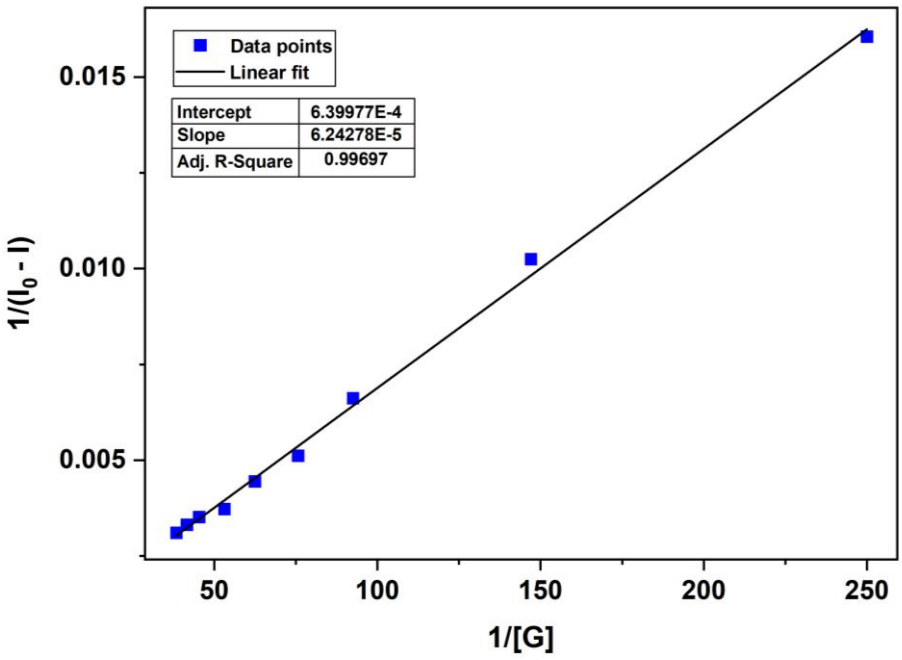

Figure 4.59. Benesi-Hildebrand plot for the emission quenching of host **4** (at 346 nm) with an increase in the concentration of benzene in DCM.

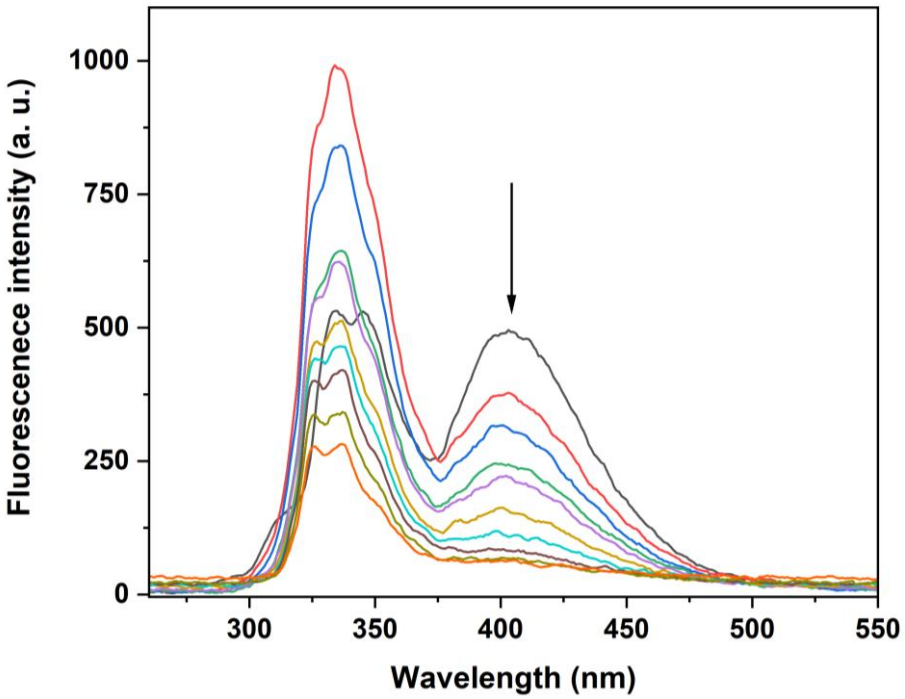

Figure 4.60. Changes in the emission spectra of **4** (2×10^{-6} M, λ_{exc} = 240 nm) with the addition of naphthalene in DCM. The arrow indicates the quenching of the emission intensity by addition of an appropriate aliquot of naphthalene.

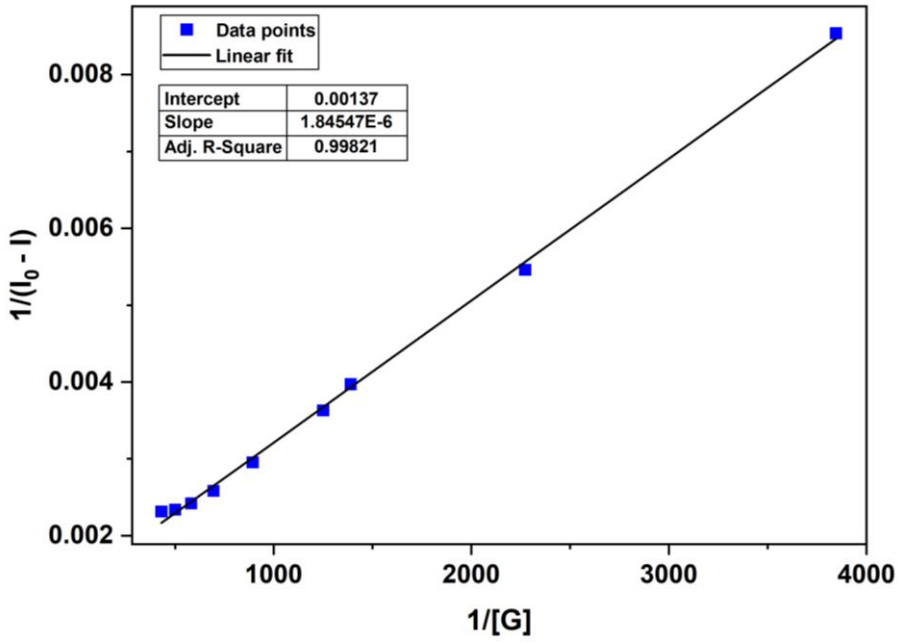

Figure 4.61. Benesi-Hildebrand plot for the emission quenching of host **4** (at 403 nm) with an increase in the concentration of naphthalene in DCM.

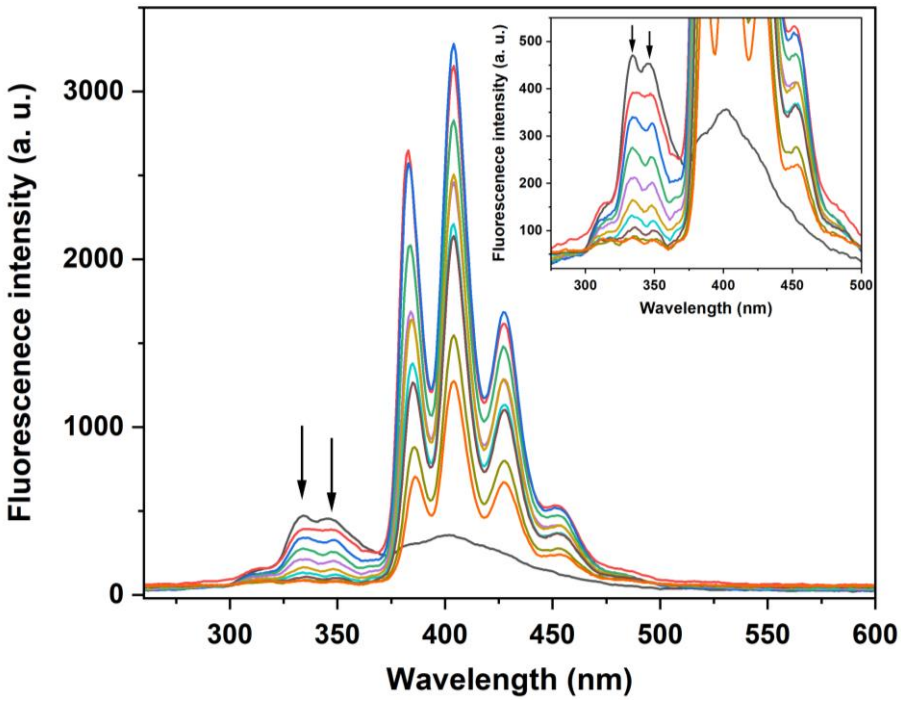

Figure 4.62. Changes in the emission spectra of **4** (2×10^{-6} M, λ_{exc} = 240 nm) with the addition of anthracene in DCM. The arrows indicate the quenching of the emission intensity by addition of an appropriate aliquot of anthracene.

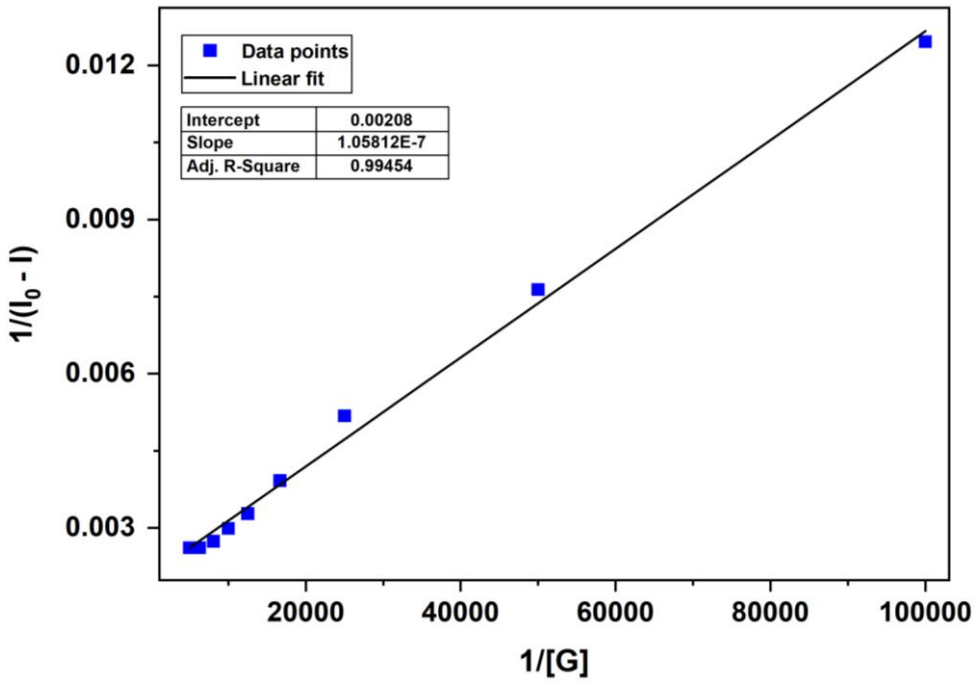

Figure 4.63. Benesi-Hildebrand plot for the emission quenching of host **4** (at 346 nm) with an increase in the concentration of anthracene in DCM.

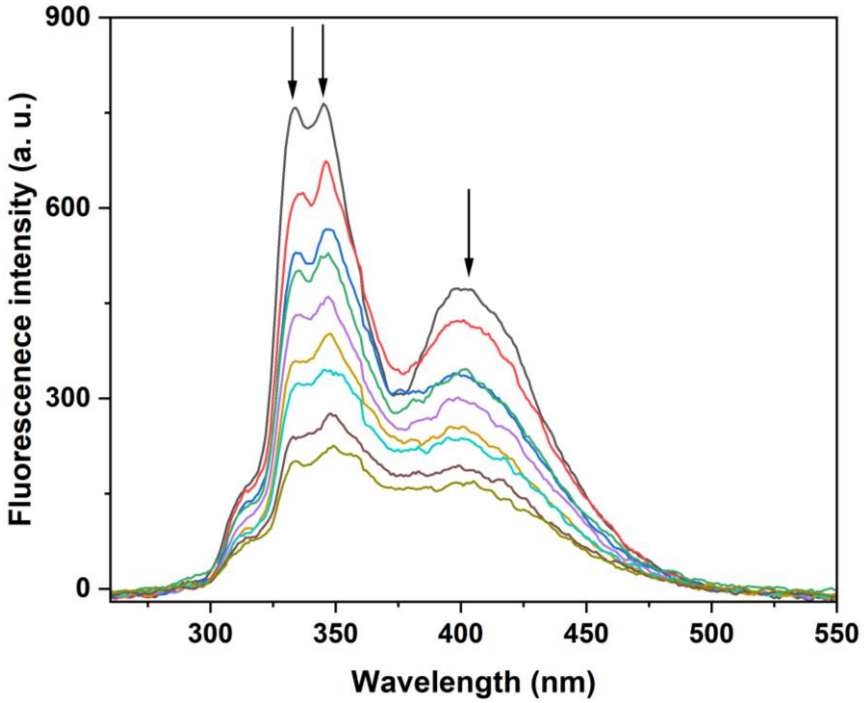

Figure 4.64. Changes in the emission spectra of **4** (2×10^{-7} M, λ_{exc} = 240 nm) with the addition of imidazole in DCM. The arrows indicate the quenching of the emission intensity by addition of an appropriate aliquot of imidazole.

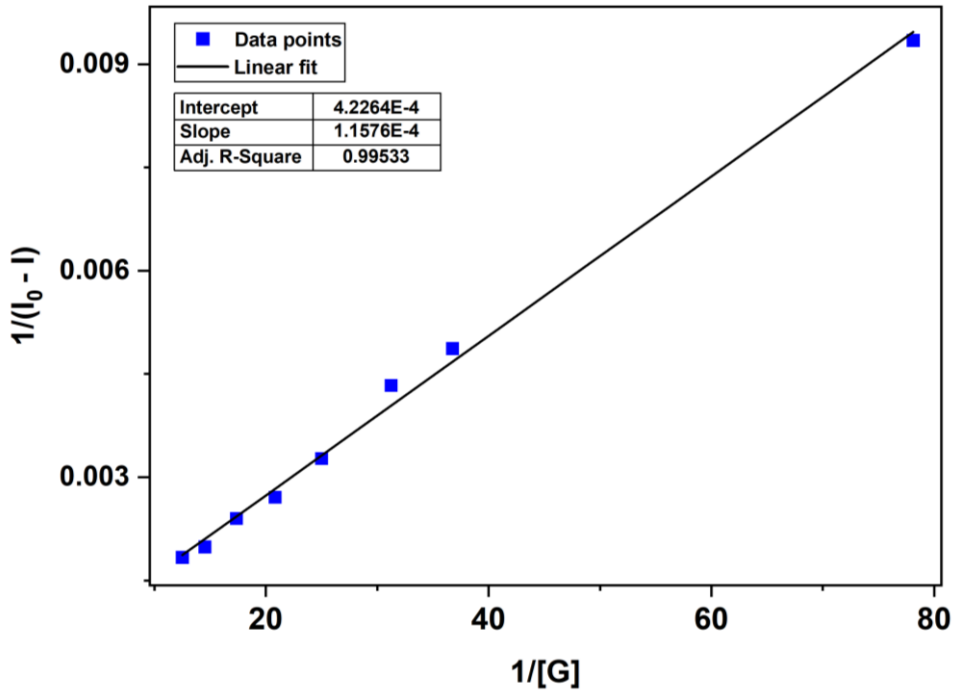

Figure 4.65. Benesi-Hildebrand plot for the emission quenching of host **4** (at 344 nm) with an increase in the concentration of imidazole in DCM.

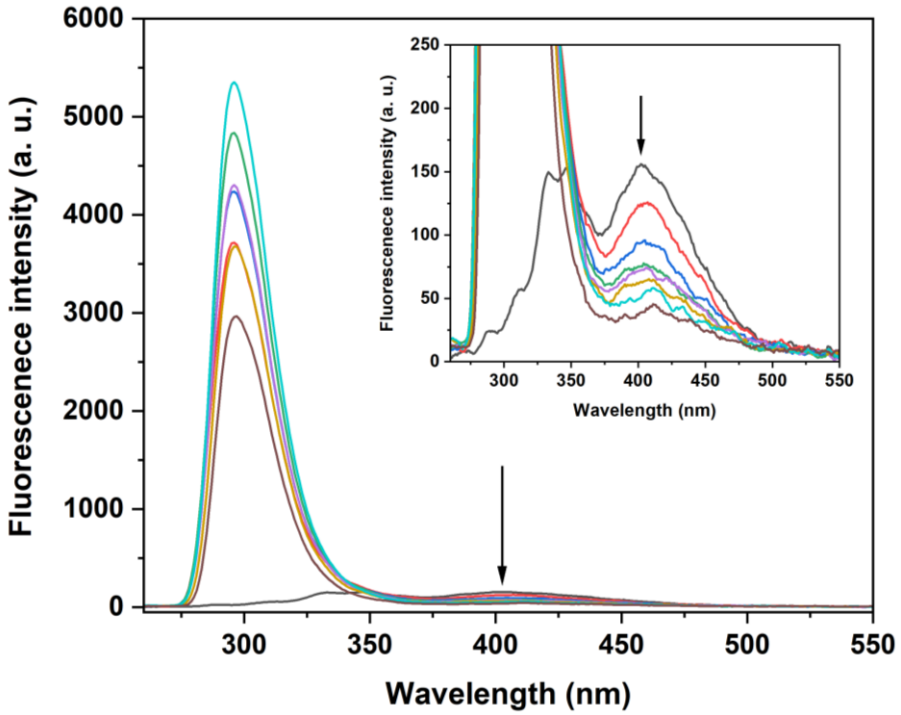

Figure 4.66. Changes in the emission spectra of **4** (2×10^{-5} M, λ_{exc} = 240 nm) with the addition of benzimidazole in DCM. The arrows indicate the quenching and enhancement of the emission intensity randomly by addition of an appropriate aliquot of benzimidazole.

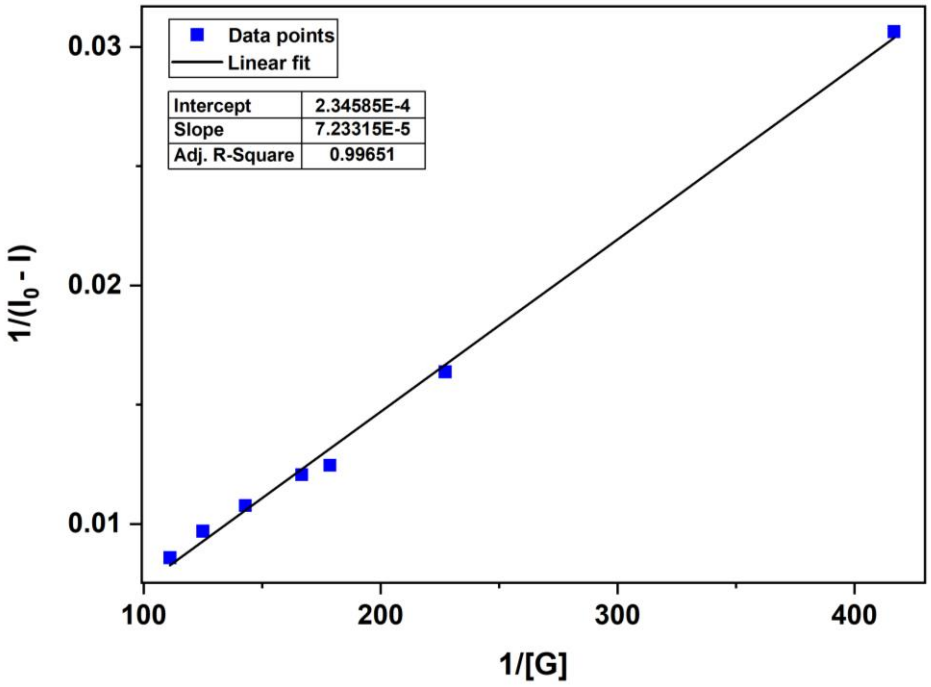

Figure 4.67. Benesi-Hildebrand plot for the emission quenching of host **4** (at 403 nm) with an increase in the concentration of benzimidazole.

4.5 Conclusion

In conclusion, technetium supramolecules analogous to calix[4]arene were self-assembled using $(NBu_4)[Tc_2(\mu\text{-}Cl)_3(CO)_6]$ and neutral flexible ditopic nitrogen donors. Structurally similar rhenium metallocavitands were assembled from $[Re(CO)_5X]$ (X= Cl, Br) and L^n. The solid-state structures of the supramolecules reveal that these molecules adopt bowl-shaped structures. To the best of our knowledge, the technetium complexes are the first examples of *fac*-$[Tc(CO)_3]^+$ core-based SCCs analogous to calix[4]arenes and the second Tc-containing metallomacrocycles. The results enable the design of unique *fac*-$[Tc(CO)_3]^+$ core-based supramolecules and extend the entry into the field of supramolecules. In the future, the suitable design of *fac*-$[Tc(CO)_3]^+$ core-based supramolecules may find potential utility in the medicinal fields due to the combined properties of the technetium core and guest encapsulation properties of the macrocyclic cavity.

4.6 References

1. Alberto, R.; Schibli, R.; Waibel, R.; Abram, U.; Schubiger, A. P. Basic aqueous chemistry of $[M(OH_2)_3(CO)_3]^+$ (M=Re, Tc) directed towards radiopharmaceutical application. *Coord. Chem. Rev*. **1999**, *190-192*, 901-919. (b) Alberto, R.; Schibli, R.; Egli, A.; Schubiger, P. A.; Abram, U.; Kaden, T. A. A Novel Organometallic Aqua Complex of Technetium for the Labeling of Biomolecules: Synthesis of $[^{99m}Tc(OH_2)_3(CO)_3]^+$ from $[^{99m}TcO_4]^-$ in Aqueous Solution and Its Reaction with a Bifunctional Ligand. *J. Am. Chem. Soc.* **1998**, *120*, 7987-7988. (c) Waibel, R.; Alberto, R.; Willuda, J.; Finnern, R.; Schibli, R.; Stichelberger, A.; Egli, A.; Abram, U.; Mach, J. – P.; Plückthun, A.; Schubiger, P. A. Stable one-step technetium-99m labeling of His-tagged recombinant proteins with a novel Tc(I)–carbonyl complex. *Nature Biotechnol*. **1999**, *17*, 897-901.
2. Abram, U.; Alberto, R. Technetium and rhenium: coordination chemistry and nuclear medical applications. *J. Braz. Chem. Soc.* **2006**, *17*, 1486-1500. (b) Morais, G. R.; Paulo, A.; Santos, I. Organometallic Complexes for SPECT Imaging and/or Radionuclide Therapy. *Organometallics* **2012**, *31*, 5693-5714. (c) Dilworth, J. R.; Parrott, S. The biomedical chemistry of technetium and rhenium. *J. Chem. Soc. Rev.* **1998**, *27*, 43-55. (d) Makris, G.; Bandari, R. P.; Kuchuk, M.; Jurisson, S. S.; Smith, C. J.; Hennkens, H. M. Development and Preclinical Evaluation of ^{99m}Tc- and ^{186}Re-Labeled NOTA and

NODAGA Bioconjugates Demonstrating Matched Pair Targeting of GRPR-Expressing Tumors. *Mol. Imaging Biol.* **2021**, *23*, 52-61. (e) Papagiannopoulou, D. Technetium-99m radiochemistry for pharmaceutical applications. *J. Labelled Comp. Radiopharm.* **2017**, *60*, 502-520.

3. Morais, M.; Paulo, A.; Gano, L.; Santos, I.; Correia, J. D. G. Target-specific $Tc(CO)_3$-complexes for *in vivo* imaging *J. Organomet. Chem.* **2013**, *744*, 125-139.
4. Alberto, R. The "Carbonyl Story" and Beyond; Experiences, Lessons and Implications. *ChemMedChem*. **2012**, *16*, 84-91
5. Gasser, G.; Metzler Nolte, N. The potential of organometallic complexes in medicinal chemistry. *Cur. Opinion Chem. Biol*. **2012**, *16*, 84-91.
6. Schibli, R.; Schwarzbach, R.; Alberto, R.; Ortner, K.; Schmalle, H.; Dumas, C.; Egli, A.; Schubiger, P. A. Steps toward High Specific Activity Labeling of Biomolecules for Therapeutic Application: Preparation of Precursor $[^{188}Re(H_2O)_3(CO)_3]^+$ and Synthesis of Tailor-Made Bifunctional Ligand Systems. *Bioconjug. Chem*. **2002**, *13*, 750-756.
7. Bhattachrayya, S.; Dixon, M. Metallic radionuclides in the development of diagnostic and therapeutic radiopharmaceuticals. *Dalton Trans.* **2011**, *40*, 6112-6128.
8. Figueiredo, D.; Fernandes, C.; Silva, F.; Palma, E.; Raposinho, P.; Belchior, A.; Vaz, P.; Paulo, A. Synthesis and Biological Evaluation of ^{99m}Tc(I) Tricarbonyl Complexes Dual-Targeted at Tumoral Mitochondria. *Molecules* **2021**, *26*, 441.
9. Argibay-Otero, S.; Gano, L.; Fernandes, C.; Paulo, A.; Carballo, R.; Vázquez-López, E. M. Chemical and biological studies of Re(I)/Tc(I) thiosemicarbazonate complexes relevant for the design of radiopharmaceuticals. *J. Inorg. Biochem*. **2020**, *203*, 110917.
10. Paparidis, G.; Akrivou, M.; Tsachouridou, V.; Shegani, A.; Vizirianakis, I. S.; Pirmettis, I.; Papadopoulos, M. S.; Papagiannopoulou, D. Synthesis and evaluation of ^{99m}Tc/Re-tricarbonyl complexes of the triphenylphosphonium cation for mitochondrial targeting *Nucl. Med. Biol.* **2018**, *57*, 34-41.
11. Day, A. H.; Domarkas, J.; Nigam, S.; Renard, I.; Cawthorne, C.; Burke, B. P.; Bahra, G. S.; Oyston, P. C. F.; Fallis, I. A.; Archibald, S. A.; Pope, S. J. Towards dual SPECT/optical bioimaging with a mitochondrial targeting, ^{99m}Tc(I) radiolabelled 1,8-naphthalimide conjugate. *Dalton Trans*. **2020**, *49*, 511-523.
12. Kasten, B. B.; Ma, X.; Cheng, K.; Bu, L.; Slocumb, W. S.; Hayes, T. R.; Trabue, S.; Cheng. Z.; Benny, P. D. Isothiocyanate-Functionalized Bifunctional Chelates and *fac*-$[M^I(CO)_3]^+$ (M = Re, ^{99m}Tc) Complexes for Targeting uPAR in Prostate Cancer. *Bioconjug. Chem*. **2016**, *27*, 130-142.

13. Imstepf, S.; Pierroz, V.; Raposinho, P.; Felber, M.; Fox, T.; Fernandes, C.; Gasser, G.; Santos, I.; Alberto, R. Towards ^{99m}Tc-based imaging agents with effective doxorubicin mimetics: a molecular and cellular study. *Dalton Trans*. **2016**, *45*, 13025-13033.
14. Yazdani, A.; Janzen, N.; Czorny, S.; Valliant, J. F. Technetium(I) Complexes of Bathophenanthrolinedisulfonic Acid. *Inorg. Chem*. **2017**, *56*, 2958-2965.
15. Pereiras-Gabián, G.; Vázquez-López, E. M.; Braband, H.; Abram, U. Mono- and Dinuclear Tricarbonyltechnetium(I) Complexes with Thiosemicarbazones. *Inorg. Chem.* **2005**, *44*, 834-836.
16. Saucedo Anaya, S. A.; Hagenbach, A.; Abram, U. Tricarbonylrhenium(I) and -technetium(I) complexes with bis(2-pyridyl)phenylphosphine and tris(2-pyridyl)phosphine. *Polyhedron* **2008**, *27*, 3587-3592.
17. (a) Lorenz, B.; Findeisen, M.; Olk, B.; Schmidt, K. Technetium(I)-Komplexe $Tc(CO)_3BrL_2$ (L = Phosphine, Pyridinderivate, Isocyanide). *Z. Anorg. Allg. Chem*. **1988**, *566*, 160-168. (b) Li, B.; Hildebrandt, S.; Hagenbach, A.; Abram, U. Tricarbonylrhenium(I) and -technetium(I) Complexes with Tris(1,2,3-triazolyl)phosphine Oxides. *Z. Anorg. Allg. Chem*. **2021**, *647*, 1070-1076. (c) Mikhalev, V. A. ^{99}Tc NMR Spectroscopy, *Radiochemistry* **2005**, *47*, 319−333.
18. Coogan, M. P.; Doyle, R. P.; Valliant, J. F.; Babich, J. W.; Zubieta. J. Single amino acid chelate complexes of the $M(CO)_3^+$ core for correlating fluorescence and radioimaging studies (M = ^{99m}Tc or Re). *J. Labelled Comp. Radiopharm*. **2014**, *57*, 255-261.
19. (a) Bauer, E. B.; Haase, A. A.; Reich, R. M.; Crans, D. C.; Kühn, F. E. Organometallic and coordination rhenium compounds and their potential in cancer therapy. *Coord. Chem. Rev.* **2019**, *393*, 79-117. (b) Haase, A. A.; Bauer, E. B.; Kühn, F. E.; Crans, D. C. Speciation and toxicity of rhenium salts, organometallics and coordination complexes. *Coord. Chem. Rev*. **2019**, *394*, 135-161.
20. (a) Ramakrishna, B.; Nagarajaprakash, R.; Veena, V.; Sakthivel, N.; Manimaran. B. Self-assembly of oxamidato bridged ester functionalised dirhenium metallastirrups: synthesis, characterisation and cytotoxicity studies. *Dalton Trans.* **2015**, *44*, 17629-17638. (b) Orsa, D. K.; Haynes, G. K.; Pramanik, S. K.; Iwunze, M. O.; Greco, G. E.; Krause, J. A.; Ho, D.; Williams, A. L.; Hill, D. A.; Mandal, S. K. Synthesis, characterization, and fluorescence and cytotoxicity studies of a tetrarhenium molecular rectangle. *Inorg. Chem. Commun.* **2007**, *10*, 821-824. (c) Gupta, D.; Sathiyendiran, M. Rhenium-Carbonyl-Based Supramolecular Coordination Complexes: Synthesis, Structure and Properties. *ChemistrySelect* **2018**, *3*, 7439-7458 and references cited therein (d) Balasingham, R. G.;

Thorp-Greenwood, F. L.; Williams, C. F.; Coogan, M. P.; Pope, S. J. A. Biologically Compatible, Phosphorescent Dimetallic Rhenium Complexes Linked through Functionalized Alkyl Chains: Syntheses, Spectroscopic Properties, and Applications in Imaging Microscopy. *Inorg. Chem*. **2012**, *51*, 1419−1426. (e) Gupta, D.; Singh, V.; Hohloch, S.; Sathiyendiran, M.; Tedin, K.; Sarkar, B. Utilizing a series of *fac*-$Re(CO)_3$ core based quinonoid containing complexes for photophysical and cell imaging studies. *Polyhedron* **2015**, *100*, 243-250.

21. (a) Dinolfo, P. H.; Hupp, J. T. Supramolecular coordination chemistry and functional microporous molecular materials. *Chem. Mater*. **2001**, *13*, 3113–3125. (b) Rohacova, J.; Ishitani, O. Photofunctional Multinuclear Rhenium(I) diimine Carbonyl Complexes. *Dalton Trans*. **2017**, *46*, 8899–8919. (c) Thanasekaran, P.; Lee, C. C.; Lu, K. L. One-Step Orthogonal-Bonding Approach to the Self-Assembly of Neutral Rhenium-Based Metallacycles: Synthesis, Structures, Photophysics, and Sensing Applications. *Acc. Chem. Res*. **2012**, *45*, 1403–1418. (d) Kumar, A.; Sun, S. S.; Lees, A. J. Directed Assembly Metallocyclic Supramolecular Systems for Molecular Recognition and Chemical Sensing. *Coord. Chem. Rev*. **2008**, *252*, 922–939.
22. Bhol, M.; Shankar, B.; Sathiyendiran, M. Rhenium(I) based irregular pentagonal-shaped metallacavitands. Dalton *Trans*. **2018**, *47*, 4794-4500.
23. Davison, A.; Trop, H. S.; de Pamphilis, D. V.; Jones, A. G.; Thomas, R. W.; Jurisson, S. S. Tetrabutylammonium Tetrachlorooxotechnetate(V). *Inorg. Synth*. **2007**, *21*, 160-162.
24. Hildebrandt, S. $(NBu_4)[Tc_2(\mu\text{-}Cl)_3(CO)_6]$ als Startverbindung für Technetiumtricarbonylkomplexe. PhD Thesis, FU Berlin, **2018.**
25. Angelici, J. R. REAGENTS FOR TRANSITION METAL COMPLEX AND ORGANOMETALLIC SYNTHESES. *Inorg. Synth*. **1990**, *28*, 162–163.
26. Marker, S. C.; MacMillan, S. N.; Zipfel, W. R.; Li, Z.; Ford, P. C.; Wilson, J. J. Photoactivated in Vitro Anticancer Activity of Rhenium(I) Tricarbonyl Complexes Bearing Water-Soluble PhosphinesInorg. *Chem*. **2018**, *57*, 1311– 1331.
27. Grobler, I.; Smith, V. J.; Bhatt, P. M.; Herber, S. A.; Barbour, L. J. Tunable Anisotropic Thermal Expansion of a Porous Zinc(II) Metal–Organic Framework. *J. Am. Chem. Soc.* **2013**, *135*, 6411– 6414.
28. Zhao, X. -L.; Sun, D.; Hu, T. -P.; Yuan, S.; Gu, L. -C.; Cong, H. -J.; Hea, H. –Y.; Sun, D. –F. Phase transfer catalyst supported, room-temperature biphasic synthesis:a facile approach to the synthesis of coordination polymers. *Dalton Trans*. **2012**, *41*, 4320– 4323.

29. Chahen, L.; Therrien, B.; Suss-Fink, G. Square-planar dichloro palladium complexes with trans-configurated phosphine ligands avoiding ortho-metallation: Ligand design, complex synthesis, molecular structure and catalytic potential for Suzuki cross-coupling reactions. *J. Organomet. Chem*. **2006**, *691*, 4257– 4264.
30. (a) Sheldrick, G. M. A short history of SHELX. *Acta Crystallogr., Sect. A: Found. Crystallogr.* **2008**, *64*, 112– 122. (b) Sheldrick, G. M. Crystal structure refinement with SHELXL. *Acta Crystallogr., Sect. C: Struct. Chem*. **2015**, *71*, 3–8.
31. (a) Jr, A. V. Ultrafast Excited-State Processes in Re(I) Carbonyl-Diimine Complexes: From Excitation to Photochemistry. *Top. Organomet. Chem.* **2010**, *29*, 73–114. (b) Giordano, P. J.; Wrighton, M. S. The Nature of the Lowest Excited State in *fac*-Tricarbonylhalobis(4-phenylpyridine) rhenium (I) and *fac*- Tricarbonylhalobis(4, 4'-bipyridine) rhenium(I) : Emissive Organometallic Complexes in Fluid Solution *J. Am. Chem. Soc*. **1979**, *101*, 2888 – 2897.
32. (a) Frischmann, P. D.; MacLachlan, M. J. Metallocavitands: an emerging class of functional multimetallic host molecules. *Chem. Soc. Rev*. **2013**, *42*, 871-890. (b) Lippert, B.; Sanz Miguel, P. J. Metallatriangles and metallasquares: the diversity behind structurally characterized examples and the crucial role of ligand symmetry. *Chem. Soc. Rev*. **2011**, *40*, 4475-4487. (c) Kulesza, J.; Barros, B. S.; Junior, S. A. Organic–inorganic hybrid materials: Metallacalixarenes. Synthesis and applications. *Coord. Chem. Rev.* **2013**, *257*, 2192-2212. (d) Díaz-Ramírez, M. L.; Huggins, H.; Donnadieu, B.; Lopez, N.; Muñoz-Hernández, M. -Á. The Quest for Large Group 13 Metallacalixarenes Based on Benzymidazolyl Ligands and Al and Ga Alkyls. *Eur. J. Inorg. Chem*. **2021**, 3896-3902 (e) Karges, J.; Seo, H.; M. Cohen, S. Synthesis of tetranuclear rhenium(I) tricarbonyl metallacycles. *Dalton Trans*. **2021**, *50*, 16147- 16155.
33. (a) Benesi, H. A.; Hildebrand, J. H. A Spectrophotometric Investigation of the Interaction of Iodine with Aromatic Hydrocarbons. *J. Am. Chem. Soc*. **1949**, *71*, 2703 -2707. (b) Murakami, Y.; Kikuchi, J. I.; Suzuki, M.; Matsuura, T. Syntheses of macrocyclic enzyme models. Part 6. Preparation and guest-binding behaviour of octopus cyclophanes. *J. Chem. Soc., Perkin Trans.1* **1988**, 1289 -1299.
34. (a) Sathiyendiran, M.; Tsai, C. C.; Thanasekaran, P.; Luo, T. T.; Yang, C. I.; Lee, C. H.; Peng, S. M. Lu, K. L. Organometallic Calixarenes: Syceelike Tetrarhenium(I) Cavitands with Tunable Size, Color, Functionality, and Coin–Slot Complexation. *Chem. Eur. J.* **2011**, *17*, 3343 – 3346. (b) Lakshmi, S.K.; Corinne, L. D.; Gibb, B. C.; Ramamurthy, V.

A Hydrophobic Nanocapsule Controls the Photophysics of Aromatic Molecules by Suppressing Their Favored Solution Pathways. *J. Am. Chem. Soc.* **2005**, *127*, 3674-3675.

35. Manimaran, B.; Lai, L. J.; Thanasekaran, P.; Wu, J. Y.; Liao, R. T.; Tseng, T. W.; Liu, Y. H.; Lee, G. H.; Peng, S. M.; Lu, K. L. CH···π Interaction for Rhenium-Based Rectangles: An Interaction That Is Rarely Designed into a Host−Guest Pair. *Inorg. Chem*. **2006**, *45*, 8070-8077.

Chapter 5

Self-Assembly and Photophysical Properties of Rheniumtricarbonyl-Based Helicates and Mesocates

Abstract

The self-assembly of five rheniumtricarbonyl core based supramolecular coordination complexes (SCCs), *fac*-[$Re(CO)_3(\mu\text{-}L)(\mu\text{-}L')Re(CO)_3$] (**1**–**5**) was assembled using $Re_2(CO)_{10}$, rigid/flexible bis-chelating ligand (HO∩N–Ph–N∩OH (L^1) / HO∩N–CH_2–mesitylene–CH_2–N∩OH (L^2), where HO∩N = 2-hydroxyphenylbenzimidazolyl), and flexible ditopic N donor (L^3 = bis(3-((1H-benzoimidazol-1-yl)methyl)-2,4,6-trimethylphenyl)methane, L^4 = bis(3-((1H-naphtho[2,3-d]imidazol-1-yl)methyl)-2,4,6-trimethylphenyl)methane, L^5 = bis(4-(benzimidazol-1-ylmethyl)phenyl)methane, L^6 = bis(4-(naphtho[2,3-d]imidazol-1-ylmethyl)phenyl)methane) via a one-pot approach. The dinuclear SCCs adopt heteroleptic double stranded helical/meso-helical architectures in the solid-state. The supramolecular structures of the complexes closely remain in the solution based on the ^1H NMR and ESI-mass analysis. The photophysical properties of the complexes were studied both in solution and solid state. All the supramolecules display emission both in solution and solid state.

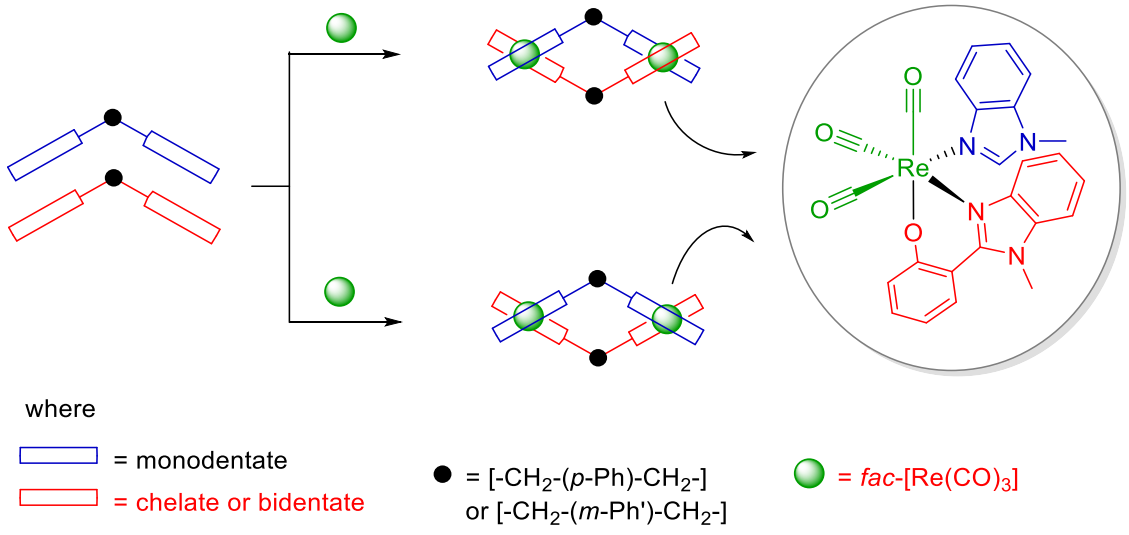

5.1. Introduction

The design and synthesis of discrete metallosupramolecules such as helicates, mesocates, 2D and 3D metallocycles with/without cavities and cages have attracted much attention not only due to their potential applications in various fields, but also for providing hitherto unknown aesthetically pleasing simple to complex molecular architectures via simple combinations of pre-designed ligands and suitable metal ions or complex motifs.[1-15] Among the various metal ion sources, $Re_2(CO)_{10}$ and $[Re(CO)_5X]$ where X = Cl or Br are two of the versatile organometallic complexes used as pre-designed metal sources for assembling various types of *fac*-$[Re(CO)_3]$- and *fac*–$[Re(CO)_3X]$-cores based supramolecules.[7-13] Due to their intrinsic properties such as kinetic stability and phosphorescence and their importance in host-guest chemistry, catalysis, photosensitizers in hydrogen evolution, carbon dioxide reduction, bioimaging, and anticancer agents, the research are being directed towards making new functional rheniumcarbonyl-based metallosupramolecules.[7-13] Although error-free synthetic principles are currently available to make desired rheniumcarbonyl-core based molecular squares, rectangles, prisms, bowls, spheroids and other cavity containing metallomacrocycles,[8a-b, 9, 10a, 11-15] the synthetic approaches for self-assembling mononuclear-, dinuclear-, trinuclear-, and polynuclear-helicates are scarce.[13] However, helicates based on other metal ions and organic ligand strands are well-known and prevalent.[1-4] To the best of our knowledge, only a handful of *fac*–$[Re(CO)_3]$-core based helicates are known till now.[13]

We first demonstrated the combination of two types of flexible ligands i.e., neutral flexible bis(monodentate) ligand N-donor (pbenzbix) and bis(bidentate) NO donor (H_2–pBC), incorporating a flexible *p*-xylene motif (–CH_2–Ph–CH_2–) between two donors with $Re_2(CO)_{10}$ for assembling dinuclear heteroleptic helicate (Scheme 5.1 and Figure 5.1).[13a] The spacer p-phenylene motif in both the ligands (pbenzbix and H_2–pBC) plays an important role in adopting helical structure. This was evident when the spacer motif in the ligand strands was changed to *m*-xylene motif which results in the mesohelical structure.[13a] Though the above design principle can be applied to generate *fac*–$[Re(CO)_3]$ core-based dinuclear helicates with similar types of ligands, many examples have to be prepared to validate the synthetic approach. We decided modulating the length of the spacer motif from "phenylene or mesitylene" spacer by longer and more flexible spacer unit such as biphenylmethane (–Ph–CH_2–Ph–) or bimesitylmethane (–mesitylene–CH_2–mesitylene–) motif in the neutral

bi(dentate) ligand and combining with semirigid bis(bidentate) ligand H_2–mBC ((H_2–mBC = *p*-phenylene(benzimidazolylphenol)$_2$))or rigid bis(bidentate) ligand (H_2–RBC = *p*-phenylene(benzimidazolylphenol)$_2$) and $Re_2(CO)_{10}$ in order explore the helicate architecture. Ligands **1-6** have ability to adopt helical twisting along Re···Re axis due to the rotatable nature of terminal donors with respect to *m*- (or) *p*-phenyl spacer.

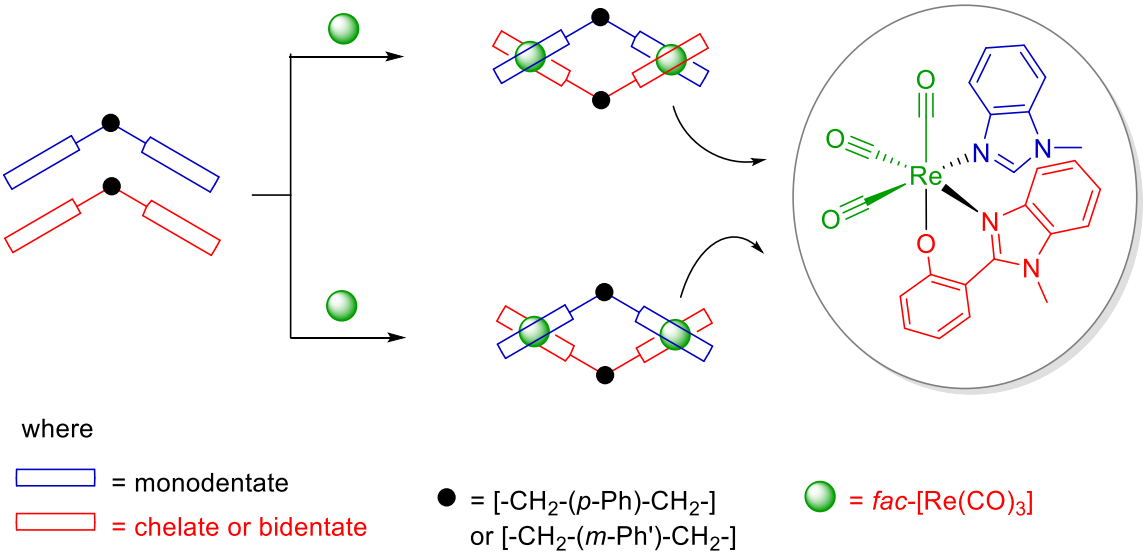

Scheme 5.1. Cartoon Representation of Self-Assembly of *fac*-Re(CO)$_3$ Core–Based Neutral Unsaturated Heteroleptic Dinuclear Double-Stranded Helicate and Mesocate.

In this chapter, two new *fac*–[Re(CO)$_3$]core- based helicates (**1-2**) and three mesocates (**3-5**) are reported. The metallosupramolecules were characterized by ATR-IR, ESI-MS, 1D and 2D NMR spectroscopic methods. The molecular structures of the metallosupramolecules were confirmed by single-crystal X-ray analysis. The photophysical properties of the complexes were studied in both solution and solid state. All the supramolecules display emission both in solution and solid state.

5.2. Experimental Section

5.2.1. Materials

All starting materials and products were found to be stable towards moisture and air, and nonspecific precautions were taken to rigorously exclude air when solvothermal methods were used. Starting materials such as $Re_2(CO)_{10}$, 1,4-dibromobenzene, CuI, Cs_2CO_3, 1,10-

phenanthroline, H_3PO_4, HBr in acetic acid 33%, paraformaldehyde, acetic acid glacial, formic acid, benzimidazole, KOH and NaH were procured from commercial sources and used as received. Then 2-(2-Hydroxyphenyl)-1H-benzimidazole,[16] naphtho[2,3-d]imidazole,[17] 2,4-bis(bromomethyl)-1,3,5-trimethylbenzene,[18] bis-(mesityl)methane,[19] and bis(3-(bromomethyl)-2,4,6-trimethylphenyl)methane [20] were synthesized as described by literature methods. Bis(3-((1H-benzoimidazol-1-yl)methyl)-2,4,6-trimethylphenyl)methane (L^3),[21] bis(3-((1H-naphtho[2,3-d]imidazol-1-yl)methyl)-2,4,6-trimethylphenyl)methane (L^4),[21] bis(4-(benzimidazol-1-ylmethyl)phenyl)methane (L^5),[22] bis(4-(naphtho[2,3-d]imidazol-1-ylmethyl)phenyl)methane (L^6),[22] 1,4-Bis(2-(2-hydroxyphenyl)benzimidazole-1-ylmethyl)benzene (H_2-pBC),[23] 1,3-Bis(2-(2-hydroxyphenyl)benzimidazole-1-ylmethyl)-2,4,6-trimethibenzene (H_2-mBC)[13a] were synthesized from previously reported methods. Toluene, hexane and THF were purified and distilled by conventional procedure. LR grade solvents like DMF, mesitylene and HPLC acetone were obtained from Sigma Aldrich and used directly. Conventional synthetic methods were routinely carried out in room atmosphere.

5.2.2 Physical Measurement

A Bruker ALPHA II FTIR Spectrometer was used to record the FT -IR spectra. ^{1}H NMR spectra were obtained by using Bruker AvanceIII 500 and 400 spectrometers. All NMR spectra were recorded using DMSO-d_6 as solvent. HR-MS spectra were recorded on a Bruker maXis mass spectrometer. The UV-Vis spectra were performed on a Shimadzu UV-VIS-NIR (UV-3600) spectrophotometer. A JASCO (FP-8500) spectrofluorometer was used to record emission spectra.

5.2.3 X-ray Crystallography.

A single crystal X-ray structural study of **1**, **2**, **3** and **5** was performed on a Rigaku Oxford XtaLAB Synergy or a Bruker D8 Quest diffractometer. Data were collected at low temperature or room temperature using Mo Kα radiation [λ(Mo Kα) = 0.71073 Å]. The structure was solved by direct methods using SHELXS-97[24] and refined by full matrix least squares with SHELXL-2018/[24b,c] All non-hydrogen atoms were refined anisotropically. The remaining hydrogen atoms were placed in geometrically constrained positions and refined with isotropic temperature factors.

5.2.4 Synthesis of Complexes

Synthesis of [{(CO)$_3$Re(μ−pBC)Re(CO)$_3$}(μ−L^3)] (1).

A mixture of $Re_2(CO)_{10}$ (50 mg, 0.0766 mmol), H_2-pBC (38 mg, 0.0766 mmol), L^3 (40 mg, 0.0766 mmol), and toluene (6 mL) in a Teflon flask was placed in a steel bomb. The bomb was kept in an oven, maintained at 160 °C for 48 h and then cooled to 30 °C. Light gray powder with yellow colour crystals was obtained. The product was filtered, washed with distilled hexane and air-dried. Yield: 41% (48 mg). ^{1}H NMR (500 MHz, DMSO-d_6): δ 8.50 (s, 2H, Ph^o), 8.29 (d, J_{HH} = 8.3 Hz, 2H, H^4), 7.95 (d, J_{HH} = 8.2 Hz, 2H, H^7), 7.75 (t, J_{HH} = 7.9 Hz, 2H, H^6), 7.63 (t, J_{HH} = 7.8 Hz, 2H, H^5), 7.39 (t, J_{HH} = 7.6 Hz 2H, H^b), 7.29 (d, J_{HH} = 8.1 Hz, 2H, H^a), 7.18-7.13 (m, 6H, H$^{c\text{-}d}$, H^C), 7.04 (s, 2H, H^9), 6.91 (d, J_{HH} = 8.0 Hz, 2H, H^A), 6.78 (d, J_{HH} = 8.2 Hz, 2H, H^D), 6.52 (t, J_{HH} = 7.7, Hz, 2H, H^B), 5.61(s, 2H, H^2), 5.50 (s, 2H, Ph^i), 5.21 (dd, J_{HH} = 14.7 Hz, 4H, H^8, -CH_2-), 3.87 (s, 2H, H^{13}, -CH_2-), 2.32 (s, 6H, -CH_3), 0.88 (s, 6H, -CH_3), and 0.69 (s, 6H, -CH_3). ESI-HR-MS. Calcd for $C_{73}H_{56}N_8O_8Re_2$ $[M+H]^+$: *m/z* 1547.3414 Found: m/z 1547.3038. FT-IR (cm^{-1}): 2012 (s), 1888 (s) and 1858 (s).

Synthesis of [{(CO)$_3$Re(μ−pBC)Re(CO)$_3$}(μ−L^4)] (2).

A mixture of Re_2 $(CO)_{10}$ (50 mg, 0.0766 mmol), H_2-pBC (38 mg, 0.0766 mmol), L^4 (47 mg, 0.0766 mmol), and toluene (6 mL) in a Teflon flask was placed in a steel bomb. The bomb was kept in an oven, maintained at 160 °C for 48 h and then cooled to 30 °C. Dark gray powder with dark brown colour crystals was obtained. The product was filtered, washed with distilled hexane and air-dried. Yield: 56% (70 mg). ^{1}H NMR (500 MHz, DMSO-d_6): δ 8.80 (s, 2H, H^4), 8.52 (s, 4H, H^4, Ph^o), 8.37- 8.35 (m, 2H, H^5), 8.20-8.18 (m, 2H, H^8), 7.67- 7.65 (m, 4H, H^{6,7}), 7.37 (pseudo t, J_{HH} = 7. 7 Hz, 2H, H^b), 7.31-7.29 (m, 4H, H$^{a,\ d}$), 7.16-7.09 (m, 6H, H^{11,C}, H^c), 6.93 (d, J_{HH} = 7.9 Hz, 2H, H^A), 6.81 (d, J_{HH} = 8.3 Hz, 2H, H^D) 6.54 (t, J_{HH} = 7.6 Hz, 2H, H^B), 5.65 (s, 2H, H^2), 5.53 (s, 2H, Ph^i), 5.30 (dd, J_{HH} = 14.5 Hz, 4H, H^{10}, -CH_2-), 3.90 (s, 2H, H^{15}, -CH_2-), 2.36 (s, 6H, -CH_3), 0.92 (s, 6H, -CH_3), and 0.72 (s, 6H, -CH_3). ESI-HR-MS. Calcd for $C_{81}H_{60}N_8O_8Re_2$ $[M+H]^+$: *m/z* 1647.8410 Found: m/z 1647.3723. FT-IR (cm^{-1}): 2011 (s), 1890 (s) and c 1862(s).

Synthesis of [{(CO)$_3$Re(μ−pBC)Re(CO)$_3$}(μ−L^6)] (3).

A mixture of Re_2 $(CO)_{10}$ (100 mg, 0.1532 mmol), H_2-pBC (75.77 mg, 0.1532 mmol), L^6 (80.99 mg, 0.1532 mmol), and toluene (12 mL) in a Teflon flask was placed in a steel bomb.

The bomb was kept in an oven, maintained at 160 °C for 48 h and then cooled to 30 °C. Light gray powder with brown crystals + yellow crystals was obtained. The product was filtered, washed with distilled hexane and air-dried. Yield: 65% (155 mg). ^{1}H NMR (400 MHz, DMSO-d_6): δ 8.85 (d, J_{HH} = 20 .7 Hz, 2H), 8.74 (s, 1H), 8.37 (s, 1H), 8.27-8.15 (m, 4H), 8.08-7.99 (m, 3H), 7.92 (d, J_{HH} = 7.4 Hz, 3H), 7.79 (s, 2H), 7.67 (s, 2H), 7.56- 7.45 (m, 8H), 7.06- 7.00 (m, 4H), 6.90- 6.75 (m, 6H), 6.62 (d, J_{HH} = 7.6 Hz, 2H), 6.43 (t, J_{HH} = 7.6 Hz, 1H), 6.30 (d, J_{HH} = 6.1 Hz, 2H), 6.17 (d, J_{HH} = 7.4 Hz, 1H), 5.53-5.31 (m, 4H, H^{10}, -CH_2-), and 3.58 (s, 2H, H^{15}, -CH_2-).ESI-HR-MS. Calcd for $C_{75}H_{48}N_8O_8Re_2$ $[M+H]^+$: *m/z* 1563.2788 Found: m/z 1563.2436. FT-IR (cm^{-1}): 2010 (s) and 1867 (s).

Synthesis of [{(CO)$_3$Re(μ−mBC)Re(CO)$_3$}(μ−L^5)] (4).

A mixture of $Re_2(CO)_{10}$ (50 mg, 0.0766 mmol), H_2-mBC (43 mg, 0.0766 mmol), L^5 (33 mg, 0.0766 mmol), and mesitylene:acetone (10 mL: 1 mL) in a Teflon flask was placed in a steel bomb. The bomb was kept in an oven, maintained at 160 °C for 48 h and then cooled to 30 °.The product was obtained as gray powder, filtered at hot conditions and washed with distilled hexane. Yield: 44% (55 mg). ^{1}H NMR (500 MHz, DMSO-d_6): δ 8.36 (s, 2H, H^2), 7.64-7.63 (m, 2H, H^7), 7.59 (d, J_{HH} = 8.0 Hz, 2H, H^D), 7.49-7.47 (m, 2H, H^4), 7.43-7.35 (m, 4H, H^{b,d}), 7.20- 7.09 (m, 14H, H$^{5\text{-}6,\ 9\text{-}12}$, H^c), 7.05 -7.01 (m, 2H, H^a), 6.94 (t, J_{HH} = 7.5 Hz, 2H, H^c), 6.90 (s, 1H, H^E), 6.85 (t, J_{HH} = 8.1 Hz, 2H, H^B), 6.50 (d, J_{HH} = 8.3 Hz, 2H, H^A), 5.41 (s, 4H, H^8, -CH_2-), 5.27 (s, 4H, H^F, -CH_2-), 3.83 (s, 2H, H^{13}, -CH_2-), 2.04 (s, 6H, -CH_3), 1.74 (s, 3H, -CH_3). ESI-HR-MS. Calcd for $C_{72}H_{54}N_8O_8Re_2$ $[M+H]^+$: *m/z* 1533.3263 Found: m/z 1533.2883. FT-IR (cm^{-1}): 2009 (s), 1892 (s) and 1861 (s).

Synthesis of [{(CO)$_3$Re(μ−mBC)Re(CO)$_3$}(μ−L^6)] (5).

A mixture of $Re_2(CO)_{10}$ (50 mg, 0.0766 mmol), H_2-mBC (43 mg, 0.0766 mmol), L^6 (41 mg, 0.0766 mmol), and mesitylene:acetone (10 mL: 0.5 mL) refluxed for 6 h in a round bottom flask. Compound 4 was obtained as gray powder. The product was filtered at hot conditions and washed with distilled hexane. Yield: 44% (55 mg). ^{1}H NMR (500 MHz, DMSO-d_6): δ 8.62 (s, 2H, H^4), 8.50 (s, 2H, H^9), 8.19 (s, 2H, H^2), 8.09-8.07 (m, 2H, H^{13}), 7.99- 7.97 (m, 2H, H^8), 7.95 (s, 2H, H^E), 7.89-7.87 (m, 2H, H^5), 7.60-7.58 (m, 2H, H^{14}), 7.42 (d, J_{HH} = 8.1 Hz, 4H, H^{a,d}), 7.36-7.34 (m, 4H, H^{6,7}), 7.26-7.19 (m, 10H, H^{11,A,C},H$^{b,\ c}$), 7.16- 7.12 (m, 6H, H^{12,B,D}), 5.70 (s, 4H, H^F), 5.50 (s, 4H, H^{10}, -CH_2-), 4.25-4.22 (m, 2H, H^{15}, -CH_2-), 2.28 (s, 3H, -CH_3), 2.07 (s, 3H, -CH_3), 1.21 (s, 3H, -CH_3).Crystals obtained from mesitylene and

acetone mixture *via* a solvothermal approach. ESI-HR-MS. Calcd for $C_{80}H_{58}N_8O_8Re_2$ $[M+H]^+$: *m/z* 1633.3571 Found: m/z 1633.3389. FT-IR (cm^{-1}): 2010 (s), 1894 (s) and 1869 (s).

5.3. Results and Discussion

5.3.1. *Synthesis and characterization of Helicates and Mesocates (1-5).*

Helicates **1** and **2** were self-assembled from $Re_2(CO)_{10}$, L^1 and L^3 or L^4 via a one-pot solvothermal approach (Scheme 5.2). Similarly, mesocates (**3**–**5**) were prepared from $Re_2(CO)_{10}$, L^1 or L^2, and L^5 or L^6. All the metallosupramolecules are air- and moisture-stable, and are completely soluble in DMSO. The ATR-IR spectra of **1**–**5** display three strong bands around 2012-1858 cm^{-1} of almost similar pattern which are the characteristic of *fac*-[$Re(CO)_3$] motif in an asymmetric coordination geometry.[13,25] The above IR data further indicate that the electronic environments around the rhenium centres in **1-5** are similar. The ESI-mass analysis of **1-5** showed signals that correspond to molecular ion peaks (m/z 1547.3039 for [**1** + H]$^+$; 1647.3723 for [**2** + H]$^+$; 1563.2499 for [**3** + H]$^+$; 1533.2883 for [**4** + H]$^+$;1633.3389 for [**5** + K]$^+$) with an experimental isotope pattern that matches the calculated values.

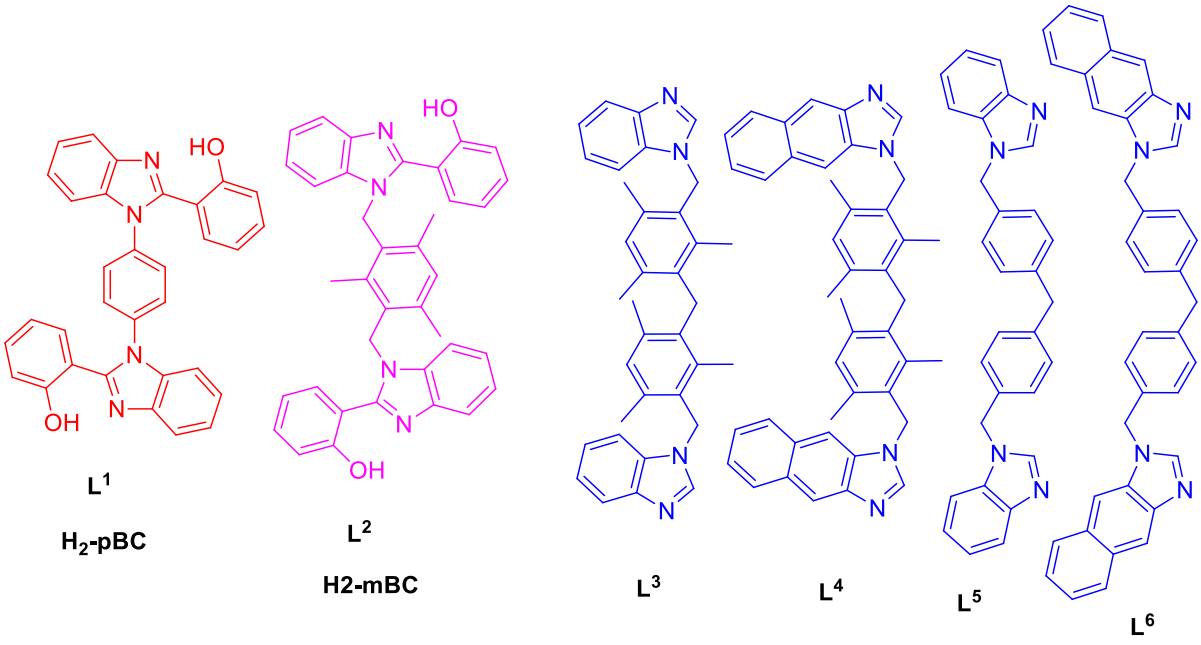

Figure 5.1. Ligands used in this work.

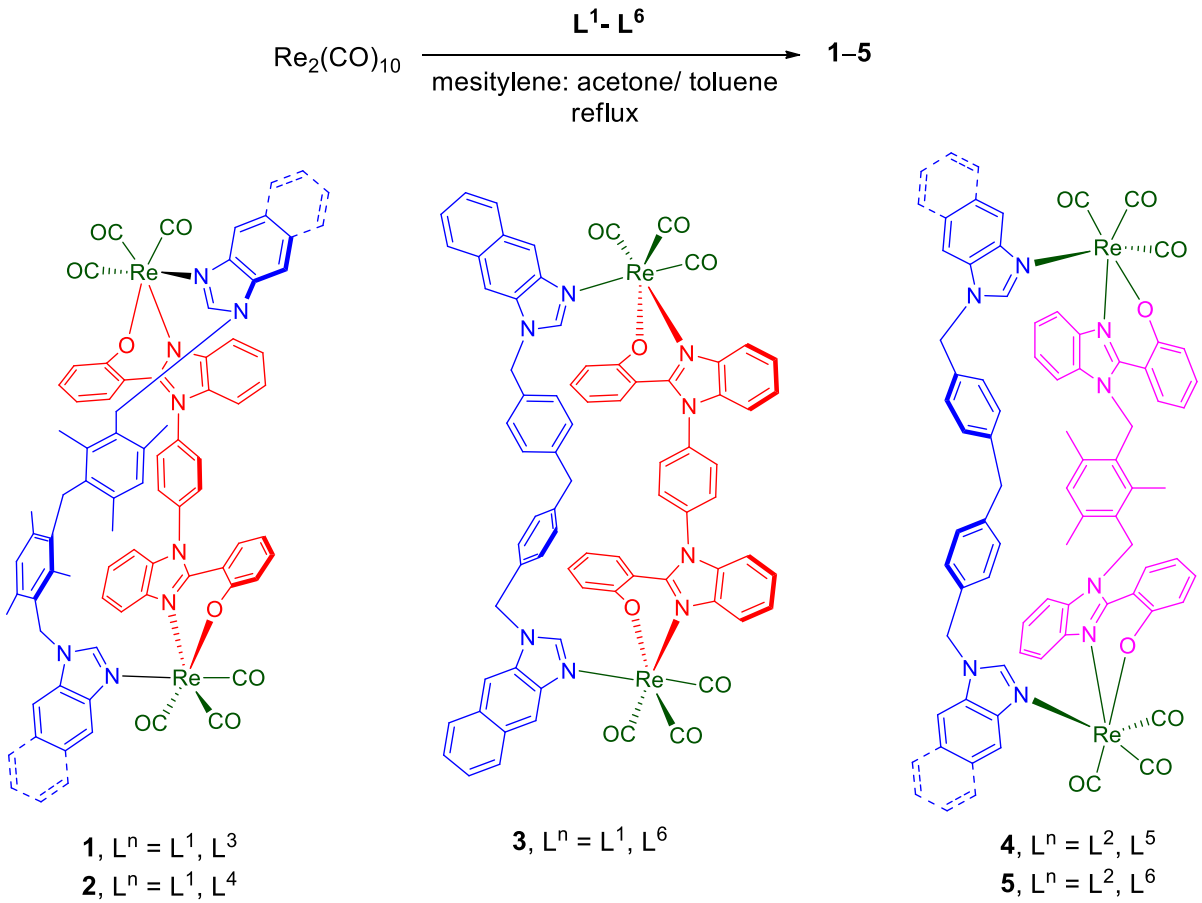

Scheme 5.2. Self-assembly of Helicates (1-2) and Mesocates (3-5).

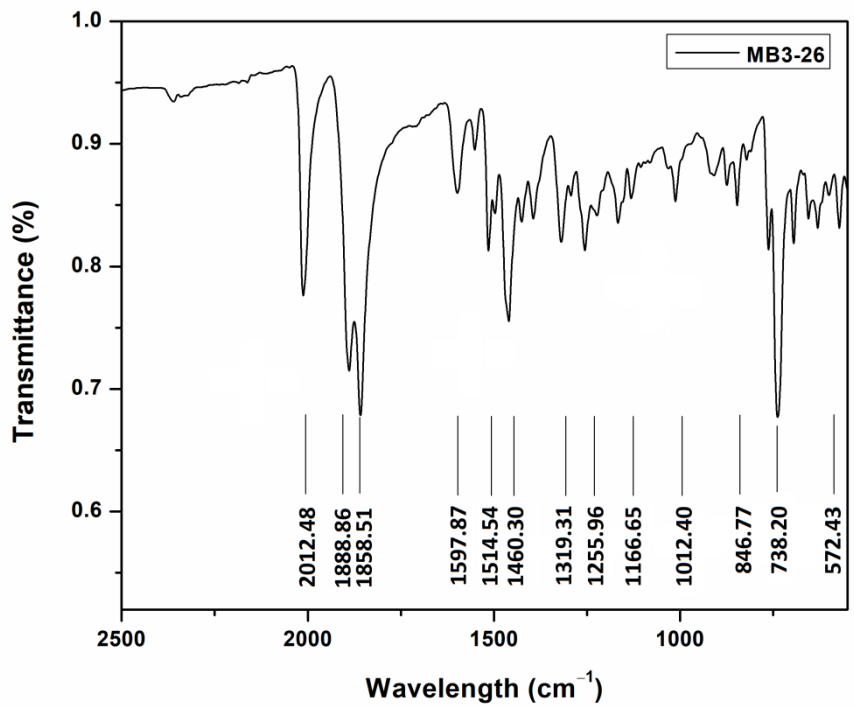

Figure 5.2. ATR- IR spectrum of **1**.

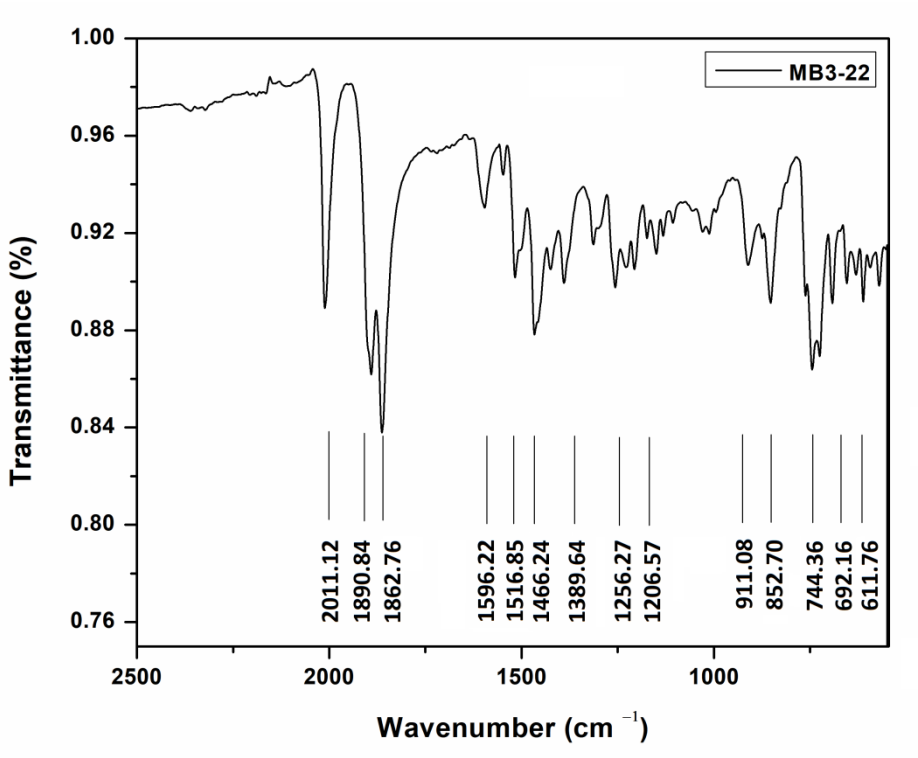

Figure 5.3. ATR- IR spectrum of **2**.

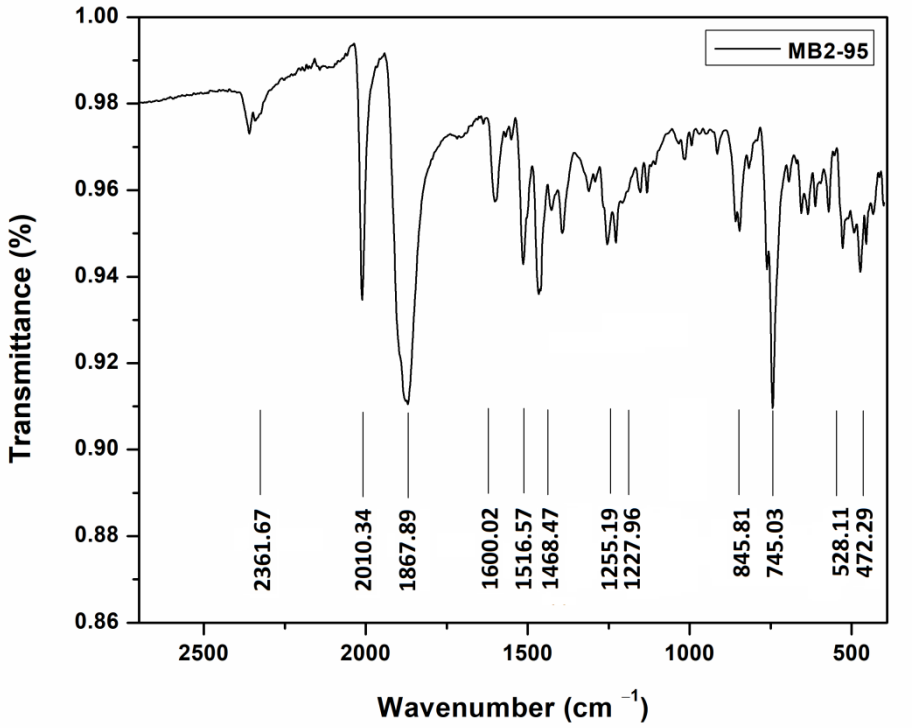

Figure 5.4. ATR- IR spectrum of **3.**

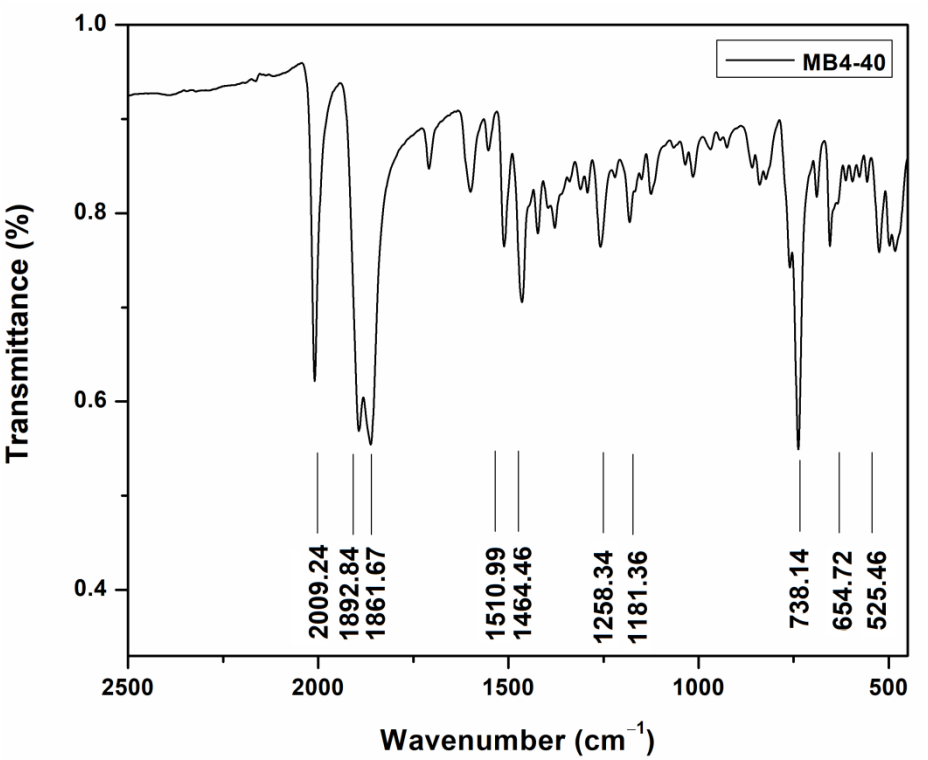

Figure 5.5. ATR- IR spectrum of **4.**

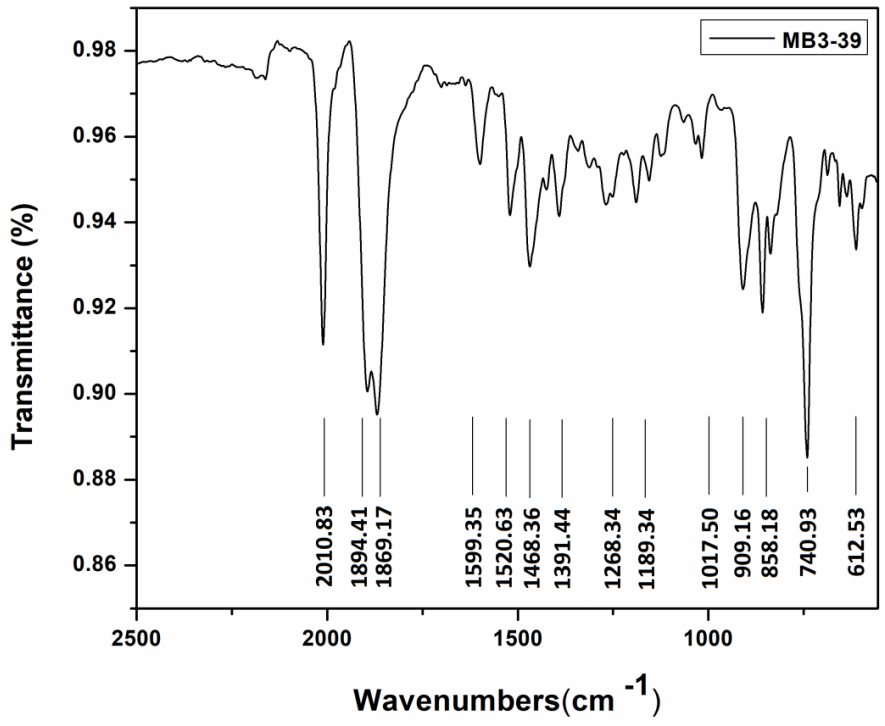

Figure 5.6. ATR- IR spectrum of **5**.

UOH -SCHOOL OF CHEMISTRY -HRMS

Analysis Info

Analysis Name	D:\Data\2019\PROF.MS\FEB\MB3-26.d	Acquisition Date	2/4/2019 3:36:28 PM
Method	tune_wide_Pos.m	Operator	UOH-Chemistry
Sample Name	MB3-26	Instrument	maXis 10138
Comment			

Acquisition Parameter

Source Type	ESI	Ion Polarity	Positive	Set Nebulizer	0.3 Bar
Focus	Not active	Set Capillary	3800 V	Set Dry Heater	180 €C
Scan Begin	700 m/z	Set End Plate Offset	-500 V	Set Dry Gas	4.0 l/min
Scan End	3500 m/z	Set Collision Cell RF	2500.0 Vpp	Set Divert Valve	Source

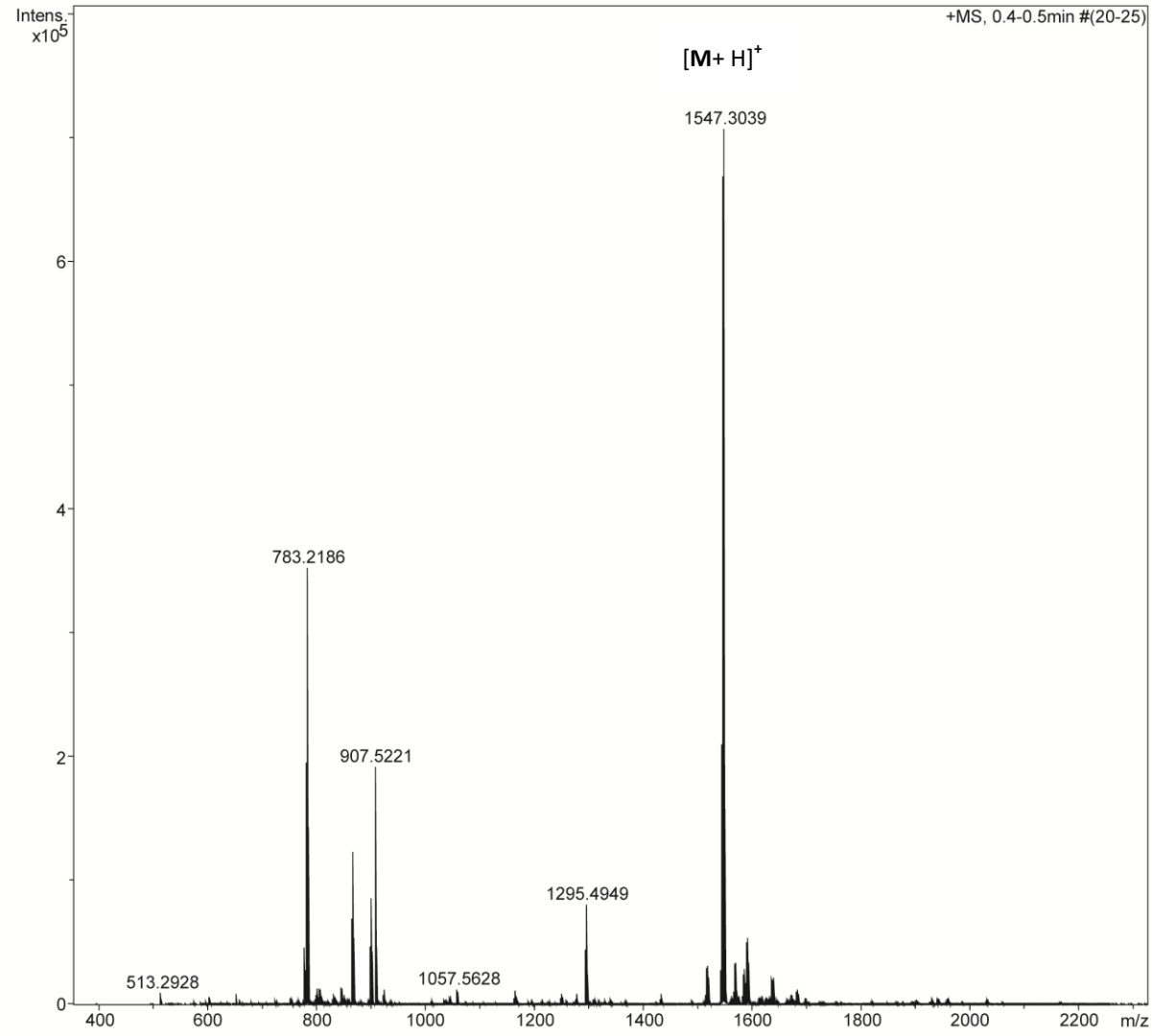

Bruker Compass DataAnalysis 4.0 printed: 2/5/2019 4:47:01 PM Page 1 of 1

Figure 5.7. ESI mass spectrum of **1** in positive ion mode.

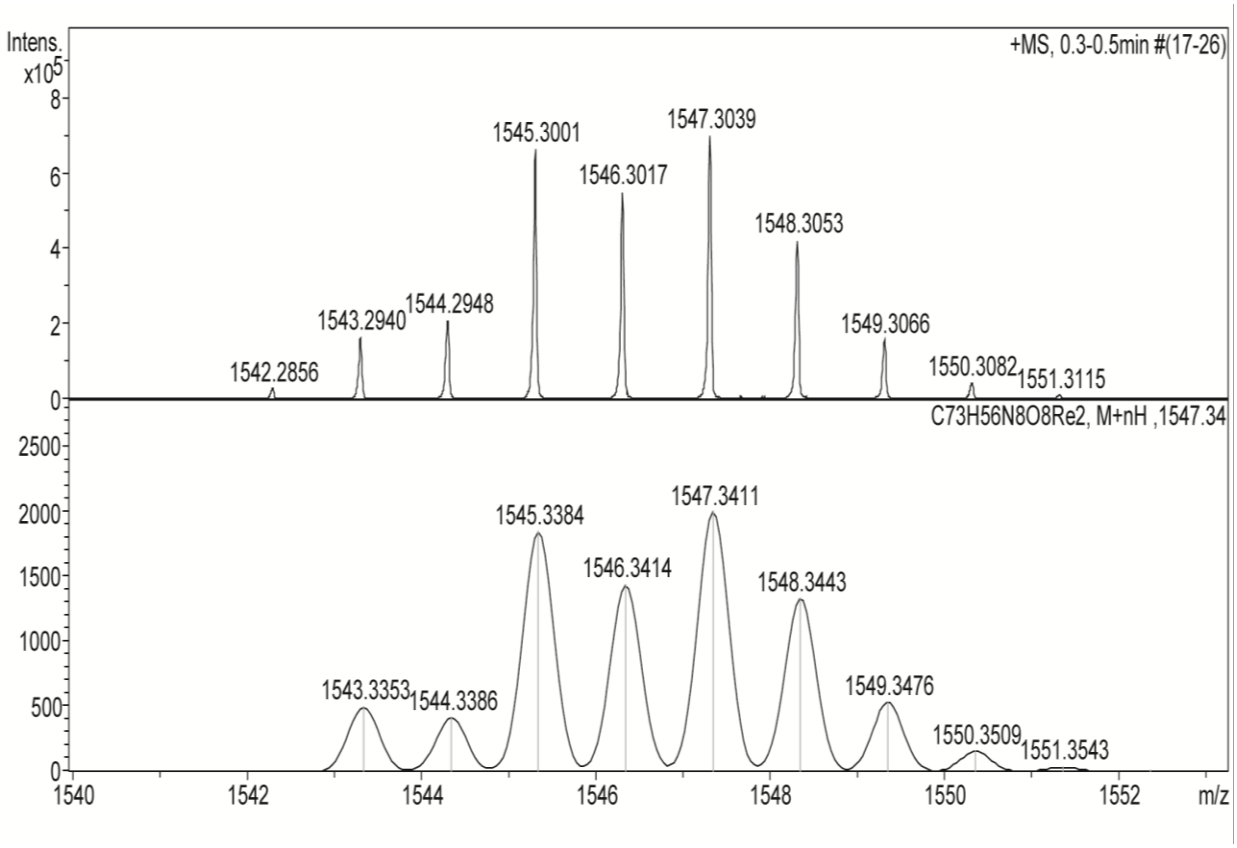

Figure 5.8. Experimental (top) and calculated (below) ESI mass spectrum of **1** in positive ion mode.

UOH -SCHOOL OF CHEMISTRY -HRMS

Analysis Info

Analysis Name	D:\Data\2018\PROF MS\DEC\MB3-22.d	Acquisition Date	12/10/2018 3:15:30 PM
Method	tune_wide_Pos.m	Operator	UOH-Chemistry
Sample Name	MB3-22	Instrument	maXis 10138
Comment			

Acquisition Parameter

Source Type	ESI	Ion Polarity	Positive	Set Nebulizer	0.3 Bar
Focus	Not active	Set Capillary	3800 V	Set Dry Heater	180 °C
Scan Begin	700 m/z	Set End Plate Offset	-500 V	Set Dry Gas	4.0 l/min
Scan End	3500 m/z	Set Collision Cell RF	2500.0 Vpp	Set Divert Valve	Source

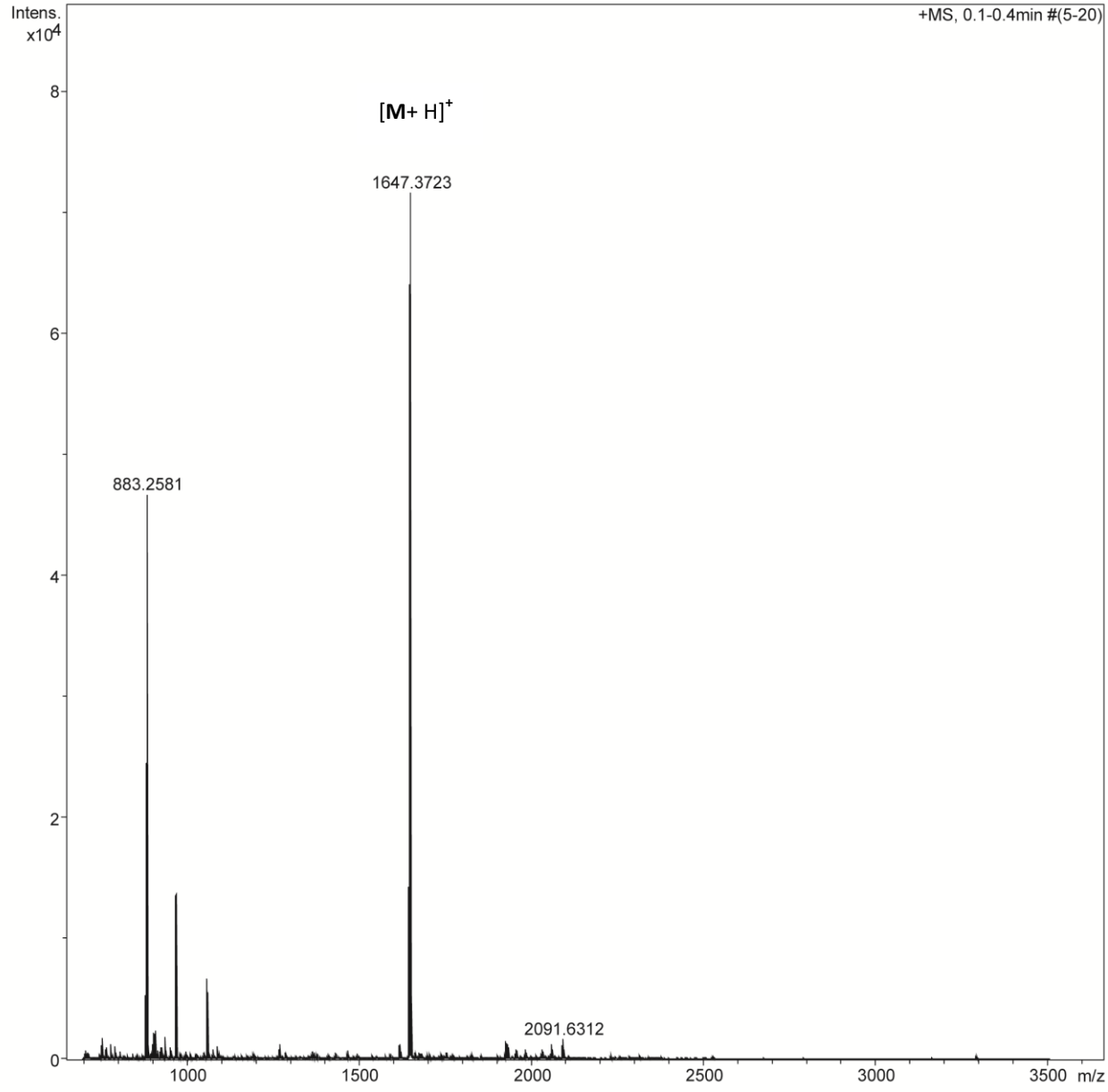

Bruker Compass DataAnalysis 4.0 printed: 12/10/2018 4:02:17 PM Page 1 of 1

Figure 5.9. ESI mass spectrum of **2** in positive ion mode.

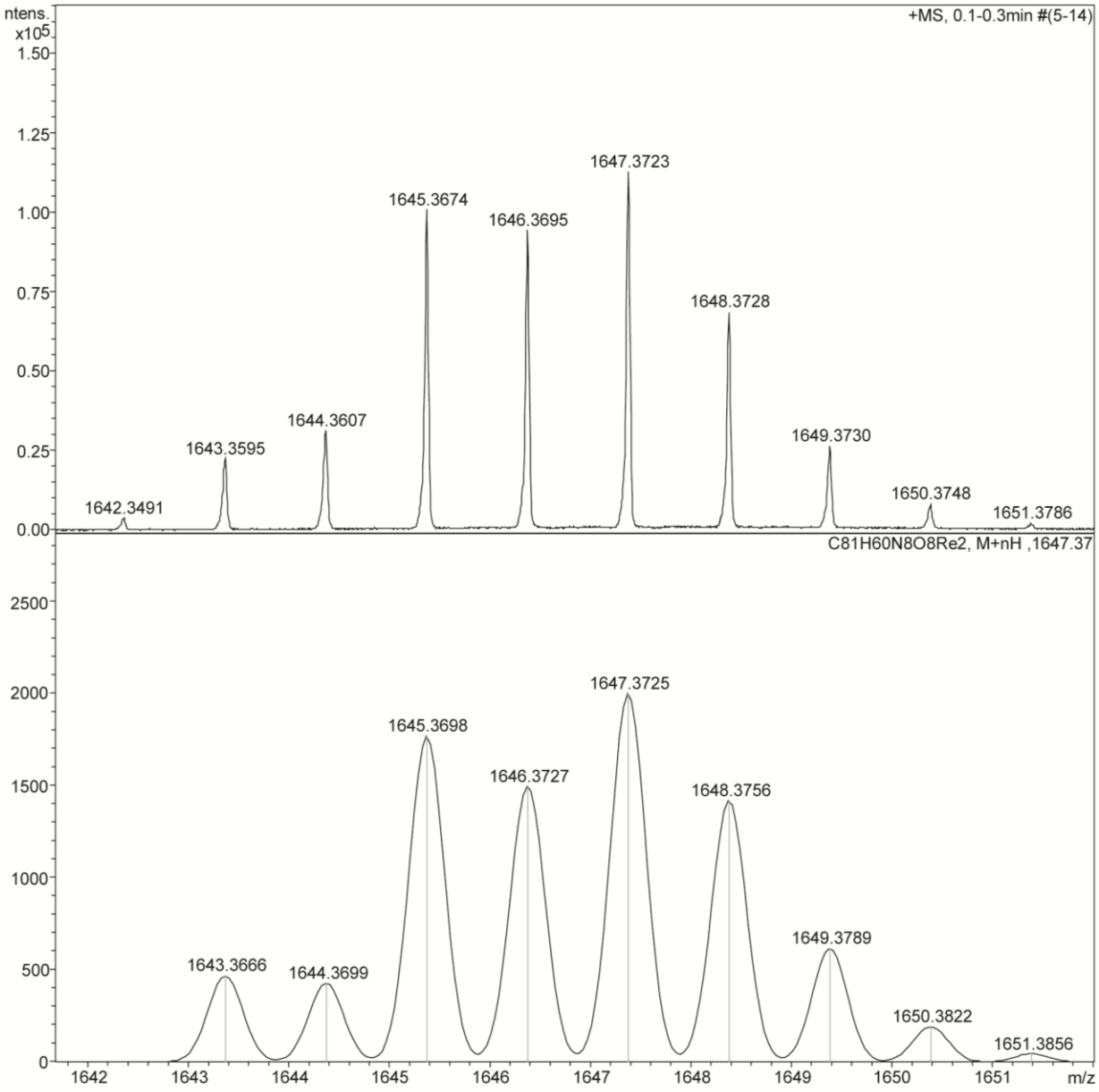

Figure 5.10. Experimental (top) and calculated (below) ESI mass spectrum of **2** in positive ion mode.

UOH -SCHOOL OF CHEMISTRY -HRMS

Analysis Info

Analysis Name	D:\Data\2017\DR. SATHIYENDIRAN\JULY\MB2-95.d	Acquisition Date	7/28/2017 3:47:24 PM
Method	tune_wide_Pos.m	Operator	Rajesh Vashisth
Sample Name	MB-2-95	Instrument	maXis 10138
Comment			

Acquisition Parameter

Source Type	ESI	Ion Polarity	Positive	Set Nebulizer	0.3 Bar
Focus	Not active	Set Capillary	3800 V	Set Dry Heater	180 °C
Scan Begin	280 m/z	Set End Plate Offset	-500 V	Set Dry Gas	4.0 l/min
Scan End	3500 m/z	Set Collision Cell RF	2500.0 Vpp	Set Divert Valve	Source

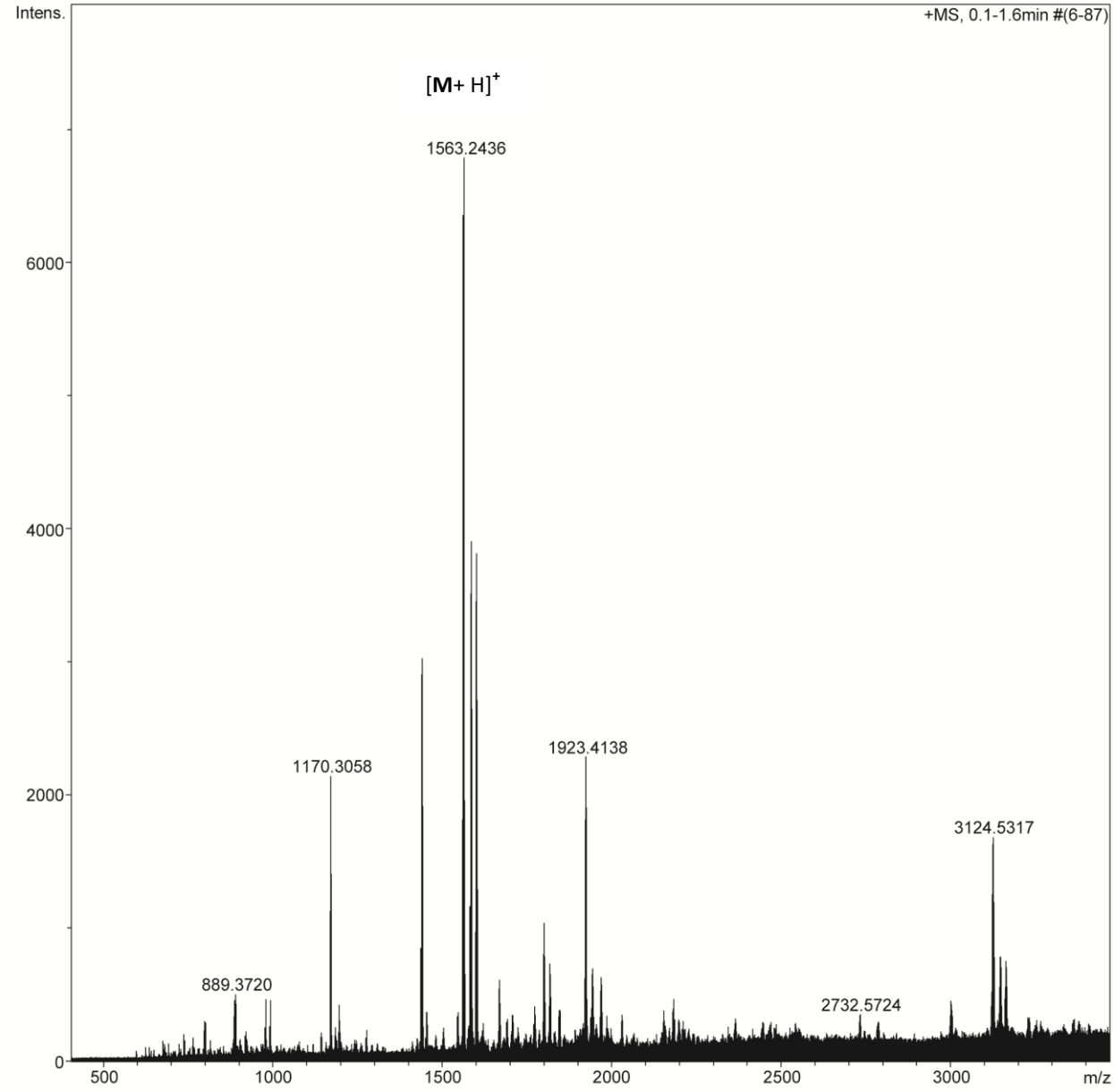

Bruker Compass DataAnalysis 4.0 printed: 11/30/2018 4:04:49 PM Page 1 of 1

Figure 5.11. ESI mass spectrum of **3** in positive ion mode.

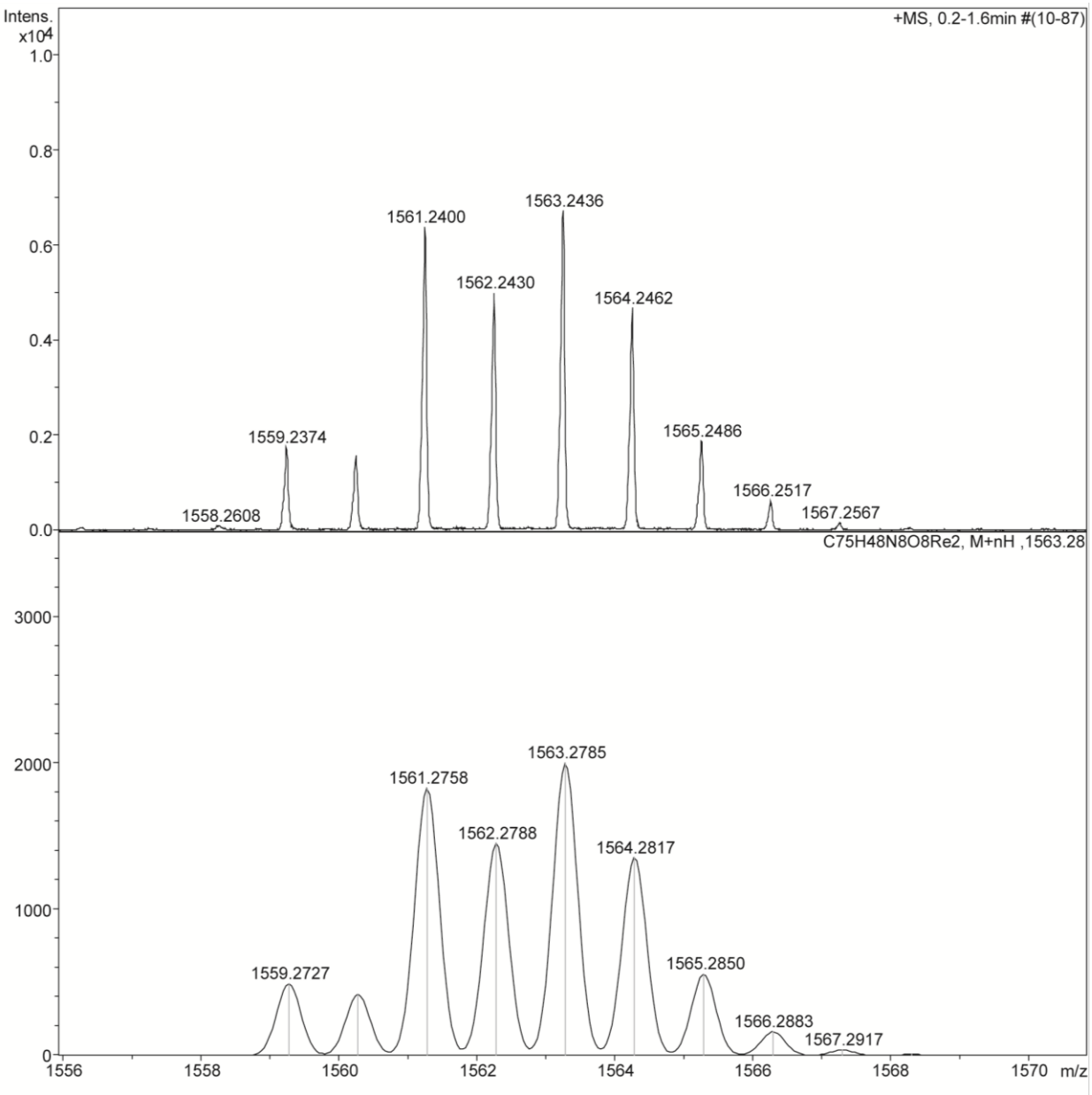

Figure 5.12. Experimental (top) and calculated (below) ESI mass spectrum of **3** in positive ion mode.

Display Report

Analysis Info

Analysis Name	D:\Data\D\Data\Finaltest\2021\MS\FEB\MB-4-40.d	Acquisition Date	2/24/2021 1:16:20 PM
Method	tune_wide_Pos.m	Operator	UOH
Sample Name	MB-4-40	Instrument	maXis 255552.10138
Comment			

Acquisition Parameter

Source Type	ESI	Ion Polarity	Positive	Set Nebulizer	0.3 Bar
Focus	Not active	Set Capillary	3800 V	Set Dry Heater	180 °C
Scan Begin	500 m/z	Set End Plate Offset	-500 V	Set Dry Gas	4.0 l/min
Scan End	3500 m/z	n/a	n/a	Set Divert Valve	Source
		Set Corona	0 nA	Set APCI Heater	0 °C

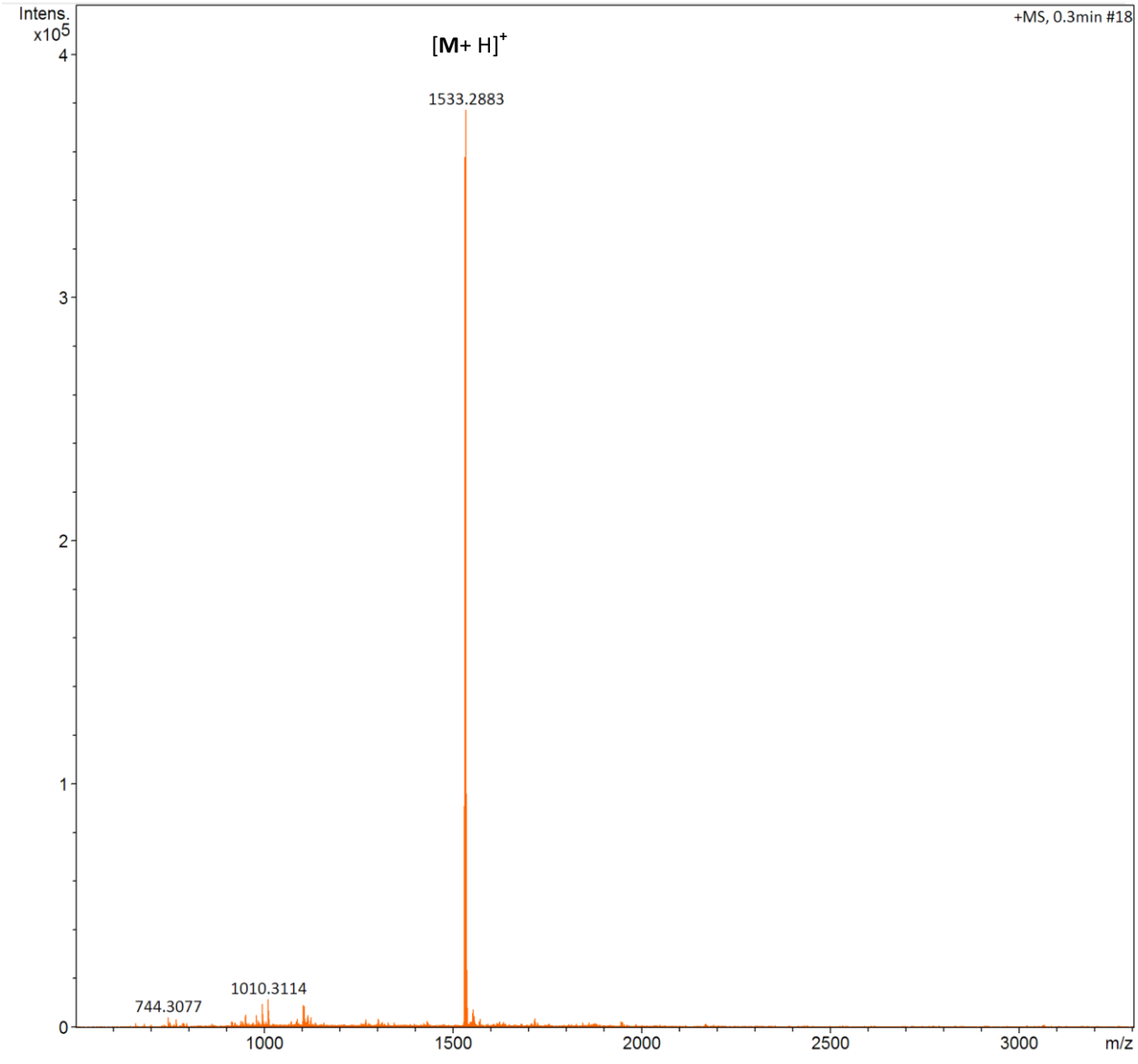

MB-4-40.d

Bruker Compass DataAnalysis 4.2 printed: 2/9/2022 5:11:39 PM by: BDAL Page 1 of 1

Figure 5.13. ESI mass spectrum of **4** in positive ion mode.

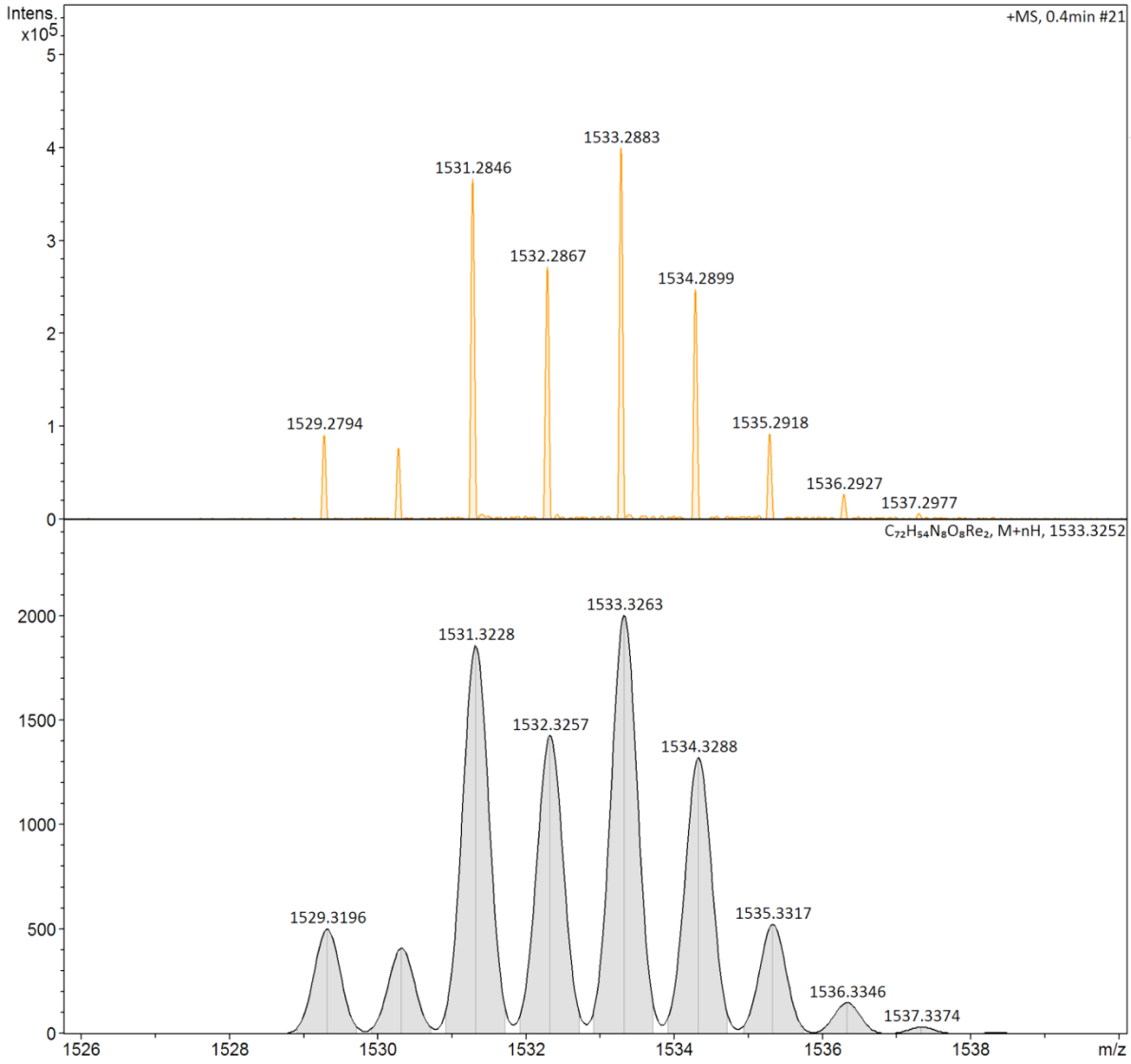

Figure 5.14. Experimental (top) and calculated (below) ESI mass spectrum of **4** in positive ion mode.

UOH -SCHOOL OF CHEMISTRY -HRMS

Analysis Info

Analysis Name	D:\Data\2019\PROF.MS\FEB\MB3-39-1.d	Acquisition Date	2/13/2019 3:29:18 PM
Method	tune_high_Pos.m	Operator	UOH-Chemistry
Sample Name	MB3-39	Instrument	maXis 10138
Comment			

Acquisition Parameter

Source Type	ESI	Ion Polarity	Positive	Set Nebulizer	0.3 Bar
Focus	Not active	Set Capillary	3800 V	Set Dry Heater	180 €C
Scan Begin	700 m/z	Set End Plate Offset	-500 V	Set Dry Gas	4.0 l/min
Scan End	3500 m/z	Set Collision Cell RF	2500.0 Vpp	Set Divert Valve	Waste

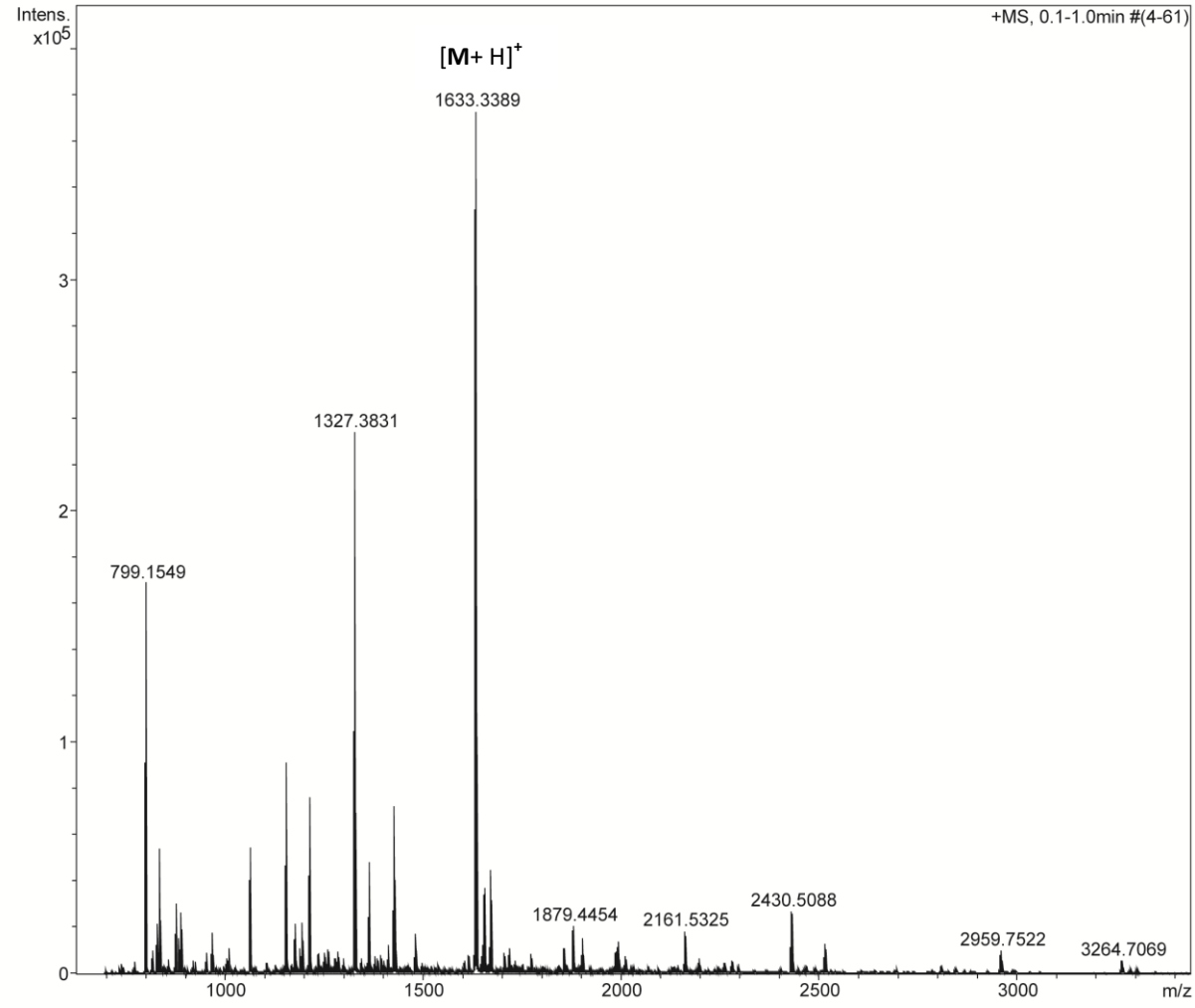

Bruker Compass DataAnalysis 4.0 printed: 2/13/2019 3:42:07 PM Page 1 of 1

Figure 5.15. ESI mass spectrum of **5** in positive ion mode.

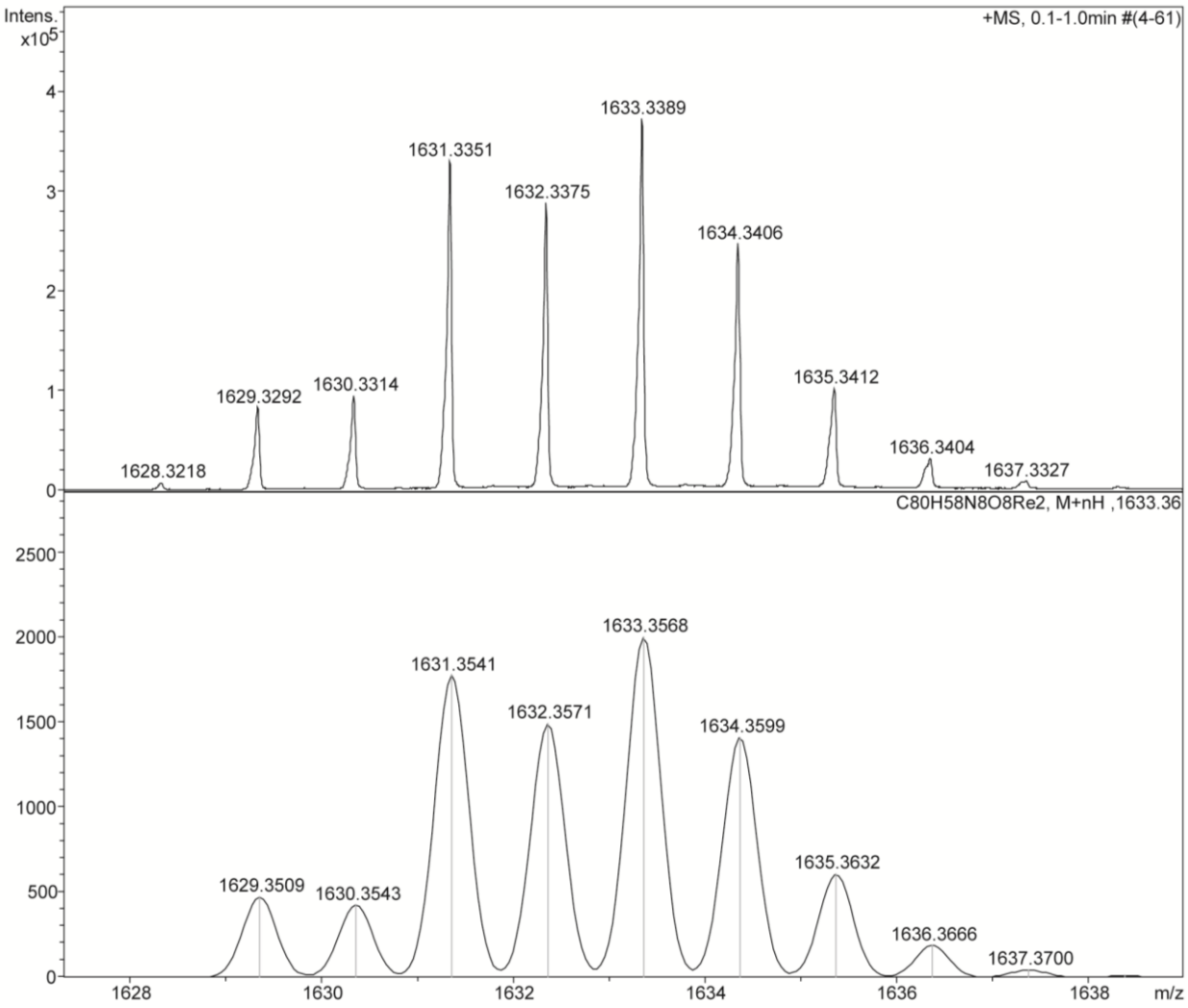

Figure 5.16. Experimental (top) and calculated (below) ESI mass spectrum of **5** in positive ion mode.

^{1}H NMR Analysis of Complexes 1-5.

The ^{1}H NMR spectra of **1** and **2** displayed well-separated chemical resonances for the protons of both the ligands in d_6-DMSO. All the protons of the complexes are assigned based on ^{1}H–^{1}H COSY spectrum. The presence of a single complex in the solution was further confirmed by DOSY experiment. The signals in region 3.7 to 7.45 ppm are similar for both complexes **1** and **2**. This clearly indicates that both complexes **1** and **2** adopt a highly symmetrical structure in the solution and are structurally similar to each other. The proton signals of **1** and **2** differ only in the region above 7.45 ppm, which are assigned to the terminal benzimidazolyl/naphthanoimidazolyl motifs of L^3/L^4 in the complexes. This is expected obviously because complex **1** differs from complex **2** based on terminal coordination donor motif. The methylene protons for both the complexes appeared as doublet of doublets with coupling constant 14.6 Hz. due to geminal coupling. In both the cases, the H_2–proton (N–C^2*H*–N of benzimidazolyl/naphthanoimidazolyl) is shifted upfield remarkably in comparison with the corresponding free ligands, indicating that the H^2 proton is directed to the nearby aromatic face in the complex and experiences the ring current effect. This indicates that the metallocycles remain intact in the solution.

The proton ^{1}H NMR spectrum of **3** displayed more number of signals than expected for the complex. Interpreting the ^{1}H-^{1}H COSY NMR spectrum of **3** also proved to be fruitless. The methylene protons appeared as multiplets in the spectrum which may be due to the flexible and flipping nature of the two *p*-phenylene units resulting in back and forth movement of the units in solution. This may result in various conformers which rapidly interconvert in solution in the NMR timescale.

The proton ^{1}H NMR spectrum of **5** displayed simple, sharp, and mostly well-separated peaks for the protons of the ligand frameworks. The methylene protons of both ligand strands appeared as two distinguished singlets due to the flexible nature of the ligand frameworks. In case of **4**, both the ligand strands displayed a similar chemical resonance pattern to that of complex **4**. The H^2 proton of the benzimidazolyl /naphthanoimidazolyl motif of L^5 /L^6 displayed a singlet at 8.4 ppm and 8.2 ppm in the complex spectra of **4** and **5**, respectively. These data indicates that metallocycle **4** and **5** adopt mesocate structures in solution.

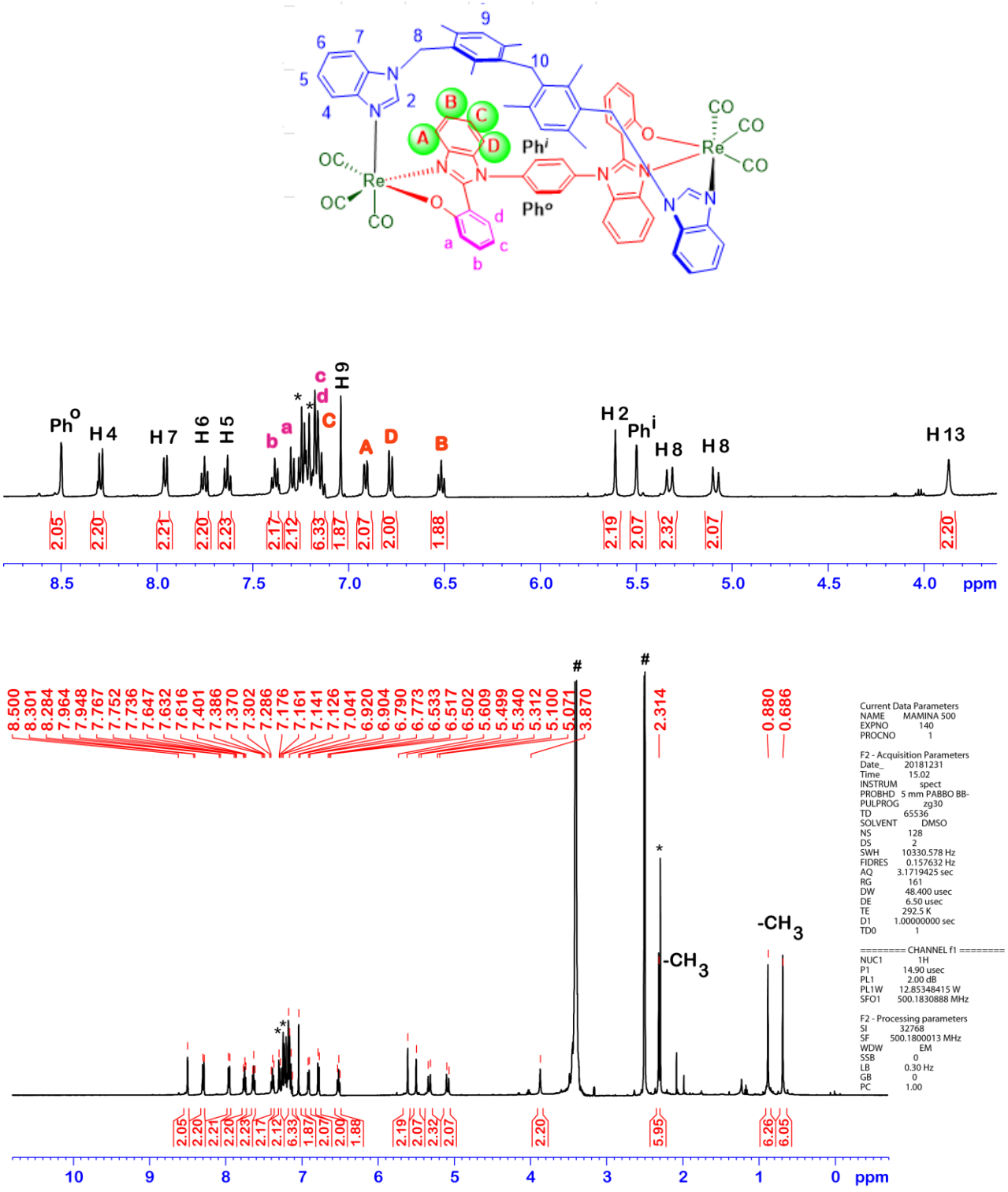

Figure 5.17. ^{1}H NMR spectra of **1** in DMSO-d_6.

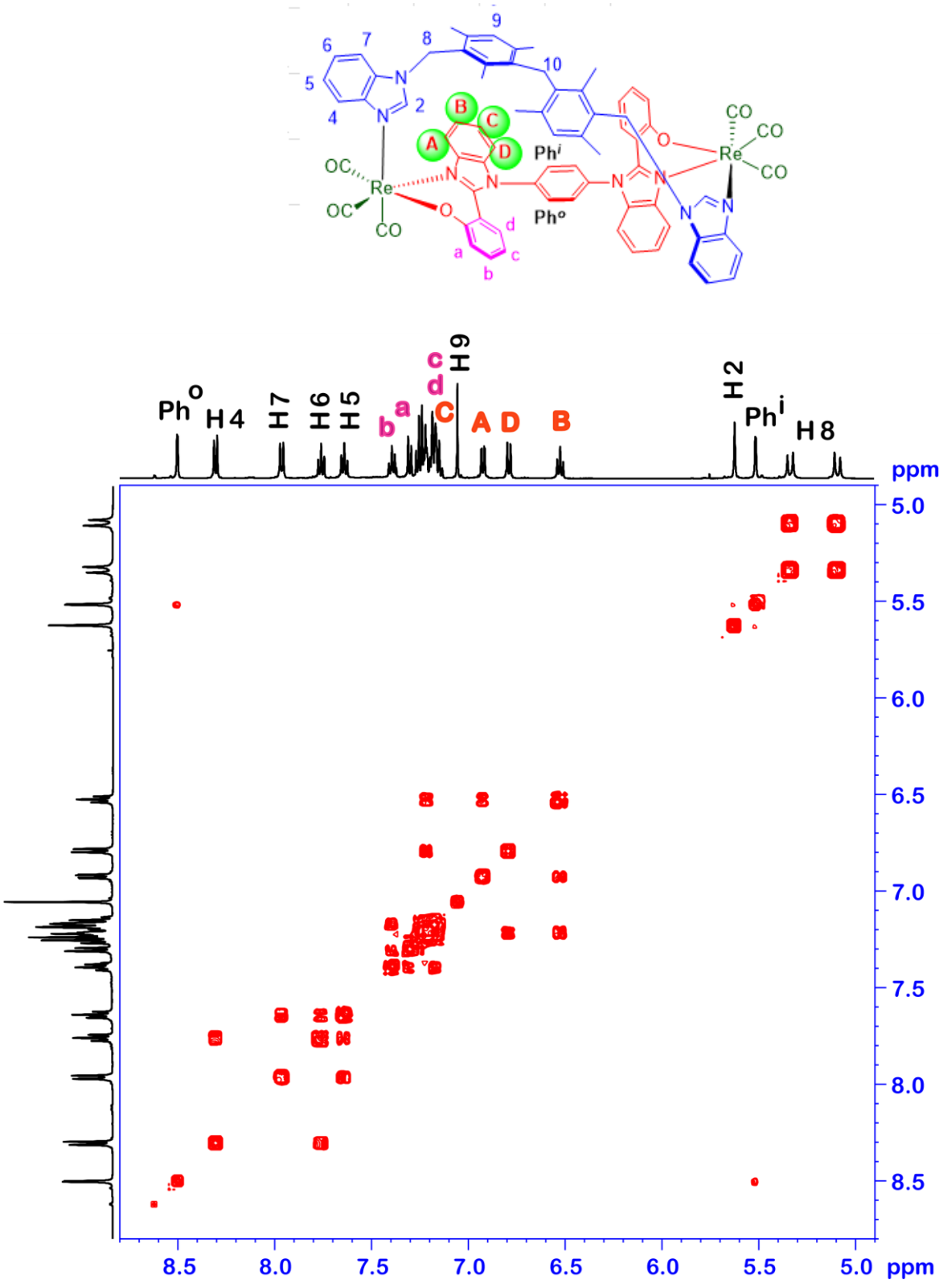

Figure 5.18. Partial ^{1}H- ^{1}H COSY NMR spectrum of **1** in DMSO-d_6.

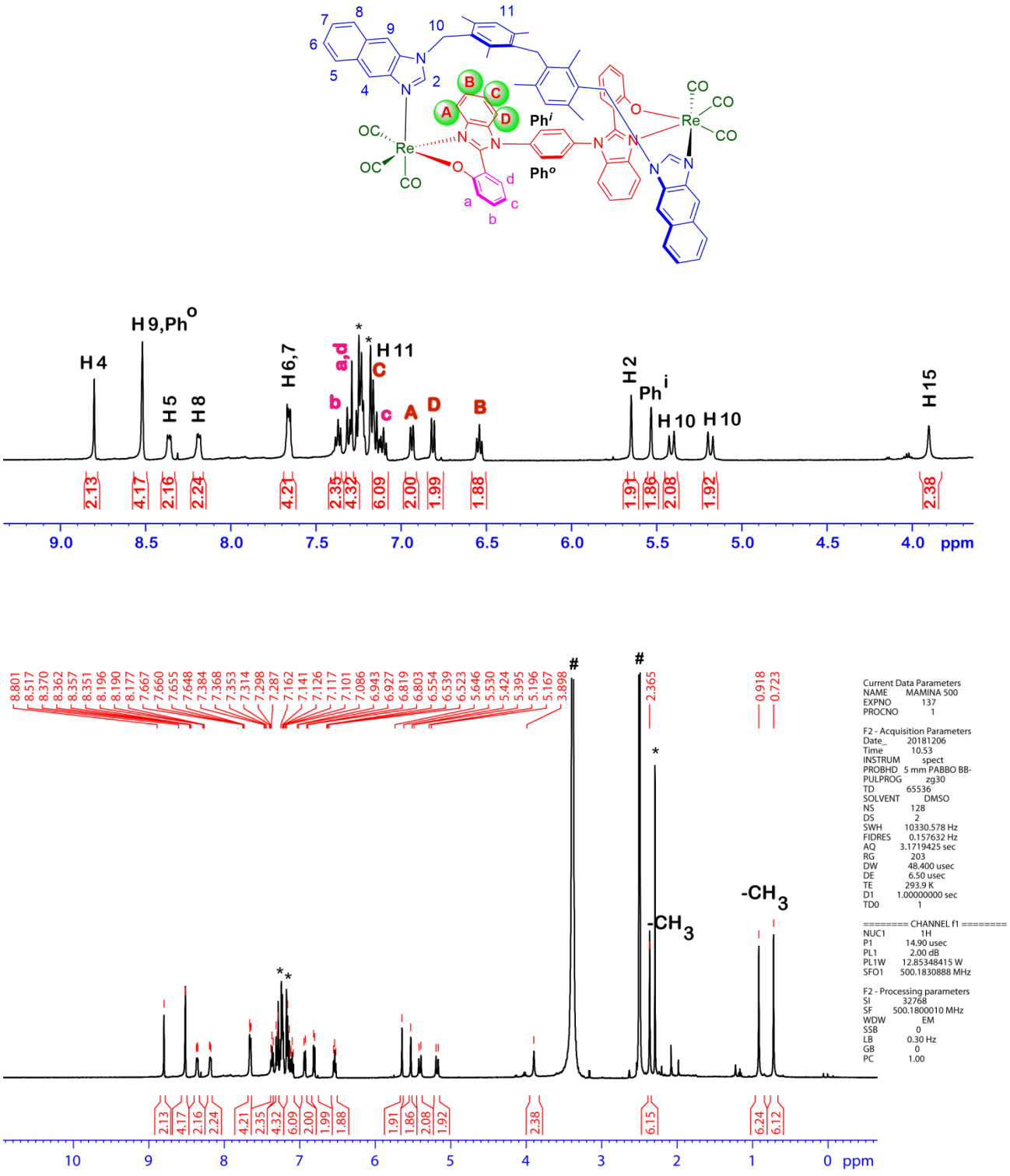

Figure 5.19. ^{1}H NMR spectra of **2** in DMSO-d_6.

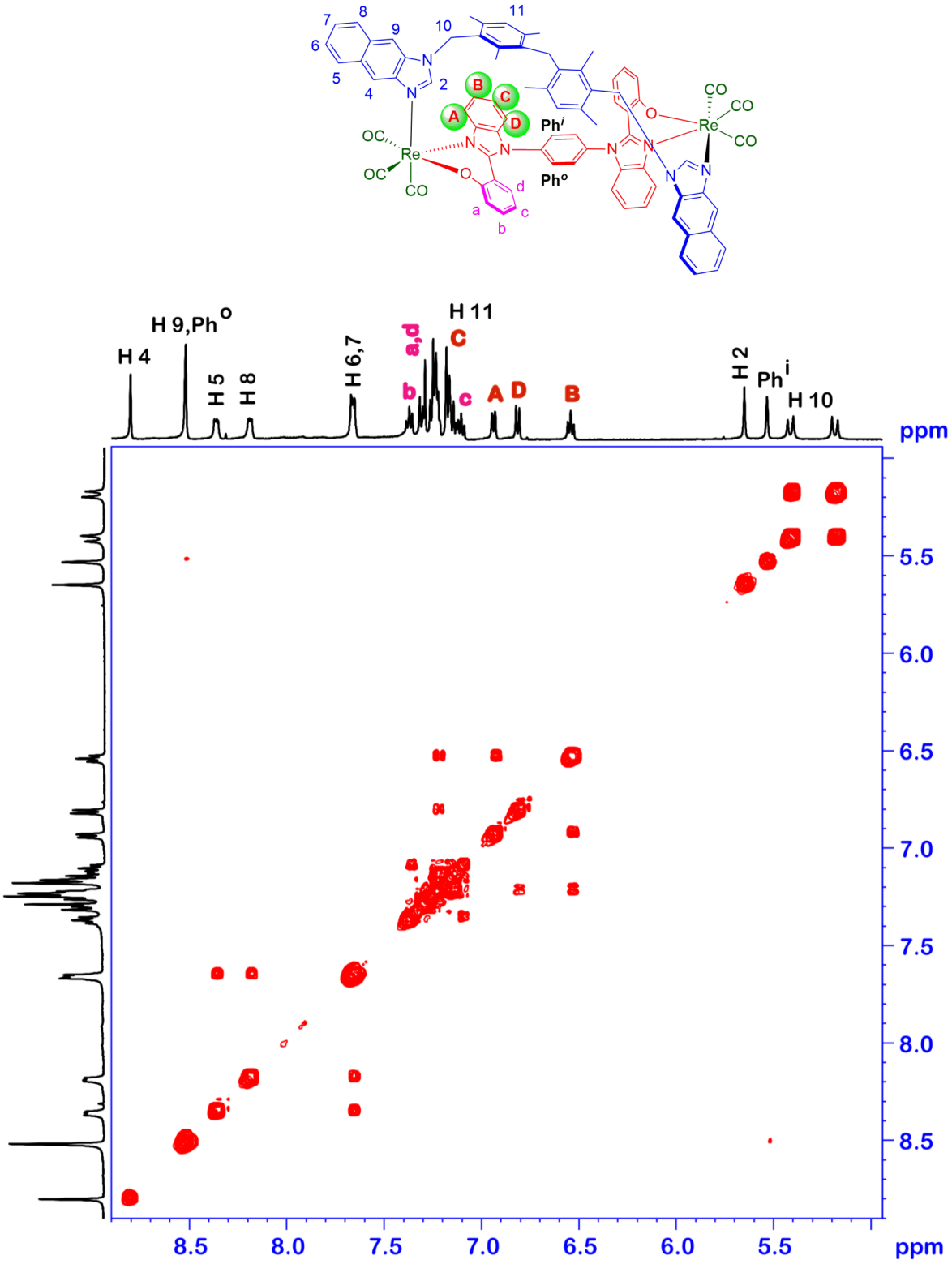

Figure 5.20. Partial ^{1}H- ^{1}H COSY NMR spectrum of **2** in DMSO-d_6.

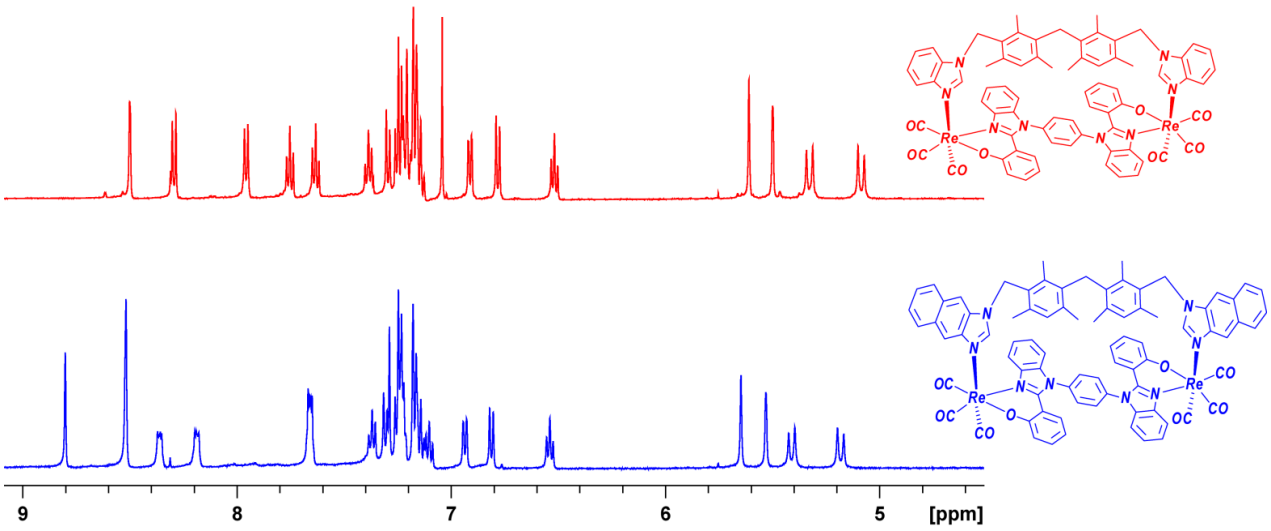

Figure 5.21. ^{1}H NMR spectra of **1** (bottom) and **2** (top) in DMSO-d_6.

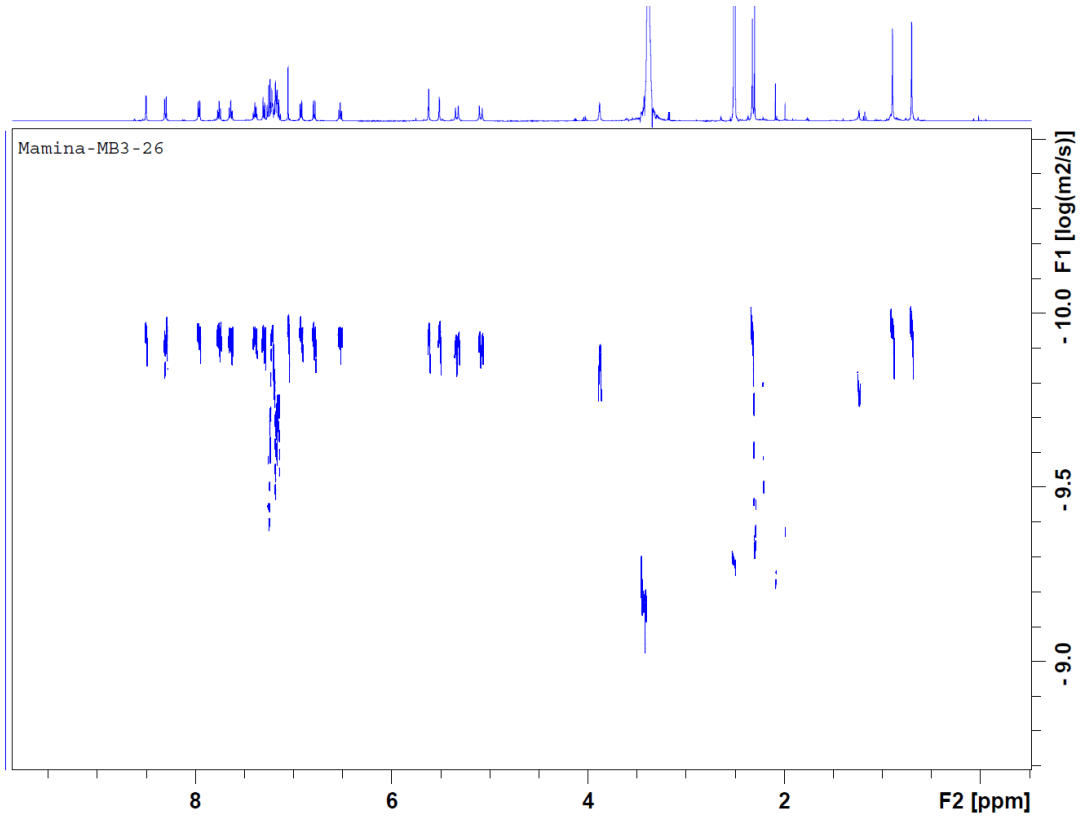

Figure 5.22. ^{1}H DOSY NMR spectrum of **1** in DMSO-d_6.

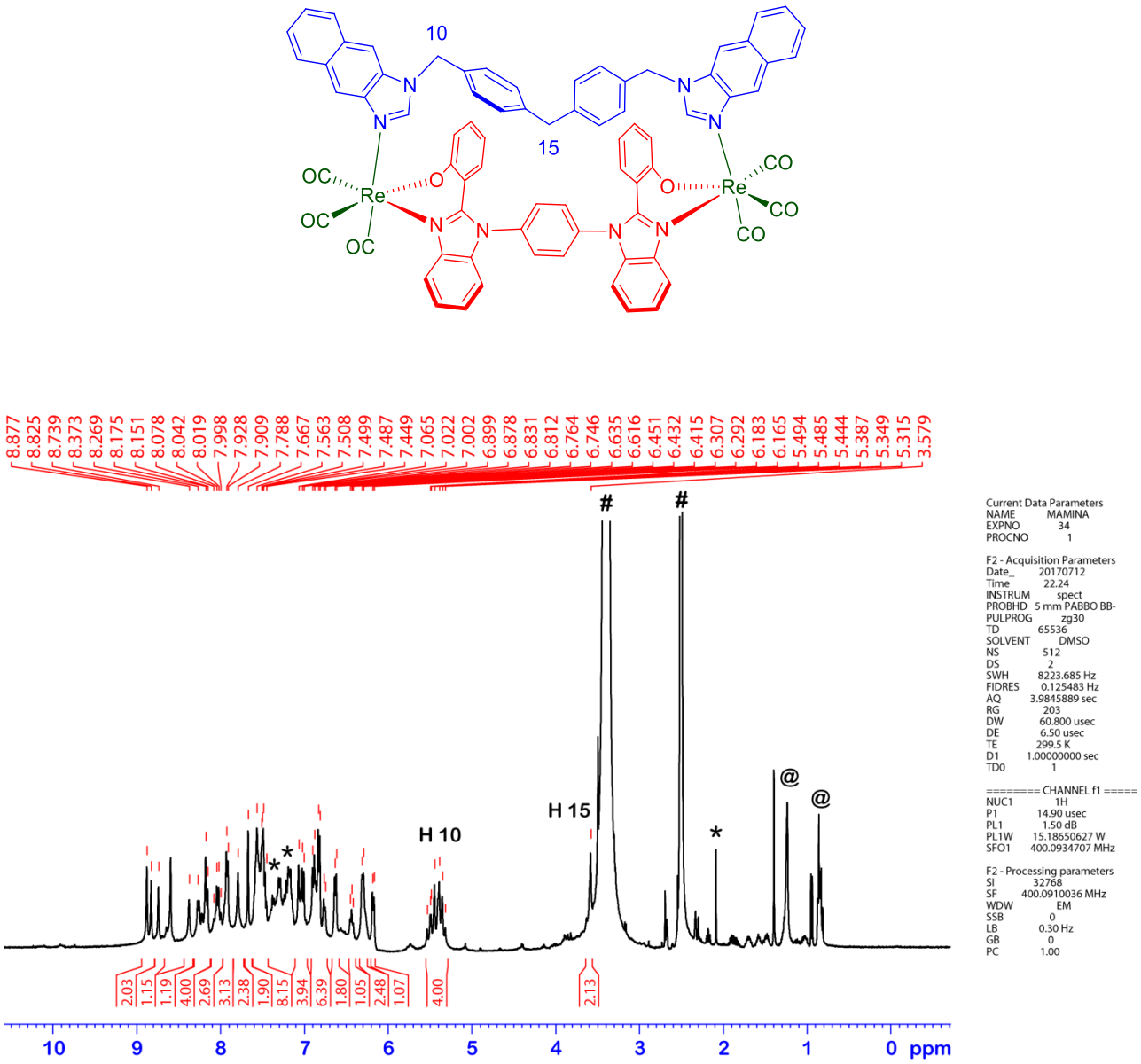

Figure 5.23. ^{1}H NMR spectrum of **3** in DMSO-d_6.

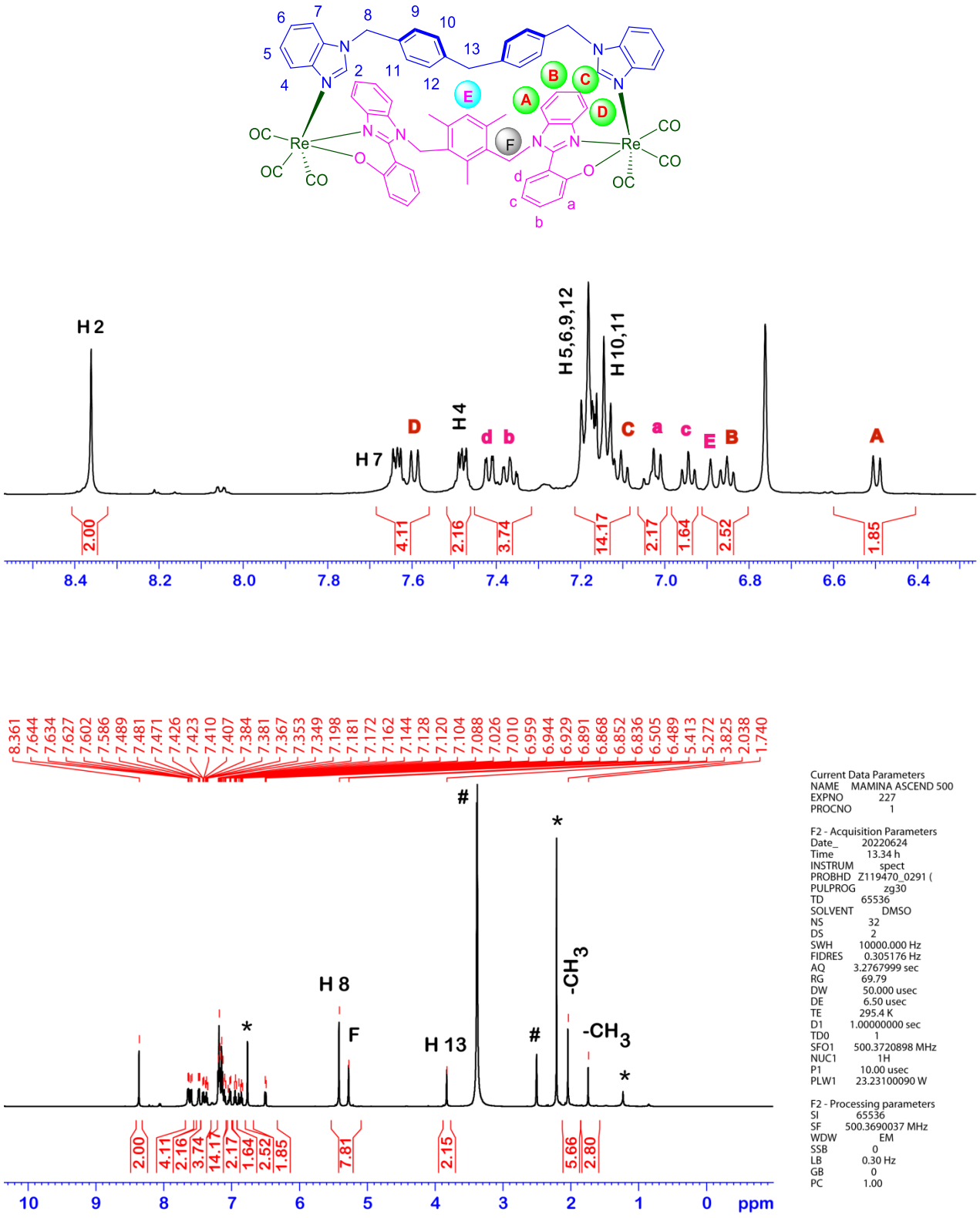

Figure 5.24. ^{1}H NMR spectra of **4** in DMSO-d_6.

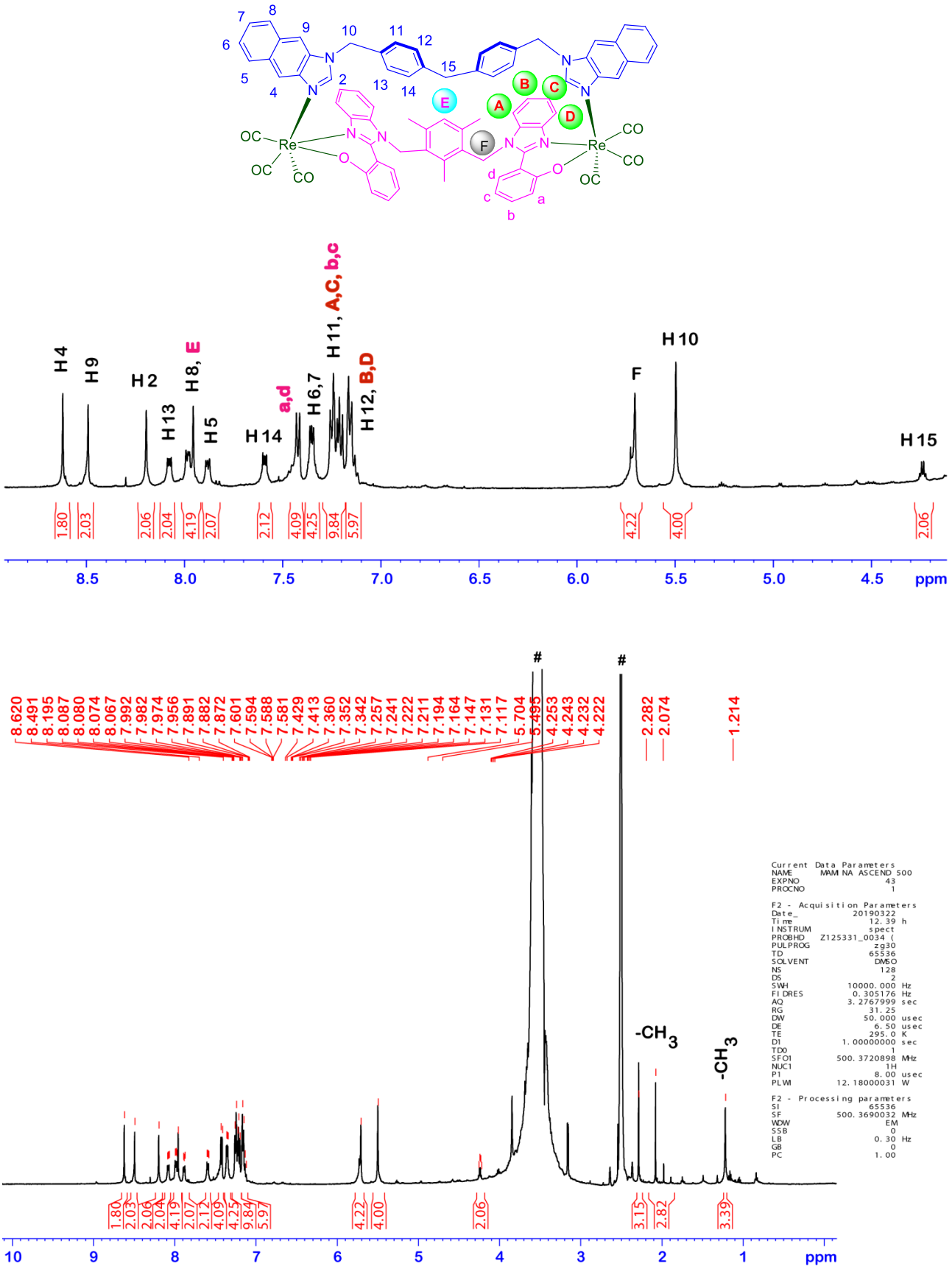

Figure 5.25. ^{1}H NMR spectra of **5** in DMSO-d_6.

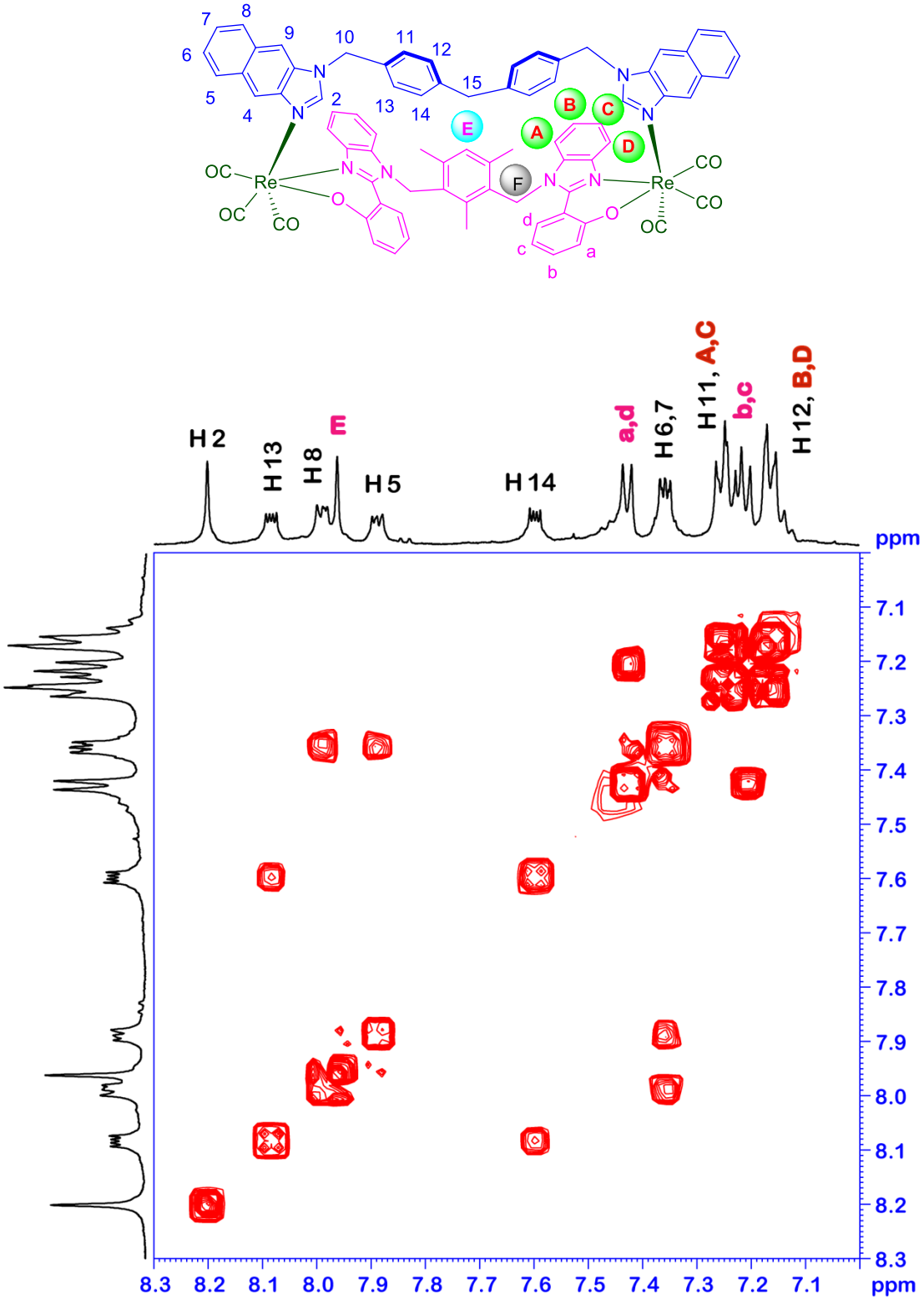

Figure 5.26. Partial ^{1}H- ^{1}H COSY NMR spectrum of **5** in DMSO-d_6.

5.3.2. Crystal Structure of Complexes 1-3 and 5.

Molecular structures of the complexes were determined by single-crystal X-ray diffraction analysis. Complexes **1**–**2** adopt a helical architecture, whereas complexes **3** and **5** adopt mesocate structures. In all the complexes Re(I) ion is coordinated by a N∩O chelating unit from the bis-chelating motif, a nitrogen atom from neutral nitrogen donor benzimidazolyl/naphthanoimidazolyl, and three oxygen atoms from three carbonyl groups. The overall size of helicates **1** and **2** are ~21.2 (length) × ~10.5 (width) for **1**, and ~25.8 (length) × ~10.5 (width) for **2**. The length is calculated from two terminal hydrogen atoms along the helical axis. The width of the helicates is calculated from the two terminal hydrogen atoms of the benzimidazolyl-phenolate motif. Both the ligand strands wrap around the Re···Re axis in a helical manner. In helicate **1**, the rigid ligand as well as the neutral N donor wrap around the helical axis in a left-handed way with twist angles of 84° (the dihedral angle between the planes of the two Re–O(Chel)–N(Chel) units) and ~87° (the dihedral angle between the two Re-N(benzimidazolyl) motifs). The opposite trend was observed in the case of helicate **2** with closely similar twisting.

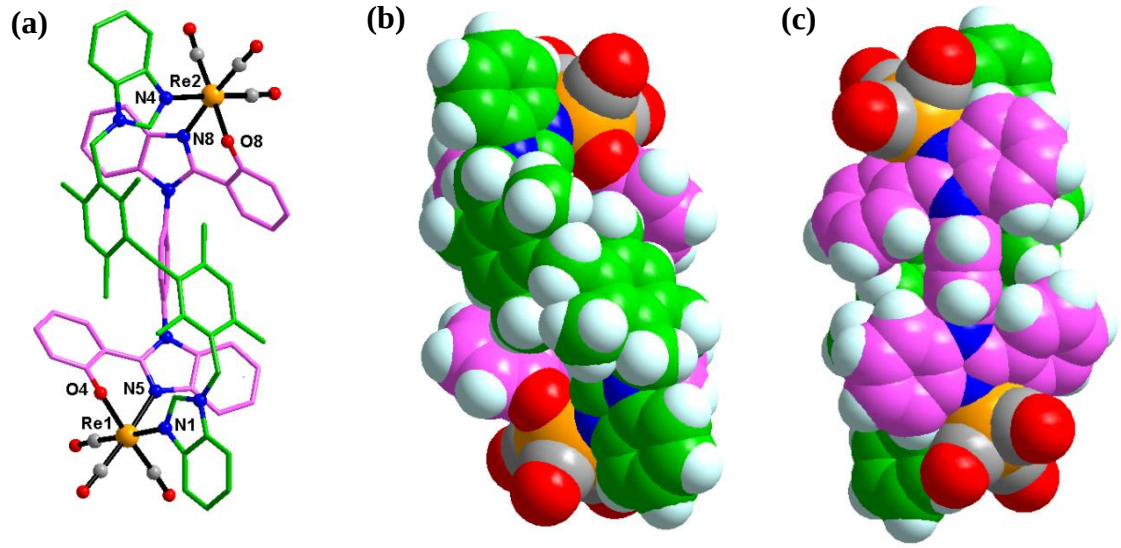

Figure 5.27. (a) Molecular structure of **1** (hydrogen atoms are omitted for clarity). (b & c) Different space fill representation, the carbon atoms of the two strands and CO atoms are differently colored for clarity (green = pink = gray = C, blue = N, red = O, light blue = H, orange = Re).

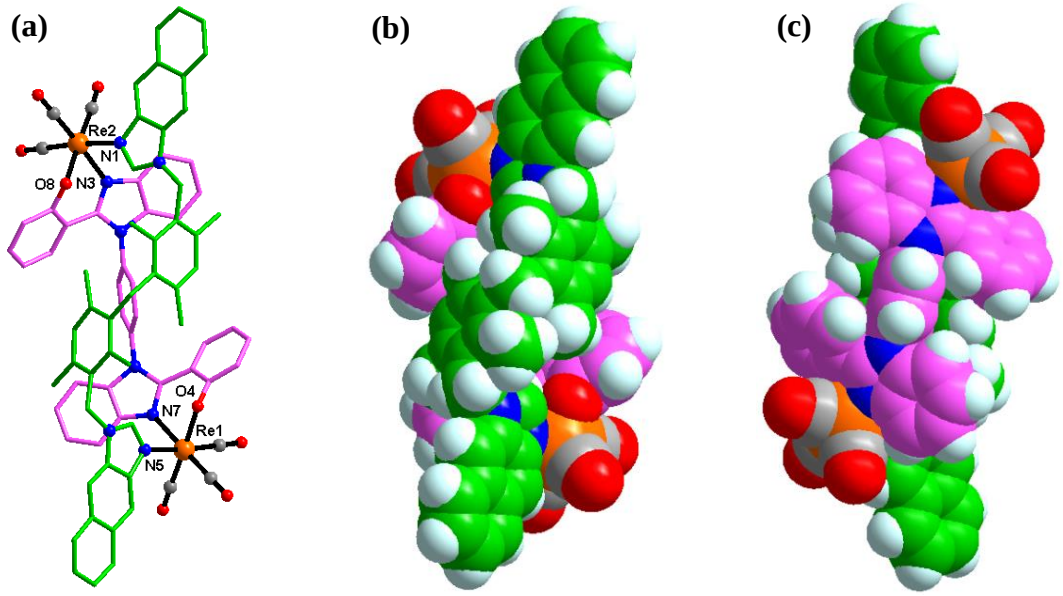

Figure 5.28 (a) Molecular structure of **2** (hydrogen atoms are omitted for clarity). (b & c) Different space fill representation, the carbon atoms of the two strands and CO atoms are differently colored for clarity (green = pink = gray = C, blue = N, red = O, light blue = H, orange = Re).

Single-crystal X-ray diffraction method reveals that metallacycles **3** and **5** adopt M_2LL'-type mesohelical architecture in which both dianionic bis-chelating and neutral bidentate ligand strands are arranged parallel to each other along the Re···Re axis. Though mesocate **3** and helicate **1** or **2** have same bis-chelating motifs, no helical twisting was observed in **3**. The dihedral angle between two [Re–$O_{(Chel)}$–$N_{(Chel)}$]units is ~1°. The bis(p-phenylene) spacer adopt v-shaped geometry and their plane was parallel to the Re…Re axis as well as central phenylene unit of bis-chelating motif of **3**. The two naphthanoimidazolyl motifs are directed their fused arene core along the Re···Re axis, resulting the longer size mesocate structure i.e., length of mesocate is ~26.3 Å. The dihedral angle between the two line of Re-N(naphthaimidazolyl) is ~1°, indicating the non-helical nature of flexible ligand in **3**. Similar to **3**, in mesocate **5** both the ligands are arranged parallel to each other along the Re…Re axis. The neutral ligand conformation in **5** is slightly different from that of in **3**. The plane of the bis-phenylene spacer is perpendicular to the Re···Re axis and is almost parallel to the terminal naphthanoimidazolyl planes. The four hetero(arene) motifs of neutral ligand in **5** are

arranged like 'W"-shaped structure. The length of mesocate is ~21.3 Å and the Re…Re axis distance is ~15 Å.

In crystal packing of **1** and **2**, the adjacent metallocycles are held together by various intermolecular non-covalent interactions including parallel displaced π···π interactions, edge-to-face C–H···π interactions, C(H)···O≡C−Re non-classical hydrogen bonding interactions. In case of **2** solvent molecule mesitylene resides in the lattice void created by three adjacent helicate molecules and stabilized by C–H···π and π···π interactions. In the crystal structures of **3** and **5**, the neighbouring molecules interact with each other *via* edge-to-face C–H···π interactions and C(H)···O≡C−Re non-classical hydrogen bonding interactions. In case of **5**, the solvent mesitylene molecules sit in the crystal lattice void created by two neighbouring mesocate molecules in a AA pattern and held with the metallocycle framework by C–H···π interactions. Further solvent acetone and the disordered mesitylene molecules occupies the lattice void in the 2D arrangement and are stabilized by non-classical H-bonding interactions C(H)···O≡C–Re and C–H···π interactions, respectively.

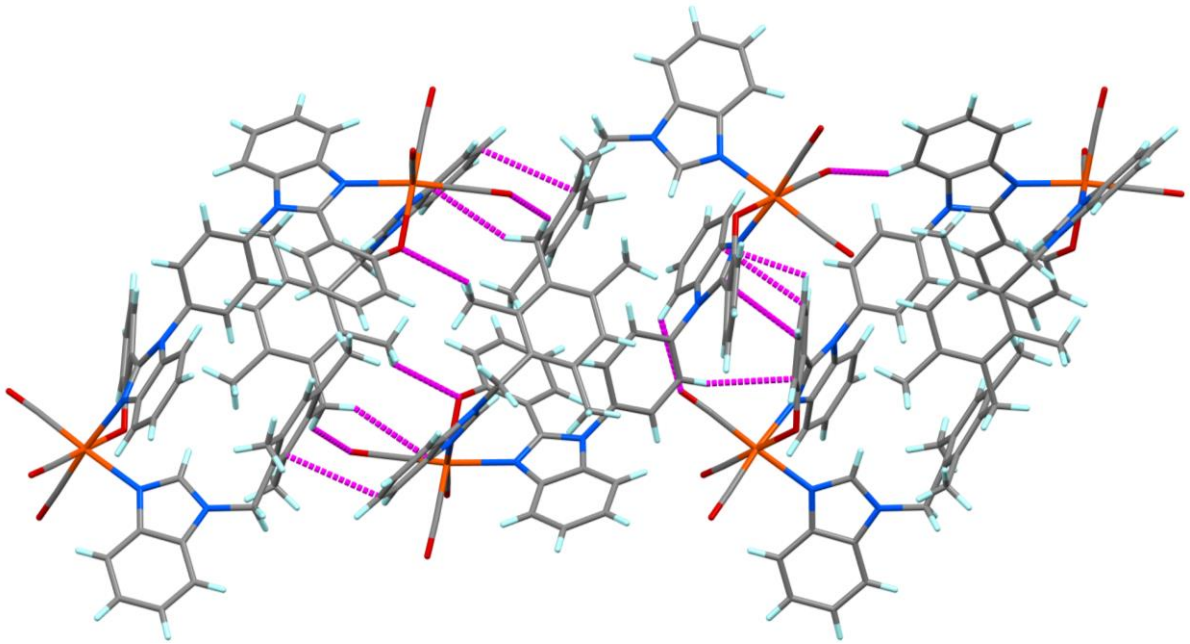

Figure 5.29. (a) Partial packing diagram of **1** showing a 1D sheet along b-axis constructuted by various non-covalent interactions (Gray = C, blue = N, red = O, light blue = H, orange = Re).

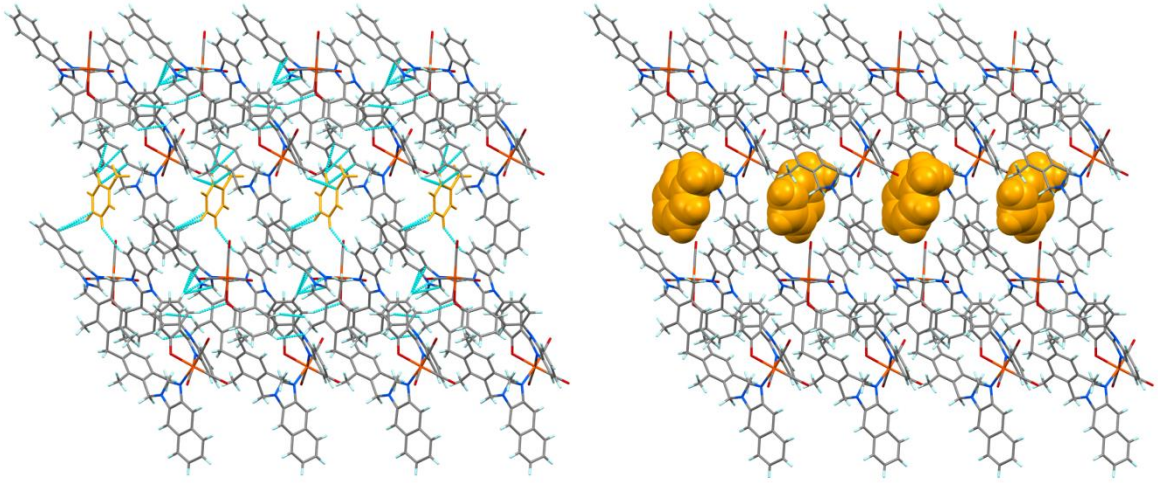

Figure 5.30. Partial packing diagram of **2** showing a 2D sheet along b-axis (Gray = C, blue = N, red = O, light blue = H, orange = Re, guest toluene = yellow).

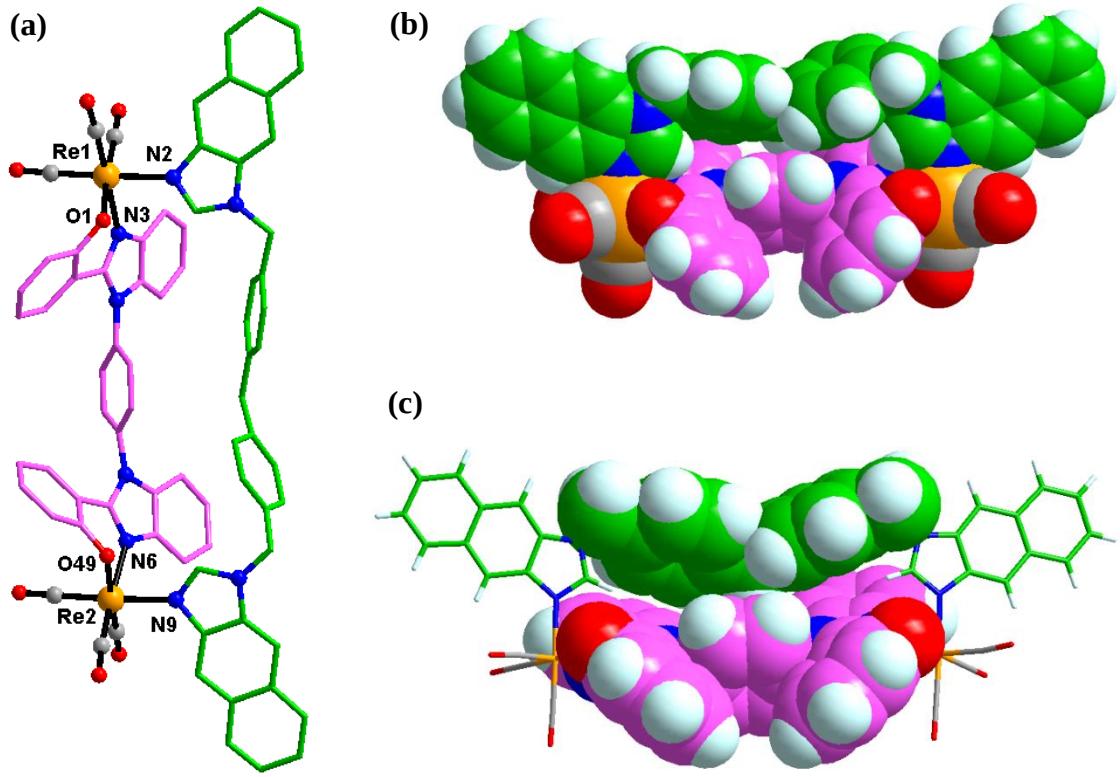

Figure 5.31. (a) Molecular structure of **3** (hydrogen atoms are omitted for clarity). (b & c) Different space fill representation, the carbon atoms of the two strands and CO atoms are differently colored for clarity (green = pink = gray = C, blue = N, red = O, light blue = H, orange = Re)

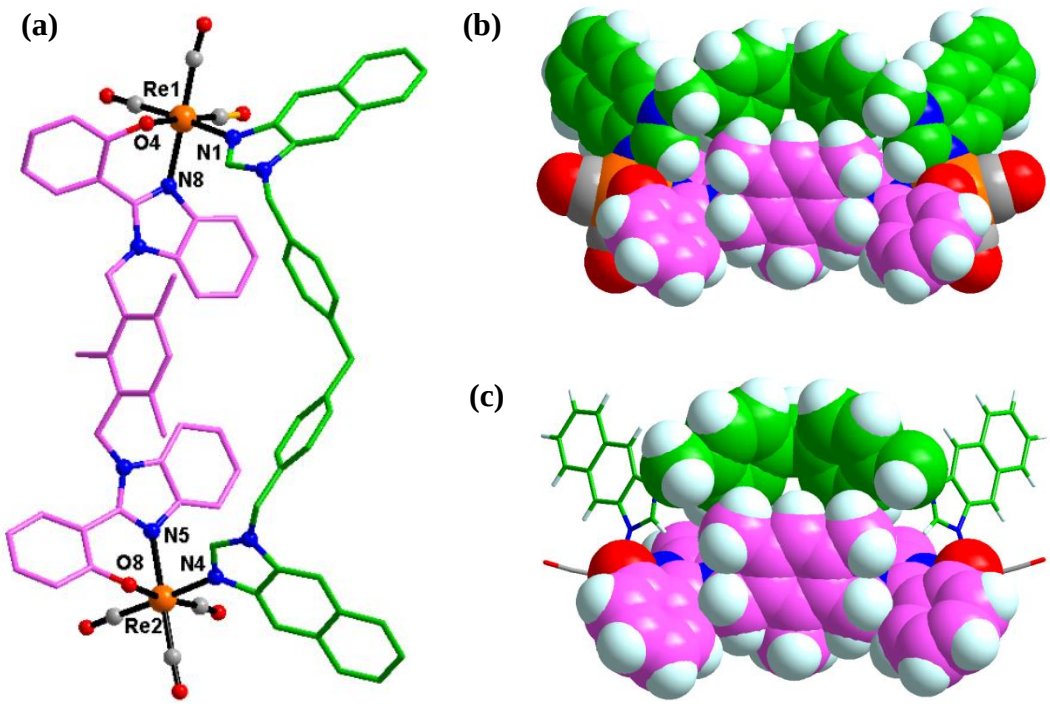

Figure 5.32. (a) Molecular structure of **5** (hydrogen atoms are omitted for clarity). (b & c) Different space fill representation, the carbon atoms of the two strands and CO atoms are differently colored for clarity (green = pink = gray = C, blue = N, red = O, light blue = H, orange = Re).

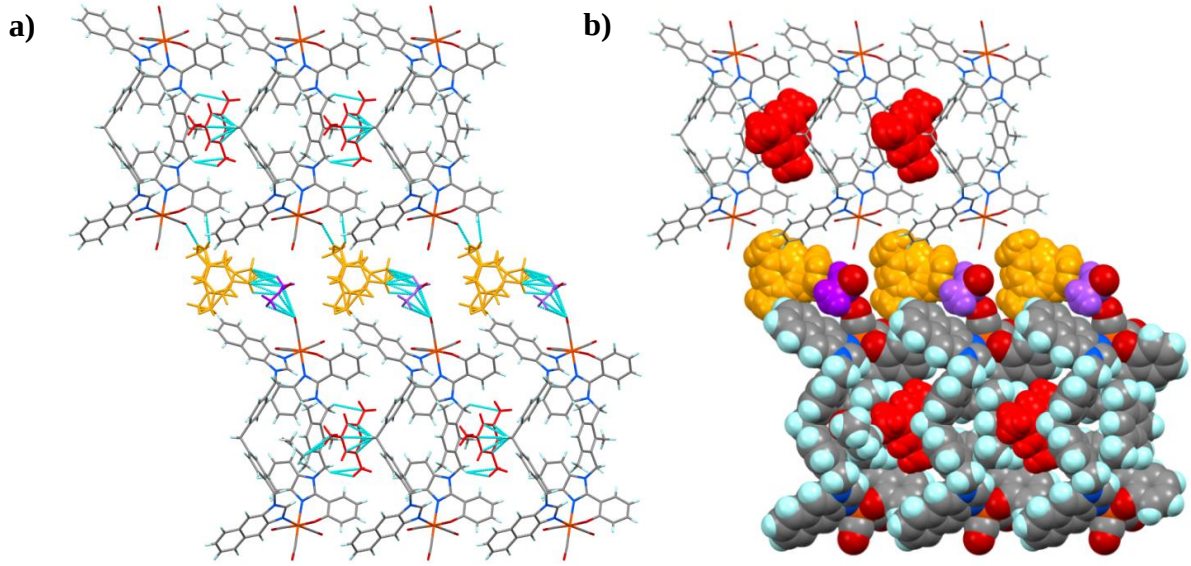

Figure 5.33. (a/b) Partial packing diagram of **5** showing a 2D sheet along c-axis (Gray = C, blue = N, red = O, light blue = H, orange = Re, guest mesitylene = red, lattice mesitylene = yellow, acetone= purple and red).

Table 5.1. Some Important Parameters of the Complexes

	1	**2**	**3**	**5**
Size of the complex				
[a]length (Å)	~21.17	~25.79	~26.32	~21.25
[b]width (Å)	~10.46	~10.46	~10.46	~10.46
Re···Re (Å)	~13.56	~13.34	~13.59	~15.2
τ(N donor to N donor in L^n) (deg)	~87	~86	~10.7	~86.9
τRe–N (L^n) (deg)	~89.6	~80.9	~0.9	~34.5
τRe–O(chel)–N(chel) (deg)	~84.2	~80.8	~14.6	~20.0
Arrangement of two benzimidazolylphenolate	anti	anti	syn	syn

[a]distance between two terminal hydrogen atoms along the Re···Re axis

[b]distance between two terminal hydrogen atoms of benzimidazolylphenolate motif

τ = dihedral angle

5.3.3 Photophysical properties of helicates 1-2 and mesocates 3-5 in solution and solid-state.

The photophysical properties of complexes (**1-5**) were studied in both solution (DMSO) and solid-state. The absorption spectra of **1**, **2**, **3**, **5**, and **4** display bands in the range of 254-373 nm and 256-362 nm, respectively. Benzimidazolyl moiety-based complexes (**1** and **4**) showed one type of absorption pattern, whereas naphthoimidazolyl moiety-based complexes (**2**, **3**, and **5**) displayed another type of absorption pattern. The high energy bands (λ_{max} = 256, 273, ~280, 292 nm for **1** and **4**; ~254, 292, 323, ~338, 353 for **2**, **3**, and **5**) corresponds to spin-allowed π–π* electronic transitions and intra-ligand charge transfer (ILCT), whereas low energy bands (λ_{max} = 373 nm for **1**, **3**, **4**, **5**, and 362 for **2**) are assigned to spin-allowed metal-to-ligand charge transfer (MLCT) transitions. The assignment of electronic transitions is

based on the literature report.[13a, 22] All the complexes show ligand-centred emission in the presence of oxygen and nitrogen at room temperature. The emission profile is quenched in the presence of air; the effect is more in the case of complex **1** than in other complexes. The benzimidazolyl moiety-based complexes (λ_{max} = ~518 nm for **1**, and λ_{max} = ~504 nm for **4**) showed a similar structureless emission profile. In contrast, naphthoimidazolyl moiety-based complexes (**2**, **3**, and **5**) displayed a similar pattern of structured emission in the range of ~356-547 nm. The appearance of broad emission shoulder at 455 nm for **2** and 437/464 (b) for **3** is due to the presence of L^1 (H_2-pBC), whereas it is absent in the case of **5**. The minor shoulder peak at ~493 nm for **1** may due to the nature of the H_2-pBC motifs, which is absent in complex **4**. The solid-state absorption spectra of the complexes are observed almost in the same range (~250-450 nm) as the solution state. All the complexes displayed a structureless emission pattern. The luminescence rigidochromic effect is more in the case of **1**, while other complexes show a more or less similar shift in both solid and solution states. The nature of the N-donor ditopic ligands and bischelating anionic donor ligands, the substituents and spacer units on them impact the luminescence behaviour of the complexes both in solution as well as solid state.

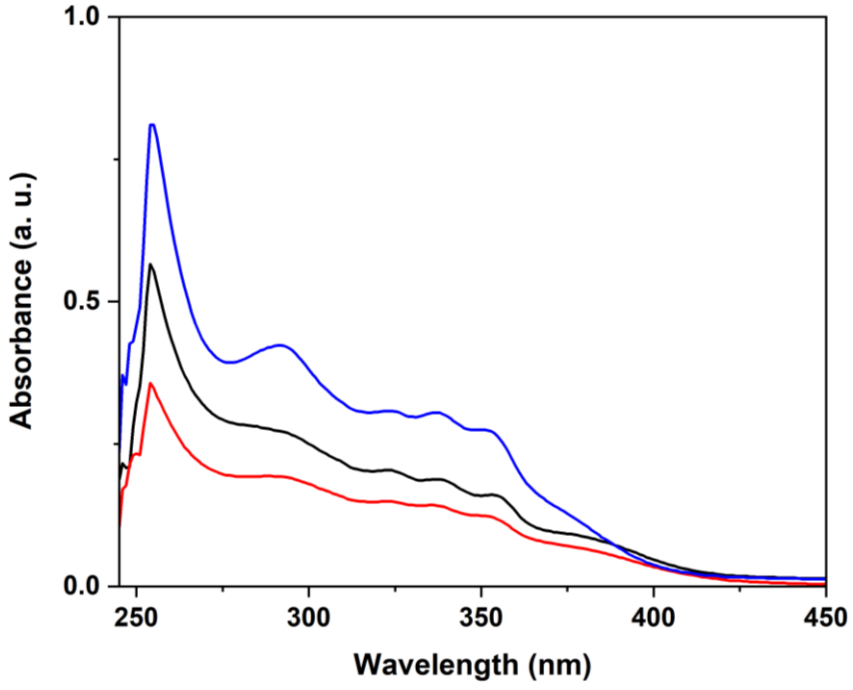

Figure 5.34. Absorption spectra of complex **2** (1.2×10^{-5} M, middle), **3** (1.0×10^{-5} M, bottom), and **5** (1.0×10^{-5} M, top) in DMSO.

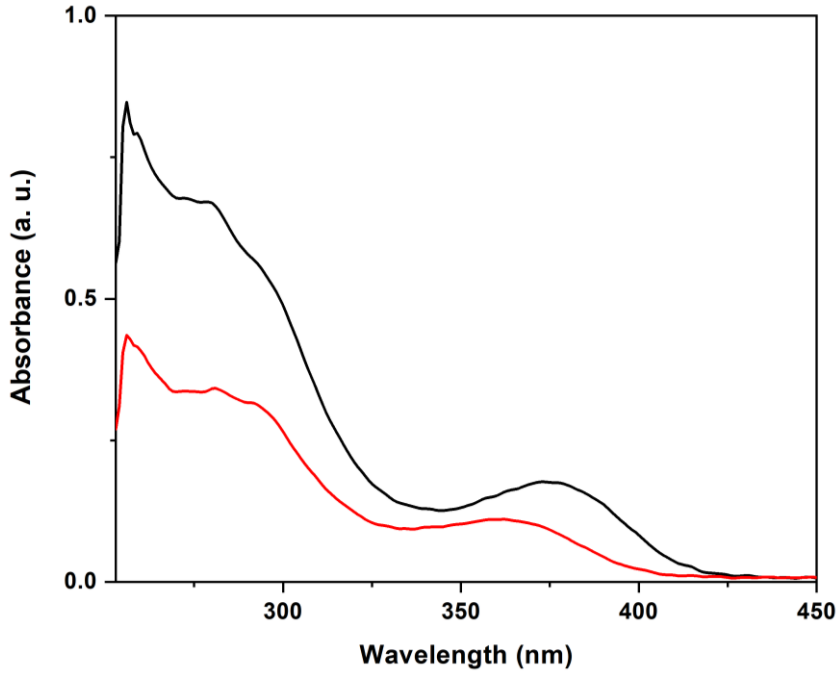

Figure 5.35. Absorption spectra of complex **1** (1.0×10^{-5} M, top) and **4** (1.2×10^{-5} M, bottom) in DMSO.

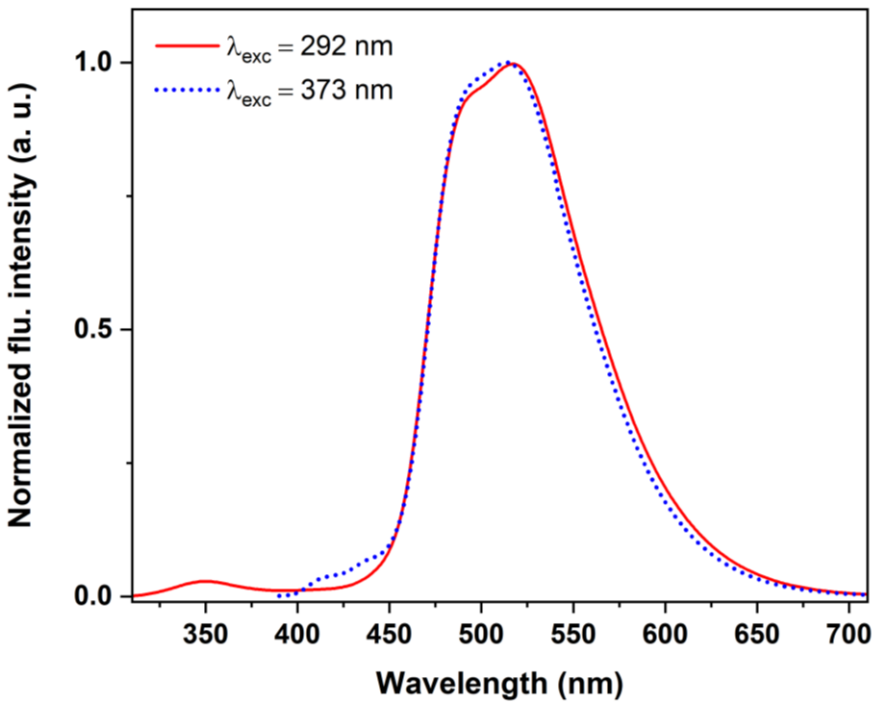

Figure 5.36. Emission spectra of complex **1** (1.16×10^{-4} M) in DMSO.

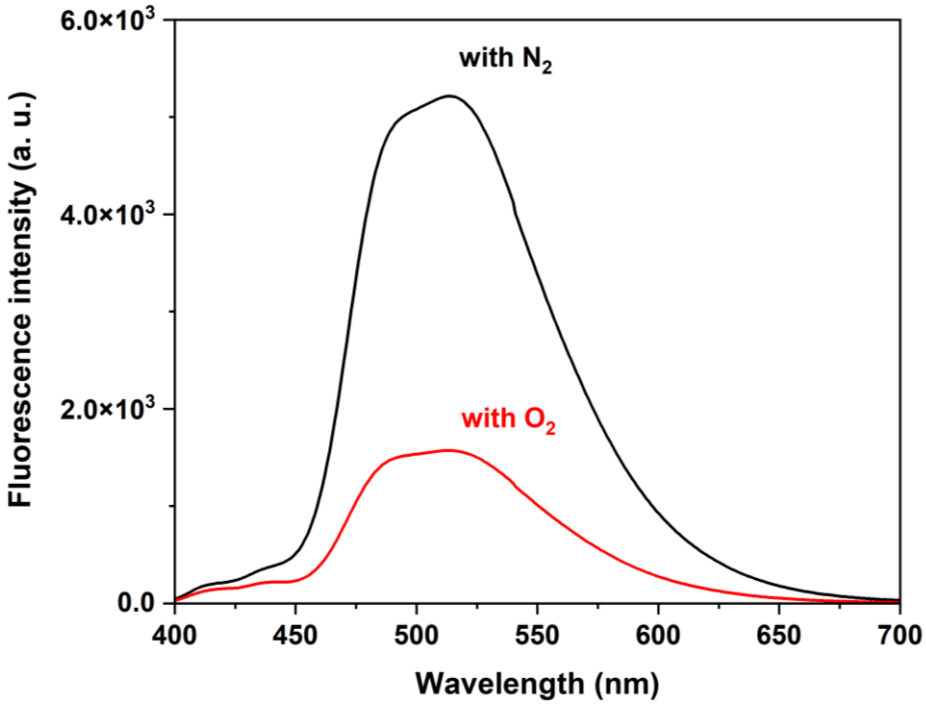

Figure 5.37. Emission spectra of complex **1** (1.16×10^{-4} M) in DMSO.

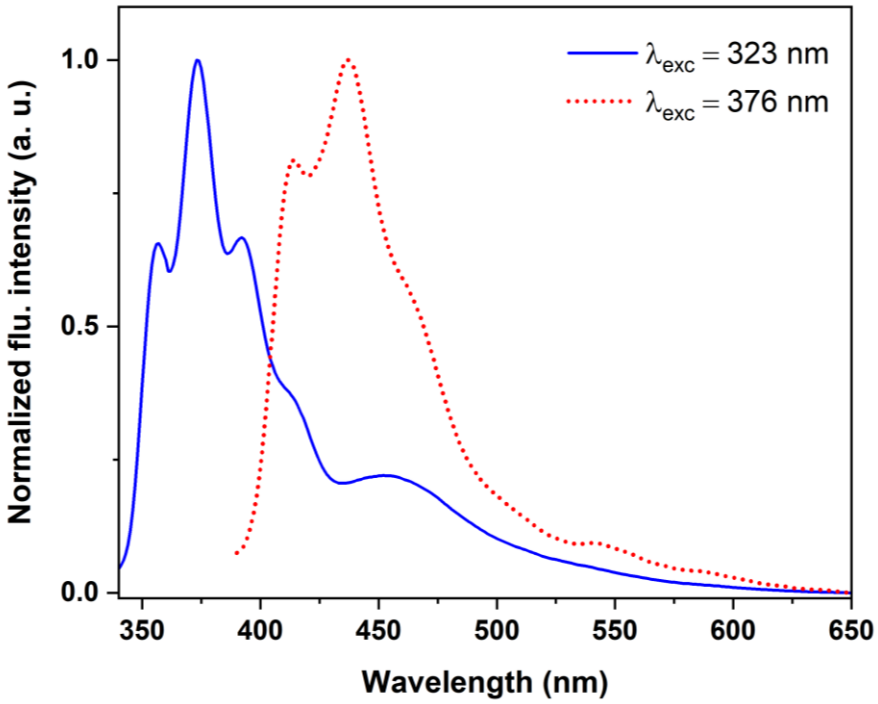

Figure 5.38. Emission spectra of complex **2** (6.10×10^{-5} M) in DMSO.

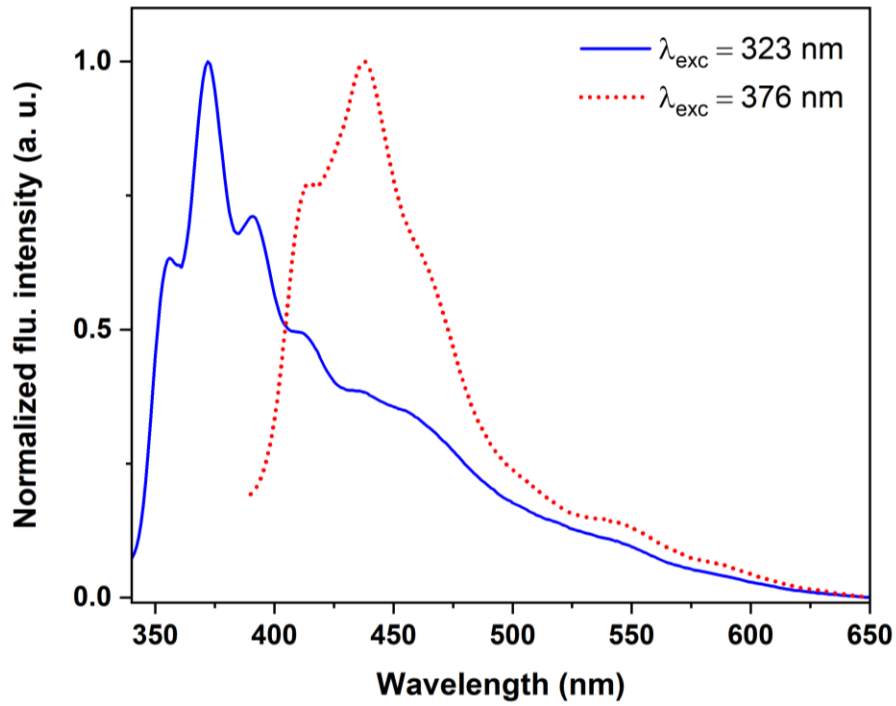

Figure 5.39. Emission spectra of complex **3** (6.40×10^{-5} M) in DMSO.

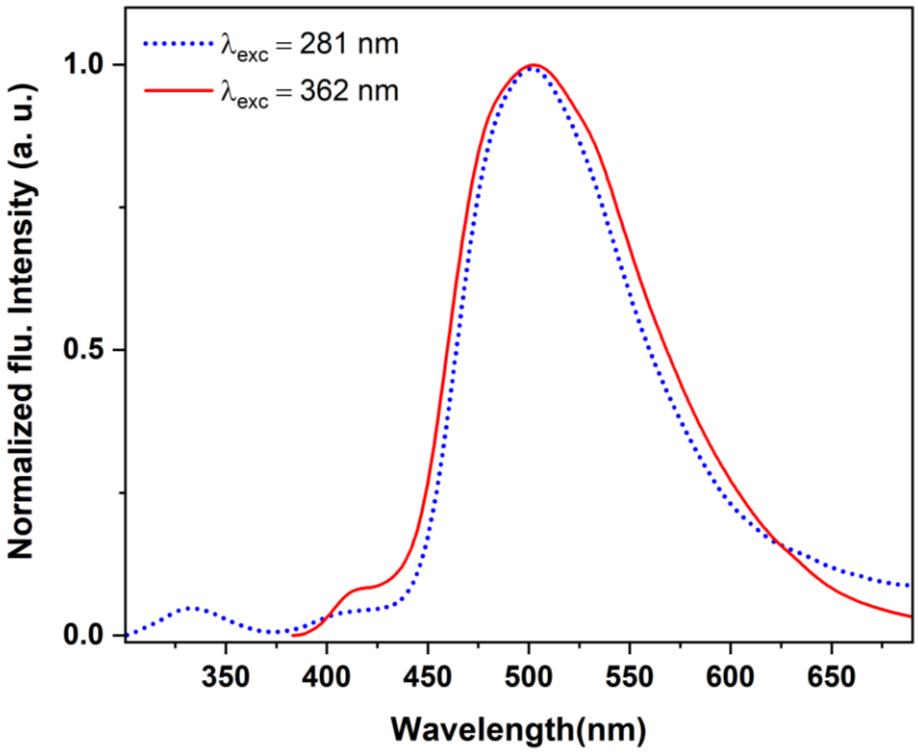

Figure 5.40. Emission spectra of complex **4** (9.13×10^{-5} M) in DMSO.

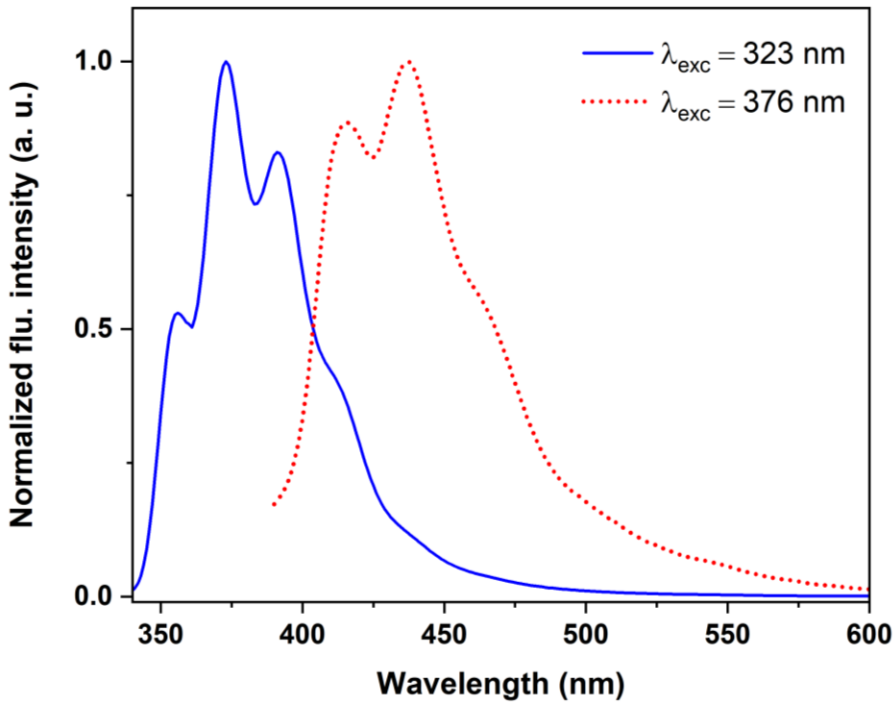

Figure 5.41. Emission spectra of complex **5** (6.13×10^{-5} M) in DMSO.

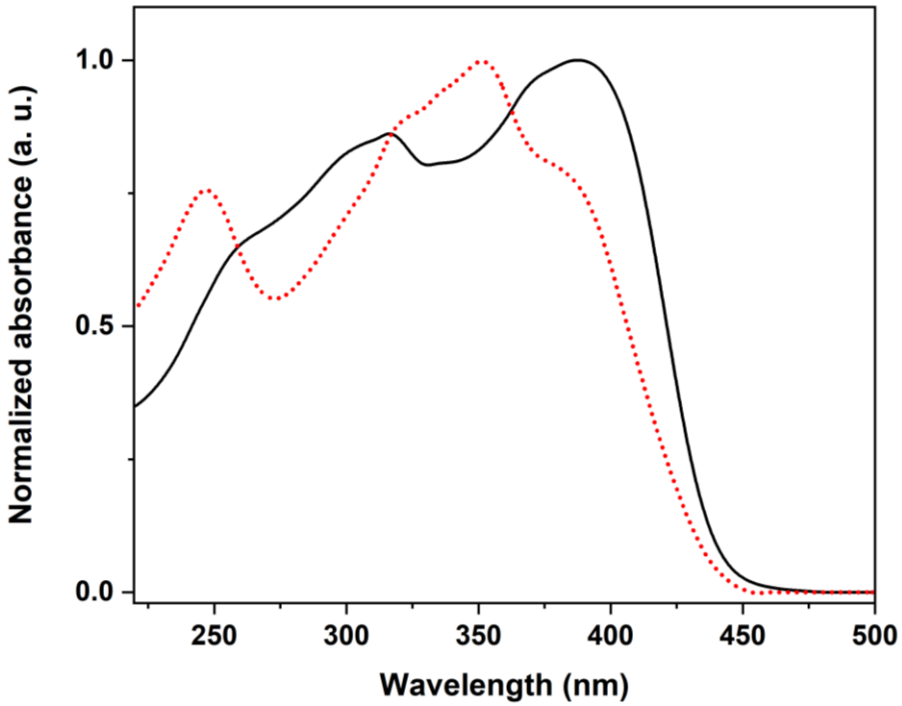

Figure 5.42. Absorption spectra of complex **1** (solid line, black) and **4** (⋯, red) in solid state.

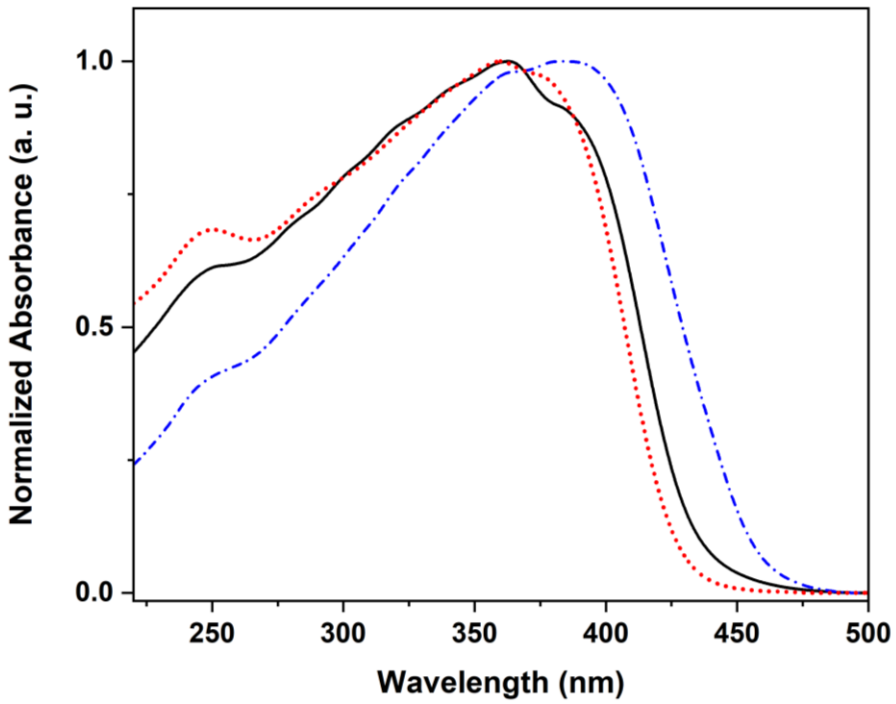

Figure 5.43. Absorption spectra of complex **2** (solid line, black), **3** (–·–·, blue), and **5** (···, red) in solid state.

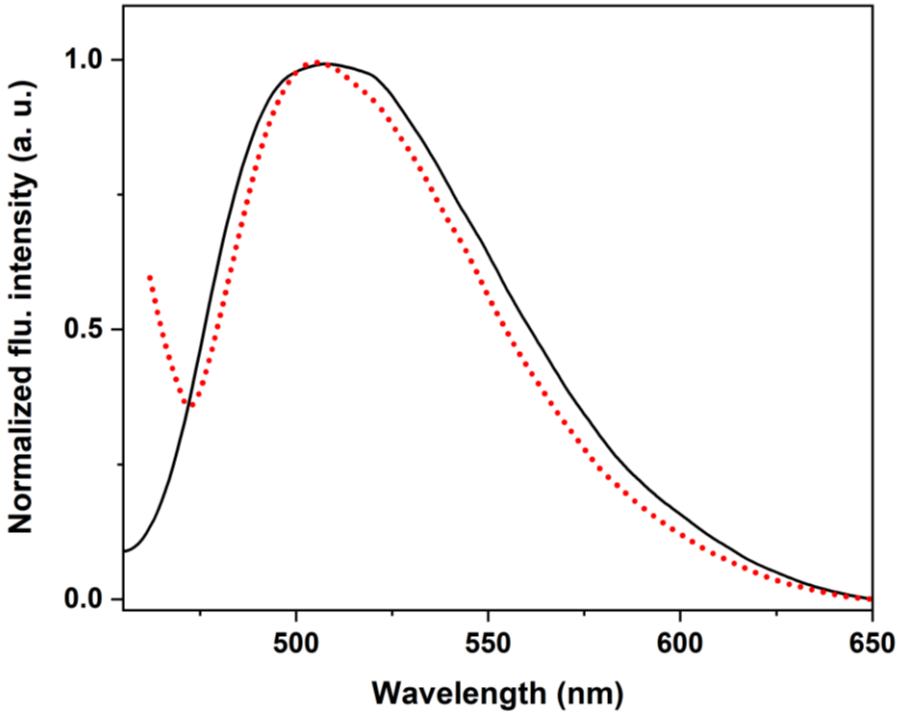

Figure 5.44. Emission spectra of complex **1** (solid line, black) and **4** (···, red) in solid state.

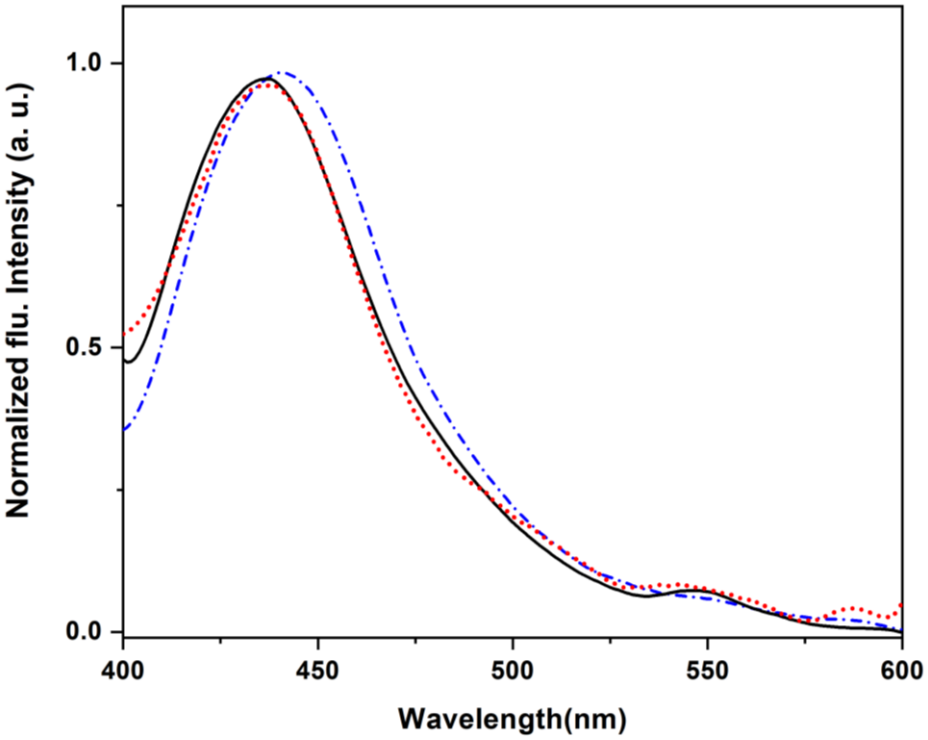

Figure 5.45. Emission spectra of complex **2** (solid line, black), **3** (–·–·, blue), and **5** (···, red) in solid state.

Table 5.2. Solid State Absorption and Emission Spectral Data for 1–5 in DMSO at 298

compounds	absorption	emission	
	λ_{max} (nm)	λ_{exc} (nm)	$\lambda_{em,\ max}$ (nm)
1	261, 300, 317, 388	420	509
2	252, 363, 385	363	436
3	250, 362, 384	362	440
4	247, 321, 351, 386	420	506
5	250, 360, 378	360	436

Table 5.3. Solution State Absorption and Emission Spectral Data for 1–5 in DMSO at 298 K.

complexes	absorption	emission	
	λ_{max} (nm)	λ_{exc} (nm)	$\lambda_{em,\ max}$ (nm)
1	256, 273, 280, 292, 373 (b)	292	350 (less intensity), 494, 518 (b, MLCT)
		373	414/436 (less intensity), 493 514 (b, MLCT)
2	254, 292, 323, 338, 353, 376	323	356, 373, 392, 415, 455(b)
		376	414, 437, 466, 544 (less intensity)
3	254, 292, 323, 336, 352, 376	323	356, 372, 391, 412, 437/464 (b), 546 (less intensity)
		376	414, 438, 466, 547 (less intensity)
4	256, 273, 281, 292, 362 (b)	281	332 (less intensity), 401(less intensity), 503 (b, MLCT)
		362	413 (less intensity), 504 (b, MLCT)
5	256, 292, 323, 338, 353, 373(b)	323	356, 373, 391, 414
		376	416, 437, 470

5.4 Conclusion

The self-assembly of rheniumtricarbonyl core based SCCs, **1**–**5** was achieved using $Re_2(CO)_{10}$, rigid/flexible bis-chelating HO∩N donor ligands and flexible ditopic N donor ligands via a one-pot approach. The metallosupramolecules were characterized by ATR-IR, ESI-MS, 1D and 2D NMR spectroscopy. The supramolecular structures of the complexes closely remain in the solution based on the ^{1}H NMR and ESI-mass analysis. Single-crystal X-ray analysis reveals that the dinuclear SCCs adopt heteroleptic double stranded helical and mesocate architectures in the solid-state. The photophysical properties of the complexes were studied both in solution and solid state. All the supramolecules display emission both in solution and solid state.

5.5 References

1. (a) Lehn, J. -M. Supramolecular Chemistry—Concepts and Perspectives, VCH, Weinheim, **1995**. (b) Lehn, J. -M. Perspectives in chemistry—steps towards complex matter. *Angew. Chem., Int. Ed*. **2013**, *52*, 2836-2850. (c) Hannon, M. J.; Childs, L. J. Helices and Helicates: Beautiful Supramolecular Motifs with Emerging Applications. *J. Supramol. Chem*. **2004**, *16*, 7-22. (d) Albrecht, M. Let's Twist Again–Double-Stranded, Triple-Stranded, and Circular Helicates *Chem. Rev*. **2001**, *101*, 3457–3498. (e) Piguet, C.; Bernardinelli, G.; Hopfgartner, G.; Helicates as Versatile Supramolecular Complexes. *Chem. Rev*. **1997**, *97*, 2005−2062.
2. (a) Paneerselvan, A. P.; Mishra, S. S.; Chand, D. K. Linear and circular helicates: A brief review. *J. Chem. Sci*. **2018**, *130*, 1–18. (b) Lehn, J. M.; Rigault, A.; Siegel, J.; Harrowfield, J.; Chevrier, B.; Moras, D. Spontaneous assembly of double-stranded helicates from oligobipyridine ligands and copper(I) cations: Structure of an inorganic double helix. *Proc. Natl. Acad. Sci. USA*. **1987**, *84*, 2565-2569. (c) Naranthatta, C. M.; Bandi, S.; Jagan R.; Chand, K. D.; Double-Stranded Binuclear Helicates and Helicity Modulation. *Cryst. Growth Des*. **2016**, 16, 6722−6728. (d) Ayme, J. F.; Lehn, J. M.; Bailly, C.; Karmazin, L. Simultaneous Generation of a [2 × 2] Grid-Like Complex and a Linear Double Helicate: a Three-Level Self-Sorting Process. *J. Am. Chem. Soc*. **2020**, 142, 5819–5824.
3. (a) Martínez-Calvo, M.; Romero M. J.; Pedrido. R.; González-Noya A. M.; Zaragozac. G. Bermejoa. M. R. Metal self-recognition: a pathway to control the formation of dihelicates and mesocates *Dalton Trans*. **2012**, *41*, 13395-13404. (b) Zhanga, Z.; Dolphin, D. A triple-stranded helicate and mesocate from the same metal and ligand. *Chem. Commun*. **2009**, 6931-6933. (c) Cui, F.; Li, S.; Jia, C.; Mathieson, J. S.; Cronin, L.; Yang, X.-J.; Wu, B. Anion-Dependent Formation of Helicates versus Mesocates of Triple-Stranded M_2L_3 (M = Fe^{2+}, Cu^{2+}) Complexes. *Inorg. Chem*. **2012**, *51*, 179–187. (d) Allison, S. J.; Cooke, D.; Davidson, F. S.; Elliott, P. I. P.; Faulkner, R. A.; Griffiths, H. B. S.; Harper, O. J.; Hussain, O.; Owen-Lynch, P. J.; Phillips, R. M.; Rice, C. R.; Shepherd, S. L.; Wheelhouse, R. T. Ruthenium-Containing Linear Helicates and Mesocates with Tuneable p53-Selective Cytotoxicity in Colorectal Cancer Cells. *Angew. Chem. Int. Ed*. **2018**, *57*, 9799-9804.
4. (a) Li, X.; Wu, J.; Wang, L.; He, C.; Chen, L.; Jiao, Y.; Duan, C. Mitochondrial DNA-targeted Ir^{III}-Containing Metallohelices with Tunable Photodynamic Therapy Efficacy in

Cancer Cells. Angew. Chem. Int. Ed. **2020**, *59*, 6420- 6427. (b) Li, X.; Shi, Z.; Wu, J.; Wu, J.; C, He.; Haoa, X.; Duan, C. Lighting up metallohelices: from DNA binders to chemotherapy and photodynamic therapy *Chem. Commun*. **2020**, 56, 7537-7548

5. (a) Cook, T. R.; Vajpayee, V.; Lee, M. H.; Stang, P. J.; Chi, K. -W. Biomedical and Biochemical Applications of Self-Assembled Metallacycles and Metallacages. *Acc. Chem. Res*. **2013**, *46*, 2464–2474. (b) Casini, A.; Woods, B.; Wenzel, M. The Promise of Self-Assembled 3D Supramolecular Coordination Complexes for Biomedical Applications. *Inorg. Chem*. **2017**, *56*, 14715−14729. (c) Gao, W. -X.; Zhang. H. N.; Jin, G. -X. Supramolecular catalysis based on discrete heterometallic coordinationdriven metallacycles and metallacages. *Coord. Chem. Rev*. **2019**, *386*, 69–84. (d) Chakrabarty, R.; Mukherjee, P. S.; Stang, P. J. Supramolecular Coordination: Self-Assembly of Finite Two- and Three-Dimensional Ensembles. *Chem. Rev*. **2011**, *111*, 6810–6918.
6. (a) Frischmann, P. D.; MacLachlan, M. J. Metallocavitands: an emerging class of functional multimetallic host molecules. *Chem. Soc. Rev.* **2013**, *42*, 871-890 and references therein. (b) Lippert, B.; Sanz Miguel, P. J. Metallatriangles and metallasquares: the diversity behind structurally characterized examples and the crucial role of ligand symmetry. *Chem. Soc. Rev*. **2011**, *40*, 4475-4487 and references therein. (c) Han, Y. F.; Li, H.; Jin, G. X. Host–guest chemistry with bi-and tetra-nuclear macrocyclic metallasupramolecules. *Chem. Commun.* **2010**, *46*, 6879-6890. (d) Therrien, B. Drug Delivery by Water-Soluble Organometallic Cages *Top. Curr. Chem*. **2012**, 319, 35-55. (e) Smulders, M. M. J.; Riddell, I. A.; Browne, C.; Nitschke, J. R. Building on architectural principles for three-dimensional metallosupramolecular construction. *Chem. Soc. Rev.* **2013**, *42*, 1728−1754. (f) Cook, T. R.; Stang, P. J. Recent Developments in the Preparation and Chemistry of Metallacycles and Metallacages via Coordination. *Chem. Rev*. **2015**, *115*, 7001–7045.
7. (a) Bauer, E. B.; Haase, A. A.; Reich, R. M.; Crans, D. C.; Kühn, F. E. Organometallic and coordination rhenium compounds and their potential in cancer therapy. *Coord. Chem. Rev.* **2019**, *393*, 79-117. (b) Haase, A. A.; Bauer, E. B.; Kühn, F. E.; Crans, D. C. Speciation and toxicity of rhenium salts, organometallics and coordination complexes. *Coord. Chem. Rev*. **2019**, *394*, 135-161.
8. (a) Ramakrishna, B.; Nagarajaprakash, R.; Veena, V.; Sakthivel, N.; Manimaran. B. Self-assembly of oxamidato bridged ester functionalised dirhenium metallastirrups: synthesis, characterisation and cytotoxicity studies. *Dalton Trans.* **2015**, *44*, 17629-17638. (b) Gupta, D.; Sathiyendiran, M. Rhenium-Carbonyl-Based Supramolecular Coordination

Complexes: Synthesis, Structure and Properties. *ChemistrySelect* **2018**, *3*, 7439-7458 and references cited therein. (c) Orsa, D. K.; Haynes, G. K.; Pramanik, S. K.; Iwunze, M. O.; Greco, G. E.; Krause, J. A.; Ho, D.; Williams, A. L.; Hill, D. A.; Mandal, S. K. Synthesis, characterization, and fluorescence and cytotoxicity studies of a tetrarhenium molecular rectangle. *Inorg. Chem. Commun.* **2007**, *10*, 821-824. (d) Balasingham, R. G.; Thorp-Greenwood, F. L.; Williams, C. F.; Coogan, M. P.; Pope, S. J. A. Biologically Compatible, Phosphorescent Dimetallic Rhenium Complexes Linked through Functionalized Alkyl Chains: Syntheses, Spectroscopic Properties, and Applications in Imaging Microscopy. *Inorg. Chem*. **2012**, *51*, 1419−1426. (e) Gupta, D.; Singh, V.; Hohloch, S.; Sathiyendiran, M.; Tedin, K.; Sarkar, B. Utilizing a series of *fac*-Re$(CO)_3$ core based quinonoid containing complexes for photophysical and cell imaging studies. *Polyhedron* **2015**, *100*, 243-250. (f) Govindarajan, R.; Nagarajaprakash, R.; Veena,V.; Sakthivel, N.; Manimaran, B. One-pot reaction of amide functionalized Re(I) based dinuclear metallacycles: Synthesis, characterization and evaluation for anticancer potential. *Polyhedron*. **2018**, *139*, 229–236.

9. (a) Dinolfo, P. H.; Hupp, J. T. Supramolecular coordination chemistry and functional microporous molecular materials. *Chem. Mater*. **2001**, *13*, 3113–3125. (b) Hupp, J. T. Rhenium-Linked Multiporphyrin Assemblies: Synthesis and Properties. *Struct. Bonding*, **2006**, *121*, 145-165. (c) Rohacova, J.; Ishitani, O. Photofunctional Multinuclear Rhenium(I) diimine Carbonyl Complexes. *Dalton Trans*. **2017**, *46*, 8899–8919. (d) Thanasekaran, P.; Lee, C. C.; Lu, K. L. One-Step Orthogonal-Bonding Approach to the Self-Assembly of Neutral Rhenium-Based Metallacycles: Synthesis, Structures, Photophysics, and Sensing Applications. *Acc. Chem. Res*. **2012**, *45*, 1403–1418. (e) Kumar, A.; Sun, S. S.; Lees, A. J. Directed assembly metallocyclic supramolecular systems for molecular recognition and chemical sensing, *Coord. Chem. Rev*. **2008**, *252*, 922-939.
10. (a) Sato, S.; Ishitani, O. Photochemical reactions of fac-rhenium(I) tricarbonyl complexes and their application for synthesis. *Coord. Chem. Rev*. **2015**, *282–283*, 50–59. (b) Cancelliere, A. M.; Puntoriero, F.; Serroni, S.; Campagna, C.; Tamaki, Y.; Saito, D.; Ishitani, O. Efficient trinuclear Ru(ii)–Re(i) supramolecular photocatalysts for CO_2 reduction based on a new tris-chelating bridging ligand built around a central aromatic ring. *Chem. Sci*. **2020**, 11, 1556–1563. (c) Sinha, D.; Parua, S. P.; Rajak, K. K. Synthesis and characterization of acrylate cyanide bridged dimeric fac-Rhenium(I) complex: Photophysical, selective CO_2 adsorption and theoretical studies. *J. Organomet.*

Chem. **2019**, *889*, 62–69.Dilworth, J. R. Rhenium chemistry – Then and Now. *Coord. Chem. Rev*. **2021**, *436*, 213822.

11. (a) Tseng, T. W.; Luo, T. T.; Liao, S. H.; Lu, K. H.; Lu, K. L. Isorecticular Synthesis of Dissectible Molecular Bamboo Tubes of Hexarhenium(I) Benzene-1,2,3,4,5,6-hexaolate Complexes. *Angew. Chem., Int. Ed*. **2016**, *55*, 8343-8347. (b) Coogan, M. P.; Fernndez-Moreira, V.; Kariuki, B. M.; Pope, S. J. A.; Thorp-Greenwood, F. L. A Rhenium Tricarbonyl 4′-Oxo-terpy Trimer as a Luminescent Molecular Vessel with a Removable Silver Stopper. *Angew. Chem., Int. Ed*. **2009**, *48*, 4965-4968. (c) Sathiyendiran, M.; Liao, R. T.; Thanasekaran, P.; Luo, T. T.; Venkataramanan, N. S.; Lee, G. H.; Peng, S. M.; Lu, K. L. Gondola-Shaped Luminescent Tetrarhenium Metallacycles with Crown-Ether-like Multiple Recognition Sites. *Inorg. Chem.*, **2006**, *45*, 10052-10054. (d) Sathiyendiran, M.; Tsai, C. C.; Thanasekaran, P.; Luo, T. T.; Yang, C. I.; Lee, G. H.; Peng, S. M.; Lu, K. L. Organometallic Calixarenes: Syceelike Tetrarhenium(I) Cavitands with Tunable Size, Color, Functionality, and Coin–Slot Complexation. *Chem. – Eur. J*. **2011**, *17*, 3343-3346.
12. (a) Shankar, B.; Marimuthu, R.; Sathiyashivan, S. D.; Sathiyendiran, M. Spheroid metallacycles and metallocavitands with calixarene-and/or cleft-shaped receptors on the surface. *Inorg. Chem.* **2016**, *55*, 4537-4544. (b) Gupta, D.; Rajakannu, P.; Shankar, B.; Hussain, F.; Sathiyendiran, M. Synthesis and crystal structure of a wheel-shaped supramolecular coordination complex. *J. Chem. Sci.*, **2014**, *126*, 1501-1506.
13. (a) Shankar, B.; Sahu, S.; Deibel, N.; Schweinfurth, D.; Sarkar, B.; Elumalai, P.; Gupta, D.; Hussain, F.; Krishnamoorthy, G.; Sathiyendiran, M. Luminescent Dirhenium(I)-Double-Heterostranded Helicate and Mesocate. *Inorg. Chem*. **2014**, *53*, 922−930. (b) Saxena, P.; Shankar, B.; Sathyanarayana, A.; Prabusankar G.; Sathiyendiran, M. Rhenium(i)-based Double-heterostranded Helicates. *Chimia*. **2015**, *69*, 675–677. (c) Soumya, K. R.; Arumugam, R.; Shankar B.; Sathiyendiran, M.; *Inorg. Chem*. **2018**, *57*, 10718–10725. (d) Shankar, B.; Elumalai, P.; Jackmil, P. J.; Kumar, P.; Singh, S.; Sathiyendiran, M. Synthesis of rhenium-based M_2LL^0-type supramolecular coordination complexes from flexible ligands. *J. Organomet. Chem.* **2013**, *743*, 109-113.
14. (a) Botana, E.; Silva, E. D.; Benet-Buchholz, J.; Ballester, P.; de Mendoza, Inclusion of Cavitands and Calix[4]arenes into a Metallobridged para -(1H -Imidazo[4,5-f][3,8]phenanthrolin-2-yl)-Expanded Calix[4]arene. *Angew. Chem., Int. Ed*. **2007**, *46*, 198-201. (b) Lu, Z. Z.; Lee, C. C.; Velayudham, M.; Lee, L. W.; Wu, J. Y.; Kuo, T. S.; Lu, K. L. Control of Light-Promoted [2+2] Cycloaddition Reactions by a Remote

Ancillary Regulatory Group That Is Covalently Attached to Rhenium Rectangles. *Chem. – Eur. J.* **2012**, *18*, 15714-15721. (c) Su, C. Y.; Cai, Y. P.; Chen, C. L.; Smith, M. D.; Kaim, W.; zur Loye, H. C. Ligand-Directed Molecular Architectures: Self-Assembly of Two-Dimensional Rectangular Metallacycles and Three-Dimensional Trigonal or Tetragonal Prisms. *J. Am. Chem. Soc.* **2003**, *125*, 8595-8613.

15. (a) Slone, R. V.; Benkstein, K. D.; Bélanger, S.; Hupp, J. T.; Guzei, I. A.; Rheingold, A. L. Luminescent transition-metal-containing cyclophanes ("molecular squares"): covalent self-assembly, host-guest studies and preliminary nanoporous materials applications. *Coord. Chem. Rev*. **1998**, 171, 221-243. (b) Sun, S. S.; Lees, A. J. Transition metal based supramolecular systems: synthesis, photophysics, photochemistry and their potential applications as luminescent anion chemosensors. *Coord. Chem. Rev.* **2002**, *230*, 171-192.
16. Han, X.; Ma, H.; Wang, Y. A Simple and Efficient Synthesis of 2-Aryl-Substituted Benzimidazoles. *Russ. J. Org. Chem*. **2008**, *44*, 872-874.
17. Grobler, I.; Smith, V. J.; Bhatt, P. M.; Herber, S. A.; Barbour, L. J. Tunable Anisotropic Thermal Expansion of a Porous Zinc(II) Metal–Organic Framework. *J. Am. Chem. Soc.* **2013**, *135*, 6411– 6414.
18. van der Made, A. W.; van der Made, R. H. A Convenient Procedure for Bromomethylation of Aromatic Compounds, Selective Mono-, Bis-, or Trisbromomethylation. *J. Org. Chem.* **1993**, *58*, 1262-1263.
19. Zhao, X. -L.; Sun, D.; Hu, T. -P.; Yuan, S.; Gu, L. -C.; Cong, H. -J.; Hea, H. –Y.; Sun, D. –F. Phase transfer catalyst supported, room temperature biphasic synthesis:a facile approach to the synthesis of coordination polymers. *Dalton Trans*. **2012**, *41*, 4320– 4323.
20. Chahen, L.; Therrien, B.; Suss-Fink, G. Square-planar dichloro palladium complexes with trans-configurated phosphine ligands avoiding ortho-metallation: Ligand design, complex synthesis, molecular structure and catalytic potential for Suzuki cross-coupling reactions. *J. Organomet. Chem*. **2006**, *691*, 4257– 4264.
21. Bhol, M.; Claude, G.; Jungfer, M. R.; Abram, U.; Sathiyendiran, M. Calix[4]arene-Analogous Technetium Supramolecules. *Inorg. Chem*. **2022**, *61*, 5173–5177.
22. Bhol, M.; Shankar, B.; Sathiyendiran, M. Rhenium(I) based irregular pentagonal-shaped metallacavitands. *Dalton Trans.* **2018**, *47*, 4494−4500.
23. Arumugam, R.; Shankar, B.; Soumya, K. R.; Sathiyendiran, M. fac-Re(CO)3-based neutral heteroleptic tetrahedrons. *Dalton Trans*. **2019**, *48*, 7425-7431.

24. (a) Sheldrick, G. M. "SHELXS-97 and SHELXL-97, Program for Crystal Structure Solution and Refinement," University of Gottingen, Gottingen, 1997. (b) Sheldrick, G. M. A short history of SHELX. *Acta Crystallogr., Sect. A: Found. Crystallogr.* **2008**, *64*, 112–122. (c) Sheldrick, G. M. Crystal structure refinement with SHELXL. *Acta Crystallogr., Sect. C: Struct. Chem*. **2015**, *71*, 3–8.
25. (a) Vlcek, A. Ultrafast Excited-State Processes in Re(I)Carbonyl-Diimine Complexes: From Excitation to Photochemistry. *Top. Organomet. Chem*. **2009,** *29*, 115−158. (b) Giordano, P. J.; Wrighton, M. S. The Nature of the Lowest Excited State in *fac*-Tricarbonylhalobis(4-phenylpyridine) rhenium (I) and *fac*-Tricarbonylhalobis(4, 4' -bipyridine) rhenium(I): Emissive Organometallic Complexes in Fluid Solution. *J. Am. Chem. Soc.* **1979**, *101*, 2888−2897.

Chapter 6

Conclusion and Future Prospects

Abstract

The thesis entitled "Rhenium- and Technetium-tricarbonyl Core-based Supramolecular Metallocavitands and Helicates" discusses the design, and synthetic principles for the construction of novel neutral, flexible bidentate nitrogen donor ligands with diarylmethane spacers and their corresponding [*fac*-M(CO)$_3$]$^+$ (M = Re/Tc) core-based supramolecular architectures, which include mononuclear rhenium/technetium homoleptic metallacalix[4]arenes, dinuclear rhenium heteroleptic metallacalix[5]arenes, and dinuclear rhenium heterostranded helicates and mesohelicates. In this chapter, the thesis is summarized, and the possible future direction of the present work and potential future application of the rhenium- and technetiumtricarbonyl complexes are briefly discussed.

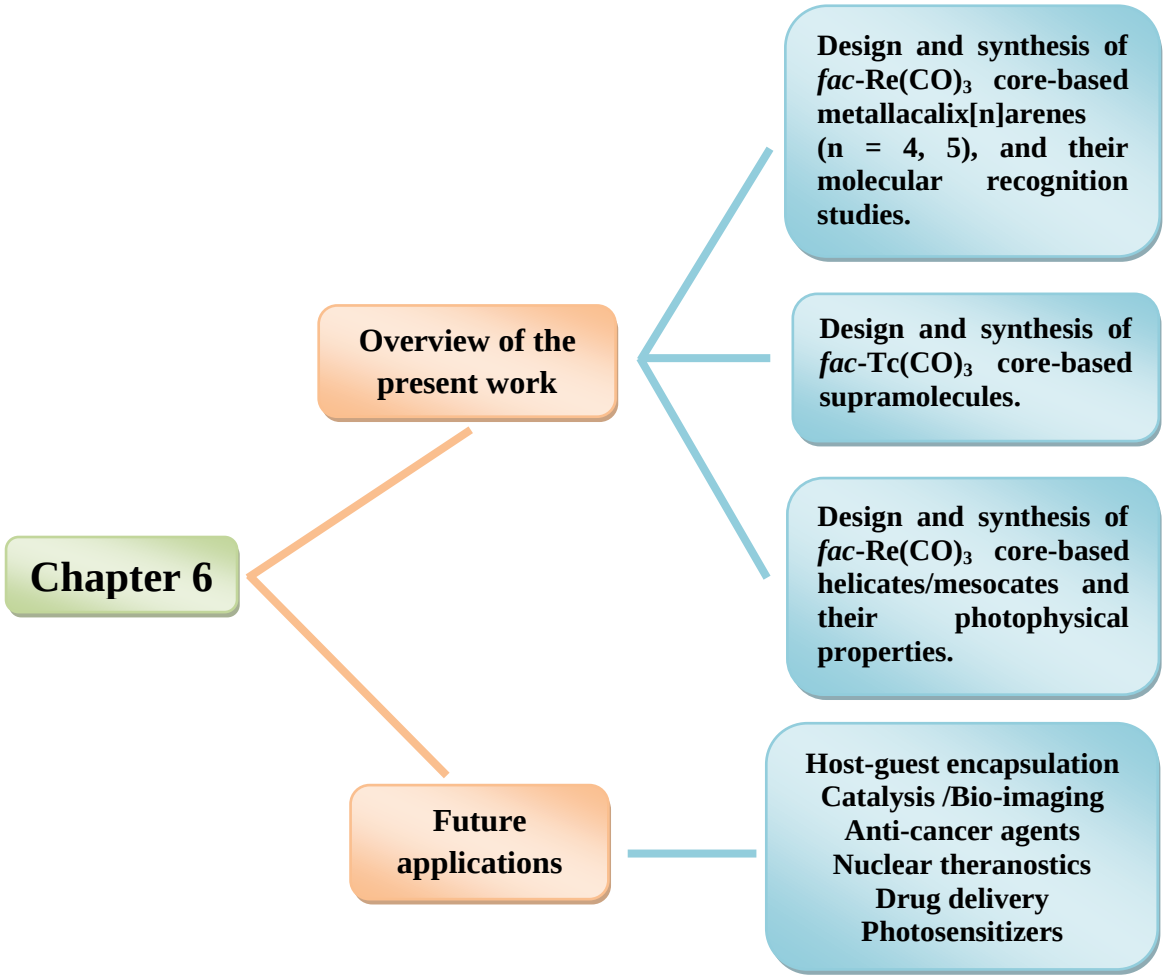

6.1. Overview of the present work

The facial rheniumtricarbonyl core-based metallomacrocycles exhibit a distinctive class of stable, functional, and robust metal-based cyclic architectures to form neutral 2D and 3D metallocycles.[1-3] The *fac*-$Re(CO)_3$ fragment is kinetically inert and biocompatible, which makes it a very significant unit in the medicinal field. [1-4] Further, the *fac*-$Re(CO)_3$ core-based SCCs display potential applications in molecular recognition, as photoluminescence quenching probes, cavity-controlled catalysis, anticancer agents, photo- and electro-chemical sensing.[1-3] The appropriate choice of nitrogen donors with/without ancillary ligands and rhenium metal precursors can achieve various shapes and sizes of metallocycles. Due to virtually identical chemical and physical properties of Re and Tc (Atomic radii: Re- 1.37 Å; Tc- 1.36 Å, lipophilicity, ionic mobility and formal charge), advances in the *fac*-$Re(CO)_3$ based chemistry can be exploited for the designing and development of new stable and kinetically inert *fac*-$[M(CO)_3]^+$ (M = ^{99m}Tc/ $^{186/188}$Re) core-based radiopharmaceuticals as diagnostic and therapeutic agents.[5-6] Though a considerable amount of research has focused on acyclic systems with *fac*-$Tc(CO)_3$ core, till now, only one example has been reported for Tc(I) core containing metallomacrocycles.

The flexible benzimidazolyl and its structural analogous based ditopic N-donors have attracted attention as versatile structural framework for making cavity-containing *fac*-$[Re(CO)_3]$ core-based metallacalix[4]arenes. Although a variety of rhenium heteroleptic, neutral metallacalixarenes are reported, the hydrophobic cavity is small to accommodate guest molecules entirely or partially. This research focuses on increasing the cavity size by modulating the spacer on N-donor ligands which can accommodate potential guest molecules entirely inside their hydrophobic cavity. Rhenium(I) based metallocavitands analogous to calix[5]arene framework with larger cavity were synthesized by using $Re_2(CO)_{10}$, rigid bis-chelating donor, and neutral ditopic flexible N-donor ligands possessing bis(4-methylphenyl)methane spacer via solvothermal approach. These metallocavitands adopt tubular structure, accommodate toluene molecule in the solid state, and are able to recognize the guest molecules, including nitroaromatic compounds and polyaromatic hydrocarbons in the solution. We are successful in making *fac*-$[Re(CO)_3]$ core-based metallocavitands analogous to calix[5]arene and have a larger hydrophobic cavity than the metallocavitand

similar to calix[4]arene framework. To the best of our knowledge, this is the first example of rhenium-core based metallocavitands analogous to calix[5]arene. This study provides a way to prepare metallocavitands with a tunable cavity and functional group via a simple one-pot method.

The internal cavity size of the *fac*-[$Re(CO)_3$] core-based metallocavitands can be further tuned by modifying the N-donor ligands or/and by changing the bis-chelating motifs. The heteroleptic *fac*-[$Re(CO)_3$] core-based metallocavitands analogous to calix[5]arene were synthesized using two new neutral, flexible ditopic nitrogen donors, bis-chelating ligands and $Re_2(CO)_{10}$ *via* one-pot synthesis. These metallocavitands adopt tubular structure, accommodate acetone, mesitylene, toluene, and chlorobenzene guest molecules in the solid state and are able to recognize substituted phenol and nitrobenzene as guest molecules in the solution. To the best of our knowledge, this is the second example of rhenium-core based metallocavitands similar to calix[5]arene from our research group. This study provides an easy synthetic approach for assembling neutral, heteroleptic pentagonal toroid-shaped *fac*-[$Re(CO)_3$] core-based host molecules.

This research work provides a new synthetic strategy to design and synthesize *fac*- $Tc(CO)_3$ core-based supramolecules analogous to calix[4]arene. Two new types of neutral, flexible ditopic nitrogen donor ligands with bismesitylene spacer were designed and synthesized. Further, N-donor ligands are utilized to assemble technetium supramolecules using $(NBu_4)[Tc_2(\mu\text{-}Cl)_3(CO)_6]$. Isostructural rhenium macrocycles were also assembled from $[Re(CO)_5X]$ (X= Cl, Br) and L^n. The solid-state structures of the supramolecules reveal that these molecules adopt bowl-shaped structures. The molecular recognition studies of rhenium macrocycles were studied with potential guest molecules, including benzene, naphthalene, anthracene, imidazole, and benzimidazole. To the best of our knowledge, the technetium complexes are the first examples of *fac*-$[Tc(CO)_3]^+$ core-based SCCs analogous to calix[4]arenes and the second Tc-containing metallomacrocycles. The results enable the design of unique *fac*-$[Tc(CO)_3]^+$ core-based supramolecules and extend the entry into the field of supramolecules.

The nature and length of the spacer motifs in the organic ligand frameworks play an essential role in getting the helicate or meso-helicate architectures. This research focuses on the design principles of synthesizing *fac*–[$Re(CO)_3$] core-based dinuclear helicates and mesocates. The helicates/ meso-helicates were self-assembled using $Re_2(CO)_{10}$, rigid/flexible bis-chelating HO∩N donor ligands, and flexible ditopic N donor ligands via a one-pot approach. Photo-physical properties show that all the supramolecules display emissions in solution and solid states. We have successfully synthesized *fac*–[$Re(CO)_3$] core-based dinuclear helicates and mesocates, which may have the potential application in biology.

6.2. Future directions

The development of new synthetic approaches is still under process to increase the width of the *fac*-[$Re(CO)_3$] and *fac*-[$Tc(CO)_3$] core-based metallocavitands, tuning functional groups at the periphery as well as to make calix[n]arene (n = 6,7)-shaped metallocavitands. Host-guest properties will be studied in both solid and solution states with various potential guest molecules, including biomolecules. In future, the suitable design of fac-$[Tc(CO)_3]^+$ core-based supramolecules may find potential utility in the medicinal fields due to the combined properties of the technetium core and guest encapsulation properties of the macrocyclic cavity. DNA recognition properties of the helicates/mesocates will be carried out, and the photophysical properties will be studied by using the time-dependent density functional theory.

The stable and kinetically inert *fac*-$[M(CO)_3]^+$ (M = ^{99m}Tc/ $^{186/188}$Re) core-based complexes have been gaining continuous research interest for the development of new radiopharmaceuticals as diagnostic and therapeutic agents.[4-5] The low spin d^6 electronic configuration of Re(I) and Tc(I) makes their complexes kinetically inert and biocompatible, providing high advantages in the medicinal field.[1-5] In addition to their kinetic inertness, thermal and phot-stability, luminescence, membrane permeability, and large stoke's shift properties offer numerous opportunities for developing novel supramolecules for applications in host-guest encapsulation, bio-imaging, transport through the cell membrane, DNA recognition, anti-cancer activities, and light-harvesting systems.[1-3]

6.3. References

1. (a) Thanasekaran, P.; Lee, C. C.; Lu, K. L. One-Step Orthogonal-Bonding Approach to the Self-Assembly of Neutral Rhenium-Based Metallacycles: Synthesis, Structures, Photophysics, and Sensing Applications. *Acc. Chem. Res*. **2012**, *45*, 1403–1418. (b) Dinolfo, P. H.; Hupp, J. T. Supramolecular coordination chemistry and functional microporous molecular materials. *Chem. Mater*. **2001**, *13*, 3113–3125. (c) Gupta, D.; Sathiyendiran, M. Rhenium-Carbonyl-Based Supramolecular Coordination Complexes: Synthesis, Structure and Properties. *ChemistrySelect*. **2018**, *3*, 7439-7458 and references cited there in.
2. (a) Cook, T. R.; Vajpayee, V.; Lee, M. H.; Stang, P. J.; Chi, K. W. Biomedical and Biochemical Applications of Self-Assembled Metallacycles and Metallacages. *Acc. Chem. Res.* **2013**, *46*, 2464-2474. (b) Cook, T. R.; Stang, P. J. Recent Developments in the Preparation and Chemistry of Metallacycles and Metallacages via Coordination. *Chem. Rev*. **2015**, *115*, 7001-7045.
3. (a) Bauer, E. B.; Haase, A. A.; Reich, R. M.; Crans, D. C.; Kühn, F. E. Organometallic and coordination rhenium compounds and their potential in cancer therapy. *Coord. Chem. Rev.* **2019**, *393*, 79-117. (b) Ramakrishna, B.; Nagarajaprakash, R.; Veena, V.; Sakthivel, N.; Manimaran. B. Self-assembly of oxamidato bridged ester functionalised dirhenium metallastirrups: synthesis, characterisation and cytotoxicity studies. *Dalton Trans.* **2015**, *44*, 17629-17638. (c) Balasingham, R. G.; Thorp-Greenwood, F. L.; Williams, C. F.; Coogan, M. P.; Pope, S. J. A. Biologically Compatible, Phosphorescent Dimetallic Rhenium Complexes Linked through Functionalized Alkyl Chains: Syntheses, Spectroscopic Properties, and Applications in Imaging Microscopy. *Inorg. Chem*. **2012**, *51*, 1419−1426. (d) Sato, S.; Ishitani, O. Photochemical reactions of fac-rhenium(I) tricarbonyl complexes and their application for synthesis. *Coord. Chem. Rev*. **2015**, *282–283*, 50–59.
4. Fernandez-Moreira, V.; Thorp-Greenwood, F. L.; Coogan, M. P. Application of d^6 transition metal complexes in fluorescence cell imaging. *Chem. Commun*. **2010**, *46*, 186-202.
5. a) Alberto, R.; Schibli, R.; Waibel, R.; Abram, U.; Schubiger, A. P. Basic aqueous chemistry of $[M(OH_2)_3(CO)_3]^+$ (M=Re, Tc) directed towards radiopharmaceutical

application. *Coord. Chem. Rev*. **1999**, *190-192*, 901-919. (b) Waibel, R.; Alberto, R.; Willuda, J.; Finnern, R.; Schibli, R.; Stichelberger, A.; Egli, A.; Abram, U.; Mach, J. –P.; Plückthun, A.; Schubiger, P. A. Stable one-step technetium-99m labeling of His-tagged recombinant proteins with a novel Tc(I)–carbonyl complex. *Nature Biotechnol*. **1999**, *17*, 897-901.

6. (a) Abram, U.; Alberto, R. Technetium and rhenium: coordination chemistry and nuclear medical applications. *J. Braz. Chem. Soc.* **2006**, *17*, 1486-1500. (b) Papagiannopoulou, D. Technetium-99m radiochemistry for pharmaceutical applications. *J. Labelled Comp. Radiopharm.* **2017**, *60*, 502-520.

Publications

A. Publications from thesis work:

1. **Bhol, M.**; Shankar, B.; Sathiyendiran, M. Rhenium(I) based irregular pentagonal-shaped metallacavitands. *Dalton Trans.* **2018**, *47*, 4494-4500.
2. **Bhol, M.**; Claude, G.; Roca Jungfer, M.; Abram, U.; Sathiyendiran. M. Calix[4]arene-Analogous Technetium Supramolecules. *Inorg. Chem.* **2022**, *61*, 5173−5177.
3. **Bhol, M.**; Shankar, B.; Sathiyendiran, M. Rhenium(I) Based Heteroleptic Pentagonal Toroid Shaped Metallocavitands: Self-Assembly and Molecular Recognition Studies. *Inorg. Chem.* **2022**, DOI:10.1021/acs.inorgchem.2c02061.
4. **Bhol, M.**; Shankar, B.; Wolff, M.; Sathiyendiran, M. Self-Assembly and Photophysical Properties of Rheniumtricarbonyl-Based Helicates and Mesocates (*To be communicated*).

B. Other Publications:

1. **Bhol, M.**; Priyatharsini, M.; Krishnakumar, R. V.; Sathiyendiran, M. Solid state structure and photophysical properties of monoanionic 2-(2′-hydroxyphenyl)benzimidazole as an anionic core in rhenium complex. *J. Organomet. Chem.* **2019**, *889*, 27-32.
2. Mishra, I.; † **Bhol. M.**; † Kalimuthu. P.; Sathiyendiran. M. Emerging Spacers-Based Ligands for Supramolecular Coordination Complexes. *Chem. Rec.* **2021**, *21*, 594-614 (†Equal Contribution).

Poster and Oral Presentations

1. **Poster:** *NMSTC-2017: National Meeting of Synthetic and Theoretical Chemists***,** University of Hyderabad, Telangana, India; 2017 Oct. 13-14.
2. **Poster:** *ICCCS-2017: 8th International Collaborative & Cooperative Chemistry Symposium*, University of Hyderabad, Telangana, India; 2017 Dec 18-19.
3. **Poster:** *CHEMFEST-2018: 15th Annual in- House Symposium*, University of Hyderabad, Telangana, India; 2018 Mar. 9-10 **(Best Poster Award).**
4. **Poster:** *CHEMFEST-2019: 16th Annual in- House Symposium*, University of Hyderabad, Telangana, India; 2019 Feb. 22-23 **(Best Poster Award).**
5. **Oral:** *ACST-2019: International Conference on Advances in Chemical Sciences and Technologies*, National Institute of Technology, Warangal, India; 2019 Sep. 23-25.
6. **Poster**: *MTIC 2019: International Conference on Modern Trends In Inorganic Chemistry-XVIII*, Indian Institute of Technology Guwahati, Assam, India; 2019 Dec.11-14.
7. **Poster:** *CHEMFEST-2020: 17th Annual in- House Symposium*, University of Hyderabad, Telangana, India; 2020 Feb. 27-28.
8. **Oral:** *CHEMFEST-2020: 19th Annual in- House Symposium*, University of Hyderabad, Telangana, India; 2022 Apr. 22-23 **(Best Oral Presentation Award by RSC).**

Rhenium- and Technetium-tricarbonyl Core-based Supramolecular Metallocavitands and Helicates

by Mamina Bhol

Submission date: 15-Jul-2022 12:38PM (UTC+0530)
Submission ID: 1870784185
File name: Mamina_Bhol_Thesis_16CHPH14.pdf (1.57M)
Word count: 16861
Character count: 92054

Rhenium- and Technetium-tricarbonyl Core-based Supramolecular Metallocavitands and Helicates

ORIGINALITY REPORT

51%	18%	50%	2%
SIMILARITY INDEX	INTERNET SOURCES	PUBLICATIONS	STUDENT PAPERS

PRIMARY SOURCES

1	Mamina Bhol, Bhaskaran Shankar, Malaichamy Sathiyendiran. "Rhenium(I)-Based Heteroleptic Pentagonal Toroid-Shaped Metallocavitands: Self-Assembly and Molecular Recognition Studies", Inorganic Chemistry, 2022 Publication	20%
2	Mamina Bhol, Guilhem Claude, Maximilian Roca Jungfer, Ulrich Abram, Malaichamy Sathiyendiran. "Calix[4]arene-Analogous Technetium Supramolecules", Inorganic Chemistry, 2022 Publication	12%
3	pubs.rsc.org Internet Source	11%
4	Mamina Bhol, Bhaskaran Shankar, Malaichamy Sathiyendiran. " Rhenium( ) based irregular pentagonal-shaped metallacavitands ", Dalton Transactions, 2018 Publication	1%

M. Sathiyendiran
Dr. M.Sathiyendiran
Professor
School of Chemistry
University of Hyderabad
Hyderabad - 500 046, India.

5	Submitted to University of Hyderabad, Hyderabad Student Paper	1 %
6	Deepak Gupta, Malaichamy Sathiyendiran. "Rhenium - Carbonyl - Based Supramolecular Coordination Complexes: Synthesis, Structure and Properties", ChemistrySelect, 2018 Publication	1 %
7	www.pubfacts.com Internet Source	1 %
8	docksci.com Internet Source	<1 %
9	Antonio Shegani, Myrto Ischyropoulou, Ioanna Roupa, Christos Kiritsis et al. "Synthesis and evaluation of new mixed "2 + 1" Re, 99mTc and 186Re tricarbonyl dithiocarbamate complexes with different monodentate ligands", Bioorganic & Medicinal Chemistry, 2021 Publication	<1 %
10	Bhaskaran Shankar, Palani Elumalai, Ramasamy Shanmugam, Malaichamy Sathiyendiran. "Neutral heteroleptic rhenium-based M3L3L' type metallacycles: Synthesis, structural characterization and DFT/TDDFT studies", Journal of Organometallic Chemistry, 2014 Publication	<1 %

M. Sathiyendiran.
Dr. M.Sathiyendiran
Professor
School of Chemistry
University of Hyderabad
Hyderabad - 500 046, India.

11	K. R. Soumya, Ramar Arumugam, Bhaskaran Shankar, Malaichamy Sathiyendiran. "Sulfate Donor Based Dinuclear Heteroleptic Triple-Stranded Helicates from Sulfite and Ditopic Nitrogen Donor Ligands and Their Transformation to Dinuclear Homoleptic Double-Stranded Mesocates", Inorganic Chemistry, 2018 Publication	<1 %
12	Isha Mishra, Maruthupandiyan Priyatharsini, Malaichamy Sathiyendiran. "Synthesis and characterization of binuclear manganese carbonyl complex of 1,4-bis(2-(2'-hydroxyphenyl)benzimidazol-1-yl)benzene and dimethylaminopyridine", Journal of Organometallic Chemistry, 2021 Publication	<1 %
13	Bhaskaran Shankar, Palani Elumalai, Shankar Deval Sathiyashivan, Malaichamy Sathiyendiran. "Spheroid Metallocavitands with Eight Calixarene-Shaped Receptors on the Surface", Inorganic Chemistry, 2014 Publication	<1 %
14	Isha Mishra, Malaichamy Sathiyendiran. "Luminescent [fac-Re(CO)3-N∩O-phenylimidazole] complexes with parallel arrangement of twisted ligand motifs", Journal of Organometallic Chemistry, 2019	<1 %

Publication

15	Submitted to Higher Education Commission Pakistan Student Paper	<1%
16	"Calixarenes and Beyond", Springer Science and Business Media LLC, 2016 Publication	<1%
17	vital.seals.ac.za:8080 Internet Source	<1%
18	Palanisamy Rajakannu, Bhaskaran Shankar, Malaichamy Sathiyendiran. "fac -Re(CO) 3 -based organometallic supramolecular coordination complexes using thiophene motif decorated flexible ditopic benzimidazolyl donor", Journal of Organometallic Chemistry, 2018 Publication	<1%
19	pubs.acs.org Internet Source	<1%
20	www.linknovate.com Internet Source	<1%
21	Bhaskaran Shankar, Firasat Hussain, Malaichamy Sathiyendiran. "Synthesis of rhenium-based M3L3L'-type metallacycle from benzimidazole and flexible tri(benzimidazole) ligands", Journal of Organometallic Chemistry, 2012	<1%

Publication

22	Upasana Phukan, Priya Maruthupandian, Malaichamy Sathiyendiran. "Self-assembly of rhenium core-based conjoined bicyclic supramolecule from pyrazole and flexible hexatopic pyrazolyl ligands", Journal of Organometallic Chemistry, 2020 Publication	<1 %
23	Genin Gary Huang, Chung-Jay Lee, Jyisy Yang, Zong-Zhan Lu et al. "Cavity-containing rhenium metallacycle treated evanescent wave infrared chemical sensors for the selective determination of odorous amines in the atmosphere", Sensors and Actuators B: Chemical, 2018 Publication	<1 %
24	scholar.uwindsor.ca Internet Source	<1 %
25	Casanova, Massimo, Ennio Zangrando, Fabio Munini, Elisabetta Iengo, and Enzo Alessio. "fac-[Re(CO)3(dmso-O)3](CF3SO3): a new versatile and efficient Re(i) precursor for the preparation of mono and polynuclear compounds containing fac-[Re(CO)3]+ fragments", Dalton Transactions, 2006. Publication	<1 %
26	Deepak Gupta, Vikash Singh, Stephan Hohloch, Malaichamy Sathiyendiran, Karsten	<1 %

Tedin, Biprajit Sarkar. "Utilizing a series of fac-Re(CO)3 core based quinonoid containing complexes for photophysical and cell imaging studies", Polyhedron, 2015
Publication

27	Isha Mishra, Maruthupandiyan Priyatharsini, Malaichamy Sathiyendiran. "Rhenium(I) complexes from 2-(2'-hydroxyphenyl)benzimidazolyl based bis-chelating ligand and 4-(amino)pyridine/4-(dimethylamino)pyridine", Journal of Organometallic Chemistry, 2020 Publication	<1 %
28	coek.info Internet Source	<1 %
29	www.science.gov Internet Source	<1 %
30	George Makris, Lauren L. Radford, Marina Kuchuk, Fabio Gallazzi, Silvia S. Jurisson, Charles J. Smith, Heather M. Hennkens. " NOTA and NODAGA [Tc]Tc- and [Re]Re-Tricarbonyl Complexes: Radiochemistry and First Example of a [Tc]Tc-NODAGA Somatostatin Receptor-Targeting Bioconjugate ", Bioconjugate Chemistry, 2018 Publication	<1 %
31	Kathleen V. Kilway, Shiping Deng, Sean Bowser, Joseph Mudd, Laronda Washington,	<1 %

Douglas M. Ho. "Molecular assembly of 1,3,5-tris(cyanomethyl) and 1,4-bis(cyanomethyl)arenes with silver triflate", Pure and Applied Chemistry, 2006
Publication

---

32 Thanasekaran, P.. "Metal-containing molecular rectangles: synthesis and photophysical properties", Coordination Chemistry Reviews, 200505 — <1%
Publication

---

33 www.cochemist.com — <1%
Internet Source

---

34 Bhaskaran Shankar, Saugata Sahu, Naina Deibel, David Schweinfurth et al. "Luminescent Dirhenium(I)-Double-Heterostranded Helicate and Mesocate", Inorganic Chemistry, 2014 — <1%
Publication

---

35 infoscience.epfl.ch — <1%
Internet Source

Exclude quotes	On	Exclude matches	< 14 words
Exclude bibliography	On		

Dalton Transactions

PAPER

View Article Online
View Journal | View Issue

Cite this: *Dalton Trans.*, 2018, **47**, 4494

Rhenium(I) based irregular pentagonal-shaped metallacavitands†

Mamina Bhol, Bhaskaran Shankar and Malaichamy Sathiyendiran *

Received 10th February 2018,
Accepted 23rd February 2018

DOI: 10.1039/c8dt00574e

rsc.li/dalton

Neutral ditopic flexible N-donor ligands (L^n = bis(4-(naphtho[2,3-*d*]imidazol-1-ylmethyl)phenyl)methane, L^1 bis(4-(benzimidazol-1-ylmethyl)phenyl)methane, L^2 or bis(4-(2-nonylbenzimidazol-1-ylmethyl)phenyl) methane, L^3) possessing a bis(4-methylphenyl)methane spacer with two imidazolyl donor units were designed and synthesized. The ligands were utilized to develop metallacavitands analogous to irregular pentagonal-shaped metallacavitands with larger cavities. The metallacavitands **1–4** were assembled from $Re_2(CO)_{10}$, a rigid bis-chelating donor (1,4-dihydroxy-9,10-anthraquinone or chloranilic acid) and L^n *via* a solvothermal approach. The ligands and the metallacavitands were characterized by analytical and spectroscopic methods. The molecular structures of **1** and **4** were further confirmed by single crystal X-ray diffraction analysis which revealed that a toluene molecule resides in the hydrophobic cavity. L^n and **1–4** are emissive in DMSO at room temperature. The internal cavity of the metallacavitand acts as a host for aromatic guest molecules. The host–guest interaction properties of **1** with anthracene, naphthalene, nitrobenzene, 2-nitrotoluene, 4-nitrotoluene and 2,4-dinitrotoluene were studied by an emission spectroscopic method.

Introduction

The design and synthesis of metallacavitands similar to calixarenes is a growing area due to their applications in the fields of molecular recognition, catalysis, selective reactivity and biology.[1–4] Most of the studies in the area are focused on making neutral/ionic metallacalix[*n*]arenes (*n* = 3 and 4) to tune the hydrophobic cavity and functional groups at the rim.[5–8] Further, various approaches *i.e.*, various metal ions and organic building units have been used to modulate the properties. Till now attempts to make a neutral metallacavitand framework larger than calix[4]arene are scarce. It is likely that the expected conformationally rigid metallacavitand may display properties similar to calix[5]arene/pillar[5]arene and may possess a larger hydrophobic cavity.[9,10] Herein, we report a simple synthetic approach to a metallacavitand with a larger cavity. The neutral heteroleptic metallacavitands were assembled using $Re_2(CO)_{10}$, rigid bis-chelating donors and flexible ditopic N-donor ligands possessing a bis(4-methylphenyl)methane spacer, *via* a solvothermal approach. Though the approach is similar to the synthesis of a dirhenium-based metallacalix[4]arene *i.e.*, combining ditopic ligands containing a "phenylene(CH_2-heterocycle)$_2$" flexible framework, a rigid bis-chelating donor, and $Re_2(CO)_{10}$,[11,12] this approach uses a "CH_2-(phenylene-CH_2-heterocycle)$_2$" framework that results in a metallacavitand with a solvent-accessible hydrophobic cavity (Scheme 1).

Results and discussion

Synthesis and molecular structure of ligands

Neutral nitrogen donor ligands (L^1–L^3) were obtained using bis(4-bromomethylphenyl)methane and a heterocyclic motif (naphthanoimidazole, H-nimz; benzimidazole, H-bimz; 2-nonylbenzimidazole, H-nbimz) in the presence of base.[11] The ^{1}H NMR spectra of L^n displayed a single set of signals for all of the protons. In particular, two singlet signals in the aliphatic region correspond to two methylene protons (~5–6 ppm for

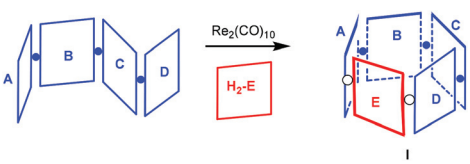

Scheme 1 Synthesis of an irregular pentagonal-shaped metallacavitand (**I**). A = D = heterocyclic nitrogen donor; B = C = phenylene; H_2E = bis-chelating unit; ● = CH_2; ○ = *fac*-$Re(CO)_3$.

School of Chemistry, University of Hyderabad, Hyderabad-500 046, India.
E-mail: msathi@uohyd.ac.in

†Electronic supplementary information (ESI) available: Experimental section and crystallographic data of L^1, L^2, **1** and **4**. CCDC 1587398, 1587399, 1587406 and 1587407. For ESI and crystallographic data in CIF or other electronic format see DOI: 10.1039/c8dt00574e

Inorganic Chemistry

pubs.acs.org/IC

Article

Rhenium(I)-Based Heteroleptic Pentagonal Toroid-Shaped Metallocavitands: Self-Assembly and Molecular Recognition Studies

Mamina Bhol, Bhaskaran Shankar, and Malaichamy Sathiyendiran*

Cite This: https://doi.org/10.1021/acs.inorgchem.2c02061

Read Online

ACCESS | Metrics & More | Article Recommendations | Supporting Information

ABSTRACT: A family of neutral, heteroleptic, dinuclear M_2LL'-type pentagonal toroid-shaped metallomacrocycles (**1**–**8**) were synthesized using flexible ditopic N donors ($L^n = L^1$–L^2), rigid bis-chelating ligands (H_2–L′ = H_2–E), and $Re_2(CO)_{10}$ in a one-pot solvothermal self-assembly approach. The ligands and the metallomacrocycles were characterized using ATR-IR, electrospray ionization mass spectrometry, nuclear magnetic resonance, ultraviolet–visible, and emission spectroscopy methods. The molecular structures of **1**, **2**, **4**, **6**, and **7** were confirmed by an X-ray diffraction study and are similar to those of calix[5]arene. The cyclic inner cavities of the metallomacrocycles accommodate toluene/mesitylene/acetone/chlorobenzene as guest molecules that are stabilized by cumulative C–H···π and π···π interactions with the cyclic framework of metallomacrocycle. The photophysical properties of the ligands and the metallomacrocycles were studied. The host–guest recognition properties of metallocavitands **1**, **2**, **7**, and **8** as a model host with phenol and nitrobenzene derivatives as guest molecules were studied by emission spectroscopy methods.

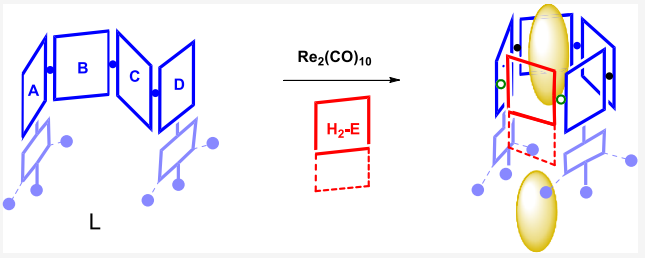

INTRODUCTION

The design and synthesis of metallomacrocycles similar to calixarene-shaped geometry have been attracting significant research interest because of their potential applications in host–guest encapsulation, catalysis, selective reactivity, sensing, and biomimetic structures.[1−5] Naked metal ions and complexes containing partially protected metal ions are employed along with pre-designed organic ligands to self-assemble calixarene-shaped complexes.[6−10] These metallomacrocycles are commonly called as metallocavitands, more specifically metallocalix[*n*]arenes.[1] Among various metal ions and metal complexes, $Re_2(CO)_{10}$/$[Re(CO)_5X]$, where X = Cl or Br, provides a way to make neutral, heteroleptic metallocalix[*n*]arenes.[11−15] Until now, neutral ditopic donors including 4,7-phenanthroline, imidazole, and semi-rigid ditopic N-donor ligands containing the phenyl ($-C_6H_4-$) spacer and rigid bis-chelating ligands are utilized for assembling tunable rhenium tricarbonyl-based metallocalix[3]arenes and metallocalix[4]arenes.[11,13,14] Recently, the focus in the area has shifted to make functional and cavity-tunable metallocalixarenes. To the best of our knowledge, the design approach for making rhenium-core-based metallocavitands similar to calix[5]arene is limited.[16] We have recently designed and employed diphenylmethane ($-C_6H_4-CH_2-C_6H_4-$) spacer-based semi-rigid ditopic N-donor ligands along with the rigid bis-chelating ligand and $Re_2(CO)_{10}$ to assemble irregular pentagonal-shaped metallocavitands.[16] These metallocavitands adopt a tubular structure, accommodate toluene molecules in the solid state, and are able to recognize the guest molecules including nitroaromatic compounds and polyaromatic hydrocarbons in the solution. The central cyclic framework, that is, annulus of the metallocavitand, consists of two phenyl motifs, two imidazolyl motifs, and a bis-chelating ligand. The size of the cavity, thereby the chemistry associated with molecular cavity, can be tuned by increasing the fused arene motif(s) either by modifying the imidazolyl motif and/or by changing the bis-chelating motifs. In continuation of our research in this field, we envision that introducing the 4-methoxyphenyl/3,4,5-trimethoxyphenyl motif at the 2-position of the benzimidazolyl unit in the ditopic N donor would result in metallocavitands with a more extended cavity suitable to accommodate various types of guest molecules (Scheme 1). In addition, the solubility of the metallocavitands in general organic solvents would be increased due to the presence of methoxy units at the periphery of the metallocavitands.

Herein, we report two new flexible neutral ditopic nitrogen donors (L^1/L^2) consisting of two terminal 4-methoxyphenyl benzimidazolyl/3,4,5-trimethoxyphenyl benzimidazolyl nitrogen donors and diphenylmethane spacer and eight new neutral heteroleptic dinuclear metallocavitands (**1**–**8**) in a one-pot approach. The molecular structures of the five metallocavitands (**1**, **2**, **4**, **6**, and **7**) are unambiguously determined

Received: June 14, 2022

Inorganic Chemistry

pubs.acs.org/IC

Communication

Calix[4]arene-Analogous Technetium Supramolecules

Mamina Bhol, Guilhem Claude, Maximilian Roca Jungfer, Ulrich Abram,* and Malaichamy Sathiyendiran*

Cite This: *Inorg. Chem.* 2022, 61, 5173−5177

Read Online

ACCESS | Metrics & More | Article Recommendations | Supporting Information

ABSTRACT: Calix[4]arene-analogous technetium supramolecules (**1** and **2**) were assembled using $(NBu_4)[Tc_2(\mu\text{-}Cl)_3(CO)_6]$ and neutral flexible bidentate nitrogen-donor ligands (L^1 and L^2) consisting of four arene units covalently joined via methylene units. The neutral homoleptic technetium macrocycles adopt a partial cone/cone-shaped conformation in the solid state. These supramolecules are the first example of *fac*-$[Tc(CO)_3]^+$ core-based metallocalix[4]arenes and second example of *fac*-$[Tc(CO)_3]^+$ core-based metallomacrocycles. Structurally similar *fac*-$[Re(CO)_3]^+$ core-based macrocycles (**3** and **4**) were also prepared using $[Re(CO)_5X]$ (where X = Cl or Br) and L^1 or L^2. The products were characterized spectroscopically and by X-ray analysis.

The design and synthesis of stable and kinetically inert *fac*-$[M(CO)_3]^+$ (M = ^{99m}Tc/$^{186/188}$Re) core-based complexes have been gaining continuous research interest for the development of new radiopharmaceuticals as diagnostic and therapeutic agents.[1−17] ^{99m}Tc is still the workhorse of nuclear diagnostics because of its ideal nuclear decay properties ($t_{1/2}$ = 6.02 h, pure γ emitter, and E_γ = 140 keV, 89%), whereas the β-emitting rhenium nuclides ^{188}Re ($t_{1/2}$ = 17 h and E_β = 2.12 MeV) and ^{186}Re ($t_{1/2}$ = 89.3 h and E_β = 1.07 MeV) have potential for therapy.[2] Isostructural technetium and rhenium complexes are good candidates for nuclear medical theranostics, and procedures exist for the synthesis of aqua complexes $[^{99m}Tc/^{188}Re(CO)_3(H_2O)_3]^+$ as appropriate precursor molecules.[1c,2b,4,6] Several attempts have been made toward the synthesis of organometallic technetium complexes using various types of heterocyclic ligands because of their importance in medicinal fields.[1−17] Recently, efforts have been directed toward the design and synthesis of *fac*-$[Re(CO)_3]^+$ core-based metal−organic macrocycles, i.e., supramolecular coordination complexes or metallomacrocycles, because of their potential applications as bioimaging and anticancer agents.[18−20]

We envision that the synthesis of *fac*-$[Tc(CO)_3]^+$ core-based macrocycles may result in a new class of supramolecules that may find potential utility in medicinal fields because of the combined properties of the technetium(I) tricarbonyl core and discrete 2D/3D supramolecular structures. In general, the known synthetic approaches for making *fac*-$[Re(CO)_3]^+$ core-based discrete supramolecules can be applied to create structurally analogous *fac*-$[Tc(CO)_3]^+$ core-based supramolecules.[20−22] To the best of our knowledge, *fac*-$[\{Tc(CO)_3Cl\}_2(ptc)_2]$ [ptc = 4-pyridylthiosemicarbazone = $C_6H_5N\text{-}C(CH_3)=N\text{-}NH\text{-}C(S)\text{-}NH_2$], is the only known example for a metallomacrocycle based on the *fac*-$[Tc(CO)_3]^+$ core.[15] Here, we report *fac*-$[Tc(CO)_3Cl]$ core-based supramolecules analogous to calix[4]arenes. The metallomacrocycles *fac*-$[Tc(CO)_3Cl(L^n)]$ (**1** and **2**) were self-assembled via the reaction between $(NBu_4)[Tc_2(\mu\text{-}Cl)_3(CO)_6]$ and neutral flexible bidentate nitrogen donors (L^1 for **1** and L^2 for **2**; Scheme 1).

Scheme 1. Synthesis of Technetium Metallocalix[4]arenes

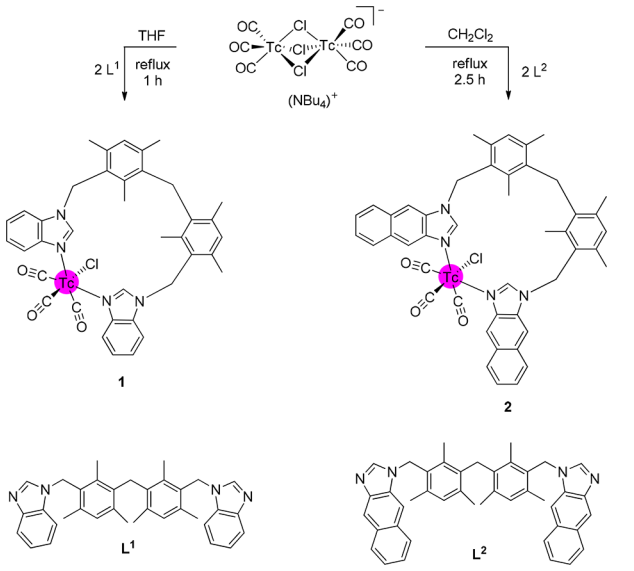

Isostructural rhenium macrocycles *fac*-$[Re(CO)_3X(L^n)]$ (**3a**, **3b**, and **4**) were assembled using $[Re(CO)_5X]$ and the nitrogen-donor ligands of Scheme 1 (X = Cl and L^n = L^1 for **3a**; X = Br and L^n = L^1 for **3b**; X = Br and L^n = L^2 for **4**). The molecular structures of the metallomacrocycles were unambig-

Received: November 27, 2021
Published: March 23, 2022

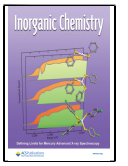

Journal of Organometallic Chemistry 889 (2019) 27–32

Contents lists available at ScienceDirect

Journal of Organometallic Chemistry

journal homepage: www.elsevier.com/locate/jorganchem

Solid state structure and photophysical properties of monoanionic 2-(2′-hydroxyphenyl)benzimidazole as an anionic core in rhenium complex

Mamina Bhol [a], Maruthupandiyan Priyatharsini [b], Rajaputi Venkatraman Krishnakumar [b, **], Malaichamy Sathiyendiran [a, *]

[a] School of Chemistry, University of Hyderabad, Hyderabad, 500046, India
[b] Department of Physics, Thiagarajar College, Madurai, 625009, India

ARTICLE INFO

Article history:
Received 9 February 2019
Received in revised form
13 March 2019
Accepted 15 March 2019
Available online 20 March 2019

Keywords:
bis(diphenylphosphino)ethane
2-(2′-phenol)benzimidazole
Luminescence
Hydrogen bonding
Rhenium

ABSTRACT

A monoanionic 2-(2′-phenolate)benzimidazole ($HPBI^-$) stabilized in organometallic complex $[Re(CO)_2(dppe)_2](HPBI)$ (**1**) which was obtained by treating 2-(2′-hydroxyphenyl)benzimidazole (H_2—PBI), 1,2-bis(diphenylphosphino)ethane (dppe), and $Re_2(CO)_{10}$, in toluene using a one-pot approach. Solid state structure of complex was determined using a single crystal X-ray diffraction analysis. The monoanionic $HPBI^-$ in **1** is nearly planar and adopts *trans*-anion conformation i.e., both oxygen atom and NH proton are on the same side and are stabilized by the intramolecular N—H···O hydrogen bonding interaction. The photophysical properties of **1** in solution are corroborated with the monoanionic $HPBI^-$ anion generated in situ from neutral H_2PBI by adding base. The solid state emission of **1** is red-shifted in compared to that of **1** in the solution. The monoanionic $HPBI^-$ in **1** was transformed into dianionic PBI^{2-} in the complex, {$[Re(CO)_2(dppe)_2](HPBI)$ (**1**) → $(Bu_4N)[Re(CO)_2(dppe)_2](PBI)$ (**2**)}, by adding tetrabutylammonium fluoride (Bu_4NF) without decomposing the coordination complex.

1. Introduction

Research on synthesis, structural characterization and photophysical studies of 2-(2′-hydroxyphenyl)benzimidazole H_2—PBI and its analogues have been gaining great importance due to their potential applications in the photoactive materials including photoactive switches, fluorescence sensors, and laser dyes [1–8]. The photophysical properties of neutral H_2PBI were studied both in the solid state and in the solution state [3,6a]. In particular, photophysical studies of neutral H_2PBI in various solvents, different temperatures and different pH conditions were studied thoroughly by various groups. Recently, the anionic forms, monoanionic $HPBI^-$ or dianionic PBI^{2-}, were generated in situ by adding a base in the solution of neutral H_2PBI. The ground state and excited state photophysical properties of monoanionic $HPBI^-$ or dianionic PBI^{2-} are studied [6]. Similar to neutral H_2PBI, these anions can adopt a different conformation in the solution depending upon the solvents, and base and display unique emission properties. In particular, each conformer, which originated due to the rotation, displays a unique absorptions and emission properties. Though the solid state structure of neutral H_2PBI was determined using single crystal X-ray diffraction data (SCXRD), solid state structure of the monoanionic $HPBI^-$ was not studied. The isolation of monoanionic $HPBI^-$ or dianionic PBI^{2-} with an ion which should not interact/influence the conformation of the monoanionic $HPBI^-$ or dianionic PBI^{2-} will be useful to get benchmark photophysical data.

Herein, we report on the synthesis, solid state structural characterization of 2-(2′-phenolate)benzimidazole ($HPBI^-$), which is stabilized by non-coordinating counter coordination complex. The complex $[Re(CO)_2(dppe)_2](H\text{-}PBI)$ (**1**) was obtained by treating neutral H_2PBI, dppe and $Re_2(CO)_{10}$ in a one-pot approach serendipitously. The monoanionic $HPBI^-$ adopts *trans*-conformation both in solid and solution states. The complex **1** was characterized using SCXRD analysis, FT-IR, and ^1H NMR spectroscopy. The photophysical properties of **1** in both solution state and solid state were studied. The monoanionic $HPBI^-$ in **1** was transformed into dianionic PBI^{2-} in the complex, {$[Re(CO)_2(dppe)_2](HPBI)$ (**1**) → $(Bu_4N)[Re(CO)_2(dppe)_2](PBI)$ (**2**)}, by adding tetrabutylammonium

* Corresponding author.
** Corresponding author.
E-mail addresses: mailtorvkk@yahoo.co.in (R.V. Krishnakumar), msathi@uohyd.ac.in (M. Sathiyendiran).

https://doi.org/10.1016/j.jorganchem.2019.03.013
0022-328X/

Record Review

THE CHEMICAL RECORD

DOI: 10.1002/tcr.202000150

Emerging Spacers-Based Ligands for Supramolecular Coordination Complexes

Isha Mishra,[a] Mamina Bhol,[a] Palanisamy Kalimuthu,*[b] and Malaichamy Sathiyendiran*[a]

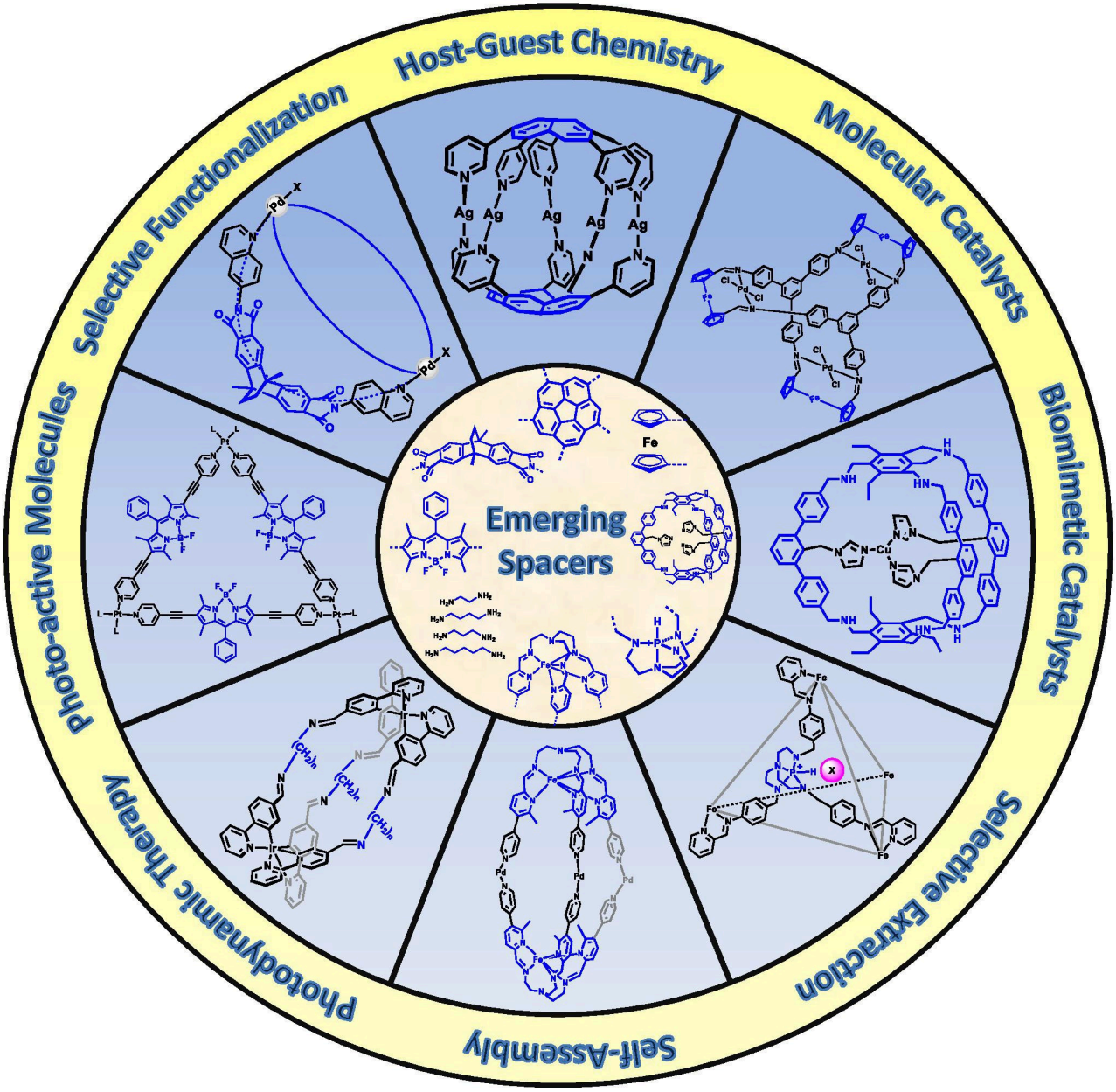

Abstract: The design and self-assembly of supramolecular coordination complexes (SCCs) i.e., discrete cyclic metalloarchitectures such as cycles, cages, mesocates, and helicates with desired size, shape, and properties have been increasing exponentially owing to their potential applications in molecular sensors, molecular cargos, molecular recognition, and catalysis. The introduction of the organic motifs and metal complexes as a spacer provides functionality to the metalloarchitecture. This review mainly focusses on newly evolving spacer based ligands employed to yield simple to high-order metallosupramolecular assemblies using straight-forward approaches. The new spacers including corannulene, organic cyclic framework, bicyclic organic motifs, aliphatic chain, metalloligands, triarylboron, BODIPY, azaphosphatrane, phosphine, and thio/selenophosphates offer a great set of properties and in-built functionalities to the metalloarchitectures which are discussed in this review.

Keywords: Supramolecular chemistry, Self-assembly, Molecular recognition, Schiff bases, Sandwich complexes

1. Introduction

The design and synthesis of supramolecular coordination complexes (SCCs) such as metallosupramolecules,[1] metallocages,[2–3] metallomacrocycles[4] using complementary motifs of predesigned ligands and metal precursors through self-assembly approach have been increasing tremendously day by day.[1–4] The continuous increase of research in this area is owing to the ease of preparation of the SCCs and their potential applications including molecular sensors,[5] selective purification of molecules,[6] molecular vessels for selective functionalization of guest molecules,[7] molecular catalysts by providing cavity as well as catalytic cores,[8] photoactive molecules,[3] cell imaging agents,[3a–d,9] and molecular drugs.[10] The simple cyclic structures to aesthetically pleasing high-order complex structures can be obtained by mixing the predesigned motifs and metal precursor, at appropriate conditions.[11] The careful selection of metal precursor and ligand design play the crucial role in achieving the desired self-assembly of SCCs. In particular, the predesign of the ligands by incorporating different types of organic spacer motifs has been elevating the field to an advanced level by providing in-built functionality.[1,11] There are two types of ligands often used in metal-directed assembly. The first one is organic coordinating motifs (Example: 4,4′-bipyridyl ligand) which are directly linked to each other and are used as the structural framework for constructing a variety of metal-core based cyclic assemblies.[12] Another type of ligand framework is spacer based coordinating motif in which the spacer separates the coordinating donor units. A typical example is alkene spacer-based 1,2-di(pyridin-4-yl)ethene which is a structural and functional analog of 4,4′-bipyridine.[13] The spacer units provide unique flexibility/rigidity and directionality for the ligands to achieve desired geometry of SCCs with distinct features.[1–13] Our review focuses on the work that appeared in the literature from the year 2018 onwards till now and includes SCCs based on newly evolving spacer-based ligands. Herein, we discuss metalloarchitecures constructed based on corannulene, organic cyclic framework, bicyclic organic motifs, aliphatic chain, metalloligands, triarylboron, boron dipyrromethene (BODIPY), azaphosphatrane, phosphine, and thio/selenophosphates as spacers-based ligands.

2. Corannulene Spacer Based Ligands and its SCCs

Corannulene is a polycyclic aromatic hydrocarbon and adopts bowl-shaped structure.[14,15] This unique arrangement with π-conjugation gives the corannulene a curved aromatic surface. The periphery of the corannulene offers a rare opportunity to synthesize symmetrical pentatopic ligands.[16] The predesigned corannulene spacer based ligands are good candidates for assembling spherical metallacages due to their unique curvature. The spherical cages with corannulene motifs are suitable host for molecules like fullerenes due to the expected complementary concave-convex noncovalent aromatic stacking interactions.

The unique properties of corannulene were utilized by Jiang and co-workers to synthesize a spectacular spherical ionic coordination cage $[Ag_5(L^1)_2]^{5+}$ (**1**) from a pentatopic ligand possessing corannulene spacer (L^1).[17] The ligand was ration-

[a] *I. Mishra,[+] M. Bhol,[+] Dr. M. Sathiyendiran*
School of Chemistry
University of Hyderabad, Hyderabad 500 046, India
E-mail: msathi@uohyd.ac.in
[b] *Dr. P. Kalimuthu*
Department of Chemistry
The Gandhigram Rural Institute (Deemed to be University)
Gandhigram-624 302, Tamil Nadu, India
E-mail: pakalimuthu@gmail.com
[+] *Both IM and MB are contributed equally.*

